Studies in Systems, Decision and Control 24

Xinghuo Yu
Mehmet Önder Efe *Editors*

Recent Advances in Sliding Modes: From Control to Intelligent Mechatronics

Springer

Studies in Systems, Decision and Control

Volume 24

Series editor

Janusz Kacprzyk, Polish Academy of Sciences, Warsaw, Poland
e-mail: kacprzyk@ibspan.waw.pl

About this Series

The series "Studies in Systems, Decision and Control" (SSDC) covers both new developments and advances, as well as the state of the art, in the various areas of broadly perceived systems, decision making and control- quickly, up to date and with a high quality. The intent is to cover the theory, applications, and perspectives on the state of the art and future developments relevant to systems, decision making, control, complex processes and related areas, as embedded in the fields of engineering, computer science, physics, economics, social and life sciences, as well as the paradigms and methodologies behind them. The series contains monographs, textbooks, lecture notes and edited volumes in systems, decision making and control spanning the areas of Cyber-Physical Systems, Autonomous Systems, Sensor Networks, Control Systems, Energy Systems, Automotive Systems, Biological Systems, Vehicular Networking and Connected Vehicles, Aerospace Systems, Automation, Manufacturing, Smart Grids, Nonlinear Systems, Power Systems, Robotics, Social Systems, Economic Systems and other. Of particular value to both the contributors and the readership are the short publication timeframe and the world-wide distribution and exposure which enable both a wide and rapid dissemination of research output.

More information about this series at http://www.springer.com/series/13304

Xinghuo Yu · Mehmet Önder Efe
Editors

Recent Advances in Sliding Modes: From Control to Intelligent Mechatronics

Springer

Editors
Xinghuo Yu
RMIT University
Carlton, Victoria
Australia

Mehmet Önder Efe
Hacettepe University
Beytepe
Turkey

ISSN 2198-4182 ISSN 2198-4190 (electronic)
Studies in Systems, Decision and Control
ISBN 978-3-319-18289-6 ISBN 978-3-319-18290-2 (eBook)
DOI 10.1007/978-3-319-18290-2

Library of Congress Control Number: 2015937480

Springer Cham Heidelberg New York Dordrecht London

Printed on acid-free paper

Springer International Publishing AG Switzerland is part of Springer Science+Business Media (www.springer.com)

To Professor Okyay Kaynak to commemorate his life time impactful research and scholarly achievements and his services to the profession

Foreword

It is a pleasure for me to write this foreword for the book dedicated to Okyay Kaynak to commemorate his lifetime impactful research and scholarly achievements and outstanding services to profession.

Okyay has been a long time friend and colleague at my university. I have been following his activities and achievements with admiration. He has been the scientific ambassador of my university and Turkey in the international circles. He appears to have friends all over the world. Although we are in somewhat different fields, wherever I visit, I have often received the remark, “Oh, we know Okyay Kaynak from your university!".

Okyay got his Ph. D. degree at a very early age, when he was only 24 years old. He spent the following 6 years in industry and then joined my university. The industrial exposure has contributed positively to his teaching and research activities, as well as to the administrative responsibilities that he has carried, such as the founding Chairman of Computer Engineering Department, Director of Biomedical Engineering Institute, Chairman of EEE Dept., Director of Mechatronics Research and Application Center and the holder of the UNESCO Chair on Mechatronics (a title conferred on him at our campus by the Director General of UNESCO; Federico Mayor), to name a few. He has introduced the field of mechatronics to his colleagues and made a reputation of being the guru of mechatronics in Turkey. Thanks to his efforts, we now have a secondary graduate program in this field.

At the early stages of his career, Okyay has designed and delivered together with his colleagues many continuing education courses to industry through Bogazici University Foundation. This has resulted in considerable amount of income to the Foundation. In later years, he has cooperated with an industrial company in delivering mechatronics related courses. A certificate program on mechatronics has been continuing for a number of years.

Okyay has been one of most prolific members of my university; in recent years he has been publishing at a rate of 6-8 high quality journal papers per year in collaboration with many colleagues from many different parts of the world, as varied as UK, US, Australia, Israel, Bulgaria, Japan, Hungary, Kazakhstan, Iran and China. Some of his coauthors have spent sabbaticals at his department.

In addition to his recognized scientific contributions, Okyay has organized many conferences in Istanbul. Thanks to him, we have had very large groups of people visiting our campus. This has helped to increase the recognition of our university throughout the world.

Okyay is known not only with his impactful scientific research but also with the leadership and guidance he has provided to his colleagues. His apparently boundless energy, insight, and leadership are well known among his international peers throughout the world. He serves as a role model for his colleagues not only in Turkey but also around the world.

Thanks Okyay for what you have done for Bogazici University.

Professor Dr. Gülay Barbarosoğlu
Rector
Bogazici University
Istanbul, Turkey

Preface

The volume is dedicated to Professor Okyay Kaynak to commemorate his life time impactful research and scholarly achievements and outstanding services to profession.

Professor Kaynak has graduated with a first class honours and PhD degrees from the University of Birmingham, UK, in 1969 and 1972, respectively. Before joining the academia, he spent some years in industry, which has been an advantage for him in later years during his academic life, causing his research activities to be more application oriented, with a strong footing. So far, he has authored or coauthored more than 400 papers that have appeared in various journals, books and conference proceedings. Professor Kaynak is very well known for his work on Variable Structure Systems and Sliding Mode Control. He started his research activities in these topics while he was in Japan in early 1980s. His 1987 publication on Discrete-Time Sliding Mode Control is seminal, having received close to 300 WoS citations. Although close to 30 years has passed since its publication, it is still being cited (20, 22 and 11 citations in 2012, 2013 and 2014 respectively) - an indication of its seminality.

In recent years, Professor Kaynak has concentrated on the fusion of computationally intelligent methodologies and sliding mode control. With a paper that combines the artificial neural networks and sliding mode control, he has coined the word "neurosliding." He contributes to the scientific literature not only with his doctoral students from Turkey but also with students and colleagues from many different parts of the world, the collaborations being achieved through internet and short visits.

In addition to his research activities, Professor Kaynak has also made significant contributions to the profession internationally, in particular, his leading role in the IEEE (Institute of Electrical and Electronics Engineers) - the world's largest professional organization with over 400,000 members worldwide. He served as the President of IEEE Industrial Electronics Society during 2002-2003, and has been a leading person in the group who conceived, designed, developed and brought to life two very successful major interdisciplinary IEEE publications, namely, IEEE/ASME Transactions on Mechatronics and IEEE Transactions on Industrial Informatics. He was in the Management Committee of the first one for a number of years, and the Editor in Chief of the latter for 2005-2006. Currently he is the Editor-in-Chief of IEEE/ASME Transaction on Mechatronics.

Professor Kaynak's outstanding achievements have been recognized by a number of awards and prizes, including the prestigious Dr. - Ing Eugene Mittelmann Achievement Award of IEEE Industrial Electronics Society, and fellowships from Alexander von Humboldt Foundation of Germany and Matusumae International. He was award an IEEE fellowship in 2003 "for contributions to variable structure systems theory and its applications in mechatronics."

His accomplishments are more remarkable considering they have all been achieved in his home country, Turkey where he has worked almost all his life, with his students and colleagues in Turkey where the conditions may have been less favorable as compared to some western countries, especially perhaps before the last decade.

The 21 invited chapters in this volume have been written by leading researchers who, in the past, have had association with Professor Kaynak as either his students and associates or colleagues and collaborators. The focal theme of the volume is the Sliding Modes and their applications from Control to Intelligent Mechatronics.

The volume is opened with a touching article by Professor Vadim Utkin acknowledging significant contributions that Professor Kaynak has made to the engineering fields and profession. The rest of the chapters cover a broad scope of topics in Sliding Modes from theoretical investigations to significant applications.

Chapters 2-11 are focused on theoretical investigations. Chapter 2 examines the development of the Sliding Mode Control (SMC) theory in the last decades, and proposes arbitrary-order continuous SMC algorithms which can significantly reduce chattering and improve precision. Chapter 3 presents a decentralised SMC strategy for some nonlinear interconnected systems using only local information. In Chapter 4, control issues for multi-input uncertain non-affine systems are examined and integral SMC is adopted as an effective approach. Chapter 5 explores various dynamical behaviours of discretised fast terminal SMC systems and conditions are obtained to ensure convergent steady states. In Chapter 6, a new class of nonlinear reaching laws are developed for discrete-time SMC and applied successfully to solve an inventory supply chain problem. Chapter 7 further studies the sliding mode adaptation and convergence-time regulation by revealing a connection between the sliding mode accuracy and homogeneous high-order sliding modes. In Chapter 8, a new class of SMC, the event-triggering SMC, is proposed and sufficient event conditions are derived to guarantee finite-time sliding mode to occur. In Chapter 9, a non-homogeneous continuous super-twisting algorithm for higher-order dynamical systems is proposed and conditions to ensure finite-time stability are obtained. Chapter 10 proposes an output feedback sliding mode controller to solve the global exact output tracking problem for a class of uncertain multivariable nonlinear systems using norm observes. In Chapter 11, the SMC of switched stochastic hybrid systems is fully explored, including sliding surface design, stability and SMC law synthesis.

The remaining chapters are about applications of SMC. Chapter 12 fully examines the SMC of unmanned aerial vehicles (UAVs) and outlines their future challenges and issues. In Chapter 13, a hybrid SMC with feedback linearization control is proposed for voltage source inverter-fed induction motors which shows to be very effective. Chapter 14 proposes a tensor product model transformation based SMC for linear control systems which is applied to a DC serve gear motor control problem. In Chapter 15, a

novel SMC strategy is developed for controlling a robotic fish. Chapter 16 extends the super-twisting algorithm to control an under-actuated five degrees of freedom parametrically excited crane. Chapter 17 integrates SMC-based learning algorithms and fuzzy neural networks for controlling helicopters. In Chapter 18, fuzzy SMC of direct drive manipulators done over the years in Professor Kaynak's laboratory is reviewed and the role of controller parameter adaptation for SMC is discussed. Chapter 19 develops a reduced model that is proposed for controlling the temperature on the wafer in a rapid thermal processing system and subsequently a SMC strategy is developed. Chapter 20 examines the development of sliding surfaces and their applications. Finally, Chapter 21 proposes a terminal SMC for controlling a quadrotor type UAV.

As the organizers of this volume who have worked with Professor Kaynak in various capacities, we would like to thank him for having such a wonderful impact on the particular field and for the service he provided to the society in many different forms. We would also like to express our sincere thanks to the chapter contributors for their support to our book project. Special thanks are directed to Prof. Janusz Kacprzyk, the Editor of Springer Book Series "Studies in Systems, Decision and Control" for his encouragement and support to edit this volume. Thanks also go to Dr. Thomas Ditzinger and Dr. Leontina Di Cecco, both from Springer Applied Sciences and Engineering, for their support during implementation of this project. Finally, we are very thankful to our families for their cooperation.

Xinghuo Yu
Mehmet Önder Efe
Editors

Contents

My Friend, Professor Okyay Kaynak

Vadim Utkin

Professor Okyay Kaynak is an internationally recognized scientist with significant contributions into several engineering areas: control theory, industrial electronics, mechatronics etc. He deserves great respect of colleagues for his many year activity including: research; teaching; work as chairman, president, vice-president of many international committees and societies, as chairman and director of departments and research centers; membership in editorial boards of scientific journals; organizing numerous international conferences.

We met for the first time in1989 during our sabbatical stay at Institute of Industrial Sciences of University of Tokyo (Figure 1). We shared an office with Okyay and since then keep close professional and personal contacts.

Fig. 1. First time meeting with Okyay and Japanese colleagues in 1989

Within last 30 years Prof. Kaynak has been working in the area of my main professional interest – variable structure systems and sliding mode control. Research in this area was initiated in the former USSR in 60's and only 10 years later colleagues of different countries showed interest and included this topic into the scope of their research programs. Prof. Kaynak was a key figure of this process. He was invited to Tokyo University in early 80's as a visiting scholar. The head of the department Prof. Harashima offered him several topics for future joint research and Okyay selected variable structure systems (VSS) with sliding mode control, practically unknown area for Japanese colleagues. His decision was the starting point for intensive development of different sections of theory and applications for this class of control systems in Japan.

The sliding mode control exhibits low sensitivity with respect to different types of uncertainties in operation conditions such as unknown disturbances, parameter variations. In addition it enables decoupling complex systems into independent subsystems of lower dimension, which is important for control of high order nonlinear

X. Yu and M. Önder Efe (eds.), *Recent Advances in Sliding Modes,*
Studies in Systems, Decision and Control 24, DOI: 10.1007/978-3-319-18290-2_1

dynamic plants, in particular manipulators and mobile robots. The colleagues working with Prof. Kaynak were the first who demonstrated efficiency of the sliding mode control methodology in robotics. The robot in Figure 2 did not look so naïve 30 years ago as it does now.

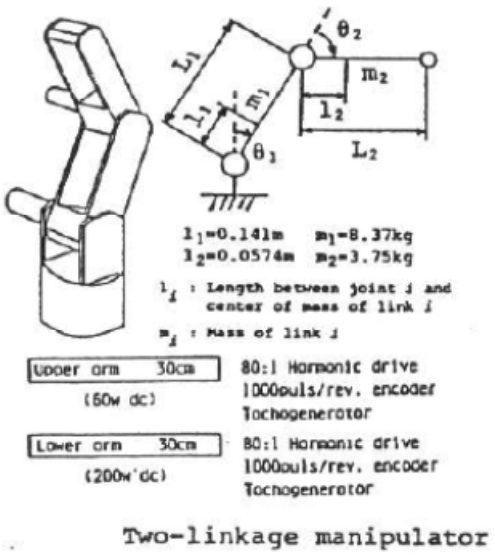

Fig. 2. Sliding mode control of a robotic manipulator

Two papers published in co-authorship with Prof. F. Harashima and Prof. H. Hashimoto served as background for the implementation of sliding mode control for the manipulator shown in Figure 2.

In 80's interest to sliding mode control increased considerably. It resulted in high level of publications by authors from different universities and research centers of many countries and we could speak about international community of researchers working in this area. The role of Prof. Kaynak in establishing of the community would hardly be overestimated. He was among the organizers of the first international workshop on VSS, held in Sarajevo in 1990. It was the historical event in the life of the community. As I know, until now Prof. Kaynak keeps the menu of the restaurant, where the meeting of the organizing committee was held, signed by the committee members. The workshop was so successful that many volunteers offered to organize the next one in their countries. Since then the workshop was held every two years in England, Italy, Japan, Australia, USA, Spain, Mexico, India, the last one in France in 2014 and of course one of them was held in Turkey and organized by Prof. Kaynak. He was a member of organizing committees of majority of them. Thanks to the activity of the leading figures in the area, including Prof. Kaynak, the sliding mode control methodology was recognized as a chapter of the nonlinear control theory and now it can be found in many modern control text books. Finally IEEE Technical Committee on Variable Structure and Sliding Mode Control was established in 2000.

The sections on sliding mode control are included into programs of the most prestigious control conferences (IFAC congresses, ACC, CDC). But not control conferences only. I will explain why. Sliding mode control implies discontinuous control actions. Electronic power converters serve as actuators in many control systems of modern technology and on-off is the only acceptable mode for them. It means that sliding mode is a natural and prospective tool to control power converters. Prof. Kaynak is an expert in industrial electronics and did a lot of "advertising efforts". Now you can find many papers on sliding mode applications in journals and conferences on industrial electronics. I am thankful to Okyay for promoting my IEEE fellowship in IEEE Industrial Electronics Society.

I am happy to pay tribute to my good friend Okyay for his outstanding scientific achievements and multifarious service to our control community, heading numerous national and international organizations and meetings, involving young scientists of many countries to research activity (reflected in his joint publications with colleagues of UK, US, Australia, Bulgaria, Japan, Hungary, Kazakhistan, Iran, China).

Dear Okyay, all of us, your friends and colleagues, believe that your retirement is symbolic and we will enjoy collaboration and personal contacts with you for many years.

Vadim Utkin
Ohio State University

Continuous Nested Algorithms : The Fifth Generation of Sliding Mode Controllers

Leonid Fridman[1], Jaime A. Moreno[2], Bijnan Bandyopadhyay[3], Shyam Kamal[3], and Asif Chalanga[3]

[1] Facultad de Ingeniería Universidad Nacional Autónoma de México (UNAM)
Coyoacán D.F. 04510, Mexico
lfridman@unam.mx

[2] Instituto de Ingeniería Universidad Nacional Autónoma de México (UNAM)
Coyoacán. 04510, Mexico
JMorenoP@ii.unam.mx

[3] Systems and Control Engineering, Indian Institute of Technology Bombay,
Mumbai-400 076, India
{bijnan,shyam,asif}@sc.iitb.ac.in

Abstract. The history and evolution of Sliding Mode Controllers in the last three decades is revisited. The new generation of continuous sliding-mode controllers, and continuous nested sliding-mode controllers is presented. Such controllers generate an continuous control signal, ensuring, for the systems with relative degree r, the finite–time convergence to the $(r+1)-th$ sliding-mode set using only information on the sliding output and its derivatives up to the $(r-1)$ order.

In this book it is natural to recall the past and to think about the future. This chapter is an attempt to give a viewpoint on the stages of development of the Sliding-Mode Control(SMC) theory in the last decades. We will show that each decade the SMC community has been able to generate families of controllers with much better properties than before, and propose arbitrary-order continuous SMC algorithms which can significatively reduce the chattering and improve the precision.

1 The First Generation of Sliding Modes Controllers

The classical theory of first order SMC was established by 1980 and later reported in Prof. Utkin's monograph in Russian, in 1981 (English version [35]). In his monograph Porfessor Utkin clearly stated the two-step procedure for sliding-mode control design:

1. Sliding surface design;
2. Discontinuous (relay or unit) controllers ensuring the sliding modes.

The main advantages of the first order SMC are the following:

- theoretically exact compensation (insensitivity) w.r.t. bounded matched uncertainties [7];

X. Yu and M. Önder Efe (eds.), *Recent Advances in Sliding Modes*,
Studies in Systems, Decision and Control 24, DOI: 10.1007/978-3-319-18290-2_2

- reduced order of sliding equations;
- finite–time convergence to the sliding surface.

However, the following disadvantages were evident:

- chattering;
- the sliding variables converge in finite–time but the state variables only converge asymptotically;
- the sliding surface design is restricted to have relative degree one with respect to the control, i.e., higher order derivatives are required for the sliding surface design.

2 The Second Generation of SMC: Second Order Sliding Modes

By the early 80's, the control community had understood that the main disadvantage of SMC is the "chattering" effect [35],[36]. It has been shown that this effect is mainly caused by unmodelled cascade dynamics which increase the system's relative degree, and perturb the ideal sliding mode [3],[14],[36], i.e. in order to adjust the chattering it is necessary that not only the sliding variable tends to zero, but also its derivative.

2.1 Second Order Sliding Modes

The second order sliding modes (SOSM) concept was introduced in the Ph.D. dissertation of A. Levant (Levantovskii).

Consider a second order uncertain system

$$\ddot{\sigma} = f\left(\sigma, \dot{\sigma}, t\right) + g\left(\sigma, \dot{\sigma}, t\right) \nu,$$

where σ and $\dot{\sigma}$ are the system state, $\sigma = x_1$ is the system output, $\nu \in R$ is the scalar control and $f\left(\sigma, \dot{\sigma}, t\right)$ represents unknown uncertainties/perturbations. It is also assumed that all the partial derivatives of $f(\sigma, \dot{\sigma}, t)$ are bounded on compacts and $g\left(\sigma, \dot{\sigma}, t\right) \neq 0$ is known. Then, one can write

$$\begin{cases} \dot{x}_1 &= x_2 \\ \dot{x}_2 &= f\left(x, t\right) + g\left(x, t\right) \nu, \end{cases} \tag{1}$$

where $x_2 = \dot{\sigma}$ and $x = [x_1, x_2]^T$. For simplicity, it will be assumed that $g(x, t) > 0$ for all t, x. Defining $\nu = g^{-1}(x, t)u$, system (2.1) can be written as

$$\begin{cases} \dot{x}_1 &= x_2 \\ \dot{x}_2 &= u + f(x, t). \end{cases} \tag{2}$$

The main objective of SOSM was to design a control u such that the origin of system (2) is finite-time stable, in spite of the uncertainties/perturbations $f(x, t)$, with $|f(x, t)| < f^+$ for all t, x. For the above mentioned goal, a controller is proposed in the next section.

Here, and always below, the solution of the all systems will be understood in the sense of A. Filippov[12].

2.2 Twisting Algorithm

The first and simplest SOSM algorithm is the so-called "Twisting Algorithm"(TA)[10]. For a relative degree two system the TA takes the form

$$u = -a\,\mathrm{sign}(x_2) - b\,\mathrm{sign}(x_1),\ b > a + f^+, a > f^+.$$

Under the assumption of known bounds for f^+, and with parameters a and b of the controller chosen appropriately [10], the twisting algorithm ensures finite-time exact convergence of both x_1 and x_2, i.e. there exists $T > 0$ such that, for all $t > T$, $x_1(t) = x_2(t) = 0$. Thus, the TA is said to be a SOSM control algorithm since it provides a (stable) "second order sliding mode" at the origin. An example trajectory can be seen in the Figure 1.

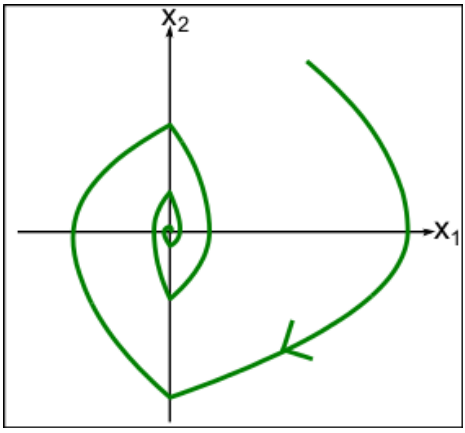

Fig. 1. Example trajectory of the Twisting algorithm

2.3 Terminal Algorithm and Singularity of Switching Surface

Consider the second order system

$$\dot{x}_1 = x_2, \quad \dot{x}_2 = u(x), \tag{3}$$

where the terminal sliding mode control input u is given by [27],[39].

$$u(x) = -\alpha\,\mathrm{sign}(s(x)), \quad s(x) = x_2 + \beta\sqrt{|x_1|}\,\mathrm{sign}(x_1). \tag{4}$$

By taking the time derivative of the switching surface, it is obtained

$$\dot{s}(x) = \dot{x}_2 + \beta\frac{x_2}{2\sqrt{|x_1|}} = -\alpha\,\mathrm{sign}(s(x)) + \beta\frac{x_2}{2\sqrt{|x_1|}}. \tag{5}$$

This means that the derivative of the switching surface $s(x)$ is singular for $x_1 = 0$, and, consequently, **the relative degree of the switching surface does not**

exist. From now on, we will call the switching surface $s(x)$, singular. On the switching surface $x_2 = -\beta\sqrt{|x_1|}\,\mathrm{sign}(x_1)$, it occurs that

$$\dot{s} = -\alpha\,\mathrm{sign}(s(x)) - \frac{\beta^2}{2}\,\mathrm{sign}(x_1).$$

It is clear that under condition $\beta^2 < 2\alpha$, the sliding on the surface $s(x) = 0$ exists, and two types of behavior for the solution of the system are possible [24], [33], [34]:

Terminal Mode. For the case when $\beta^2 < 2\alpha$, the trajectories of the system reach the surface $s(x) = 0$ and remain there for all the future time. This kind of behavior can be seen in Figure 2.

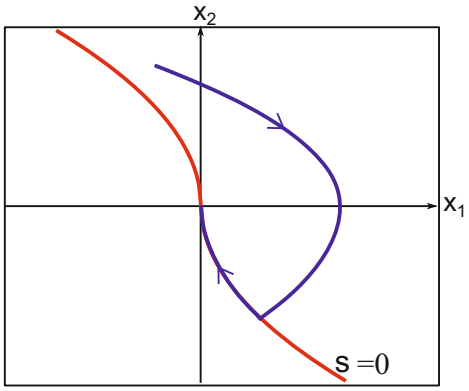

Fig. 2. Terminal mode with $\beta = 3,\ \alpha = 5$

The ideal sliding and computational chattering start when the solution reaches $s(x) = x_2 + \beta\sqrt{|x_1|}\,\mathrm{sign}(x_1)$.

Twisting Mode. When the controller parameters are chosen such that $\beta^2 > 2\alpha$, the trajectories of the system do not slide on the surface $s(x) = 0$. This behavior is exemplified in Figure 3. Note that the computational chattering does not start until the states reach the system's origin.

As it has been seen from (5), there is an issue of singularity of the switching surface. Such issue has been overcame by rewriting the function s as follows [11]

$$\bar{s}(x) = \beta^2 x_1 + x_2^2\,\mathrm{sign}(x_2).$$

Note that $s(x) = 0$, and $\bar{s}(x) = 0$ describe the same switching surface.

Precision of SOSM. The main advantage of SOSM is that they are homogeneous, with weights {2,1} ([1],[30]). As it is shown in [19], the order of precision, determined by the weights of homogeneity in terms of the discretization step δ,

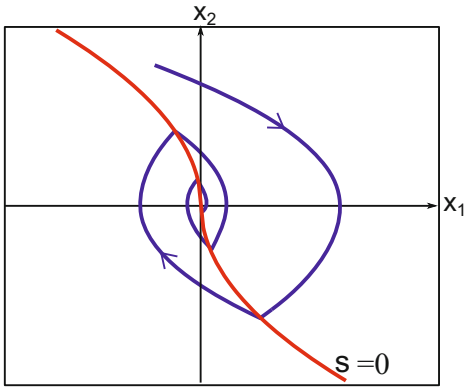

Fig. 3. Twisting mode with $\beta = 4,\ \alpha = 5$

is $O(\delta^2)$ with respect to the sliding output and $O(\delta)$ with respect to its derivative. Moreover, in the presence of fast actuator dynamics with time constant μ, the precision order is $O(\mu^2)$ with respect to the sliding output and $O(\mu)$ with respect to its derivative [5],[26].

2.4 Discussion about SOSM

Advantages of SOSM

1. **SOSM ensures the quadratic precision of convergence with respect to the sliding output.**
2. For one degree of freedom mechanical systems, both the Twisting and the Terminal controllers provide dynamic collapse, i.e. the sliding surface design is no longer needed.
3. For systems with relative degree r, the order of the sliding dynamics is reduced up to $(r-2)$. The design of the sliding surface of order $(r-2)$ is still necessary.

However, the following problems remain open:

- **SOSM algorithms for systems with relative degree two still produce a discontinuous control signal, i.e., they can not reduce the chattering substantially.**
- The problem of exact finite-time stabilization (dynamic collapse) and exact disturbance compensation for SISO systems with arbitrary relative degree still persists.

Chattering Attenuation Strategy Based on SOSM. Under additional assumptions regarding the smoothness of the system, the SOSM controllers(see also [2]) have been used to attenuate chattering in systems with relative

degree one, by including an integrator in the control input. Consider the following system

$$\dot{X} = F(t, X) + G(t, X)u, X \in R^n, u \in R$$
$$\dot{u} = v,$$

where F is a function with known upper bound. The relative degree one switching variable $\sigma(X)$ is designed such that it satisfies the equation $\dot{\sigma} = f(x,t)+g(x,t)u$. Then, defining for example a Twisting-like control $v = -a\,\mathrm{sign}(\dot{\sigma}(X)) - b\,\mathrm{sign}(\sigma(X))$, or a Terminal-like control $v = -\alpha\,\mathrm{sign}(s(\sigma(X)))$, and selecting appropriate parameters, we will have an continuous control signal u, ensuring finite-time convergence to the surface $\sigma(X) = 0$.

2.4.1 The First Criticism of SOSM

In the end of the 80's, the SOSM were strongly criticized. The main point of this criticism is the that anti-chattering strategy for a first order sliding mode uses the derivative $\dot{\sigma}$. Thus, if by any reason it is possible to measure $\dot{\sigma} = f(t,\sigma)+g(t,\sigma)u$ and, additionally, $g(t,\sigma)$ is also known, then the uncertainty $f(t,\sigma) = \dot{\sigma}-g(t,\sigma)u$ is also known and can be compensated without any discontinuous control! In this case, what is the reason for theq use of a SMC?

In the late eighties it was clear that, in order to adjust the chattering for a relative degree one sliding variable, an continuous control signal should be generated without requiring information on the derivative of the sliding variable, i.e. on the perturbations.

3 Third Generation of Sliding Modes Controllers: The Super-Twisting Algorithm

The Super–Twisting Algorithm (STA)[19]:

$$\begin{aligned} \dot{x} &= f(t,x) + g(t,x)u, \\ u &= -k_1|x|^{\frac{1}{2}}\,\mathrm{sign}(x) + v, \\ \dot{v} &= -k_2\,\mathrm{sign}(x), \end{aligned} \tag{6}$$

where f is any Lipschitz bounded uncertainty/disturbance, for some constants k_1 and k_2, ensures [19] exact finite time convergence to the second sliding-mode set $x(t) = \dot{x}(t) = 0$, $\forall t \geq T$ without usage of $\dot{x}$. If we consider system (6) having x as the measured output, the STA is an output-feedback controller for a system of one dimension.

3.0.2 Robust Exact Differentiator

This last property of the STA allowed to construct the "robust exact" sliding-mode differentiator [20] and gave further impetus to the development of the mathematical theory and applications of SOSM algorithms. We now briefly describe the idea behind it. Let $f(t)$ be a signal to be differentiated and assume

that $|\ddot{f}(t)| \leq L$, with L being a known constant. Take $x_1 = f, x_2 = \dot{f}$; then the problem can be reformulated as finding an observer for

$$\dot{x}_1 = x_2, \quad \dot{x}_2 = \ddot{f}, \quad y = x_1,$$

where $\ddot{f}(t)$ is considered as a bounded perturbation. Since the STA does not require derivatives, which in this case would be the state x_2, it only uses output injection and results particularly useful in the form of a STA observer

$$\begin{aligned} \dot{\hat{x}}_1 &= -k_1|\hat{x}_1 - y|^{\frac{1}{2}} \operatorname{sign}(\hat{x}_1 - y) + \hat{x}_2, \\ \dot{\hat{x}}_2 &= -k_2 \operatorname{sign}(\hat{x}_1 - y)\,. \end{aligned}$$

Once the constants k_1 and k_2 are appropriately chosen, the convergence of the STA ensures that the equalities $(f - \hat{x}_1) = (\dot{f} - \hat{x}_2) = 0$ are established after a finite-time transient. Thus $\hat{x}_2$ is an estimate for the derivative $\dot{f}(t)$ and turns out to be the best possible one ([20]) in the sense of [18] when (bounded Lebesgue-measurable) noise or discretization are present. However, the difficult geometrical proof of the STA convergence remained as the main disadvantage for this algorithm, thereby preventing further generalizations.

3.0.3 Recapitulations

The use of the Super Twisting Algorithm for Lipschitz systems allows substituting a discontinuous control by means of an continuous one. Additionally, their use offers:

1. Chattering attenuation (but not its complete removal![4]).
2. Differentiator obtained using the STA:
   - finite-time exact estimation of derivatives in the absence of both noise and sampling;
   - the best possible approximation in the sense of [18] of order $O(\delta)$ w.r.t. discrete sampling and of order $O(\sqrt{\varepsilon})$ w.r.t. deterministic Lebesgue-measurable noise bounded by ε.

However, there are some disadvantages:

1. For systems with relative degree $r = 2$, the design of a sliding surface is still needed. Hence, there is finite-time convergence to the surface, but the convergence of the states to the origin is asymptotic. Moreover, in this case, the usage of STA based differentiator for the sliding surface design is not enough [6] because the reconstructed switching surface should have at least Lipschitz derivative.
2. The first order sliding mode controllers with constant gains could compensate Lebesgue but bounded perturbations. The STA is insensible to perturbations whose time derivative is bounded. However, these perturbations could grow no more fast than linear function of time, i.e., they do not need to be bounded.

4 Fourth Generation of Sliding Mode Controllers: Arbitrary Order Sliding Mode Controllers

Consider the uncertain dynamical system:

$$\dot{X} = F(t, X) + G(t, X)u, X \in R^n, u \in R$$
$$\sigma = \sigma(X, t), \in R.$$

Let the output σ have a fixed and known relative degree r. In such a case, the control problem is translated into the finite-time stabilization of an uncertain differential equation or, equivalently, of the following differential inclusion

$$\sigma^{(r)} \in [-C, C] + [K_m, K_M]u, \tag{7}$$

where C, K_m and K_M are known constants parameterizing the uncertainty of the original system.

4.1 Nested Arbitrary Order Sliding-Mode Controllers

In 2001, the first arbitrary order SM controller was introduced [21], combining relay controller with hierarchical terminal sliding modes [38]. Such controllers solve the finite-time exact stabilization problem for an output with an arbitrary relative degree, in the presence of bounded Lebesgue measurable uncertainties.

Given the relative degree r of the output, "Nested" higher order sliding-mode(HOSM) controllers are constructed using a recursion, generalizing the singular Terminal Algorithm. The following is the recursion for the Singular Terminal Algorithm. Let p be the least common multiple of $1, 2, \ldots, r$. Also let

$$u = -\alpha \operatorname{sign}\left(\varphi_{r-1,r}(\sigma, \dot{\sigma}, \ldots, \sigma^{(r-1)})\right), \tag{8}$$

where $\varphi_{0,r} = \sigma,\ N_{1,r} = |\sigma|^{\frac{r-1}{r}}$ and

$$\varphi_{i,r} = \sigma^{(i)} + \beta_i N_{i,r} \operatorname{sign}(\varphi_{i-1,r}),\ N_{i,r} = \left(|\sigma|^{\frac{p}{r}} + \cdots + |\sigma^{(i-1)}|^{\frac{p}{r-1+1}}\right)^{\frac{r-i}{p}}.$$

The parameters β_i can be selected in advance in such a way that only the gain of the controller α has to be selected large enough. The algorithm provides for the finite-time stabilization of $\sigma = 0$ and, therefore, of its successive derivatives up to $r-1$. Thus, it provides for the existence of an r-th order sliding mode in the set $S_r = \{\sigma = \dot{\sigma} = ... = \sigma^{(r-1)} = 0\}$. In Figure 4 it is exemplified the trajectories and states for the Nested controller with $r = 3$. Since controller (8) uses the output and its successive derivatives, the HOSM arbitrary order differentiator, introduced in [23], was instrumental for the applicability of HOSM controllers. Let $\sigma(t)$ be a signal to be differentiated $k-1$ times and assume that $|\sigma^{(k)}| \leq L$,

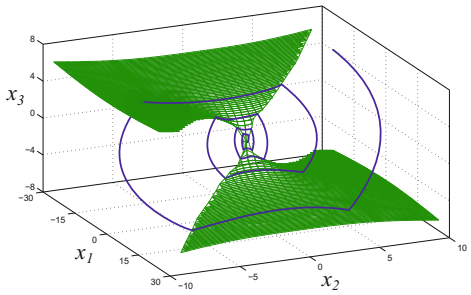

Fig. 4. System trajectory of Nested algorithm for $r = 3$

with L being a known constant. Then, the $(k-1)$-th order HOSM differentiator takes the following form

$$\begin{aligned}
\dot{z}_0 &= v_0 = -\lambda_k L^{\frac{1}{k+1}} |z_0 - \sigma|^{\frac{k}{k+1}} \operatorname{sign}(z_0 - \sigma) + z_1, \\
\dot{z}_1 &= v_1 = -\lambda_{k-1} L^{\frac{1}{k}} |z_1 - v_0|^{\frac{k-1}{k}} \operatorname{sign}(z_1 - v_0) + z_2, \\
&\vdots \\
\dot{z}_{k-1} &= v_{k-1} = -\lambda_1 L^{\frac{1}{2}} |z_{k-1} - v_{k-2}|^{\frac{1}{2}} \operatorname{sign}(z_{k-1} - v_{k-2}) + z_k \\
\dot{z}_k &= -\lambda_0 L \operatorname{sign}(z_k - v_{k-1})
\end{aligned} \tag{9}$$

where z_i is the estimation of the true derivative $\sigma^{(i)}(t)$. The differentiator ensures the finite-time exact differentiation under ideal conditions of exact measurement in continuous time. The only information needed is an upper bound, L, for $|\sigma^{(k+1)}|$. Then a parametric sequence $\{\lambda_i\} > 0$, $i = 0, 1, \ldots, k$, is recursively built, which provides for the convergence of the differentiators for each order k. In particular, the parameters $\lambda_0 = 1.1$, $\lambda_1 = 1.5$, $\lambda_2 = 2$, $\lambda_3 = 3$, $\lambda_4 = 5$, $\lambda_5 = 8$ are enough up until the 5-th differentiation order. With discrete sampling, the differential equations are replaced by their Euler approximations. This differentiator provides for the best possible asymptotic accuracy in the presence of input noises or discrete sampling [19,18] for the rth derivative:

- order $O(\delta)$ with respect to discrete sampling,
- order $O(\varepsilon^{\frac{1}{r+1}})$ with respect to bounded deterministic Lebesgue measurable noise.

The use of the HOSM arbitrary order differentiator together with the HOSM arbitrary order controller allowed the design and the implementation of a nested arbitrary-order HOSM output-feedback controller for uncertain single-input single-output (SISO) systems ensuring the finite-time output stabilization in spite of disturbances. The block diagram for implementation of the output-feedback nested HOSM controller is presented in Figure 5.

4.1.1 Discussion about Nested HOSM

Nested HOSM algorithm ensures exact finite-time stabilization (dynamic collapse) of the output σ and exact disturbance compensation for SISO systems with relative degree r, using information on $\sigma, \dot{\sigma}, ..., \sigma^{(r-1)}$.

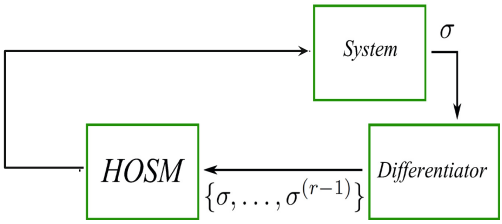

Fig. 5. The implementation of the output-feedback nested HOSM controller

Some of its advantages are:

- **SOSM ensure the r-th order precision for the sliding output with respect to the discretization step and fast parasitic dynamics [22],[26].**
  item The sliding surface design is no longer needed.

However, the nested HOSM algorithms for relative degree r systems still produces a discontinuous control signal, i.e., they can not reduce the chattering substantially.

5 Fifth Generation of SMC: Continuous Arbitrary Order Sliding-Mode Controllers

In this section we propose an arbitrary order Continuous Nested Sliding Mode Algorithm(CNSMA). The CNSMA provides, for relative degree r systems with respect to the output,

- continuous control signal;
- finite-time convergence to the $(r+1)$-th order sliding-mode set;
- derivatives of the output up to the $(r-1)$ order.

Firstly for the systems with relative degree two we will introduce two versions of the Continuous Terminal Sliding Mode Algorithm(CTSMA), as a combination of Super-Twisting with both versions of Terminal Algorithm: singular and nonsingular. It will be shown that the CTSMA has also the above mentioned properties of the CNSMA for the systems with relative degree two. The possibilities to prove their convergence will be discussed.

Than the CNSMA for the systems with arbitrary relative degree is suggested.

In this section the following notation is used, for a real variable $z \in \mathbb{R}$ to a real power $p \in \mathbb{R}$, $\lfloor z \rceil^p = |z|^p sgn(z)$, therefore $\lfloor z \rceil^2 = |z|^2 sgn(z) \neq z^2$. If p is an odd number, this notation does not change the meaning of the equation, i.e. $\lfloor z \rceil^p = z^p$. Therefore

$$\begin{aligned} &\lfloor z \rceil^0 = sgn(z), \quad \lfloor z \rceil^0 z^p = |z|^p, \quad \lfloor z \rceil^0 |z|^p = \lfloor z \rceil^p \\ &\lfloor z \rceil^p \lfloor z \rceil^q = |z|^p sgn(z) |z|^q sgn(z) = |z|^{p+q} \end{aligned} \tag{10}$$

5.1 Continuous Terminal Sliding Mode Algorithm

Continuous terminal sliding-mode algorithms are defined in the following way:

(a) Continuous Singular Terminal Sliding Mode Algorithm (CSTSMA);
(b) Continuous Nonsingular Terminal Sliding Mode Algorithm (CNTSMA).

Continuous Singular Terminal Sliding Mode Algorithm (CSTSMA)

Suppose that the control input u is defined as

$$u = -k_1 \lfloor \phi \rceil^{1/2} - k_3 \int_0^t \lfloor \phi \rceil^0 d\tau, \tag{11}$$

or

$$u = -k_1 \lfloor \phi \rceil^{1/2} + L, \quad \dot{L} = -k_3 \lfloor \phi \rceil^0, \tag{12}$$

where $\phi = \left(x_2 + k_2 \lfloor x_1 \rceil^{2/3}\right)$, and k_1, k_2, k_3 are appropriate positive gains. Substituting the control (12) into (2), the closed loop system becomes

$$\begin{cases} \dot{x}_1 &= x_2 \\ \dot{x}_2 &= -k_1 \lfloor \phi \rceil^{1/2} + L + f(x,t) \\ \dot{L} &= -k_3 \lfloor \phi \rceil^0. \end{cases} \tag{13}$$

Suppose $x_3 = L + f(x,t)$, then one can rewrite (13) as

$$\begin{cases} \dot{x}_1 &= x_2 \\ \dot{x}_2 &= -k_1 \lfloor \phi \rceil^{1/2} + x_3 \\ \dot{x}_3 &= -k_3 \lfloor \phi \rceil^0 + \rho, \end{cases} \tag{14}$$

where $\rho = \frac{\partial f}{\partial x}\dot{x} + \frac{\partial f}{\partial t}$, and it is assumed that it satisfies $|\rho| \leq \Delta$.

Proposed algorithm (14) can be interpreted as a combination of the Super-Twisting algorithm with the Singular Terminal Sliding mode.

5.2 Continuous Nonsingular Terminal Sliding Mode Algorithm (CNTSMA)

Suppose that the control input u is defined as

$$u = -k_1 \lfloor \phi_N \rceil^{1/3} - k_3 \int_0^t \lfloor \phi_N \rceil^0 d\tau, \tag{15}$$

or

$$u = -k_1 \lfloor \phi_N \rceil^{1/3} + L, \quad \dot{L} = -k_3 \lfloor \phi_N \rceil^0, \tag{16}$$

where, $\phi_N = \left(x_1 + k_2 \lfloor x_2 \rceil^{3/2}\right)$ and $k_1, k_2,\ k_3$ are appropriate positive gains. Substituting the control (16) into (2), the closed loop system becomes

$$\begin{cases} \dot{x}_1 &= x_2 \\ \dot{x}_2 &= -k_1 \lfloor \phi_N \rceil^{1/3} + L + f(x,t) \\ \dot{L} &= -k_3 \lfloor \phi_N \rceil^{0}. \end{cases} \tag{17}$$

Suppose $x_3 = L + f(x,t)$, then one can rewrite (17) as

$$\begin{cases} \dot{x}_1 &= x_2 \\ \dot{x}_2 &= -k_1 \lfloor \phi_N \rceil^{1/3} + x_3 \\ \dot{x}_3 &= -k_3 \lfloor \phi_N \rceil^{0} + \rho, \end{cases} \tag{18}$$

where $\rho = \frac{\partial f}{\partial x}\dot{x} + \frac{\partial f}{\partial t}$ and assume that it satisfy $|\rho| \leq \Delta$.

Proposed algorithm (18) can be viewed as a combination of the Super-Twisting algorithm with the Nonsingular Terminal Sliding Mode algorithm.

5.2.1 Discussion about the CSTSMA and CNSTMA

Continuous singular/nonsingular terminal sliding-mode algorithms (14) and (18) are homogeneous of degree $\delta_f = -1$, with weights $\varrho = \{3, 2, 1\}$. The main advantage of this algorithm is that, the only information needed, for the finite time convergence of all three variables x_1, x_2 and x_3, is the output (x_1) and its derivative (x_2). It is also obvious that $\dot{x}_2 = 0$ because ϕ, which is a function of x_1, x_2 and x_3, equals to zero. The precision of the output tracking $\sigma, \dot{\sigma}$ and $\ddot{\sigma}$, corresponding to a 3^{rd} order sliding mode.

The parameters used in the simulation of were

- initial conditions $x_1(0) = 2$ and $x_2(0) = -7$
- gains $k_1 = 6, k_2 = 5$ and $k_3 = 6$

After substituting the control u in (2), the closed loop system is the same as in (14). Figure 6 shows that the convergence and precision of the states x_1, x_2 and x_3 are $10^{-9}, 10^{-6}$ and 10^{-3} respectively, when the simulation step of the Euler algorithm is set to $\tau = 10^{-3}$. It evident from the simulation that the precision corresponds to a third order sliding mode.

Figure (7) shows the convergence of the states, the phase portrait, the control input and the perturbation estimation of a second order uncertain plant with 3-CSTSMC as a controller. It is noticeable from the phase portrait in Fig. (7)(b) that switching surface $\phi = 0$ does not seem to be a sliding surface, and shows a behavior typical of the second order sliding mode known as Twisting controller.

The time evolution of the states of system (18) with u as a Continuous Nonsingular Terminal Sliding Mode Control(CNTSMC) are given in Figure 9, where the value of perturbation is again taken as $f = 2 + 4\sin(t/2) + 0.6\sin(10t)$ and gains are selected as $k_1 = 13.4$, $k_2 = 3.3$, $k_3 = 25$. It is clear from the figure that all the states converge to zero, despite of the perturbation f. Figure 10 shows the precision of each of the states when the simulation step of the Euler

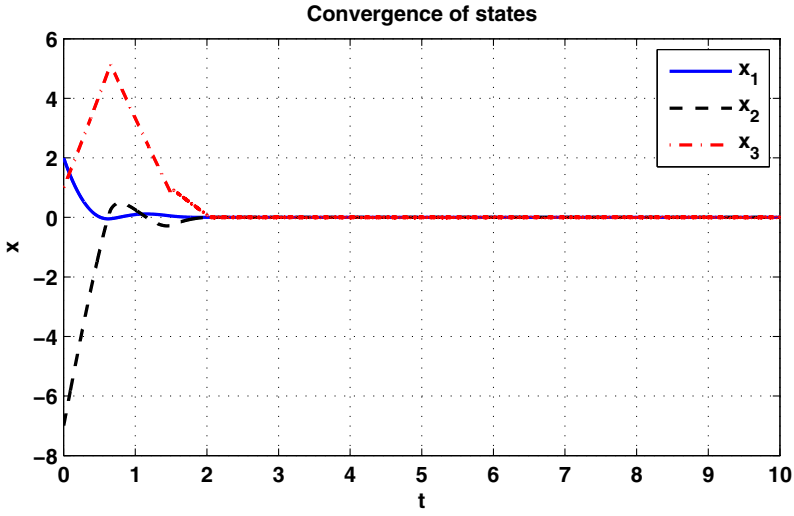

(a)

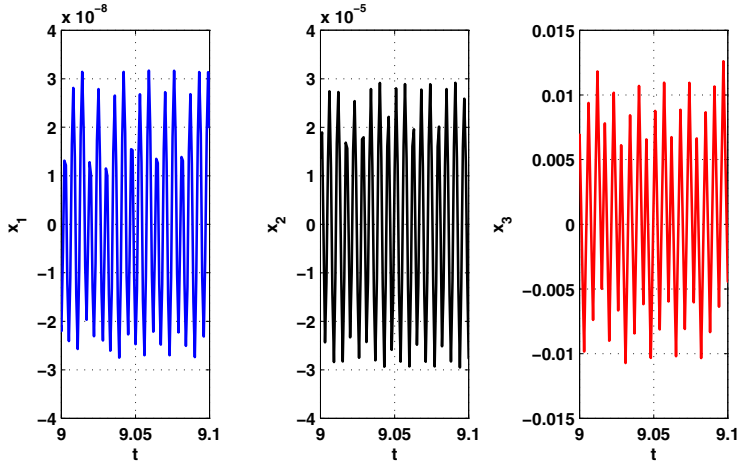

(b)

Fig. 6. Convergence and precision of states with $\tau = 0.001$ for 3-CSTSMA

algorithm is set to $\tau = 10^{-3}$ (Fig. 10a), or $\tau = 10^{-4}$ (Fig. 10b). From them we can calculate the (precision) coefficients: $\nu_3 = 80$, $\nu_2 = 80$ and $\nu_1 = 1200$. They show that the precision corresponds to a third-order sliding mode.

In Figure 11 the phase portrait of the plant's states x_1 and x_2 is shown, along with the switching curve $\phi_N = 0$. It is noticeable that the trajectory reaches the switching surface and then slides along it, until the origin is reached in finite time. This is also clear from the behavior of $\phi = \phi_N$ in Figure 9, that also appears

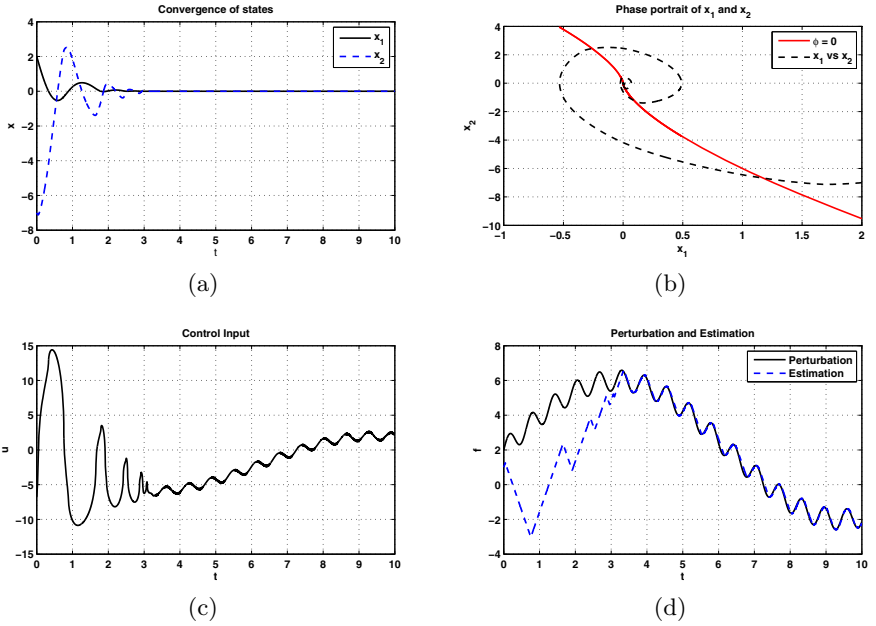

Fig. 7. Numerical example uncertain double integrator

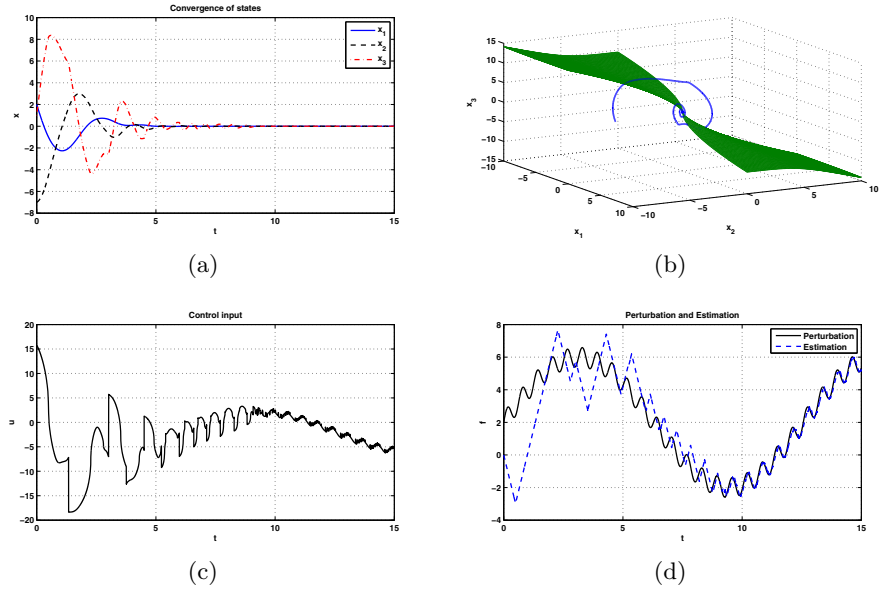

Fig. 8. Numerical example uncertain triple integrator

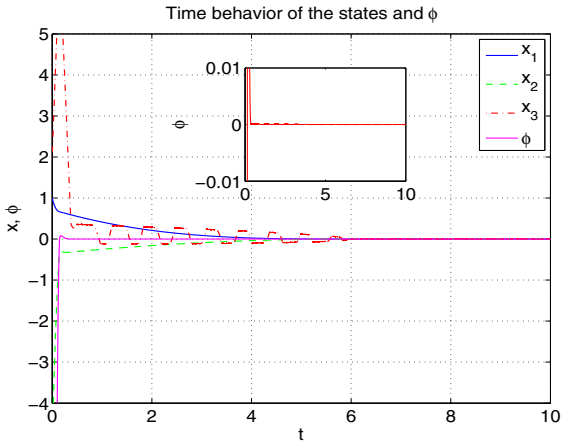

Fig. 9. Time evolution of the sates x_1, x_2, x_3 and of the switching variable $\phi = \phi_N$ under a non vanishing perturbation f

zoomed in the same picture. This behavior is similar to the one of the classical second-order sliding mode known as Terminal (or Prescribed) Controller.

Figure 13 presents again the phase portrait of the plant's states x_1 and x_2 with the same CNTSMC, but with different gains: $k_1 = 6$, $k_2 = 1/6$, $k_3 = 6$. Trajectories in Figure 13 have a rather undamped behavior compared to the ones in Figure 11. In this case, the convergence to the switching surface $\phi = \phi_N = 0$ has a twisting-like convergence to the switching surface (see Fig. 11 and Fig. 13).

6 Convergence Conditions for the Continuous Terminal Sliding Mode Algorithm

The proposed controllers (12) and (16) are able to stabilize system (2) in finite time if the following Proposition is satisfied.

Proposition 1. *System* (14) *is finite time stable at the origin, with appropriate gains* k_1, k_2 *and* k_3*, in spite of bounded perturbations* $|\rho| \leq \Delta$.

of the bounded perturbation ρ.

6.1 Lyapunov Function for Continuous Singular Terminal Sliding Mode Algorithm (CSTSMA)

Consider the following continuous Lyapunov function candidate for the stability analysis of (14)

$$V(x) = p_1|x_1|^{\frac{4}{3}} - p_{12}\lfloor x_1 \rceil^{\frac{2}{3}} \left(x_2 + k_2\lfloor x_1 \rceil^{2/3}\right) + p_2 \left|x_2 + k_2\lfloor x_1 \rceil^{2/3}\right|^2 + p_{13}\lfloor x_1 \rceil^{\frac{2}{3}}\lfloor x_3 \rceil^2 - p_{23}\left(x_2 + k_2\lfloor x_1 \rceil^{2/3}\right)\lfloor x_3 \rceil^2 + p_3|x_3|^4. \quad (19)$$

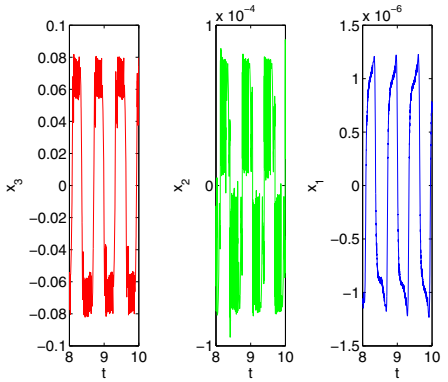

Fig. 10. Precision of the state variables x_1, x_2, x_3 corresponding to a 3-order Sliding Mode

$V(x)$ is homogeneous of degree $\delta_V = 4$, with weights $\varrho = [3, 2, 1]$. It is differentiable everywhere, but it is not locally Lipschitz at $x_1 = 0$. Our main goal is to derive conditions for the coefficients $(p_1, p_{12}, p_2, p_{13}, p_{23}, p_3)$, and for the gains (k_1, k_2, k_3) of the continuous terminal sliding-mode algorithm (14), such that $V(x) > 0$ and time derivative of (19), along (14), is negative definite ($\dot{V} < 0$ for all $x \in \mathbb{R}^3, x \neq 0$).

Function (19) can also be expressed as a quadratic form, with the vector $\Xi^T = \left[\lfloor x_1 \rceil^{\frac{2}{3}} \quad \phi \quad \lfloor x_3 \rceil^2\right]$, where $\phi = \left(x_2 + k_2 \lfloor x_1 \rceil^{2/3}\right)$, i.e.

$$V(x) = \Xi^T P \Xi, \quad \text{where} \quad P = \begin{bmatrix} p_1 & -\frac{1}{2}p_{12} & \frac{1}{2}p_{13} \\ -\frac{1}{2}p_{12} & p_2 & -\frac{1}{2}p_{23} \\ \frac{1}{2}p_{13} & -\frac{1}{2}p_{23} & p_3 \end{bmatrix} \tag{20}$$

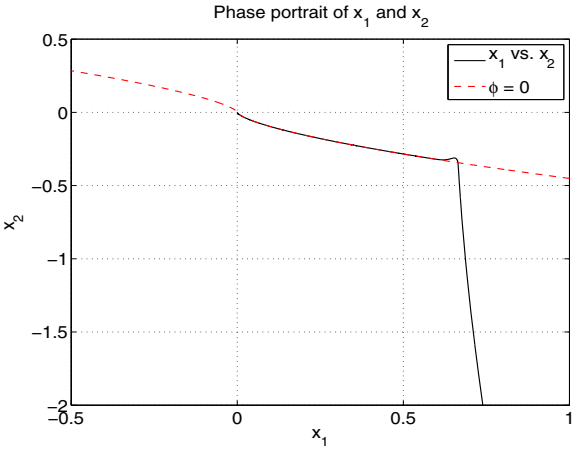

Fig. 11. Phase portrait of Plant's states x_1 and x_2, and locus of the switching curve $\phi = \phi_N = 0$, showing a Sliding-Like behavior of the CTSM controller

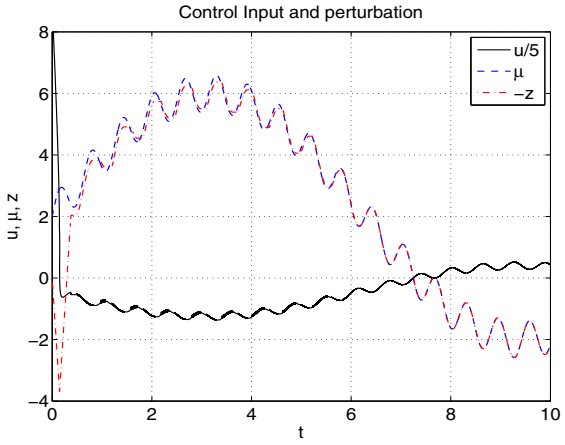

Fig. 12. Time behavior of the continuous control signal u_2, and (finite-time) estimation of the perturbation f by the controller state $-L = -z$

$V(x)$ is positive definite and radially unbounded if and only if $P > 0$, which is true if the following inequalities are satisfied

$$\begin{cases} p_1 > 0, \quad p_1 p_2 > \frac{1}{4} p_{12}^2, \\ p_1 \left(p_2 p_3 - \frac{1}{4} p_{23}^2 \right) + \frac{p_{12}}{2} \left(-\frac{p_{12} p_3}{2} + \frac{p_{13} p_{23}}{4} \right) \\ + \frac{p_{13}}{2} \left(\frac{p_{12} p_{23}}{4} - \frac{p_2 p_{13}}{2} \right) > 0 \end{cases} \tag{21}$$

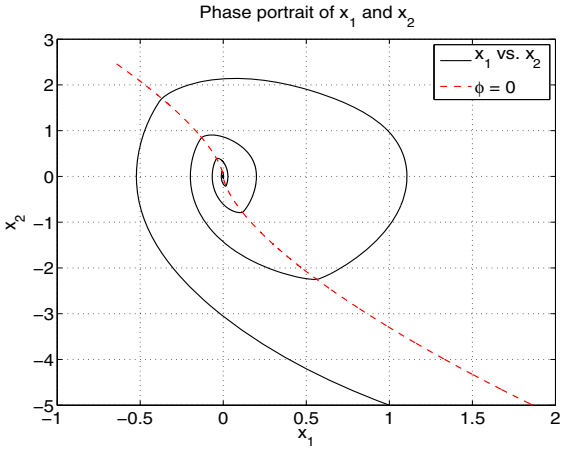

Fig. 13. Phase portrait of Plant's states x_1 and x_2, and locus of the switching curve $\phi = \phi_N = 0$, showing a Twisting-Like behavior of the CNTSM controller

The derivative of (19), along the system (14), is

$$\begin{aligned}\dot{V}(x) = {} & q_1 \lfloor x_1 \rceil^{\frac{1}{3}} x_2 - q_2 |x_1|^{-\frac{1}{3}} x_2^2 - 2k_1 p_2 |\phi|^{\frac{3}{2}} - p_{23} |x_3|^3 \\ & - q_3 |x_1|^{-\frac{1}{3}} x_2 \lfloor x_3 \rceil^2 + k_1 p_{12} \lfloor x_1 \rceil^{\frac{2}{3}} \lfloor \phi \rceil^{\frac{1}{2}} - \bar{q}_4 \lfloor x_1 \rceil^{\frac{2}{3}} x_3 \\ & + \bar{q}_5 x_3 \phi + p_{23} k_1 \lfloor \phi \rceil^{\frac{1}{2}} \lfloor x_3 \rceil^2 - \bar{q}_6 \lfloor x_3 \rceil^3 \lfloor \phi \rceil^0 \end{aligned} \tag{22}$$

where

$$\begin{cases} q_1 & = \frac{4p_1}{3} - \frac{4k_2 p_{12}}{3} + \frac{4p_2 k_2^2}{3} \\ q_2 & = \frac{2p_{12}}{3} - \frac{4p_2 k_2}{3} \\ q_3 & = \frac{2p_{23} k_2}{3} - \frac{2p_{13}}{3} \\ \bar{q}_4 & = p_{12} + 2p_{13} k_3 \lfloor \phi \rceil^0 \lfloor x_3 \rceil^0 - 2p_{13} \lfloor x_3 \rceil^0 \rho \\ \bar{q}_5 & = 2p_2 + 2p_{23} k_3 \lfloor \phi \rceil^0 \lfloor x_3 \rceil^0 - 2p_{23} \lfloor x_3 \rceil^0 \rho \\ \bar{q}_6 & = 4k_3 p_3 - 4p_3 \rho \lfloor \phi \rceil^0 \end{cases} \tag{23}$$

when $\rho = 0$, then let us define

$$\begin{cases} q_4 & = p_{12} + 2p_{13} k_3 \lfloor \phi \rceil^0 \lfloor x_3 \rceil^0 \\ q_5 & = 2p_2 + 2p_{23} k_3 \lfloor \phi \rceil^0 \lfloor x_3 \rceil^0 \\ q_6 & = 4k_3 p_3 \end{cases} \tag{24}$$

The following Definition and Lemma are presented to prove the stability of system (14) without disturbances i.e., $\rho = 0$

Definition 1. *Functions $\beta(\alpha,\lambda)$ and $\vartheta(\alpha)$ are the real valued function of the real variable $\alpha > 0$ and any value of λ, $\beta(\alpha,\lambda)$ satisfied $\vartheta(\alpha) \geq \beta(\alpha,\lambda)$ for all λ, where the function $\beta(\alpha,\lambda)$ is defined as*

$$\beta(\alpha,\lambda) = \begin{cases} max(0,\beta_1(\alpha,\lambda)) & for \;\; \lambda \geq -\sqrt{3\alpha} \\ max(0,\beta_2(\alpha,\lambda)) & for \;\; \lambda < -\sqrt{3\alpha} \end{cases} \tag{25}$$

where

$$\begin{cases} \beta_1(\alpha,\lambda) & = -\alpha r_1^3(\alpha,\lambda) + \lambda r_1^2(\alpha,\lambda) + r_1(\alpha,\lambda) \\ \beta_2(\alpha,\lambda) & = \alpha r_2^3(\alpha,\lambda) - \lambda r_2^2(\alpha,\lambda) + r_2(\alpha,\lambda) \end{cases} \tag{26}$$

and

$$r_1(\alpha,\lambda) = \frac{\lambda + \sqrt{|\lambda|^2 + 3\alpha}}{3\alpha}, r_2(\alpha,\lambda) = \frac{\lambda - \sqrt{|\lambda|^2 - 3\alpha}}{3\alpha} \tag{27}$$

One of the main results of the chapter which guarantee the finite time stability of proposed algorithm (14) when $\rho = 0$ is stated in the following lemma :

Lemma 1. *Consider the continuous and homogeneous function $V(x)$ given by* (20)*. $V(x)$ goes to zero in finite time if the following conditions are satisfied*

$$\begin{cases} p_1 + p_2 k_2^2 > k_2 p_{12},\;\; p_{12} = 2p_2 k_2,\;\; p_{23} k_2 = p_{13} \\ p_{12} > 2p_{13} k_3,\;\; p_2 > p_{23} k_3,\;\; k_3 > 0, \end{cases} \tag{28}$$

and there exists some $\alpha_1, \alpha_2 > 0$ such that

$$\begin{cases} q_1 k_1 k_2 p_{12} - k_1 p_{12} - \sqrt{\frac{2^2|q_4|^3}{3^3(p_{23}-|q_6|)}} > \alpha_1 > 0 \\ \vartheta(\alpha_1) \geq \beta(q_1,\alpha_1) \\ \frac{2k_1^2 p_2 p_{23} - \alpha_2}{k_1^3 p_{23} p_{12}} > \vartheta(\alpha_1) > 0, \end{cases} \tag{29}$$

$$\begin{cases} 2k_1^2 p_2 p_{23} > \alpha_2 > 0 \\ \vartheta(\alpha_2) \geq max\{\beta(\lambda_1,\alpha_2), \beta(\lambda_2,\alpha_2)\} \\ \frac{1}{(k_1 p_{12})^2}\left(p_{23} - |q_6| - \frac{2^2|q_4|^3}{3^3\left(q_1 k_2 - \frac{\alpha_1}{k_1 p_{12}}\right)^2}\right) > \vartheta(\alpha_2) > 0, \end{cases} \tag{30}$$

where $\lambda_1 = 2p_2 + 2p_{23}k_3$ and $\lambda_2 = 2p_2 - 2p_{23}k_3$. In this case $V(x)$ satisfies the differential inequality

$$\dot{V} \leq -\kappa V^{3/4} \tag{31}$$

for some positive κ and it is a Lyapunov function for the system (14)*, whose trajectories converges in finite time to the origin $x = 0$, for every value of the perturbation $\rho = 0$. The convergence time of a trajectory starting at the initial condition x_0 can be estimated as*

$$T(x_0) \leq \frac{4}{\kappa} V^{\frac{1}{4}}(x_0). \tag{32}$$

Lemma 1 provides conditions for the existence of a Lyapunov function for system (14), when $\rho = 0$. However, it is not obvious a priori that there exist indeed values of the parameters $k_1, k_2, k_3, p_1, p_2, p_3, p_{12}, p_{13}, p_{23}, \alpha_1, \alpha_2$ for which the conditions imposed in the Lemma 1 are satisfied, i.e. if the system of inequalities are feasible. Using the next Theorem it will be shown that there are indeed sets of values for the parameters, that fulfill the conditions of the Theorem in the both case when $\rho = 0$ or $\rho \neq 0$. This Theorem is the main contribution of the chapter, which also gives the proof of the Proposition 1.

Theorem 1. *Let us suppose that the origin $x = 0$ of system (14) is finite time stable for a set of gains k_1, k_2, k_3, and (19) is the Lyapunov function $V(x)$, with a set of parameters $p_1, p_2, p_3, p_{12}, p_{13}, p_{23}$ in the unperturbed case. Then, the origin $x = 0$ of (14) remains finite time stable for a set of gains l^3k_1, l^2k_2, l^6k_3 and that $V(x)$ in (19) is a Lyapunov function for the set of parameters $l^{-8}p_1, l^{-12}p_2, l^{-24}p_3, l^{-10}p_{12}, l^{-16}p_{13}, l^{-18}p_{23}$, for the sufficiently large positive real number l in the both perturbed and unperturbed case.*

Table 1. Parameters of the Lyapunov function when $\rho = 0$

k_1	6	6
k_2	1	2
k_3	6	6
p_1	20	20
p_2	0.5	0.5
p_3	0.01	0.01
p_{12}	1	2
p_{13}	0.05	0.1
p_{23}	0.05	0.05

6.1.1 Lyapunov Function Validation

After finding the conditions on the gains k_1, k_2, k_3, as given by (28), based on the Lyapunov function parameters of (20), $p_1, p_2, p_3, p_{12}, p_{13}, p_{23}$ that makes system (14) finite time stable at the origin, it is still not quite obvious that system inequalities (21) and (28) to (30) are feasible. Therefore, we have to find at least one set of numerical values of k_1, k_2, k_3, $p_1, p_2, p_3, p_{12}, p_{13}, p_{23}$ and inequalities for α_1 and α_2 such that inequalities (21) and (28) to (30) are feasible. Other sets of gains can easily be found using Theorem 1, by simply tuning the positive real value l.

One of the Possible Choice for Validation:

Using (28) to (30) and some particular $k_i, i = 1, 2, 3$ and $p_1, p_2, p_3, p_{12}, p_{13}, p_{23}$, one can write $\alpha_2 = \eta_1\alpha_1$ where $0 < \eta_1 < 1$. Figures 14 (a) and (b) show the graphs of the functions $\vartheta(\alpha_1)$, $\beta(\alpha_1, \lambda)$ and $\vartheta(\alpha_2)$, $\beta(\alpha_2, \lambda_1)$ along with $\beta(\alpha_2, \lambda_2)$, respectively, for the parameters of the first column of Table 1 parameters which satisfy (29) and (30).

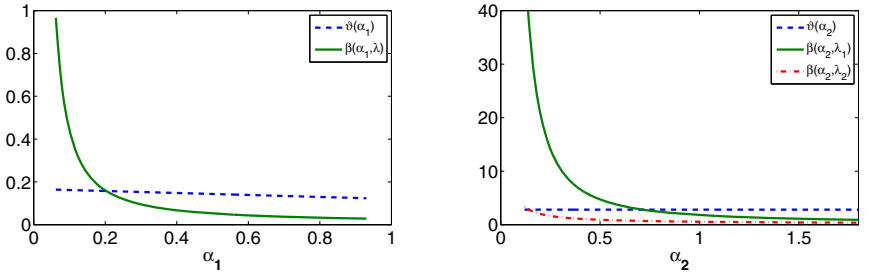

(a) Graph of $\vartheta(\alpha_1)$, $\beta(\alpha_1, \lambda)$ (b) Graph of $\vartheta(\alpha_2)$, $\beta(\alpha_2, \lambda_1)$ and $\beta(\alpha_2, \lambda_2)$

Fig. 14. Inequalities for the Lyapunov Function Validation

6.2 Lyapunov Analysis of Continuous Nonsingular Terminal Sliding Mode Algorithm (CNTSMA)

The Lyapunov function candidate for system (18) is proposed as

$$V(x) = \beta |x_1|^{\frac{5}{3}} + x_1 x_2 + \frac{2}{5} k_2 |x_2|^{\frac{5}{2}} - \frac{1}{k_1^3} x_2 x_3^3 + \gamma_3 |x_3|^5 ,$$

which is homogeneous (of degree $\delta_V = 5$) and continuously differentiable. We will show that $V(x)$ is decrescent, and that selecting $\beta > 0$ and $\gamma_3 > 0$ sufficiently large it is also positive definite.

For this, recall the classical Young's inequality [16]: for any real values $p > 1$, $q > 1$ such that $\frac{1}{p} + \frac{1}{q} = 1$ and any positive real numbers a, b, c the inequality $ab \leq c^p \frac{a^p}{p} + c^{-q} \frac{b^q}{q}$ holds. Using this inequality it follows that

$$\begin{aligned} V(x) \geq & \left(\beta - \frac{3}{5} c_1^{\frac{5}{3}} \right) |x_1|^{\frac{5}{3}} + \frac{2}{5} \left(k_2 - c_1^{-\frac{5}{2}} - c_2^{-\frac{5}{2}} \frac{1}{k_1^3} \right) |x_2|^{\frac{5}{2}} \\ & + \left(\gamma_3 - \frac{3}{5} \frac{1}{k_1^3} c_2^{\frac{5}{3}} \right) |x_3|^5 . \end{aligned}$$

V is positive definite if all its coefficients are positive. This can be achieved by selecting e.g. $c_1 = \left(\frac{4}{k_2} \right)^{\frac{2}{5}}$, $c_2 = \left(\frac{4}{k_2 k_1^3} \right)^{\frac{2}{5}}$, and

$$\beta > \frac{3}{5} \left(\frac{4}{k_2} \right)^{\frac{2}{3}} , \tag{33}$$

$$k_1^5 \gamma_3 > \frac{3}{5} \left(\frac{4}{k_2} \right)^{\frac{2}{3}} . \tag{34}$$

It is straight forward to verify that V is decrescent for any values of the parameters if the following conditions are satisfied

$$\begin{aligned} k_3 &> \Delta \\ \beta &> \frac{3}{5k_2^{\frac{2}{3}}} \\ k_1 &> 5\gamma_3 k_1^5 \kappa \left(1+\frac{\Delta}{k_3}\right) + \frac{\left(\frac{3}{2}\right)^2 (\frac{k_3}{k_1})^2}{\left(\frac{5}{3}\beta k_2^{\frac{2}{3}}-1\right)} \left(1+\frac{\Delta}{k_3}\right)^2 \\ \gamma_3 k_1^5 &> \frac{\left(\frac{5}{3}2^{\frac{1}{3}}\beta + 3\frac{k_3}{k_1}\left(1+\frac{\Delta}{k_3}\right)\right)^2}{20\frac{k_3}{k_1}\left(1-\frac{\Delta}{k_3}\right)\left(\frac{5}{3}\beta k_2^{\frac{2}{3}}-1\right)} \end{aligned} \tag{35}$$

7 Continuous Nested Sliding Mode Algorithm

In this section a generalization of the Continuous Singular Terminal Sliding Mode Algorithm (CSTSMA) is presented. Due to the nested structure of the algorithm, it is also referred to as continuous nested terminal sliding-mode algorithm.

CSTSMA is proposed as follows

$$\begin{aligned} \dot{x}_1 &= x_2 \\ \dot{x}_2 &= -k_1 \left|\phi_1\right|^{1/2} \mathrm{sign}\left(\phi_1\right) + x_3 \\ \dot{x}_3 &= -k_3 \mathrm{sign}\left(\phi_1\right) + \rho \end{aligned} \tag{36}$$

where $\phi_1 = x_2 + k_2|x_1|^{2/3}\mathrm{sign}(x_1)$ x_1, x_2, x_3 represent the states, and the perturbation ρ satisfies $|\rho| \leq \Delta$.

4-CSNSMA is proposed as follows

$$\begin{aligned} \dot{x}_1 &= x_2 \\ \dot{x}_2 &= x_3 \\ \dot{x}_3 &= -k_1 \left|\phi_2\right|^{1/2} \mathrm{sign}\left(\phi_2\right) + x_4 \\ \dot{x}_4 &= -k_4 \mathrm{sign}\left(\phi_2\right) + \rho \end{aligned} \tag{37}$$

where

$$\phi_2 = x_3 + k_3 \left(|x_1|^3 + |x_2|^4\right)^{\frac{1}{6}} \mathrm{sign}\left(x_2 + k_2|x_1|^{\frac{3}{4}}\mathrm{sign}(x_1)\right) \tag{38}$$

and x_1, x_2, x_3, x_4 represent the states, and the perturbation ρ satisfies $|\rho| \leq \Delta$.

Similarly, 5-CSNSMA is proposed as follows

$$\begin{aligned}
\dot{x}_1 &= x_2 \\
\dot{x}_2 &= x_3 \\
\dot{x}_3 &= x_4 \\
\dot{x}_4 &= -k_1 \left|\phi_3\right|^{1/2} \operatorname{sign}(\phi_3) + x_5 \\
\dot{x}_5 &= -k_5 \operatorname{sign}(\phi_3) + \rho
\end{aligned} \tag{39}$$

where

$$\phi_3 = x_4 + k_4 \left[\left(|x_1|^{12} + |x_2|^{15} + |x_3|^{20} \right)^{\frac{1}{30}} \operatorname{sign}(l_1) \right]$$

and

$$l_1 = x_3 + k_3 \left(|x_1|^{12} + |x_2|^{15} \right)^{\frac{1}{20}} \operatorname{sign}\left(x_2 + k_2 |x_1|^{\frac{4}{5}} \operatorname{sign}(x_1) \right)$$

and $x_1, x_2,\ x_3,\ x_4, x_5$ represent the states, and the perturbation ρ satisfies $|\rho| \leq \Delta$.

The generalized r-CSNSMA is proposed as follows

$$\begin{aligned}
\dot{x}_1 &= x_2 \\
\dot{x}_2 &= x_3 \\
&\vdots \\
\dot{x}_{r-1} &= -k_1 \left|\phi_{r-2}\right|^{1/2} \operatorname{sign}(\phi_{r-2}) + x_r \\
\dot{x}_r &= -k_r \operatorname{sign}(\phi_{r-2}) + \rho
\end{aligned} \tag{40}$$

where $x_1, x_2, \cdots, x_r$ represent the states, and the perturbation ρ satisfies $|\rho| \leq \Delta$. Variable ϕ_{r-2} is defined as:

- $$R_{1,r-1} = |x_1|^{\frac{r}{r+1}}$$
  where r represents the relative degree of the algorithm with respect to x_1.
- $$R_{i,r-1} = \left| |x_1|^{r_1} + |x_2|^{r_2} + \cdots + |x_{i-2}|^{r_{i-2}} \right|^{q_i},$$
  where $i = 2, 3, \cdots, (r-1)$, $r_1, r_2, \cdots, r_{i-2}$, and q_i is a parameter designed based on the homogeneity weight of x_{i+1}.
- $$S_{0,r-1} = x_1$$
  $$S_{1,r-1} = x_2 + k_2 R_{1,r-1} \operatorname{sign}(x_1)$$
  $$S_{i,r-1} = x_{i+1} + k_{i+1} R_{i,r-1} \operatorname{sign}(S_{i-1,r-1})$$
  where $i = 2, 3, \cdots, (r-1)$
- Finally $\phi_{r-2} = s_{r-1,r-1}$.

For example, if we want to select r_1, r_2 and q_2 for the 4-CSNSMA (r=3), firstly we have to check its weighted homogeneity. Our aim is to design a 4-CSNSMA that has homogeneous weights $\{4, 3, 2, 1\}$. The design of parameters r_1, r_2, and q_2 is fully dependent on the weight assigned to x_3. Here, we have chosen its value as 2, therefore, it is necessary to adjust r_1, r_2 and q_2 such that after homogenous scaling, one can get the desired value 2 for x_3. There are several ways to select these parameters, one of them consists on calculating the LCM (lowest common factor) of 4 and 3, which is 12, and then adjusting the power of the terms $|x_1|$, and $|x_2|$, such that the weight of x_3 is equal to 2. It is obvious that by selecting $r_1 = 3, r_2 = 4$ and $q_2 = 6$ it is possible to maintain the homogeneity of the algorithm with weights $\{4, 3, 2, 1\}$. Similarly, one can generalize the 4-CSNSMA till the r-CSNSMA.

Evolution of the states for the STA, where STA is given as follows [19], [28]

$$\begin{aligned} \dot{x}_1 &= -k_1|x_1|^{\frac{1}{2}}\text{sign}(x_1) + x_2 \\ \dot{x}_2 &= -k_2\text{sign}\,(x_1) + \rho, \end{aligned} \tag{41}$$

where x_1, x_2 represent the states, and the perturbation ρ satisfies $|\rho| \leq \Delta$. The CSTSMA, and 4-CSNSMA are shown in Fig. 15-Fig. 16, with the following values for the initial conditions and gains

- STA
  - initial conditions $x_1(0) = 2$, $x_2(0) = -7$
  - gains $k_1 = 3, k_2 = 4$
- CSTSMA
  - initial conditions $x_1(0) = 2$, $x_2(0) = -7$ and $x_3(0) = 1$
  - gains $k_1 = 6, k_2 = 2$ and $k_3 = 6$
- 4-CSNSMA
  - initial conditions $x_1(0) = 2, x_2(0) = -7$, $x_3(0) = 1$ and $x_4(0) = -1$
  - gains $k_1 = 4, k_2 = 1, k_3 = 2$ and $k_4 = 4$

Remark 1. The properties of the proposed algorithms are the same as those of the terminal sliding mode, therefore it is referred to as r^{th} order continuous terminal sliding-mode algorithm (r-CSNSMA).

Discussion about CTSMA and Other Generalized CSNSMA. The CTSMA (36) is homogeneous of degree $\delta_f = -1$ with weights $\varrho = \{3, 2, 1\}$. The main advantage of this algorithm is that the only information that it needs to maintain finite time convergence of all three variables x_1, x_2 and x_3 is the output (x_1) and its derivative (x_2). The proposed algorithm can work as a controller for an uncertain system with relative degree 2 with respect to its output, in the case of CSTSMA. Similarly, the r-CSNSMA is homogeneous of degree $\delta_f = -1$, with weights $\varrho = \{r, r-1, \cdots, 2, 1\}$, and it can be used for an uncertain system with relative degree $r-1$ with respect to output. The main idea behind the construction of this algorithm is to add one extra discontinuous integral term, which is able to reconstruct the perturbation and also nullify it. The CSNSMA is insensible to perturbations whose time derivative is bounded. These perturbations

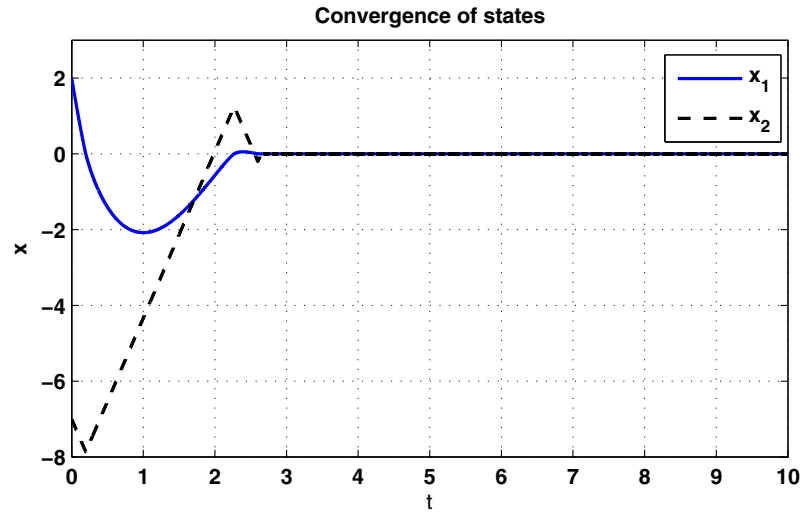

(a)

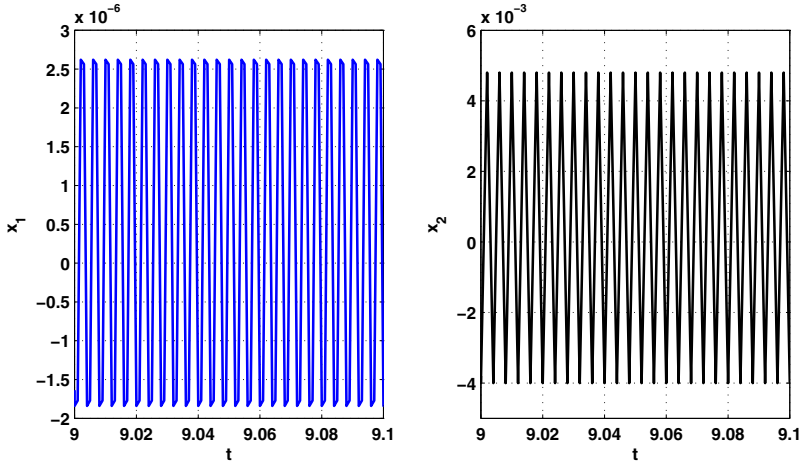

(b)

Fig. 15. STA and states precision with $\tau = 0.001$

could grow no more fast than linear function of time, i.e., they do not need to be bounded. In comparison the nested HOSM controller can compensate bounded Lebesgue measurable perturbations. Comparison of the properties of the principal SMC strategies for the second order uncertain system is given in the Table 2.

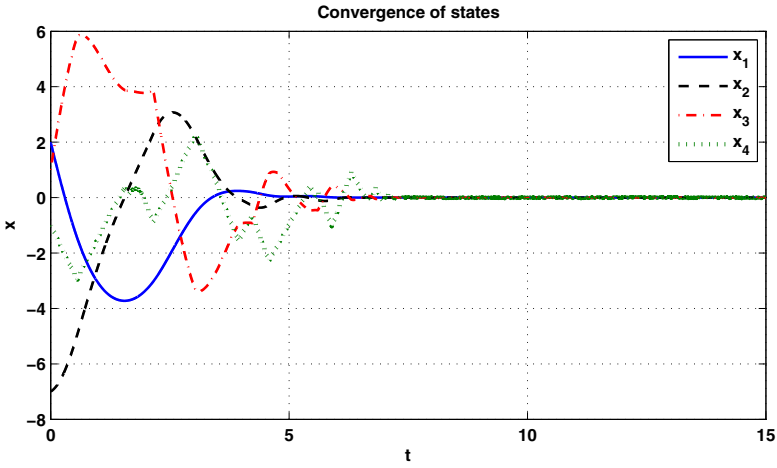

(a)

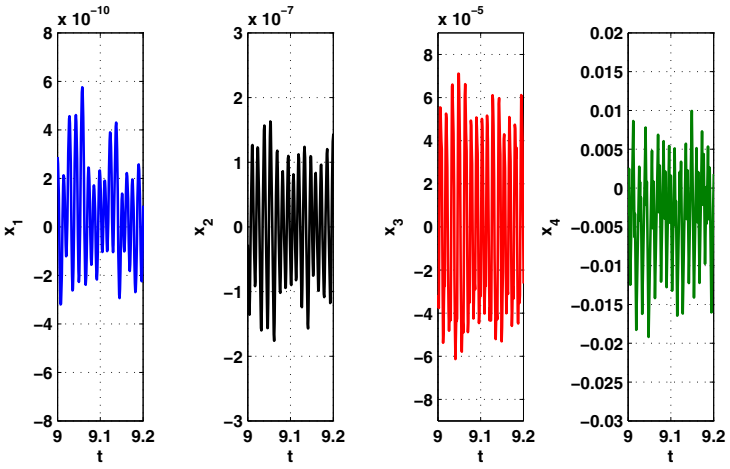

(b)

Fig. 16. CSTSMA and states precision with $\tau = 0.001$

Simulation Results. In order to verify the proposed technique of the r-CSNSMA, the following second and third order systems are considered

$$\begin{aligned} \dot{x}_1 &= x_2 \\ \dot{x}_2 &= u + f \end{aligned} \tag{42}$$

Table 2. Comparison of the properties of the different SMC strategies for the second order uncertain system with output σ

Algorithm	Control Signal	Information	Stability	Chattering	Order of sliding w.r.t. σ
First SMC	Discontinuous	$\sigma, \dot{\sigma}$	Asymptotic	Yes	1
Twisting	Discontinuous	$\sigma, \dot{\sigma}$	Finite time	Yes	2
Terminal SMC	Discontinuous	$\sigma, \dot{\sigma}$	Finite time	Yes	2
STC	Continuous	$\sigma, \dot{\sigma}$	Asymptotic	No	2
Third SMC	Continuous	$\sigma, \dot{\sigma}, \ddot{\sigma}$	Finite time	No	3
Continuous Terminal SMC	**Continuous**	$\sigma, \dot{\sigma}$	**Finite time**	**No**	3

where x_1, x_2 are the states, u is the control and $f = 2 + 4sin(t/2) + 0.6sin(10t)$ is the Lipschitz (in time) disturbance. Similarly,

$$\begin{aligned} \dot{x}_1 &= x_2 \\ \dot{x}_2 &= x_3 \\ \dot{x}_3 &= u + f \end{aligned} \tag{43}$$

where x_1, x_2, x_3 are the states, u is the control and $f = 2+4sin(t/2)+0.6sin(10t)$ is the Lipschitz (in time) disturbance. The controller for systems (42) and (43) are designed as

$$u = -k_1 \left|\phi_1\right|^{1/2} \text{sign}\left(\phi_1\right) - \int_0^t k_3 \text{sign}\left(\phi_1\right) d\tau \tag{44}$$

and

$$u = -k_1 \left|\phi_2\right|^{1/2} \text{sign}\left(\phi_1\right) - \int_0^t k_4 \text{sign}\left(\phi_2\right) d\tau \tag{45}$$

where ϕ_1 and ϕ_2 are defined as in (14) and (37), respectively. The following parameters are used for the simulation

- uncertain double order integrator (42)
  - initial conditions $x_1(0) = 2$ and $x_2(0) = -7$
  - gains $k_1 = 6, k_2 = 5$ and $k_3 = 6$
- uncertain third order integrator (43)
  - initial conditions $x_1(0) = 2, x_2(0) = -7$ and $x_3(0) = 1$
  - gains $k_1 = 5, k_2 = 1, k_3 = 2$ and $k_4 = 4$

How to Implement CSNSMA? The main specific feature of CSNSMA as well as of STA, CSTSMA and CNTSMA is that the part of control signal responsable for the compensation of Lipschitz perturbation is continuous. As a consequence of this, they are only able to compensate, theoretically exactly, Lipschitz perturbations, but they also need a Lipschitz signal to follow. This means that the switching surfaces estimated by the differentiators should be smooth and have Lipschitz derivatives. This is the reason why even the CSNSMA requires only $(r-1)$ derivatives of the sliding output, and the derivative of order $(r-1)$

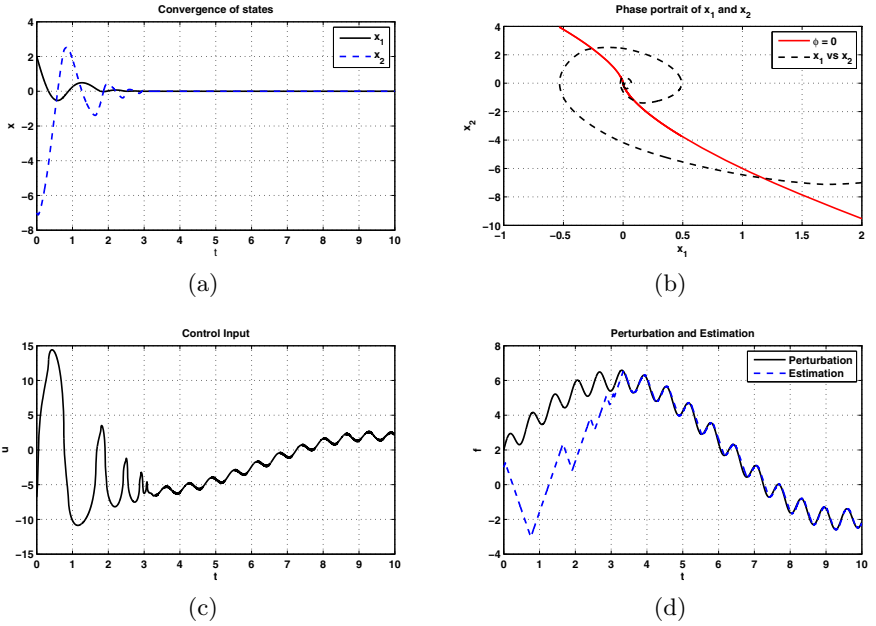

Fig. 17. Numerical example uncertain double integrator

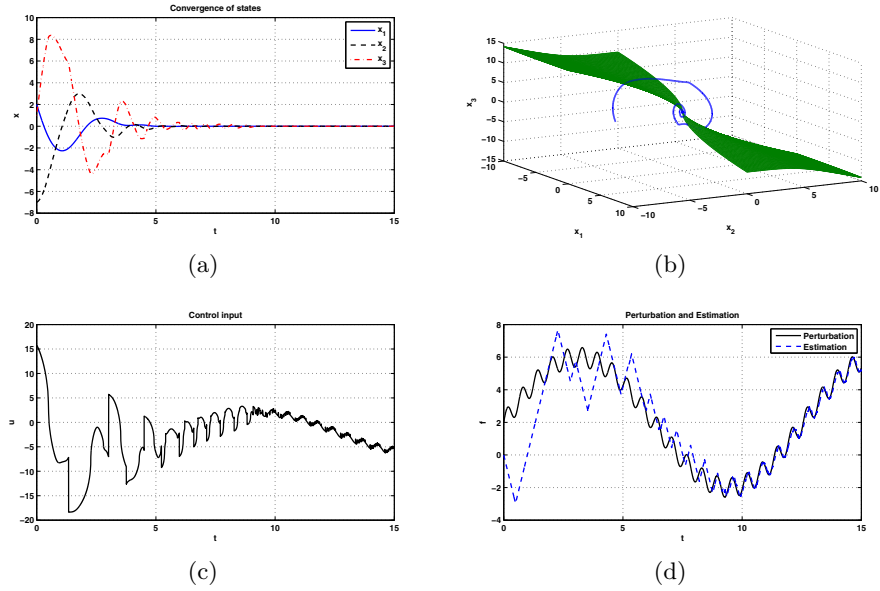

Fig. 18. Numerical example uncertain triple integrator

should be approximated by smooth signal with Lipschitz derivatives. This could be achieved by a differentiator of order r so, in order to implement the CSNSMA it is necessary to use r-order robust exact differentiators [22], but using only the derivatives that it produces up to the order $(r-1)$. By doing so, all the necessary signals for the r-CSNSMA will be smooth, with Lipschitz derivative. The block diagram for the implementation of CSNSMA is shown in next Figure.

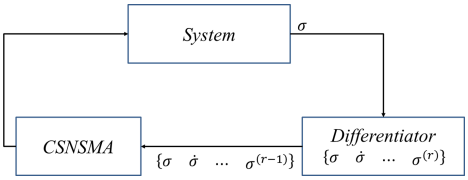

Fig. 19. CSNSMA implementation

8 Conclusion

In this chapter, the historical overview of the development of SMC is presented. We have shown that in the last three decades the Sliding Mode Community has created new generations of controllers:

- second order sliding mode controllers(1985);
- super-twisting controllers(1993);
- arbitrary sliding-mode controllers(2001,2005).

In this chapter we have presented the next generation: two families of continuous nested sliding-mode controllers, that can be used on Lipschitz systems with relative degree r, providing the continuous control signal. This new controllers ensure a finite-time convergence of the sliding output to the $(r+1)-th$-order sliding set using information on the sliding output and its derivatives up to the order $(r-1)$,

Anknowledgements. With this chapter the authors want to acknowledge the contribution of Professor Okyay Kaynak in the development of sliding mode control. His energy, his willing and abilities to help to all of colleagues, the excellent organization VSS08 workshop pushing the VSS community to reach the high level results. **Thank you Okyay!**

The authors also want to acknowledge to the joint scientific program Mexico-India, CONACyT- DST/INT/MEX/RPO-02/2008, the CONACyT grant 132125, PAPIIT grants 113613 and 113614 of UNAM and Fondo de Colaboracion II-FI the grant IIGSBAS-122-2014.

References

1. Baccioti, A., Rosier, L.: Lyapunov functions and stability in control theory, 2nd edn. Springer, New York (2005)
2. Bartolini, G., Ferrara, A., Usai, E.: Chattering avoidance by second-order sliding-mode control. IEEE Transactions on Automatic Control 43(2), 241–246 (1998)
3. Bondarev, A.G., Bondarev, S.A., Kostyleva, N.E., Utkin, V.I.: Sliding modes in systems with asymptotic state observers. Automation and Remote Control 5, 5–11 (1985)
4. Boiko, I., Fridman, L.: Analysis of chattering in continuous sliding mode controllers. IEEE Transaction on Automatic Control 50(11), 1442–1446 (2005)
5. Boiko, I., Fridman, L., Pisano, A., Usai, E.: Analysis of chattering in systems with second-order sliding modes. IEEE Transactions on Automatic Control 52(11), 2085–2102 (2007)
6. Chalanga, A., Kamal, S., Fridman, L., Bandyopadhyay, B., Moreno, J.A.: How to implement Super-Twisting Controller based on sliding mode observer? In: Proc. of 13th IEEE Workshop on Variable Structure Systems, Nantes (2014), doi:10.1109/VSS.2014.6881145
7. Drazenovic, B.: The invariance conditions in variable structure systems. Automatica 5(3), 287–295 (1969)
8. Edwards, C., Spurgeon, S.: Sliding Mode Control. Taylor and Francis, London (1998)
9. Efimov, D.: Global sliding-mode observer with adjusted gains for locally Lipschitz systems. Automatica 47(3), 565–570 (2011)
10. Emel'yanov, S.V., Korovin, S.K., Levantovski, L.V.: Higher-order sliding modes in binary control systems. Sov. Phys. Dokl 31(4), 291–293 (1986)
11. Feng, Y., Yu, X., Man, Z.: Non-singular terminal sliding mode control of rigid manipulators. Automatica 38(12), 2159–2167 (2002)
12. Filippov, A.F.: Diffrential equations and discontinuous right hand side. Kluwer, Dordrecht, The Netherlands (1988)
13. Fridman, L.: Sliding mode enforcement after 1990: Main results and some open problems. In: Fridman, L., Moreno, J., Iriarte, R. (eds.) Sliding Modes. LNCIS, vol. 412, pp. 3–57. Springer, Heidelberg (2011)
14. Fridman, L.: On robustness of sliding mode systems with discontinuous control function. Automatika i Telemechanica (Automation & Remote Control 5, 172–175 (1985)
15. Gonzalez, T., Moreno, J., Fridman, L.: Variable Gain Super-Twisting Sliding Mode Control. IEEE Transactions on Automatic Control 57(8), 2100–2105 (2012)
16. Hardy, G.H., Littlewood, J.E., Plya, G.: Inequalities, 2nd edn. Cambridge University Press, London (1988)
17. Kamal, S., Chalanga, A., Moreno, J.A., Fridman, L., Bandyopadhyay, B.: Higher order super-twisting algorithm. In: Proc. of 13th IEEE Workshop on Variable Structure Systems, Nantes (2014), doi:10.1109/VSS.2014.6881129
18. Kolmogorov, A.N.: On inequalities between upper bounds of consecutive derivatives of an arbitrary function defined on an infinite interval. Amer. Math. Soc. Transl. 2(9), 233–242 (1962)
19. Levant, A.: Sliding order and sliding accuracy in sliding mode control. International Journal of Control 58(6), 1247–1263 (1993)
20. Levant, A.: Robust exact differentiation via sliding mode technique. Autmatica 34(3), 379–384 (1998)

21. Levant, A.: Universal single-input-single-output (SISO) sliding-mode controllers with finite-time convergence. IEEE Transactions on Automatic Control 6(9), 1447–1451 (2001)
22. Levant, A.: Higher-order sliding modes,differentiation and output-feedback control. Int. J. Control 76(9), 924–941 (2003)
23. Levant, A.: Homogeneity approach to high-order sliding mode design. Automatica 41(5), 823–830 (2005)
24. Levant, A.: Principles of 2-sliding mode design. Automatica 43(4), 576–586 (2007)
25. Levant, A.: Chattering analysis. IEEE Transaction on Automatic Control 55(6), 1380–1389 (2010)
26. Levant, A., Fridman, L.: Accuracy of homogeneous Sliding Modes in the Presence of Fast Actuators. IEEE Transactions on Automatic Control 55(3), 810–814 (2010)
27. Man, Z., Paplinski, A.P., Wu, H.R.: A robust MIMO terminal sliding mode control scheme for rigid robotic manipulators. IEEE Transaction on Automatic Control 39(12), 2464–2469 (1994)
28. Moreno, J.A., Osorio, M.: Strict Lyapunov functions for the Super-twsiting algorithm. IEEE Transactions on Automatic Control 57(4), 1035–1040 (2012)
29. Moreno, J.A.: Lyapunov function for Levant's second order differentiator. In: Proceedings of the 51st IEEE Conference on Decision and Control Maui, Hawaii, December 10–13 (2012)
30. Orlov, Y.: Discontinuous systems: Lyapunov analysis and robust synthesis under uncertainty conditions. Springer (2008)
31. Orlov, Y., Aoustin, Y., Chevallereau, C.: Finite time stabilization of a perturbed double integrator—Part I: Continuous sliding mode-based output feedback synthesis. IEEE Transactions on Automatic Control 56(3), 614–618 (2011)
32. Polyakov, A., Poznyak, A.: Reaching time estimation for super-twisting second order sliding mode controller via Lyapunov function designing. IEEE Transactions on Automatic Control 54(8), 1951–1955 (2009)
33. Polyakov, A., Poznyak, A.: Unified Lyapunov function for a finite–time stability analysis of relay second–order sliding mode control systems. IMA Journal of Mathematical Control and Information 29(4), 529–550 (2012)
34. Sanchez, T., Moreno, J.A.: Lyapunov functions for Twisting and Terminal controllers. In: Proceedings of the 13th International Workshop on Variable Structure Systems Nantes, France (2014)
35. Utkin, V.: Sliding modes in control and optimization. Springer (1992); (translated from Russian edition 1981)
36. Utkin, V.: Variable structure systems- Present and future. Automation and Remote Control 44(9), 1105–1120 (1984)
37. Utkin, V.: First Stage of VSS: people and events. In: Yu, X., Xu, J.-X. (eds.) Variable Structure Systems: Towards the 21st Century. LNCS, vol. 274, pp. 1–32. Springer, Heidelberg (2002)
38. Yu, X., Man, Z.: Fast terminal sliding mode control design for nonlinear dynamic systems. IEEE Transactions on Circuits and Systems Part I 39(2), 261–264 (2002)
39. Yu, X., Man, Z.: Model reference adaptive control systems with terminal sliding modes. International Journal of Control 64(6), 1165–1176 (1996)

Decentralised Sliding Mode Control for Nonlinear Interconnected Systems with Application to a Continuously Stirred Tank Reactor

Jianqiu Mu, Xing-Gang Yan, and Sarah K. Spurgeon

Instrumentation, Control and Embedded Systems Research Group, School of Engineering & Digital Arts, University of Kent, Canterbury, CT2 7NT, United Kingdom
{jm838,x.yan,s.k.spurgeon}@kent.ac.uk

Abstract. In this chapter, a decentralised control strategy based on sliding mode techniques is proposed for a class of nonlinear interconnected systems. Both matched uncertainties in the isolated subsystems and mismatched uncertainties associated with the interconnections are considered in the problem formulation. Under mild conditions, sliding mode controllers for each subsystem are designed in a decentralised manner by only employing local information. Conditions are determined which enable information on the interconnections to be employed within the decentralised controller design process in order to reduce conservatism. The developed results are applied to a continuously stirred-tank reactor (CSTR) system. Simulation results are presented which demonstrate the effectiveness of the approach.

1 Introduction

A class of complex systems, such as multi-machine power systems ([5, 15]), chemical reactor systems [7] and multi-agent systems [6], can be modelled as a collection of subsystems with appropriate interconnections. Such classes of systems are called large scale interconnected systems. The interconnections among subsystems together with the inherent nonlinearity of the coupled dynamics inevitably result in complex dynamics. Moreover, such classes of system are frequently distributed in space. This may make control design using a centralised strategy difficult [16] as such an approach requires that information about each subsystem is available to the other subsystems for use by the controller. Problems such as network failure or failure of communication channels may prevent information transfer among subsystems. Even if information transfer is possible, the time delay caused by information transfer may compromise system performance. This has motivated the development of decentralised control strategies in which each subsystem is controlled independently. The control is based only on local information, which not only enhances system reliability but also reduces the cost of implementing systems to transfer information between subsystems.

It is well known that uncertainties or modelling errors may seriously affect control system performance. Specifically, for large scale interconnected systems, uncertainties experienced by one subsystem not only affect its own performance but usually affect the other subsystems' performance as well due to the interactions among subsystems. Sliding mode control has been recognised as a powerful approach in dealing with uncertainties.

X. Yu and M. Önder Efe (eds.), *Recent Advances in Sliding Modes*,
Studies in Systems, Decision and Control 24, DOI: 10.1007/978-3-319-18290-2_3

When in the sliding mode, a closed loop system is completely insensitive to matched uncertainties [4, 13]. The sliding mode approach can also be used to deal with the systems in the presence of unmatched uncertainty [17] although the property of total insensitivity is frequently lost. However, in contrast to the case of centralised control, decentralised control can only use local information and thus the uncertainties within the interconnections may not be rejected, even if they are matched. Designing a decentralised control scheme to reject the effect of uncertainties in the interconnection terms is challenging.

The problem of robust decentralised controller design has received much attention and many results have been obtained. In [1,3,9,19], only matched uncertainties are considered and bounds on the matched uncertainties are assumed to be linear or polynomial. In terms of mismatched uncertainties, in order to achieve asymptotic stability, some limitations are unavoidable. Mismatched uncertainties have been considered in [12, 17] where centralised dynamical feedback controllers are designed which need more resources to exchange information between subsystems. A class of constraints called integral quadratic constraints is imposed on the considered systems to limit the structure of the original systems [12]. In some cases, adaptive techniques are applied to estimate an upper bound on the mismatched uncertainty to counteract the effects [2]. This approach may be powerful when the uncertainty satisfies a linear growth condition. In [10], although the uncertainties are assumed to be functions, the system needs to be transformed into a special triangular structure. All of the literature which considers mismatched uncertainties mentioned above inevitably requires extra resources and increases the system complexity. This may be unattractive from the viewpoint of implementation.

In this chapter, a decentralized control strategy for a class of nonlinear interconnected systems is presented based on a sliding mode control paradigm. In terms of robustness, both matched and unknown interconnections with mismatched uncertainties are considered. Moreover, the uncertainties are assumed to be bounded by known functions which are employed within the control design to counteract the effects of the uncertainties. The bounds on the uncertainties take more general forms when compared with existing work. Based on the approach proposed in [4], a sliding surface for each subsystem is designed which when combined constitute a composite sliding surface for the interconnected system. A set of sufficient conditions is developed such that the corresponding sliding motion is asymptotically stable when the system is restricted to the designed sliding surface. Then, a decentralised sliding mode control is designed to drive the large-scale interconnected system to the sliding surface in finite time. It is shown that if the uncertainties/interconnections possess a superposition property, a decentralised control scheme may be designed to counteract the effect of the uncertainty. Finally, the developed decentralised control scheme is applied to a continuously stirred-tank reactor system. Simulation results relating to this system show that the obtained results are effective.

2 System Description

Consider a nonlinear large-scale interconnected system composed of N subsystems where the i-th subsystem is described by

$$\dot{x}_i = A_i x_i + B_i\big(u_i + \phi_i(t, x_i)\big) + \sum_{j=1}^{N} \Xi_{ij}(t, x_j) + \psi_i(t, x) \qquad i = 1, 2, \ldots, N \tag{1}$$

where $x_i \in \mathcal{D}_i \subset \mathcal{R}^{n_i}$, $u_i \in \mathcal{R}^{m_i}$ denote the state variables and inputs of the i-th subsystem, respectively. The matrix pairs (A_i, B_i) are constant with appropriate dimensions. The matched uncertainties are denoted by $\phi_i(t, x_i)$. The term $\sum_{j=1}^{n} \Xi_{ij}(t, x_j)$ describe the known interconnection of the i-th subsystem. The nonlinear functions $\psi_i(t, x)$ represent the uncertain interconnections where $x = \text{col}(x_1, x_2, \ldots, x_n)$. It is assumed that all the nonlinear functions are sufficiently smooth such that the unforced system has a unique continuous solution. It should be noted that

$$\sum_{j=1}^{N} \Xi_{ij}(t, x_j) = \Xi_{ii}(t, x_i) + \sum_{\substack{j \neq i \\ j=1}}^{N} \Xi_{ij}(t, x_j) \tag{2}$$

In this case, $\Xi_{ii}(t, x_i)$ can be considered the known nonlinearity in the ith subsystem and the term $\sum_{\substack{j \neq i \\ j=1}}^{N} \Xi_{ij}(t, x_j)$ the known interconnection within the ith subsystem. It will be shown that that such a class of interconnections can be employed in decentralised controller design to reduce conservatism.

The objective is to design a decentralised control scheme for system (1) based on sliding mode techniques such that the corresponding closed-loop system is asymptotically stable. The following assumption is first imposed on the system (1).

Assumption 1. The matrix pairs (A_i, B_i) are controllable and $\text{rank}(B_i) = m_i$ for $i = 1, 2, \ldots, N$.

Under the condition that $\text{rank}(B_i) = m_i$ in Assumption 1, there exists an invertible matrix $\tilde{T}_i \in \mathcal{R}^{(n_i \times n_i)}$ such that following the coordinate transformation $\tilde{x}_i = \tilde{T}_i x_i$, the matrix pairs (A_i, B_i) with respect to the new coordinates $\tilde{x}_i$ have the following structure

$$\tilde{A}_i = \begin{bmatrix} \tilde{A}_{i1} & \tilde{A}_{i2} \\ \tilde{A}_{i3} & \tilde{A}_{i4} \end{bmatrix} = \tilde{T}_i A_i \tilde{T}_i^{-1} \tag{3}$$

$$\tilde{B}_i = \begin{bmatrix} 0 \\ \tilde{B}_{i2} \end{bmatrix} = \tilde{T}_i B_i \tag{4}$$

where $\tilde{A}_{i1} \in \mathcal{R}^{(n_i - m_i) \times (n_i - m_i)}$ and the matrix $\tilde{B}_{i2} \in \mathcal{R}^{m_i \times m_i}$ is nonsingular for $i = 1, 2, \ldots, N$. It should be noted that the matrix $\tilde{T}_i$ can be obtained using basic matrix theory.

As (A_i, B_i) is controllable from Assumption 1, from [4], it follows that the matrix pair $(\tilde{A}_{i1}, \tilde{A}_{i2})$ in (3) is controllable. Then, there exists a matrix $K_i \in \mathcal{R}^{(n_i - m_i) \times m_i}$ such that $\tilde{A}_{i1} - K_i \tilde{A}_{i2}$ is Hurwitz stable. Considering the system (1), introduce a new transformation matrix as follows:

$$T_i = \begin{bmatrix} I_{n_i - m_i} & 0 \\ K_i & I_{m_i} \end{bmatrix} \tilde{T}_i \tag{5}$$

It is clear that the matrix T_i is nonsingular. Define $z = \text{col}(z_1, z_2, \ldots, z_N)$ where $z_i = T_i x_i$. Then in this new coordinate system, system (1) has the following form

$$\begin{aligned}\dot{z}_i = &\begin{bmatrix} A_{i1} & A_{i2} \\ A_{i3} & A_{i4} \end{bmatrix} z_i + \begin{bmatrix} 0 \\ \tilde{B}_{i2} \end{bmatrix} \big(u_i + g_i(t, z_i)\big) \\ &+ \sum_{j=1}^{N} \Gamma_{ij}(t, z_j) + \delta_i(t, z) \end{aligned} \tag{6}$$

where $z_i = T_i(D_i) := \Omega_i$, $A_{i1} = \tilde{A}_{i1} - \tilde{A}_{i2}K_i$ is stable with K_i given in (5), $T^{-1} \equiv: \text{diag}\{T_1^{-1}, T_2^{-1}, \ldots, T_N^{-1}\}$ and for $i, j = 1, 2, \ldots, N$

$$g_i(t, z_i) = \phi_i(t, T_i^{-1} z_i) \tag{7}$$

$$\Gamma_{ij}(t, z_j) \triangleq \begin{bmatrix} \Gamma_{ij}^a(t, z_j) \\ \Gamma_{ij}^b(t, z_j) \end{bmatrix} = T_i \Xi_{ij}(t, T_j^{-1} z_j) \tag{8}$$

$$\delta_i(t, z) \triangleq \begin{bmatrix} \delta_i^a(t, z) \\ \delta_i^b(t, z) \end{bmatrix} = T_i \psi_i(t, T^{-1} z) \tag{9}$$

where

$$\begin{matrix} \Gamma_{ij}^a(t, z_j), & \delta_i^a(t, z) \in \mathcal{R}^{(n_i - m_i)} \\ \Gamma_{ij}^b(t, z_j), & \delta_i^b(t, z) \in \mathcal{R}^{m_i} \end{matrix}$$

For further analysis, now partition $z_i = \text{col}(z_i^a, z_i^b)$ where $z_i^a \in \mathcal{R}^{n_i - m_i}$ and $z_i^b \in \mathcal{R}^{m_i}$. Then the system (6) can be rewritten in the following form

$$\dot{z}_i^a = A_{i1} z_i^a + A_{i2} z_i^b + \sum_{j=1}^{N} \Gamma_{ij}^a(t, z_j) + \delta_i^a(t, z) \tag{10}$$

$$\begin{aligned}\dot{z}_i^b = &A_{i3} z_i^a + A_{i4} z_i^b + \tilde{B}_{i2}\big(u_i + g_i(t, z_i)\big) \\ &+ \sum_{j=1}^{N} \Gamma_{ij}^b(t, z_j) + \delta_i^b(t, z) \end{aligned} \tag{11}$$

where the matrix A_{i1} in (10) is stable.

The following assumption is now imposed on the uncertainty.

Assumption 2. There exist known continuous functions $\rho_i(t, z_i)$, $\eta_i^a(t, z)$ and $\eta_i^b(t, z)$ such that for $i, j = 1, 2, \ldots, N$

$$\begin{aligned} &\text{(i)} \ \|g_i(t, z_i)\| \le \rho_i(t, z_i) \\ &\text{(ii)} \ \|\delta_i^a(t, z)\| \le \eta_i^a(t, z)\|z\| \\ &\text{(iii)} \ \|\delta_i^b(t, z)\| \le \eta_i^b(t, z) \end{aligned}$$

Remark 1. Assumption 2 is a limitation on all the uncertainty experienced by the system. It is required that bounds on the uncertainties are known. These bounds will be employed in the control design to reject the effects of the uncertainty. It should be emphasised that the bounds on the uncertainties in Assumption 2 have a more general form

when compared with existing work. Assumption 2 also shows that it is only required that the uncertainties $\delta_i^a(\cdot)$ vanish at the origin, but it is not required that $g_i(\cdot)$ and $\delta_i^b(\cdot)$ vanish at the origin.

3 Stability Analysis of the Sliding Mode Dynamics

In this section, a sliding surface is designed for the system (10)-(11) and the stability of the corresponding sliding motion is analysed. A set of sufficient conditions is provided such that the sliding motion is asymptotically stable. By inspection, the system (10)-(11) has regular form. Choose the local sliding surface for the ith subsystem of the large-scale interconnected system (6) as follows:

$$\sigma_i(z_i) \equiv: z_i^b = 0, \qquad i = 1, 2, \ldots, N. \tag{12}$$

Then, the composite sliding surface for the interconnected system (6) is chosen as

$$\sigma(z) = 0 \tag{13}$$

where $\sigma(z) \equiv: \text{col}\left(z_1^b, z_2^b, \ldots, z_N^b\right)$

Since A_{i1} in (10) is stable, for any $Q_i > 0$, the following Lyapunov equation has a unique solution $P_i > 0$ such that

$$A_{i1}^\tau P_i + P_i A_{i1} = -Q_i, \qquad i = 1, 2, \ldots, N. \tag{14}$$

During sliding motion, $z_i^b = 0$ for $i = 1, 2, \ldots, N$. Then, the sliding mode dynamics for the system (10)-(11) associated with the designed sliding surface (13) can be described by

$$\dot{z}_i^a = A_{i1} z_i^a + \sum_{j=1}^{n} \Gamma_{ij}^s(t, z_j^a) + \delta_i^s(t, z_1^a, z_2^a, \ldots, z_N^a) \tag{15}$$

where

$$\Gamma_{ij}^s(t, z_j^a) := \Gamma_{ij}^a(t, z_j)|_{z_j^b = 0} \tag{16}$$

$$\delta_i^s(t, z_1^a, z_2^a, \ldots, z_N^a) := \delta_i^a(t, z)|_{(z_1^b, z_2^b, \ldots, z_N^b) = 0} \tag{17}$$

Here $\Gamma_{ij}^a(t, z_j)$ and $\delta_i^a(t, z)$ are defined in (8) and (9) respectively.

Assumption 3. The function $\Gamma_{ij}^s(\cdot)$ has the following decomposition:

$$\Gamma_{ij}^s(t, z_j^a) = \tilde{\Gamma}_{ij}^s(t, z_j^a) z_j^a \tag{18}$$

where $\tilde{\Gamma}_{ij}^s(t, z_j^a)$ is an appropriately-dimensioned matrix function for $i, j = 1, 2, \ldots, N$.

Remark 2. If the term $\Xi_{ij}(t, x_j)$ in system (1) is sufficiently smooth with $\Xi_{ij}(t, 0) = 0$, then $\Gamma_{ij}^s(t, z_j^a)$ will be smooth enough with $\Gamma_{ij}^s(t, 0) = 0$. From [14], it is straightforward to see that the decomposition (18) holds. It should be noted that in this chapter, it

is only required that $\Gamma_{ij}^s(\cdot)$ has the decomposition in (18). This is different to existing work reported in [1, 10, 12, 14, 16] where it is required that $\Xi_{ij}(t, x_j)$ in (1) vanish at the origin.

It follows that, under Assumptions 1-3, a reduced order interconnected system composed of N subsystems with dimension $n_i - m_i$ is obtained as follows

$$\dot{z}_j^a = A_{i1} z_j^a + \sum_{j=1}^{n} \tilde{\Gamma}_{ij}^s(t, z_j^a) z_j^a + \delta_i^s(t, z_1^a, z_2^a, \ldots, z_N^a) \tag{19}$$

which represents the sliding mode dynamics relating to the sliding surface (13), where $z_i^a \in \mathcal{R}^{n_i - m_i}$ and $\tilde{\Gamma}_{ij}^s(t, z_j^a)$ satisfy equation (18).

Lemma 1. *For the terms $\delta_i^s(t, z_1^a, z_2^a, \ldots, z_N^a)$ in system (19), if condition (ii) in Assumption 2 holds, then there exist continuous functions $\gamma_{ij}(\cdot)$ such that*

$$\|\delta_i^s(t, z_1^a, z_2^a, \ldots, z_N^a)\| \leq \sum_{j=1}^{N} \gamma_{ij}(t, z^a) \|z_j^a\| \tag{20}$$

where $z^a = \mathrm{col}(z_1^a, z_2^a, \ldots, z_N^a)$.

Proof. From the definition of $\delta_i^s(\cdot)$ in (16), it follows that

$$\delta_i^s(t, z_1^a, z_2^a, \ldots, z_N^a) = \delta_i^a(t, z_1^a, 0, z_2^a, 0, \ldots, z_N^a, 0) \tag{21}$$

From condition (ii) in Assumption 2,

$$\|\delta_i^a(t, z)\| \leq \eta_i^a(t, z) \|z\| \tag{22}$$

From (21) and (22), it follows that

$$\begin{aligned} \|\delta_i^s(t, z_1^a, z_2^a, \ldots, z_N^a)\| &= \|\delta_i^a(t, z_1^a, 0, z_2^a, 0, \ldots, z_N^a, 0)\| \\ &\leq \eta_i^a(t, z_1^a, 0, z_2^a, 0, \ldots, z_N^a, 0) \|z^a\| \\ &\leq \sum_{j=1}^{N} \eta_i^a(t, z_1^a, 0, z_2^a, 0, \ldots, z_N^a, 0) \|z_j^a\| \\ &\leq \sum_{j=1}^{N} \gamma_{ij}(t, z_j^a) \|z_j^a\| \end{aligned} \tag{23}$$

where $\gamma_{ij}(t, z_j^a) = \eta_i^a(t, z_1^a, 0, z_2^a, 0, \ldots, z_N^a, 0)$ for $i = 1, 2, \ldots, N$. Hence the result follows. □

The following result can now be presented.

Theorem 1. *Consider the sliding mode dynamics given in equation (19). Under Assumptions 1-3, the sliding motion governed by (19) is asymptotically stable if there exists a domain Ω_{z^a} of the origin in $z^a \in \mathcal{R}^{\sum_{i=1}^{N}(n_i - m_i)}$ such that*

$$M^\tau + M > 0$$

in $\Omega_{z^a}\backslash\{0\}$ *where* $M = (m_{ij})_{N\times N}$ *and for* $i, j = 1, 2, \ldots, N$

$$m_{ij} = \begin{cases} \lambda_{min}(Q_i) - 2\|P_i\|\gamma_{ii}(t, z_i^a) - \varsigma_{ii}(t, z_i^a), & i = j \\ -\varsigma_{ij}(t, z_j^a) - 2\|P_i\|\gamma_{ij}(t, z_j^a), & i \neq j \end{cases}$$

where P_i *and* Q_i *satisfy (14), and the functions* $\varsigma_{ij}(\cdot)$ *are defined by*

$$\varsigma_{ij}(t, z_j^a) :\equiv \|P_i\tilde{\Gamma}_{ij}^s(t, z_j^a) + (\tilde{\Gamma}_{ij}^s)^\tau(t, z_j^a)P_i\|$$

with $\tilde{\Gamma}_{ij}^s(t, z_j^a)$ *given by (18), and* $\gamma_{ij}(t, z_j^a)$ *determined by (20).*

Proof. For system (19), consider the Lyapunov function candidate

$$V(t, z_1^a, z_2^a, \ldots, z_N^a) = \sum_{i=1}^{N}(z_j^a)^\tau P_i z_j^a \tag{24}$$

where P_i satisfies equation (14)

Then, the time derivative of $V(t, z_1^a, z_2^a, \ldots, z_N^a)$ along the trajectories of system (19) is given by

$$\begin{aligned} \dot{V} = \sum_{i=1}^{N}\Big\{ & -(z_j^a)^\tau Q_i z_i^a + 2(z_j^a)^\tau P_i \delta_i^s(t, z_1^a, z_2^a, \ldots, z_N^a) \\ & + \sum_{j=1}^{n}(z_j^a)^\tau\Big(P_i\tilde{\Gamma}_{ij}^s(t, z_j^a) + (\tilde{\Gamma}_{ij}^s)^\tau(t, z_j^a)P_i\Big)z_j^a\Big\} \end{aligned} \tag{25}$$

where (14) is used above. From (20), it follows that

$$\begin{aligned} \dot{V} &\leq \sum_{i=1}^{N}\Big\{ -\lambda_{min}(Q_i)\|z_i^a\|^2 + 2\|z_i^a\|\|P_i\|\|\delta_i^s(t, z_1^a, z_2^a, \ldots, z_N^a)\| \\ &\quad + \sum_{j=1}^{N}\Big\|P_i\tilde{\Gamma}_{i1}^s(t, z_j^a) + (\tilde{\Gamma}_{ij}^s(t, z_j^a))^\tau z_j^a P_i\Big\|\|z_i^a\|\|z_j^a\|\Big\} \\ &\leq \sum_{i=1}^{N}\Big\{ -\lambda_{min}(Q_i)\|z_i^a\|^2 + \sum_{j=1}^{N}\varsigma_{ij}(t, z_j^a)\|z_i^a\|\|z_j^a\| \\ &\quad + 2\|z_i^a\|\|P_i\|\sum_{j=1}^{N}\gamma_{ij}(t, z_j^a)\|z_j^a\|\Big\} \\ &= -\sum_{i=1}^{N}\Big\{\lambda_{min}(Q_i) - 2\|P_i\|\gamma_{ii}(t, z_i^a) - \varsigma_{ii}(t, z_i^a)\Big\}\|z_i^a\|^2 + \\ &\quad \sum_{i=1}^{N}\sum_{\substack{j=1 \\ j\neq i}}^{N}\Big\{\varsigma_{ij}(t, z_j^a) + 2\|P_i\|\gamma_{ij}(t, z_j^a)\Big\}\|z_i^a\|\|z_j^a\| \\ &= -\frac{1}{2}Y^\tau(M^\tau + M)Y \leq 0 \end{aligned} \tag{26}$$

where $Y \equiv: \text{col}(\|z_1^a\|, \ldots, \|z_N^a\|)$.

Thus, the conclusion follows from $M^\tau + M > 0$. □

Theorem 1 shows that the designed sliding motion is asymptotically stable. Conditions to ensure that this sliding motion is attained and maintained will now be developed.

4 Decentralised Sliding Mode Control Design

A sliding mode control is designed to drive the system to the sliding surface. It is well known that an appropriate reachability condition is described by

$$\sigma^\tau(z)\dot{\sigma}(z) < 0$$

for a centralised system with switching surfaces $\sigma(z) = 0$. For the nonlinear interconnected system (1), the corresponding condition is described by

$$\sum_{i=1}^{N} \frac{\sigma_i^\tau(z_i)\dot{\sigma}_i(z_i)}{\|\sigma_i(z_i)\|} < 0 \tag{27}$$

where $\sigma_i(z_i)$ is defined by (13). It should be noted that the condition (27) is proposed in [8] and has been widely used [14, 18].

In order to reduce the effects of the unknown interconnection $\delta_i^b(\cdot)$, consider the expression

$$\eta_i^b(t,z) = \sum_{j=1}^{N} \mu_{ij}(t,z_j) + \nu_i(t,z) \tag{28}$$

where $\nu_i(t,z)$ represents all the coupling terms which cannot be included in the term $\sum_{j=1}^{N} \mu_{ij}(t,z_j)$

The objective is to design a decentralised sliding mode controller such that the reachability condition (27) is satisfied. For $i = 1, 2, \ldots, N$, the following control scheme is proposed:

$$\begin{aligned} u_i = &-\tilde{B}_{i2}^{-1}\Big\{A_{i3}z_i^a + A_{i4}z_i^b + \sum_{j=1}^{N} \Gamma_{ji}^b(t, T_i^{-1}z_i)\Big\} \\ &-\tilde{B}_{i2}^{-1}\text{sgn}(z_i^b)\Big\{\|\tilde{B}_{i2}\|\rho_i(t,z_i) \\ &+\sum_{j=1}^{N} \mu_{ji}(t,z_i) + \zeta_i(t,z_i)\Big\} \end{aligned} \tag{29}$$

where the $\rho_i(t,z_i)$ are defined in Assumption 2, $\mu_{ji}(t,z_i)$ satisfy (28) and $\zeta_i(t,z_i)$ is a reachability function which will be defined later.

Theorem 2. *Consider the nonlinear interconnected system (6). Under Assumptions 1-3, the decentralised control (29) is able to drive the system (1) to the composite sliding surface (13) and maintain a sliding motion on it thereafter if in the considered domain $\Omega = \Omega_1 \times \Omega_2 \cdots \times \Omega$, the functions $\zeta_i(t, z_i)$ in (29) satisfy*

$$\sum_{i=1}^{N} \zeta_i(t, z_i) > \sum_{i=1}^{N} \nu_i(t, z)$$

in $\Omega \backslash \{0\}$ for all $t > 0$ with $\nu_i(t, z)$ defined in (28).

Proof. From the analysis above, all that needs to be proved is that the composite reachability condition (27) is satisfied. From (13), for $i = 1, 2, \ldots, N$

$$\begin{aligned}\dot{\sigma}_i(z_i) = \dot{z}_i^b = A_{i3} z_i^a + A_{i4} z_i^b \\ + \tilde{B}_{i2}\big(u_i + \phi_i(t, T_i^{-1} z_i)\big) \\ + \sum_{j=1}^{N} \Gamma_{ij}^b(t, z_j) + \delta_i^b(t, z)\end{aligned} \tag{30}$$

Substituting (29) into (30),

$$\begin{aligned}\sum_{i=1}^{N} \frac{\sigma_i^\tau(z_i)\dot{\sigma}_i(z_i)}{\|\sigma_i(z_i)\|} &= \sum_{i=1}^{N} \Big\{ \frac{(z_i^b)^\tau}{\|z_i^b\|}\big\{\delta_i^b(t, z) + \tilde{B}_{i2}\phi_i(t, T_i^{-1} z_i)\big\} \\ &\quad - \|\tilde{B}_{i2}\|\rho_i(t, z_i) - \sum_{j=1}^{N} \mu_{ji}(t, z_i) - \zeta_i(t, z_i)\Big\} \\ &\quad + \frac{(z_i^b)^\tau}{\|z_i^b\|}\big\{ \sum_{i=1}^{N}\sum_{j=1}^{N} \Gamma_{ij}^b(t, z_j) - \sum_{i=1}^{N}\sum_{j=1}^{N} \Gamma_{ji}^b(t, z_i)\big\} \\ &\leq \sum_{i=1}^{N} \|\tilde{B}_{i2}\phi_i(t, T_i^{-1} z_i)\| + \sum_{i=1}^{N} \|\delta_i^b(t, z)\| \\ &\quad - \sum_{i=1}^{N} \|\tilde{B}_{i2}\|\rho_i(t, z_i) - \sum_{i=1}^{N}\sum_{j=1}^{N} \mu_{ji}(t, z_i) \\ &\quad - \sum_{i=1}^{N} \zeta_i(t, z_i)\end{aligned} \tag{31}$$

From Assumption 3,

$$\begin{aligned}\sum_{i=1}^{N} \|\delta_i^b(t, T^{-1} z)\| &\leq \sum_{i=1}^{N}\sum_{j=1}^{N} \mu_{ij}(t, z_j) + \sum_{i=1}^{N} \nu_i(t, z) \\ &= \sum_{i=1}^{N}\sum_{j=1}^{N} \mu_{ji}(t, z_i) + \sum_{i=1}^{N} \nu_i(t, z)\end{aligned} \tag{32}$$

and

$$\begin{aligned}\|\tilde{B}_{i2}\phi_i(t,T_i^{-1}z_i)\| &\leq \|\tilde{B}_{i2}\|\|\phi_i(t,T_i^{-1}z_i)\| \\ &\leq \|\tilde{B}_{i2}\|\rho_i(t,z_i) \end{aligned} \tag{33}$$

Substituting inequalities (32) and (33) into (31)

$$\sum_{i=1}^{N}\frac{\sigma_i^{\tau}\dot{\sigma}_i}{\|\sigma_i\|} \leq -\sum_{i=1}^{N}\zeta_i(t,z_i)+\sum_{i=1}^{N}\nu_i(t,z) < 0 \tag{34}$$

Then the reachability condition (31) is satisfied. Hence, the result follows. □

From sliding mode control theory, Theorems 1 and 2 together guarantee that the closed-loop system formed by applying the decentralised controller (29) to the interconnected system (6) is asymptotically stable in the domain Ω. From the relationship between (1) and (6), it follows that the control (29) with the transformation

$$\mathrm{col}(z_i^a, z_i^b) = T_i x_i$$

can stabilize the system (1) asymptotically in the domain $\mathcal{D} := \mathcal{D}_1 \times \mathcal{D}_2 \times \mathcal{D}_N$.

5 Case Study —Control of a Continuously Stirred Tank Reactor (CSTR)

To illustrate the algorithm, a system composed of three cascaded non-isothermal continuously stirred-tank reactors (CSTRs) with recycling as presented in [11] is considered. The overview of the system is shown in Fig.1.

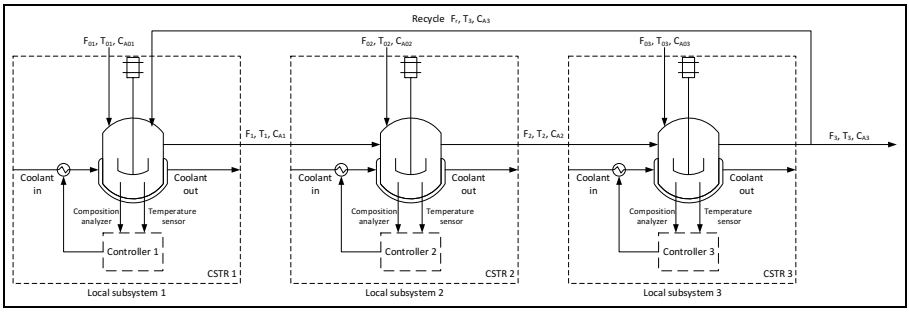

Fig. 1. Schematic diagram of the CSTR system

The output of local subsystem CSTR 3 is passed through a separator that recycles unreacted products back to the CSTR 1 subsystem. The reactant species are consumed in each reactor by three parallel, irreversible exothermic reactions. Due to the non-isothermal nature of the reactions, a jacket is used to remove/provide heat to each

reactor. A plant model based on material and energy balance is described as follows (see [11] for full details):

$$\frac{dT_1}{dt} = \frac{F_1^0}{V_1}(T_1^0 - T_1) + \frac{F_r}{V_1}(T_r - T_1) + \sum_{i=1}^{3} \frac{-\Delta H_i}{\rho c_p} R_i(C_{A1}, T_1) + \frac{Q_1}{\rho c_p V_1} \tag{35}$$

$$\frac{dC_{A1}}{dt} = \frac{F_1^0}{V_1}(C_{A1}^0 - C_{A1}) + \frac{F_r}{V_1}(C_{Ar} - C_{A1}) - \sum_{i=1}^{3} R_i(C_{A1}, T_1) \tag{36}$$

$$\frac{dT_2}{dt} = \frac{F_2^0}{V_2}(T_2^0 - T_2) + \frac{F_1}{V_2}(T_1 - T_2) + \sum_{i=1}^{3} \frac{-\Delta H_i}{\rho c_p} R_i(C_{A2}, T_2) + \frac{Q_2}{\rho c_p V_2} \tag{37}$$

$$\frac{dC_{A2}}{dt} = \frac{F_2^0}{V_2}(C_{A2}^0 - C_{A2}) + \frac{F_1}{V_2}(C_{A1} - C_{A2}) - \sum_{i=1}^{3} R_i(C_{A2}, T_2) \tag{38}$$

$$\frac{dT_3}{dt} = \frac{F_3^0}{V_3}(T_3^0 - T_3) + \frac{F_2}{V_3}(T_2 - T_3) + \sum_{i=1}^{3} \frac{-\Delta H_i}{\rho c_p} R_i(C_{A3}, T_3) + \frac{Q_3}{\rho c_p V_3} \tag{39}$$

$$\frac{dC_{A3}}{dt} = \frac{F_3^0}{V_3}(C_{A3}^0 - C_{A3}) + \frac{F_2}{V_3}(C_{A2} - C_{A3}) - \sum_{i=1}^{3} R_i(C_{A3}, T_3) \tag{40}$$

where T_i, C_{Ai}, Q_j and V_j denote the temperature, the reactant concentration, the rate of heat, and the volume of the ith reactor, respectively. The terms

$$R_i(C_{Aj}, T_j) = k_{i0} e^{\frac{-E_i}{RT_j}} C_{Aj}, \qquad i = 1, 2, 3$$

represent the reaction rate of the ith reaction. F_i^0 denotes the flow rate of a fresh feed stream associated with the ith reactor. F_r represents the flow rate of the recycle stream. It should be noted that the temperature and the reactant concentration of the recycle stream are assumed to be equal to the temperature and the concentration of the CSTR 3 subsystem as the recycled product is directly separated from CSTR 3. ΔH_i, k_i and E_i for $i = 1, 2, 3$ denote the enthalpy, pre-exponential constants and activation energies of the three reactions respectively. The symbols c_p and ρ denote the heat capacity and density of fluid in the reactor. As in [11], it is assumed that the recycle ratio is $r = 0.5$ and the system parameters are given in Table 1. The corresponding steady state operating conditions are presented in Table 2 (see [11]).

Table 1. System Parameters

Parameters	Value	Parameters	Value
F_1^0	4.998 m^3/h	V_1	1.0 m^3
F_2^0	30 m^3/h	V_2	3.0 m^3
F_3^0	60 m^3/h	V_3	9.0 m^3
T_1^0	300.0 K	C_{A1}^0	4.0 kmol/m^3
T_2^0	300.0 K	C_{A2}^0	3.0 kmol/m^3
T_3^0	300.0 K	C_{A3}^0	2.0 kmol/m^3
ΔH_1	-5.0 $\times$ 10^4 KJ/kmol	k_{10}	3.0 $\times$ 10^6 h^{-1}
ΔH_2	-5.2 $\times$ 10^4 KJ/kmol	k_{20}	3.0 $\times$ 10^5 h^{-1}
ΔH_3	-5.4 $\times$ 10^4 KJ/kmol	k_{30}	3.0 $\times$ 10^5 h^{-1}
E_1	5.0 $\times$ 10^4 KJ/kmol	ρ	1000.0 kg/m^3
E_2	7.53 $\times$ 10^4 KJ/kmol	c_p	0.231 KJ/kg K
E_3	7.53 $\times$ 10^4 KJ/kmol	F_r	94.998 m^3/h

Note: $F_r = rF_3$ where r is the recycle ratio.

The objective is to design a decentralised control strategy to stabilise the CSTR system asymptotically. Let

$$x_{i1} = C_{Ai} - C_{Ai}^s$$
$$x_{i2} = T_i - T_i^s$$

for $i = 1, 2, 3$. Then, the CSTR system can be described in the form of (1) by

$$\dot{x}_1 = \underbrace{\begin{bmatrix} -99.996 & 0 \\ 0 & -99.996 \end{bmatrix}}_{A_1} x_1 + \underbrace{\begin{bmatrix} 0 \\ 0.00433 \end{bmatrix}}_{B_1} (u_1 + \phi_1(t, x_1)) + \underbrace{\begin{bmatrix} 94.998 & 0 \\ 0 & 94.998 \end{bmatrix}}_{\Xi_{13}} x_3 + \underbrace{\begin{bmatrix} f_{11}(t, x_1) \\ f_{12}(t, x_1) \end{bmatrix}}_{\Xi_{11}} + \psi_1(t, x) \tag{41}$$

Table 2. System Steady State Operating Conditions

State	Equilibrium Point	State	Equilibrium Point
T_1^s	432.8113 K	C_{A1}^s	1.8864 kmol/m^3
T_2^s	422.1458 K	C_{A2}^s	2.0510 kmol/m^3
T_3^s	427.8888 K	C_{A3}^s	1.8302 kmol/m^3

$$\dot{x}_2 = \underbrace{\begin{bmatrix} -43.332 & 0 \\ 0 & -43.332 \end{bmatrix}}_{A_2} x_2 + \underbrace{\begin{bmatrix} 0 \\ 0.00144 \end{bmatrix}}_{B_2} (u_2 + \phi_2(t, x_2)) + \underbrace{\begin{bmatrix} 33.332 & 0 \\ 0 & 33.332 \end{bmatrix}}_{\Xi_{21}} x_1 + \underbrace{\begin{bmatrix} f_{21}(t, x_2) \\ f_{22}(t, x_2) \end{bmatrix}}_{\Xi_{22}} + \psi_2(t, x) \tag{42}$$

$$\dot{x}_3 = \underbrace{\begin{bmatrix} -21.111 & 0 \\ 0 & -21.111 \end{bmatrix}}_{A_3} x_3 + \underbrace{\begin{bmatrix} 0 \\ 0.000481 \end{bmatrix}}_{B_3} (u_3 + \phi_3(t, x_3)) + \underbrace{\begin{bmatrix} 14.444 & 0 \\ 0 & 14.444 \end{bmatrix}}_{\Xi_{32}} x_2 + \underbrace{\begin{bmatrix} f_{31}(t, x_3) \\ f_{32}(t, x_3) \end{bmatrix}}_{\Xi_{33}} + \psi_3(t, x) \tag{43}$$

where

$$\begin{aligned}
f_{11}(t, x_1) &= \Big(-3 \times 10^6 \exp(\frac{-6013.952}{x_{12} + 432.8113}) \\
&\quad -6 \times 10^5 \exp(\frac{-9057.012}{x_{12} + 432.8113}) \Big)(x_{11} + 1.8864) + 5.2249 \\
f_{12}(t, x_1) &= \Big(6.494 \times 10^8 \exp(\frac{-6013.952}{x_{12} + 432.8113}) \\
&\quad +1.377 \times 10^8 \exp(\frac{-9057.012}{x_{12} + 432.8113}) \Big)(x_{11} + 1.8864) \\
&\quad -1131.4185 \\
f_{21}(t, x_2) &= \Big(-3 \times 10^6 \exp(\frac{-6013.952}{x_{22} + 422.1458}) \\
&\quad -6 \times 10^5 \exp(\frac{-9057.012}{x_{22} + 422.1458}) \Big)(x_{21} + 2.051) + 4.0035 \\
f_{22}(t, x_2) &= \Big(6.494 \times 10^8 \exp(\frac{-6013.952}{x_{22} + 422.1458}) \\
&\quad +1.377 \times 10^8 \exp(\frac{-9057.012}{x_{22} + 422.1458}) \Big)(x_{21} + 2.051) \\
&\quad -865.9556 \\
f_{31}(t, x_3) &= \Big(-3 \times 10^6 \exp(\frac{-6013.952}{x_{32} + 427.8888}) \\
&\quad -6 \times 10^5 \exp(\frac{-9057.012}{x_{32} + 427.8888}) \Big)(x_{31} + 1.8302) + 4.3212 \\
f_{32}(t, x_3) &= \Big(6.494 \times 10^8 \exp(\frac{-6013.952}{x_{32} + 427.8888}) \\
&\quad +1.377 \times 10^8 \exp(\frac{-9057.012}{x_{32} + 427.8888}) \Big)(x_{31} + 1.8302) \\
&\quad -935.5439
\end{aligned}$$

The unknown matched uncertainty $\phi_i(t, x_i, t)$ is assumed to satisfy

$$\|\phi_1(t, x_1)\| \leq 1000|x_{11}| + 800|x_{12}| \tag{44}$$
$$\|\phi_2(t, x_2)\| \leq 2000|x_{21}| + 600|x_{22}| \tag{45}$$

Consider the system (41)-(43) in the domain

$$D = \{x_i \in \mathcal{R}^3 | x_{i1} \geq -C_{Ai}^s, |x_{i2}| \leq 100\}$$

It should be noted that since the concentration of each tank cannot be negative and the temperature is upper and lower limited by practical bounds, the domain considered covers a reasonable range from the practical point of view.

By using the algorithm in [4], the coordinate transformation $z_i = T_i x_i$ for $i = 1, 2, 3$ can be obtained with T_i defined by

$$T_i = \begin{bmatrix} 1 & 0 \\ -0.1 & 1 \end{bmatrix}$$

Then the system (41)-(43) is transformed into the form in (10)-(11) as

$$\begin{aligned} \dot{z}_1 = & \begin{bmatrix} -99.996 & 0 \\ 0 & -99.996 \end{bmatrix} z_1 + \begin{bmatrix} 0 \\ 0.00433 \end{bmatrix} (u_1 + g_1(t, z_1, t)) \\ & + \underbrace{\begin{bmatrix} 94.998 & 0 \\ 0 & 94.998 \end{bmatrix} z_3}_{\Gamma_{13}(t, z_3)} + \begin{bmatrix} \Gamma_{11}^a(t, z_1) \\ \Gamma_{11}^b(t, z_1) \end{bmatrix} + \begin{bmatrix} \delta_1^a(t, z) \\ \delta_1^b(t, z) \end{bmatrix} \end{aligned} \tag{46}$$

$$\begin{aligned} \dot{z}_2 = & \begin{bmatrix} -43.332 & 0 \\ 0 & -43.332 \end{bmatrix} z_2 + \begin{bmatrix} 0 \\ 0.00144 \end{bmatrix} (u_2 + g_2(t, z_2, t)) \\ & + \underbrace{\begin{bmatrix} 33.332 & 0 \\ 0 & 33.332 \end{bmatrix} z_1}_{\Gamma_{21}(t, z_1)} + \begin{bmatrix} \Gamma_{22}^a(t, z_2) \\ \Gamma_{22}^b(t, z_2) \end{bmatrix} + \begin{bmatrix} \delta_2^a(t, z) \\ \delta_2^b(t, z) \end{bmatrix} \end{aligned} \tag{47}$$

$$\begin{aligned} \dot{z}_3 = & \begin{bmatrix} -21.111 & 0 \\ 0 & -21.111 \end{bmatrix} z_3 + \begin{bmatrix} 0 \\ 0.000481 \end{bmatrix} (u_3 + g_3(t, z_3, t)) \\ & + \underbrace{\begin{bmatrix} 14.444 & 0 \\ 0 & 14.444 \end{bmatrix} z_2}_{\Gamma_{32}(t, z_2)} + \begin{bmatrix} \Gamma_{33}^a(t, z_3) \\ \Gamma_{33}^b(t, z_3) \end{bmatrix} + \begin{bmatrix} \delta_3^a(t, z) \\ \delta_3^b(t, z) \end{bmatrix} \end{aligned} \tag{48}$$

where

$$\begin{aligned} \Gamma_{ii}^a(t, z_i) &= f_{i1}(T_i^{-1} z_i) \\ \Gamma_{ii}^b(t, z_i) &= f_{i2}(T_i^{-1} z_i) - 0.1 f_{i1}(T_i^{-1} z_i) \end{aligned}$$

for $i = 1, 2, 3$ and $j = 1, 2$, and the unknown interconnections are assumed to satisfy

$$\begin{aligned}
\delta_1^a(t,z) &\leq 5\sin^2(z_{11})\|z\| \\
\delta_1^b(t,z) &\leq \underbrace{0.5\sin^2(z_{11})\|z_1\|}_{\mu_{11}(t,z_2)} + \underbrace{0.5\sin^2(z_{11})\|z_2\| + 0.5\sin^2(z_{11})\|z_3\|}_{\nu_1(t,z)} \\
\delta_2^b(t,z) &\leq \underbrace{6|z_{21}| + 5|z_{22}|}_{\mu_{22}(t,z_2)} \\
\delta_3^a(t,z) &\leq 2\cos^2(z_{31})\|z3\| \\
\delta_3^b(t,z) &\leq \underbrace{0.2\cos^2(z_{11})\|z_3\|}_{\mu_{31}(t,z_1)} + \underbrace{0.7|z_{22}|}_{\mu_{32}(t,z_2)}
\end{aligned}$$

During sliding motion, $z_{i2} = 0$ and $\Gamma_{ii}^s(t, z_i)$ is given by

$$\Gamma_{11}^s(t, z_{11}) = \xi_{11}(t, z_{11})z_{11} + 1.8864\xi_{11}(t, z_{11}) + 5.2249 \tag{49}$$

$$\Gamma_{22}^s(t, z_{21}) = \xi_{21}(t, z_{21})z_{11} + 2.051\xi_{21}(t, z_{21}) + 4.0035 \tag{50}$$

$$\Gamma_{33}^s(t, z_{31}) = \xi_{31}(t, z_{31})z_{11} + 1.8302\xi_{31}(t, z_{31}) + 4.3212 \tag{51}$$

where

$$\begin{aligned}
\xi_{11}(t, z_{11}) &= -3 \times 10^6 \exp\left(\frac{-6013.952}{0.1z11 + 432.8113}\right) \\
&\quad -6 \times 10^5 \exp\left(\frac{-9057.012}{0.1z11 + 432.8113}\right) \\
\xi_{11}(t, z_{21}) &= -3 \times 10^6 \exp\left(\frac{-6013.952}{0.1z21 + 422.1458}\right) \\
&\quad -6 \times 10^5 \exp\left(\frac{-9057.012}{0.1z21 + 422.1458}\right) \\
\xi_{11}(t, z_{31}) &= -3 \times 10^6 \exp\left(\frac{-6013.952}{0.1z31 + 427.8888}\right) \\
&\quad -6 \times 10^5 \exp\left(\frac{-9057.012}{0.1z31 + 427.8888}\right)
\end{aligned}$$

It is straightforward to verify that the term $1.8864\xi_{11}(t, z_{11}) + 5.2249$ in (49) vanishes to 0 when $x_{11} = 0$, which means that the term can be approximated with a Taylor series. By using a Taylor series of order 6, the term can be expressed as follows:

$$1.8864\xi_{11}(t, z_{11}) + 5.2249 = d_1(t, z_{11})z_{11} \tag{52}$$

where

$$\begin{aligned}
d_1(t, z_{11}) &= 1.43 \times 10^{-15} z_{11}^4 + 7.27 \times 10^{-12} z_{11}^3 \\
&\quad +1.73 \times 10^{-8} z_{11}^2 + 2.31 \times 10^{-5} z_{11} + 0.0168
\end{aligned} \tag{53}$$

With the same procedure, the Taylor series' expansions for similar terms in $\Gamma_{22}^s(t, z_2)$ and $\Gamma_{33}^s(t, z_3)$ can also be expressed with $d_2(t, z_{21})$ and $d_3(t, z_{31})$

$$\begin{aligned}
d_2(t, z_{21}) &= 7.67 \times 10^{-16} x_{22}^4 + 3.45 \times 10^{-12} x_{22}^3 \\
&\quad +7.61 \times 10^{-9} x_{22}^2 + 9.55 \times 10^{-6} x_{22} + 0.00658
\end{aligned} \tag{54}$$

$$d_3(t, z_{31}) = 7.64 \times 10^{-16} x_{32}^4 + 3.67 \times 10^{-12} x_{32}^3 + 8.42 \times 10^{-9} x_{32}^2 + 1.09 \times 10^{-5} x_{32} + 0.00776 \quad (55)$$

Thus the known nonlinearity $\Gamma_{ii}^s(t, z_{i1})$ in (46)-(48) can be expressed as

$$\Gamma_{ii}^s(t, z_{i1}) = \underbrace{(\xi_{i1}(t, z_{i1}) + d_i(t, z_{i1}))}_{\tilde{\Gamma}_{ii}^s(t, z_{i1})} z_{i1}$$

It is clear that the known nonlinear interconnections $\Gamma^s ij(t, z_{j1})$ can be expressed as

$$\Gamma_{13}^s(t, z_{31}) = 94.998 z_{31}$$
$$\Gamma_{21}^s(t, z_{11}) = 33.332 z_{31}$$
$$\Gamma_{32}^s(t, z_{21}) = 14.444 z_{31}$$

From Lemma 1,

$$\delta_1^a(t, z_{11}, z_{21}, z_{31}) \leq \sum_{j=1}^{3} 5 \sin^2(z_{21}) \|z_{11}\|$$
$$\delta_3^a(t, z_{11}, z_{21}, z_{31}) \leq 2 \cos^2(z_{31}) \|z_{31}\|$$

Choosing $Q_i = I_2$ for $i = 1, 2, 3$ and solving the Lyapunov equation (14) yields

$$P_1 = -0.005$$
$$P_2 = -0.0115$$
$$P_3 = -0.0237$$

Then, the matrix function M will be

$$\begin{bmatrix} 1 - \frac{\|\tilde{\Gamma}_{11}^s(t, z_{11})\|}{99.996} - 0.05 \sin^2(z_{11}) & -0.05 \sin^2(z_{11}) & -0.95 - 0.05 \sin^2(z_{11}) \\ -0.7692 & 1 - \frac{\|\tilde{\Gamma}_{22}^s(t, z_{21})\|}{43.332} & 0 \\ 0 & -0.6842 & 1 - \frac{\|\tilde{\Gamma}_{33}^s(t, z_{31})\|}{21.11} - 0.0947 \cos^2(z_{31}) \end{bmatrix}$$

By direct computation, it is straightforward to verify that in the domain D,

$$M^\tau + M > 0$$

It follows from Theorem 1 that the designed sliding mode is asymptotically stable. From Theorem 2, define the following decentralised control law

$$\begin{aligned} u_1(t,z_1) &= 15395.8441z_{12} - 230.9469\Gamma_{11}^b(t,z_1) \\ &\quad -\text{sgn}(z_{13})\Big\{1000|z_{11}| + 800|z_{12} - 0.1z_{11}| \\ &\quad +115.47\sin^2(z_{11})\|z_1\| + 230.9469\zeta_1(z_1)\Big\} \qquad (56) \\ u_2(t,z_2) &= 20014.7806z_{22} - 692.8406\Gamma_{22}^b(t,z_2) \\ &\quad -\text{sgn}(z_{23})\Big\{2000|z_{21}| + 600|z_{22} - 0.1z_{21}| \\ &\quad +692.8406\zeta_2(z_2)\Big\} \qquad (57) \\ u_3(t,z_3) &= -153575.7506z_{32} - 2078.5219\Gamma_{11}^b(t,z_3) \\ &\quad -\text{sgn}(z_{33})\Big\{415.70348\cos^2(z_{31})\|z_3\| + 2078.5219\zeta_3(z_3)\Big\} \qquad (58) \end{aligned}$$

where $\zeta_1(z_1) = 250 + 0.5\|z_1\|$, $\zeta_2(z_2) = 100$, and $\zeta_3(z_3) = 100$.

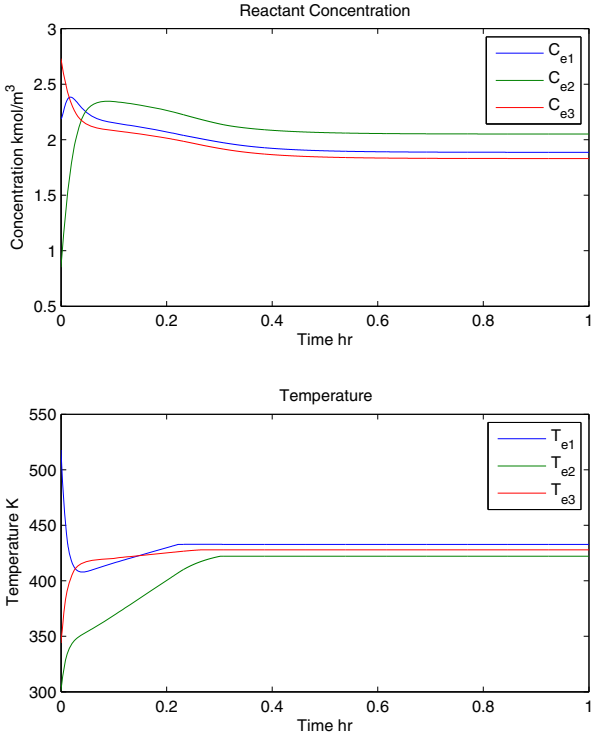

Fig. 2. Time response of the states of the CSCTR system from (35)-(40)

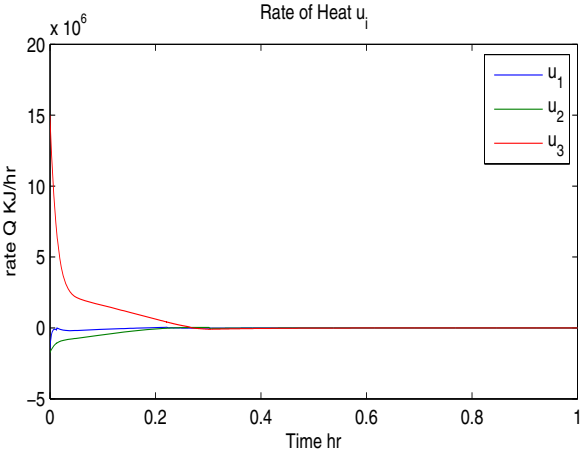

Fig. 3. Time response of the control input signals

By direct computation, it follows that the condition $\sum_{i=1}^{N} \zeta_i(z_i) \geq \sum_{i=1}^{N} \nu_i(t,z)$ is satisfied in the domain D, and thus the designed controllers (56)–(58) stabilise the system (41)-(43) asymptotically. The time responses of the system states of the CSCTR described in equations (35)-(40) are given in Figure 2 where the upper figure shows the reactant concentration while the lower figure shows the tank temperature. The time response of the control input signals are shown in Figure 3. The simulation results show that the proposed approach is effective.

6 Conclusions

In this chapter, a decentralised state feedback sliding mode control law has been proposed to stabilise a class of nonlinear interconnected systems with known and unknown interconnections asymptotically in the considered domain. Both matched and mismatched uncertainties are considered. The bounds on the uncertainty can be functions instead of constants or being restricted to having purely polynomial bounds, which is different to previous work. Both known interconnections and the bounds on the unknown interconnections have been fully considered in the control design to reduce the conservatism. The developed results are applicable to a wide class of interconnected systems. Design and simulation for a CSTR system has been presented to demonstrate the effectiveness of the results obtained.

Acknowledgement. This book is dedicated to the career and work of Professor Okyay Kaynak whose commitment to pushing the boundaries of control application oriented work has been a source of inspiration for discontinuous control teams both at the University of Leicester and the University of Kent in the UK. Okyay has also been a tremendous host to the research community and the events he has organised in Turkey are

memorable both for the quality of the academic dialogue as well as the great hospitality and insight into the history and culture of the country.

References

1. Aldeen, M., Trinh, H.: Decentralised feedback controllers for uncertain interconnected dynamic systems. IEE Proc. Part D: Control Theory Appl. 140(6), 429–434 (1993)
2. Cheng, C.C., Chang, Y.: Design of decentralised adaptive sliding mode controllers for large-scale systems with mismatched perturbations, Int. J. Control 81(10), 1507–1518 (2008)
3. Cheng, C.-F.: Disturbances attenuation for interconnected systems, Int. J. Control 66(2), 213–224 (1997)
4. Edwards, C., Spurgeon, S.K.: Sliding mode control: Theory and applications. Taylor & Francis, London (1998)
5. Giuseppe, F., Mario, R.: Design of Decentralized Robust Controller for Voltage Regulation and Stabilization of Multimachine Power systems. Int. J. Control 11(2), 277–285 (2013)
6. Ha, Q.P., Trinh, H.: Observer-based control of multi-agent systems under decentralized information structure, Int. J. Systems Science 35(12), 719–728 (2004)
7. Hua, C.-C., Leng, J., Guan, X.-P.: Decentralized MRAC for large-scale interconnected systems with time-varying delays and applications to chemical reactor systems. J. Process Control 22, 1985–1996 (2012)
8. Hsu, K.C.: Decentralized variable-structure control design for uncertain large-scale systems with series nonlinearities. Int. J. control 68(6), 1231–1240 (1997)
9. Jiang, L., Wu, Q.H., Wen, J.W.: Decentralized nonlinear adaptive control for multimachine power systems via high-gain perturbation observer. IEEE Trans. on Circuits and Systems (I) 51(10), 2052–2059 (2004)
10. Jiang, Z.-P.: Recent developments in decentralised nonlinear control. In: 8th Int. Conf. on Control, Automation, Robotics and Vision, Kunming, China (2004)
11. Sun, Y., El-Farra, N.H.: Resource aware quasi-decentralized control of networked process systems over wireless sensor networks. Chemical Engineering Science 69, 93–106 (2012)
12. Ugrinovskii, V.A., Petersen, I.R., Savkin, A.V., Ugrinovskaya, E.Y.: Decentralised state-feedback stabilization and robust control of uncertain large-scale systems with intergrally constrained interconnection. Systems and Control Letters 41(2), 107–119 (2000)
13. Utkin, V., Guldner, J., Shijun, M.: Sliding Mode Control in Electro-mechanical Systems. Taylor & Francis, London (1998)
14. Yan, X.-G., Edwards, C., Spurgeon, S.K.: Decentralised robust sliding mode control for a class of nonlinear interconnceted systems by static output feedback. Automatica 40(4), 613–620 (2004)
15. Yan, X.-G., Edwards, C., Spurgeon, S.K., Bleijs, J.A.M.: Decentralised sliding-mode control for multimachine power systems using only output information. IEE Proc.-Control Theory Appl. 151, 627–635 (2004)
16. Yan, X.-G., Spurgeon, S.K., Edwards, C.: Decentralized output feedback sliding mode control of nonlinear large-scale systems with uncertainties. J. Optimization Theory and Appl. 119(3), 597–614 (2003)
17. Yan, X.-G., Spurgeon, S.K., Edwards, C. (2005) Dynamic sliding mode control for a class of systems with mismatched uncertainty, European J. European J. Control 11(1), 1–10 (2005)
18. Yan, X.-G., Spurgeon, S.K., Edwards, C.: Decentralised stabilisation for nonlinear time delay interconnected systems using static output feedback. Automatica 49(2), 633–641 (2013)
19. Yang, M., Yang, F., Wang, C.-S., Wang, P.: Decentralised sliding mode load frequency control for multi-area power systems. IEEE Trans. on Power Systems 28(4), 4301–4309 (2013)

Integral Sliding Mode Control of Multi-input Nonlinear Uncertain Non-affine Systems

Giorgio Bartolini[1] and Elisabetta Punta[2]

[1] CNR-IEIIT, Via De Marini 6, 16149 Genova, Italy
giorgio.bartolini@ieiit.cnr.it
[2] CNR-IEIIT, Politecnico di Torino, Corso Duca degli Abruzzi 24, 10129 Torino, Italy
elisabetta.punta@ieiit.cnr.it

Abstract. This chapter is devoted to examine the control of multi-input uncertain non affine systems. Despite the great importance of this subject the literature has relatively few contributions, often not fully satisfactory. The authors attempt to identify the reasons for this in the difficulties of dealing with uncertain and time and state dependent matrices multiplying the control in the sliding output dynamics called High Frequency Gain matrices. For constant nonsingular matrices it would seem sufficient to know a set of matrices, the so-called unmixing set, and use enumerative techniques to identify on line the element which serves to make effective the control algorithm. The problem up to now is the cardinality of this set which is the product of factorial and exponential of the dimension of the matrix making impractical this approach even for low scale systems. The issue becomes more complicated if the matrix HFG is state-dependent and time. In this case the best that, in the current state of the research, can be done is to assume the above matrix with eigenvalues in the positive half-plane for any value of its arguments, and adopt a particular technique called integral sliding mode. Generalization to nonsingular matrices seems to be a very hard task since everything must be time and state varying.

1 Introduction

In this chapter recent results regarding the sliding mode control of multi-input nonlinear systems with uncertainties in the state equation are presented. It is well known that the sliding mode control problem can be also viewed as a stabilization problem for an I/O system with an artificial output (the sliding output) zeroing which the relevant control problem turns out to be solved. This assumption obviously implies the stability of the so called zero-dynamics. The I/O relationship of interest does not need to be perfectly known as will be more clearly stated in the sequel.

In order to clarify which is the main contribution of this chapter we start considering the case in which the relationship between the time derivative of the sliding output and the control is affine. This means that the dynamics of the sliding output is described by a first order differential equation whose R.H.S is the sum of a time and state dependent disturbance term, the drift vector field, and the product of a matrix of suitable dimension with the control vector. We call this matrix High Frequency Gain Matrix (HFGM) in analogy with the linear time invariant case. While uncertainties in the drift term can

X. Yu and M. Önder Efe (eds.), *Recent Advances in Sliding Modes*,
Studies in Systems, Decision and Control 24, DOI: 10.1007/978-3-319-18290-2_4

be managed exploiting the knowledge of norm upper bounds, the lack of knowledge of the HFG matrix implies the ignorance of the direction in which the control action is exerted on the sliding output dynamics . The perfect knowledge of this matrix, on the other hand, allows the perfect decoupling of the multi input control in a set of single input control problem much more tractable. Between the two extreme cases of perfect knowledge and total ignorance the problem is to investigate if there are classes of uncertain matrices for which a control strategy causing the convergence of the sliding output to zero exist. This is one of the most important object of the research on the control of multi input nonlinear uncertain systems.

Even when dealing with the single input systems the situation in which the sign of the high frequency gain is unknown has been, for some time, considered a challenging case of study by many researchers, mainly in the field of adaptive control community. The structure of a simple first order parameter adaptive control with constant control gain with uncertain sign has been considered $\dot{x} = f(x) + g(x)u$ with the nonlinear drift term $f(x)$ upper bounded in modulus by a non necessarily known function and the non zero gain $g(x)$ with unknown sign and with known lower bound of its modulus. The design of a control strategy effective with systems with drift term of general type (so that the uncontrolled system can be characterized by any form of undesired behaviour ranging from instability to finite escape time etc..), and insensitive to the control direction has been often denominated as the universal control problem. The solution of such kind of problem is not so trivial if Morse in [13] raised the famous conjecture that even in the case of linear system $\dot{x} = x + bu$ where $b \neq$ is unknown with unknown sign cannot be globally stabilized by a smooth adaptive control law. In [11] and [12] Martensson on the basis of results in [24] disproved such a conjecture showing the existence of a globally asymptotically stable control law with integral adaptive mechanism characterized by suitable nonlinear gains named Nussbaum functions. These functions, roughly speaking, grow in modulus faster than the norm of the drift term as function of the state norm while their sign is commuted the quicker the higher the state norm. Many papers appeared in the literature, starting from the simpler case in [24] to the design of universal stabilizer that is control systems with negligible a priori knowledge about the plant dynamics [1].

Relaxing the requirement of smooth control law, which was the main concern of the researcher in adaptive control, and allowing any form of discontinuous control law, a sliding mode control insensitive to the sign of the control gain is presented in [1] which can be considered a very simple example of Knowledge Based controller. Similar switching logic can be found in [14] based on the implicit identification of the sign of the control gain as a consequence of of the use of the so called monitoring function, that is a time varying function that commutes the sign of the control gain and abruptly increases its initial conditions as an upper bound of the absolute value of the output cross it.

The generalization to the multi-variable case is not trivial due to the above mentioned ignorance of the direction of the control action and to make the problem tractable some assumption on the uncertain HFG matrix structure must be made .

In Section 2 we consider the case of constant HFG matrices in order to present the results proposed in literature for such case and the intrinsic implementation difficulties

as the dimension of the system increases. In Section 3 the considered control system is presented, together with the relevant assumptions. It is analyzed the case of nonlinear uncertain systems non-affine in the control with nonlinear sliding manifold. For this kind of systems the control direction is defined in implicit form. In such case the considered sliding output is suitably modified and integrators are introduced in the input channel and the augmented system turns out to be affine with respect to the new control, which is first time derivative of the actual control. The resulting HFG matrix is, in general, time and state dependent. In Section 4 an effective use of the integral Sliding Mode method is proposed. In Section 5 some assumptions previously posed in the chapter are discussed and analyzed together with their implications. A numerical example is provided in Section 6. Finally some concluding remarks are provided.

All the proofs are collected in the Appendix.

Throughout this chapter a prime denotes transpose and $|\cdot|$ is the Euclidean norm or the induced matrix norm.

Moreover, let ρ be a function in μ and γ, then the symbols ρ_μ, $\rho_{\mu\mu}$ and $\rho_{\mu\gamma}$ denote, respectively, the first-order partial derivatives $\frac{\partial}{\partial\mu}\rho$, the second-order partial derivatives $\frac{\partial^2}{\partial\mu^2}\rho$, and the second-order mixed partial derivatives $\frac{\partial^2}{\partial\mu\partial\gamma}\rho$.

In this chapter any solution of a differential equation with discontinuous r.h.s. must be interpreted in the Filippov sense, [7], and it is assumed to exist on the whole $[0, +\infty)$.

2 The Nonlinear Sliding Mode Control Systems with Constant HFG Matrix

In this section we briefly present some previous results in literature regarding sliding mode control systems with constant HFG matrices.

Let us consider nonlinear uncertain systems affine in the control law

$$\dot{x}_1 = A_1(t,x_1) + B_1 u_1, \quad x_1 \in R^n, \quad u_1 \in R^m, \quad t \geq 0, \tag{1}$$

and a sliding output

$$s_1(t,x_1) = C_0(t) + C_1 x_1, \quad s_1 \in R^m, \tag{2}$$

where the term $C_0(t)$ and the constant matrix C_1 are perfectly known. The state x_1 is available to the controller. The sliding output (2) is designed such that a system motion, constrained in finite time by the condition

$$s_1(t,x_1) = 0, \tag{3}$$

fulfills the prescribed control objectives. The constraint (3) is often referred to as the sliding manifold.

The first time derivative of the sliding output s_1 can be expressed as

$$\dot{s}_1(t,x_1) = s_{1t} + s_{1x_1}[A_1(t,x_1) + B_1 u_1] = \dot{C}_0(t) + C_1[A_1(t,x_1) + B_1 u_1] \tag{4}$$

We assume that the relative degree of the sliding output s_1 with respect to the control u_1 is uniformly one, i.e. $\det(C_1B_1) \neq 0$. Then (4) can be rewritten as

$$\dot{s}_1(t,x_1) = G_1[\Phi_1(t,x_1) + u_1], \tag{5}$$

where $G_1 = C_1B_1$, $G_1 \in R^{m\times m}$, and $\Phi_1(t,x_1) = G_1^{-1}[s_{1t} + C_1A_1(t,x_1)]$, $\Phi_1 \in R^m$.

The nonlinear control system (1) is uncertain. If G_1 is perfectly known and the norm of the drift term $\Phi_1(t,x_1)$ is upper bounded by a known function of the same arguments, classical sliding mode method can solve easily the control problem. Indeed if the control is chosen, for example

$$u_{1i} = -G_{1i}^{-1}\left[F_1(t,x_1) + k^2\right]\operatorname{sign}(s_1),$$

where G_{1i}^{-1} is the i-th row of the matrix G_1^{-1}, $F_1(t,x_1) \geq |\Phi_1(t,x_1)|$, $k \neq 0$ is a chosen constant, and $\operatorname{sign}(s_1) \in R^m$ is defined as the vector $\operatorname{sign}(s_1) = [\operatorname{sign}(s_1),\ldots,\operatorname{sign}(s_m)]'$, then it suffices to guarantee the standard condition $s_1's_1 \leq -k^2|s_1|$ and s_1 is steered to zero in finite time. The multi-input control problem is decoupled in single-input ones.

While uncertainties in the drift term $\Phi_1(t,x_1)$ can be quite easily managed if suitable upper-bounds are known, uncertainties in the matrix G_1 often make the problem formidable even for sliding mode control approach. Uncertainties in the matrix G_1 affect directly the possibility of decoupling the system and, therefore, represent a difficult obstacle to the achievement of the control objectives.

In the sequel we summarize the control strategies proposed in literature and effective for systems with uncertain and constant matrices G_1 featuring specific structural properties. Three cases are presented characterized by increasing generality. The solution of the control problem in the three cases is based on the choice of a suitable Lyapunov function candidate, the time derivative of which must be evaluated according to the Filippov's solution concept due to possible discontinuities in the r.h.s. of the state equation (1).

Case 1. The HFG matrix is positive definite, i.e. $G_1 > 0$.

The following Lyapunov function is chosen

$$V_1 = \frac{1}{2}s_1'G_1^{-1}s_1.$$

The control vector is designed as

$$u_1 = -\rho_1(t,x_1)\operatorname{sign}(s_1),$$

where the control gain is $\rho_1(t,x_1) = \left[F_1(t,x_1) + k^2\right]$ and $k \neq 0$ is a chosen constant.

The first time derivative of the function V_1 satisfies the following inequalities

$$\dot{V}_1 = s_1'[\Phi_1 + u_1] \leq -k^2 s_1'\operatorname{sign}(s_1) \leq -k^2\sqrt{s_1's_1} \leq -\frac{k^2}{\sqrt{\lambda_{max}\left(G_1^{-1}\right)}}\sqrt{V_1},$$

where $\lambda_{max}(G_1^{-1})$ indicates the maximum eigenvalue of the matrix G_1^{-1}; as a consequence s_1 converges to zero in finite time.

Case 2. The HFG matrix is such that $G_1 + G_1' > 0$.

The Lyapunov function is chosen as follows

$$V_2 = s_1' s_1.$$

The control vector u_1 is designed as a unit vector control of this kind

$$u_1 = -\rho_1(t,x_1)\frac{s_1(t,x_1)}{|s_1(t,x_1)|},$$

where the control gain is as in the previous case $\rho_1(t,x_1) = \left[F_1(t,x_1) + k^2\right]$, $k \neq 0$.

The first time derivative of the function V_2 satisfies the following inequalities

$$\begin{aligned}\dot{V}_2 &= s_1' G_1(\Phi_1 + u_1) + (\Phi_1 + u_1)' G_1' s_1 \\ &\leq -\tfrac{k^2}{|s_1|}\lambda_{min}(G_1 + G_1') s_1' s_1 + 2 s_1' G_1\left(\Phi_1 - F_1 \tfrac{s_1}{|s_1|}\right),\end{aligned}$$

since it can be shown that the vectors s_1 and $G_1\left(\Phi_1 - F_1\frac{s_1}{|s_1|}\right)$ form an obtuse angle, it results

$$\dot{V}_2 \leq -\frac{k^2}{|s_1|}\lambda_{min}\left(G_1 + G_1'\right) s_1' s_1 \leq -k^2\lambda_{min}\left(G_1 + G_1'\right)\sqrt{s_1' s_1} \leq -k^2\lambda_{min}\left(G_1 + G_1'\right)\sqrt{V_2},$$

where $\lambda_{min}(G_1 + G_1')$ indicates the minimum eigenvalue of the matrix $(G_1 + G_1')$; as a consequence s_1 converges to zero in finite time.

Case 3. The HFG matrix is such that $-G_1$ is Hurwitz .

The Lyapunov function is chosen as follows

$$V_3 = s_1' P_1 s_1,$$

where $P_1 \in R^{m\times m}$ is the unique symmetric positive definite solution to the equation

$$-P_1 G_1 - G_1' P_1 = -I.$$

The control vector u_1 is designed as a unit vector control of this kind

$$u_1 = -\rho_1(t,x_1)\frac{s_1(t,x_1)}{|s_1(t,x_1)|},$$

where the control gain is chosen as $\rho_1(t,x_1) = \left[F_1(t,x_1) + k^2\right]$, $k \neq 0$.

The first time derivative of the function V_3 satisfies the following inequalities

$$\dot{V}_3 = s_1' P_1 G_1(\Phi_1 + u_1) + (\Phi_1 + u_1)' G_1' P_1 s_1 \leq -\frac{k^2}{|s_1|} s_1' s_1 + 2 s_1' P_1 G_1\left(\Phi_1 - F_1\frac{s_1}{|s_1|}\right),$$

since it can be shown that the vectors s_1 and $P_1 G_1\left(\Phi_1 - F_1\frac{s_1}{|s_1|}\right)$ form an obtuse angle, it results

$$\dot{V}_3 \leq -\frac{k^2}{|s_1|} s_1' s_1 \leq -k^2\sqrt{s_1' s_1} \leq -\frac{k^2}{\lambda_{max}(P_1)}\sqrt{V_3}$$

where $\lambda_{max}(P_1)$ indicates the maximum eigenvalue of the matrix P_1; as a consequence s_1 converges to zero in finite time.

It is also possible to complement the previous results, effective for constant HFG matrices G_1, by considering for all the cases a norm bounded time and state dependent perturbation, $\Delta G_1(t,x_1)$, provided some constraint of the type

$$\left|G_1^{-1}\Delta G_1(t,x_1)\right| \leq \gamma < 1.$$

The scalar γ is assumed known to the designer and slight modifications of the above control amplitude $\rho_1(t,x_1)$ solves the problem.

In recent years further steps for more general cases of uncertainties of the matrix G_1 have been performed. We refer to [17] in which the eigenvalues of the uncertain matrix G_1 are assumed arbitrarily located in the complex plane except on a boundary layer of the imaginary axis.

The method is based on the knowledge of a suitable set $S = S_1 ... S_i ... S_{n_m}$ of matrices, the so called unmixing set [12] having the following property:
given an arbitrary real nonsingular $m \times m$ matrix M there exists at least one element S_i of the set such that the product $-MS_i$ is Hurwitz.

As a consequence let S_{G_1} an element of the unmixing set corresponding to G_1, if we chose

$$u_1 = S_{G_1} w_1, \quad w_1 = -\rho_1(t,x_1)\frac{s_1(t,x_1)}{|s_1(t,x_1)|},$$

the situation would coincide, with respect to the new control w_1, with the Case 3.

The finite cardinality unmixing set has been proved to exist, [12], [17], and it is assumed to be known by the designer. Since G_1 is not known, in [17] a time-varying estimate of S_{G_1} is provided by a time-varying convex combination of the elements of this set. An adaptation mechanism for the coefficients provides a facility for cycling through the elements of the set dwelling on each element for a progressively longer time intervals. As a result, by using contradiction argumentation like in the single input case, the asymptotic stability is guaranteed. Similar approach based on the knowledge of an unmixing set has been recently proposed in the area of sliding mode control [15] in which the sliding manifold is reached in a finite number of trial(in the worst case equal to the cardinality of the unmixing set). The procedure to identify the matrix S_{G_1} is, in both cases, heuristic and the door for different searching procedure based on intelligent and learning techniques [26,23] is open.

In the following we shall present some consideration regarding the implication of the fundamental assumption that the unmixing set is known. Indeed this assumption hides the fact that only the existence of an unmixing set has been proved and no general methods to build it have been provided until now so we can consider the problem relevant to the case of constant uncertain non singular HFG matrices a relatively open problem. The cardinality of an unmixing set for matrices of rather general structure has been evaluated in [25] according to the next proposition.

Proposition 1. *For any non singular real matrix M of order $m \leq 3$ there exists a permutation matrix P_{mj} and an Identity variant I_{mj} (a diagonal matrix whose elements can be $+1$ or -1) to such that the product $MP_{mj}I_{mj}$ has positive eigenvalues. Therefore the set of the products of any permutation matrix for any Identity variants is an unmixing spectrum at least for $m \leq 3$.*

The cardinality of such a set is consequently equal to $m!2^m$.

A conjecture relevant to the extension to $m > 3$ has been disproved for $m = 65$ with no guarantee that its validity is extended to lesser values. In any case even if the conjecture were true the cardinality of the unmixing set would be non polynomial bounded with m as (NP-complete) making any enumerative technique impractical even for systems of low dimension. Therefore, dealing for medium/large scale system the problem is not solved in practice (the examples in [14] are for $m = 2$) and deserves further investigations encouraged by the fact that some particular matrices (e.g. triangular, block triangular, in companion form [20], [8]) can be characterized by surprisingly lower dimensional unmixing set.

To conclude this section on systems with constant HFG matrices we can stress the fact that up to now there is no well defined constructive methodology to support the basic assumption in [17], [14].

3 The Nonlinear Sliding Mode Control System

Consider the control system

$$\dot{y} = f(t, y, v), \qquad t \geq 0, \tag{6}$$

with the control vector $v \in R^m$, the state variable $y \in R^k$ and the dynamics $f : [0, +\infty) \times R^k \times R^m \to R^k$. A sliding manifold is defined by

$$\sigma(t, y) = 0 \tag{7}$$

with $\sigma : [0, +\infty) \times R^k \to R^m$, $m \leq k$, which fulfills prescribed control aims. The objective is to control the state variables $y(t)$, $t \geq 0$, of the control system (6) in order to exponentially guarantee the sliding property $\sigma[t, y(t)] = 0$ with uncertain dynamics f.

3.1 The Nonlinear Control System with Chattering Reduction

In order to reduce chattering in the control system (6) and sliding manifold (7) due to the discontinuous nature of the Sliding Mode control v, the augmented control system is defined as

$$\dot{y} = f(t, y, v), \qquad \dot{v} = u, \qquad t \geq 0, \tag{8}$$

with augmented state variable $x = (y', v')' \in R^n$, $n = k + m$, and control variable $u \in R^m$. The state x and the control u are available. If the new control u is discontinuous, then the vector v turns out to be (absolutely) continuous and the corresponding state x of (8) must be intended in the Filippov sense, [7].

Discussion.

If the control objective is satisfied, then the sliding motion on $\sigma(t, y) = 0$ is exponentially achieved by applying a continuous control v.

This fact implicitly defines the class of nonlinear non-affine systems, which can be suitably dealt with by the methodology which is proposed in this chapter.

Indeed it is necessary that:

- the continuous control v_*, solution to the equation $\sigma_t(t,y)+\sigma_y(t,y)f(t,y,v_*(t,y))=0$, exists and is unique;
- the constrained dynamical system (6)–(7), implicitly defining the zero-dynamics, is stable with $v=v_*$ (minimum–phase), [9,5];
- the motion of system (6) in a boundary layer of the sliding manifold $\sigma(t,y)=0$ is practically stable, [27].

The augmented dynamics

$$\dot{x}=A(t,x)+Bu, \tag{9}$$

where $A(t,x)=\begin{bmatrix} f(t,y,v) \\ 0 \end{bmatrix}$ and $B=\begin{bmatrix} 0 \\ I \end{bmatrix}$.

Assume that f, σ are both of class C^2 everywhere. Then

$$\dot{\sigma}(t,x)=M(t,x), \tag{10}$$

with $M(t,x)=\sigma_t(t,y)+\sigma_y(t,y)f(t,y,v)$, and

$$\ddot{\sigma}(t,x,u)=E(t,x)+G(t,x)u, \tag{11}$$

where $E=\sigma_{tt}+2\sigma_{ty}f+f'\sigma_{yy}f+\sigma_y f_t+\sigma_y f_y f$, the term $f'\sigma_{yy}f$ denotes the vector of components $f'\sigma_{jyy}f$, $j=1,\ldots,m$, and $G=\sigma_y f_v$.

Fix a constant $m\times m$ matrix $C=\operatorname{diag}(c_i)$, $c_i>0$, $\quad i=1,\ldots,m$, $i=1,\ldots,m$, and consider

$$\zeta(t,x)=\dot{\sigma}(t,x)+C\sigma(t,x). \tag{12}$$

Remark 1. We assume that the sliding output ζ, hence σ and $\dot{\sigma}$ are available to the controller for feedback purposes. Actually, $\dot{\sigma}$ cannot be directly computed since it is affected by the uncertainties of the system. In [2] a second order sliding mode (SOSM) observer was introduced to solve this kind of problem. It was proven, [2], that this SOSM observer can exactly estimate $\dot{\sigma}(t,x)$ in finite time, provided the availability of a known function Q such that $|\ddot{\sigma}|\le Q(t,x,u)$.

Then for almost every t

$$\begin{aligned}\dot{\zeta}(t,x,u) &= \ddot{\sigma}(t,x,u)+C\dot{\sigma}(t,x) \\ &= E(t,x)+G(t,x)u+CM(t,x) \\ &= L(t,x)+G(t,x)u,\end{aligned} \tag{13}$$

where $L=\zeta_t+\zeta_x A=E+CM$, $G=\zeta_x B$ and L, G are continuous.

Let us consider system (9) with sliding output vector (12), the time derivative of which is expressed by (13). Let D be an open subset of R^n and suppose that A, $B\in C^0(D)$, $\zeta\in C^1([0,+\infty)\times D)$.

We make the following assumption.

Assumption 1. *Let $\lambda_i(G)$, $i=1,\ldots,m$, be the real parts of the eigenvalues of the matrix $G(t,x)$, $t\ge 0$ and $x\in D$. There exist two continuous functions α and ω such that for all t and x*

$$0<\alpha(t,x)\le\lambda_i(G)\le\omega(t,x), \qquad i=1,\ldots,m. \tag{14}$$

Remark 2. Assumption 1 implies that the real parts of the eigenvalues of the matrix G are positive and bounded by two continuous functions $\alpha(t,x)$ and $\omega(t,x)$ according to (14). The two functions $\alpha(t,x)$ and $\omega(t,x)$ are assumed to exist. In this chapter neither the two functions $\alpha(t,x)$ and $\omega(t,x)$, nor bounding functions for them are assumed to be known.

If condition (14) holds (see [3] and [10]), then for all $t \geq 0$ and x there exists a unique solution $P(t,x) > 0$ to the Lyapunov equation

$$-G'(t,x)P(t,x) - P(t,x)G(t,x) = -I. \tag{15}$$

If $G(t,x)$ were known, then $P(t,x)$ could be computed by solving an algebraic equation, [10]. In this chapter we assume not to know the matrix $G(t,x)$, therefore we cannot obtain $P(t,x)$. The proposed control strategy does not rely on the availability of $P(t,x)$.

Even though we do not know the matrix $P(t,x)$, we can write its time derivative $\frac{dP(t,x)}{dt}$ as the sum of two terms

$$\frac{dP(t,x)}{dt} = H_1(t,x) + H_2(t,x,u), \tag{16}$$

where $H_1 = P_t + P_x A$ and $H_2 = P_x B u$.

Remark 3. Assumption 1 is similar to the Hurwitz condition presented by [4] for Sliding Mode control of multi-variable linear systems, which does not impose upper bounds on the norm of HFGM. In [4] a constant HFGM is considered and a lower bound of the unknown positive eigenvalues is sufficient. Here the HFGM $G(t,x)$ is time and state dependent. It is necessary to take into account the first time derivative of the matrix $P(t,x)$, given by (16). This requires the knowledge of the existence of an upper bound of the unknown positive eigenvalues of $G(t,x)$. Therefore the results, which we propose here and the ones of [4], even if they are related, cannot be directly compared.

Suppose that the sliding manifold (7) and the system (9) are such that the following assumption holds.

Assumption 2. *$G \in C^1([0,+\infty) \times D)$ and there exist three continuous functions k_0, k_1, k_2 such that for every t and x one has*

$$|A| + |B| \leq k_0(t,x), \qquad |G_x| \leq k_1(t,x), \qquad |G_t| \leq k_2(t,x). \tag{17}$$

Under the previously posed conditions we can state the following proposition.

Proposition 2. *Let Assumption 1 and 2 hold. Then there exists a continuous scalar $\gamma_1(t,x)$ such that*

$$\zeta' H_1(t,x)\zeta \leq \gamma_1(t,x)|\zeta|^2 \tag{18}$$

and a continuous positive scalar $\gamma_2(t,x)$ such that

$$\left|\zeta' H_2(t,x,u)\zeta\right| \leq \gamma_2(t,x)|\zeta|^2|u|, \tag{19}$$

for every t, x, u, ζ.

Proof. See the proof of Proposition 2.3 in [3].

Remark 4. The three continuous functions $k_0(t,x)$, $k_1(t,x)$ and $k_2(t,x)$ are assumed to exist. This assumption is required for the proof of Proposition 2. In this chapter neither the functions $k_0(t,x)$, $k_1(t,x)$, $k_2(t,x)$, $\gamma_1(t,x)$ and $\gamma_2(t,x)$, nor bounding functions for them are assumed to be known, since they are not necessary to the proposed control procedure.

4 The Unit Vector Integral Sliding Mode Control

In this section we introduce an Integral Sliding Mode control method. This Sliding Mode approach was proposed so far, [22], [21], [16], and it is based on the idea to determine a sliding manifold such that the state trajectories of the controlled system start on the sliding surface at the initial time $t = 0$. Provided a sliding condition is guaranteed by the applied control for $t \geq 0$, the sliding mode is obtained without reaching phase together with the exact rejection of the uncertainties since the initial time $t = 0$.

The Integral Sliding Output

Let us define a new integral sliding output

$$s(t,x) = \zeta(t,x) + c_0 \left[-\frac{1}{c\,0} \zeta(0,x(0)) + \int_0^t \zeta(\tau,x)\, d\tau \right], \tag{20}$$

where c_0 is an arbitrary positive constant.

Remark 5. The sliding output s can always be computed since all the terms in (20) are available. From (20) it appears that $s(0,x(0)) = 0$.

Remark 6. If the condition $s(t,x) = 0$ is identically fulfilled for $t \geq 0$, the original sliding output $\zeta(t,x)$ vanishes arbitrarily exponentially fast

$$\zeta(t,x) = \zeta(0,x(0))\, e^{-c_0 t}.$$

The dynamics of the sliding output s, considering (13) and (20), is given by

$$\dot{s}(t,x) = c_0 \zeta(t,x) + G(t,x)\left[\Phi(t,x) + u\right], \tag{21}$$

where $\Phi(t,x) = G^{-1}(t,x) L(t,x)$.

$$u = -\rho(t,x) \frac{s(t,x)}{|s(t,x)|}. \tag{22}$$

The following theorem is proven.

Theorem 1. *Consider system (9) with sliding output $s(t,x)$ given by (20) under Assumptions 1 and 2. Assume to know $\Phi^*(t,x)$ such that for every $t \geq 0$ and x*

$$\Phi^*(t,x) \geq 2\left|P(t,x)\, G(t,x)\, \Phi(t,x)\right| + 2c_0 \left|P(t,x)\, \zeta(t,x)\right|. \tag{23}$$

The unit vector control (22) with amplitude

$$\rho(t,x) \geq 2\left[\varepsilon^* + \Phi^*(t,x)\right], \tag{24}$$

$\varepsilon^* > 0$, *guarantees that* $s(t,x) = 0$ *for* $t \geq 0$. *The sliding manifold* $s(t,x) = 0$ *is invariant and locally stable within the ball* $|s| < \dfrac{1}{2\gamma_2(t,x)}$, *where the unknown function* $\gamma_2(t,x) > 0$ *is given by (19).*

Proof of Theorem 1. See the Appendix.

Remark 7. The augmented control system (9) is defined such that $\dot{v} = u$; the actual control v is included in the augmented state $x = (y', v')'$ and the new control vector is u. According to Theorem 1 the sliding motion on $s(t,x) = 0$ is guaranteed by applying the discontinuous control u given by (22). The corresponding control v turns out to be continuous and the corresponding state x solution of (9) must be intended in the Filippov sense, [7]. The actual control v, which is part of the state x solution of (9), is guaranteed to be bounded if the zero-dynamics defined by the dynamical system (9) constrained on $s(t,x) = 0$ is stable.

5 Upper Bounds of the Norm of the Solution of the Continuous Algebraic Lyapunov Function

The computation of the drift term $\Phi^*(t,x)$ implies the availability of an upper bounds of the norm of the matrix $P(t,x)$ for any (t,x). In the sequel it will be proved that $\Phi^*(t,x)$ is the only information required to carry out the design of the control system and therefore it make sense to analyze the literature regarding the solutions bound to the Lyapunov equation.

Assumption 1 guarantees that an unique positive definite solution to the following equation exists

$$G'(t,x)P(t,x) + P(t,x)G(t,x) = I. \tag{25}$$

The question is which is the minimum amount of information, regarding the set of matrix $G(t,x)$, sufficient to provide the required norm bound for $P(t,x)$.

In principle the required upper bound is computable once the minimum singular value $\sigma_{min}(G'(t,x) \oplus G'(t,x))$ of the Kronecker sum of $G'(t,x)$ with itself is available according to

$$\mathrm{vec}(P(t,x)) = \left[\left(I \otimes G'(t,x)\right) + \left(G'(t,x) \otimes I\right)\right]^{-1}\mathrm{vec}(I) = \left(G'(t,x) \oplus G'(t,x)\right)^{-1}\mathrm{vec}(I)$$

$$|(P(t,x))| \leq |\mathrm{vec}(P(t,x))| \leq \left(\sigma_{min}\left(G'(t,x) \oplus G'(t,x)\right)\right)^{-1}|\mathrm{vec}(I)|.$$

In case of known matrix $G(t,x)$ the computation can be performed on line exploiting some form of symbolic algorithm. It is still an open problem the generalization of such an approach to the case of norm bounded uncertainties with respect to a nominal known $G(t,x)$ despite of the broad literature relevant to robust Lyapunov stability.

An upper bound of $P(t,x)$ can be expressed in terms of the bounds of the eigenvalues of $G(t,x)$ exploiting the following integral form of the solution of the Lyapunov equation, which, for any (t,x), can be expressed as

$$P(t,x) = \int_0^{+\infty} e^{-G(t,x)'\tau} e^{-G(t,x)\tau} d\tau,$$

From this integral form it follows that $P(t,x) \in C^1([0,\infty) \times D)$.

The first consequence of this latter expression for $P(t,x)$ and the Assumption 1 is that

$$|P(t,x)| \leq c \int_0^{+\infty} e^{-2\alpha\tau} d\tau = \frac{c}{2\alpha}, \tag{26}$$

where c, which always exists due to Assumption 1, is such that

$$ce^{-\alpha} \geq \left| e^{-G(t,x)} \right|.$$

Different bounds requiring less a priori knowledge about the matrix $G(t,x)$ have been provided in the literature.

According to previous notations let

- $\lambda_1(P) \geq \lambda_2(P) \geq \ldots \lambda_m(P)$ the eigenvalues of $P(t,x)$;
- $\sigma_1(G) \geq \sigma_2(G) \geq \ldots \sigma_m(G)$ the singular values of the matrix $G(t,x)$;
- $\lambda_1(G_s) \geq \lambda_2(G_s) \geq \ldots \lambda_m(G_s)$ the eigenvalues of the symmetric part $\frac{G(t,x)+G'(t,x)}{2} = G_s(t,x)$ of $G(t,x)$.

The former result of was attained for the restricted class of matrices $G(t,x)$ with $\lambda_m(G_s) > 0$ which, as previously remarked, is considered of little interest for this paper. The bound presented in [19] is

$$\lambda_1(P) \leq \frac{1}{\lambda_m(G_s)}.$$

Slightly more general result has been presented in [6]. The class of system is extended to that for which $\lambda_m(G_s)$ is not necessarily positive but there exist a positive definite matrix F such that the minimum eigenvalue of the symmetric part of $F^{\frac{1}{2}} G(t,x) F^{-\frac{1}{2}} + G'(t,x)$ is greater than a known positive number $\mu_F(G)$. In that case a computable upper bound of the norm of $P(t,x)$ is

$$\lambda_1(P) \leq \frac{\lambda_1(F)\lambda_m(F)}{\mu_F(G)}$$

A more general class of uncertain matrices for which it is possible to compute an upper bound of the norm of $P(t,x)$ is presented in [18] and will be here detailed and adapted to the considered case. Consider the polar decomposition of the invertible matrix $G(t,x)$

$$G(t,x) = \left(G(t,x)G'(t,x)\right)^{\frac{1}{2}} \left(G(t,x)G'(t,x)\right)^{-\frac{1}{2}} G(t,x) = H(t,x)R(t,x),$$

where $H(t,x) = (G(t,x)G'(t,x))^{\frac{1}{2}} > 0$ is the symmetric positive definite factor of $G(t,x)$ and $R(t,x) = (G(t,x)G'(t,x))^{-\frac{1}{2}} G(t,x)$ is the orthogonal factors of $G(t,x)$ (indeed $R(t,x)R'(t,x) = I$).

The required Assumptions are that R has eigenvalues with positive real parts and $\det(R) = +1$, that is $R \in SO(m)$.

R, we drop the arguments for notation simplicity sake, can be factorized according to Schur theorem as

$$R = XShX' \qquad XX' = I$$

and Sh is a block diagonal matrix with 2×2 diagonal blocks Sh_i,

$$Sh_i = \begin{bmatrix} \cos\theta_i & -\sin\theta_i \\ \sin\theta_i & \cos\theta_i \end{bmatrix} \tag{27}$$

where by assumption $\cos\theta_i > 0$.

As a result for the symmetric part of R

$$\frac{R+R'}{2} = XCX' \qquad C = \operatorname{diag} c_i$$

and

$$c_i = \begin{bmatrix} \cos\theta_i & 0 \\ 0 & \cos\theta_i \end{bmatrix} \tag{28}$$

Therefore

$$1 \geq \lambda_1\left(\frac{R+R'}{2}\right) \geq \lambda_m\left(\frac{R+R'}{2}\right) \geq \min_i \cos\theta_i.$$

The posed assumptions imply that a possibly time and state dependent strictly positive scalar $c_m \leq \min_i \cos\theta_i$ is available to the designer.

Let

$$H^{-1} = \left(GG'\right)^{-1/2} \qquad H^{-1}G = R$$

and

$$\frac{R+R'}{2} = \frac{H^{-1}G + G'H^{-1}}{2}.$$

Note that $GH^{-1} = HRH^{-1}$ and $\frac{GH^{-1}+H^{-1}G'}{2}$ have the same eigenvalue of R and $\frac{R+R'}{2}$ respectively.

Consider now the Lyapunov equation (25) and multiply both sides by H^{-1} as follows

$$H^{-1}PG + H^{-1}G'P = H^{-1}$$

$$H^{-1}PGH^{-1}H + H^{-1}G'P = H^{-1}.$$

The two terms in the left hand side are similar and therefore have the same trace

$$2\operatorname{trace}\left(H^{-1}G'P\right) = \operatorname{trace}\left(H^{-1}\right),$$

since $\operatorname{trace}(AB) \geq \lambda_m(A)\operatorname{trace}(B)$ and, due to the previous remark $\operatorname{trace}\left(GH^{-1}\right) = \operatorname{trace}(R)$

$$2\lambda_m(R)\operatorname{trace}(P) = \operatorname{trace}\left(H^{-1}\right)$$

since the eigenvalues of H are the singular values of G it results:

$$\text{trace}\left(H^{-1}\right) \leq \frac{m}{\sigma_m(G)},$$

$$\lambda_1(P) \leq \text{trace}(P) \leq \frac{m}{2c_m\sigma_m(G)}. \tag{29}$$

If $G(t,x)$ has spectrum in C^+ , its orthogonal factor $R(t,x)$ has positive eigenvalues, known lower bounds of the singular values of $G(t,x)$ and of the eigenvalues of $R(t,x)$ are sufficient to provide an upper bound (29) of the norm of the solution of the Lyapunov equation (25).

6 Example

Consider the control system (6) with

$$f(t,y,v) = \begin{bmatrix} y_3 \\ y_4 \\ -f_5(y_1,y_3)\, f_6(v_2) \\ f_7(y_1,y_3)\, v_1 + [f_5(y_1,y_3) + f_8(y_2,y_4)]\, f_6(v_2) \end{bmatrix}, \tag{30}$$

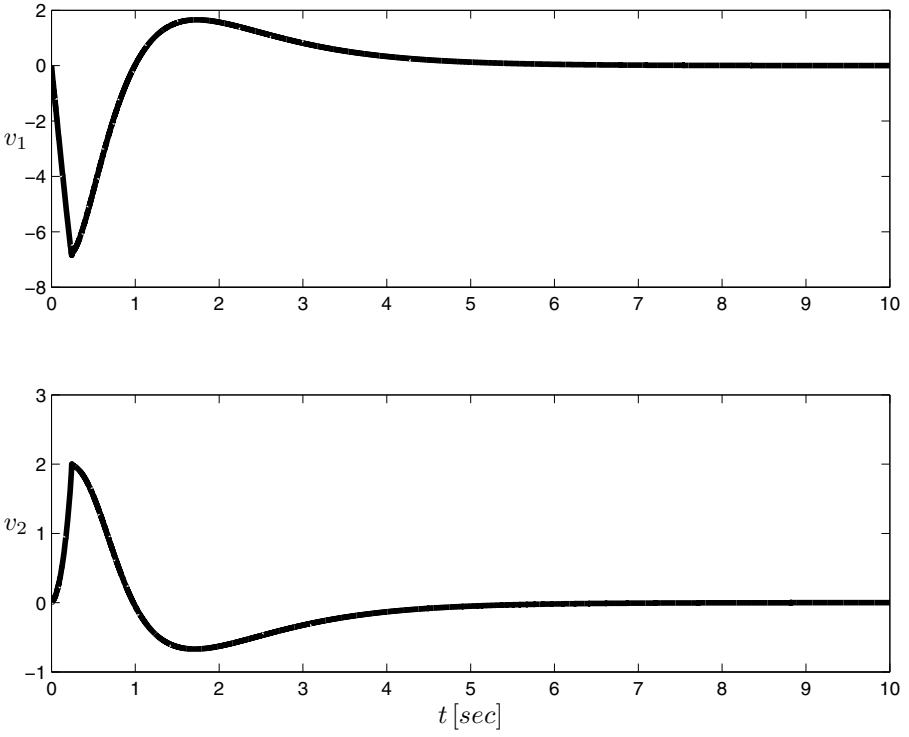

Fig. 1. The applied continuous control actions v_i, $i = 1,2$

$f_5(y_1,y_3) = \frac{2.5}{\sqrt{5.25}}\sqrt{10+.02|y_1+y_3|^3}$, $f_6(v_2) = \left(v_2+.03v_2^3\right)$,
$f_7(y_1,y_3) = \frac{\sqrt{5.25}}{2.5}\sqrt{10+.02|y_1+y_3|}$, $f_8(y_2,y_4) = .1\sqrt{10+.02|y_2+y_4|^3}$, the control vector $v \in R^2$, the state variable $y \in R^4$ and the dynamics $f : [0,+\infty) \times R^4 \times R^2 \to R^4$. The sliding manifold is defined by

$$\sigma(t,y) = \begin{bmatrix} y_1+y_3 \\ y_2+y_4 \end{bmatrix} = 0. \tag{31}$$

The sliding output σ is exploited to define ζ and s according to (12) and (20) respectively, with $C = \text{diag}(4,4)$ and $c_0 = 2$. We define the augmented dynamics

$$\dot{x} = g(t,x,u) = A(t,x) + Bu, \tag{32}$$

with augmented state variable $x = (y',v')' \in R^6$, control variable $u \in R^2$, and dynamics $g(t,x,u) = (f'(t,x),u')'$.

The HFGM results $G(t,x) = \begin{bmatrix} 0 & -f_5\left(1+.09v_2^2\right) \\ f_7\ (f_5+f_8)\left(1+.09v_2^2\right) \end{bmatrix}$. It is easy to verify that $G(t,x)$ has positive eigenvalues for all $t \geq 0$ and x. Assumption 1 holds, then for all

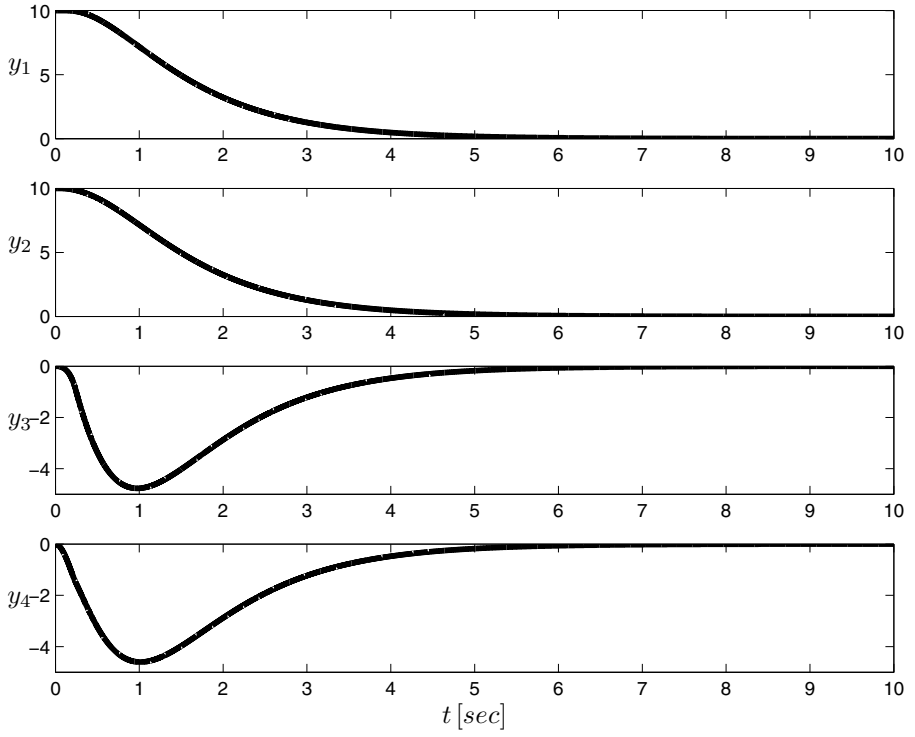

Fig. 2. The state variables y_i, $i = 1,\ldots,4$

$t \geq 0$ and x there exists a unique solution $P(t,x) > 0$ to the Lyapunov equation (15). The matrix $G(t,x)$ is assumed not to be known, therefore we do not compute $P(t,x)$. The proposed control strategy does not rely on the availability of $P(t,x)$.

The previously posed conditions and assumptions hold for system (30), sliding manifold (31), and augmented dynamics (32).

We design the control switching logic according to the unit vector control algorithm (22). The applied control actions v_i, $i = 1,2$, are continuous, Figure 1. The state variables y_i, $i = 1,\ldots,4$, are presented in Figure 2.

Conclusions

The control of uncertain multi-input systems has been considered.

The case of system with constant HFG has been analyzed first. The concept of unmixing set is introduced and its role in motivating an enumerative technique to deal with simply nonsingular HFG matrices has been outlined. The Curse of Dimensionality of this approach and the heuristic nature of the proposed methodologies open the door to alternative solutions possibly more feasible.

The attempt to generalize to time and state dependent HFG matrices with eigenvalues in the positive half-plane for any value of their arguments the control method adopted for constant HFG matrices(with the same spectral features) turns out to be not satisfactory. Indeed with the same choice of the Lyapunov function candidate the application of the same unit vector control method leads to the rather poor result that the convergence cannot be guaranteed outside a boundary layer of the sliding manifold whose size depends on the system uncertainties in a very involved way and therefore not available to the designer.

The situation is made more complicated by the fact that the system originally non affine in the control is made affine by the introduction of integrators in the Input Channel.

The use of the Integral Sliding Mode control, consisting instead in the introduction of integrators in the Output Channel, (whose initial conditions can be arbitrarily assigned) allows the elimination of the so called reaching condition and the sliding motion is established from the initial time whichever the size of the boundary layer.

Acknowledgement. This book is a special volume dedicated to Professor Okyay Kaynak to commemorate his lifetime impactful research and scholarly achievements and his services to the profession. With this chapter the authors want to outline the original contribution of Professor Kaynak to make Sliding Mode Theory an important tool to solve problems ranging from robotics and other advanced engineering applications, to mathematical programming and optimization. This impression of vastness and variety of research interests, for Giorgio Bartolini, dates back at the first meeting with Okyay Kaynak during the IEEE International Workshop on Intelligent Motion Control in August 1990 in Istanbul.

Appendix

The proof of Theorem 1 requires the following lemma.

Lemma 1. *Let $V(t)$ be absolutely continuous on every interval $[0,T]$, $T>0$, such that $V(t)\geq 0$ for every $t\geq 0$ and*

$$\frac{dV(t)}{dt}\leq -p(t)\sqrt{V(t)}+q(t)V(t), \tag{33}$$

where p and q are nonnegative integrable functions on every $[0,T]$, $T>0$. Then $V(t)=0$ for every t sufficiently large provided

$$V(0)\leq \frac{1}{4}\left(\int_0^{t^*} p(t)\,e^{-Q(t)}dt\right)^2 \tag{34}$$

for some $t^*>0$, where

$$Q(t)=\frac{1}{2}\int_0^t q(s)\,ds.$$

Moreover, if there exists $\bar{t}\geq 0$ such that $V(\bar{t})=0$, then $V(t)=0$ for every $t\geq\bar{t}$.

The proof of Lemma 1 can be found in [3].

Proof of Theorem 1. Let us choose the following Lyapunov function candidate

$$V(t,x)=s'(t,x)P(t,x)s(t,x), \tag{35}$$

where $P(t,x)>0$ is the unknown matrix solution to (15).

By using (13), (21) and (35)

$$\begin{array}{l}\frac{dV}{dt}=2c_0s'P(t,x)\zeta+s'P(t,x)G(t,x)[\Phi(t,x)+u]\\ +[\Phi(t,x)+u]'G'(t,x)P(t,x)s+s'\frac{dP(t,x)}{dt}s.\end{array} \tag{36}$$

The equation (36) implies

$$\begin{array}{l}\frac{dV}{dt}\leq s'P(t,x)G(t,x)[\Phi(t,x)+u]+\\ \quad+[\Phi(t,x)+u]'G'(t,x)P(t,x)s+\\ \quad 2c_0s'P(t,x)\zeta+\gamma_2(t,x)|s|^2|u|+\gamma_1(t,x)|s|^2,\end{array} \tag{37}$$

where the unknown functions $\gamma_1(t,x)$ and $\gamma_2(t,x)>0$ are given by (18) and (19).

The unit vector control strategy (22), [3], discontinuous on $s(t,x)=0$, can be applied

$$u=-\rho(t,x)\frac{s}{|s|}.$$

By virtue of the unit vector control (22) and since (15) holds, the Lyapunov equation (37) implies

$$\begin{array}{l}\frac{dV}{dt}\leq -s'\left[\rho(t,x)\frac{s}{|s|}-2P(t,x)G(t,x)\Phi(t,x)+2c_0P(t,x)\zeta\right]+\\ \quad+\gamma_2(t,x)\rho(t,x)|s|^2+\gamma_1(t,x)|s|^2.\end{array} \tag{38}$$

By (23) we can write

$$\frac{dV}{dt} \leq -\left[\rho(t,x)\left(1-\gamma_2(t,x)|s|\right)-\Phi^*(t,x)\right]|s|+\gamma_1(t,x)|s|^2. \tag{39}$$

For any $\varepsilon^* > 0$, within the ball $|s| < \frac{1}{2\gamma_2}$, if $\rho(t,x)$ fulfills (24), then

$$\frac{dV}{dt} \leq -\varepsilon^*|s|+\gamma_1(t,x)|s|^2. \tag{40}$$

Denote by $\lambda_{min} = \lambda_{min}(t,x)$, $\lambda_{max} = \lambda_{max}(t,x)$ the minimum and maximum eigenvalue of $P(t,x)$. Taking into account (35), (40) implies that

$$\frac{dV}{dt} \leq -\frac{\varepsilon^*}{\sqrt{\lambda_{max}}}\sqrt{V}+\frac{\gamma_1}{\lambda_{min}}V.$$

From this inequality, according to Lemma 1, it follows that the application of the unit vector control (22) guarantees $s(t,x) = 0$ for $t \geq 0$. □

References

1. Bartolini, G., Ferrara, A., Giacomini, L.: A switching controller for systems with hard uncertainties. IEEE Trans. on Circuit and Systems I: Fundamental Theory and Applications 50(8), 984–990 (2003)
2. Bartolini, G., Punta, E., Zolezzi, T.: Simplex sliding mode methods for the chattering reduction control of multi-input nonlinear uncertain systems. Automatica 45, 1923–1928 (2009)
3. Bartolini, G., Punta, E., Zolezzi, T.: Multi-input sliding mode control of nonlinear uncertain affine systems. Int. J. Control 84(5), 867–875 (2011)
4. Cunha, J., Hsu, L., Costa, R., Lizarralde, F.: Output-feedback model-reference sliding mode control of uncertain multivariable systems. IEEE Trans. on Automatic Control 48(12), 2245–2250 (2003)
5. Ebenbauer, C., Allgöwer, F.: Stability analysis of constrained control systems: An alternative approach. Systems & Control Letters 56, 93–98 (2007)
6. Fang, Y., Loparo, K., Feng, X.: New estimates for solutions of Lyapunov equations. IEEE Trans. on Automatic Control 42(3), 408–411 (1997)
7. Filippov, A.F.: Differential Equations with Discontinuous Right-Hand Sides. Kluwer (1988)
8. Imai, A., Costa, R., Hsu, L., Tao, G., Kokotovic, P.: Multivariable adaptive control using high-frequency gain matrix factorization. IEEE Trans. on Automatic Control 49(7), 1152–1157 (2004)
9. Kravaris, C., Niemiec, M., Kazantzis, N.: Singular pdes and the assignment of zero dynamics in nonlinear systems. Systems & Control Letters 51, 67–77 (2004)
10. Laub, A.: Matrix analysis for scientists and engineers. SIAM (2005)
11. Martensson, B.: Adaptive stabilization of multivariable linear systems. Contemporary Mathematics 68, 191–225 (1987)
12. Martensson, B.: The unmixing problem. IMA Journal of Mathematical Control and Information 8(4), 367–377 (1991)
13. Morse, A.: New directions in parameter adaptive control systems. In: Proceedings 23rd IEEE Conf. on Decision and Control, pp. 1566–1568 (1984)

14. Oliveira, T., Peixoto, A., Hsu, L.: Sliding mode control of uncertain multivariable nonlinear systems with unknown control direction via switching and monitoring function. IEEE Trans. on Automatic Control 55(4), 1028–1034 (2010)
15. Oliveira, T., Peixoto, A., Leite, A., Hsu, L.: Sliding mode control of uncertain multivariable nonlinear systems applied to uncalibrated robotics visual servoing. In: Proceedings American Contr. Conf. (2009)
16. Posznyak, A., Fridman, L., Bejarano, F.: Minimax integral sliding-mode control for multimodel linear uncertain systems. IEEE Trans. on Automatic Control 49(1), 97–102 (2004)
17. Ryan, E.: Adaptive stabilization of multi-input nonlinear systems. Int. Journal of Robust and Nonlinear Systems 3(2), 169–181 (1993)
18. Savov, S., Popchev, I.: New upper estimates for the solution of the continuous algebraic Lyapunov equation. IEEE Trans. on Automatic Control 49(10), 1841–1842 (2004)
19. Shapiro, E.: On the Lyapunov matrix equation. IEEE Trans. on Automatic Control 19(5), 594–596 (1974)
20. ShiNung, C., Davison, E.: Spectral unmixing of classes of arbitrary nonsingular matrices. In: Proceedings IFAC Symposium on System Structure and Control, pp. 84–89 (2004)
21. Utkin, V., Guldner, J., Shijun, M.: Sliding Modes in Electromechanical Systems. Taylor & Francis, London (1999)
22. Utkin, V., Shi, J.: Integral sliding mode in systems operating under uncertainty conditions. In: Proceedings 35th IEEE Conf. Decision Control, pp. 4591–4596. Kobe, Japan (1996)
23. Wilamowski, B., Cotton, N., Kaynak, O., Dündar, G.: Computing gradient vector and jacobian matrix in arbitrarily connected neural networks. IEEE Trans. on Industrial Electronics 55(10), 3784–3790 (2008)
24. Willems, J., Byrnes, G.: Global adaptive stabilization in the absence of information on the sign of the high frequency gain. In: Bensoussan, A., Lions, J. (eds.) Analysis and Optimization of Systems. LNCIS, vol. 62, pp. 49–57. Springer, Heidelberg (1984)
25. Yarlagadda, R.: Stabilization of matrices. Linear Algebra and its Applications 21, 271–288 (1978)
26. Yu, X., Kaynak, O.: Sliding-mode control with soft computing: A survey. IEEE Trans. on Industrial Electronics 56(9), 3275–3285 (2009)
27. Zolezzi, T.: Real states of stable sliding mode control systems. Systems & Control Letters 57, 778–783 (2008)

Dynamical Behaviors of Discrete-Time Fast Terminal Sliding Mode Control Systems

Haibo Du[1], Xinghuo Yu[2,3], and Shihua Li[3]

[1] School of Electrical Engineering and Automation
Hefei University of Technology, Hefei, Anhui 230009, China
[2] Platform Technologies Research Institute,
RMIT University, Melbourne VIC 3001, Australia
[3] School of Automation, Southeast University, Nanjing, Jiangsu 210096, China

Abstract. In this chapter, the dynamical behaviors of discrete-time fast terminal sliding mode control systems are studied. Based on Euler's discretization, the approximate discrete-time model is obtained. Using a recursive analysis method, the boundedness for the steady states of the discrete-time system is established. Theoretical analysis shows that the discrete-time fast terminal sliding mode control method can offer a higher output tracking precision than the discrete-time linear sliding mode control method. As an application of the proposed theoretical results, the control problem for the DC-DC buck converters via discrete-time fast terminal sliding mode control is investigated. Simulation results are given to demonstrate the effectiveness of the proposed method.

Keywords: Dynamical behaviors, Euler discretization, Fast terminal sliding mode.

1 Introduction

In recent years, the sliding mode control (SMC) has been extensively studied and successfully applied in practice. This is due to its many attractive features, such as simplicity, invariance, and robustness to parameters uncertainties and external disturbances [1–4]. In general, in order to realize a SMC, a switching surface or a sliding mode surface is first defined, and then a SMC law is designed to drive the system state to the sliding mode surface. Once the sliding mode is reached and retained, the dynamic behaviors of system are determined by the sliding mode.

In the literature, most sliding mode surfaces only guarantee that the system state converges to the equilibrium asymptotically with infinite convergence time. To improve the dynamic response of the closed-loop system, a direct way is to introduce nonlinear sliding surfaces. One of such nonlinear sliding surfaces is the terminal sliding mode (TSM) surface [5, 6], which can ensure the finite-time convergence during the sliding mode stage. Such TSM control methods have been developed in [5–8], which can guarantee that the systems states converge to the equilibrium in finite time. To overcome the shortcoming that the TSM has a

X. Yu and M. Önder Efe (eds.), *Recent Advances in Sliding Modes*,
Studies in Systems, Decision and Control 24, DOI: 10.1007/978-3-319-18290-2_5

slower convergence rate than the linear sliding mode (LSM) when the system state is far away from the equilibrium, a fast terminal sliding mode (FTSM) control method was proposed in [9]. The FTSM control method combines the advantages of the TSM control and the conventional LSM control together so that fast (finite-time) transient convergence both at a distance from and at a close range of the equilibrium can be obtained. Actually, the finite-time control of dynamical systems is of interest because the systems with finite-time convergence demonstrate some nice features such as faster convergence rate, and better robustness and disturbance rejection properties [10]. Nevertheless, the aforementioned results on TSM control (TSMC) or FTSM control (FTSMC) are obtained in the continuous-time domain.

In practice, since more and more controllers are implemented using digital computers, how to design a digital controller becomes imperative. Many researchers have studied the discretization effect on continuous-time SMC systems, i.e., discrete-time SMC systems. Due to limited switching frequencies of discrete-time SMC, the celebrated invariance property for continuous-time SMC systems no longer holds [11, 12]. In this case, the complex dynamical behaviors (e.g., periodic behaviors) of discrete-time SMC may occur which were explored for different SMC systems [13–17].

Although many works have been done on discretized SMC systems, less studies exist on the analysis of discrete-time TSMC systems. However, since the TSM controller is an inherent nonlinear controller, how to design digitized TSMC and derive conditions to ensure the asymptotical convergence and stability of this kind of systems is very challenging even for the first-order case. In [18], for a first-order discrete-time TSMC system, it was shown that the system's steady state behaviors are period-2 cycle. In [19, 20], for a second-order discrete-time TSMC system, the boundedness for the system's steady states was established. Nevertheless, these results are only focused on lower-order TSMC systems. In [21], the authors considered the problem of discretization of continuous-time high-order TSMC systems and redesigned a class of discrete-time finite-time convergent control laws by imposing certain assumptions. However, they did not analyze the dynamical behavior of discretization of continuous-time high-order TSMC systems although there are many works about continuous-time TSMC, see for example [6, 7]. To this end, in [22], we studied the dynamical behaviors of a class of discrete-time higher-order TSMC systems based on Euler's discretization.

Considering the superior control performance of FTSMC than TSMC and LSMC in continuous-time domain, this chapter will further investigate the dynamical behaviors of a class of discrete-time higher-order FTSMC systems. Due to the introduction of fractional powers in the recursive FTSM surfaces, it is very challenging to analyze the complex dynamical behaviors of discretized higher-order FTSMC systems. By a recursive analysis, we give the explicit boundedness for the steady states of the system, which builds a relationship between control parameters (including the fractional powers and sampling period) and the boundedness of steady states. We will show that the discrete-time FTSMC

systems can offer a higher output tracking precision than the discrete-time linear SMC systems. Finally, an example about the control problem of buck type DC-DC converters is provided to show the potential of the proposed techniques.

2 System Description and SMC System

Consider the following single-input-single-output (SISO) system:

$$\begin{aligned} \dot{x} &= Ax + Bu, \\ y &= Cx, \end{aligned} \tag{1}$$

where $x = [x_1, x_2, \cdots, x_n]^T \in R^n$ is the system state, $y \in R$ is the system output, and u is the control input. Without loss of generality, assume that A, B, C are in the controllable observable canonical form as

$$A = \begin{bmatrix} 0 & 1 & 0 & \cdots & 0 \\ 0 & 0 & 1 & \cdots & 0 \\ \vdots & & & \ddots & \\ 0 & 0 & 0 & \cdots & 1 \\ -a_1 & -a_2 & -a_3 & \cdots & -a_n \end{bmatrix}, \quad B = \begin{bmatrix} 0 \\ 0 \\ \vdots \\ 0 \\ 1 \end{bmatrix}, \quad C = \begin{bmatrix} 1\, 0 \cdots 0\, 0 \end{bmatrix}, \tag{2}$$

where $a_i (i = 1, \cdots, n)$ are known constants.

Let us first review the well-known equivalent control-based SMC method in continuous-time domain. A linear sliding mode surface is chosen as:

$$s = c^T x \quad \text{with} \quad c = [\underline{c} \;\; 1]^T = [c_1 \;\; c_2 \;\; \cdots \;\; c_{n-1} \;\; 1]^T, \tag{3}$$

where $c_1, c_2, \cdots, c_{n-1}, 1$ are coefficients of a Hurwitz polynomial

$$\lambda^{n-1} + c_{n-1}\lambda^{n-2} + \cdots + c_2\lambda + c_1 = 0. \tag{4}$$

Then an equivalent control based SMC is given as:

$$u = u_{eq} + u_s \tag{5}$$

with

$$u_{eq} = -c^T Ax, \quad u_s = -\alpha \text{sgn}(s) \quad \text{with} \quad \alpha > \rho, \tag{6}$$

where ρ is a positive constant. Under the SMC law, the sliding mode state will converge to zero in a finite time. After then, the system behavior is determined by the sliding mode surface, which is determined by the following closed-loop system

$$\begin{bmatrix} \dot{x}_1 \\ \vdots \\ \dot{x}_{n-2} \\ \dot{x}_{n-1} \end{bmatrix} = \begin{bmatrix} 0 & 1 & \cdots & 0 \\ \vdots & & \ddots & \\ 0 & \cdots & 0 & 1 \\ -c_1 & \cdots & -c_{n-2} & -c_{n-1} \end{bmatrix} \begin{bmatrix} x_1 \\ \vdots \\ x_{n-2} \\ x_{n-1} \end{bmatrix}. \tag{7}$$

Clearly the selection of parameters $c_1, c_2, \cdots, c_{n-1}$ will determine the closed-loop system's eigenvalues and dynamical behavior.

In practice, since more and more controllers are implemented using digital computers, it is very important to study the dynamical behaviors of SMC systems in discrete-time domain. It is well-known that Euler's discretization is a very popular discretization method which is widely used. Thus, we consider Euler's discretization of SMC systems.

3 Discrete-Time Linear Sliding Mode Control (LSMC) Systems

In this section, we will investigate the discrete implementation of SMC system (1) with (5) using Euler's discretization. The Euler's discretization model of system (1) is

$$\begin{aligned} x_1(k+1) &= x_1(k) + hx_2(k), \\ &\vdots \\ x_{n-1}(k+1) &= x_{n-1}(k) + hx_n(k), \\ x_n(k+1) &= x_n(k) - h[a_1x_1(k) + a_2x_2(k) + \cdots + a_nx_n(k)] + hu(k), \end{aligned} \tag{8}$$

where h is the sampling period. For this discrete-time system, the continuous-time LSMC law (5) becomes a discrete-time LSMC law which is given by:

$$u(k) = -c^T Ax(k) - \alpha \mathrm{sgn}(c^T x(k)) = \sum_{i=1}^{n} a_i x_i(k) - \alpha \mathrm{sgn}(c^T x(k)). \tag{9}$$

Under the discrete-time LSMC law (9), the steady-state behavior of system (8) will be a period orbit. The main result and proof are given in [14]. Here, we only present the main theorem.

Theorem 1. *For the discrete-time closed-loop system (8)-(9), if all the eigenvalues of the matrix $I + hB_c$ are located within the unit circle, then every trajectory of the closed-loop system converges to a period-2 orbit whose coordinates are bounded by:*

$$\begin{aligned} |x_1(k)| &\le \frac{\alpha h}{2c_1}\left(1 + \frac{c_1}{|1+S|}\left(\frac{h}{2}\right)^{n-1}\right), \\ |x_j(k)| &\le \frac{\alpha}{|1+S|}\left(\frac{h}{2}\right)^{n-j+1}, \quad j = 2, 3, \cdots, n, \end{aligned} \tag{10}$$

where $B_c = \begin{bmatrix} 0 & 1 & \cdots & 0 \\ \vdots & \vdots & \ddots & \vdots \\ 0 & 0 & \cdots & 1 \\ -c_1 & -c_2 & \cdots & -c_{n-1} \end{bmatrix}$ *and* $S = \sum_{i=1}^{n-1} c_i(-\frac{h}{2})^{n-i}$.

4 Discrete-Time Fast Terminal Sliding Mode Control (FTSMC) Systems

4.1 Continuous-Time TSMC

Note that LSMC only guarantee that the system state converges to the equilibrium asymptotically with infinite convergence time. To improve the convergence rate, the TSMC method was introduced in [5, 6], which can ensure the finite-time convergence during the sliding mode stage. The aim of TSMC is to design a control law such that state x reaches zero in a finite time. Specifically, as shown in [6], a recursive TSM surface is first constructed:

$$s_{i+1} = \dot{s}_i + \beta_{i+1} s_i^{q_{i+1}/p_{i+1}}, \quad i = 0, 1, \cdots, n-2, \tag{11}$$

where $s_0 = x_1, p_i, q_i$ are both odd positive integers with $q_i < p_i$ and $\beta_i > 0$ for every $i = 1, \cdots, n-1$. Clearly, if $s_{n-1} = 0$ is achieved in a finite time, by a simple deduction, it can be concluded that s_{n-2} will reach zero in a finite time. By an inductive deduction, it can be proven that $s_i, i = 0, 1, \cdots, n-3$, will reach zero in a finite time, i.e., the equilibrium $s_i = 0$ is a terminal attractor [6]. Hence, the task of TSMC law is to guarantee the sliding mode surface $s_{n-1} = 0$ is achieved in a finite time and kept on it for ever. Based on this idea, in [6], the TSMC law is proposed as

$$u(t) = \sum_{i=1}^{n} a_i x_i(t) - \sum_{i=0}^{n-2} \beta_{i+1} \frac{\mathrm{d}^{n-i-1}}{\mathrm{d}t^{n-i-1}} (s_i^{q_{i+1}/p_{i+1}}) - K \mathrm{sgn}(s_{n-1}), \tag{12}$$

where $K > \rho$ with a positive constant ρ. In order to avoid the singularity, the parameters p_i, q_i should be chosen carefully [6], that is, if $\frac{q_{k+1}}{p_{k+1}} > \frac{n-k-1}{n-k}$, then the control u is bounded when $s_k \to 0$ sequentially from $k = n-2$ to $k = 0$.

4.2 Continuous-Time FTSMC

For the previous TSMC, when the system state is far away from the equilibrium, the TSMC does not prevail over the LSMC on the convergence rate. To this end, a fast TSMC method was proposed in [9], which employs the following FTSM surface

$$s_{i+1} = \dot{s}_i + \beta_{i+1} s_i^{q_{i+1}/p_{i+1}} + \gamma_{i+1} s_i, \quad i = 0, 1, \cdots, n-2, \tag{13}$$

where $\gamma_{i+1} > 0$. Based on the FTSM (13), the FTSMC law is designed as

$$\begin{aligned} u(t) = & \sum_{i=1}^{n} a_i x_i(t) - \sum_{i=0}^{n-2} \beta_{i+1} \frac{\mathrm{d}^{n-i-1}}{\mathrm{d}t^{n-i-1}} (s_i^{q_{i+1}/p_{i+1}}) - \sum_{i=0}^{n-2} \gamma_{i+1} \frac{\mathrm{d}^{n-i-1}}{\mathrm{d}t^{n-i-1}} (s_i) \\ & - K \mathrm{sgn}(s_{n-1}), \end{aligned} \tag{14}$$

where $K > 0$, which can guarantee that the system state converges to the equilibrium in a finite time with a faster convergence rate no matter when the system state is far away from or close to the equilibrium.

4.3 Euler's Discretization of FTSMC Systems

In this subsection, we will investigate the discrete implementation of FTSMC system by using Euler's discretization. Note that in [22], the dynamical behaviors of discrete-time system (8) with discrete-time TSMC law (12) is investigated. In this chapter, the main aim is to study the dynamical behaviors of discrete-time systems (8) under discrete-time FTSMC law (14).

For convenience, let $\triangle$ denote forward difference operator, i.e.,

$$\triangle^1 s(k) \equiv \triangle\, s(k) = \frac{s(k+1) - s(k)}{h},\ \forall s(k) \in R. \tag{15}$$

Based on this notation, define $\triangle^i := \triangle(\triangle^{i-1})$ with $i = 2, 3, ..., n$.

Since the FTSMC law (14) is designed based on the recursive FTSM structure (13), then we obtain Euler's discretization of FTSM structure (13) as follows:

$$\begin{aligned} s_{i+1}(k) &= \frac{s_i(k+1) - s_i(k)}{h} + \beta_{i+1} s_i^{q_{i+1}/p_{i+1}}(k) + \gamma_{i+1} s_i(k) \\ &= \triangle s_i(k) + \beta_{i+1} s_i^{q_{i+1}/p_{i+1}}(k) + \gamma_{i+1} s_i(k), \quad i = 0, 1, \cdots, n-2, \end{aligned} \tag{16}$$

where $s_0(k) = x_1(k)$. By (15) and (16), we obtain the discrete-time FTSMC law as follows:

$$\begin{aligned} u(k) = &\sum_{i=1}^{n} a_i x_i(k) - \sum_{i=0}^{n-2} \beta_{i+1} \triangle^{n-i-1}(s_i^{q_{i+1}/p_{i+1}}(k)) - \sum_{i=0}^{n-2} \gamma_{i+1} \triangle^{n-i-1}(s_i(k)) \\ &- K \mathrm{sgn}(s_{n-1}(k)), \end{aligned} \tag{17}$$

where $K > \rho$.

Remark 1. Note that in continuous-time controllers (12) and (14), the fractional powers should be carefully chosen to avoid the singularity problem. Here, it should be pointed out that for the discrete-time FTSMC law (17), to avoid the singularity, the conditions for fractional powers should also be satisfied. The detailed explanation will be given in subsection D.

Next, we will analyze the stability of the closed-loop system (8) with (17). First, we will show that the finite-time convergence property of FTSM structure (13) is not guaranteed.

A. Analysis of Discrete-Time FTSM Structure

The design of continuous-time FTSMC law is mainly based on the fact that when $s_{n-1} = 0$ is reached and kept it on for ever, then $s_{n-2} = 0$ will reach zero in a finite time. However, in the case of design of discrete-time FTSMC law, this does not hold. Specifically, if $s_{n-1}(k) = 0$, it follows from (16) that

$$s_{n-2}(k+1) = s_{n-2}(k) - h\beta_{n-1} s_{n-2}^{q_{n-1}/p_{n-1}}(k) - h\gamma_{n-1} s_{n-2}(k). \tag{18}$$

We first show that it is impossible that the discrete-time system (18) is finite-time stable, even asymptotically stable. The proof of Lemma 1 is given in the Appendix.

Lemma 1. *For the discrete-time system (18), there is a 2-orbit equilibrium*

$$s_{n-2} = \Big(\pm \frac{h\beta_{n-1}}{2 - h\gamma_{n-1}} \Big)^{1/(1-q_{n-1}/p_{n-1})}. \tag{19}$$

Due to the existence of non-zero equilibrium for the discrete-time system (18), $s_{n-2}(k)$ will not reach zero in a finite number of sampling instants. Although the finite-time convergence property of discrete-time FTSMC is not possible, issues such as the stability and the boundedness of the discrete-time system (8) with (17) should be studied. In the sequel, we will give an answer to these questions.

B. Analysis of Steady-State Behaviors

1) Analysis of steady state of discrete-time FTSM surface
In this subsection, we will analyze the steady-state behavior of sliding mode surfaces s_i, $i = 0, \cdots, n-1$. Before moving on, we give the following two lemmas.

Lemma 2. *[15] For the scalar dynamical system* $z(k+1) = z(k) + g(k) - \varepsilon \mathrm{sgn}(z(k))$, *if* $|g(k)| < \gamma, \gamma > 0$, *and* $\gamma < \varepsilon$, *then there is a finite number* $K^* > 0$ *such that* $|z(k)| \le \varepsilon + \gamma < 2\varepsilon$, $\forall k \ge K^*$.

Lemma 3. *Consider the scalar dynamical system*

$$z(k+1) = z(k) - l_1 z^{\alpha}(k) - l_2 z(k) + g(k), \tag{20}$$

where $l_1 > 0$, $0 < l_2 < 1$, *and* $0 < \alpha < 1$ *is a ratio of odd integers. If* $|g(k)| \le \gamma, \gamma > 0$, *then there is a finite number* $K^* > 0$ *such that*

$$|z(k)| \le \psi(\alpha) \cdot \max\Big\{ \Big(\frac{\gamma}{l_1}\Big)^{1/\alpha}, \Big(\frac{l_1}{1-l_2}\Big)^{\frac{1}{1-\alpha}} \Big\}, \quad \forall k \ge K^*, \tag{21}$$

where function $\psi(\alpha)$ is defined as

$$\psi(\alpha) = 1 + \alpha^{\frac{\alpha}{1-\alpha}} - \alpha^{\frac{1}{1-\alpha}}. \tag{22}$$

The proof of this lemma is in the Appendix and the plot of function $\psi(\alpha)$ is shown in Fig. 1.

With the help of these two lemmas, we present the first result.

Theorem 2. *For system (8), if the sliding mode surface is defined as (16) and the control law is designed as (17), then there is a finite number* $K^* > 0$ *such that*

$$|s_i(k)| \le \rho_i, \quad i = 0, \cdots, n-1, \quad \forall k \ge K^*, \tag{23}$$

where $\rho_{n-1} = h(K)$ *and*

$$\rho_i = \psi(\frac{q_{i+1}}{p_{i+1}}) \cdot \max\Big\{ \Big(\frac{\rho_{i+1}}{\beta_{i+1}}\Big)^{p_{i+1}/q_{i+1}}, \Big(\frac{h\beta_{i+1}}{1 - h\gamma_{i+1}}\Big)^{\frac{1}{1-q_{i+1}/p_{i+1}}} \Big\}, i = n-2, \cdots, 0. \tag{24}$$

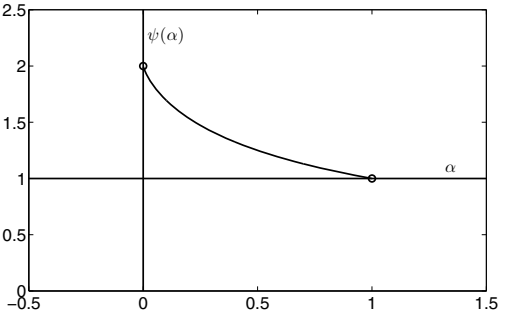

Fig. 1. The plot of function $\psi(\alpha)$

Proof. We first consider s_{n-1}. It follows from (16) that

$$\begin{aligned} & s_{n-1}(k+1) - s_{n-1}(k) \\ &= \triangle s_{n-2}(k+1) + \beta_{n-1} s_{n-2}^{q_{n-1}/p_{n-1}}(k+1) + \gamma_{n-1} s_{n-2}(k+1) \\ &\quad - \triangle s_{n-2}(k) - \beta_{n-1} s_{n-2}^{q_{n-1}/p_{n-1}}(k) - \gamma_{n-1} s_{n-2}(k) \\ &= h \triangle^2 s_{n-2}(k) + h\beta_{n-1} \triangle [s_{n-2}^{q_{n-1}/p_{n-1}}(k)] + h\gamma_{n-1} \triangle s_{n-2}(k). \end{aligned} \tag{25}$$

Since $s_i(k) = \triangle s_{i-1}(k) + \beta_i s_{i-1}^{q_i/p_i}(k) + \gamma_i s_{i-1}(k)$ for $i = n-1, n-2, \cdots, 1$, then $\triangle^l s_i(k) = \triangle^{l+1} s_{i-1}(k) + \beta_i \triangle^l [s_{i-1}^{q_i/p_i}(k)] + \gamma_i \triangle^l s_{i-1}(k)$. With this relation in mind, it follows from (25) that

$$\begin{aligned} s_{n-1}(k+1) - s_{n-1}(k) =& h \triangle^n s_0(k) + h \sum_{i=0}^{n-2} \beta_{i+1} \triangle^{n-i-1} [s_i^{q_{i+1}/p_{i+1}}(k)] \\ &+ h \sum_{i=0}^{n-2} \gamma_{i+1} \triangle^{n-i-1} s_i(k). \end{aligned} \tag{26}$$

Meanwhile, from (8), we have

$$\triangle^n s_0(k) = -a_1 x_1(k) - a_2 x_2(k) - \cdots - a_n x_n(k) + u(k). \tag{27}$$

Substituting (27) and (17) into (26) yields

$$s_{n-1}(k+1) - s_{n-1}(k) = -hK \mathrm{sgn}(s_{n-1}(k)). \tag{28}$$

By Lemma 2, there is a finite number $K_1^* > 0$ such that $|s_{n-1}(k)| \leq hK = \rho_{n-1}, \forall k \geq K_1^*$.

Next, let us consider sliding mode surface s_{n-2}. According to (16), we obtain

$$s_{n-2}(k+1) = s_{n-2}(k) - h\beta_{n-1} s_{n-2}^{q_{n-1}/p_{n-1}}(k) - h\gamma_{n-1} s_{n-2}(k) + h s_{n-1}(k). \tag{29}$$

By Lemma 3 and noticing $|s_{n-1}(k)| \leq \rho_{n-1}$, it follows from (29) that there is a finite number $K_2^* > 0$ such that

$$|s_{n-2}(k)| \leq \rho_{n-2} = \psi(\frac{q_{n-1}}{p_{n-1}}) \cdot \max\left\{\left(\frac{\rho_{n-1}}{\beta_{n-1}}\right)^{p_{n-1}/q_{n-1}}, \left(\frac{h\beta_{n-1}}{1-h\gamma_{n-1}}\right)^{\frac{1}{1-q_{n-1}/p_{n-1}}}\right\}, \quad \forall k \geq K_2^*.$$

Similarly, consider s_{n-3}. According to (16), we obtain

$$s_{n-3}(k+1) = s_{n-3}(k) - h\beta_{n-2}s_{n-3}^{q_{n-2}/p_{n-2}}(k) - h\gamma_{n-2}s_{n-3}(k) + hs_{n-2}(k). \tag{30}$$

And there is a finite number $K_3^* > 0$ such that

$$|s_{n-3}(k)| \leq \rho_{n-3} = \psi(\frac{q_{n-2}}{p_{n-2}}) \cdot \max\left\{\left(\frac{\rho_{n-2}}{\beta_{n-2}}\right)^{p_{n-2}/q_{n-2}}, \left(\frac{h\beta_{n-2}}{1-h\gamma_{n-2}}\right)^{\frac{1}{1-q_{n-2}/p_{n-2}}}\right\}, \quad \forall k \geq K_3^*.$$

Recursively, we can complete the proof. □

2) Analysis of steady state of $x(k)$
Next, let us estimate the state $x(k)$. Before moving on, we need the following lemmas.

Lemma 4. *[23] If $0 < p = p_1/p_2 \leq 1$, where $p_1 > 0, p_2 > 0$ are positive odd integers, then $|x^p - y^p| \leq 2^{1-p}|x-y|^p$.*

Based on this lemma, we have the following propositions. The proofs are in the Appendix.

Proposition 1. *For $j = 1, \cdots, n, i = 1, \cdots, n-1$, the following inequality holds:*

$$\left| \triangle^i \left[s_{j-1}^{q_j/p_j}(k)\right]\right| \leq (\frac{2}{h})^{i-q_j/p_j} |\triangle s_{j-1}(k)|^{q_j/p_j}. \tag{31}$$

Proposition 2. *For $i = 0, \cdots, n-2, j = 1, \cdots, n-1-i$, the following inequality holds:*

$$\begin{aligned} |\triangle^{j+1} s_i(k)| \leq & |\triangle^j s_{i+1}(k)| + \beta_{i+1}(\frac{2}{h})^{j-q_{i+1}/p_{i+1}} |\triangle s_i(k)|^{q_{i+1}/p_{i+1}} \\ & + \gamma_{i+1} |\triangle^j s_i(k)|. \end{aligned} \tag{32}$$

Theorem 3. *For system (8), if the sliding mode surface is defined as (16) and the control law is designed as (17), then it can be found a finite number $K^* > 0$ such that*

$$|x_1(k)| \leq \rho_0, \quad |x_i(k)| = |\triangle^{i-1} s_0(k)| \leq \delta_{0,i-1}, \quad i = 2, \cdots, n, \quad \forall k \geq K^*, \tag{33}$$

where

$$\delta_{i,1} = \rho_{i+1} + \beta_{i+1}\rho_i^{q_{i+1}/p_{i+1}} + \gamma_{i+1}\rho_i, \quad i = 0, \cdots, n-2,$$
$$\delta_{i,j+1} = \delta_{i+1,j} + \beta_{i+1}(\frac{2}{h})^{j-q_{i+1}/p_{i+1}}\delta_{i,1}^{q_{i+1}/p_{i+1}} + \gamma_{i+1}\delta_{i,j},$$
$$j = 1, \ldots, n-2, i = 0, \cdots, n-1-j. \quad (34)$$

Proof. First, we consider $\triangle s_i(k), i = 0, \cdots, n-2$. By (16),

$$\triangle s_i(k) = s_{i+1}(k) - \beta_{i+1}s_i^{q_{i+1}/p_{i+1}}(k) - \gamma_{i+1}s_i(k). \quad (35)$$

By Theorem 2,

$$\begin{aligned} |\triangle s_i(k)| \leq & |s_{i+1}(k)| + \beta_{i+1}|s_i(k)|^{q_{i+1}/p_{i+1}} + \gamma_{i+1}|s_i(k)| \\ \leq & \rho_{i+1} + \beta_{i+1}\rho_i^{q_{i+1}/p_{i+1}} + \gamma_{i+1}\rho_i := \delta_{i,1}, \quad \forall k \geq K^*. \end{aligned} \quad (36)$$

Second, we consider $\triangle^2 s_i(k), i = 0, \cdots, n-3$. By (36), it follows from Proposition 2 that

$$\begin{aligned} |\triangle^2 s_i(k)| \leq & |\triangle s_{i+1}(k)| + \beta_{i+1}(\frac{2}{h})^{1-q_{i+1}/p_{i+1}}|\triangle s_i(k)|^{q_{i+1}/p_{i+1}} + \gamma_{i+1}|\triangle s_i(k)| \\ \leq & \delta_{i+1,1} + \beta_{i+1}(\frac{2}{h})^{1-q_{i+1}/p_{i+1}}\delta_{i,1}^{q_{i+1}/p_{i+1}} + \gamma_{i+1}\delta_{i,1} \\ := & \delta_{i,2}, \quad \forall k \geq K^*. \end{aligned} \quad (37)$$

Recursively, assume $|\triangle^j s_i(k)| \leq \delta_{i,j}, j = 3, \ldots, n-2, i = 0, \cdots, n-1-j, \forall k \geq K^*$. Now, let us consider $|\triangle^{j+1} s_i(k)|, i = 0, \cdots, n-2-j$. By Proposition 2, we have

$$\begin{aligned} |\triangle^{j+1} s_i(k)| \leq & |\triangle^j s_{i+1}(k)| + \beta_{i+1}(\frac{2}{h})^{j-q_{i+1}/p_{i+1}}|\triangle s_i(k)|^{q_{i+1}/p_{i+1}} \\ & + \gamma_{i+1}|\triangle^j s_i(k)| \\ \leq & \delta_{i+1,j} + \beta_{i+1}(\frac{2}{h})^{j-q_{i+1}/p_{i+1}}\delta_{i,1}^{q_{i+1}/p_{i+1}} + \gamma_{i+1}\delta_{i,j} \\ := & \delta_{i,j+1}, \quad \forall k \geq K^*. \end{aligned}$$

Next, let us analyze $x_i(k), i = 1, \cdots, n$. According to (8) and (16), we get

$$x_1(k) = s_0(k), \quad x_i(k) = \triangle^{i-1}s_0(k), i = 2, \cdots, n. \quad (38)$$

□

C. Output Tracking Precision Using Discrete-Time FTSMC and Linear Sliding Mode Control (LSMC)

Consider system (1) with output $y = x_1$. Assume the desired output signal is y_r and $y_r, \dot{y}_r, \cdots, y_r^{(n)}$ are bounded. Define $e = y - y_r$ as the output tracking error and let $e_1 = e, e_2 = \dot{e}_1, \cdots, e_n = \dot{e}_{n-1}$. Then, it follows from (1) that

$$\dot{e}_i = e_{i+1}, \quad i = 1, \cdots, n-1, \quad \dot{e}_n = -a_1x_1 - a_2x_2 - \cdots - a_nx_n + u - y_r^{(n)}. \quad (39)$$

On one hand, according to Theorems 2 and 3, for the Euler's discretization model of system (39), if we design the following discrete-time FTSMC law:

$$u(k) = \sum_{i=1}^{n} a_i x_i(k) - \sum_{i=0}^{n-2} \beta_{i+1} \triangle^{n-i-1}(s_i^{q_{i+1}/p_{i+1}}(k)) - \sum_{i=0}^{n-2} \gamma_{i+1} \triangle^{n-i-1} s_i(k) - K\mathrm{sgn}(s_{n-1}(k)) + y_r^{(n)}, \tag{40}$$

with $s_0(k) = e(k), s_{i-1}(k) = \triangle s_{i-2}(k) + \beta_{i-1} s_{i-2}^{q_{i-1}/p_{i-1}}(k) + \gamma_{i-1} s_{i-2}(k), i = 2, \cdots, n$, then the tracking error e is ultimately bounded and the bound is

$$|e(k)|_{FTSMC} \leq \rho_0, \qquad \text{with} \tag{41}$$

$$\rho_{n-1} = hK, \rho_i = \psi(\frac{q_{i+1}}{p_{i+1}}) \cdot \max\left\{ \left(\frac{\rho_{i+1}}{\beta_{i+1}}\right)^{p_{i+1}/q_{i+1}}, \left(\frac{h\beta_{i+1}}{1 - h\gamma_{i+1}}\right)^{\frac{1}{1-q_{i+1}/p_{i+1}}} \right\}, \quad i = n-2, \cdots, 0. \tag{42}$$

On the other hand, if we employ linear sliding mode surfaces, under the LSMC law (9), according to Theorem 1, the output tracking error e is also ultimately bounded and the bound is

$$|e(k)|_{LSMC} \leq \frac{\alpha h}{2c_1} \left(1 + \frac{c_1}{|1+S|} \left(\frac{h}{2}\right)^{n-1}\right), \tag{43}$$

where $S = \sum_{i=1}^{n-1} c_i (-\frac{h}{2})^{n-i}$ and h is the sampling period.

Based on (41) and (43), we can compare the output tracking precisions under these two discrete-time SMC laws. In the following, as in [15], the big $\mathcal{O}$ notation is used. A function $f(h)$ is said to be of order $g(h)$ as $h \to 0$ and denoted as $f(h) = \mathcal{O}(g(h))$, if there exist $\delta > 0$ and $M > 0$ such that $|f(h)| < M|g(h)|$ for $|h| < \delta$.

First, with the big $\mathcal{O}$ notation in mind, according to (41)-(42), we have $\rho_{n-1} = \mathcal{O}(h)$. Then

$$\rho_{n-2} = \psi(\frac{q_{n-1}}{p_{n-1}}) \cdot \max\left\{ \left(\mathcal{O}(h)\right)^{p_{n-1}/q_{n-1}}, \left(\mathcal{O}(h)\right)^{\frac{1}{1-q_{n-1}/p_{n-1}}} \right\}. \tag{44}$$

Since $\frac{1}{2} < \frac{q_{n-1}}{p_{n-1}} < 1$, then $1 < \frac{p_{n-1}}{q_{n-1}} < \frac{1}{1-q_{n-1}/p_{n-1}}$, which leads to $\rho_{n-2} = \mathcal{O}(h^{p_{n-1}/q_{n-1}})$. By a similar analysis and using the inductive method, it can be concluded that

$$\lim_{k\to\infty} |e(k)|_{FTSMC} \leq \rho_0 = \mathcal{O}(h^{\frac{p_{n-1}}{q_{n-1}} \cdots \frac{p_2}{q_2} \cdot \frac{p_1}{q_1}}). \tag{45}$$

Second, it follows from (43) that

$$\lim_{k\to\infty} |e(k)|_{LSMC} = \mathcal{O}(h). \tag{46}$$

According to (45)-(46) and noticing $\frac{p_i}{q_i} > 1, i = 1, \cdots, n-1$, we can adjust the fractional powers $\frac{p_i}{q_i}, i = 1, \cdots, n-1$, such that $\lim_{k\to\infty} |e(k)|_{FTSMC}$ is much smaller than $\lim_{k\to\infty} |e(k)|_{LSMC}$, which demonstrates the superiority of FTSMC.

Remark 2. It should be pointed out that the estimated ultimate bound in Theorems 2 and 3 is for the discrete-time system (8) based on Euler's discretization, rather than the continuous-time model (1). The trajectories of the Euler-discretized system are different from those of the original continuous-time counterpart system with piecewise constant control. This statement also applies to system (39). In section 5, we will use simulations to demonstrate the difference between Euler-discretized model and exact-discretized model.

D. Analysis of Singularity Problem in Discrete-Time FTSMC Law
Note that in the continuous-time controller (12) and (14), the fractional powers should be carefully chosen to avoid the singularity problem. Here, as in [6, 7, 9], the singularity of the control is referred to the phenomenon when $s_i \to 0, u \to \infty$. Actually, for the discrete-time controller (17), to avoid the singularity, the same conditions should also be satisfied. That is if $q_{k+1}/p_{k+1} > (n-k-1)/(n-k)$, then there is no singularity in the control law (17) when s_k enters the region $\{s_k : |s_k| \leq \rho_k\}$ sequentially from $k = n-1$ to $k = 0$, (i.e., s_{n-1} first enters the region $\{s_{n-1} : |s_{n-1}| \leq \rho_{n-1}\}$, s_{n-2} then enters the region $\{s_{n-2} : |s_{n-2}| \leq \rho_{n-2}\}$, and so on). The proof is similar to that of Ref. [22], which is omitted here.

Remark 3. Note that it is possible there is another kind of singularity problem as that for the continuous-time FTSMC in [9]. That is there may exist such a case when $|s_i(t_0)| > \rho_i$ and $|s_j(t_0)| \leq \rho_j$ for $0 \leq j < i \leq (n-1)$ at the initial time. Actually, in practice, to avoid this singularity problem, as suggested in [8] for the continuous-time TSMC, we can replace $s_j(t_0)$ with the following mapping function: $\mathrm{Map}(s_j(t_0)) = \begin{cases} s_j(t_0), & \text{for } |s_j(t_0)| > \rho_j; \\ \delta, & \text{for } |s_j(t_0)| \leq \rho_j, \end{cases}$ where $\delta > 0$.

5 Application to a DC-DC Buck Converter System

Consider the buck type DC-DC converter which is shown in Fig. 2. V_{in} is a DC input voltage source, S is a controlled switch, D is a diode, V_o is sensed output voltage, and L, C, R are the inductance, capacitance, load resistance, respectively. The buck type DC-DC converters are used in applications where the required output voltage is smaller than the input voltage. If the switching frequency for S is sufficiently high, the dynamic of DC-DC converters can be described by an average state space model [24]. Based on the average state space model [24], the dynamic equation for the buck converter is:

$$\begin{aligned} \dot{i}_L &= \frac{1}{L}(uV_{in} - V_o), \\ \dot{V}_o &= \frac{1}{C}(i_L - \frac{V_o}{R}), \end{aligned} \tag{47}$$

where u is the control input and $u \in [0, 1]$. Let V_{ref} be the desired DC output voltage and $x_1 = V_{ref} - V_o$ be the output voltage error. It follows from (47) that the error dynamic equation is:

$$\begin{aligned} \dot{x}_1 &= x_2 = -\dot{V}_o, \\ \dot{x}_2 &= -\frac{1}{LC}x_1 - \frac{1}{RC}x_2 - \frac{V_{in}}{LC}u + \frac{V_{ref}}{LC}, \\ y &= x_1. \end{aligned} \tag{48}$$

Based on this model, the control objective is to design a control law such that the tracking error x_1 converges to zero.

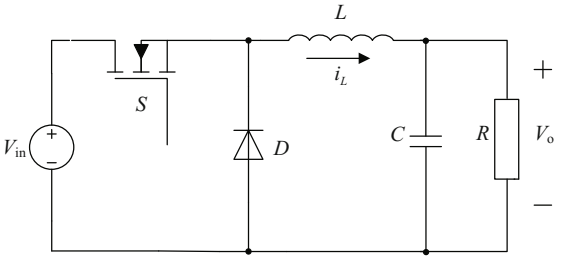

Fig. 2. DC-DC Buck converter

By Euler's discretization, the discrete-time model of system (48) is:

$$\begin{aligned} x_1(k+1) &= x_1(k) + hx_2(k), \\ x_2(k+1) &= x_2(k) - h[a_1x_1(k) + a_2x_2(k)] + h\mu(k), \end{aligned} \tag{49}$$

where $a_1 = \frac{1}{LC}, a_2 = \frac{1}{RC}, \mu = -\frac{V_{in}}{LC}u + \frac{V_{ref}}{LC}$. By Theorem 2, the corresponding discrete-time FTSMC law is

$$\mu(k) = a_1x_1(k) + a_2x_2(k) - \beta_1 \triangle(s_0^{q_1/p_1}(k)) - \gamma_1 \triangle s_0(k) - K\text{sgn}(s_1(k)) \tag{50}$$

with

$$s_0(k) = x_1(k), s_1(k) = \triangle s_0(k) + \beta_1 s_0^{q_1/p_1}(k) + \gamma_1 s_0(k), \tag{51}$$

where $\beta_1 > 0, \gamma_1 > 0, K > 0, 1/2 < q_1/p_1 < 1$. In simulation, the components values of the DC-DC buck converter are given as: Input Voltage $V_{in} = 20V$, Desired Output Voltage $V_{ref} = 15V$, Inductance $L = 100mH$, Capacitance $C = 0.1F$, Load Resistance $R = 10\Omega$.

Choose $\beta_1 = \gamma_1 = K = 1$ and $q_1 = 3, p_1 = 5$. By Theorem 3, the steady state x is bounded by:

when $h = 0.01$(sec), then $\lim_{k\to\infty} |x_1(k)| \leq 0.00055, \lim_{k\to\infty} |x_2(k)| \leq 0.0216$;
when $h = 0.1$(sec), then $\lim_{k\to\infty} |x_1(k)| \leq 0.0255, \lim_{k\to\infty} |x_2(k)| \leq 0.2363$.

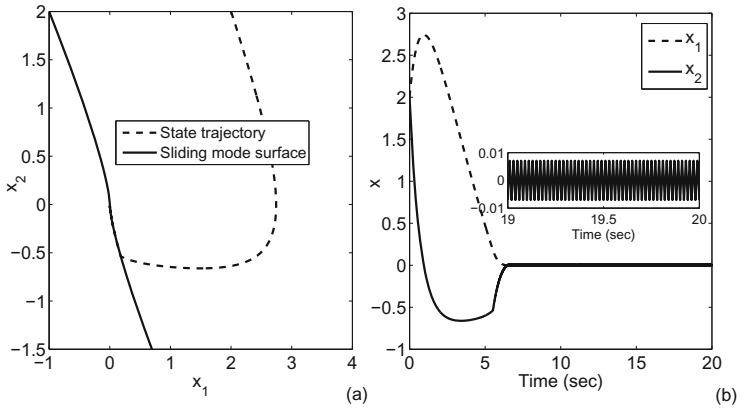

Fig. 3. Response curves of Euler-discretized model (49) under the FTSMC law (50) with $h = 0.01$(sec) and $(x_1(0), x_2(0)) = (2, 2)$. (a) Phase plane of state x and sliding mode surface $0 = x_2 + x_1^{3/5} + x_1$. (b) Time histories of states x_1, x_2.

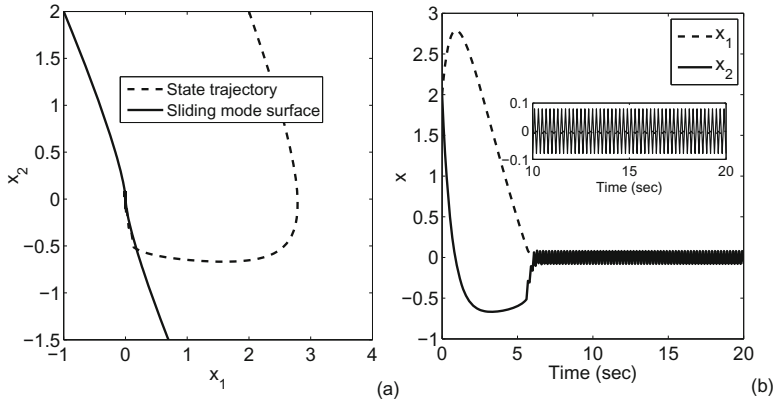

Fig. 4. Response curves of Euler-discretized model (49) under the FTSMC law (50) with $h = 0.1$(sec) and $(x_1(0), x_2(0)) = (2, 2)$. (a) Phase plane of state x and sliding mode surface $0 = x_2 + x_1^{3/5} + x_1$. (b) Time histories of states x_1, x_2.

The response curves of Euler-discretized system (49)-(50) are shown in Fig. 3 and Fig. 4, where the sampling period $h = 0.01$(sec) and $h = 0.1$(sec).

Note that Euler's discretization is only the approximate discretization of continuous-time model under a piecewise constant control. To further investigate the difference between Euler-discretized model and exact-discretized model, in Fig. 5, we do some simulations for continuous-time model (48) under a sampling control law (50) via a sampler and zero-order hold device, i.e., exact-discretized model. By comparisons, it can be found that Euler's discretization is a good approximate discretization when the sampling period is relatively small.

6 Conclusions

This chapter has studied the dynamical behaviors of discrete-time FTSMC systems based on Euler's discretization. By a rigorous theoretic analysis, we have found bounds for the steady state, which allow us to estimate the maximum chattering amplitude when using a given value of the time step. Further work includes the study of more complex discretization behaviors of FTSMC systems with uncertain parameters.

Acknowledgements. The authors are honoured to have the opportunity to contribute to this book which is dedicated to Professor Okyay Kaynak for his long term outstanding and inspiring contributions to his profession and the research field of Sliding Modes and their Applications. The second author in particular wishes to express his sincere thanks to Professor Okyay Kaynak for his support and friendship over the many years since they first met in Sarajevo during the first International Workshop on Variable Structure Systems in March 1990, and it has been a privilege to have this professional and personal association. Heartfelt Congratulations to Professor Okyay Kaynak on this important milestone of his career, and we are looking forward to continuing our cooperation in the years to come.

Appendix

This appendix includes Lemma 1, Lemma 3, and the proofs for Propositions 1-2.

Proof of Lemma 1: Without loss of generality, let

$$s_{n-2}(k) = \Big(\frac{h\beta_{n-1}}{2-h\gamma_{n-1}}\Big)^{1/(1-q_{n-1}/p_{n-1})},$$

which results into

$$s_{n-2}^{1-q_{n-1}/p_{n-1}}(k) = \frac{h\beta_{n-1}}{2-h\gamma_{n-1}}. \tag{A.1}$$

As a result,

$$(2-h\gamma_{n-1})s_{n-2} = h\beta_{n-1}s_{n-2}^{q_{n-1}/p_{n-1}}(k), \tag{A.2}$$

that is

$$s_{n-2}(k+1) = (1-h\gamma_{n-1})s_{n-2}(k) - h\beta_{n-1}s_{n-2}^{q_{n-1}/p_{n-1}}(k) = -s_{n-2}(k). \tag{A.3}$$

Using a similar deduction leads to

$$s_{n-2}(k+2) = s_{n-2}(k).$$

The proof is completed. □

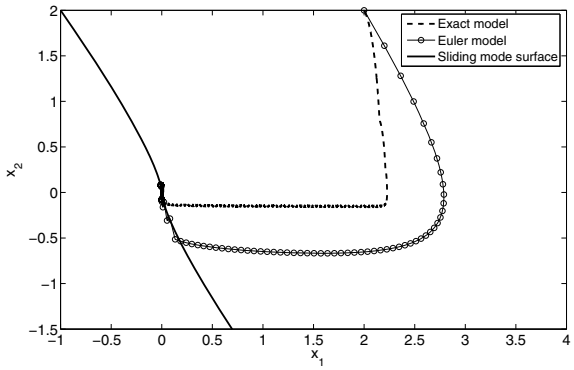

(a)

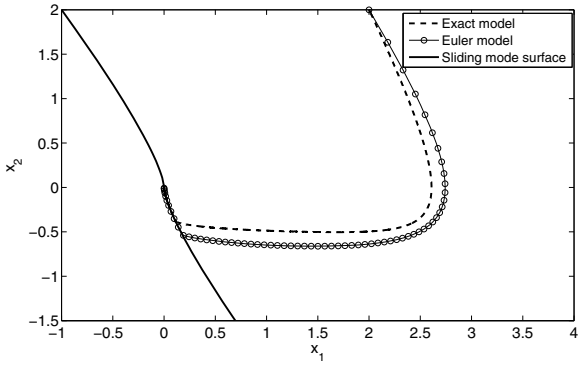

(b)

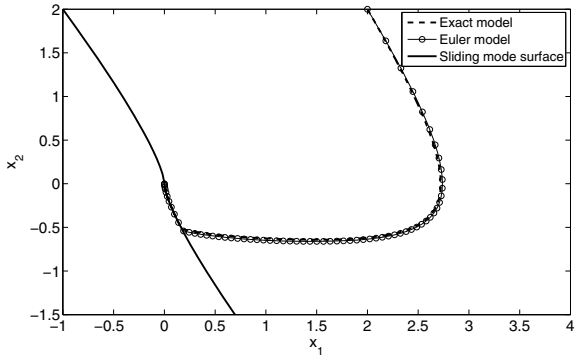

(c)

Fig. 5. Phase plane of Euler-discretized model (49)-(50) and Exact–discretized model (48) with (50) when (a) $h = 0.1$(sec), (b) $h = 0.01$(sec), (c) $h = 0.001$(sec).

Lemma 5. *If $0 < \alpha < 1$ and the function $\psi(\alpha)$ is defined in (22), then*

$$x\psi(\alpha) - x^{\alpha}\psi(\alpha)^{\alpha} + \psi(\alpha) - 1 \geq 0 \quad \text{for any } x \in [0,1].$$

Proof. Denote $F(x) = x\psi(\alpha) - x^{\alpha}\psi(\alpha)^{\alpha} + \psi(\alpha) - 1$. Next, we will calculate the minimum of $F(x)$ when $x \in [0,1]$. First of all, according to the definition of $\psi(\alpha)$, it is clear that $\psi(\alpha) > 1$, which implies that $F(0) = \psi(\alpha) - 1 > 0$ and $F(1) = \psi(\alpha) - \psi(\alpha)^{\alpha} + \psi(\alpha) - 1 > 0$. Secondly, by a calculation of $\dot{F}(x) = 0$, we have $x = \frac{\alpha^{\frac{1}{1-\alpha}}}{\psi(\alpha)}$. Substituting it into $F(x)$ and according to the values of $F(0), F(1)$, we obtain $\min_{x\in[0,1]} F(x) = 0$, which completes the proof. □

Proof of Lemma 3: Denote

$$\Omega = \left\{ |z| \leq \max\left\{ \psi(\alpha)\Big(\frac{\gamma}{l_1}\Big)^{1/\alpha}, \psi(\alpha)\Big(\frac{l_1}{1-l_2}\Big)^{\frac{1}{1-\alpha}} \right\} \right\}.$$

The following proof is divided into two steps. First, we show that the state z will enter the region Ω in a finite time. Second, we prove that once there $z \in \Omega$, then it will stay there forever.

Step 1. Choosing Lyapunov function $V(k) = z^2(k)$, it follows from (20) that

$$\begin{aligned} \triangle V(k) &= V(k+1) - V(k) \\ &= -\Big(l_1 z^{\alpha}(k) + l_2 z(k) - g(k)\Big)\Big(2z(k) - l_1 z^{\alpha}(k) - l_2 z(k) + g(k)\Big). \end{aligned} \tag{A.4}$$

Next, we will show that if $z(k) \notin \Omega$, then $\triangle V(k) \leq -c$, where c is a small positive constant.

If $z(k) \notin \Omega$, there are two cases for $z(k)$.

Case 1: $z(k) > \max\left\{ \psi(\alpha)\Big(\frac{\gamma}{l_1}\Big)^{1/\alpha}, \psi(\alpha)\Big(\frac{l_1}{1-l_2}\Big)^{\frac{1}{1-\alpha}} \right\}$.

On one hand, since $z(k) > \psi(\alpha)\Big(\frac{\gamma}{l_1}\Big)^{1/\alpha}$, then $l_1 z^{\alpha}(k) > \psi^{\alpha}(\alpha)\gamma$. By noticing that $|g(k)| \leq \gamma$, we obtain $l_1 z^{\alpha}(k) - |g(k)| > [\psi^{\alpha}(\alpha) - 1]\gamma := \mu$, which implies

$$l_1 z^{\alpha}(k) + l_2 z(k) - g(k) > \mu, \tag{A.5}$$

where μ is a positive constant since $\psi(\alpha) > 1$ and $\gamma > 0$.

On the other hand, since $z(k) > \psi(\alpha)\Big(\frac{l_1}{1-l_2}\Big)^{\frac{1}{1-\alpha}}$, then $(1-l_2)z^{1-\alpha}(k) > \psi^{1-\alpha}(\alpha)l_1$, which implies that $(1-l_2)z(k) > \psi^{1-\alpha}(\alpha)l_1 z^{\alpha}(k) \geq l_1 z^{\alpha}(k)$. Hence,

$$z(k) > l_1 z^{\alpha}(k) + l_2 z(k). \tag{A.6}$$

It follows from this inequality and (A.5) that

$$2z(k) - l_1 z^{\alpha}(k) - l_2 z(k) + g(k) > l_1 z^{\alpha}(k) + l_2 z(k) + g(k) > \mu. \tag{A.7}$$

Substituting this inequality and (A.5) into (A.4) results in $\triangle V(k) < -\mu^2 := -c$.

Case 2: $z(k) < -\max\left\{\psi(\alpha)\left(\frac{\gamma}{l_1}\right)^{1/\alpha}, \psi(\alpha)\left(\frac{l_1}{1-l_2}\right)^{\frac{1}{1-\alpha}}\right\}$.
A similar proof can prove that $\triangle V(k) \leq -c$ still holds. Hence, the state z will enter the region Ω in a finite time.

Step 2. Although in Step 1 we show that $\triangle V(k)$ is negative when $z(k) \notin \Omega$, it is possible the states may escape from Ω after entering it, since in Ω, $\triangle V(k) < 0$ is no longer guaranteed. So in this step, we will show that once $z \in \Omega$, then it will stay there forever. Without loss of generality, assume $z(k) \in \Omega$. Next, we will prove that $z(k+1) \in \Omega$.

Case 1: $\left(\frac{\gamma}{l_1}\right)^{1/\alpha} \geq \left(\frac{l_1}{1-l_2}\right)^{\frac{1}{1-\alpha}}$.
In this case, $\Omega = \{|z| \leq \psi(\alpha)\left(\frac{\gamma}{l_1}\right)^{1/\alpha}\}$. First assume that

$$z(k) = \psi(\alpha)\theta\left(\frac{\gamma}{l_1}\right)^{1/\alpha}, 0 \leq \theta \leq 1.$$

It follows from (20) that

$$\begin{aligned} z(k+1) =& \psi(\alpha)\theta\left(\frac{\gamma}{l_1}\right)^{1/\alpha} - (\psi(\alpha)\theta)^{\alpha}\gamma - l_2\psi(\alpha)\theta\left(\frac{\gamma}{l_1}\right)^{1/\alpha} + g(k) \\ \leq& (1-l_2)\psi(\alpha)\theta\left(\frac{\gamma}{l_1}\right)^{1/\alpha} - (\psi(\alpha)\theta)^{\alpha}\gamma + \gamma. \end{aligned} \tag{A.8}$$

If $\psi(\alpha)\theta \geq 1$, it follows from (A.8) that

$$z(k+1) \leq \psi(\alpha)\theta\left(\frac{\gamma}{l_1}\right)^{1/\alpha} \leq \psi(\alpha)\left(\frac{\gamma}{l_1}\right)^{1/\alpha}. \tag{A.9}$$

If $0 \leq \psi(\alpha)\theta \leq 1$, it follows from (A.8) that

$$z(k+1) \leq (1-l_2)\psi(\alpha)\theta\left(\frac{\gamma}{l_1}\right)^{1/\alpha} + [1-(\psi(\alpha)\theta)^{\alpha}]\gamma. \tag{A.10}$$

Since $\left(\frac{\gamma}{l_1}\right)^{1/\alpha} \geq \left(\frac{l_1}{1-l_2}\right)^{\frac{1}{1-\alpha}}$, then $\gamma \geq l_1^{\frac{1}{1-\alpha}}\left(\frac{1}{1-l_2}\right)^{\frac{\alpha}{1-\alpha}}$, which yields $\gamma^{1-\alpha} \geq l_1\left(\frac{1}{1-l_2}\right)^{\alpha}$. By a further calculation, it can be obtained that $\frac{\gamma}{l_1} \geq \left(\frac{\gamma}{1-l_2}\right)^{\alpha}$. Thus,

$$\frac{\gamma}{1-l_2} \leq \left(\frac{\gamma}{l_1}\right)^{1/\alpha}. \tag{A.11}$$

In addition, since $0 < \alpha < 1$ and $0 \leq \psi(\alpha)\theta \leq 1$, then $\psi(\alpha)\theta \leq (\psi(\alpha)\theta)^{\alpha}$. With this fact and (A.11) in mind, it follows from (A.10) that

$$\begin{aligned} z(k+1) &\leq (1-l_2)\psi(\alpha)\theta\left(\frac{\gamma}{l_1}\right)^{1/\alpha} + [1-(\psi(\alpha)\theta)^{\alpha}](1-l_2)\left(\frac{\gamma}{l_1}\right)^{1/\alpha} \\ &\leq (1-l_2)\left(\frac{\gamma}{l_1}\right)^{1/\alpha} \leq \left(\frac{\gamma}{l_1}\right)^{1/\alpha}. \end{aligned} \tag{A.12}$$

Thus $z(k+1) \leq \psi(\alpha)(\frac{\gamma}{l_1})^{1/\alpha}$.

On the other hand, with (A.11) in mind, it follows from (A.8) that

$$\begin{aligned} z(k+1) \geq & (1-l_2)\psi(\alpha)\theta\Big(\frac{\gamma}{l_1}\Big)^{1/\alpha} - (\psi(\alpha)\theta)^{\alpha}\gamma - \gamma \\ \geq & (1-l_2)[\psi(\alpha)\theta - (\psi(\alpha)\theta)^{\alpha} - 1]\Big(\frac{\gamma}{l_1}\Big)^{1/\alpha}. \end{aligned} \tag{A.13}$$

By noticing $0 < \alpha < 1$, if $\psi(\alpha)\theta \geq 1$, then $\psi(\alpha)\theta - (\psi(\alpha)\theta)^{\alpha} - 1 \geq -1$. If $0 \leq \psi(\alpha)\theta < 1$, then it follows from Lemma 5 that

$$\psi(\alpha)\theta - (\psi(\alpha)\theta)^{\alpha} - 1 \geq -\psi(\alpha).$$

Thus,

$$z(k+1) \geq -(1-l_2)\psi(\alpha)\Big(\frac{\gamma}{l_1}\Big)^{1/\alpha} \geq -\psi(\alpha)\Big(\frac{\gamma}{l_1}\Big)^{1/\alpha}. \tag{A.14}$$

As a result, $z(k+1) \in \Omega$. A similar proof will show that the assumption of $z(k) = \psi(\alpha)\theta\Big(\frac{\gamma}{l_1}\Big)^{1/\alpha}, -1 \leq \theta \leq 0$, will also lead to the conclusion that $z(k+1) \in \Omega$.

Case 2: $\Big(\frac{\gamma}{l_1}\Big)^{1/\alpha} \leq \Big(\frac{l_1}{1-l_2}\Big)^{\frac{1}{1-\alpha}}$. By a similar proof as that in Case 1, we can prove that $z(k+1) \in \Omega$, which is omitted here. □

Proof of Proposition 1: An inductive argument is employed. At the first step, for $i = 1$, it follows from Lemma 1 that

$$\begin{aligned} \Big| \triangle [s_{j-1}^{q_j/p_j}(k)]\Big| &= \Big|\frac{s_{j-1}^{q_j/p_j}(k+1) - s_{j-1}^{q_j/p_j}(k)}{h}\Big| \\ &\leq (\frac{2}{h})^{1-q_j/p_j}\Big|\frac{s_{j-1}(k+1) - s_{j-1}(k)}{h}\Big|^{q_j/p_j} \\ &= (\frac{2}{h})^{1-q_j/p_j}|\triangle s_{j-1}(k)|^{q_j/p_j}. \end{aligned} \tag{A.15}$$

At the inductive step, assume that the relation (31) holds for $i = m \geq 2$. With this assumption in mind, we have for $i = m+1$

$$\begin{aligned} \Big| \triangle^{m+1} [s_{j-1}^{q_j/p_j}(k)]\Big| &= \Big|\frac{\triangle^m[s_{j-1}^{q_j/p_j}(k+1)] - \triangle^m[s_{j-1}^{q_j/p_j}(k)]}{h}\Big| \\ &\leq (\frac{2}{h})^{m+1-q_j/p_j}|\triangle s_{j-1}(k)|^{q_j/p_j}, \end{aligned} \tag{A.16}$$

which completes the proof. □

Proof of Proposition 2: Since $\triangle s_i(k) = s_{i+1}(k) - \beta_{i+1}s_i^{q_{i+1}/p_{i+1}}(k) - \gamma_{i+1}s_i(k)$ from (16), then

$$\begin{aligned} |\triangle^{j+1} s_i(k)| &= |\triangle^j s_{i+1}(k) - \beta_{i+1}\triangle^j [s_i^{q_{i+1}/p_{i+1}}(k)] - \gamma_{i+1}\triangle^j s_i(k)| \\ &\leq |\triangle^j s_{i+1}(k)| + \beta_{i+1}|\triangle^j [s_i^{q_{i+1}/p_{i+1}}(k)]| + \gamma_{i+1}|\triangle^j s_i(k)|. \end{aligned}$$

By Proposition 1, we can complete the proof. □

References

1. Drazenovic, B.: The invariance conditions in variable structure systems. Automatica 5, 287–295 (1969)
2. Utkin, V.I.: Sliding Modes in Control Optimization. Springer (1992)
3. Edwards, C., Spurgeon, S.: Sliding Mode Control: Theory and Applications. Taylor and Francis, London (1998)
4. Perruquetti, W., Barbot, J.P. (eds.): Sliding Modes Control in Engineering. Marcel Dekker, New York (2002)
5. Man, Z., Paplinski, A.P., Wu, H.R.: A robust MIMO terminal sliding mode control scheme for rigid robotic manipulators. IEEE Transactions on Automatic Control 39(12), 2464–2469 (1994)
6. Yu, X., Man, Z.: Model reference adaptive control systems with terminal sliding modes. International Journal of Control 64, 1165–1176 (1996)
7. Wu, Y., Yu, X., Man, Z.: Terminal sliding mode control design for uncertain dynamic systems. Systems and Control Letters 34(5), 281–287 (1998)
8. Yu, X., Man, Z.: Multi-input uncertain linear systems with terminal sliding-mode control. Automatica 34(3), 389–392 (1998)
9. Yu, X., Man, Z.: Fast terminal sliding-mode control design for nonlinear dynamical systems. IEEE Transactions on Circuits and Systems I: Fundamental Theory and Applications 49(2), 261–264 (2002)
10. Bhat, S.P., Bernstein, D.S.: Finite-time stability of continuous autonomous systems. SIAM Journal on Control and Optimization 38(3), 751–766 (2000)
11. Sarpturk, Z., Istefanopulos, Y., Kaynak, O.: On the stability of discrete time sliding mode control systems. IEEE Transactions on Automatic Control 32(10), 930–932 (1987)
12. Yu, X., Wang, B., Li, X.: Computer-controlled variable structure systems: The state of the art. IEEE Transactions on Industrial Informatics 8(2), 197–205 (2012)
13. Xia, X., Zinober, A.S.I.: Delta-modulated feedback in discretization of sliding mode control. Automatica 42(5), 771–776 (2006)
14. Galias, Z., Yu, X.: Euler's discretization of single input sliding-mode control systems. IEEE Transactions on Automatic Control 52(9), 1726–1730 (2007)
15. Yu, X., Wang, B., Galias, Z., Chen, G.: Discretization effect on equivalent control-based multi-input sliding-mode control systems. IEEE Transactions on Automatic Control 53(6), 1563–1569 (2008)
16. Su, W.C., Drakunov, S.V., Ozguner, U.: An $O(T^2)$ boundary layer in sliding mode for sampled-data systems. IEEE Transactions on Automatic Control 45(3), 482–485 (2000)
17. Levant, A.: Finite differences in homogeneous discontinuous control. IEEE Transactions on Automatic Control 52(7), 1208–1217 (2007)
18. Yu, X., Xu, J.-X., Hong, Y., Yu, S.: Analysis of a class of discrete-time systems with power rule. Automatica 43(3), 562–566 (2007)
19. Abidi, K., Xu, J., She, J.: A discrete-time terminal sliding-mode control approach applied to a motion control problem. IEEE Transactions on Industrial Electronics 56(9), 3619–3627 (2009)
20. Galias, Z., Yu, X.: Dynamical behaviors of discretized second-order terminal sliding-mode control systems. IEEE Transactions on Circuits and Systems-Part II: Express Briefs 59(9), 597–601 (2012)
21. Janardhanan, S., Bandyopadhyay, B.: On discretization of continuous-time terminal sliding mode. IEEE Transactions on Automatic Control 51(9), 1532–1536 (2006)

22. Li, S., Du, H., Yu, X.: Discrete-time terminal sliding mode control systems based on Euler's discretization. IEEE Transactions on Automatic Control 59(2), 546–552 (2014)
23. Qian, C., Lin, W.: A continuous feedback approach to global strong stabilization of nonlinear systems. IEEE Transactions on Automatic Control 46(7), 1061–1079 (2001)
24. Tan, S.C., Lai, Y.M., Tse, C.K.: Sliding Mode Control of Switching Power Converters. CRC Press (2011)

A New Class of Non-linear Reaching Laws for Sliding Mode Control of Discrete Time Systems

Piotr Lesniewski and Andrzej Bartoszewicz

Institute of Automatic Control, Technical University of Lodz,
18/22 Stefanowskiego St., 90-924 Lodz, Poland
piotr.lesniewski2@gmail.com, andrzej.bartoszewicz@p.lodz.pl

Abstract. In this chapter we investigate the reaching law based approach to the discrete time sliding mode control of dynamical systems. We present a particular class of recently introduced controllers designed according to this approach and we thoroughly discuss their properties. The common idea of all the controllers considered in this chapter, is to obtain the desired convergence rate of the systems' state to a vicinity of the sliding hyperplane and to maintain the state in the vicinity, once the state has entered it. The vicinity is called the quasi sliding mode band and its width may serve as a good measure of the closed loop system robustness. Furthermore, we apply the proposed controllers to the periodic review inventory management problem. Even though in this chapter we focus our attention on the inventory system control, the presented reaching laws can be effectively applied to any linear discrete time plant subject to disturbance and parameter uncertainty.

Keywords: sliding mode control, discrete time systems, reaching law.

1 Introduction

Sliding mode methodology [4,11,12,23,24,32] is an effective regulation and tracking control technique that can be applied to a wide class of nonlinear, uncertain, time-varying dynamic systems. Because of its computational efficiency and robustness [10,13] it has rapidly gained much interest in the automation science and engineering community. Furthermore, since an overwhelming majority of control algorithms are nowadays implemented in digital hardware, discrete time sliding mode controllers [2,14,19,21,27,28,30,33] have recently become increasingly popular.

In general, there are two fundamental methods of designing sliding mode controllers. The first one involves stating a control law and then demonstrating that it guarantees a stable sliding motion in the considered system. The second approach to the design of sliding mode controllers is based on the reaching law method. This technique begins with defining the desired evolution of the sliding variable. Then the control law which ensures, that the system follows the specified profile of this variable is determined. This method has originally been developed for continuous time systems in [17]. Then the results were extended

X. Yu and M. Önder Efe (eds.), *Recent Advances in Sliding Modes*,
Studies in Systems, Decision and Control 24, DOI: 10.1007/978-3-319-18290-2_6

[18] and further analysed [3] for discrete time systems. A number of other interesting and practically important reaching laws for discrete time systems have also been proposed and successfully applied [19], but the one presented in [18] still maintains its importance and is often used as a benchmark for currently developed algorithms.

Unfortunately, as we will show in Section 4 the reaching law developed by Gao *et al.* cannot be directly applied to some systems, due to generating negative, as well as positive control signals in order to ensure the zigzag motion of the representative point about the sliding hyperplane. Therefore, in this chapter we will present several reaching law approaches, that do not have this disadvantage.

We will apply the presented reaching laws to the periodic review inventory management problem. The control theoretic approach to this issue has in recent years become an important research topic. An overview of the approaches used in the field and the obtained results can be found in [8,20,22,29]. The control theory methods were first applied to the management of logistic processes in the early 1950s when Simon [31] used servomechanism control algorithm to find an efficient strategy of replenishing goods in continuous time, single product inventory control systems. Several years later the discrete time servomechanism control algorithm for the problem of efficient goods replenishment has been developed [34]. Since then numerous solutions have been presented, and therefore, we are able to mention only several, arbitrarily chosen examples of solutions proposed over the last few decades. In [15] and [16] autoregressive moving average (ARMA) system structure has been used to model uncertain demand. Then model predictive control of supply chain has been proposed in [1] and [26]. In [9] a robust controller for the continuous time system with uncertain processing time and delay has been designed by minimizing H_∞-norm. However, obtaining the control law parameters of the strategy described in [9] requires application of numerical methods, which limits the analytical tractability of this approach.

The remainder of this chapter is organised as follows. In Section 2 we present the periodic review inventory system. In Section 3 we develop a basic, dead-beat type controller for this system. Such a controller generates a very high value of the control signal in the first time instant. Therefore, in Section 4 we try to apply the well-known reaching law developed by Gao. Unfortunately, this reaching law is unsuitable for the considered system, as it cannot guarantee generating a non-negative control signal. In sections 5-8 we develop the non-switching, inverse tangent based, hyperbolic tangent based and variable structure reaching laws. We demonstrate, that each of these reaching laws ensures generating a non-negative and upper bounded control signal, eliminates the need for costly emergency storage, and can, with an adequate warehouse capacity, guarantee full consumers' demand satisfaction. In Section 9 the performance of the obtained reaching law based sliding mode controllers is verified in computer simulations. Section 10 presents the conclusions of the chapter.

2 Inventory System Model

In this section we will consider a periodic review inventory system, depicted in Figure 1. The system consists of a distribution center and m distant commodity suppliers. Every provider p is characterized by the maximum amount of goods $u_{\max p}$ it can send during a single review period T. Supplier p delivers goods with a lead time L_p. We assume, that each lead time L_p is a multiple of the review period, i.e. $L_p = \mu_p T$, where μ_p is a positive integer. Inevitably, during the transport, some goods are broken, so that only α_p of the goods sent by supplier p arrive at the distribution center, where $\alpha_p \in (0, 1]$ for $p = 1, \ldots, m$. The goods are then stored and used to satisfy an a priori unknown, time-varying consumers' demand $d(kT)$. Only the upper bound of $d(kT)$ is known in advance, and we denote it by $d_{\max}$. As the warehouse on hand stock may be insufficient to fully satisfy the consumers' demand, we introduce an additional function $h(kT)$, which corresponds to the amount of goods actually sold at time kT. Therefore,

$$0 \leq h(kT) \leq d(kT) \leq d_{\max}. \tag{1}$$

The replenishment orders are generated by the controller placed at the distribution center. Its output $u(kT)$ corresponds to the total amount of goods requested from all of the providers. This value is divided among the suppliers in proportion to their output capabilities, i.e. each supplier p receives $u_{\max p} \Big/ \sum_{i=1}^{m} u_{\max i}$ of the total order.

The stock level at time kT is denoted by $y(kT)$. The warehouse is empty at the beginning of the control process, i.e. $y(kT < 0) = 0$, and the first resupply order is generated at $kT = 0$, i.e. $u(kT < 0) = 0$. We can express the on hand stock level for any $kT > 0$ as the difference between incoming and outgoing amounts of goods

$$y(kT) = \sum_{p=1}^{m} \sum_{j=0}^{k-1} \frac{u_{\max p}}{\sum_{i=1}^{m} u_{\max i}} \alpha_p u\left(jT - L_p\right) - \sum_{j=0}^{k-1} h(jT). \tag{2}$$

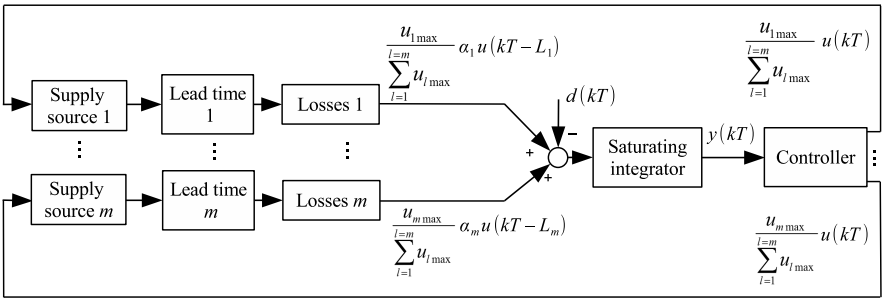

Fig. 1. Inventory supply model

We can simplify the model, by representing all suppliers with equal lead times as a single provider. The amount of goods, that will arrive at the distribution center from this provider is equal to $a_i u$, where $a_i = \sum_{p:\mu_p=i} u_{\max p} \Big/ \sum_{j=1}^{m} u_{\max j}$ for $i = 1, \ldots, n-1$, and $n = \max(\mu_p) + 1$. If there is no supplier with a particular lead time iT, then the corresponding coefficient a_i is equal to zero. Now the stock level can be expressed in the following form

$$y(kT) = \sum_{i=1}^{n-1} \sum_{j=0}^{k-1} a_i u[(j-i)T] - \sum_{j=0}^{k-1} h(jT). \tag{3}$$

We express the system dynamics in the standard state space form

$$\begin{aligned} \boldsymbol{x}[(k+1)T] &= \boldsymbol{A}\boldsymbol{x}(kT) + \boldsymbol{b}u(kT) + \boldsymbol{o}h(kT) \\ y(kT) &= \boldsymbol{q}^T \boldsymbol{x}(kT), \end{aligned} \tag{4}$$

where $\boldsymbol{x}(kT) = [x_1(kT)\ x_2(kT)\ \ldots\ x_n(kT)]^T$ is the state vector, $y(kT) = x_1(kT)$ is the warehouse stock level. The remaining state variables are the delayed values of the control signal, i.e. for $i = 2, \ldots, n$

$$x_i(kT) = u[(k-n+i-1)T]. \tag{5}$$

$\boldsymbol{A}$ is $n \times n$ state matrix, and $\boldsymbol{b}$, $\boldsymbol{o}$, and $\boldsymbol{q}$ are $n \times 1$ vectors

$$\boldsymbol{A} = \begin{bmatrix} 1 & a_{n-1} & a_{n-2} & & a_1 \\ 0 & 0 & 1 & \cdots & 0 \\ & \vdots & & \ddots & \vdots \\ 0 & 0 & 0 & \cdots & 1 \\ 0 & 0 & 0 & & 0 \end{bmatrix}, \quad \boldsymbol{b} = \begin{bmatrix} 0 \\ 0 \\ \vdots \\ 0 \\ 1 \end{bmatrix}, \quad \boldsymbol{o} = \begin{bmatrix} -1 \\ 0 \\ \vdots \\ 0 \\ 0 \end{bmatrix}, \quad \boldsymbol{q} = \begin{bmatrix} 1 \\ 0 \\ \vdots \\ 0 \\ 0 \end{bmatrix}. \tag{6}$$

The demand state of the system is $\boldsymbol{x_d} = [y_d\ \ 0\ \ \ldots\ \ 0]$, where y_d is the desired on hand stock level.

3 Dead-Beat Controller

In this section we will design a basic dead-beat sliding mode controller for the described inventory system. Then, we will analyse the properties of the closed loop system with the application of this controller.

We begin, by introducing a sliding hyperplane described by the following equation

$$s(kT) = \boldsymbol{c}^T \boldsymbol{e}(kT) = 0, \tag{7}$$

where $\boldsymbol{c}^T = [c_1\ c_2\ \ldots\ c_n]$ satisfies $\boldsymbol{c}^T \boldsymbol{b} \neq 0$ and $\boldsymbol{e}(kT) = \boldsymbol{x_d} - \boldsymbol{x}(kT)$ is the closed loop system error. By substituting (4) and (6) into $s[(k+1)T] = 0$ we obtain the following control signal

$$u(kT) = \left(\boldsymbol{c}^T \boldsymbol{b}\right)^{-1} \boldsymbol{c}^T [\boldsymbol{x_d} - \boldsymbol{A}\boldsymbol{x}(kT)]. \tag{8}$$

When this control signal is applied, the closed loop system state matrix has the following form $\boldsymbol{A_c} = [\boldsymbol{I_n} - \boldsymbol{b}\left(\boldsymbol{c}^T\boldsymbol{b}\right)^{-1}\boldsymbol{c}^T]\boldsymbol{A}$. We find the characteristic polynomial of this matrix

$$\det(z\boldsymbol{I_n} - \boldsymbol{A_c}) = z^n + \frac{c_1a_1 + c_{n-1} - c_n}{c_n}z^{n-1} + \\ + \cdots + \frac{c_1a_{n-2} + c_2 - c_3}{c_n}z^2 + \frac{c_1a_{n-1} - c_2}{c_n}z. \tag{9}$$

Condition $\boldsymbol{c}^T\boldsymbol{b} \neq 0$ implies, that all denominators in (9) are not equal to zero. In order to ensure asymptotic stability, all of the eigenvalues of the system must be located inside a unit circle. Furthermore, to obtain finite time error convergence to zero, the characteristic polynomial (9) must satisfy

$$\det\left(z\boldsymbol{I_n} - \boldsymbol{A_c}\right) = z^n. \tag{10}$$

We find, that (10) is satisfied when the following vector $\boldsymbol{c}$ is chosen

$$c_1 = 1, \;\; c_i = \sum_{j=1}^{i-1} a_{n-j} \;\; \text{for} \;\; i = 2, \ldots, n. \tag{11}$$

Substituting (6) and (11) into (8) we get

$$u(kT) = \left[y_d - x_1(kT) - \sum_{i=2}^{n} c_i x_i(kT)\right] \Bigg/ \sum_{j=1}^{n-1} a_j. \tag{12}$$

This concludes the design of the basic, dead-beat controller. Further in this section we will analyse some of its properties. In the first theorem we demonstrate, that the control signal is always non-negative and upper bounded. This control signal directly corresponds to the replenishment orders sent to the suppliers. Each supplier always has some maximum replenishment order, that it can fulfil during a single review period. Obviously, the provider also cannot send a negative amount of goods. Thus, both of these properties are crucial for implementation in a real system.

Theorem 1. *Control signal (12) for any $k \geq 0$ satisfies*

$$0 \leq u(kT) \leq \max\left(y_d, d_{\max}\right) \Bigg/ \sum_{j=1}^{n-1} a_j. \tag{13}$$

Proof. We observe, that the control signal at the initial instant is

$$u(0) = y_d \Bigg/ \sum_{j=1}^{n-1} a_j. \tag{14}$$

Next, from (11) we get

$$c_i = c_{i-1} + a_{n-i+1}, \tag{15}$$

for any $i = 3, \ldots, n$. Using (15) and (12) we obtain

$$u[(k+1)T] = \frac{1}{c_n}\left\{y_d - x_1[(k+1)T] - \sum_{i=2}^{n-1} c_i x_i[(k+1)T]\right\} - u(kT) =$$
$$= \frac{1}{c_n}\left\{y_d - x_1[(k+1)T] - \sum_{i=2}^{n-1} c_i x_i[(k+1)T]\right\} + \tag{16}$$
$$- \frac{1}{c_n}\left[y_d - x_1(kT) - \sum_{i=2}^{n} c_i x_i(kT)\right] = h(kT) \Big/ \sum_{j=1}^{n-1} a_j,$$

for any $k \geq 0$. Taking into account (1), (14) and (16) we observe, that (13) indeed holds. This ends the proof. □

The costs of emergency storage are usually quite high. Therefore, it would be advantageous, if we could calculate an a priori known size, that the on hand stock will never exceed. Then, by assigning an inventory capacity equal to, or greater than this value, we would ensure, that all incoming shipments will be accommodated inside the warehouse. In this way, the need for emergency storage would be eliminated.

Theorem 2. *When the dead-beat controller is applied, the on hand stock level will never exceed its demand value.*

Proof. Using (5) with (12) we obtain for any $k \geq 0$

$$y_d - x_1(kT) = u(kT) \sum_{i=1}^{n-1} a_i + \sum_{i=2}^{n} c_i u[(k-n+i-1)T]. \tag{17}$$

All of the parameters c_i are positive, and as shown in Theorem 1, the control signal is always non-negative. Therefore, the right hand side of (17) is non-negative, which ends the proof. □

Remark 1. Since the warehouse stock level cannot exceed its demand value, then $h(kT) \leq y_d$, for any choice of y_d. Therefore, taking into account (16), inequality (13) actually simplifies to $0 \leq u(kT) \leq y_d / \sum_{j=1}^{n-1} a_j$.

In order to maximize profit, it is crucial to eliminate lost sales. Therefore, the consumers' demand, if possible, should be fully satisfied. In the following theorem, we will calculate the minimum value of the demand stock level, that guarantees that after some initial time, the warehouse will never be empty. This implies full satisfaction of the consumers' demand.

Theorem 3. *If the demand value of the on hand stock satisfies*

$$y_d > d_{\max} \sum_{i=1}^{n-1} a_i(i+1) \Big/ \sum_{j=1}^{n-1} a_j, \tag{18}$$

then the warehouse will never be empty for any $k > \max(\mu_p) + 1$.

Proof. As we have already mentioned, $u(kT<0)=0$. *Therefore, using (16) we can write (3) for* $k>\max(\mu_p)+1$ *as*

$$y(kT)=\sum_{i=1}^{n-1}\left\{a_i\sum_{j=0}^{k-1}u[(j-i)T]\right\}-\sum_{j=0}^{k-1}h(jT)=$$

$$=\sum_{i=1}^{n-1}\left\{a_i\sum_{j=0}^{i-1}u[(j-i)T]+a_iu(0)+a_i\sum_{j=i+1}^{k-1}u[(j-i)T]\right\}-\sum_{j=0}^{k-1}h(jT)= \quad (19)$$

$$=y_d-\frac{\sum_{i=1}^{n-1}\left[a_i\sum_{j=k-i-1}^{k-1}h(jT)\right]}{\sum_{j=1}^{n-1}a_j}\geq y_d-d_{\max}\frac{\sum_{i=1}^{n-1}a_i(i+1)}{\sum_{j=1}^{n-1}a_j}.$$

This ends the proof. □

Let us notice, that if the warehouse is never empty for any $k>\max(\mu_p)+1$, then the consumers' demand is fully satisfied after this initial period.

The basic dead-beat controller generates a very large control signal in the first time instant, which would be problematic in a real application. Therefore, in the following chapters we will propose several reaching law based controllers which eliminate this problem. The common idea of these controllers is to define an appropriate way in which the representative point will converge, starting from any initial position, to the vicinity of the sliding hyperplane $s(kT)=0$, and in this way to decrease the required amplitude of the control signal.

4 Gao's Reaching Law

We will begin by applying a well-known reaching law developed in [18] to the problem considered in this chapter. In that work, the authors first define the quasi sliding mode as a motion with the following properties:

1. Starting from any initial state, the representative point will converge monotonically to the switching plane and cross it in finite time.
2. After reaching the plane the representative point will cross it in each successive step.
3. The size of each zigzagging step is non-increasing, and the representative point stays within a specified band around the hyperplane $s(kT)=0$.

A perturbed system is described by the following difference state equation

$$\boldsymbol{x}[(k+1)T]=\boldsymbol{A}\boldsymbol{x}(kT)+\boldsymbol{\Delta A}\boldsymbol{x}(kT)+\boldsymbol{b}u(kT)+\boldsymbol{f}(kT), \quad (20)$$

where $\boldsymbol{\Delta A}$ represents system parameter uncertainty and $\boldsymbol{f}(kT)$ is an external disturbance. In order to satisfy conditions 1-3 the authors propose the following reaching law

$$s[(k+1)T]=(1-q)s(kT)-(S_2+F_2+\epsilon)\,\mathrm{sgn}[s(kT)]+$$
$$-\tilde{S}(kT)-\tilde{F}(kT)+S_1+F_1, \quad (21)$$

where function

$$\operatorname{sgn}(x) = \begin{cases} -1 \text{ if } x \leq 0 \\ 1 \text{ if } x > 0 \end{cases} \tag{22}$$

$q \in (0, 1]$ is a convergence rate factor, and $\epsilon > 0$ is used to satisfy the second condition. Furthermore

$$\tilde{S}(kT) = \tilde{S}[\boldsymbol{x}(kT)] = \boldsymbol{c}^T \boldsymbol{\Delta A x}(kT) \tag{23}$$

is the influence of parameter uncertainty on the sliding variable, and

$$\tilde{F}(kT) = \boldsymbol{c}^T \boldsymbol{f}(kT) \tag{24}$$

is the effect of external disturbance on this variable. Constants S_1 and F_1 are the average values of $\tilde{S}(kT)$ and $\tilde{F}(kT)$, i.e.

$$S_1 = (S_U + S_L)/2, \quad F_1 = (F_U + F_L)/2, \tag{25}$$

where S_U, F_U are the upper, and S_L, F_L are the lower bounds of $\tilde{S}$ and $\tilde{F}$

$$S_L \leq \tilde{S} \leq S_U, \quad F_L \leq \tilde{F} \leq F_U. \tag{26}$$

Moreover, S_2 and F_2 correspond to the greatest possible deviation of $\tilde{S}$ and $\tilde{F}$ from their nominal values S_1, F_1

$$S_2 = (S_U - S_L)/2, \quad F_2 = (F_U - F_L)/2. \tag{27}$$

Using (20) and (21) we obtain the following control signal

$$\begin{aligned} u(kT) = -\left(\boldsymbol{c}^T \boldsymbol{b}\right)^{-1} \{ & (1-q)s(kT) + \boldsymbol{c}^T \boldsymbol{A x}(kT) + \\ & -\boldsymbol{c}^T \boldsymbol{x_d} + S_1 + F_1 - (\epsilon + S_2 + F_2)\operatorname{sgn}[s(kT)] \}. \end{aligned} \tag{28}$$

According to [3], if parameters q, ϵ are chosen to satisfy

$$\frac{q\epsilon}{2(1-q)} > S_2 + F_2, \tag{29}$$

then this reaching law ensures, that the sliding variable will change its sign in every successive control period and converge to the band

$$|s(kT)| \leq \epsilon/(1-q). \tag{30}$$

For the system considered in this chapter

$$S_1 = S_2 = 0, \quad \tilde{F}(kT) = -h(kT), \quad F_1 = -d_{\max}/2, \quad F_2 = d_{\max}/2. \tag{31}$$

Using (6), (11) and (31) with (28) we get

$$u(kT) = \{qs(kT) + (\epsilon + d_{\max}/2)\operatorname{sgn}[s(kT)] + d_{\max}/2\} \Big/ \sum_{i=1}^{n-1} a_i. \tag{32}$$

Theorem 4. *With the application of Gao's reaching law, the control signal is bounded by*

$$-\frac{\epsilon}{(1-q)\sum_{i=1}^{n-1} a_i} \leq u(kT) \leq \frac{qy_d + \epsilon + d_{\max}}{\sum_{i=1}^{n-1} a_i}. \tag{33}$$

Proof. The sliding variable will start from the initial value $s(0) = \boldsymbol{c}^T \boldsymbol{x_d} = y_d$ *and will converge to the band (30). Therefore, during the whole control process the value of the sliding variable*

$$s(kT) \in \left[\frac{-\epsilon}{1-q}, y_d\right]. \tag{34}$$

The value of the control signal (32) always increases with the increase of $s(kT)$*. Therefore, in order to obtain the minimum and maximum possible values of* $u(kT)$ *we simply substitute the bounds of interval (34) into (32) and find that (33) indeed holds.* □

We now observe, that the application of Gao's reaching law to the considered system has allowed to significantly reduce the maximum absolute value of the control signal when compared with the dead-beat sliding mode controller. Unfortunately, since $q \in (0, 1]$ and $\epsilon > 0$ it is not possible to find a combination of the controller parameters that would ensure generating a non-negative control signal. As this control signal represents the replenishment orders sent to the suppliers, this approach is therefore not feasible for the application considered in this chapter.

5 Non-switching Reaching Law

The application of Gao's reaching law is not possible for the considered inventory system, as was shown in the previous section. Therefore, in this section we will present another approach to this problem [6]. We begin by defining the quasi sliding mode in a slightly different way. We still require that the representative point of the controlled system should, from any initial position, converge monotonically toward the vicinity of the sliding hyperplane $s(kT) = 0$. However, after reaching the vicinity of $s(kT) = 0$ the representative point does not have to cross the hyperplane in each successive step as it was required in Gao's definition. We only require, that it does not leave a band around $s(kT) = 0$, which is further called the quasi sliding mode band. This allows us to discard the discontinuous term from the control signal, which was needed to ensure the zigzagging motion. We also replace the constant convergence rate factor q with the following variable one

$$q[s(kT)] = \frac{s_0}{s_0 + |s(kT)|}, \tag{35}$$

where $s_0 > S_2 + F_2$ is a design parameter used to obtain a satisfactory compromise between fast convergence and feasible amplitude of the control signal. This second modification allows us to reduce the value of the control signal when

$s(kT)$ is large, while still maintaining fast convergence in the neighbourhood of the sliding hyperplane. Finally, we express the modified reaching law for a general discrete-time system as follows

$$s[(k+1)T] = \{1 - q[s(kT)]\}\, s(kT) - \tilde{S}(kT) - \tilde{F}(kT) + F_1 + S_1. \tag{36}$$

We will now demonstrate, that reaching law (36) ensures the existence and reachability of the quasi sliding mode.

Theorem 5. *If the following inequality*

$$|s(kT)| \leq \frac{s_0\,(S_2 + F_2)}{s_0 - (S_2 + F_2)} \tag{37}$$

is satisfied for some $k = k_0$, then it also holds for any $k > k_0$.

Proof. From (36) we observe, that $|s[(k+1)T]|$ always increases with the increase of $|s(kT)|$. Therefore, even if we assume the most disadvantageous influence of the model uncertainty and external disturbance, if (37) is satisfied for some k, then from (36) we get

$$\begin{aligned} |s[(k+1)T]| &\leq \frac{s_0^2\,(S_2 + F_2)^2 \,/\, [s_0 - (S_2 + F_2)]^2}{s_0\,(S_2 + F_2) \,/\, [s_0 - (S_2 + F_2)] + s_0} + S_2 + F_2 = \\ &= \frac{(S_2 + F_2)^2}{s_0 - (S_2 + F_2)} + S_2 + F_2 = \frac{s_0\,(S_2 + F_2)}{s_0 - (S_2 + F_2)}. \end{aligned} \tag{38}$$

Using the principle of mathematical induction, we conclude, that (37) indeed holds for any $k > k_0$. □

Theorem 6. *If $|s(kT)|$ is greater than the right hand side of (37), then $s(kT)$ converges, at least asymptotically to the band specified by (37).*

Proof. We introduce a positive δ, that corresponds to the distance between the value of $s(kT)$ and the quasi sliding mode band (37). The proof will consist of two cases, in the first one we will consider positive, and in the second negative values of $s(kT)$.

Case 1. If

$$s(kT) = \frac{s_0\,(S_2 + F_2)}{s_0 - (S_2 + F_2)} + \delta > \frac{s_0\,(S_2 + F_2)}{s_0 - (S_2 + F_2)} > 0, \tag{39}$$

then we get

$$\begin{aligned} s[(k+1)T] - s(kT) = &- \frac{s_0^2 \left[S_2 + F_2 + \tilde{S}(kT) + \tilde{F}(kT) - S_1 - F_1\right]}{s_0^2 + \delta\,[s_0 - (S_2 + F_2)]} + \\ &- \frac{\delta\,(s_0 - S_2 - F_2)\left[s_0 + \tilde{S}(kT) + \tilde{F}(kT) - S_1 - F_1\right]}{s_0^2 + \delta\,[s_0 - (S_2 + F_2)]} \leq \\ \leq &- \frac{\delta\,(s_0 - S_2 - F_2)\left[s_0 + \tilde{S}(kT) + \tilde{F}(kT) - S_1 - F_1\right]}{s_0^2 + \delta\,[s_0 - (S_2 + F_2)]}. \end{aligned} \tag{40}$$

Taking into account that $s_0 > S_2+F_2$ *and* $S_2+F_2 \geq \left|\tilde{S}(kT)+\tilde{F}(kT)-S_1-F_1\right|$, *we observe, that* $s[(k+1)T]-s(kT)$ *is negative, and it approaches zero only if* $\delta \to 0$. *Therefore, if the initial value* $s(0) > 0$, *then it will asymptotically converge to the band (37).*

Case 2. If

$$s(kT) = -\frac{s_0\,(S_2+F_2)}{s_0-(S_2+F_2)} - \delta < -\frac{s_0\,(S_2+F_2)}{s_0-(S_2+F_2)} < 0, \tag{41}$$

then, we use (36) and obtain

$$\begin{aligned} s[(k+1)T]-s(kT) &= \frac{s_0^2\left[S_2+F_2-\tilde{S}(kT)-\tilde{F}(kT)+S_1+F_1\right]}{s_0^2+\delta\left[s_0-(S_2+F_2)\right]}+ \\ &+\frac{\delta\,(s_0-S_2-F_2)\left[s_0-\tilde{S}(kT)-\tilde{F}(kT)+S_1+F_1\right]}{s_0^2+\delta\left[s_0-(S_2+F_2)\right]} \geq \\ &\geq \frac{\delta\,(s_0-S_2-F_2)\left[s_0+\tilde{S}(kT)+\tilde{F}(kT)-S_1-F_1\right]}{s_0^2+\delta\left[s_0-(S_2+F_2)\right]}. \end{aligned} \tag{42}$$

Since $s_0 > S_2+F_2$ *and* $S_2+F_2 \geq \left|\tilde{S}(kT)+\tilde{F}(kT)-S_1-F_1\right|$ *we conclude, that if (41) is true, then the difference* $s[(k+1)T]-s(kT)$ *is positive, and it approaches zero only if* $\delta \to 0$. *Taking into account the results for cases 1 and 2 we conclude, that if s(kT) is outside of the band (37), then it will, at least asymptotically, converge to this band.*

□

Taking into account (31) we rewrite (36) for the analysed inventory system as

$$s[(k+1)T] = \{1-q[s(kT)]\}\,s(kT)+h(kT)-d_{\max}/2. \tag{43}$$

Using (4) and (43) we obtain the following control law

$$u(kT) = \left\{q[s(kT)]s(kT)+d_{\max}/2\right\} \Big/ \sum_{i=1}^{n-1} a_i. \tag{44}$$

Having obtained the controller, in the following three theorems, we will demonstrate its properties. The significance of these properties for the inventory replenishment system has been justified in Section 3.

Theorem 7. *Control signal (44) will, for any* $k \geq 0$ *satisfy*

$$0 \leq u(kT) \leq \left[s_0 y_d/\,(y_d+s_0)+d_{\max}/2\right] \Big/ \sum_{i=1}^{n-1} a_i. \tag{45}$$

Proof. As we have shown in Theorems 5 and 6, the absolute value of the sliding variable will decrease in each step, unless (37) is satisfied. Moreover, once (37) is satisfied, it holds for the rest of the control process. Since $s(0) = \boldsymbol{c}^T \boldsymbol{x_d} = y_d$*, taking into account (31), we observe that*

$$s(kT) \in \left[-s_0 d_{\max} / \left(2s_0 - d_{\max}\right), y_d\right]. \tag{46}$$

As the control signal (44) always increases with the increase of $s(kT)$*, we substitute the limits of interval (46) into (44) and find that (45) is true.* □

Theorem 8. *With the application of the proposed non-switching reaching law based controller, the warehouse stock level will always satisfy*

$$y(kT) \leq y_d + s_0 d_{\max} / \left(2s_0 - d_{\max}\right). \tag{47}$$

Proof. From (46) we obtain

$$s(kT) \geq -s_0 d_{\max} / \left(2s_0 - d_{\max}\right) \tag{48}$$

for all $k \geq 0$*. Using (5) and (7) we can rewrite (48) as*

$$y(kT) \leq y_d + \frac{s_0 d_{\max}}{2s_0 - d_{\max}} - \sum_{i=2}^{n} c_i u[(k-n+i-1)T]. \tag{49}$$

The coefficients c_i *are positive, and, as shown in Theorem 7, the control signal is always non-negative. Therefore (49) implies (47).* □

Theorem 9. *If the demand warehouse stock level satisfies*

$$y_d > d_{\max} \sum_{i=1}^{n-1} i a_i \Bigg/ \sum_{i=i}^{n-1} a_i + \frac{s_0 d_{\max}}{2s_0 - d_{\max}}, \tag{50}$$

then $y(kT) > 0$ *for any* $k \geq k_0 + n - 1$*, where* k_0 *is the first time instant in which (37) is satisfied.*

Proof. Using (37), we get

$$y(kT) \geq y_d - \sum_{i=2}^{n} c_i u[(k-n+i-1)T] - \frac{s_0 d_{\max}}{2s_0 - d_{\max}} \tag{51}$$

for any $k \geq k_0$*. Moreover, using (37) with (44), we obtain*

$$u(kT) \leq d_{\max} \Bigg/ \sum_{i=1}^{n-1} a_i \tag{52}$$

also for any $k \geq k_0$*. Using (51) and (52) we get*

$$y(kT) \geq y_d - d_{\max} \sum_{i=1}^{n-1} i a_i \Bigg/ \sum_{i=1}^{n-1} a_i - \frac{s_0 d_{\max}}{2s_0 - d_{\max}} \tag{53}$$

for any $k \geq k_0 + n - 1$*. If (50) is true, then the right hand side of (53) is always strictly positive.* □

6 Inverse Tangent Based Reaching Law

The non-switching reaching law approach demonstrated in the previous section shows some promising results. In this section, we consider a similar reaching law, however this time based on a trigonometric function [7]. The reaching law has the following form

$$s[(k+1)T] = s(kT) - g\text{arctg}\left[s(kT)/g\right] - \tilde{S}(kT) - \tilde{F}(kT) + S_1 + F_1, \quad (54)$$

where

$$g > 2\left(S_2 + F_2\right)/\pi \quad (55)$$

is a parameter used to find a compromise between fast convergence and reasonable magnitude of the control signal. We will begin by showing, that this reaching law ensures existence and reachability of the quasi sliding mode.

Theorem 10. *If inequality*

$$|s(kT)| \leq g\text{tg}\left[\left(S_2 + F_2\right)/g\right] \quad (56)$$

is satisfied for some $k = k_0$, then it also holds for all $k > k_0$.

Proof. First we demonstrate that if (56) holds, then

$$s[(k+1)T] \leq g\text{tg}\left[\left(S_2 + F_2\right)/g\right]. \quad (57)$$

We can observe from (54) that the value of $|s[(k+1)T]|$ always increases with the increase of $|s(kT)|$. Using (54) and (56) we obtain

$$\begin{aligned} s[(k+1)T] \leq\ & g\text{tg}\left[\left(S_2 + F_2\right)/g\right] + \\ & - g\text{arctg}\left\{\text{tg}\left[\left(S_2 + F_2\right)/g\right]\right\} - \tilde{S}(kT) - \tilde{F}(kT) + S_1 + F_1. \end{aligned} \quad (58)$$

In the considered case, the most disadvantageous values of perturbations are $\tilde{S}(kT) = S_L$ and $\tilde{F}(kT) = F_L$. Under these conditions, the terms in the second line of (58) cancel each other out. This means, that (58) implies (57). We will now show, that if (56) is satisfied, then

$$s[(k+1)T] \geq -g\text{tg}\left[\left(S_2 + F_2\right)/g\right]. \quad (59)$$

Using (54) and (56) we obtain

$$\begin{aligned} s[(k+1)T] \geq\ & -g\text{tg}\left[\left(S_2 + F_2\right)/g\right] + \\ & - g\text{arctg}\left\{-\text{tg}\left[\left(S_2 + F_2\right)/g\right]\right\} - \tilde{S}(kT) - \tilde{F}(kT) + S_1 + F_1. \end{aligned} \quad (60)$$

The most disadvantageous values of perturbations for this case are $\tilde{S}(kT) = S_U$ and $\tilde{F}(kT) = F_U$. For this worst possible case, the terms in the second line of (60) cancel out. Therefore, (60) implies (59).

Taking into consideration (57) and (59), using the principle of mathematical induction, we conclude that indeed once (56) is satisfied, it will remain true for the rest of the control process. □

Theorem 11. *If the proposed reaching law is applied, then the value of* $|s(kT)|$ *will converge, at least asymptotically, to the band (56).*

Proof. We introduce a positive δ*, which corresponds to the distance of* $s(kT)$ *from the band (56). We will show, that* $|s(k+1)T|$ *is always closer to this band than* $|s(kT)|$ *by an amount, that can drop to zero only if* $\delta \to 0$*. This property means, that* $s(kT)$ *will converge, in the worst case asymptotically, to the band (56).*

Case 1. First, we consider positive values of $s(kT)$*, i.e.*

$$s(kT) = g\mathrm{tg}\left[\left(S_2 + F_2\right)/g\right] + \delta. \tag{61}$$

We calculate the rate of change of variable s *by using (61) and (54)*

$$\begin{aligned} s[(k+1)T] - s(kT) &= -g\mathrm{arctg}\left\{\mathrm{tg}\left[\left(S_2 + F_2\right)/g\right] + \delta/g\right\} + S_1 + F_1 + \\ &-\tilde{S}(kT) - \tilde{F}(kT) \leq S_2 + F_2 - g\mathrm{arctg}\left\{\mathrm{tg}\left[\left(S_2 + F_2\right)/g\right] + \delta/g\right\}. \end{aligned} \tag{62}$$

Since function arctg(.) *is monotonic, we notice that the right hand side of (62) is strictly negative, and approaches zero only for* $\delta \to 0$*.*

Case 2. We now assume, that

$$s(kT) = -g\mathrm{tg}\left[\left(S_2 + F_2\right)/g\right] - \delta. \tag{63}$$

From (54) we get

$$\begin{aligned} s[(k+1)T] - s(kT) &= -g\mathrm{arctg}\left\{-\mathrm{tg}\left[\left(S_2 + F_2\right)/g\right] - \delta/g\right\} + S_1 + F_1 + \\ &-\tilde{S}(kT) - \tilde{F}(kT) \geq -S_2 - F_2 + g\mathrm{arctg}\left\{\mathrm{tg}\left[\left(S_2 + F_2\right)/g\right] + \delta/g\right\} \end{aligned} \tag{64}$$

We observe, that the right hand side of (64) is strictly positive, and approaches zero only if $\delta \to 0$*. Taking into consideration (62) and (64) we conclude, that* $s(kT)$ *will converge, in the worst case scenario asymptotically, to the band (56).* □

This concludes the demonstration of existence and reachability of the quasi sliding mode. We will now derive a controller for the considered system based on the presented reaching law.

Using (4), (7) and (31) with (54) we obtain

$$u(kT) = \left\{g\mathrm{arctg}\left[s(kT)/g\right] + d_{\max}/2\right\} \Big/ \sum_{i=1}^{n-1} a_i. \tag{65}$$

In the remainder of this section, we will demonstrate some important properties of this control law. The meaning of these properties for an actual logistic system has already been described in Section 3.

Theorem 12. *Control signal (65) is non-negative and upper bounded, i.e.*

$$0 \leq u(kT) \leq \left[g\text{arctg}\left(y_d/g\right) + d_{\max}/2\right] \Big/ \sum_{i=1}^{n-1} a_i \tag{66}$$

for any $k \geq 0$.

Proof. As shown in Theorems 10 and 11, the magnitude of $s(kT)$ *will decrease in each step, unless (56) is satisfied. Moreover, once (56) is satisfied, it will hold for the rest of the control process. Since* $s(0) = y_d$, *this means that the sliding variable*

$$s(kT) \in \left[-g\text{tg}\left[d_{\max}/(2g)\right], y_d\right] \tag{67}$$

for all $k \geq 0$. *The control signal (65) always increases with the increase of* $s(kT)$. *Therefore, to obtain its maximum and minimum values, we simply substitute the limits of interval (67) into (65) and find that (66) indeed holds.* □

Theorem 13. *The on hand stock, for all* $k \geq 0$, *satisfies the following inequality*

$$y(kT) \leq y_d + g\text{tg}\left[d_{\max}/(2g)\right]. \tag{68}$$

Proof. From (67) we obtain

$$s(kT) \geq -g\text{tg}\left[d_{\max}/(2g)\right] \tag{69}$$

for all $k \geq 0$. *Moreover, we can rewrite (69) using (7) and (5) as*

$$y(kT) \leq y_d + g\text{tg}\left[d_{\max}/(2g)\right] - \sum_{i=2}^{n} c_i u[(k-n+i-1)T]. \tag{70}$$

All the coefficients c_i *are positive. Furthermore, as demonstrated in Theorem 12, the control signal is non-negative. This allows us to conclude that (70) implies (68).* □

Theorem 14. *If the demand stock level satisfies*

$$y_d > d_{\max} \sum_{i=1}^{n-1} i a_i \Big/ \sum_{i=1}^{n-1} a_i + g\text{tg}\left[d_{\max}/(2g)\right], \tag{71}$$

then the warehouse will never be empty for any $k \geq k_0 + n - 1$, *where* k_0 *is the first review period in which (56) is satisfied.*

Proof. From (56) we obtain

$$y(kT) \geq y_d - \sum_{i=2}^{n} c_i u[(k-n+i-1)T] - g\text{tg}\left[d_{\max}/(2g)\right] \tag{72}$$

for any $k \geq k_0$. Moreover, since $u(kT)$ increases with the increase of $s(kT)$, using (56) with (65) we obtain

$$u(kT) \leq d_{\max} \Big/ \sum_{i=1}^{n-1} a_i \tag{73}$$

again, for all $k \geq k_0$. By combining (72) and (73) we arrive at

$$y(kT) \geq y_d - d_{\max} \sum_{i=1}^{n-1} i a_i \Big/ \sum_{i=1}^{n-1} a_i - g\mathrm{tg}\left[d_{\max}/(2g)\right] \tag{74}$$

for any $k \geq k_0 + n - 1$. If (71) is true, then the right hand side of (74) is always strictly positive, which ends the proof. □

7 Hyperbolic Tangent Based Reaching Law

In this section we take into consideration the reaching law based on the hyperbolic tangent function [25]. This reaching law can be presented as

$$s[(k+1)T] = s(kT) - r\tanh\left[s(kT)/r\right] - \tilde{S}(kT) - \tilde{F}(kT) + S_1 + F_1 \tag{75}$$

with $r > S_2 + F_2$ which plays a similar role to g in the inverse tangent based reaching law.

We will begin by demonstrating that reaching law (75) ensures the existence and reachability of the quasi sliding mode for any discrete time system that can be described by (20).

Theorem 15. *If the following inequality*

$$|s(kT)| \leq r\left[\ln\left(r + S_2 + F_2\right) - \ln\left(r - S_2 - F_2\right)\right]/2 \tag{76}$$

is satisfied for some $k = k_0$, then it is also true for any $k > k_0$.

Proof. From (75) we obtain

$$\left|s[(k+1)T]\right| \leq \left|s(kT) - r\tanh\left[s(kT)/r\right]\right| + \left|F_1 + S_1 - \tilde{S}(kT) - \tilde{F}(kT)\right|. \tag{77}$$

Considering (25), (26) and (27) the second term on the right hand side of (77) is always smaller than or equal to $S_2 + F_2$. Moreover, the value of the first term always increases with the increase of $|s(kT)|$. Thus, taking into account (76), we get

$$\begin{aligned} |s(k+1)T| \leq r\Big\{&\left[\ln\left(r + S_2 + F_2\right) - \ln\left(r - S_2 - F_2\right)\right]/2 + \\ &- \frac{e^{\left[\ln(r+S_2+F_2) - \ln(r-S_2-F_2)\right]/2} - e^{-\left[\ln(r+S_2+F_2) - \ln(r-S_2-F_2)\right]/2}}{e^{\left[\ln(r+S_2+F_2) - \ln(r-S_2-F_2)\right]/2} + e^{-\left[\ln(r+S_2+F_2) - \ln(r-S_2-F_2)\right]/2}}\Big\} + S_2 + F_2 = \\ r\left[\ln\left(r + S_2 + F_2\right) - \ln\left(r - S_2 - F_2\right)\right]/2 \end{aligned} \tag{78}$$

which ends the proof. □

Theorem 16. *The sliding variable will converge, at least asymptotically to the band described by (76).*

Proof. We express the distance of $|s(kT)|$ *from the band (76) by a positive value* δ*. Therefore, any value of* $|s(kT)|$ *outside of this band can be represented as*

$$|s(kT)| = r\left[\ln\left(r + S_2 + F_2\right) - \ln\left(r - S_2 - F_2\right)\right]/2 + \delta. \tag{79}$$

We observe, that $|s(kT)| \geq |r\tanh[s(kT)/r]|$ *for any value of s(kT). This allows us to use (77) to express the rate of change of the sliding variable as*

$$\begin{aligned} |s[(k+1)T]| - |s(kT)| \leq\ & S_2 + F_2 + \\ & - r\tanh\left\{\left[\ln\left(r + S_2 + F_2\right) - \ln\left(r - S_2 - F_2\right)\right]/2 + \delta/r\right\}. \end{aligned} \tag{80}$$

Because $\tanh(.)$ *is a monotonic function of its argument, and*

$$\tanh\left\{\left[\ln\left(r + S_2 + F_2\right) - \ln\left(r - S_2 - F_2\right)\right]/2\right\} = \frac{S_2 + F_2}{r}, \tag{81}$$

then the right hand side of inequality (80) is negative and approaches zero only for $\delta \to 0$*. Therefore,* $s(kT)$ *will in fact converge to the band (76).* □

Using (4) and (11) we write the control signal for the considered system as

$$u(kT) = \left\{r\tanh\left[s(kT)/r\right] + d_{\max}/2\right\} \Big/ \sum_{i=1}^{n-1} a_i. \tag{82}$$

In the three theorems that follow, we will describe the properties of the system with the application of the obtained controller. The importance of these properties has been explained in the section concerning the dead-beat controller.

Theorem 17. *The control signal (82) satisfies*

$$0 \leq u(kT) \leq \left[r\tanh\left(y_d/r\right) + d_{\max}/2\right] \Big/ \sum_{i=1}^{n-1} a_i \tag{83}$$

for all $k \geq k_0$*.*

Proof. It follows from Theorems 15 and 16 that the absolute value of the sliding variable will decrease in each period, unless (76) is satisfied. Furthermore, once (76) becomes satisfied, it will hold for the rest of the control process. As $s(0) = y_d$*, we observe, that for any* $k \geq 0$

$$s(kT) \in \left[-r\left[\ln\left(r + d_{\max}/2\right) - \ln\left(r - d_{\max}/2\right)\right]/2, y_d\right]. \tag{84}$$

Control signal (82) always increases with the increase of $s(kT)$*. By substituting the limits of interval (84) into (82) we obtain the maximum and minimum values of* $u(kT)$ *and find that (83) indeed holds.* □

Theorem 18. *The stock level in the distribution center always satisfies the following inequality*

$$y(kT) \leq y_d + r\left[\ln\left(r + d_{\max}/2\right) - \ln\left(r - d_{\max}/2\right)\right]/2. \tag{85}$$

Proof. From (84) we have

$$s(kT) \geq -r\left[\ln\left(r + d_{\max}/2\right) - \ln\left(r - d_{\max}/2\right)\right]/2 \tag{86}$$

for all $k \geq 0$. By substituting (5) and (7) into (86) we get

$$y(kT) \leq \\ \leq y_d - \sum_{i=2}^{n} c_i u[(k-n+i-1)T] + \frac{r}{2}\left[\ln\left(r + \frac{d_{\max}}{2}\right) - \ln\left(r - \frac{d_{\max}}{2}\right)\right]. \tag{87}$$

The control signal, as shown in Theorem 17 is always non-negative, and all the elements of vector $\mathbf{c}$ are positive. Therefore, we conclude that (87) implies (86). □

Theorem 19. *If the demand stock level is chosen to satisfy*

$$y_d > d_{\max} \sum_{i=1}^{n-1} i a_i \Bigg/ \sum_{i=1}^{n-1} a_i + \frac{r}{2}\left[\ln\left(r + \frac{d_{\max}}{2}\right) - \ln\left(r - \frac{d_{\max}}{2}\right)\right], \tag{88}$$

then the on hand stock level will never drop to zero for any $k > k_0 + n - 1$, where k_0 is the first review period in which (76) is satisfied.

Proof. By using (5) with (76) we obtain

$$y(kT) \geq y_d - \sum_{i=2}^{n} c_i u[(k-n+i-1)T] - \frac{r}{2}\left[\ln\left(r + \frac{d_{\max}}{2}\right) - \ln\left(r - \frac{d_{\max}}{2}\right)\right] \tag{89}$$

for all $k \geq k_0$. As $u(kT)$ always increases with the increase of $s(kT)$ we use (76) and (82) to get

$$u(kT) \leq d_{\max} \Bigg/ \sum_{i=1}^{n-1} a_i \tag{90}$$

also for any $k \geq k_0$. By combining (89) and (90) we arrive at

$$y(kT) \geq y_d - d_{\max} \sum_{i=1}^{n-1} i a_i \Bigg/ \sum_{i=1}^{n-1} a_i - \frac{r}{2}\left[\ln\left(r + \frac{d_{\max}}{2}\right) - \ln\left(r - \frac{d_{\max}}{2}\right)\right] \tag{91}$$

for any $k > k_0 + n - 1$. If (88) is satisfied, then the right hand side of (91) is strictly positive, and this observation ends the proof. □

8 Variable Structure Reaching Law

In some inventory systems it would be advantageous if the controller output would always be equal either to some defined a priori value, or to zero. This corresponds to making a delivery request for some specific amount of goods (for example one truckload) or no request at all. In order to obtain such an inventory management policy, we propose the following reaching law [5]

$$s[(k+1)T] = s(kT) - 0.5Q\{1 + \mathrm{sgn}[s(kT)]\} + h(kT), \tag{92}$$

where sgn(.) is defined by (22) and parameter

$$Q > d_{\max}. \tag{93}$$

We notice from (92) and (93) that if $s(kT) > 0$, then $s[(k+1)T] \geq s(kT) - Q$. On the other hand, if $s(kT) \leq 0$, then $s[(k+1)T] \geq s(kT)$. Therefore

$$s(kT) > -Q \tag{94}$$

for all $k \geq 0$. We define k_1 as the first time instant when the representative point reaches or crosses the hyperplane. We observe from (92), (93), and $s(0) = y_d > 0$, that the value of $s(kT)$ will decrease in each step, at least by $Q - d_{\max}$, unless $s(kT) \leq 0$ becomes satisfied. Therefore, we can upper bound k_1 by

$$k_1 < \lceil y_d / (Q - d_{\max}) \rceil. \tag{95}$$

Now we will consider the value of $s(kT > k_1 T)$. If $s(kT) \leq 0$, then $s[(k+1)T] \leq s(kT) + d_{\max} \leq d_{\max}$. If on the other hand $s(kT) > 0$, then $s[(k+1)T] \leq s(kT) - Q + d_{\max} < s(kT)$. Therefore, for any $k \geq k_1$

$$s(kT) \leq d_{\max}. \tag{96}$$

Taking into account (94) and (96) we conclude, that for all $k \geq k_1$ the value of the sliding variable will satisfy $s(kT) \in (-Q, d_{\max}]$.

By substituting (4) and (7) into (92) we obtain the following control signal

$$u(kT) = Q\{1 + \mathrm{sgn}[s(kT)]\} \Bigg/ \left(2 \sum_{i=1}^{n-1} a_i \right). \tag{97}$$

As we easily observe the replenishment orders generated by the controller are always equal to either $Q / \sum_{i=1}^{n-1} a_i$ or to zero. In the next theorem we will demonstrate, that the stock level is always upper bounded, and therefore, the risk of costly emergency storage can be eliminated by choosing an appropriate warehouse size.

Theorem 20. *When the proposed controller is applied, the on hand stock level satisfies*

$$y(kT) < y_d + Q \tag{98}$$

for any $k \geq 0$.

Proof. Using (5) we transform (94) to the following form

$$y(kT) < y_d + Q - \sum_{i=2}^{n} c_i u[(k-n+i-1)T]. \tag{99}$$

Because all parameters c_i are positive, and the control signal is non-negative, we conclude, that (99) implies (98). □

In the next theorem, we show that with a sufficiently large demand stock level, our control strategy ensures full satisfaction of consumers' demand and therefore maximizes profit.

Theorem 21. *If the demand stock level satisfies*

$$y_d > d_{\max} + Q \sum_{i=1}^{n-1} i a_i \Bigg/ \sum_{j=1}^{n-1} a_j, \tag{100}$$

then the on hand stock level will be strictly positive for any $k \geq k_1$.

Proof. Inequality (96) holds for all $k \geq k_1$. We can rewrite it as follows

$$y(kT) \geq y_d - d_{\max} - \sum_{i=2}^{n} c_i u[(k-n+i-1)T] \geq y_d - d_{\max} - Q \sum_{i=1}^{n-1} i a_i \Bigg/ \sum_{j=1}^{n-1} a_j \tag{101}$$

If (100) holds, then the right hand side of (101) is strictly positive, which ends the proof. □

9 Simulation Results

In order to verify the properties of the proposed controllers, and to compare their performance, computer simulations were performed. The maximum consumers' demand $d_{\max} = 100$ items and the review period $T = 1$ day. The actual consumers' demand $d(kT)$ in the simulations is shown in Fig. 2. It exhibits sudden changes between small and large values, which corresponds to the most difficult conditions in the inventory system. There are three suppliers in the system and their description is shown in Table 1. This set of parameters characterising the suppliers results in the following values of coefficients: $a_3 = 0.156$, $a_5 = 0.309$, $a_8 = 0.476$, and the remaining a_i are equal to zero. As we have already demon-

Table 1. System parameters

p	L_p [days]	α_p	$u_{\max p}$ [items]
1	3	0.97	18
2	5	0.96	36
3	8	0.92	58

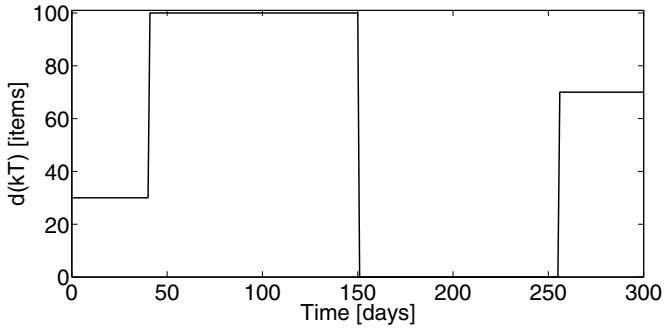

Fig. 2. Consumers' demand

strated in Theorem 4 it is impossible to guarantee generating a non-negative control signal with the application of Gao's reaching law, which means that this approach cannot be used in practice. Therefore, we omit the Gao's reaching law in the simulations presented in this section. The parameters of each controller are chosen so that the control signal will not exceed $\sum_{i=1}^{3} u_{\max} = 112$ items (apart from the dead-beat controller where this is not possible). In each case the minimum demand stock level y'_d that ensures full consumers' demand satisfaction has been calculated, and a slightly larger value, y_d has been used. Furthermore, for each controller, we have obtained the stock level $y_{\max}$, that will never be exceeded. This information, useful for choosing an appropriate warehouse size, is shown in Table 2.

For each controller we will present the control signal, the inventory stock level, and the value of the sliding variable. The simulation results for the dead-beat controller are shown in figures 3, 4 and 5, for the non-switching reaching law in figures 6, 7 and 8, for the inverse tangent based reaching law in figures 9, 10 and 11, for the hyperbolic tangent based reaching law in figures 12, 13 and 14 and for the variable structure controller in figures 15, 16 and 17.

Observing the figures 3-17 we notice, that all of the controllers satisfy the properties, which have been demonstrated analytically in the previous sections. They all generate a non-negative and upper bounded control signal and ensure that the stock level does not exceed an a priori known value. By choosing an

Table 2. Controllers parameters

Controller	Parameters	y'_d [items]	y_d [items]	$y_{\max}$ [items]
Dead-beat	None	719	730	730
Non-switching reaching law	$s_0 = 59.02$ items	946	960	1287
Inverse tangent reaching law	$g = 36.3$ items	804	810	995
Hyperbolic tangent reaching law	$r = 55.4$ items	701	710	792
Variable structure reaching law	$Q = 105.4$ items	752	760	865

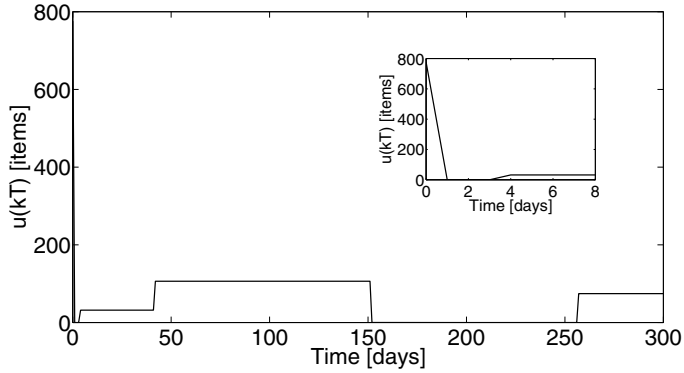

Fig. 3. Control signal for the dead-beat controller ($u(0) = 775.7$ items)

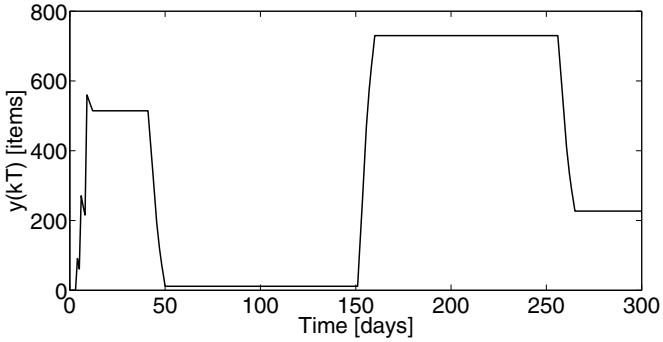

Fig. 4. On hand stock level for the dead-beat controller

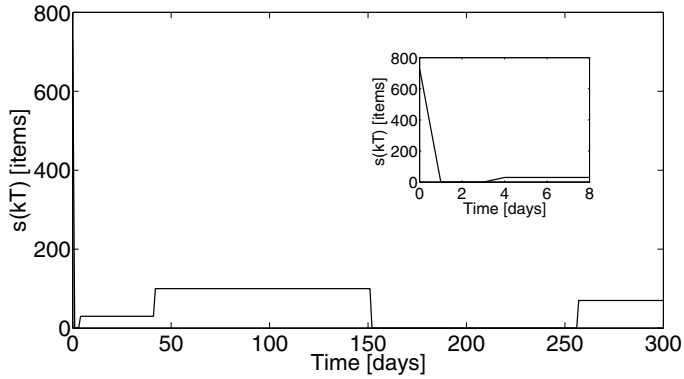

Fig. 5. Evolution of the sliding variable for the dead-beat controller.

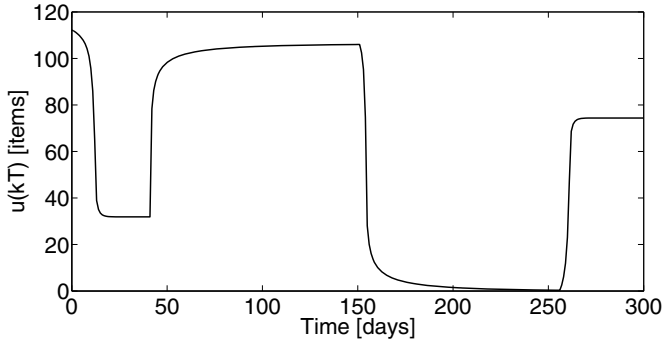

Fig. 6. Replenishment orders generated by the non-switching reaching law controller

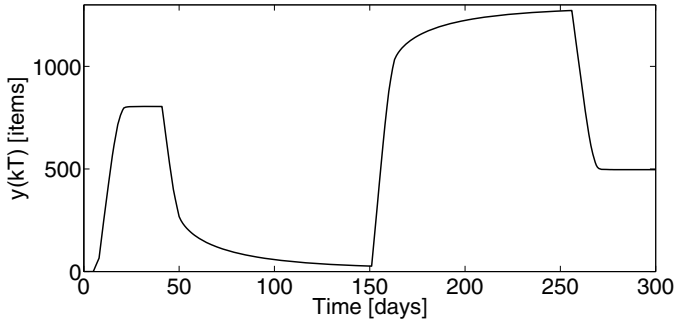

Fig. 7. Stock level for the non-switching reaching law controller

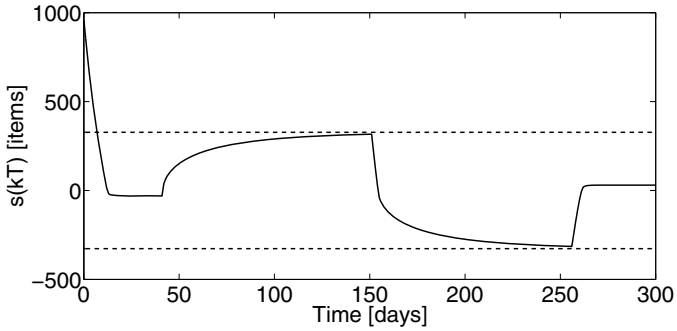

Fig. 8. Sliding variable evolution for the non-switching reaching law controller (the QSMB bounds equal to ±327 items are shown with dashed lines)

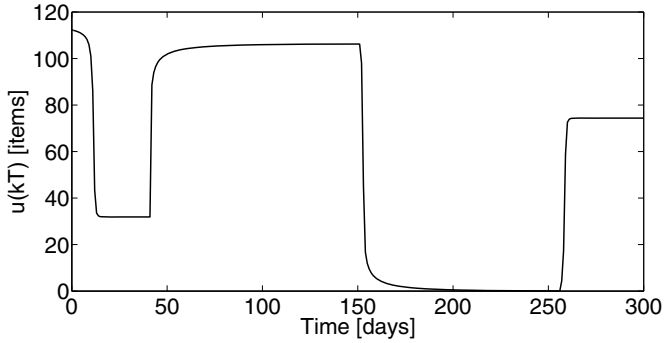

Fig. 9. Replenishment orders generated by the inverse tangent reaching law controller

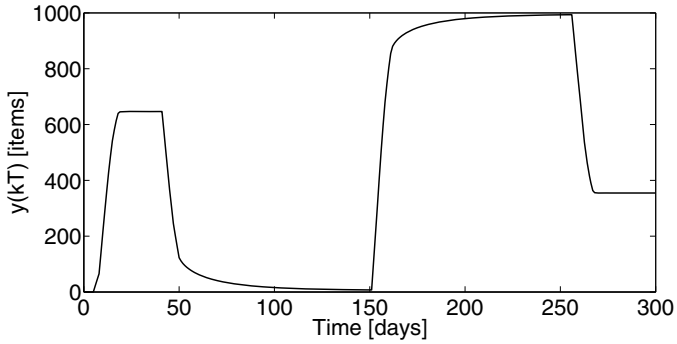

Fig. 10. Stock level for the inverse tangent reaching law controller

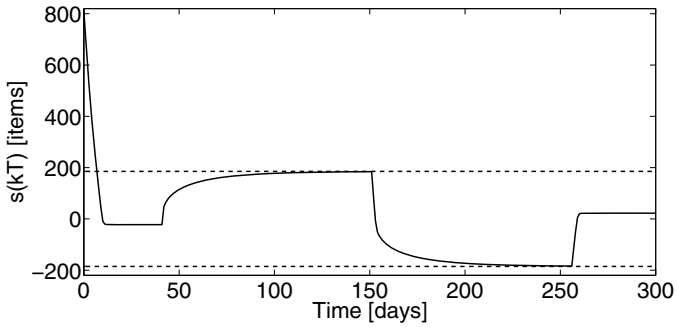

Fig. 11. Sliding variable evolution for the inverse tangent reaching law controller (the QSMB bounds equal to ±185 items are shown with dashed lines)

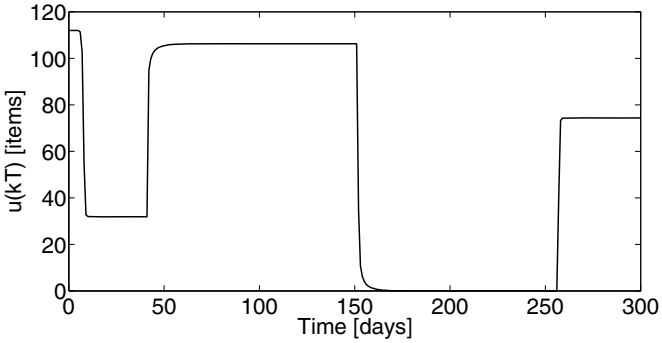

Fig. 12. Replenishment orders generated by the hyperbolic tangent reaching law controller

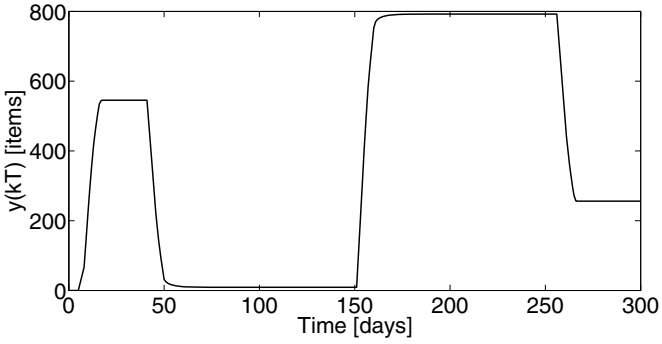

Fig. 13. Stock level for the hyperbolic tangent reaching law controller

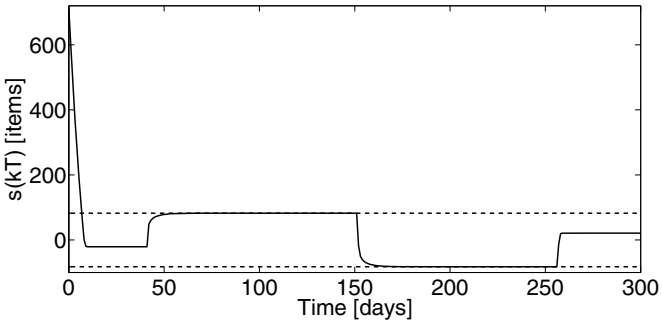

Fig. 14. Sliding variable evolution for the hyperbolic tangent reaching law controller (the QSMB bounds equal to ±82.3 items are shown with dashed lines)

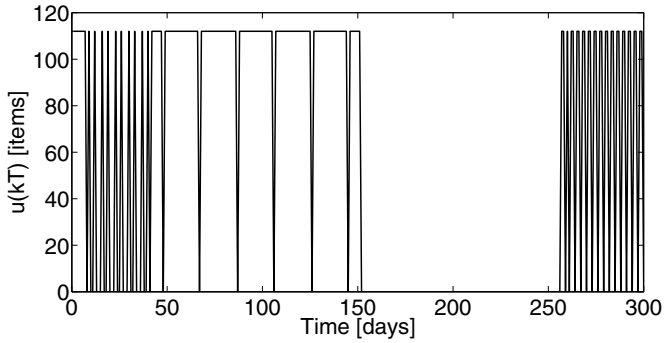

Fig. 15. Replenishment orders generated by the variable structure controller

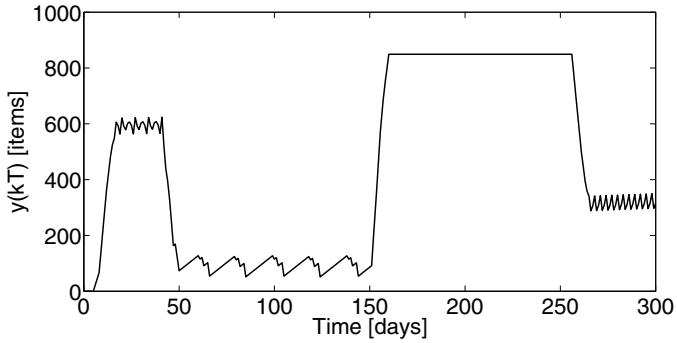

Fig. 16. Stock level for the variable structure controller

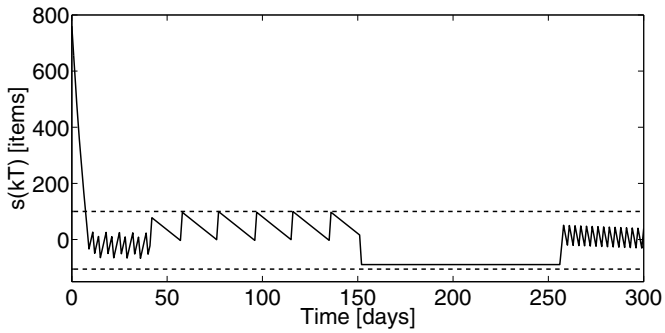

Fig. 17. Sliding variable evolution for the variable structure controller (the bounds equal to $d_{\max} = 100$ items and $-Q = -105.4$ items are shown with dashed lines)

appropriately large value of the demand stock level for each controller, we have eliminated the risk of lost sales.

Comparing the results obtained with the different controllers we immediately notice, that the basic dead-beat strategy generates an unacceptably large value of the control signal in the first time instant. Therefore, the reaching law approaches are needed to overcome this drawback. As we can observe, the non-switching, inverse tangent and hyperbolic tangent reaching law approaches give different results, even when their parameters are chosen to obtain the same bound on the magnitude of the control signal. The non-switching reaching law generates the smoothest control signal of the three, making it easy to follow by the suppliers. Unfortunately, in order to ensure full consumers' demand satisfaction it requires the largest warehouse size. On the other side of the spectrum, the hyperbolic tangent reaching law requires the least amount of inventory space, but the generated replenishment orders change quite rapidly. Therefore, the undesirable bullwhip effect in this case is only slightly reduced. The properties of the inverse tangent reaching law lie between the other two. The choice between one of these three strategies for a specific application can be motivated by comparing the cost of storage of a particular ware and the willingness of the providers to fulfil rapidly changing replenishment orders.

The variable structure controller generates orders that are always equal to either zero, or some specified a priori value. Therefore, it seems best fitted for cases in which a decision whether to send or not to send a transport of a particular quantity of goods (for example one truckload) has to be reached. This kind of situation could arise, when the transportation costs are high when compared to the value of goods themselves, or when a transport between wholesalers is considered. The drawback of this strategy is that it would also require considerable storage capabilities on the side of the supplier, so that it would be able to comply with the incoming shipment requests.

10 Conclusions

In this work, we have chosen a definition of the quasi sliding mode that, in contrast to the seminal work of Gao, does not require crossing the sliding hyperplane in each control step. In our definition, it is sufficient, that the representative point remains in a pre-defined band around the sliding hyperplane. This modification allowed us to eliminate chattering and obtain tighter bounds on the control signal. We have presented four reaching laws for linear discrete time systems subject to parameter uncertainties and disturbances. For each of the presented reaching laws we have demonstrated the conditions ensuring the existence and reachability of the quasi sliding mode.

We have shown, that for some systems, e.g. the inventory supply chains, the reaching law of Gao cannot be applied, because it does not guarantee generating a non-negative control signal. On the other hand, all of the recently proposed reaching laws can satisfy this important condition. We have also demonstrated, that by applying the proposed reaching laws, we obtain controllers that eliminate

the need for costly emergency storage, and can, with a sufficiently large warehouse capacity, ensure complete satisfaction of the consumers' demand. These important properties have been both proved analytically and verified in computer simulations.

The variable structure reaching law is the most suited to problems, in which it is advantageous to generate a control signal that is equal either to zero, or to some known, specified a priori value. Choosing between one of the remaining reaching laws for a specific case one should take into account the requirements on the system robustness (reflected by the maximum admissible width of the quasi sliding mode band) and the limits on the control signal rate of change.

Acknowledgements. This work has been performed in the framework of a project "Optimal sliding mode control of time delay systems" financed by the National Science Centre of Poland decision number DEC 2011/01/B/ST7/02582. Kind support provided by the Foundation for Polish Science under Mistrz grant is also acknowledged. This chapter is dedicated to Professor Okyay Kaynak to commemorate his extraordinary research and scholarly achievements and his unparalleled service to the control engineering community. The second author of this chapter had a unique opportunity to collaborate with Professor Okyay Kaynak in the years of 2007-2009 and benefited greatly from his extensive experience and kind advice.

References

1. Aggelogiannaki, E., Doganis, P., Sarimveis, H.: An adaptive model predictive control configuration for production-inventory systems. International J. of Production Economics 114, 165–178 (2008)
2. Bandyopadhyay, B., Janardhanan, S.: Discrete-Time Sliding Mode Control. LNCIS, vol. 323. Springer, Heidelberg (2006)
3. Bartoszewicz, A.: Remarks on 'Discrete-time variable structure control systems'. IEEE T. on Industrial Electronics 43, 235–238 (1996)
4. Bartoszewicz, A., Kaynak, O., Utkin, V.: Guest Editorial. IEEE T. on Industrial Electronics 55, 3806–3808 (2008)
5. Bartoszewicz, A., Lesniewski, P.: Variable structure flow controller for connection-oriented communication networks. In: Proceedings of the 14th International Carpathian Control Conference, pp. 5–10 (2013)
6. Bartoszewicz, A., Lesniewski, P.: Reaching law approach to the sliding mode control of periodic review inventory systems. IEEE T. on Automation Science and Engineering 11, 810–817 (2014)
7. Bartoszewicz, A., Lesniewski, P.: A new reaching law based sliding mode flow controller for connection-oriented data transmission networks. In: Proceedings of the 13th International Workshop on Variable Structure Systems, pp. 1211–1216 (2014)
8. Boccadoro, M., Martinelli, F., Valigi, P.: Supply chain management by H-infinity control. IEEE T. on Automation Science and Engineering 5, 703–707 (2008)
9. Boukas, E.K., Shi, P., Agarwal, R.K.: An application of robust technique to manufacturing systems with uncertain processing time. Optimal Control Applications and Methods 21, 257–268 (2000)

10. Drazenovic, B.: The invariance conditions in variable structure systems. Automatica 5, 287–295 (1969)
11. Edwards, C., Spurgeon, S.: Sliding Mode Control: Theory and Applications. Taylor & Francis, London (1998)
12. Efe, M.O., Kaynak, O., Unsal, C., Yu, X.: Sliding mode control of a class of uncertain systems. In: Proceedings of 2003 IEEE Conference on Control Applications, pp. 78–82 (2003)
13. Erbatur, K., Kaynak, M., Sabanovic, A.: A study on robustness property of sliding-mode controllers: a novel design and experimental investigations. IEEE T. on Industrial Electronics 46, 1012–1018 (1999)
14. Furuta, K.: Sliding mode control of a discrete system. Systems & Control Letters 14, 145–152 (1990)
15. Gaalman, G., Disney, S.M.: State space investigation of the bullwhip problem with ARMA(1,1) demand processes. International J. of Production Economics 104, 327–339 (2006)
16. Gaalman, G.: Bullwhip reduction for ARMA demand: the proportional order-up-to policy versus the full-state-feedback policy. Automatica 42, 1283–1290 (2006)
17. Gao, W., Hung, J.: Variable structure control of nonlinear systems: a new approach. IEEE T. on Industrial Electronics 40, 45–55 (1993)
18. Gao, W., Wang, Y., Homaifa, A.: Discrete-time variable structure control systems. IEEE T. on Industrial Electronics 42, 117–122 (1995)
19. Golo, G., Milosavljevic, C.: Robust discrete-time chattering free sliding mode control. Systems & Control Letters 41, 19–28 (2000)
20. Hoberg, K., Bradley, J.R., Thonemann, U.W.: Analyzing the effect of the inventory policy on order and inventory variability with linear control theory. European J. of Operations Research 176, 1620–1642 (2007)
21. Janardhanan, S., Bandyopadhyay, B.: Multirate output feedback based robust quasi-sliding mode control of discrete-time systems. IEEE T. on Automatic Control 52, 499–503 (2007)
22. Karaesmen, I., Scheller-Wolf, A., Deniz, B.: Managing perishable and aging inventories: review and future research directions. In: Kempf, K., Keskinocak, P., Uzsoy, R. (eds.) Handbook of production planning, Dordrecht, Kluwer (2008)
23. Kayacan, E., Oniz, Y., Kaynak, O.: A grey system modeling approach for sliding-mode control of antilock braking system. IEEE T. on Industrial Electronics 56, 3244–3252 (2009)
24. Kaynak, O., Bartoszewicz, A., Utkin, V.: Guest Editorial. IEEE T. on Industrial Electronics 56, 3271–3274 (2009)
25. Lesniewski, P., Bartoszewicz, A.: Discrete time sliding mode inventory management - hyperbolic tangent reaching law based approach. In: Proceedings of the 19th International Conference on Methods and Models in Automation and Robotics, pp. 276–281 (2014)
26. Li, X., Marlin, T.E.: Robust supply chain performance via Model Predictive Control. Computers & Chemical Engineering 33, 2134–2143 (2009)
27. Mehta, A., Bandyopadhyay, B.: Frequency-shaped sliding mode control using output sampled measurements. IEEE T. on Industrial Electronics 56, 28–35 (2009)
28. Milosavljevic, C.: General conditions for the existence of a quasi-sliding mode on the switching hyperplane in discrete variable structure systems. Autom. Remote Control 46, 307–314 (1985)
29. Sarimveis, H., Patrinos, P., Tarantilis, C.D., Kiranoudis, C.T.: Dynamic modeling and control of supply chain systems: a review. Computers and Operations Research 35, 3530–3561 (2008)

30. Sarpturk, S.Z., Istefanopulos, Y., Kaynak, O.: On the stability of discrete-time sliding mode control systems. IEEE T. on Automatic Control 32, 930–932 (1987)
31. Simon, H.A.: On the application of servomechanism theory in the study of production control. Econometrica 20, 247–268 (1952)
32. Utkin, V.: Variable structure systems with sliding modes. IEEE T. on Automatic Control 22, 212–222 (1977)
33. Utkin, V., Drakunov, S.V.: On discrete-time sliding mode control. In: IFAC Conference on Nonlinear Control, pp. 484–489 (1989)
34. Vassian, H.J.: Application of discrete variable servo theory to inventory control. Arthur D. Little, Inc., Cambridge Massachusetts (1954)

Sliding Mode Order and Accuracy in Sliding Mode Adaptation and Convergence Acceleration

Yaniv Dvir and Arie Levant

Tel Aviv University, Tel Aviv, Israel
yanivdvi@gmail.com, levant@post.tau.ac.il

Abstract. Fundamental properties of Sliding Mode (SM) Control (SMC) are considered. The best and worst possible SM accuracy of Single-Input Single-Output (SISO) and Multi-Input Multi-Output (MIMO) systems is shown to be directly determined by the number of continuous derivatives of the sliding variables. The best SM accuracy is obtained in the both SISO and MIMO cases by homoneous SMs. SM adaptation is to be based on the detection of a real SM. Such detection is based on the observation of the above best possible accuracy in the presence of noises and discrete sampling. Convergence to SM is accelerated by control, which is piece-wise homogeneous on successive time segments. It allows feedback application of homogeneous SM-based differentiators with piece-wise constant parameters, providing for arbitrarily fast convergence and preserving the optimal accuracy featuring homogeneous SMs. Simulation results show the feasibility of the proposed methods and demonstrate their asymptotic accuracy.

1 Introduction

The idea of the Sliding Mode Control (SMC) approach is very intuitive. One tries to remove the dynamics uncertainty by establishing and keeping an appropriate connection $\sigma = 0$ between the system variables. Due to the system uncertainty the proposed way is to shift the system towards the constraint, and to switch the control each time this goal appears to be missed. It results in high-frequency switching of the control, and the corresponding motion mode $\sigma \equiv 0$ is called Sliding Mode (SM), whereas σ is called the sliding variable [65,21,57,59].

The main advantages and disadvantages of the approach are immediately seen: on the one hand the control method is simple and effective, on the other hand the resulting control becomes discontinuous on the constraint manifold and theoretically features infinite-frequency switching. Such switching can cause dangerous system vibrations (the chattering effect [65,7,25]).

High-Order Sliding Modes (HOSMs) were historically proposed to overcome the above chattering-effect problem. Describe that approach. Suppose that the equality $\sigma = 0$ is kept on the solutions of a closed-loop system. The sliding order r is the lowest integer r, such that the rth-order total time derivative $\sigma^{(k)}$

X. Yu and M. Önder Efe (eds.), *Recent Advances in Sliding Modes*,
Studies in Systems, Decision and Control 24, DOI: 10.1007/978-3-319-18290-2_7

is not a continuous function of the state variables and time (see [31,32]. The corresponding motion $\sigma \equiv 0$ is called rth-order SM, and for brevity is called r-sliding mode (r-SM).

The standard SMs [21,65] are of the first order, i.e. $\sigma = 0$ is held, whereas already $\dot{\sigma}$ contains discontinuous control u, $r = 1$. The idea of the HOSM-based chattering attenuation of standard SMs is to introduce the virtual control $\dot{u}$, so as to keep $\sigma = \dot{\sigma} = 0$ by means of a discontinuous virtual control $\dot{u}$ [9,31,15]. The control u itself is formally included in the system variables. As the result, the sliding order is increased from 1 to 2. Note that the chattering reduction is not due to the continuity of the corresponding control $u(t)$, but due to simultaneously keeping continuous functions of system variables σ and $\dot{\sigma}$ at zero [35]. Nothing theoretically prevents using $u^{(k)}$ providing for the $(k+1)$-SM keeping $\sigma = \dot{\sigma} = \ldots = \sigma^{(k)} = 0$ [35], $k = 1, 2, \ldots$. HOSMs are also typically characterized by high accuracy in the presence of small switching imperfections and noises [31,33].

Relative degree is defined as the lowest total derivative order of the output σ which explicitly contains control [28]. Families of universal controls are recursively constructed and solve the problem for any relative degree r [33,59] of the output σ by means of r-SM. In particular, the finite-time stabilization of σ is possible by means of control, continuous everywhere except the manifold $\sigma = \dot{\sigma} = \cdots = \sigma^{(r-1)} = 0$ [34]. The controllers are complemented by the robust exact SM-based differentiators in finite time providing for the unavailable derivatives of σ [32]. SM control is proved to be insensitive to disturbances in the control channel (matched disturbances), robust with respect to sampling noises and small delays. Homogeneous SMs [33] are proved to be robust to small disturbances, including those which change the relative degree [43], and to the presence of fast stable sensors and actuators [26,35].

The results described above constitute a solid foundation for extensive applications of SMC for solution of various control and observation problems under uncertainty conditions [3,8,11,15,19,20,24,27,29,46,45,51,57,49,61]. The new emerging areas of SMC theory deal with nonhomogeneous SMC and observation [18,39], robustness and discretization issues [6,26,40,43], approximability features [12]. Lyapunov functions are found and used for HOSM controllers [47,55,56,17].

Usually the uncertainties are assumed to be bounded, whereas the bounds serve as the SM control parameters. The SM adaptation is needed, if these bounds exist, but are unknown. The next-level adaptation is required, if the bounds are variable, but change with some bounded speed, etc. SM adaptation is one of the hot topics of the modern SMC [50,53,52,60,2,63,66].

It is well-known that though the transient time to SM of the homogeneous SM controllers is finite, the convergence is slow at large distances. The convergence time is very important, since the system uncertainty is suppressed only after the SM is established. Intensive efforts have been made to shorten the transient. In that context one has to especially single out the controllers with fixed-time convergence, i.e. with the convergence times bounded from above by some constant independent of initial conditions [17,4,54]. Unfortunately, recent study shows

that realization of such systems is problematic, if the sampling rate is a-priory bounded [36]. Therefore, it seems more realistic to regulate the convergence time so that it will not exceed a prescribed function of initial conditions.

In this chapter we discuss some fundamental properties of the SMC, review and extend the recent results by the authors in SM adaptation and convergence-time regulation. In this context new general results on the SM accuracy, homogeneous Multi-Input Multi-Output (MIMO) SMC and its acceleration are presented. The main idea of this chapter is that the best possible accuracy defined by the SM order is not only to be obtained both in the Single-Input Single-Output (SISO), and MIMO cases by homogeneous HOSMs, but also can be used for the detection of homogeneous HOSMs kept in practical systems. The accelerated control is homogeneous over successive time intervals, which also allows the feedback application of the robust finite-time convergent differentiators [32]. Simulation results show the feasibility of the proposed methods and demonstrate their asymptotic accuracy.

2 General SMC Problem

Consider an uncertain smooth nonlinear system of the form $\dot{x} = f(t, x, u),\ x \in \mathbb{R}^n$, $u \in \mathbb{R}^m$, with a smooth output $\sigma(t, x) \in \mathbb{R}^l$. By the SMC problem we understand the problem of establishing and afterwards keeping a proper constraint $\sigma(t, x) = 0$ which solves or facilitates the main control problem. Introducing a new auxiliary control $\dot{u} = v$ obtain the new *affine-in-control* system $\begin{pmatrix} \dot{x} \\ \dot{u} \end{pmatrix} = \begin{pmatrix} f(t,x,u) \\ 0 \end{pmatrix} + \begin{pmatrix} 0 \\ 1 \end{pmatrix} v$. Further we only deal with affine-in-control systems. We also usually assume that the system has a well-defined relative degree.

Recall that a scalar output $\sigma(t, x)$ of a smooth SISO system

$$\dot{x} = a(t, x) + b(t, x)u, \tag{1}$$

has a relative degree r, if the rth total time derivative of σ is the first to explicitly contain the control, and the corresponding control coefficient does not vanish. In the MIMO case the dimensions of u and σ are to be equal, a partial relative degree r_i with respect to some control component is to exist for each component σ_i of the output, and the matrix $\left(\frac{\partial \sigma^{(r_i)}}{\partial u_j}\right)$ is to be nonsingular [28].

Finite-Time Stability. We say that the SM $\sigma \equiv 0$ is finite-time stable, if $\sigma \equiv 0$ is established in finite time. In the sequel we mainly consider finite-time stable SMs (FTSSMs). One frequently doubts the advantages of systems with FTSSMs over asymptotically stable SMs (ASSMs). Indeed, in practice exact convergence is never possible. Nevertheless the difference is significant.

The practical accuracy of a FTSSM is determined by present small disturbances and is obtained in a finite time known in advance, whereas the transient time of a practical ASSM tends to infinity, if the disturbances gradually vanish.

The disturbed steady-state motion of a FTSSM is close to the ideal SM over any compact time interval [23], which often practically finishes the analysis. On

the other hand, the disturbed motions of an ASSM are close to undisturbed transient motions over closed finite time intervals, but since the undisturbed transient never ends, some special convergence analysis is inevitable.

3 Sliding Order and Restrictions of SM Accuracy

Realization of SM control inevitably includes discrete switching [58] and noisy measurements. Here we estimate the worst and the best possible realization accuracy of HOSMs in the presence of noises and discrete switching, and show that possible practical SM accuracies are strictly determined by the numbers of the output derivatives in which the discontinuity appears for the first time.

3.1 Accuracy of SMs in the Absence of Noises

The following lemma actually describes SM accuracy in the presence of discrete control swithing. It extends a similar result of [31].

Lemma 1. *Let $\omega(t)$ be a scalar function having continuous derivative $\omega^{(l)}$ on the segment $[0,\tau]$, $\tau > 0$. Then for each natural number l there exist such $c_0, c_1, ..., c_{l-1} > 0$ and $d_1, d_2, ..., d_{l-1} > 0$ that for any $\delta > 0$*

1. *if $|\omega^{(l)}| \le \delta$ holds on the segment, then*

$$\max|\omega| \le c_0\delta\tau^l, \max|\dot{\omega}| \le c_1\delta\tau^{l-1}, ..., \max|\omega^{(l-1)}| \le c_{l-1}\delta\tau; \qquad (2)$$

2. *if $|\omega^{(l)}| \le \delta$ and $|\omega| \le d_0\delta\tau^l$ hold over the segment $[0,\tau]$ for some d_0, then*

$$\max|\dot{\omega}| \le (d_0d_1+1)\delta\tau^{l-1}, ..., \max|\omega^{(l-1)}| \le (d_0d_{l-1}+1)\delta\tau. \qquad (3)$$

Obviously the second statement of the Lemma provides for a rather crude estimation, since with $d_0 = 0$ all derivatives of ω should vanish.

Proof of Statement 1. The statement is trivial with $l = 1$. Let the statement be true with some $l = k > 0$, i.e. the corresponding set c_i be chosen. Transition from $l = k$ to $l = k+1$ is as follows.

Obviously $\dot{\omega}$ satisfies the statement with $l = k$. Thus, only ω is to be evaluated. Prove that $\max|\omega| \ge 2^{-(k+1)}3^{-(k+1)^2}\delta\tau^{k+1}$. Indeed, let it be wrong and $|\omega| < 2^{-(k+1)}3^{-(k+1)^2}\delta\tau^{k+1}$ hold. The points of the whole segment can be written in the ternary number system as numbers $\tau\cdot 0.b_1b_2\ldots$ with $b_j \in \{0,1,2\}$. Consider only points with $b_j \in \{0,2\}$, $j = 1,\ldots,k+1$. They constitute 2^{k+1} subsegments of the length $3^{-k-1}\tau$. Take one internal point at each such subsegment. The distance between each two neighbor points with the same b_j, $j = 1,\ldots,k$, is not less than $3^{-(k+1)}\tau$, and the difference of the values of ω does not exceed $|\omega| < 2^{-k}3^{-(k+1)^2}\delta\tau^{k+1}$. Hence, according to the Lagrange Theorem, there is a point between them, where $|\dot{\omega}| < 2^{-k}3^{-k(k+1)}\delta\tau^k$. These 2^k second-generation points belong to the set of points with $b_j \in \{0,2\}$, $j = 1,\ldots,k$, and the distance between successive points is not less than $3^{-k}\tau > 3^{-(k+1)}\tau$. Apply once more the same procedure and get $2^{(k-1)}$ third-generation points with the distance between

them not less than $3^{-(k+1)}\tau$. After $k+1$ steps get a point in the original segment, where $|\omega^{(k+1)}| < \delta$, which is a contradiction to the Lemma condition.

Proof of Statement 2. Applying the same procedure as for statement 1 get $l-1$ points t_j with $|\omega^{(j)}(t_j)| \le d_0\delta\tilde{d}_j\tau^{l-j}$, $j = 1, 2, \ldots, l-1$. Now from

$$\omega^{(l-1)}(t) = \omega^{(l-1)}(t_{l-1}) + \int_{t_{l-1}}^{t} \omega^{(l)}(t)dt$$

one gets $|\omega^{(l-1)}(t)| \le (d_0\tilde{d}_{l-1}+1)\delta\tau$. Similarly, integrating one gets $|\omega^{(l-2)}(t)| \le (d_0\tilde{d}_{l-2} + d_0\tilde{d}_{l-1} + 1)\delta\tau^2$, etc. □

Lemma 1 shows that the accuracy of keeping an output $\sigma = 0$ is directly connected with the number of its continuous total time derivatives. This naturally implies the following definition [31], directly formulated for the vector output σ.

Definition 1. *Suppose the constraint $\sigma(x) = 0$, $\sigma : \mathbb{R}^k \to \mathbb{R}^m$, is identically kept on some solutions of a dynamic system $\dot{x} = v(x)$, $x \in \mathbb{R}^k$, understood in the Filippov sense, $v(x)$ is any Lebesgue-measurable locally bounded vector-function. Then the solutions keeping $\sigma(x) = 0$ are said to be in the $(r_1, r_2, ..., r_m)$th-order sliding mode, if*

1. *$\sigma_i^{(j)}(x)$ are continuous functions of x, $j \le r_i - 1$;*
2. *the r-sliding set $L_r = \left\{x \,|\, \sigma_i^{(j)}(x) = 0,\ j \le r_i - 1,\ i = 1, ..., m\right\}$ is not empty, and locally consists of Filippov solutions;*
3. *$\sigma_1^{(r_1)}, \sigma_2^{(r_2)}, ..., \sigma_m^{(r_m)}$ are discontinuous functions of x or do not exist.*

In the non-autonomous case the time t is considered as an additional coordinate, and the equation $\dot{t} = 1$ is formally added.

It follows from the sliding-order definition that SM order is component-wise larger or equal than vector relative degree, if the latter exists. It can be higher, if, for example, the control itself features some discontinuous dynamics. An r-SM is called unstable, asymptotically stable, finite-time stable, etc., if the r-sliding manifold L_r features the same property.

Consider a MIMO dynamic system (1). Let the output $\sigma(t, x)$ and the input u be vectors, $\sigma : \mathbf{R}^{n+1} \to \mathbf{R}^m$, $u \in \mathbf{R}^l$, a, b be smooth. The system is assumed to have the partial relative degrees $r = (r_1, ..., r_m)$, $r_i > 0$, which means that the successive total time derivatives $\sigma_i^{(j)}$, $j = 0, 1, ..., r_i - 1$, $i = 1, ..., m$, do not contain controls, but controls appear in $\sigma_i^{(r_i)}$. Respectively, get a vector equation

$$\sigma^{(r)} = h(t, x) + g(t, x)u, \tag{4}$$

where $\sigma^{(r)}$ denotes $(\sigma_1^{(r_1)}, ..., \sigma_m^{(r_m)})^T$. As a direct consequence of Lemma 1 obtain the following Theorem.

Theorem 1. *Let system (1) be smooth with partial relative degrees r=$(r_1, ..., r_m)$. Then for some constants $c_{r_i,0}, ..., c_{r_i,r_i-1}$, $d_{r_i,1}, ..., d_{r_i,r_i-1} > 0$, $i = 1, ..., m$ the following is true for each component σ_i. Over any time interval of the length τ with continuous control $u(t) \in \mathbb{R}^l$*

1. *if* $|\sigma_i^{(r_i)}| \le \delta_i$ *holds on the segment for some* $\delta_i > 0$, *then*

$$\max|\sigma_i| \le c_{r_i,0}\delta_i\tau^{r_i}, \max|\dot{\sigma}_i| \le c_{r_i,1}\delta_i\tau^{r_i-1}, ..., \max|\sigma^{(r_i-1)}| \le c_{r_i,r_i-1}\delta_i\tau; \tag{5}$$

2. *if* $|\sigma_i^{(r_i)}| \le \delta_i$ *and* $|\sigma_i| \le d_{r_i,0}\delta_i\tau^r$ *hold over the segment for some* $d_{r_i,0}$ *and* $\delta_i > 0$, *then*

$$\max|\dot{\sigma}| \le (d_{r_i,0}d_{r_i,1}+1)\delta_i\tau^{r_i-1}, ..., \max|\sigma^{(r_i-1)}| \le (d_{r_i,0}d_{r_i,r_i-1}+1)\delta_i\tau. \tag{6}$$

In particular, in the case of the SISO SMC problem, it follows from the Theorem that no one can expect an accuracy better than

$$\sigma = \mathcal{O}(\tau^r), \dot{\sigma} = \mathcal{O}\left(\tau^{r-1}\right), ..., \sigma^{(r-1)}| = \mathcal{O}(\tau)$$

in the sliding mode $\sigma \approx 0$, if $\sigma^{(r)}$ is separated from zero between the switchings. On the other hand, if $\sigma^{(r)}$ exists and is bounded, then keeping $\sigma \approx 0$ implies that also $\sigma^{(j)} \approx 0$, $j = 1, \ldots, r-1$.

As follows from the second statement of the Theorem, the r-SM accuracy can be higher than $\sigma^{(j)} = O(\tau^{r-j})$, if $\sigma^{(r)}$ is kept close to zero. For example, the implicit Euler method [1] actually increases the order of the real (i.e. approximate) SM due to the on-line estimation of the equivalent control, which allows to decrease the discontinuous component of the control. Unfortunately such estimation requires some additional system knowledge.

3.2 Accuracy of Sliding Modes in the Presence of Noises

Once more consider the uncertain SMC problem (1), (4). Recall that it is possible to provide for the exact finite-time establishment of the r-SM $\sigma \equiv 0$ using only output measurements [32,33].

Theorem 2. *Suppose that the control, based on the input measurements only, provides for the exact finite-time establishment of the r-SM* $\sigma \equiv 0$ *independently of the function h, satisfying* $\|h\| \le C$. *Let* σ_i *be measured with a Lebesgue-measurable noise* $\eta_i(t)$ *of the maximal magnitude* $\varepsilon_i \ge 0$, $\eta_i(t) \le \varepsilon_i$, *with unknown features,* $i = 1, \ldots, m$. *Then the worst-case SM accuracy cannot be better than*

$$\begin{aligned} &|\sigma_i| \le \varepsilon_i, |\dot{\sigma}| \le \tilde{c}_{i,1}\varepsilon_i^{\frac{r_i-1}{r_i}}, ..., |\sigma_i^{(r_i-1)}| \le \tilde{c}_{i,r_i-1}\varepsilon_i^{\frac{1}{r_i}}, \\ &\tilde{c}_{i,j} = \left(\frac{C}{m^{\frac{1}{2}}}\right)^{\frac{j}{r_i}}, \ j = 1, \ldots, r_i, \ i = 1, \ldots, m. \end{aligned} \tag{7}$$

Proof. Let the output satisfy the equation $\sigma^{(r)} = g(t,x)u$, i.e. (4) with $\|h\| \le C$, $h \equiv 0$. Let now the measured signal $\hat{\sigma}_i$ be of the form $\hat{\sigma}_i(t,x) = \sigma_i(t,x) + \varepsilon_i \cos((m^{-1/2}C/\varepsilon)^{1/r_i}t)$, i.e. the noise be equal $\varepsilon\cos((m^{-1/2}C/\varepsilon)^{1/r_i}t)$. Then the noisy signal $\hat{\sigma}_i$ satisfies

$$\sigma_i^{(r_i)} = \left(\cos\left(\left(\frac{C}{\varepsilon m^{\frac{1}{2}}}\right)^{\frac{1}{r}}t\right)\right)^{(r)} + g(t,x)u, \left|\left(\cos\left(\left(\frac{C}{\varepsilon m^{\frac{1}{2}}}\right)^{\frac{1}{r}}t\right)\right)^{(r)}\right| \le \frac{C}{m^{\frac{1}{2}}}.$$

Respectively, according to the assumptions, the control will successfully establish and keep $\hat{\sigma}_i \equiv 0$, which corresponds to $|\sigma_i^{(j)}| \leq \left(\frac{C}{\sqrt{m}}\right)^{\frac{j}{r}} \varepsilon^{\frac{r-j}{r}}$, $j = 0, \ldots, r-1$. □

Note that both Theorems 1, 2 are true for any τ and ε_i, neither τ nor ε_i need to be small.

Under the conditions of Theorem 2 let the output σ be measured with noises of the magnitudes $\varepsilon_i > 0$ at some discrete time instants, and let the control be updated at each sampling instant and remain constant between the sampling moments. Then the inequalities (5) hold independently of the noise presence over each sampling time interval of the length τ on which the inequality $|\sigma_i^{(r_i)}| > \delta_i > 0$ is held.

The situation is more complicated, if the maximal sampling step tends to zero. Some additional assumptions are needed to ensure that the corresponding solutions uniformly converge to solutions with continuous sampling. If such a convergence takes place, then, according to (7), the worst case SM accuracy is not better than $|\sigma_i^{(j)}| = O(\varepsilon_i^{\frac{r-j}{r}})$.

Example. The output σ of the SISO system (1), (8) of the relative degree r is traditionally nullified by keeping the constraint $\Sigma = \left(\frac{d}{dt} + \lambda\right)^{r-1} \sigma = 0$ in 1-SM $\Sigma \equiv 0$ [22,65,21]. Let τ be the sampling step, then $\Sigma = \mathcal{O}(\tau)$ is the only possible accuracy according to Theorem 1. The respective overall r-SM accuracy is $\sigma = \mathcal{O}(\tau), \dot{\sigma} = \mathcal{O}(\tau), ..., \sigma^{(r-1)}| = \mathcal{O}(\tau)$ [62]. It definitely satisfies (5), but is much worse than the best possible accuracy (6).

4 Homogeneous SM Control

In this section we develop SMC which realizes the best possible asymptotic SM accuracy (6), (7) calculated in the previous section. The corresponding controllers are developed for systems featuring well-defined relative degrees and are based on the homogeneity theory [5,13,14].

Definition 2. *A function $f : \mathbb{R}^n \to \mathbb{R}$ is called homogeneous of the degree q, $\deg f = q$, with the dilation $d_\kappa : (x_1, ..., x_n) \mapsto (\kappa^{m_1} x_1, ..., \kappa^{m_n} x_n)$, if the equality $f(x) = \kappa^{-q} f(d_\kappa x)$ holds for any $x \in \mathbb{R}^n$ and $\kappa > 0$. The numbers $\deg x_i = m_i$, $m_i > 0$, are called the homogeneity degrees (weights) of x_i.*

Definition 3 ([33]). *A differential inclusion $\dot{x} \in F(x)$, $F(x) \subseteq \mathbb{R}^n$, is homogeneous of the degree q, if it is invariant with respect to the homogeneity transformation $(t, x) \mapsto (\kappa^{-q} t, d_\kappa x)$. In other words, the equality $F(x) = \kappa^{-q} d_\kappa^{-1} F(d_\kappa x)$, holds for any $x \in \mathbb{R}^n$, $\kappa > 0$.*

Remark 1. Differential equations are considered here as a particular case, when $F(x)$ has only one element. The definition is then reduced to the classic definition [5]: $\deg \dot{x}_i = \deg x_i + q$. The nonzero homogeneity degree q of a vector field can always be scaled to ± 1 by an appropriate proportional change of the weights $m_1, ..., m_n$. Note that one can formally introduce the weight $\deg t = -q$, respectively $\deg \dot{x}_i = \deg x_i - \deg t$.

The inclusion $\dot{x} \in F(x)$, $x \in \mathbb{R}^n$, is called Filippov's, if $F(x)$ is nonempty, compact, convex and upper-semicontinuous. The latter means that the maximal distance of the points of $F(x)$ from the set $F(y)$ tends to zero as x tends to y.

The following is the main result on the Filippov homogeneous differential inclusions $\dot{x} \in F(x)$, $x \in \mathbb{R}^n$ that we use. Let the inclusion homogeneity degree be negative, then [33,43]

1. The asymptotic stability is equivalent to uniform finite-time stability and to the "contractivity" property [33]. The latter means that all solutions starting in some ball centered at 0 in some finite time T gather in a ball of a smaller radius (maybe to leave it afterwards).
2. In the presence of measurement noises with magnitudes $\varepsilon_1, \ldots, \varepsilon_n \geq 0$ and variable delays not exceeding $\tau > 0$ all indefinitely-extendable-in-time solutions of the disturbed inclusion

$$\dot{x} \in F(x_1(t + [-\tau, 0]) + \varepsilon_1[-1, 1], \ldots, x_n(t + [-\tau, 0]) + \varepsilon_n[-1, 1])$$

in finite time enter a compact $|x_i| \leq c_i \delta^{m_i}$, where $c_i > 0$, $\deg x_i = m_i$, $\delta = \max[\tau, \max_i(\varepsilon_i^{1/m_i})]$, $i = 1, \ldots, n$, to stay there forever.

4.1 Homogeneous SISO SM Control

Consider the SISO SMC problem (1) with smooth functions a and b. The system is understood in the Filippov sense [23]. Let the scalar output $\sigma(t, x)$ have the relative degree r, which means that

$$\sigma^{(r)} = h(t, x) + g(t, x)u, \tag{8}$$

where h, g are uncertain smooth functions, $g(t, x) \neq 0$. As usual [31,32,33] assume that h, g are bounded,

$$|h(t, x)| \leq C, \ 0 < K_m \leq g(t, x) \leq K_M, \tag{9}$$

Such bounds are true at least for any compact operational region. Any solution of (1) is assumed infinitely extendable in time, provided σ, its derivatives and u remain bounded along the solution.

The uncertain dynamics (8) can be replaced by the concrete differential inclusion

$$\sigma^{(r)} \in [-C, C] + [K_m, K_M]u. \tag{10}$$

Most r-SM controllers are build as controllers for (10) making $\overrightarrow{\sigma} = (\sigma, \dot{\sigma}, \ldots, \sigma^{(r-1)})$ vanish in finite time.

We want the closed-loop inclusion to be homogeneous with negative homogeneity degree. It is easy to see that with $C > 0$ inevitably $\deg \sigma^{(r)} = 0$, on the other hand, $\deg \sigma^{(r)} = \deg \sigma^{(r-1)} - \deg t$. Taking the system homogeneity degree -1, $\deg t = 1$, obtain that $\deg \sigma = r, \ldots, \deg \sigma^{(r-1)} = 1$. This homogeneity is called r-sliding homogeneity [33]. Respectively, the control

$$u = U(\overrightarrow{\sigma}) \tag{11}$$

is called r-sliding homogeneous, if $\deg u = 0$, i.e.

$$u(\sigma, \dot{\sigma}, ..., \sigma^{(r-1)}) \equiv u(\kappa^r \sigma, \kappa^{r-1}\dot{\sigma}, ..., \kappa\sigma^{(r-1)}). \tag{12}$$

holds for any $\kappa > 0$, $\overrightarrow{\sigma} \in \mathbb{R}^r$. Since the control is locally bounded [23], due to (12) it is also globally bounded. The right-hand side of the inclusion (10), (11) is assumed minimally enlarged at the points of the discontinuity of (11) to satisfy the Filippov conditions [23].

Replace $\sigma \in \mathbb{R}$ with $\omega \in \mathbb{R}$ in the following formulas, enabling the further usage of the controllers for different components of the vector output σ in the MIMO case. Let $\beta_{1,r}, \ldots, \beta_{r-1,r}$ be some predefined positive coefficients, and α be the chosen control magnitude. Then the simplest family of r-sliding homogeneous controllers of the form

$$u = -\alpha \Psi_{r-1,r}(\omega, \dot{\omega}, \ldots, \omega^{(r-1)}), \tag{13}$$

called embedded SM controllers [32], are provided by the following resursion. Let $d \geq r$, define

$$\begin{array}{l} \varphi_{0,r} = \omega,\ N_{0,r} = |\omega|^{1/r},\ \Psi_{0,r} = \operatorname{sign}\omega; \\ \varphi_{j,r} = \omega^{(j)} + \beta_{j,r} N_{j-1,r}^{r-j} \Psi_{j-1,r}, \Psi_{j,r} = \operatorname{sign}\varphi_{j,r}, \\ N_{j,r} = \left(|\omega|^{d/r} + |\dot{\omega}|^{d/(r-1)} + \ldots + |\omega^{(j-1)}|^{d/(r+1-j)}\right)^{1/d}. \end{array} \tag{14}$$

The following are valid parametric sets $\{\beta_{1,r}, \ldots, \beta_{r-1,r}\}, d_r$ for $r = 2, \ldots, 4$: $r = 2$, $\{1\}$, $d_1 = 1$; $r = 3$, $\{1, 2\}$, $d_2 = 6$; $r = 4$, $\{0.5, 1, 3\}$, $d_4 = 12$. They provide for the finite-time convergence to r-SM with sufficiently large α. It is further assumed that $\beta_{1,r}, \ldots, \beta_{r-1,r}$ are always properly chosen, which means that the differential equations $\varphi_{r-1,r} = 0$ are finite-time stable [41].

Another well-known family of SM controllers, called quasi-continuous SM controllers [34], features control continuous everywhere except the r-sliding set $\omega = \dot{\omega} = \ldots = \omega^{(r-1)} = 0$. Such controllers feature considerably less chattering. Other constructions of homogeneous HOSM controllers and the choice of parameters are considered in [33,41].

4.1.1 Differentiator

Any r-sliding homogeneous controller can be combined with an $(r-1)$th-order differentiator [32] producing an output feedback controller. Its applicability in this case is possible, since $\sigma^{(r)}$ is bounded due to the boundedness of the feedback function $u = -\alpha\Psi_{r-1,r}(\overrightarrow{\sigma})$ in (10).

Let the input signal $\phi(t)$ be a function consisting of a bounded Lebesgue-measurable noise with unknown features, and of an unknown base signal $\phi_0(t)$, whose k_dth derivative has a known Lipschitz constant $L > 0$. The following differentiator is presented in a recursive form and provides for the estimations z_j of the derivatives $\phi_0^{(j)}$, $j = 0, \ldots, k_d$:

$$\begin{array}{l} \dot{z}_0 = -\lambda_{k_d} L^{1/(k_d+1)} |z_0 - \phi(t)|^{k_d/(k_d+1)} \operatorname{sign}(z_0 - \phi(t)) + z_1, \\ \dot{z}_1 = -\lambda_{k_d-1} L^{1/k_d} |z_1 - \dot{z}_0|^{(k_d-1)/k_d} \operatorname{sign}(z_1 - \dot{z}_0) + z_2, \\ \ldots \\ \dot{z}_{k_d-1} = -\lambda_1 L^{1/2} |z_{k_d-1} - \dot{z}_{k_d-2}|^{1/2} \operatorname{sign}(z_{k_d-1} - \dot{z}_{k_d-2}) + z_{k_d}, \\ \dot{z}_{k_d} = -\lambda_0 L \operatorname{sign}(z_{k_d} - \dot{z}_{k_d-1}). \end{array} \tag{15}$$

The parameters λ_i of differentiator (15) are chosen in advance for each k_d. An infinite sequence of parameters λ_i can be built, valid for all natural k_d [32]. In particular, one can choose $\lambda_0 = 1.1$, $\lambda_1 = 1.5$, $\lambda_2 = 2$, $\lambda_3 = 3$, $\lambda_4 = 5$, $\lambda_5 = 8$ [34], which is enough for $k_d \leq 5$. In the absence of noises the differentiator provides for the exact estimations in finite time. Its error dynamics is homogeneous [32]. With sampling time periods not exceeding $\tau > 0$ and the maximal possible sampling error $\varepsilon \geq 0$ the accuracy $z_j - \phi_0^{(j)} = O(\max(\tau^{k_d+1-j}, \varepsilon^{(k_d+1-j)/(k_d+1)}))$ is ensured.

4.1.2 Differentiator Initialization

Although one can take arbitrary initial values of differentiator for its feedback application, it may considerably destroy the initial system transient, since at the beginning the differentiator outputs will have no resemblance to the right derivatives. The overall performance can be drastically improved if the initial values of the differentiator are chosen right.

The most simple method is to take $z_0(t_0) = \phi(t_0)$ and $z_i(t_0) = 0$, $i = 1, \ldots, k_d$, where t_0 is the first sampling time. Then one just provides some reasonable time for the differentiator convergence prior to the control application.

Another method, which we consider preferable, is to choose some initial time increments of the length Δt, consisting of a number of real sampling intervals. The $k_d + 1$ sampling values of the input ϕ are stored for k_d such successive time increments, and then the initial values of the differentiator are calculated by divided differences. During all this period the control is not applied, i.e. is kept at zero. Then the differentiator is practically already in the steady state from the very beginning. This initialization process is robust with respect to noises of the magnitude of the order Δt^{k_d+1}. One can still add a small additional time for the initial error elimination. One can also consider non-homogeneous differentiator modifications [4,17,37] with faster convergence. In that case the global system homogeneity is lost, which can affect the further results presented in the chapter.

4.1.3 Output Feedback Control

Assuming that the sequence λ_j, $j = 0, 1, ...$, is the same over the whole chapter, denote (15) by the equality $\dot{z} = D_{k_d}(z, \phi, L)$. Incorporating the $(r-1)$th order differentiator into the feedback equations, obtain the output-feedback r-sliding controller

$$u = U(z), \;\; \dot{z} = D_{r-1}(z, \sigma, L), \tag{16}$$

where $L \geq C + K_M \sup |U|$. Obviously, provided (10), (11) is finite-time stable, the output-feedback controller (16) ensures the finite-time establishment of the r-sliding mode $\overrightarrow{\sigma} = 0$. Moreover [33], if (11) is r-sliding homogeneous, the closed-loop inclusion (10), (16) is homogeneous with $\deg z_i = \deg \sigma^{(i)} = r - i$ and the system homogeneity degree -1. Respectively, if σ is measured with the sampling accuracy $\varepsilon \geq 0$ and the sampling intervals not exceeding $\tau > 0$, then the asymptotic SM accuracy $\sigma^{(j)} = O(\max(\tau^{r-j}, \varepsilon^{(r-j)/r}))$ is obtained.

Remark 2. All the accuracies here and further are formally calculated under the assumption that, whereas the sampling is discrete, the differential equations/

inclusions still take place between the samplings. In practice the internal dynamics of the controller (16) is realized as a discrete computer system. The simplest one-step-Euler realization has been shown to destroy the asymptotic accuracy of the differentiator (15) [40]. A special modification is needed to preserve the above accuracy [44]. Nevertheless, no modification is required, if the differentiator is applied in a feedback with a homogeneous SM controller, as in (15) [43]. In that case the standard accuracy is preserved.

4.2 Homogeneous MIMO SM Control

Once more consider dynamic system (1),

$$\dot{x} = a(t,x) + b(t,x)u, \;\; \sigma = \sigma(t,x), \tag{17}$$

but let now σ and u be vectors, $\sigma : \mathbb{R}^{n+1} \to \mathbb{R}^m$, $u \in \mathbb{R}^m$. The system is assumed to have the vector relative degree $r = (r_1, ..., r_m)$, $r_i > 0$. It means that the successive total time derivatives $\sigma_i^{(j)}$, $j = 0, 1, ..., r_i - 1$, $i = 1, ..., m$, do not contain controls, and can be used as a part of new coordinates [28]. Respectively, (8) turns to be a vector equation,

$$\sigma^{(r)} = h(t,x) + g(t,x)u, \tag{18}$$

where $\sigma^{(r)}$ denotes $(\sigma_1^{(r_1)}, ..., \sigma_m^{(r_m)})^T$, the functions h, and g are unknown and smooth. The function g is a nonsingular matrix.

Let g be represented in the form $g = K\bar{g}$, where $K > 0$ defines the "size" of the matrix g, and $\bar{g}$ corresponds to the matrix "direction". A nominal "direction" matrix $G(t,x)$ is assumed nonsingular and available in real time, so that

$$g(t,x) = K(t,x)(G(t,x) + \Delta g(t,x)), \;\; \left\|\Delta g G^{-1}\right\|_1 \le p < 1. \tag{19}$$

Here Δg is the uncertain deviation of $\bar{g}$ from G, and the norm $\|\cdot\|_1$ of the matrix $A = (a_{ij})$ is defined as $\|A\|_1 = \max\limits_i \sum\limits_j |a_{ij}|$. The estimation G can be any Lebesgue-measurable function, p is a known constant. Mark that similar assumptions are adopted in [19].

Similarly to (9), assume that the uncertain vector function h and the scalar function K are bounded,

$$\|h(t,x)\| \le C, \;\; 0 < K_m \le K(t,x) \le K_M, \tag{20}$$

where C, K_m, K_M are known constants.

Note that the avaialability of $G(t,x)$ in real time does not necessarily mean that $x(t)$ is available, and G is known analitically. For example, the aerodynamic characteristics of an aircraft are usually available as approximate table functions of the observable dynamic pressure and altitude.

Introduce a virtual control v,

$$u = G(t,x)^{-1} v. \tag{21}$$

Then dynamics (18) take the form

$$\sigma^{(r)} = h(t,x) + K(t,x)(I + \Delta g(t,x)G^{-1}(t,x))v, \tag{22}$$

where I is the unit matrix.

Introduce the notation $\overrightarrow{\sigma}_i = (\sigma_i, \dots, \sigma_i^{(r_i-1)})$, $\overrightarrow{\sigma} = (\overrightarrow{\sigma}_1, \dots, \overrightarrow{\sigma}_m)$. Choose the components of $v = (v_1, \dots, v_m)^T$ in the form of the embedded r_i-sliding homogeneous controller (13), (14)

$$v_i = -\alpha \Psi_{r_i-1,r_i}(\overrightarrow{\sigma}_i),\ i = 0, 1, \dots, m,\ u = G(t,x)^{-1}v, \tag{23}$$

where $\alpha > 0$. Now the closed-loop system satisfies the decoupled $(r_1, r_2, \dots, r_m)$-sliding homogeneous inclusion

$$\sigma_i^{(r_i)} \in [-C, C] - \alpha[K_m(1-p), K_M(1+p)]\Psi_{r_i-1,r_i}(\overrightarrow{\sigma}_i),\ i = 1, \dots, m, \tag{24}$$

with the weights $\deg \sigma_i^{(j)} = r_i - j$. According to Subsection 4.1, (24) is finite-time stable with sufficiently large α.

Respectively the output-feedback control gets the form

$$\begin{aligned} &v_i = -\alpha \Psi_{r_i-1,r_i}(z_i),\ i = 0, 1, \dots, m,\ u = G(t,x)^{-1}v, \\ &\dot{z}_i = D_{r_i-1}(L, \sigma_i, z_i),\ L \geq C + 2K_M\alpha. \end{aligned} \tag{25}$$

The closed-loop inclusion is still homogeneous with $\deg \sigma_i^{(j)} = \deg z_{i,j} = r_i - j$.

Theorem 3. *Let the MIMO system* (17), (18) *satisfy conditions* (19), (20). *Then output-feedback control* (25) *provides for the finite-time establishment and keeping of the r-SM* $\sigma = 0$. *Let* σ_i *be measured with the sampling accuracy* $\varepsilon_i \geq 0$, $i = 1, 2, \dots, m$, *and the sampling intervals not exceeding* $\tau > 0$, *then the asymptotic SM accuracy* $\sigma_i^{(j)} = O(\max(\tau^{r_i-j}, \varepsilon_i^{(r_i-j)/r_i}))$ *is obtained.*

The proof is straight-forward. As we have seen, the obtained SM asymptotics are the best possible. Note that one can here use quasi-continuous controllers [34,41], but the corresponding technique is more complicated [38], though provides for superior performance.

5 Adaptation of Sliding Modes

Consider SISO (8), (9) or MIMO (18), (19), (20) SMC problem. How to solve it if C, K_m, K_M are unknown, or even are variable in time?

It is quite clear that if the bounds change continuously with bounded velocity, then developed standard controllers (13) or (23) solve the problem with sufficiently large α at least locally in the space and time. From that observation the solution strategy is clear: one needs to increase α sufficiently fast. At some point α is so large that the system starts converging to the desired SM. Then one needs to detect the moment when the SM $\sigma \equiv 0$ is established. Obviously α can be too large at that time, which means a large control effort and terrible

chattering. So one gradually decreases α until the SM is lost. Then α is once more increased. If the rates of increasing and decreasing α are chosen right, the system will remain in real (approximate) SM all the time.

The above strategy is very natural and one finds a lot of papers, where it is applied fully or partially. Often one assumes that any sufficiently large α solves the problem. Then one never needs to decrease it. The problem is that in that case one risks increasing α indefinitely. Indeed, any error in detecting SM leads to additional increase of α.

There are two conclusions: first, there always should be some stopping, preferably decreasing mechanism for α; second, one needs a robust criterion for the detection of SM. Indeed one will never observe $\sigma \equiv 0$ in real life. One of the popular methods [66] is to apply the Utkin filter [65] for extraction of the equivalent control, and to use it for the regulation of α. The problem with this approach is that both SM detection and extraction of the equivalent control remain not clear and not robust. Another approach [60] is just detecting that σ is sufficiently small. Since the derivatives of σ are not taken into account, it leads to false detection of SM. Taking the derivatives into account allows to detect a real (approximate) r-SM, but requires direct derivatives' measurements or additional information for differentiator application.

We adopt here another approach [10,63]. If α is sufficiently large with respect to uncertainties and changes with locally bounded velocity, then the dynamics around the r-SM manifold is locally homogeneous in space and time. Therefore the optimal SM accuracy asymptotics of Section 4 is to be observed. The approach requires taking into account switching imperfections and noises, which makes the approach robust from the very beginning. According to Theorem 1, the accuracy is proportional to α, provided α is at least of the order of $||h||$. Since often only σ is available, another idea is to replace calculation/observation of σ derivatives with observing the inequality $|\sigma| \leq \mu\alpha\tau^r$ for sufficiently long time. Obviously, the presence of sampling noises not exceeding $\gamma\alpha\tau^r$ in their magnitude does not interfere with this reasoning, if γ is sufficiently small compared with μ. Demonstrate this approach on the twisting-controller adaptation [10].

Consider a SISO system (1) of the relative degree 2. In other words

$$\ddot{\sigma} = h(t,x) + g(t,x)u, \tag{26}$$

where $h(t,x)$ and $g(t,x)$ are some smooth functions. It is supposed that for some positive constants h_d, h_m, g_m, g_M, $g_d > 0$ the following inequalities hold:

$$\begin{array}{l} |\dot{h}/h| \leqslant h_d \text{ with } |h| \geqslant h_m,\ |\dot{h}| \leqslant h_{dm} \text{ with } |h| \leqslant h_m, \\ g_m \leqslant g \leqslant g_M,\ |\dot{g}/g| \leqslant g_d. \end{array} \tag{27}$$

Only h_d and g_d are assumed known. Since there is no constant or functional bound of $\dot{h}$, introduction of $\dot{u}$ as a new control does not solve the problem by standard 3-sliding control methods.

Let $\tau > 0$ be the sampling period. Choose the control in the form

$$u = -\alpha(\operatorname{sign}\sigma + \beta \operatorname{sign}\dot{\sigma}),\ 0.5 < \beta < 1, \tag{28}$$

where β is a constant control parameter. With constant α a standard twisting controller [31] is obtained. Here $\dot{\sigma}$ is supposed available, the control value remains constant between the measurements. Since h/g *can be unbounded*, no concrete constant value of α solves the stated problem. The adaptation of α recently proposed by [30] is not applicable here due to the unboundedness of h. It also does not provide for the expected accuracy $O(\tau^2)$ (Sections 3, 4) characteristical for 2-sliding modes.

Introduce a real 2-sliding mode criterion. Choose a natural number N_t and some $\mu > 0$. Let $t \in [t_i, t_{i+1})$, and define

$$c_{SM}(t) = \begin{cases} 1 \text{ if } \forall t_j \in [t - N_t\tau, t] : \ |\sigma(t_j)| \leqslant \mu\alpha(t_j)\tau^2 \\ -1 \text{ if } \exists t_j \in [t - N_t\tau, t] : \ |\sigma(t_j)| > \mu\alpha(t_j)\tau^2 \end{cases}, \tag{29}$$

where t_j are the sampling instants. *The 2-sliding mode criterion is considered satisfied if* $c_{SM} = 1$.

It can be shown that with $\beta \in (0.5, 1)$ and constant α, g, h the convergence is assured with $\alpha > \frac{1}{1-\beta}|h/g|$, whereas the fast divergence is assured with $\alpha < \frac{1}{1-\beta}|h/g|$. Thus, at the moment when the divergence is detected a switch from α to $q\alpha$ is natural, where $q > \frac{1+\beta}{1-\beta}$ is a predefined constant. Then one can expect that the convergence will be immediately restored. The following adaptation law is a modification of [10].

Choose some $\alpha_m > \alpha_{mm} > 0$. Let the gradual adaptation law be

$$\dot{\alpha} = \begin{cases} \lambda_+\alpha \text{ if } \alpha > \alpha_m,\ c_{SM} = 1, \\ -\lambda_-\alpha \text{ if } \alpha > \alpha_m,\ c_{SM} = -1, \\ -c_{SM}\lambda_m \text{ if } \alpha_{mm} < \alpha \leqslant \alpha_m, \\ \lambda_m \text{ if } \alpha \leqslant \alpha_{mm}, \end{cases} \quad \alpha(0) \geq \alpha_{mm}, \tag{30}$$

where λ_+, λ_-, λ_m are positive adaptation parameters. Thus, α is never less than α_{mm}, which is taken arbitrarily small.

In addition, an instant increment is implemented at each sampling instant t_i, at which the 2-sliding criterion changes from 1 to -1:

$$\alpha(t_i) = \begin{cases} q\alpha(t_i - 0) \text{ if } c_{SM}(t_{i-1}) = 1 \,\&\, c_{SM}(t_i) = -1, \\ \alpha(t_i - 0) \text{ if } c_{SM}(t_{i-1}) \neq 1 \text{ or } c_{SM}(t_i) \neq -1. \end{cases} \tag{31}$$

Theorem 4. *Let σ be sampled with time step τ and a noise not exceeding $\gamma\tau^2$ in absolute value, where the constant $\gamma > 0$ is another parameter of the problem. Choose $\lambda_- > g_d + h_d$, $\lambda_+ > g_d + h_d$. Then for some $q_* > q/(1-\beta)$ and any sufficiently large μ and sufficiently large $N_t \geq 4$ (chosen after μ) with sufficiently small τ the positive parameter $\alpha(t)$ features local maxima, which do not exceed $\max[q_*|h|/g, K_{mm}]$ taken at the same time. Respectively the accuracy $|\sigma| \leq \nu_1\tau^2\alpha(t)$, $|\dot{\sigma}| \leq \nu_2\tau\alpha(t)$ is established in finite time. The constants q_*, ν_1, ν_2 only depend on the parameters of the algorithm and parameters of the assumptions.*

Here N_t can be chosen in advance independently of the actual system, μ depends on γ. Obviously, $\mu > \gamma$ is necessary. There are no restrictions on λ_m, α_{mm} and α_m.

It can be proved that with sufficiently large λ_m the gain $\alpha(t)$ follows $|h|/g$. If λ_m is not large enough, only peak values of α are restricted according to the Theorem. If $\dot{\sigma}$ is not available, the control is chosen in the form $u = -\alpha(\operatorname{sign}\sigma + \beta \operatorname{sign}\Delta\sigma)$, where $\Delta\sigma$ is the increment of σ over the last sampling period.

Example. Consider an academic example

$$\dot{y} = \begin{cases} \operatorname{sign} s(t) & \text{with } |y| \le 100, \\ -y & \text{with } |y| > 100, \end{cases}$$
$$\ddot{\sigma} = y + (2 + \cos t)u.$$

Here $s(t)$ is a standard Gaussian white noise with the distribution (0,1). Obviously, $\alpha = 200$ would be enough to establish 2-SM $\sigma \equiv 0$, but it would lead to strong chattering. The algorithm (28), (29), (30), (31) is applied with artificial saturation of α at 200. Without such saturation α becomes so large during the transient that its graph lacks observable details in the steady state. The parameter $\beta = 2/3$ is taken, and $q = 6 > \frac{1+\beta}{1-\beta} = 5$. Other controller parameters $\mu = 30$, $N_t = 10$, $\alpha_m = 1$, $\alpha_{mm} = 0.1$, $\lambda_- = 7$, $\lambda_+ = 2$, $\lambda_m = 4$ are taken. The initial values are $\sigma(0) = 10$, $\dot{\sigma}(0) = 1$, $y(0) = 5$, $\alpha(0) = 0.1$.

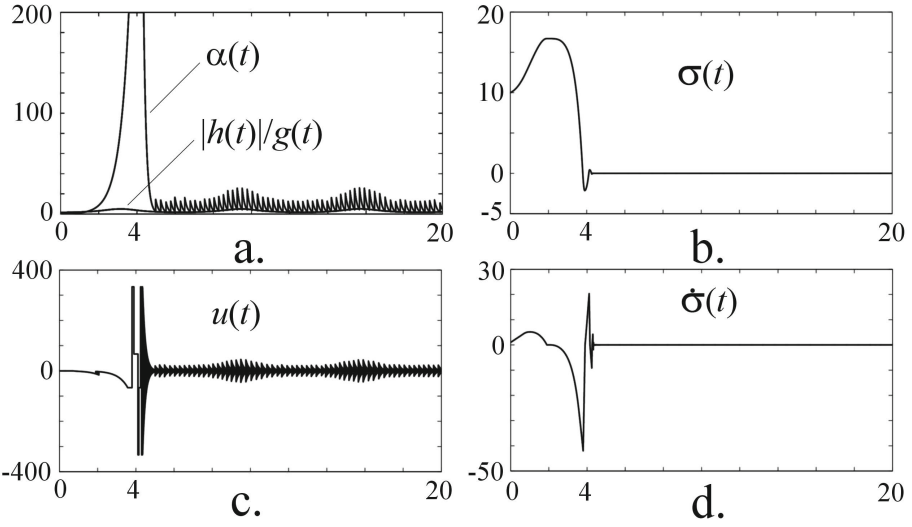

Fig. 1. 2-SM twisting adaptation: a. the adaptation gain maxima do not exceed $6|h|/g$, b. graph of σ, c. graph of $\dot{\sigma}$, d. graph of u.

The graphs of α and of $|h|/g$ are shown in Fig. 1a. For the first time the 2-sliding mode criterion is satisfied at about $t = 4.5$, and at $t = 5$ the criterion is violated. It is clearly seen from Fig. 1a that the maxima of α do not exceed $q|h|/g$, $q = 6$. The local 2-sliding accuracy of σ is proportional to τ^2 and $\alpha(t)$, and is practically equal $\mu\alpha(t)\tau^2 = 30\alpha(t)\tau^2 \approx 180|h(t)|/g(t)\tau^2$. The graphs of σ, $\dot{\sigma}$, u are demonstrated in Fig. 1b,c,d respectively.

6 Acceleration of SM Convergence

Transient time restrictions often appear important in SM control. In particular, in control of switched systems [42], the natural requirement is that the SM be established before the next switch, so that the dynamics uncertainty be effectively removed. Also in observation one often needs to know in advance when the observer transient is over.

Thus, the transient time of a HOSM controller is often required to be bounded by some predefined function of initial conditions. Ideally the maximal convergence time is to be independent of the initial conditions even for unbounded operational regions. The corresponding notions of *fixed-time* or *uniformly exact* stability and convergence were introduced in [4,16,17,54]. Meantime, such convergence has been obtained for observers [4,17] and disturbed linear time-invariant systems [54]. Unfortunately, recent results [36] show that fixed-time stable systems are not feasible over really large operational regions, if the sampling rate is apriory bounded. The reason is that even for small sampling periods, the system makes enormous jumps between the samplings at sufficiently distant points, and even can escape to infinity faster than any exponent. Therefore, the larger the region the smaller the sampling period is to be taken, and only semiglobal convergence is obtained in practice. Large fast-changing controls also usually exclude observation of the output derivatives, which makes output-feedback control impossible.

The main idea proposed here is to realize an arbitrarily fast convergence rate by successively switching from one homogeneous SM controller to another. In particular, a predefined upper bound for the convergence time to SM can be satisfied, which is provided as a function of the initial conditions. Between such switches one can apply the differentiator (15), providing for the output-feedback control. The differentiator parameters switch together with the the controller, whereas the derivative estimations are kept intact.

6.1 Twisting Acceleration

Consider a SISO system (1), (8), (9) of the relative degree $r = 2$ and the twisting controller (28) [31] with $\beta \in (0, 1)$.

With $\alpha > \frac{C}{(1-\beta)K_m}$ the function $\sigma(t)$ oscillates [31], and the trajectories rotate around the origin in the plane $\sigma, \dot{\sigma}$ (Fig. 2a). The trajectory starts at the point $(\sigma_0, \dot{\sigma}_0)$ at the moment t_0. The intersections σ_k, $k = 1, 2, ...$, of the trajectory with the σ-axis correspond to local extrema of σ at the time instants t_k. The respective intersections of the trajectory with the $\dot{\sigma}$-axis in the time range (t_k, t_{k+1}) are denoted $\dot{\sigma}_k$ (Fig. 2a). Note that with $k > 0$ the values σ_k and $\dot{\sigma}_k$ correspond to different time instants.

The problem is to provide for the needed convergence rate by properly changing the coefficient α at each intersection σ_k of the trajectory with the σ-axis at the times t_k, $k = 1, 2, ...$

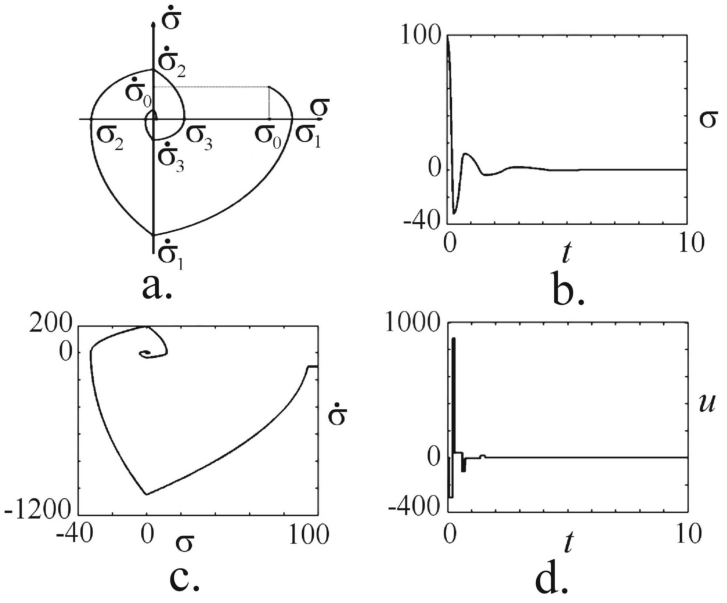

Fig. 2. Accelerated twisting controller: theoretical trajectory and notation (a), simulation with initial values $(\sigma(0), \dot{\sigma}(0)) = (100, -100)$ (b,c,d).

Let

$$(1-\beta)K_M < K_m(1+\beta),\ \omega_*(\alpha) = \frac{(1-\beta)\alpha K_M + C}{(1+\beta)\alpha K_m - C}, \tag{32}$$

and fix some α_*, such that

$$\omega_*(\alpha_*) < 1,\ \ \alpha_* > \tfrac{C}{(1-\beta)K_m}. \tag{33}$$

Theorem 5. *Let* (32), (33) *hold. Then with any* $\gamma > 0$, $q \geq 1$ *the output-feedback control*

$$u = -\alpha_k(\operatorname{sign} z_0 + \beta \operatorname{sign} z_1) \text{ with } t \in [t_k, t_{k+1}),$$
$$\alpha_k = \max\{\alpha_*, \gamma|\sigma_k|^\rho\},\ k = 0, 1, ...,$$
$$\dot{z} = D_1(z, \sigma, L_k),\ L_k = q(C + K_M\alpha_k(1+\beta))$$

provides for the fixed-time convergence to 2-SM $\sigma = 0$ *with* $\rho > 1$, *and just for accelerated finite-time convergence with* $0 < \rho \leq 1$.

The standard optimal 2-SM accuracy (Theorem 3) is obtained in the presence of noises and discrete sampling, since in a vicinity of the SM the dynamics coincides with that of a standard twisting controller. The differentiator is initialized as in Subsection 4.1.2. Note that with $\rho > 1$ a compact operational region should

be chosen [36]. The proof consists in estimation of one rotation time and showing that in the backward time the times of rotations coming from infinity are dominated from above by a converging geometric series.

6.1.1 Simulation Example

Consider an academic example

$$\ddot{\sigma} = \cos e^t + \left(2 - \sin t^2\right) u.$$

Dynamics of σ satisfy $\ddot{\sigma} \in [-C, C] + [K_m, K_M]u$, where $C = 1,\ K_m = 1,\ K_M = 3$. Integration is performed by the Euler method, being the only reliable method with discontinuous dynamics. The sampling step $\tau = 10^{-4}$ is taken equal to the integration step. Two sampling intervals of the length $\Delta t = 0.01$ are applied for the initialization of the differentiator, and additional time 0.05 is added for the final differentiator convergence with $L = 2C$, afterwards $L_k = 2(C + K_M\alpha_k)$. The sampling noise $\eta(t) = 0.005\sin(137579.23t + 0.231375)$ is introduced.

Let $\beta = \frac{2}{3}$, $\gamma = 0.6$, $\alpha_* = 6$, $\rho = 3$. The performance of the algorithm with the initial conditions $\sigma(0) = 100$, $\dot{\sigma}(0) = -100$ is demonstrated in Fig. 2b,c,d. The differentiator initialization is clearly observed in the trajectory graph Fig. 2c. The accuracies $|\sigma| \le 0.0024$, $|\dot{\sigma}| \le 0.032$ are obtained after the convergence time of about 9.

6.2 General Case: Accelerated HOSM MIMO SM Control

6.2.1 Once More on MIMO SM Homogeneity

Consider a MIMO dynamic system (17), (18), (19), (20). Recall that the relative degree is $(r_1, \dots, r_m)$ and a virtual control $v = G(t,x)u$ is introduced,

$$u = G(t,x)^{-1}v,\ v_i = -\alpha\Psi_{r_i-1,r_i}(\overrightarrow{\sigma}_i)),\ i = 0, 1, ..., m,$$

practically decoupling the system. Here Ψ_{r_i-1,r_i} is an embedded r_i-sliding homogeneous controller (14) [32,33], $\alpha > 0$, $\overrightarrow{\sigma}_i = (\sigma_i, \dot{\sigma}_i, ..., \sigma_i^{(r_i-1)})$, $\Psi_{r_i-1,r_i}(\overrightarrow{\sigma}_i) = \pm 1$. Thus, solutions of (17), (18), (19), (20), (23) satisfy the inclusion (24)

$$\sigma_i^{(r_i)} \in [-C, C] - \alpha[K_m(1-p), K_M(1+p)]\Psi_{r_i-1,r_i}(\overrightarrow{\sigma}_i),\ i = 1, \dots, m, \quad (34)$$

with the weights $\deg \sigma_i^{(j)} = r_i - j$. Inclusion (34) has the homogeneity degree -1 and is finite-time stable (Theorem 3).

6.2.2 Choosing the Convergence Rate

Define the so-called homogeneous norms

$$||\overrightarrow{\sigma}_i||_h = |\sigma_i|^{\frac{1}{r_i}} + |\dot{\sigma}_i|^{\frac{1}{r_i-1}} + ... + |\sigma_i^{(r_i-1)}|,\ i = 1, ..., m,$$
$$||\overrightarrow{\sigma}||_h = ||\overrightarrow{\sigma}_1||_h + ||\overrightarrow{\sigma}_2||_h + ... + ||\overrightarrow{\sigma}_m||_h.$$

Let R_k be an arbitrary monotonously growing sequence $R_k \to \infty$, $R_0 = 0$, $k = 0, 1, 2, ...$ And let $T(R)$ be a monotonously increasing positive-definite

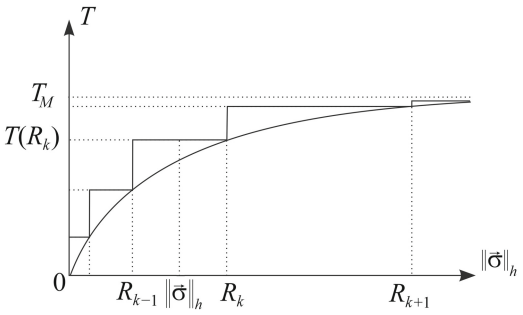

Fig. 3. The convergence-rate function T, and the piece-wise-constant convergence-time estimation. The case of the fixed-time convergence, $\lim_{R\to\infty} T(R) = T_M < \infty$.

convergence-rate function $R \geq 0,\ T(0) = 0$. The idea is to develop such a control that all trajectories starting in the region $||\overrightarrow{\sigma}||_h \leq R_k$ converge to the r-sliding mode in the time not exceeding $T(R_k)$ (Fig. 3).

Consider control of the form

$$\begin{array}{ll} r_M = \max_i r_i,\ r_m = \min_i r_i,\ \mu > 1 \\ v_i \ \ = \alpha\mu^{r_M}\Psi_{r_i-1,r_i}(\overrightarrow{\sigma}_i\mu^{-r_M})). \end{array} \tag{35}$$

Let the stabilization time of any trajectory of (34), starting within the homogeneous disk $||\overrightarrow{\sigma}||_h \leq 1$ belong to $[T_*, T^*]$, $0 < T_* \leq T^*$. Note that T_*, T^* exist due to [33,36]. The following Lemma constitutes the idea of the convergence acceleration.

Lemma 2. *Control (35) provides for the convergence of any trajectory of the system starting in the region $||\overrightarrow{\sigma}||_h \leq R$ to the r-sliding mode $\overrightarrow{\sigma} = 0$ in some time belonging to $[RT_*/\mu^{\frac{r_M}{r_m}}, RT^*/\mu]$.*

The proof is based on a time transformation [38]. Define the functions

$$n(\overrightarrow{\sigma}) = k \Leftrightarrow ||\overrightarrow{\sigma}||_h \in [R_{k-1}, R_k),\ k = 0, 1, ..., \tag{36}$$

$$\mu_M(\overrightarrow{\sigma}) = \frac{\gamma R_{n(\overrightarrow{\sigma})}}{T(R_{n(\overrightarrow{\sigma})}) - T(R_{n(\overrightarrow{\sigma})-1})},\ \gamma > 0. \tag{37}$$

Introduce the variable $\mu(t)$ that is left-hand continuous and features the dynamics

$$\begin{array}{ll} \mu(t+0) = \max\{1, \min[\mu(t), \mu_M(\overrightarrow{\sigma})]\}, \\ \mu(t_0) \ \ \ = \max\{1, \mu_M(\overrightarrow{\sigma})\}. \end{array} \tag{38}$$

It is easy to see that μ is piece-wise constant and monotonously decreases, while $\mu \geq 1$ is always preserved.

It follows from Lemma 2, Fig. 3 that the control (35), (36), (37), (38) provides for the convergence time $T_{conv}(t)$ to the SM $\sigma \equiv 0$, which satisfies $T_{conv}(t) \leq \frac{T^*}{\gamma} T(R_{n(\vec{\sigma}(t,x(t)))})$ along the trajectory [38]. The fixed-time convergence is obtained if $\lim_{R\to\infty} T(R) = T_M < \infty$.

Unfortunately, fixed-time convergence controls is difficult to realize [36]. Much "softer" acceleration is obtained, if (37) is replaced with

$$\mu_M(\overrightarrow{\sigma}) = \frac{\gamma R_{n(\overrightarrow{\sigma})}}{T(R_{n(\overrightarrow{\sigma})})},\ \gamma > 0. \tag{39}$$

Theorem 6. *Control* (35), (36), (39), (38) *features the convergence time* T_{conv} *satisfying the inequality* $T_{conv} \le \frac{T^*}{\gamma}\sum_{k=1}^{n(\overrightarrow{\sigma}(t_0))} T(R_k)$, *where* t_0 *is the initial moment. In particular, the simple estimation* $T_{conv} \le \frac{T^*}{\gamma} n(\overrightarrow{\sigma}(t_0))T_M$ *is obtained with* $\lim_{R\to\infty} T(R) = T_M < \infty$. *In the case* $R_k = R_1\lambda^{k-1}$, $k = 1, 2, \ldots$, *the estimation is*

$$T_{conv}(t) \le \frac{T^* T_M}{\gamma}\log_\lambda\left(\frac{\left\|\overrightarrow{\sigma}(t_0)\right\|_h}{R_1}\right). \tag{40}$$

Note that $\|\overrightarrow{\sigma}(t_0)\|_h$ grows slower than the Euclidian norm $\|\overrightarrow{\sigma}(t_0)\|$, so the convergence rate (40) is faster than exponential.

Proof. Consider the control (35). It follows from Lemma 2 that $\Delta t_k \le \frac{R_k T^*}{\mu}$, where Δt_k is the time needed for a trajectory starting in $\|\overrightarrow{\sigma}(t_0)\| \le R_k$ to enter $\|\overrightarrow{\sigma}(t_0)\| \le R_{k-1}$. Taking into account (39) obtain the Theorem statements. □

Fix any $q \ge 1$, then the output-feedback control gets the form

$$\begin{aligned} v_i &= \alpha\mu^{r_M}\Psi_{r_i-1,r_i}(z_i\mu^{-r_M})),\\ \dot{z}_i &= D_{r_i-1}(z_i, \sigma_i, L_k),\ L_k = q\alpha\mu^{r_M}(C + 2K_M). \end{aligned} \tag{41}$$

Mark that one needs appropriate differentiator initialization (Subsection 4.1.2). With discrete measurements the sampling period is to be small enough, which may turn the control into a semiglobal one, especially, if the fixed time convergence is imposed [36]. The standard accuracy of Theorem 3 is obtained in the presence of noises and discrete sampling.

6.2.3 Example

Consider an academic MIMO control system

$$\begin{pmatrix} \dddot{\sigma}_1 \\ \ddot{\sigma}_2 \end{pmatrix} = \begin{pmatrix} 2\cos(\sigma_1\dot{\sigma}_2 + 5.1t) \\ -\cos(\sigma_1\sigma_2 - 3.2t) \end{pmatrix} +$$
$$(1 + \tfrac{1}{2}\cos t)\begin{pmatrix} 2 + 0.1\sin\dot{\sigma}_2 + \sin t & 0.3\sin(\dot{\sigma}_2 + t) \\ 0.5\sin(\ddot{\sigma}_1 - 2t) & 3 - 0.1\sin\ddot{\sigma}_1 - \cos 1.7t \end{pmatrix}\begin{pmatrix} u_1 \\ u_2 \end{pmatrix},$$
$$G = \begin{pmatrix} 2 + \sin t & 0 \\ 0 & 3 - \cos 1.7t \end{pmatrix},\ K \in [0.5, 2.5].$$

Obviously, $r = (3, 2)$, $r_M = 3$. Standard embedded $(3, 2)$-sliding controllers [32] are taken with $\alpha = 20$. The resulting output-feedback controller is

$$u = G^{-1}v = \begin{pmatrix} 2 + \sin t & 0 \\ 0 & 3 - \cos 1.7t \end{pmatrix}^{-1}\begin{pmatrix} v_1 \\ v_2 \end{pmatrix},$$
$$v_1 = -20\mu^3\,\mathrm{sign}[s_2\mu^{-2} + 2(|s_1\mu^{-1}|^3 + s_0^2)^{1/6}\,\mathrm{sign}(s_1\mu^{-1} + |s_0|^{1/2}\,\mathrm{sign}\,s_0)],$$
$$v_2 = -20\mu^3\,\mathrm{sign}(w_1\mu^{-1} + |w_0|^{1/2}\,\mathrm{sign}\,w_0),$$

where s and w are the outputs of the differentiators (15) of the orders 1 and 2,

$$\begin{aligned}
\dot{s}_0 &= -2L^{1/3}|s_0 - \sigma_1|^{2/3}\,\mathrm{sign}(s_0 - \sigma_1) + s_1,\\
\dot{s}_1 &= -1.5L^{1/2}|s_1 - \dot{s}_0|^{1/2}\,\mathrm{sign}(s_1 - \dot{s}_0) + s_2,\\
\dot{s}_2 &= -1.1L\,\mathrm{sign}(s_2 - \dot{s}_1);\\
\dot{w}_0 &= -1.5L^{1/2}|w_0 - \sigma_2|^{1/2}\,\mathrm{sign}(w_0 - \sigma_2) + w_1,\\
\dot{w}_1 &= -1.1L\,\mathrm{sign}(w_0 - \sigma_2),\ L = 40\mu^3,
\end{aligned}$$

μ is defined by (36), (38) and (37) or (39).

The differentiators are initialized by finite differences using 3 samplings taken at the times 0, 0.01 and 0.02. The control is applied starting from $t = 1$ in order to provide some time for the differentiators' convergence. The integration is carried out according to the Euler method.

The non-accelerated convergence (with $\mu = 1$) from initial conditions $\vec{\sigma}_1(0) = (120, 100, 90)$, $\vec{\sigma}_2(0) = (-120, -100)$ takes about 70 time units. The expected accuracies are to satisfy the formula $\sigma_i^{(j)} = O(\tau^{r_i - j})$, $i = 1, 2$, $j = 0, \ldots, r_i - 1$.

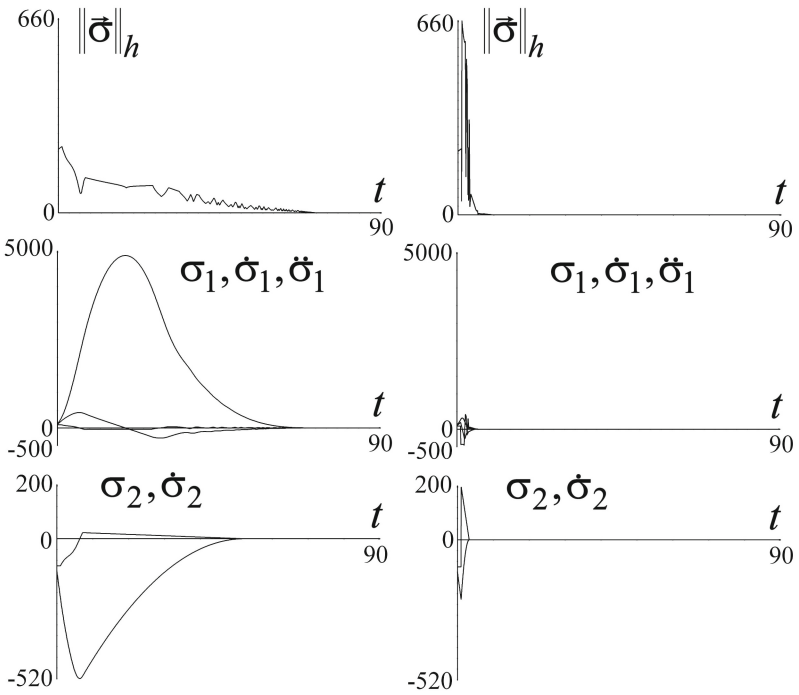

Fig. 4. Homogeneous MIMO SMC performance on the left and its acceleration on the right. The same initial conditions $(120, 100, 90)$, $(-120, -100)$ and scales are taken.

Indeed, the SM accuracies $|\sigma_1| \leq 2.8 \cdot 10^{-8}$, $|\dot{\sigma}_1| \leq 1.5 \cdot 10^{-5}$, $|\ddot{\sigma}_1| \leq 2.1 \cdot 10^{-2}$, $|\sigma_2| \leq 1.4 \cdot 10^{-5}$, $|\dot{\sigma}_2| \leq 2.0 \cdot 10^{-2}$ are obtained with $\tau = 10^{-4}$, and $|\sigma_1| \leq 2.1 \cdot 10^{-11}$, $|\dot{\sigma}_1| \leq 1.2 \cdot 10^{-7}$, $|\ddot{\sigma}_1| \leq 1.8 \cdot 10^{-3}$, $|\sigma_2| \leq 0.81 \cdot 10^{-7}$, $|\dot{\sigma}_2| \leq 1.4 \cdot 10^{-3}$ are obtained with $\tau = 10^{-5}$. Similar accuracies are got also by all accelerated algorithms.

Now take $R_k = 0.5e^k$, $\gamma = 1$ and the convergence-rate function $T(R) = 0.1RT_M/(1 + 0.1R)$, $T_M = 15$. The control (35), (37), (38) would provide here for the fixed-time convergence, but its reliable simulation requires $\tau = 10^{-8}$ or less. Instead of (37) take (39). The resulting convergence with $\tau = 10^{-5}$ is demonstrated in Fig. 4 and takes only about 10 time units. In order to clarify the comparison, the graphs for the non-accelerated and accelerated convergence are demonstrated side by side in the same scale.

7 Conclusions

The best and worst SM accuracy asymptotics are shown to be directly determined by the order of the SM, both in the SISO and MIMO cases. Homogeneous SM control is extended to the MIMO uncertain systems. Asymptotic accuracies of the output-feedback homogeneous MIMO SMC are calculated in the presence of noises and discrete sampling, and are shown to be the best possible.

The observation of the standard output accuracy of homogeneous HOSM control over a sufficiently long time interval implies keeping the standard accuracies also of its derivatives (Theorem 1). Thus, such observation can be naturally utilized for the detection of a real (approximate) HOSM, which can be used in SM adaptation. An example of such twisting-controller adaptation is presented.

Any system with a homogeneous MIMO SM can be accelerated providing for arbitrarily fast convergence to the SM. The convergence time can be kept bounded from above by a function of the homogeneous norm of initial conditions. It can be done also by output-feedback control. The optimal SM accuracy is preserved in any case.

Acknowledgement. The authors would like to express their profound respect for Professor Kaynak and utmost appreciation of his contributions to sliding-mode control theory. Professor's Kaynak results lie at the foundation of the theory. In this respect we would especially like to single out his seminal paper [58], one of the first papers to demonstrate the complicated nature of discretized sliding-mode motions. Moreover, such his recent papers as [64,67,48] indicate new developments and trends in the practical realization and application of sliding-mode control systems.

References

1. Acary, V., Brogliato, B., Orlov, Y.: Chattering-free digital sliding-mode control with state observer and disturbance rejection. IEEE Transactions on Automatic Control. 57(5), 1087–1101 (2012)
2. Alwi, H., Edwards, C.: An adaptive sliding mode differentiator for actuator oscillatory failure case reconstruction. Automatica 49(2), 642–651 (2013)

3. Angulo, M., Fridman, L., Levant, A.: Robust exact finite-time output based control using high-order sliding modes. International Journal of Systems Science 42(11), 1847–1857 (2011)
4. Angulo, M., Moreno, J., Fridman, L.: Robust exact uniformly convergent arbitrary order differentiator. Automatica 49(8), 2489–2495 (2013)
5. Bacciotti, A., Rosier, L.: Liapunov Functions and Stability in Control Theory. Springer, London (2005)
6. Bandyopadhyay, B., Sivaramakrishnan, J.: Discrete-time sliding mode control: a multirate output feedback approach. Springer (2006)
7. Bartolini, G.: Chattering phenomena in discontinuous control systems. International Journal of Systems Science 20, 2471–2481 (1989)
8. Bartolini, G., Damiano, A., Gatto, G., Marongiu, I., Pisano, A., Usai, E.: Robust speed and torque estimation in electrical drives by second-order sliding modes. IEEE Transactions on Control Systems Technology 11(1), 84–90 (2003)
9. Bartolini, G., Ferrara, A., Usai, E.: Chattering avoidance by second-order sliding mode control. IEEE Transactions on Automatic Control 43(2), 241–246 (1998)
10. Bartolini, G., Levant, A., Plestan, F., Taleb, M., Punta, E.: Adaptation of sliding modes. IMA Journal of Mathematical Control and Information 30(3), 285–300 (2013)
11. Bartolini, G., Pisano, A.E.P., Usai, E.: A survey of applications of second-order sliding mode control to mechanical systems. International Journal of Control 76(9/10), 875–892 (2003)
12. Bartolini, G., Punta, E., Zolezzi, T.: Approximability properties for second-order sliding mode control systems. IEEE Transactions on Automatic Control 52(10), 1813–1825 (2007)
13. Bhat, S., Bernstein, D.: Finite-time stability of continuous autonomous systems. SIAM Journal of Control and Optimization 38(3), 751–766 (2000)
14. Bhat, S., Bernstein, D.: Geometric homogeneity with applications to finite-time stability. Mathematics of Control, Signals and Systems 17(2), 101–127 (2007)
15. Boiko, I., Fridman, L.: Analysis of chattering in continuous sliding-mode controllers. IEEE Transactions on Automatic Control 50(9), 1442–1446 (2005)
16. Cruz-Zavala, E., Moreno, J., Fridman, L.: Second-order uniform exact sliding mode control with uniform sliding surface. In: Proc. of the 50th IEEE Conference on Decision and Control, Orlando, FL, USA, December 12-15, pp. 4616–4621 (2011)
17. Cruz-Zavala, E., Moreno, J., Fridman, L.: Uniform robust exact differentiator. IEEE Transactions on Automatic Control 56(11), 2727–2733 (2012)
18. Cruz-Zavala, E., Moreno, J., Fridman, L.: Uniform sliding mode controllers and uniform sliding surfaces. IMA Journal of Mathematical Control and Information 29(4), 491–505 (2012)
19. Defoort, M., Floquet, T., Kokosy, A., Perruquetti, W.: A novel higher order sliding mode control scheme. Systems & Control Letters 58(2), 102–108 (2009)
20. Dinuzzo, F., Ferrara, A.: Higher order sliding mode controllers with optimal reaching. IEEE Transactions on Automatic Control 54(9), 2126–2136 (2009)
21. Edwards, C., Spurgeon, S.: Sliding Mode Control: Theory And Applications. Taylor & Francis systems and control book series. Taylor & Francis (1998), http://books.google.co.il/books?id=uH2RJhIPsiYC
22. Emel'yanov, S., Utkin, V., Taran, V., Kostyleva, N.E.: Theory of variable structure systems. Nauka, Moscow (1970)
23. Filippov, A.: Differential Equations with Discontinuous Right-Hand Sides. In: Mathematics and Its Applications, Kluwer Academic Publishers, Dordrecht (1988)

24. Floquet, T., Barbot, J., Perruquetti, W.: Higher-order sliding mode stabilization for a class of nonholonomic perturbed systems. Automatica 39(6), 1077–1083 (2003)
25. Fridman, L.: Chattering analysis in sliding mode systems with inertial sensors. International Journal of Control 76(9/10), 906–912 (2003)
26. Fridman, L., Levant, A.: Accuracy of homogeneous sliding modes in the presence of fast actuators. IEEE Transactions on Automatic Control 55(3), 810–814 (2010)
27. Furuta, K., Pan, Y.: Variable structure control with sliding sector. Automatica 36(2), 211–228 (2000)
28. Isidori, A.: Nonlinear Control Systems, Second edition. Springer, New York (1989)
29. Kobayashi, S., Suzuki, S., Furuta, K.: Frequency charachteristics of Levant's differentiator and adaptive sliding mode differentiator. International Journal of Systems Science 38(10), 825–832 (2007)
30. Kochalummoottil, J., Shtessel, Y., Moreno, J., Fridman, L.: Adaptive twist sliding mode control: a Lyapunov design. In: The 50th IEEE Conference on Decision and Control and European Control Conference (CDC-ECC), Orlando, USA, December 12-15, 2011, pp. 7623–7628 (2011)
31. Levant, A.: Sliding order and sliding accuracy in sliding mode control. International J. Control 58(6), 1247–1263 (1993)
32. Levant, A.: Higher order sliding modes, differentiation and output-feedback control. International J. Control 76(9/10), 924–941 (2003)
33. Levant, A.: Homogeneity approach to high-order sliding mode design. Automatica 41(5), 823–830 (2005)
34. Levant, A.: Quasi-continuous high-order sliding-mode controllers. IEEE Trans. Aut. Control 50(11), 1812–1816 (2005)
35. Levant, A.: Chattering analysis. IEEE Transactions on Automatic Control 55(6), 1380–1389 (2010)
36. Levant, A.: On fixed and finite time stability in sliding mode control. In: Proc. of the 52 IEEE Conference on Decision and Control, Florence, Italy, December 10-13 (2013), http://www.tau.ac.il/~levant/Levant.CDC2013.FTS.corrected.pdf
37. Levant, A.: Globally convergent fast exact differentiator with variable gains. In: Proc. of the European Conference on Control, Strasbourg, France, June 24-27 (2014)
38. Levant, A., Dvir, Y.: Accelerated high-order MIMO sliding mode control. In: Proc. of the 13th International Workshop on Variable Structure Systems, Nantes, France, June 29 - July 2 (2014)
39. Levant, A., Livne, M.: Exact differentiation of signals with unbounded higher derivatives. IEEE Transactions on Automatic Control 57(4), 1076–1080 (2012)
40. Levant, A., Livne, M.: Discrete-time sliding-mode-based differentiation. Lecture Notes in Control and Information Sciences 440, 299–312 (2013)
41. Levant, A., Pavlov, Y.: Generalized homogeneous quasi-continuous controllers. International Journal of Robust and Nonlinear Control 18(4-5), 385–398 (2008)
42. Liberzon, D.: Switching in Systems and Control. Birkhäuser, Boston (2003)
43. Livne, M., Levant, A.: Accuracy of disturbed homogeneous sliding modes. In: Proc. of the 13th International Workshop on Variable Structure Systems, Nantes, France, June 29 - July 2 (2014)
44. Livne, M., Levant, A.: Proper discretization of homogeneous differentiators. Automatica 50, 2007–(2014)
45. Man, Z., Feng, Y., Yu, X.: Non-singular terminal sliding mode control of rigid manipulator. Automatica 38(12), 2159–2167 (2002)
46. Man, Z., Paplinski, A., Wu, H.: A robust MIMO terminal sliding mode control scheme for rigid robotic manipulators. IEEE Transactions on Automatic Control 39(12), 2464–2469 (1994)

47. Moreno, J.A., Osorio, M.: Strict lyapunov functions for the super-twisting algorithm. IEEE Transactions on Automatic Control 57, 1035–1040 (2012)
48. Oniz, Y., Kaynak, O.: Variable-structure-systems based approach for online learning of spiking neural networks and its experimental evaluation. Journal of the Franklin Institute 351(6), 3269–3285 (2014)
49. Pisano, A., Usai, E.: Sliding mode control: A survey with applications in math. Mathematics and Computers in Simulation 81(5), 954–979 (2011)
50. Plestan, F., Bregeault, V., Glumineau, A., Shtessel, Y., Moulay, E.: Advances in high order and adaptive sliding mode control. Theory and applications 412, 465–492 (2011)
51. Plestan, F., Glumineau, A., Laghrouche, S.: A new algorithm for high-order sliding mode control. International Journal of Robust and Nonlinear Control 18(4/5), 441–453 (2008)
52. Plestan, F., Shtessel, Y., Bregeault, V., Poznyak, A.: New mETHODOLOGIES for adaptive sliding mode control. International Journal of Control 83(9), 1907–1919 (2010)
53. Plestan, F., Shtessel, Y., Bregeault, V., Poznyak, A.: Sliding mode control with gain adaptation - application to an electropneumatic actuator. Control Engineering Practice 21(5), 679–688 (2013)
54. Polyakov, A.: Nonlinear feedback design for fixed-time stabilization of linear control systems. IEEE Transactions on Automatic Control 57(8), 2106–2110 (2012)
55. Polyakov, A., Poznyak, A.: Lyapunov function design for finite-time convergence analysis: "twisting" controller for second-order sliding mode realization. Automatica 45(2), 444–448 (2009)
56. Polyakov, A., Poznyak, A.: Unified lyapunov function for a finite-time stability analysis of relay second-order sliding mode control systems. IMA Journal of Mathematical Control and Information 29(4), 529–550 (2012)
57. Sabanovic, A.: Variable structure systems with sliding modes in motion control-a survey. IEEE Transactions on Industrial Informatics 7(2), 212–223 (2011)
58. Sarpturk, S., Istefanopulos, Y., Kaynak, O.: On the stability of discrete-time sliding mode control systems. IEEE Transactions on Automatic Control 32(10), 930–932 (1987)
59. Shtessel, Y., Edwards, C., Fridman, L., Levant, A.: Sliding mode control and observation. Birkhäuser (2014)
60. Shtessel, Y., Taleb, M., Plestan, F.: A novel adaptive-gain supertwisting sliding mode controller: methodology and application. Automatica 48(5), 759–769 (2012)
61. Shtessel, Y.B., Shkolnikov, I.A.: Aeronautical and space vehicle control in dynamic sliding manifolds. International Journal of Control 76(9/10), 1000–1017 (2003)
62. Slotine, J.J., Li, W.: Applied Nonlinear Control. Prentice Hall Int, New Jersey (1991)
63. Taleb, M., Levant, A., Plestan, F.: Pneumatic actuator control: solution based on adaptive twisting and experimentation. Control Engineering Practice 21(5), 727–736 (2013)
64. Topalov, A., Cascella, G., Giordano, V., Cupertino, F., Kaynak, O.: Sliding mode neuro-adaptive control of electric drives. IEEE Transactions on Industrial Electronics 54(1), 671–679 (2007)
65. Utkin, V.: Sliding modes in control and optimization. Springer, Berlin (1992)
66. Utkin, V., Poznyak, A.: Adaptive sliding mode control with application to supertwist algorithm: equivalent control method. Automatica 49(1), 39–47 (2013)
67. Yu, X., Kaynak, O.: Sliding-mode control with soft computing: A survey. IEEE Transactions on Industrial Electronics 56(9), 3275–3285 (2009)

Event-Triggered Sliding Mode Control for Robust Stabilization of Linear Multivariable Systems

Abhisek K. Behera, Bijnan Bandyopadhyay, Nithin Xavier, and Shyam Kamal

Systems and Control Engineering, Indian Institute of Technology Bombay, Mumbai-400 076, India
{abhisek,nithinxavier,shyam}@sc.iitb.ac.in,
bijnan@ee.iitb.ac.in

Abstract. Event-triggered sliding mode control for robust stabilization of linear systems is presented here. In event-triggered control strategy the control law is not updated in periodic manner but a specific condition is used to generate the possible triggering instant for the control update. It is seen that with the sliding mode control the sequence of triggering instants generated by event condition does not exhibit accumulation of triggering instants in the presence of disturbances. We propose the sufficient event condition for the sliding mode control that guarantees that in the finite time sliding mode occurs in the system in the vicinity of sliding surface and remains within a predesigned region. An analysis for event triggered stabilization of fractional order systems is briefly given. The same triggering condition developed for integer order systems also guarantees stability of fractional order systems. A numerical example is given to show the effectiveness of the above result.

1 Introduction

Computer-controlled systems have been widely used these days due to its numerous advantages over analog implementation. In this strategy, the states are sampled and the control is updated in period manner in time. The dynamics of the system evolves in continuous open loop manner between two consecutive control updates. This strategy is easy to design and analyse the stability of the system. Indeed, it demands the dedicated reliable feedback to send the information of the plant at periodic instants. For instance, in networked control systems the sensors and actuators communicate over the communication networks which is subjected to loss of information due to packet dropout. Another concern in classical periodic implementation is the reduced time sharing capability of the digital processor. An improved time sharing capability makes the processor to work in multi task environment. In most of the cases, states of the system changes barely require any control update subject to desired performance. Thus, it seems natural to update the control whenever the demand is made and letting the system to run in open loop manner as long as possible. So, it is always desirable to minimise the control update in digital implementation such that the closed loop system is stable.

Event-triggered strategy has shown promising system performance with reduced control updates over time of interest. Here, the triggering instant for the next control

X. Yu and M. Önder Efe (eds.), *Recent Advances in Sliding Modes*,
Studies in Systems, Decision and Control 24, DOI: 10.1007/978-3-319-18290-2_8

update is calculated based on some condition called *event*. Generally, the event uses the measurement error defined as discrepancy of evolution of states with respect to the state sampled at immediate previous instant. Compared to periodic time triggered, control update is achieved in a closed-loop manner. A detailed discussion can be seen in [1]–[6] and references therein. It has been observed that these techniques offer advantages in terms of maximum inter execution time, optimal resource use, etc. This technique has been successfully studied in many applications such as networked control system [10]–[12]. In similar context, the other control techniques has appeared in literature such as quantized feedback [7], [8], Lebesgue sampling [9], etc. In all these cases, the system is guaranteed to be input-to-state stable (ISS) with respect to measurement error. Another, approach to design the event-triggered is achieved through model based technique where an approximate model is used at the controller end for applying control and the states of the model states are updated with plant state whenever event is satisfied [18]. In these cases, the event is continuously evaluated for control update which needs a dedicated circuit to measure the state from the plant. Recently, in [17], [19] a periodic event-triggered control strategy is proposed to evaluate event at predesigned periodic time instants and ascertain the system stability.

Self triggered strategy is proposed in literatures in alternative to event triggered for generating triggering sequences [13]–[16]. Unlike periodic time implementation, in self-triggered strategy the triggering instant is calculated from the last sampled state information and hence, the continuous state information is not required. However, a tradeoff between event-triggered and self-triggered mechanism is achieved with respect to maximum inter execution time interval. Very few papers have reported the performance of event-triggered control for systems with disturbances. For instance, in [13], a self-triggered $\mathscr{H}_\infty$ controller is studied. Also, event-triggered stability of systems with uncertainties are discussed in few papers such as [5], [21]. It has been shown that the complete stabilization of the system with disturbances are not achieved and also accumulation of triggering instants might occur [20].

Here, we discuss event-triggered sliding mode control for stabilization of systems with disturbances acting on it. We consider the external disturbances enter through input channel only. Sliding mode control has the capability to reject the disturbances/uncertainities completely [24]. The implementation of sliding mode control with sampled data analysis is reported in literatures and few of them can be found in [25]–[32]. However, in all these works a constant period is assumed for digital implementation. Also the steady state boundaries are shown to be function of sampling period.

In this chapter, we analyse the performance of sliding mode algorithm in event triggered implementation. The preliminary of this work can be found in [6]. We develop a sufficient condition for stability of the system with respect to the measurement error for the sliding mode control. We show the event condition developed here guarantees the sliding trajectories to remain bounded in a region around the sliding manifold for all time. We further show that the inter execution time are bounded from below by a positive quantity and hence there is no accumulation of inter execution times. Based on these conditions, we also develop a self-triggering mechanism which does not require feedback information to guarantee the closed-loop system stability. This self-triggering mechanism requires only the information of previous state to find the next possible triggering

instant. In the next section of this chapter, we propose briefly event-triggering condition for fractional order systems. Fractional order systems has been studied since last decades extensively as it describes both integer and fractional order calculus [33], [35], [36]. The robust stabilization of fractional order systems has also been studied with sliding mode control [34], [35]. We show that with the same triggering condition developed for integer order system, the stability of the fractional system is ensured.

The rest of the chapter are as follows. Section 2 describes the preliminaries to the main result of the chapter. Here, sliding mode control and problem with digitally implementing the control law is discussed. In Section 3, the event triggered sliding mode control for integer order system is presented. Sufficient condition to ensure the sliding trajectories to remain bounded within a band is given here. Also, we show that there inter execution times are always lower bounded by finite positive quantity. Further, the event parameters must be selected such that it should not result in accumulation of triggering instants. A discussion on choosing the event design parameters are given in Section 4. A brief analysis for nonlinear systems is given in Section 5. Then, event triggered sliding mode control for fractional order systems are presented in Section 6. First, preliminaries to the fractional order systems and then the design of sliding mode control for fractional order systems are presented here. Briefly, self-triggering based sliding mode control is developed in Section 7. Finally, the simulation results and some concluding remarks are given in Sections 8 and 9, respectively.

2 Problem Statement

2.1 Notation

$\mathbb{N} = \{1, 2, \ldots, \mathtt{k}, \ldots\}$ denotes set of natural numbers. We denote $\mathbb{N}_0 = \mathbb{N} \cup \{0\}$. $\mathbb{R}$, $\mathbb{R}^n$ denote sets of real numbers, n-dimensional real vector space, respectively. Any matrix symmetric means $M = M^\top$ and $M > 0 (\geq 0)$ represents positive (positive semi) definite matrix, that is $x^\top M x > 0$ (≥ 0) for all $x \in \mathbb{R}^n$. Next, $\lambda_{\max}\{M\}$ and $\lambda_{\min}\{M\}$ are the maximum and minimum eigenvalues of M, respectively. $\|x\|$ denotes Euclidean norm (2-norm) for any $x \in \mathbb{R}^n$ and is defined as $\|x\| := \sqrt{x^\top x}$. The notion $|a|$ represents absolute value of any scalar $a \in \mathbb{R}$. A function $\alpha : [0, +\infty) \mapsto \mathbb{R}_{\geq 0}$ is called class-$\mathscr{K}$ function if it is strictly increasing and $\alpha(0) = 0$. It is called class-$\mathscr{K}_\infty$ if it belongs to class-$\mathscr{K}$ and $\alpha(t)$ tends to $+\infty$ as t does. A function $\gamma : [0, +\infty) \times [0, +\infty) \mapsto \mathbb{R}_{\geq 0}$ is called as class-$\mathscr{K}\mathscr{L}$ if for each fixed $t \geq 0$ the function $\gamma(\cdot, t)$ is a class-$\mathscr{K}$ and for every $s \geq 0$ the function $\gamma(s,t) \to 0$ as t tends to ∞.

Next, we introduce the notion of input-to-state stable (ISS) for any dynamical system. Consider a system

$$\dot{\xi} = f(\xi, w), \qquad \xi_0 := \xi(t_0) \in \mathbb{R}^n. \tag{1}$$

Here, w acts as the input to the system (1). This input is locally essentially bounded function and it may be external control or disturbance depending on the context of the problem. We introduce the following notions below used in this chapter [22].

Definition 1. *The system* (1) *is said to be ISS if there exists a class-$\mathscr{KL}$ function $\beta_1(\cdot,\cdot)$ and a class-$\mathscr{K}$ function $\gamma_1(\cdot)$ such that*

$$\|\xi\| \leq \beta_1(\|\xi_0\|,t) + \gamma_1(\|w\|_\infty) \tag{2}$$

for all $\xi \in \mathbb{R}^n$.

Definition 2. *The system* (1) *is said to be ISS in the Lyapunov sense if there exists class-$\mathscr{K}_\infty$ functions $\underline{\alpha}(\cdot)$, $\overline{\alpha}(\cdot)$, a class-$\mathscr{K}$ function $\gamma_2(\cdot)$ and a class-$\mathscr{KL}$ function $\beta_2(\cdot,\cdot)$ such that for any Lyapunov function $V : \mathbb{R}^n \to \mathbb{R}_{\geq 0}$, we have*

$$\underline{\alpha}(\|\xi\|) \leq V(\|\xi\|) \leq \overline{\alpha}(\|\xi\|) \tag{3}$$

$$\frac{\partial V}{\partial \xi}\dot{\xi} \leq \beta_2(\|\xi_0\|,t) + \gamma_2(\|w\|_\infty) \tag{4}$$

for all $\xi \in \mathbb{R}^n$.

2.2 Preliminaries

Consider a continuous linear time-invariant system

$$\dot{x}(t) = Ax(t) + Bu(t) + Dd(t) \tag{5}$$

where $x(t) \in \mathbb{R}^n$ represents the state of the system, $u(t) \in \mathbb{R}^m$ is the control input and $d(t) \in \mathbb{R}^m$ is the disturbance and it is assumed to be bounded $\|d(t)\| \leq d_{\max}$. The matrices A, B and D are of appropriate dimensions. We assume that $\texttt{range}D \subseteq \texttt{range}B$, i.e., matching condition is satisfied. The system (5) can also be represented in regular form

$$\begin{aligned} \dot{x}_1(t) &= A_{11}x_1(t) + A_{12}x_2(t) \\ \dot{x}_2(t) &= A_{21}x_1(t) + A_{22}x_2(t) + B_2u(t) + D_2d(t) \end{aligned} \tag{6}$$

where $x_1(t) \in \mathbb{R}^{n-1}$ and $x_2(t) \in \mathbb{R}^m$. In most practical cases the disturbances enter the system through the input channel e.g., measurement noises etc. so, the assumption made in this chapter seems justified. It is well known that sliding mode control can reject the disturbance completely that is acting in the input channel only.

We choose the sliding variable for the system (6) as

$$s(t) = c^\top x(t), \qquad c \in \mathbb{R}^{n\times m}. \tag{7}$$

The sliding mode control law can be designed such that the sliding variable $s(t) = 0$ is ensured in finite time. To achieve this, differentiating (7), it gives

$$\dot{s}(t) = c^\top(Ax(t) + Bu(t) + Dd(t)). \tag{8}$$

Design the sliding mode control for the system (5) as

$$u(t) = -(c^\top B)^{-1}\left(c^\top Ax(t) + K\frac{s(t)}{\|s(t)\|}\right) \tag{9}$$

where $K \geq \sup_{t\geq 0} \|c^\top Dd(t)\| + \eta$ where $\eta > 0$. This control law (9) guarantees sliding mode is enforced in the system in finite time. Therefore, during sliding i.e., $s(t) = \begin{bmatrix} c_1^\top & c_2^\top \end{bmatrix} x(t) = 0$, from (7), we obtain

$$x_2(t) = -\left(c_2^\top\right)^{-1} c_1^\top x_1(t).$$

This implies that when sliding mode takes place, the trajectories of the system corresponds to the null space of matrix $c \in \mathbb{R}^{n\times m}$ and hence system order is reduced. c can be designed such that $c_2 = I$, then the reduced dynamics can be given from (6) as

$$\dot{x}_1(t) = (A_{11} - A_{12}c_1^\top)x_1(t). \tag{10}$$

Now, if the pair (A_{11}, A_{12}) is controllable, then it is always possible to design c_1 such that $A_{11} - A_{12}c_1^\top$ is Hurwitz. Thus, the closed loop system is asymptotically stable.

2.3 Problem Setup

In practical implementation the control law is not updated continuously but at some discrete instants only. A rich analysis of sampled data system with sliding mode control has been reported in literature. Here, the control law is updated at periodic time instants. This is often regarded as time triggered implementation. If h is the constant sampling period then the control (9) can be given with $t_{i+1} = t_i + h$

$$u(t) = -(c^\top B)^{-1}\left(c^\top Ax(t_i) + K\frac{s(t_i)}{\|s(t_i)\|}\right), \quad \forall t \in [t_i, t_{i+1}[\tag{11}$$

with $s(t_i) = c^\top x(t_i)$ denotes sliding variable at t_i. At the time instant t_{i+1}, the control (11) is updated again and remains constant till the next triggering become active. However, in event-triggered strategy, the control law is not updated in periodic manner in time. The triggering instants for control is calculated based on event condition and hence the triggering sequences are aperiodic. The triggering condition developed must ensure stability of the system in appropriate sense. We report in subsequent sections that the event condition developed guarantees the sliding trajectories to remain bounded within an region in finite time. We define the measurement error of the sampled state of the system as

$$e(t) = x(t_i) - x(t), \quad \forall t \in [t_i, t_{i+1}[. \tag{12}$$

This measurement error $e(t)$ plays a significant role in achieving the accuracy of the stabilization problem. For $t = t_i$, $e(t_i) = x(t_i) - x(t_i) = 0$ since the control is updated only at this instant only, so the sliding mode will occur at this instant. However, for any $t \in]t_i, t_{i+1}[$, $e(t) \neq 0$ and consequently $s(t)$ will deviate from the sliding manifold.

In this chapter, we address the problem of achieving robust stabilization with respect to measurement error $e(t)$ by sliding mode control. This is ensured by executing simple event that makes the system stable. We also establish that with this triggering scheme there is no *Zeno Phenomena* i.e., no accumulation of control inter executions times in some time intervals $[t_i, t_{i+1}[$.

3 Event-Triggered Sliding Mode

Theorem 1. *Consider the system* (5) *and sliding variable* (7)*. Let* $\varepsilon \in (0,\infty)$ *be given. Then the control law* (11) *achieves sliding mode in the vicinity of* $s(t) = 0$ *within a band given as*

$$\left\{x(t) \in \mathbb{R}^n \ : \ \|s(t)\| \leq 2\varepsilon \|A\|^{-1}\right\} \tag{13}$$

if the following conditions are satisfied

$$\left\| c^\top A e(t) \right\| < \varepsilon \tag{14}$$

and K *is chosen as*

$$K > \sup_{t \geq 0} \left\| c^\top D d(t) \right\| + \eta + \varepsilon \tag{15}$$

where $\eta > 0$*.*

Proof. We consider the Lyapunov function for $t \in [t_i, t_{i+1}[$ as

$$V = \frac{1}{2} s^\top(t) s(t).$$

Differentiating V with respect to time along the system trajectories and using (8), yields

$$\dot{V} = s^\top(t) \left(c^\top A x(t) + c^\top B u(t) + c^\top D d(t) \right).$$

Now using (11) in the above for control, we obtain

$$\begin{aligned} \dot{V} &= s^\top(t) \left(c^\top A x(t) - c^\top A x(t_i) - K \frac{s(t_i)}{\|s(t_i)\|} + c^\top D d(t) \right) \\ &= -s^\top(t) \left(c^\top A e(t) + K \frac{s(t_i)}{\|s(t_i)\|} - c^\top D d(t) \right). \end{aligned} \tag{16}$$

It can be shown that at $t = t_i$ the Lyapunov function $\dot{V} < 0$. However, for $t \in [t_i, t_{i+1}[\backslash t_i$, invoking the conditions (14) and (15), we obtain

$$\begin{aligned} \dot{V} &< -s^\top(t) \left(K \frac{s(t_i)}{\|s(t_i)\|} - c^\top D d(t) - \varepsilon \frac{s(t)}{\|s(t)\|} \right) \\ &< -\eta s^\top(t) \frac{s(t_i)}{\|s(t_i)\|} \\ &= -\eta \|s(t_i)\| + \eta c^\top e(t) \frac{s(t_i)}{\|s(t_i)\|}. \end{aligned} \tag{17}$$

The last equality in the above follows from $s(t) = c^\top x(t) = c^\top (x(t_i) - e(t))$. Further using (14), we obtain

$$\dot{V} < -\eta \|s(t_i)\| + \eta \varepsilon \|A\|^{-1}. \tag{18}$$

Now recalling the fact that $\|s(t)\| = \|s(t_i) + c^\top e(t)\| \leq \|s(t_i)\| + \|c\|\|e(t)\|$. Using this in (18), we obtain

$$\dot{V} < -\eta\|s(t)\| + 2\eta\varepsilon\|A\|^{-1} \tag{19}$$

Define the set $\mathscr{B}_i := \{s(t), t \in [t_i, t_{i+1}) : \|s(t)\| \leq 2\varepsilon\|A\|^{-1}\}$. For $i = 0$, if $\|s(t_i)\| \in \mathscr{B}_0$, then system trajectory remain in $\mathscr{B}_0$ for all time hence. On the other hand, if $\|s(t_i)\| \notin \mathscr{B}_0$, then there exists a $p \in \mathbb{N}$ such that $\|s(t)\| \in \mathscr{B}_p$ for all $t \geq t_p$ due to (18). Since p is finite, we claim that this occurs in finite time. So, the sliding mode will occur in the vicinity of $s(t) = 0$ with an band as given in (13). This completes the proof. ■

Remark 1. It can be noted that the condition (14) must be maintained for all time the sliding trajectories to remain in a band given by (13). However, in practice we assume the following relation $\|c\|\|A\|\|e(t)\| \leq \varepsilon$ to be satisfied. This in turn respects the relation (14).

3.1 System Stability

Here, we discuss the stability of the closed loop system. When sliding trajectories remain bounded within the region given by (13), then for all time $t \geq t_p$ where t_p is the time instant where sliding trajectories enter (7), we have

$$\|s(t)\| \leq 2\varepsilon\|A\|^{-1},$$

then it can be written as

$$x_2(t) \leq -c_1^\top x_1(t) + 2\varepsilon\|A\|^{-1}.$$

The reduced order dynamics can be given as

$$\dot{x}_1(t) \leq (A_{11} - A_{12}c_1^\top)x_1(t) + 2A_{12}\varepsilon\|A\|^{-1}. \tag{20}$$

In the following, we give the stability of the closed loop system.

Proposition 1. *Consider the system* (20)*. Let the control law* (11) *bring the sliding mode in the vicinity of the sliding surface. Then the system is ISS and the trajectories remain bounded with an ultimate bound given by*

$$\mathscr{B} = \left\{x_1(t) \ : \ \lambda_{\min}\{Q\}\|x_1(t)\| \leq 4\varepsilon\|A\|^{-1}\left\|A_{12}^\top P\right\|\right\}. \tag{21}$$

Proof. Consider the Lyapunov function

$$V = x_1^\top(t)Px_1(t)$$

where P is a symmetric positive definite matrix, i.e., $P = P^\top > 0$. Differentiating V with respect to time and using (20), we write

$$\begin{aligned}\dot{V} =& \dot{x}_1(t)^\top Px_1(t) + x_1(t)^\top P\dot{x}_1(t)\\ \leq& x_1(t)^\top(A_{\text{cl}}^\top P + PA_{\text{cl}})x_1(t) + 4\varepsilon\|A\|^{-1}A_{12}^\top Px_1(t)\end{aligned} \tag{22}$$

where $A_{\text{cl}} = (A_{11} - A_{12}c_1^\top)$ is Hurtiwz. Then by converse Lyapunov Theorem, there will exist a positive definite matrix Q such that the following relation

$$A_{\text{cl}}^\top P + PA_{\text{cl}} + Q = 0$$

holds. Then

$$\dot{V} \leq -x_1^\top(t)Qx_1(t) + 4\varepsilon \|A\|^{-1} A_{12}^\top P x_1(t). \tag{23}$$

From Rayleigh's inequality for any positive definite matrix Q, we have

$$\lambda_{\min}\{Q\}\|z(t)\|^2 \leq z^\top(t)Qz(t) \leq \lambda_{\max}\{Q\}\|z(t)\|^2$$

for all $z(t) \in \mathbb{R}^n$. So,

$$\begin{aligned}
\dot{V} &\leq -\lambda_{\min}\{Q\}\|x_1(t)\|^2 + 4\varepsilon \|A\|^{-1} \left\| A_{12}^\top P x_1(t) \right\| \\
&\leq -\lambda_{\min}\{Q\}\|x_1(t)\|^2 + 4\varepsilon \|A\|^{-1} \left\| A_{12}^\top P \right\| \|x_1(t)\| \\
&= -\lambda_{\min}\{Q\} \left(\|x_1(t)\| - 4\varepsilon \|A\|^{-1} \frac{\|A_{12}^\top P\|}{\lambda_{\min}\{Q\}} \right) \|x_1(t)\|.
\end{aligned}$$

Therefore, the system (20) is ISS with respect to ε with a bound as given in (21). This completes the proof. ■

3.2 Event-Triggering Scheme

Here, we discuss event-triggering scheme for the system (5) which ensures sliding mode in the system. We see that if the condition (14) is satisfied for all time then sliding mode always occur in the vicinity of sliding surface in finite time. So, we select (14) as the triggering condition for sliding mode to occur. For any $\sigma \in]0,1]$, if we guarantee

$$\|c\|\|A\|\|e(t)\| < \sigma\varepsilon \tag{24}$$

holds for $t \in [t_i, t_{i+1}[$ and $i \in \mathbb{Z}_{\geq 0}$, then condition (14) is respected and hence the results of Theorem 1 holds for all t. So, the triggering instant is generated whenever this condition is violated, i.e., equality is satisfied,

$$\|c\|\|A\|\|e(t)\| = \sigma\varepsilon. \tag{25}$$

Thus, the triggering instant t_{i+1} can then be determined as

$$t_{i+1} = \inf\{t \in]t_i, +\infty[\ : \ \|c\|\|A\|\|e(t)\| \geq \sigma\varepsilon\} \tag{26}$$

for all $i \in \mathbb{N}_0$.

In practical cases, the control gets updated after some time instants once the states are sampled. Therefore the delay forms an important part in this analysis. So, if the delay is considered then the control (11) would be held constant for all $t \in [t_i + \Delta, t_{i+1} + \Delta[$,

$\Delta > 0$. We refer here inter execution time as time interval between two consecutive triggering instants.

It might be possible that the inter execution time may approach to zero leading to accumulation of triggering instants. This can cause inability of the processor to execute the control task and hence the stability of the system can not be ensured. In order to avoid such a situation, we show next that there always exist a positive lower bound for inter execution times.

Theorem 2. *Consider the system* (5)*. Let the control law* (11) *brings the sliding mode in the system by executing the event* (25) *for all* $t > t_i$ *for the increasing time sequence* $\{t_i\}_{i\in\mathbb{N}_0}$*, i.e.,* $t_0 < t_1 < t_2 < \cdots$*. If* t_{i+1} *is the triggering instant, then the inter execution time* $t_{i+1} - t_i = T_i > 0$ *satisfy*

$$T_i \geq \frac{1}{\tau} \ln \left(1 + \left\| c^\top A \right\|^{-1} \sigma \varepsilon \frac{\tau}{\rho(\|x(t_i)\|) + \beta} \right) \tag{27}$$

where τ *and* β *are defined as*

$$\tau := \|A\| \quad \textit{and} \quad \beta := \left\| B(c^\top B)^{-1} K \right\| + \|D\| \, d_{\max}, \tag{28}$$

and the real valued function $\rho(\|x(t_i)\|) : \mathbb{R}^n \mapsto \mathbb{R}_{\geq 0}$ *is given as*

$$\rho(\|x(t_i)\|) := \left\| A - B(c^\top B)^{-1} c^\top A \right\| \|x(t_i)\| . \tag{29}$$

Proof. Consider the set $\Gamma = \{t : \|c\|\|A\|\|e(t)\| = 0\}$. Then for time $t \in [t_i, t_{i+1}[\backslash \Gamma$, we write

$$\begin{aligned} \frac{\mathrm{d}}{\mathrm{d}t} \|e(t)\| &\leq \|\dot{e}(t)\| = \|\dot{x}(t)\| \\ &= \left\| Ax(t) - B(c^\top B)^{-1} c^\top A x(t_i) - B(c^\top B)^{-1} K \frac{s(t_i)}{\|s(t_i)\|} + Dd(t) \right\| . \end{aligned}$$

Substituting $x(t) = x(t_i) - e(t)$ in the above relation and simplifying yields

$$\begin{aligned} \frac{\mathrm{d}}{\mathrm{d}t} \|e(t)\| &\leq \|A\| \, \|e(t)\| + \left\| \left(A - B(c^\top B)^{-1} c^\top A \right) x(t_i) \right\| \\ &\quad + \left\| B(c^\top B)^{-1} K \frac{s(t_i)}{\|s(t_i)\|} \right\| + \|D\| \, d_{\max} \\ &= \|A\| \, \|e(t)\| + \left\| A - B(c^\top B)^{-1} c^\top A \right\| \|x(t_i)\| \\ &\quad + \left\| B(c^\top B)^{-1} K \right\| + \|D\| \, d_{\max} \\ &= \tau \|e(t)\| + \rho(\|x(t_i)\|) + \beta \end{aligned} \tag{30}$$

where τ, β and the function $\rho(\|x(t_i)\|)$ are defined as per (28) and (29), respectively.

Using comparison Lemma [23], the solution to the differential inequality (30) with the initial condition $e(t_i) = x(t_i) - x(t_i) = 0$ can be given as

$$\|e(t)\| \leq \frac{\rho(\|x(t_i)\|) + \beta}{\tau} \left(\mathrm{e}^{\tau(t - t_i)} - 1 \right) \tag{31}$$

where $t \in [t_i, t_{i+1}[$. Recalling the relation (25) and (26) and since $e_1(t) := c^\top A e(t)$, we write (31) as

$$\sigma\varepsilon \leq \left\| c^\top A \right\| \frac{\rho(\|x(t_i)\|) + \beta}{\tau} \left(\mathrm{e}^{\tau T_i} - 1 \right) \tag{32}$$

where $T_i = t_{i+1} - t_i$ then the lower bound for inter execution time can be obtained as given (27). Since the control (11) is an asymptotic stabilizing control law implying $\|x(t_i)\|$ never equals zero in finite time. Also $\beta > 0$. This together implies the lower bound is bounded below by strictly nonzero. This proves the Theorem. ■

Remark 2. Theorem 2 gives the existence of a positive lower bound of inter execution time. This is important to ensure the control executions are processed only after a finite time interval. Therefore, triggering instants for control signal get updated can be given as $t_{i+1} - t_i \geq T_i$. This also avoids accumulation of triggering instants, so it is practically feasible.

In many practical cases, delay Δ is inevitable, but it may not be given an attention if it is sufficiently small to neglect. However, it affects the performance, possibly increases the sliding mode band around $s(t) = 0$ for large non zero values of Δ. Let t_i be the instant at which state is sampled and after Δ instant, i.e., $t_i + \Delta$ control signal execution is finished and updated. Then the control can be given

$$u(t) = u(t_i + \Delta), \quad \forall t \in [t_i + \Delta, t_{i+1} + \Delta[. \tag{33}$$

It has been assumed constant delay for all intervals of time. In the following, we state that there exists a lower bound for delay in inter execution times. This result is reported in the following Corollary.

Corollary 1. *Consider the system* (5). *Assume that the control law* (33) *is applied to the system at $t_i + \Delta$ instants such that the sliding mode begins in some finite time. Let $\sigma_1 \in]0,1[$ be given and the increasing time sequences $\{t_i\}_{i \in \mathbb{N}_0}$ satisfy the event execution rule* (26). *Let's denote*

$$T_i^\star = \frac{1}{\tau} \ln \left(1 + \left\| c^\top A \right\|^{-1} \sigma_1 \varepsilon \frac{\tau}{\rho_1(\|x(t_{i-1})\|, \|x(t_i)\|) + \beta} \right) \tag{34}$$

where τ and β are defined as given by (28) *and $\rho_1(\|x(t_{i-1})\|, \|x(t_i)\|)$ given as*

$$\rho_1(\|x(t_{i-1})\|, \|x(t_i)\|) = \|A\| \|x(t_i)\| + \left\| B(c^\top B)^{-1} c^\top A \right\| \|x(t_{i-1})\|.$$

If

$$0 \leq \Delta \leq T_i^\star \tag{35}$$

then there exists $\sigma \in]\sigma_1, 1[$ such that sliding mode occur in the vicinity of sliding surface $s(t) = 0$.

Proof. Consider $t \in [t_i, t_i + \Delta_i)$. Then (35) guarantees that $\|c\|\|A\|\|e(t)\| = \sigma_1 \varepsilon$ for all $t \in [t_i, t_i + \Delta_i)$. Since $\sigma \in]\sigma_1, 1[$, there will exist a time from Theorem 2 such that $\|c\|\|A\|\|e(t)\| = \sigma\varepsilon$ for all $t \in [t_i + \Delta_i, t_{i+1}\Delta_{i+1})$ with initial condition for (30) can be chosen as $\|c\|\|A\|\|e(t)\| = \sigma_1\varepsilon$. Thus the sliding mode occurs due to Eqns. (14) and (25) with desired sliding band. The minimum inter execution time $T_i^\star$ exists due to Theorem 2 represents the time taken by $\|c^\top Ae(t)\|$ to grow from 0 to $\sigma_1\varepsilon$. Therefore, from Theorem 2 there exists a non zero delay as given in (35). ■

4 Admissible Triggering Signals

In this Section, we derive the conditions for admissible triggering instants that ascertain the system stability. We say that the triggering instants are *admissible* if $t_{i+1} \geq t_i + T_i$ holds for all $i \in \mathbb{N}_0$. Similarly, the closed loop system (5) and (11) is said to be *admissibility* if the corresponding triggering time sequences are admissible.

The control signal is updated whenever the triggering condition (25) is satisfied. At the mean time it must be ensured that the triggering instant generated must be admissible. If the design parameters are not chosen properly, non admissible triggering will occur and eventually *Zeno Phenomenon* results. This happens due to the unknown disturbance which governs rate of decrement of sliding variable towards the sliding manifold. Moreover, the selection of α also affects the triggering instants. The less value of ε, the more chance to lead to accumulation of triggering instants. So, a suitable value must be chosen.

5 Event-Triggered Control for Nonlinear Systems

This idea can also be extended to nonlinear systems. Here, briefly we discuss the analysis for nonlinear systems. We consider a nonlinear system

$$\dot{x}(t) = f(x(t), u(t), d(t)) \tag{36}$$

where $x(t) \in \mathscr{D} \subset \mathbb{R}^n$ and $u(t) \in \mathscr{U} \subset \mathbb{R}$. It has been assumed that the function $f(\cdot)$ is Lipschitz in $x(t) \in \mathscr{D}$ and it is also affine in control and disturbance. Further, we assume that the disturbance $d(t)$ enters the system through the input channel only. We design the sliding manifold for the system (36) as $s(t) = c^\top x(t)$. Taking the derivative of $s(t)$, we obtain

$$\dot{s}(t) = c^\top f(x(t), u(t), d(t)). \tag{37}$$

Since $f(\cdot,\cdot,\cdot)$ is affine in both control and disturbance, we write the above relation as

$$\dot{s}(t) = a_1(x(t)) + b(x(t))u(t) + a_2(x(t), d(t)). \tag{38}$$

Design the SMC for the system (36) as

$$u(t) = -b^{-1}(x(t))(a_1(x(t)) + K\text{sign}s(t)) \tag{39}$$

where $K > \sup_{t\geq 0} |a_2(x(t),d(t))|$. It can be easily shown that with the control (39), the sliding manifold is reached in finite time and is constrained to remain on this manifold for all time. Now, if the c is chosen suitably, then the reduced order system is asymptotically stable. Here, we discuss event-triggered implementation of the control law (39) such that closed loop system is ISS. Let L_1 be the Lipschitz constant of $a_1(x(t))$ and $0 < K_1 \leq \|b(x(t))\| \leq K_2$.

Theorem 3. *Consider the system* (36). *Let* $\varepsilon_1 \in (0,\infty)$ *be given and* $\{t_i\}_{i=0}^{\infty}$ *be the sequences of triggering instants. Then, the sliding mode is enforced in the system in the vicinity of the sliding manifold given by the region*

$$\{x(t) \in \mathbb{R}^n : |s(t_i)| \leq \varepsilon_0\} \tag{40}$$

if the following holds

$$K \geq \frac{K_2}{K_1}(\varepsilon_1 + \Delta_{\max}) \tag{41}$$

and

$$\frac{K_1}{K_2} L_1 \|c\| \|e(t)\| \leq \varepsilon_1 \tag{42}$$

where $\varepsilon_0 = 2\frac{K_2}{K_1}\frac{\varepsilon_1}{L_1}$.

Proof. To prove this, we consider Lyapunov function for $t \in [t_i, t_{i+1}[$ as

$$V = \frac{1}{2}s^2(t).$$

Differentiating V along the system trajectories and using the control law (39), we obtain

$$\begin{aligned}\dot{V} &= s(t)c^\top(a_1(x(t)) + b(x(t))u(t) + a_2(x(t),d(t))) \\ &= s(t)c^\top(a_1(x(t)) - b(x(t))b^{-1}(x(t_i))a_1(x(t_i)) - b(x(t))b^{-1}(x(t_i))K\text{sign}s(t_i) \\ &\quad + a_2(x(t),d(t)))\end{aligned} \tag{43}$$

It can be easily shown that if (42) holds then

$$\|c^\top(a_1(x(t)) - b(x(t))b^{-1}(x(t_i))a_1(x(t_i)))\| \leq \frac{K_1}{K_2} L_1 \|c\| \|e(t)\| \leq \varepsilon_1.$$

Then, using this, the above relation can be deduced as

$$\begin{aligned}\dot{V} &\leq -s(t)\frac{K_1}{K_2}K\text{sign}s(t_i) + |s(t)|\varepsilon_1 + |s(t)|\Delta_{\max} \\ &= -s(t)\frac{K_1}{K_2}\left(K\text{sign}s(t_i) - \frac{K_2}{K_1}(\varepsilon_1 + \Delta_{\max})\text{sign}s(t)\right) \\ &\leq -s(t)\frac{K_1}{K_2}\eta\,\text{sign}s(t_i) \\ &= -\eta\frac{K_1}{K_2}\left(|s(t_i)| - \frac{K_2}{K_1 L_1}\varepsilon_1\right).\end{aligned} \tag{44}$$

On further simplification, it yields

$$\dot{V} < -\eta \frac{K_1}{K_2} \left(|s(t)| - 2\frac{K_2}{K_1}\frac{\varepsilon_1}{L_1} \right) \tag{45}$$

It can be seen that the sliding trajectory decreases till $|s(t)| \leq \varepsilon_0$. It can be argued that there will exist a finite time $t_p \geq 0$ such that the sliding trajectory re,main bounded within the region given by (40). ■

6 Event-Triggered Control for Fractional Order Systems

An event triggered sliding mode control for fractional order systems is discussed in this section. Fractional order systems has been gaining popular as it deals with fractional order calculus. Here, sliding mode control for fractional order systems are first discussed and then its realization with event-triggering scheme is analysed. Briefly, we define the terminologies pertaining to the fractional order systems.

6.1 Preliminaries

The definition of Riemann-Liouville fractional order integrals and derivatives are stated recalled given in [33]–[36]. The Laplace transform of the Riemann-Liouville fractional order integrals and derivatives are also given.

6.1.1 Gamma Function

Gamma function $\Gamma(z)$ is defined by

$$\Gamma(z) = \int_0^\infty e^{-t} t^{z-1} \mathrm{d}t. \tag{46}$$

6.1.2 Mittag-Leffler Function

The Mittag-Leffler function in one parameter $E_\alpha(z)$ is given by

$$E_\alpha(z) = \sum_{k=0}^{\infty} \frac{z^k}{\Gamma(\alpha k + 1)}. \tag{47}$$

Mittag-Leffler function in two parameters $E_{\alpha,\beta}(z)$ is given by

$$E_{\alpha,\beta}(z) = \sum_{k=0}^{\infty} \frac{z^k}{\Gamma(\alpha k + \beta)}. \tag{48}$$

The Mittag-Leffler function in two parameters in fractional calculus plays the same role as exponential function does in integer order calculus. The Mittag-Leffler function is in fact a generalization of exponential function. For instance,

$$E_{1,1}(z) = \sum_{k=0}^{\infty} \frac{z^k}{\Gamma(k+1)} = \sum_{k=0}^{\infty} \frac{z^k}{k!} = e^z. \tag{49}$$

6.1.3 Fractional Order Integral

Riemann-Liouville fractional order integral of order $\alpha \in \mathbb{R}^+$ is defined by

$$ {}_0D_t^{-\alpha} f(t) = \frac{1}{\Gamma(\alpha)} \int_0^t \frac{f(\tau)}{(t-\tau)^{(1-\alpha)}} \mathrm{d}\tau. \tag{50} $$

6.1.4 Fractional Order Derivative

Riemann-Liouville fractional order derivative of order α is defined by

$$ \begin{aligned} {}_0D_t^{\alpha} f(t) &= {}_0D_t^m {}_0D_t^{-(m-\alpha)} f(t) \\ &= \frac{\mathrm{d}^m}{\mathrm{d}t^m} \left[\frac{1}{\Gamma(m-\alpha)} \int_0^t \frac{f(\tau)}{(t-\tau)^{(\alpha-m+1)}} \mathrm{d}\tau \right] \end{aligned} \tag{51} $$

where $\alpha \in \mathbb{R}^+$ and $m-1 < \alpha < m$, $m \in \mathbb{N}$.

6.2 Sliding Mode Control For Fractional Order Systems

This section deals with the basic concept of sliding mode control and the application of Sliding Mode Control to a LTI commensurate fractional order single system given in [35]. The solution to the fractional differential equation with discontinuous righthand side is understood in a Filippov sense. The sliding surface is selected such that the motion of the system trajectories along the sliding surface is stable and the states of the system will reach the origin asymptotically.

Consider the commensurate fractional order LTI system given as

$$ {}_0D_t^{\alpha} \bar{x}(t) = \bar{A}\bar{x}(t) + \bar{B}\big(u(t) + d(t)\big) \tag{52} $$

where $\bar{x}(t) \in \mathbb{R}^n$, $u(t) \in \mathbb{R}$ and $d(t) \in \mathbb{R}$ represent the states, control input and disturbance of the system, respectively. We assume that the system is controllable and the uncertainty entering the system is matched and bounded, i.e., $|d(t)| \leq d_{\max}$ for all $t \geq 0$.

We can always find a non singular matrix T such that a linear transformation $x(t) = T\bar{x}(t)$ will transform the equation (52) into the regular form

$$ \begin{aligned} {}_0D_t^{\alpha} x_1(t) &= A_{11}x_1(t) + A_{12}x_2(t) \\ {}_0D_t^{\alpha} x_2(t) &= A_{21}x_1(t) + A_{22}x_2(t) + B_2\big(u(t) + d(t)\big). \end{aligned} \tag{53} $$

where $x_1 \in \mathbb{R}^{n-1}$ and $x_2 \in \mathbb{R}$. The system (53) can also be represented as

$$ {}_0D_t^{\alpha} x(t) = Ax(t) + B(u(t) + d(t)). \tag{54} $$

The sliding surface for the system (53) is chosen as

$$ s(t) = {}_0D_t^{\alpha-1} Cx(t) \tag{55} $$

where $C = [c_1 \ 1]$ and $c_1 \in \mathbb{R}^{n-1}$. The matrix c_1 is selected such that motion along the sliding surface is stable. The derivative of the sliding surface $s(t)$ with respect to time can be written as

$$ \begin{aligned} \dot{s}(t) &= {}_0D_t^{\alpha} Cx(t) \\ &= C\big(Ax(t) + B\big(u(t) + d(t)\big)\big). \end{aligned} \tag{56} $$

The C is chosen such that CB is singular. Then control input can be designed as

$$u(t) = -(CB)^{-1}\left(CAx(t) + K\text{sign}(s(t))\right) \tag{57}$$

where K is selected as $K \geq |CBd_{\max}| + \eta$ and $\eta > 0$ to guarantee the existence of sliding mode.

Theorem 4. *Consider the system given in equation(53). Then the control law given by (57) guarantees the existence of sliding mode along the surface defined by equation(55).*

Proof. Consider the Lyapunov function

$$V(t) = \frac{1}{2}s^2(t).$$

Taking the derivative of $V(t)$ with respect to time and using (54) and (57), we obtain

$$\begin{aligned}
\dot{V}(t) &= s(t)\dot{s}(t) \\
&= s(t)\left(CAx(t) + CB(u(t) + d(t))\right) \\
&= -s(t)\left(K\text{sign}(s(t)) + CBd(t)\right) \\
&\leq -\eta|s(t)| \\
&= -\eta\sqrt{2}V^{1/2}(t).
\end{aligned} \tag{58}$$

This implies that the $V(t)$ converges to zero in finite time lesser than $t_0 + \frac{\sqrt{2}V^{1/2}(x(0))}{\eta}$. Hence, the sliding variable will also converges to zero in finite time.

Once the system is in sliding mode, i.e., $s(t) = 0$, the dynamics of the system during sliding motion is governed by

$${}_0D_t^{\alpha}x_1(t) = (A_{11} - A_{12}c_1)x_1(t) + A_{12}\left({}_0D_t^{1-\alpha}s(t)\right). \tag{59}$$

Since ${}_0D_t^{1-\alpha}s(t) \to 0$ in finite time, we can write the dynamics of the system as

$${}_0D_t^{\alpha}x_1(t) = (A_{11} - A_{12}c_1)x_1(t) = \hat{A}x_1(t).$$

It is always possible choose an appropriate $C = [c_1\ 1]$ matrix, so as to place the eigenvalues of $\hat{A}$ at desired location, since the $(\bar{A}, \bar{B})$ pair is controllable. In order to make the system asymptotically stable, the matrix C is chosen such that the following condition is satisfied

$$|\arg(\lambda_i(\hat{A}))| > \alpha\frac{\pi}{2} \tag{60}$$

where $\lambda_i(\hat{A})$ are the eigenvalues of $\hat{A}$. Thus the system represented by equation (52) can be stabilized by sliding mode control along with the rejection of matched disturbances.

6.3 Event Triggering Based Control for Fractional Order Systems

In event triggered based control, the control law is updated whenever event condition satisfied. The control law is given as

$$u(t) = -(CB)^{-1}\left(CAx(t_i) + K\text{sign}(s(t_i))\right) \quad \forall t \in [t_i, t_{i+1}[\tag{61}$$

where $s(t_i) = {}_0D_{t_i}^{\alpha-1}Cx(t_i)$. The control input is updated at every triggering instant when the event triggering condition is satisfied. The control input to the system is kept constant until the next triggering instant. The gain K is selected as

$$K \geq \|CBd_{\max}\| + \eta + \varepsilon \tag{62}$$

where $\eta > 0$ is a positive real number and $\beta > 0$ is a positive design parameter. Since the control is not updated continuously, the states of the system remain within an band in the vicinity of sliding surface.

Here, we use the same triggering condition (25) to ensure the stability of the closed loop system and the triggering instants are generated based on (26).

By applying the control (61), the states of the system are driven to the neighbourhood of $s(t) = 0$ and constrained to remain within a band around the sliding surface given by

$$\mathbb{B} = \left\{x \in \mathbb{R}^n : |s(t_i)| \leq {}_0D_t^{\alpha-1}\varepsilon\|A\|^{-1}\right\} \tag{63}$$

We design control to drive the system states to the band $\mathbb{B}$. Then the states of the system will be within the band $\mathbb{B}_1$ since $\mathbb{B} \subseteq \mathbb{B}_1$ where $\mathbb{B}_1$ is given by

$$\mathbb{B}_1 = \left\{x \in \mathbb{R}^n : |Cx(t_i)| \leq \varepsilon\|A\|^{-1}\right\}. \tag{64}$$

Remark 3. The sliding mode band that we discuss here is different from the quasi sliding mode band in the discrete sliding mode control. The quasi sliding mode band in DSMC depend on the disturbance bound and sampling time while the sliding mode band we discuss here depend on design parameter ε. The ε allows the designer to have a trade of between the system performance and resource utilization.

7 Self-Triggered Sliding Mode Control

Self-triggering mechanism is proposed as alternative to event-triggered control to develop triggering sequences. Here, we do not need feedback information to evaluate event continuously but at some aperiodic time instants. We propose the self-triggering mechanism which is based on the results of Theorem 2 in the following. It is observed

from Theorem 2 that the inter execution time T_i is always lower bounded by a finite positive quantity. So, it can be said that no triggering instant will appear below this time. To achieve this, we define the next triggering instant as

$$\tilde{t}_{i+1} = \tilde{t}_i + \frac{1}{\tau} \ln \left(1 + \left\| c^\top A \right\|^{-1} \sigma \varepsilon \frac{\tau}{\rho(\|x(t_i)\|) + \beta} \right). \tag{65}$$

The time instant $\tilde{t}_i$ is defined as the sampling and control update time instant. To avoid confusion, we denote sampling instant by this in self-triggered. The triggering instant is calculated as (65) gives a minimum triggering instant where triggering condition is not satisfied for all times lesser than that given in (65).

Theorem 5. *Consider the system* (5) *and the control law* (11)*. Then the triggering sequences* $\{\tilde{t}_i\}_{i=0}^{\infty}$ *generated by* (65) *guarantees closed-loop system is ISS and sliding mode occurs in the system sin finite time.*

Proof. Consider the time interval $[t_i, t_{i+1}[$. Since the triggering satisfies (65), we obtain from (27) the following $t_{i+1} \geq \tilde{t}_{i+1}$. So, the event condition (24) is respected for (65). This is also true for all $i \in \mathbb{N}_0$. We also have $t_{i+1} > t_i$ since the second term in (65) is always nonzero quantity. Thus, triggering mechanism developed ensures ISS of the system with respect to the measurement error. We also see that as (24) holds for all time, so sliding mode occurs in the finite time and the proof is completed.

8 Simulation Results

Here, we give the simulation results pertaining to the analysis derived in the previous Sections. Consider the LTI system

$$\dot{x}(t) = \begin{bmatrix} 0 & 1 & 0 \\ 0 & 0 & 1 \\ 1 & 2 & 3 \end{bmatrix} x(t) + \begin{bmatrix} 0 & 0 \\ 1 & 0 \\ 0 & 1 \end{bmatrix} \left(u(t) + \begin{bmatrix} 0.1 + 0.2\cos(5t) \\ 0.5\sin(10t) \end{bmatrix} \right).$$

Design the sliding surface as $s(t) = \begin{bmatrix} 0.7071 & 1 & 0 \\ 0 & 0 & 1 \end{bmatrix} x(t)$. The following parameters are chosen as $K = 0.8$, $\varepsilon = 0.2$, $\sigma = 0.9$. The initial condition is chosen as $x_0 = \begin{bmatrix} 3 & 2 & 1 \end{bmatrix}$. The control input for the system is given as

$$u(t) = -\left(\begin{bmatrix} 0 & 0.7071 & 1 \\ 1 & 2 & 3 \end{bmatrix} \begin{bmatrix} x_1(t_i) \\ x_2(t_i) \end{bmatrix} + 0.8 \frac{s(t_i)}{\|s(t_i)\|} \right), \quad \forall t \in [t_i, t_{i+1}[.$$

8.1 Event-Triggered Scheme

Fig. 1(a)-(d) show the plot of states of the system, sliding surface, control input and sampling intervals, respectively. It is shown that, stability of the system is guaranteed even if the control input is not updated in continuous manner. Moreover, the system achieves bounded stability as stated in previous Sections. The bounds of the states and

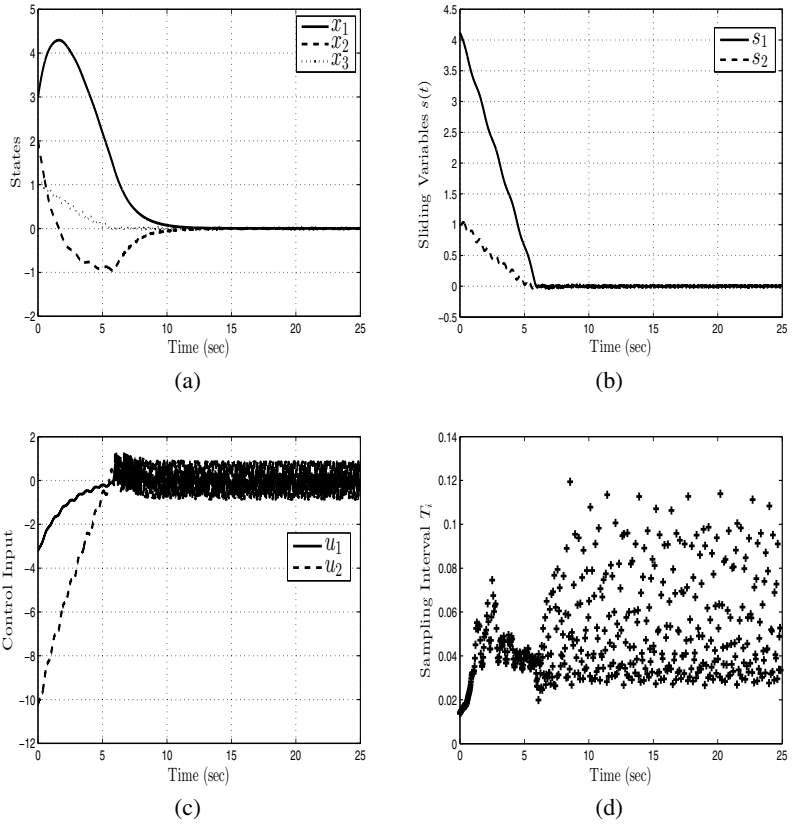

Fig. 1. Performance of system with event-triggering scheme (a) Evolution of states of the system (b) sliding surface (c) event based control input and (d) sampling interval generated by executing event condition

sliding surface can be minimized by suitably selecting the value of ε. For the given value of ε, we obtain the sliding mode band as 0.0932. It is clear from Fig. 1(b) during steady state sliding variable remains bounded within the sliding band given by (13). The plot of sampling intervals versus time is shown in Fig. 1(d). Once the sliding mode is enforced in the system, the sampling intervals are significantly increased.

8.2 Self-Triggering Scheme

Fig. 2(a)-(d) show the performances of the self-triggering strategy. Fig. 2(a) and (b) give the plot of states of the system and sliding trajectory. We observe that the sliding mode occurs in the system almost in the same time. However, in this case the sampling intervals are reduced. It is to be noted that this scheme doest not require feedback information continuously so it is more suitable in applications where reliable communication is needed.

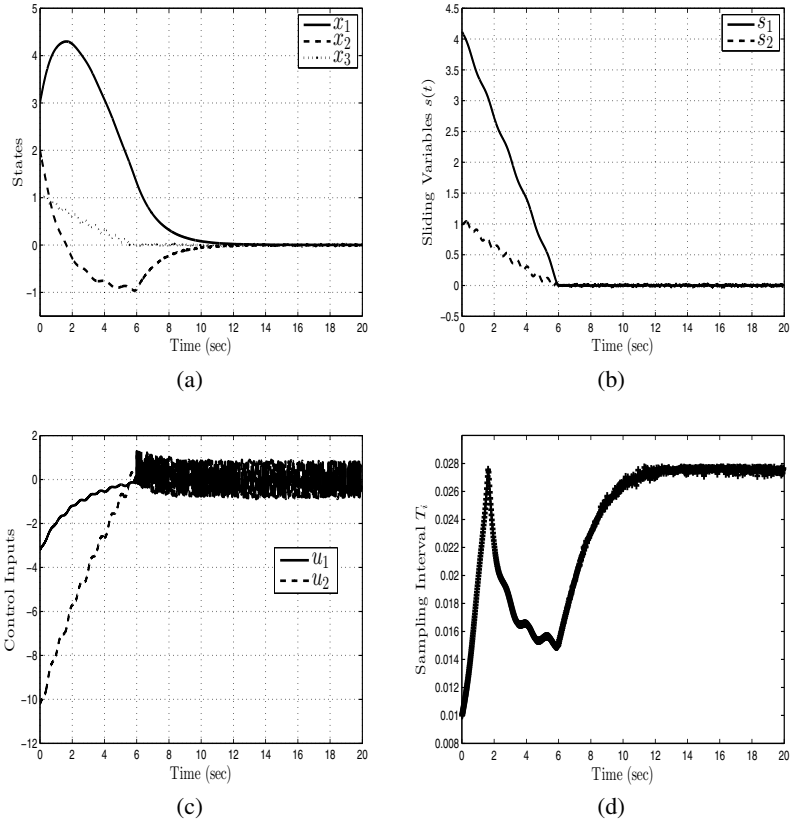

Fig. 2. Performance of system with self-triggering scheme (a) Evolution of states of the system (b) sliding surface (c) self triggered based control input and (d) sampling interval

9 Conclusion

In this chapter, event control based robust stabilization for linear time-invariant system is proposed. The event strategy possesses many advantages such as optimal resource utilization, effective use of time and cost of processor. To achieve this advantage, event triggering based sliding mode control is analysed from the practical point of view. In many situations, robustness forms one of the prime objective in stabilization problems. Here, by defining the simple triggering condition the linear system is ISS for any bounded disturbance. The robustness in the system is assured by enforcing the execution of triggering condition that ensures sliding mode in the vicinity of sliding manifold. Further, we derived the ultimate bound for the bounded stability. We also derive the minimum possible inter execution time for the control signal execution. This result is further reported by considering delays into account. The proposed strategy actually deals with real time application of sliding mode control for any linear system. Following this, we also give a self-triggering strategy with sliding mode control.

Self-triggering scheme seems to be reliable in practice as it does not need any information for triggering. In the latter part, we also state event-triggering scheme for fractional order systems. The event triggering condition developed for integer order system also guarantees the stability of fractional order systems.

Acknowledgement. B. Bandyopadhyay is formally associated with Prof. Okyay Kaynak in the editing job of IEEE/ASME Transactions on Mechatronics and he highly appreciates Prof. Kaynak, the way he keeps in personal touch with the editorial board to bring out high quality journals.

References

1. Årźen, K.E.: A simple event-based PID controller. In: Preprints 14th World Congr. IFAC, Beijing (1999)
2. Åström, A.J., Bernhardsson, B.: Comparison of riemann and lebesgue sampling for first order stochastic systems. Int. Conf. Decision and Control (2002)
3. Tabuada, P.: Event-triggered real-time scheduling of stabilizing control tasks. IEEE Trans. Autom. Control 52(9), 1680–1685 (2007)
4. Tallapragada, P., Chopra, N.: On event triggered tracking for nonlinear systems. IEEE Transactions on Automatic Control 58(9), 2343–2348 (2013)
5. Lunze, J., Lehmann, D.: A state-feedback approach to event-based control. Automatica 46(1), 211–215 (2010)
6. Behera, A.K., Bandyopadhyay, B.: Event triggered robust stabilization of linear systems. In: Proceedings of the Annual Conference of IEEE Industrial Electronics Society, Dallas, USA, 29 October-1November, pp. 133–138 (2014)
7. Brockett, R., Liberzon, D.: Quantized feedback stabilization of linear systems. IEEE Trans. Autom. Control 45(7), 1279–1289 (2000)
8. Elia, N., Mitter, S.: Stabilization of linear systems with limited information. IEEE Trans. Autom. Control 46(9), 1384–1400 (2001)
9. Xu, Y.-K., Cao, X.-R.: Lebesgue-sampling-based optimal control problems with time aggregation. IEEE Trans. Autom. Control 56(5), 1097–1109 (2011)
10. Mazo, J.M., Tabuada, P.: Decentralized event-triggered control over wireless sensor/actuator networks. IEEE Trans. Autom. Control 56(10), 2456–2461 (2011)
11. Tallapragada, P., Chopra, N.: Decentralized event-triggering for control of nonlinear systems. IEEE Trans. Autom. Control 59(12), 3312–3324 (2014)
12. Premaratne, U., Halgamuge, S.K., Mareels, I.M.Y.: Event triggered adaptive differential modulation: a new method for traffic reduction in networked control systems. IEEE Trans. Autom. Control 58(7), 1696–1706 (2013)
13. Wang, X., Lemmon, M.D.: Self-triggered feedback control systems with finite-gain $\mathscr{L}_2$ stability. IEEE Trans. Autom. Control 54(3), 452–467 (2009)
14. Wang, X., Lemmon, M.D.: Self-triggering under state-independent disturbances. IEEE Trans. Autom. Control 55(6), 1494–1500 (2010)
15. Anta, A., Tabuada, P.: To sample or not to sample: self-triggered control for nonlinear systems. IEEE Trans. Autom. Control 55(9), 2030–2042 (2010)
16. Anta, A., Tabuada, P.: Preliminary results on state-triggered stabilizing control tasks. In: 45th IEEE Proc. Conf. Decision and Control, pp. 892–897 (2010)
17. Heemels, W.P.M.H., Donkers, M.C.F., Teel, A.R.: Periodic event-trigggered control for linear systems. IEEE Trans. Autom. Control 58(4), 847–861 (2013)

18. Garcia, E., Antsaklis, P.J.: Model-based event-triggered control for systems with quantization and time-varying network delays. IEEE Trans. Autom. Control 58(2), 422–434 (2013)
19. Heemels, W.P.M.H., Donkers, M.C.F.: Model-based periodic event-triggered control for linear systems. Automatica 49(3), 698–711 (2013)
20. Borgers, D.P., Heemels, W.P.M.H.: Event-separtion propertirs of event-triggered control systems. IEEE Trans. Autom. Control 59(10), 2644–2656 (2014)
21. Donkers, M.C.F., Heemels, W.P.M.H.: Ouput-based event-triggered control with guaranteed $\mathscr{L}_\infty$-gain and improved and decntralized event-triggering. IEEE Trans. Autom. Control 57(6), 1362–1376 (2012)
22. Sontag, E.D.: Smooth stabilization implies coprime factorization. IEEE Trans. Autom. Control 34(4), 435–443 (1989)
23. Khalil, H.: Nonlinear Systems, 3rd edn. Prentice-Hall, Upper Saddle River (2002)
24. Utkin, V.I.: Variable structure systems with sliding modes. IEEE Trans. Autom. Control 22(2), 212–222 (1977)
25. Gao, W., Wang, Y., Homaifa, A.: Discret-time variable structure control systems. IEEE Trans. Ind. Electron. 42(2), 117–122 (1995)
26. Bartoszewicz, A.: Discrete-time quasi-sliding-mode control strategies. IEEE Trans. Ind. Electron. 45(4), 633–637 (1998)
27. Su, W.-C., Drakunov, S.V., Özgüner, Ü.: An $O(T^2)$ baoundary layer in sliding mode for sampled data systems. IEEE Trans. Autom. Control 45(3), 482–485 (2000)
28. Janardhanan, S., Bandyopadhyay, B.: Output feedback sliding-mode control for uncertain systems using fast output sampling technique. IEEE Trans. Ind. Electron. 53(5), 1677–1682 (2006)
29. Bandyopadhyay, B., Janardhanan, S.: Discrete-time sliding mode control- A multirate output feedback approach. LNCIS. Springer (2005)
30. Abidi, K., Xu, J.-X., Yu, X.: On the discrete-time integral sliding-mode control. IEEE Trans. Autom. Control 52(4), 709–715 (2007)
31. Saaj, M.C., Bandyopadhyay, B., Unbehauen, H.: A new algorithm for discrete-time sliding-mode control using fast output sampling feedback. IEEE Trans. Ind. Electron. 49(3), 518–523 (2002)
32. Galias, Z., Yu, X.: Euler's discretization of single-input sliding mode control systems. IEEE Trans. Autom. Control 52(9), 1726–1730 (2007)
33. Podlubny, I.: Fractional Differential Equations, 3rd edn. Mathematics in Science and Engineering, vol. 198. Academic Press (1999)
34. Kamal, S., Raman, A., Bandyopadhyay, B.: Finite-time stabilization of fractional order uncertain chain of integrators: An integral sliding mode approach. IEEE Trans. Autom. Control 58(6), 1597–1602 (2013)
35. Bandyopadhyay, B., Kamal, S.: Stabilization and Control of Fractional Order Systems: A Sliding Mode Approach. LNEE, vol. 317. Springer, Heidelberg (2015)
36. Lakshmikantham, V., Leela, S., Devi, J.V.: Theory of Fractional Dynamic Systems. Cambridge Scientific Publishers (2009)

A Nonhomogeneous Super-Twisting Algorithm*

Michael Basin[1], Pablo Rodriguez-Ramirez[1], Steven Ding[2], and Shane Dominic[2]

[1] Department of Physical and Mathematical Sciences
Autonomous University of Nuevo Leon
San Nicolas de los Garza, Nuevo Leon, Mexico
[2] Institute for Automatic Control and Complex Systems
University of Duisburg-Essen, Duisburg, Germany

Abstract. This chapter presents a nonhomogeneous continuous super-twisting algorithm for systems of dimension more than one. The conditions of finite-time convergence to the origin are obtained and the robustness of the designed algorithm is discussed. The chapter concludes with numerical simulations illustrating performance of the designed algorithms.

Keywords: Sliding mode control, super-twisting, nonhomogeneous systems.

1 Introduction

It is well known that the classical discontinuous sliding mode control provides finite-time convergence for a one-dimensional system [1]. A finite-time stabilizing control for a system of dimension two is realized using the twisting algorithm [2], where the second order sliding mode control is also discontinuous. Both algorithms are robust with respect to bounded disturbances. On the other hand, using a continuous second-order sliding mode super-twisting algorithm [3], a state of a one-dimensional system can be stabilized along with its first derivative. The super-twisting algorithm is robust with respect to unbounded disturbances satisfying a Lipschitz condition. There are a number of papers applying twisting and super-twisting algorithms to robust regulator and observer design. Various modifications of the sliding mode technique have always been actively used in industrial applications ([4,5,6,7,8,9,10]), including fault detection/correction and data-driven control and monitoring ([11,12,13,14,15,16]).

The finite-time convergence of the designed algorithms is conventionally established using geometrical techniques [2,3], direct Lyapunov method [17,18,19], or homogeneity approach [20,21,22]. The explicit Lyapunov functions for their second-order super-twisting algorithms can be found in [19]. The homogeneity approach, mentioned even in the classical book [23], was consistently developed in the mentioned papers and applied to the observer design in [24]. The homogeneity is a commonly accepted tool for establishing finite-time convergence of the control laws: for instance, the classical signum control [1] and the super-twisting algorithm [3] are homogeneous. The recent

* The authors thank the German Academic Exchange Service (DAAD) and the Mexican National Science and Technology Council (CONACyT) for financial support under Grants 57064906, 170660 and 129081.

X. Yu and M. Önder Efe (eds.), *Recent Advances in Sliding Modes*,
Studies in Systems, Decision and Control 24, DOI: 10.1007/978-3-319-18290-2_9

paper [25] presents a homogeneous continuous super-twisting algorithm for systems of dimension more than one, which assures finite-time convergence to the origin for all system states; as a consequence, it is applicable to homogeneous systems only.

This chapter corrects the indicated flaw and presents a nonhomogeneous continuous super-twisting algorithm for systems of dimension more than one, which assures finite-time convergence to the origin for all system states. First, the case of dimension two is addressed. The conditions of finite-time convergence to the origin equilibrium are obtained and the robustness of the designed algorithm is discussed. Similar results are then obtained for systems of dimension more than two. The chapter concludes with numerical simulations illustrating performance of the designed algorithms.

The chapter is organized as follows. The problem statement is given in Section 2. A nonhomogeneous super-twisting-like control algorithm for systems of dimension two is designed in Section 3. The corresponding examples are provided in Section 4. A nonhomogeneous super-twisting-like control algorithm for systems of dimension more than two is presented in Section 5 and illustrated by examples in Section 6. Section 7 concludes this study. The proofs of all theorems and lemmas are given in Appendix.

2 Control Problem Statement

Consider a conventional dynamic system of dimension two

$$\dot{x}_1(t) = x_2(t), \quad x_1(t_0) = x_{10}, \tag{1}$$

$$\dot{x}_2(t) = u(t), \quad x_1(t_0) = x_{20},$$

where $x(t) = [x_1(t), x_2(t)] \in R^2$ is the system state and $u(t) \in R$ is the control input.

In the classical second-order sliding mode control theory, a finite-time stabilizing control for the system (1) is designed using the twisting algorithm [2] in the form

$$u(t) = -k_1 sign(x_1(t)) - k_2 sign(x_2(t)), \tag{2}$$

where $k_1, k_2 > 0$ are certain positive constants, and the signum function of a scalar x is defined as $sign(x) = 1$, if $x > 0$, $sign(x) = 0$, if $x = 0$, and $sign(x) = -1$, if $x < 0$ ([23]).

On the other hand, for a scalar dynamic system

$$\dot{x}(t) = u(t), \quad x(t_0) = x_0, \tag{3}$$

a continuous finite-time stabilizing control for the system (3) can be designed using the super-twisting algorithm [3] as follows

$$u(t) = -\lambda \mid x(t) \mid^{1/2} sign(x(t)) - \alpha \int_{t_0}^{t} sign(x(s))ds, \tag{4}$$

where $\lambda > 0$, $\alpha > 0$ are certain positive constants. Note that applying the continuous control (4) to the system (3) results in a second-order sliding mode, i.e., both $x(t)$ and $\dot{x}(t)$ converge to zero for a finite time. In other words, the continuous control (4) yields finite-time convergence similar to that produced by a classical discontinuous sliding mode control $u(t) = -Ksign(x(t))$, where $K > 0$ is sufficiently large, for the system (3).

In this chapter, we propose a nonhomogeneous super-twisting-like continuous modification of the twisting control algorithm (2) as follows

$$u(t) = -\lambda_0 \mid \int_{t_0}^{t} x_1(s)ds \mid^{\gamma_0} sign(\int_{t_0}^{t} x_1(s)ds) - \lambda_1 \mid x_1(t) \mid^{\gamma_1} sign(x_1(t)) -$$

$$-\lambda_2 \mid x_2(t) \mid^{\gamma_2} sign(x_2(t)) - \alpha \int_{t_0}^{t} sign(x_2(s))ds, \tag{5}$$

where $\lambda_0, \lambda_1, \lambda_2 > 0$, $\alpha > 0$, $0 < \gamma_0, \gamma_1, \gamma_2 < 1$ are certain positive constants. It would be demonstrated that the designed continuous control (5) works similarly to the twisting control (2), i.e., results in finite-time convergence of both states $x_1(t)$ and $x_2(t)$ of the system (1) to the origin. The announced result is formalized in the next section and then proved in Appendix.

3 Nonhomogeneous Super-Twisting Algorithm for Relative Degree Two Systems

The result for the control law (5) is given as follows.

Theorem 1. Consider a dynamic system (1) of dimension two. Then, the modified nonhomogeneous super-twisting control law (5) yields finite-time convergence of both states $x_1(t)$ and $x_2(t)$ to the origin under certain conditions on control gains $\lambda_0, \lambda_1, \lambda_2 > 0$.

Proofs of all the theorems are given in Appendix.

Remark 1. In contrast to [25], sufficient conditions on the control gains in (5) are not provided explicitly. Please refer to Remark 2 at the end of Section 5 for additional comments.

Consider now a system (1) in presence of a disturbance:

$$\dot{x}_1(t) = x_2(t), \quad x_1(t_0) = x_{10}, \tag{6}$$

$$\dot{x}_2(t) = u(t) + \xi(t), \quad x_1(t_0) = x_{20},$$

where $\xi(t)$ satisfies the Lipschitz condition with a constant L. The system (6) can still be stabilized at the origin in view of the following theorem.

Theorem 2. Consider a dynamic system (6) of dimension two in presence of a disturbance $\xi(t)$ satisfying the Lipschitz condition with a constant L. Then, the modified nonhomogeneous super-twisting control law (5) yields finite-time convergence of both states $x_1(t)$ and $x_2(t)$ to the origin under certain conditions on control gains $\lambda_0, \lambda_1, \lambda_2, \alpha > 0$.

4 Examples: I. Relative Degree Two

This section presents examples of designing a finite-time stabilizing regulator for a dynamic system (1) of dimension two, based on the modified nonhomogeneous super-twisting regulator (5) in Theorems 1 and 2.

1. Consider a system (1). The modified super-twisting regulator (5) is applied with the control gains selected as $\lambda_0 = 20$, $\lambda_1 = 10$, $\lambda_2 = 5$, $\alpha = 1$ and the exponents $\gamma_0 = 1/10$, $\gamma_1 = 1/10$, $\gamma_2 = 1/5$. The initial conditions are assigned as $x_{10} = 1000$, $x_{20} = 1000$. The obtained results are shown in Fig. 1. Figure 2 depicts the graph of the control input. The results for the initial conditions $x_{10} = 1000$, $x_{20} = -1000$ are demonstrated in Figure 3. Figure 4 depicts the graph of the control input.

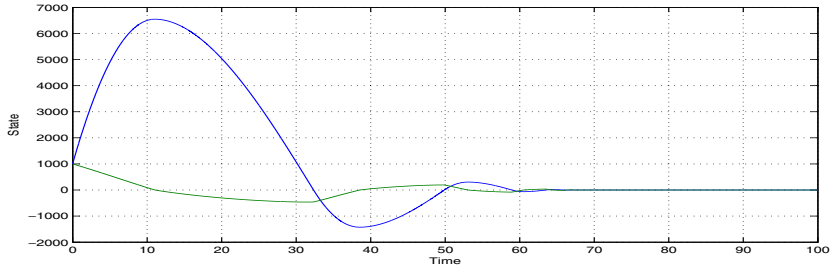

Fig. 1. Graphs of the system states (1) upon applying the control law (5) with exponents $\gamma_0 = 1/10$, $\gamma_1 = 1/10$, $\gamma_2 = 1/5$ and initial conditions $x_{10} = 1000$, $x_{20} = 1000$

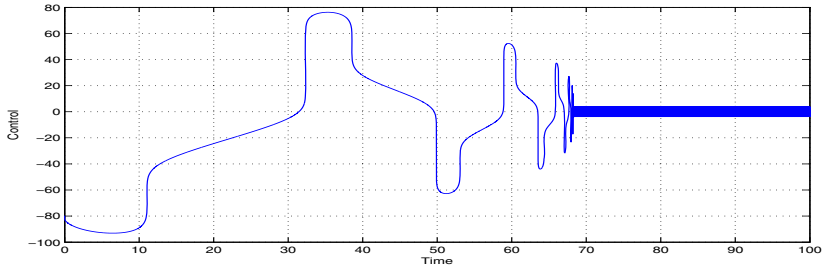

Fig. 2. Graphs of the control input (5) with exponents $\gamma_0 = 1/10$, $\gamma_1 = 1/10$, $\gamma_2 = 1/5$ for the system states (1) with initial conditions $x_{10} = 1000$, $x_{20} = 1000$

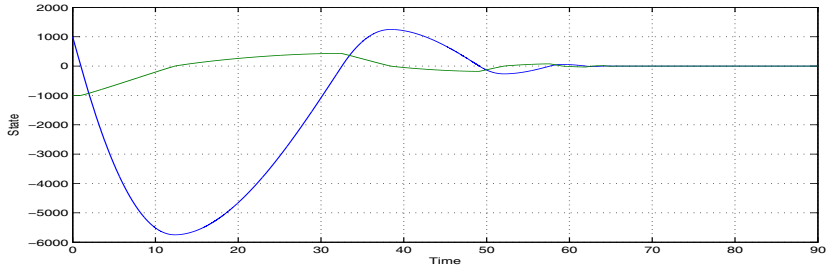

Fig. 3. Graphs of the system states (1) upon applying the control law (5) with exponents $\gamma_0 = 1/10$, $\gamma_1 = 1/10$, $\gamma_2 = 1/5$ and initial conditions $x_{10} = 1000$, $x_{20} = -1000$

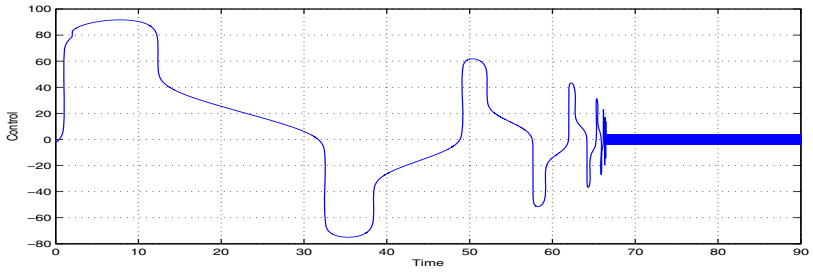

Fig. 4. Graphs of the control input (5) with exponents $\gamma_0 = 1/10$, $\gamma_1 = 1/10$, $\gamma_2 = 1/5$ for the system states (1) with initial conditions $x_{10} = 1000$, $x_{20} = -1000$

2. Consider a system (1) with another set of the control gains $\lambda_0 = 0.1$, $\lambda_1 = 20$, $\lambda_2 = 10$, $\alpha = 1$ and the exponents $\gamma_0 = \gamma_1 = \gamma_2 = 1/4$. The initial conditions are assigned as $x_{10} = 1000, x_{20} = 1000$. The obtained results are shown in Fig. 5. Figure 6 depicts the graph of the control input. The results for the initial conditions $x_{10} = 1000, x_{20} = -1000$ are demonstrated in Figure 7. Figure 8 depicts the graph of the control input.

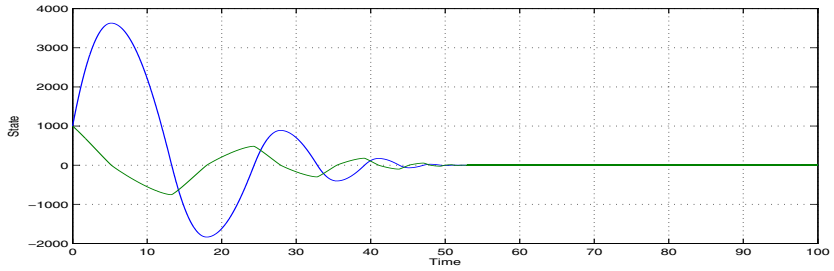

Fig. 5. Graphs of the system states (1) upon applying the control law (5) with exponents $\gamma_0 = \gamma_1 = \gamma_2 = 1/4$ and initial conditions $x_{10} = 1000$, $x_{20} = 1000$

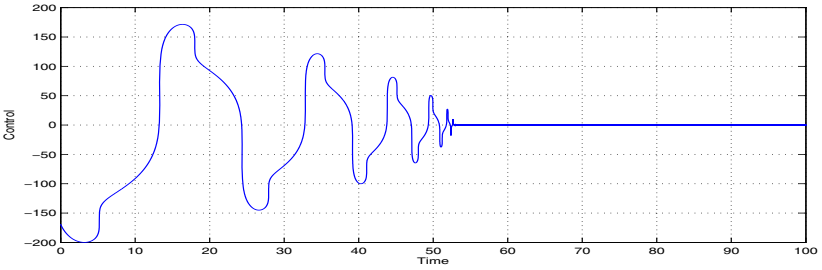

Fig. 6. Graphs of the control input (5) for the system states (1) with exponents $\gamma_0 = \gamma_1 = \gamma_2 = 1/4$ and initial conditions $x_{10} = 1000$, $x_{20} = 1000$

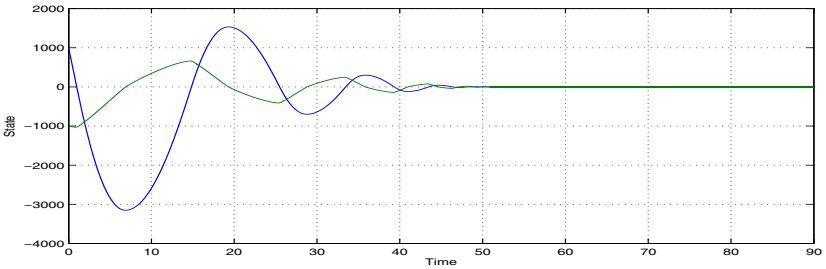

Fig. 7. Graphs of the system states (1) upon applying the control law (5) with exponents $\gamma_0 = \gamma_1 = \gamma_2 = 1/4$ and initial conditions $x_{10} = 1000$, $x_{20} = -1000$

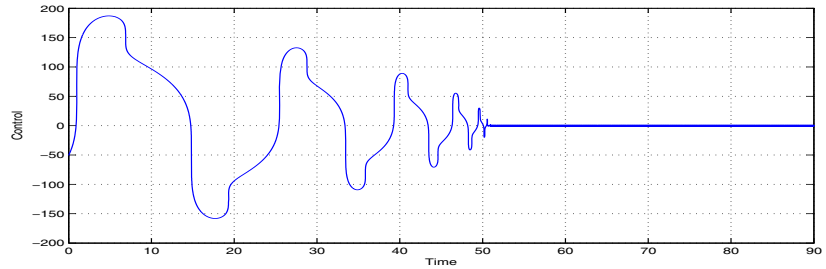

Fig. 8. Graphs of the control input (5) for the system states (1) with exponents $\gamma_0 = \gamma_1 = \gamma_2 = 1/4$ and initial conditions $x_{10} = 1000$, $x_{20} = -1000$

3. Consider a system (6) with disturbance $\xi(t) = \sin(1000t)$. Again, the modified super-twisting regulator (5) is applied with the control gains selected as $\lambda_0 = 20$, $\lambda_1 = 10$, $\lambda_2 = 5$, $\alpha = 1$ and the exponents $\gamma_0 = 1/10$, $\gamma_1 = 1/10$, $\gamma_2 = 1/5$. The initial conditions are assigned as $x_{10} = 1000$, $x_{20} = 1000$. The obtained results are shown in Fig. 9. Figure 10 depicts the graph of the control input. The results for the initial conditions $x_{10} = 1000$, $x_{20} = -1000$ are demonstrated in Figure 11. Figure 12 depicts the graph of the control input.

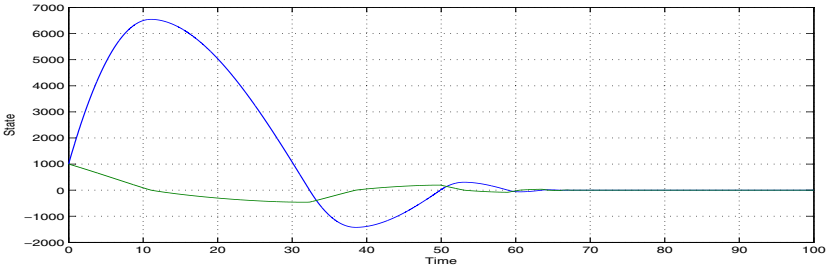

Fig. 9. Graphs of the system states (6) with disturbance $\xi(t) = \sin(1000t)$ upon applying the control law (5) with exponents $\gamma_0 = 1/10$, $\gamma_1 = 1/10$, $\gamma_2 = 1/5$ and initial conditions $x_{10} = 1000$, $x_{20} = 1000$

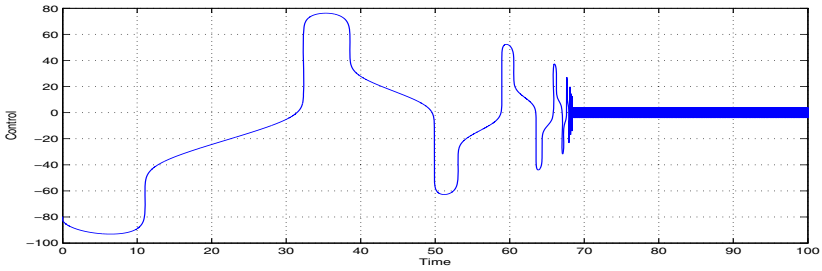

Fig. 10. Graphs of the control input (5) with exponents $\gamma_0 = 1/10$, $\gamma_1 = 1/10$, $\gamma_2 = 1/5$ for the system states (6) with disturbance $\xi(t) = \sin(1000t)$ and initial conditions $x_{10} = 1000$, $x_{20} = 1000$

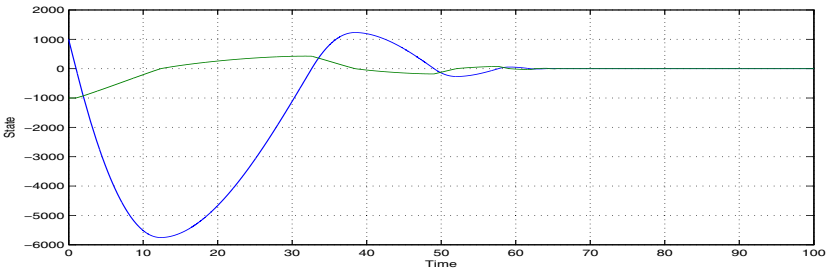

Fig. 11. Graphs of the system states (6) with disturbance $\xi(t) = \sin(1000t)$ upon applying the control law (5) with exponents $\gamma_0 = 1/10$, $\gamma_1 = 1/10$, $\gamma_2 = 1/5$ and initial conditions $x_{10} = 1000$, $x_{20} = -1000$

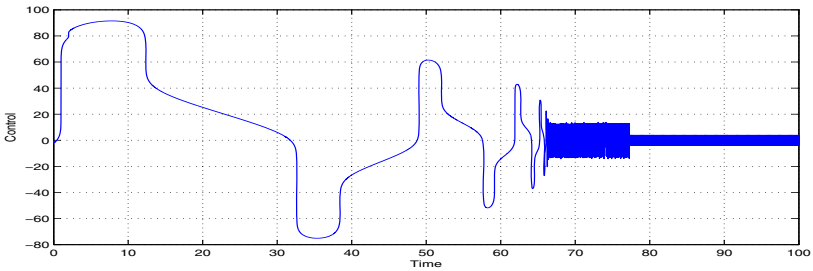

Fig. 12. Graphs of the control input (5) with exponents $\gamma_0 = 1/10$, $\gamma_1 = 1/10$, $\gamma_2 = 1/5$ for the system states (6) with disturbance $\xi(t) = \sin(1000t)$ and initial conditions $x_{10} = 1000$, $x_{20} = -1000$

4. Consider a system (6) with disturbance $\xi(t) = \sin(1000t)$ and another set of the control gains $\lambda_0 = 0.1$, $\lambda_1 = 20$, $\lambda_2 = 10$, $\alpha = 1$ and the exponents $\gamma_0 = \gamma_1 = \gamma_2 = 1/4$. The initial conditions are assigned as $x_{10} = 1000$, $x_{20} = 1000$. The obtained results are shown in Fig. 13. Figure 14 depicts the graph of the control input. The results for the initial conditions $x_{10} = 1000$, $x_{20} = -1000$ are demonstrated in Figure 15. Figure 16 depicts the graph of the control input.

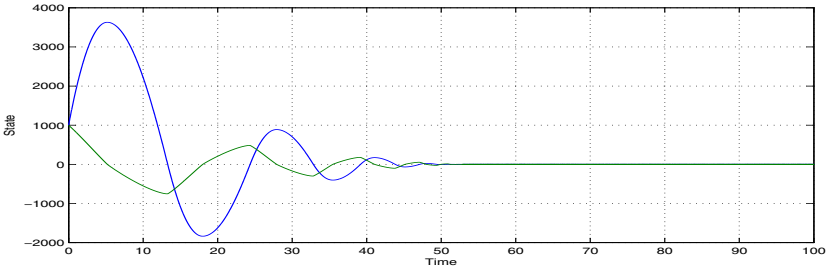

Fig. 13. Graphs of the system states (6) with disturbance $\xi(t) = \sin(1000t)$ upon applying the control law (5) with exponents $\gamma_0 = \gamma_1 = \gamma_2 = 1/4$ and initial conditions $x_{10} = 1000$, $x_{20} = 1000$

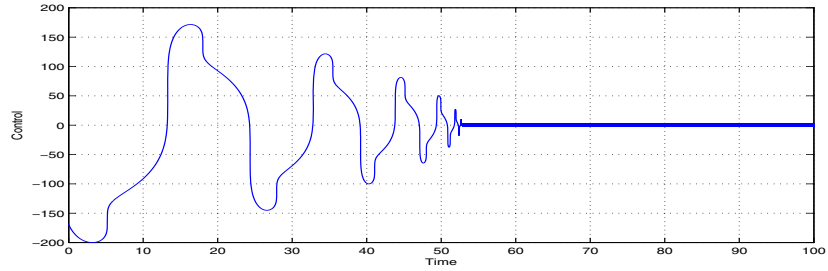

Fig. 14. Graphs of the control input (5) with exponents exponents $\gamma_0 = \gamma_1 = \gamma_2 = 1/4$ for the system states (6) with disturbance $\xi(t) = \sin(1000t)$ and initial conditions $x_{10} = 1000$, $x_{20} = 1000$

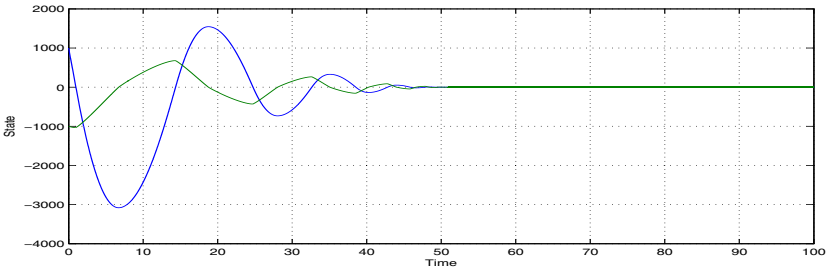

Fig. 15. Graphs of the system states (6) with disturbance $\xi(t) = \sin(1000t)$ upon applying the control law (5) with exponents $\gamma_0 = \gamma_1 = \gamma_2 = 1/4$ and initial conditions $x_{10} = 1000$, $x_{20} = -1000$

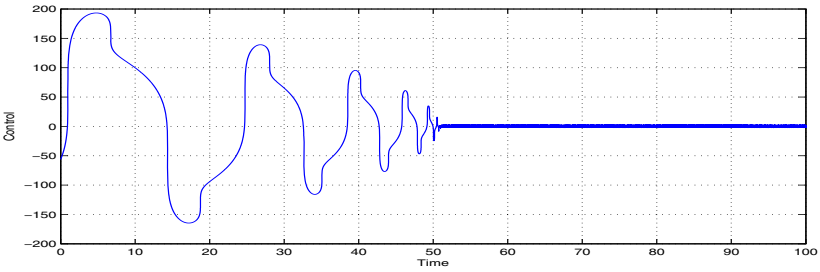

Fig. 16. Graphs of the control input (5) with exponents $\gamma_0 = \gamma_1 = \gamma_2 = 1/4$ for the system states (6) with disturbance $\xi(t) = \sin(1000t)$ and initial conditions $x_{10} = 1000$, $x_{20} = -1000$

5 Nonhomogeneous Super-Twisting Algorithm for Relative Degree More Than Two Systems

The main result can be generalized as follows. Consider a dynamic system of dimension $n > 2$

$$\begin{aligned} \dot{x}_1(t) &= x_2(t), \quad x_1(t_0) = x_{10}, \\ \dot{x}_2(t) &= x_3(t), \quad x_2(t_0) = x_{20}, \\ &\dots \\ \dot{x}_n(t) &= u(t), \quad x_n(t_0) = x_{n0}, \end{aligned} \tag{7}$$

using the notation for the system (1). We propose a generalization of the nonhomogeneous super-twisting-like continuous control algorithm (5) as follows

$$u(t) = -v_0(t) - v_1(t) - v_2(t) - \ldots - v_n(t) - v_{n+1}(t), \tag{8}$$

where

$$v_0(t) = \lambda_0 \mid \int_{t_0}^{t} x_1(s)ds \mid^{\gamma_0} sign(\int_{t_0}^{t} x_1(s)ds),\ v_i(t) = \lambda_i \mid x_i(t) \mid^{\gamma_i} sign(x_i(t)),\ i = 1, \ldots, n,$$

$$v_{n+1}(t) = \alpha \int_{t_0}^{t} sign(x_n(s))ds,$$

and $\lambda_0, \lambda_1, \ldots, \lambda_n > 0$, $\alpha > 0$ and $\gamma_i \in (0,1)$, $i = 0, \ldots, n$ are certain positive constants.

It would be demonstrated that the designed nonhomogeneous continuous control (8) works similarly to the twisting control (2), i.e., results in finite-time convergence of the states $x_1(t), x_2(t), \ldots, x_n(t)$ of the system (7) to the origin. The announced result is formalized in the next theorem and then proved in Appendix.

Theorem 3. Consider a dynamic system (7) of dimension $n > 2$. Then, the modified nonhomogeneous super-twisting control law (8) yields finite-time convergence of the

states $x_1(t),\ldots,x_{n-1}(t),x_n(t)$ to the origin under certain conditions on control gains $\lambda_0,\lambda_1,\ldots\lambda_n>0$.

Consider now a system (7) in presence of a disturbance:

$$\begin{aligned}\dot{x}_1(t)&=x_2(t),\quad x_1(t_0)=x_{10},\\ \dot{x}_2(t)&=x_3(t),\quad x_2(t_0)=x_{20},\\ &\ldots\\ \dot{x}_n(t)&=u(t)+\xi(t),\quad x_n(t_0)=x_{n0},\end{aligned}\tag{9}$$

where $\xi(t)$ satisfies the Lipschitz condition with a constant L. The system (9) can still be stabilized at the origin in view of the following theorem.

Theorem 4. Consider a dynamic system (9) of dimension $n>2$ in presence of a disturbance $\xi(t)$ satisfying the Lipschitz condition with a constant L. Then, the modified nonhomogeneous super-twisting control law (8) yields finite-time convergence of the states $x_1(t),\ldots,x_{n-1}(t),x_n(t)$ to the origin under certain conditions on control gains $\lambda_0,\lambda_1,\ldots\lambda_n,\alpha>0$.

Remark 2. In contrast to [25], sufficient conditions on the control gains in (8) are not provided explicitly. Indeed, in the nonhomogeneous case, there is no result similar to Theorem 8.1 in [20], which establishes that the system (7),(8) without terms $v_0(t)$ and $v_{n+1}(t)$ is finite-time stable, if $s^{n+1}+\lambda_n s^n+\ldots+\lambda_1 s+\lambda_0$ is a Hurwitz polynomial. Thus, it is currently unclear if the sufficient conditions obtained in [25] for the homogeneous case: 1. $s^{n+1}+\lambda_n s^n+\ldots+\lambda_1 s+\lambda_0$ is a Hurwitz polynomial, and 2. $\alpha>L$, $\lambda_n^2>2(\alpha+L)^2/(\alpha-L)$, which should be added in the presence of disturbances satisfying satisfying the Lipschitz condition with a constant L, would also be sufficient conditions in Theorems 1–4.

6 Examples: II. Relative Degree More Than Two

This section presents examples of designing a finite-time stabilizing regulator for a dynamic system (7) of dimension more than two, based on the modified nonhomogeneous super-twisting regulator (8) in Theorems 3 and 4.

5. Consider a 3D system

$$\begin{aligned}\dot{x}_1(t)&=x_2(t),\quad x_1(t_0)=x_{10},\\ \dot{x}_2(t)&=x_3(t),\quad x_2(t_0)=x_{20},\\ \dot{x}_3(t)&=u(t),\quad x_3(t_0)=x_{30},\end{aligned}\tag{10}$$

The modified nonhomogeneous super-twisting regulator (8)

$$u(t)=-\lambda_0\mid\int_{t_0}^{t}x_1(s)ds\mid^{1/5}sign(\int_{t_0}^{t}x_1(s)ds)-\lambda_1\mid x_1(t)\mid^{1/10}sign(x_1(t))$$

$$-\lambda_2\mid x_2(t)\mid^{1/10}sign(x_2(t))-\lambda_3\mid x_3(t)\mid^{1/10}sign(x_3(t))-\alpha\int_{t_0}^{t}sign(x_3(s))ds,\tag{11}$$

is applied with the control gains selected as $\lambda_0 = \lambda_1 = \lambda_2 = 20$, $\lambda_3 = 10$, $\alpha = 1$. The initial conditions are assigned as $x_{10} = x_{20} = x_{30} = 1000$. The obtained results are shown in Fig. 17. Figure 18 depicts the graph of the control input. Figure 19 shows the results for the initial conditions $x_{10} = x_{30} = 1000$, $x_{20} = -1000$. Figure 20 depicts the graph of the control input.

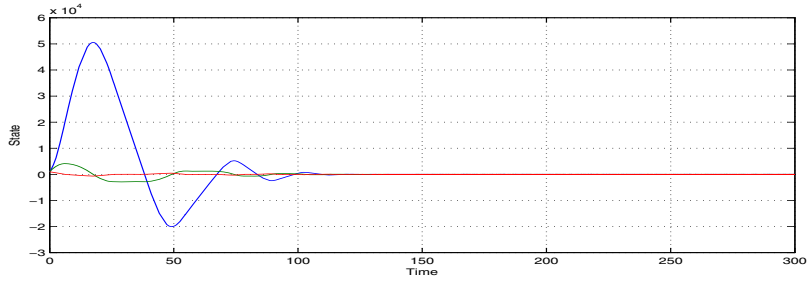

Fig. 17. Graphs of the system states (10) upon applying the control law (11) with exponents $\gamma_0 = 1/10$, $\gamma_1 = 1/10$, $\gamma_2 = 1/5$ and initial conditions $x_{10} = 1000$, $x_{20} = 1000$

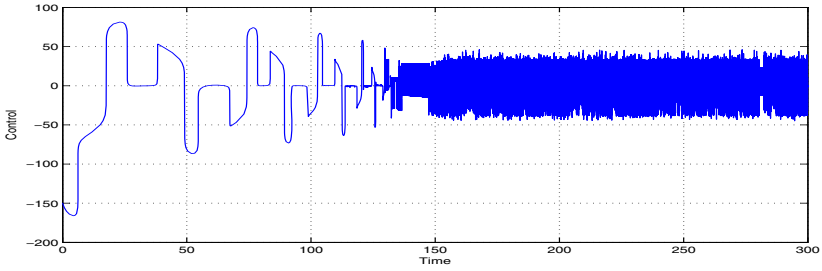

Fig. 18. Graphs of the control input (11) with exponents $\gamma_0 = 1/10$, $\gamma_1 = 1/10$, $\gamma_2 = 1/5$ for the system states (10) with initial conditions $x_{10} = 1000$, $x_{20} = 1000$

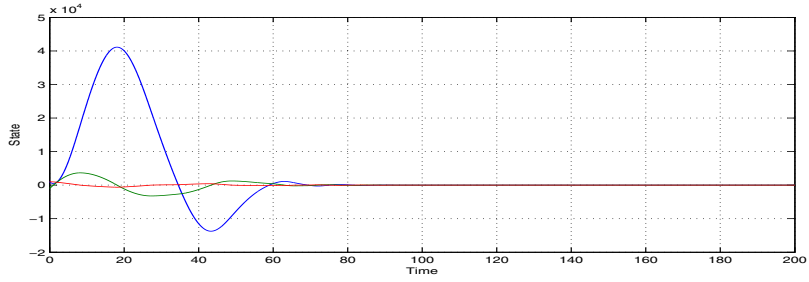

Fig. 19. Graphs of the system states (10) upon applying the control law (11) with exponents $\gamma_0 = 1/10$, $\gamma_1 = 1/10$, $\gamma_2 = 1/5$ and initial conditions $x_{10} = 1000$, $x_{20} = -1000$

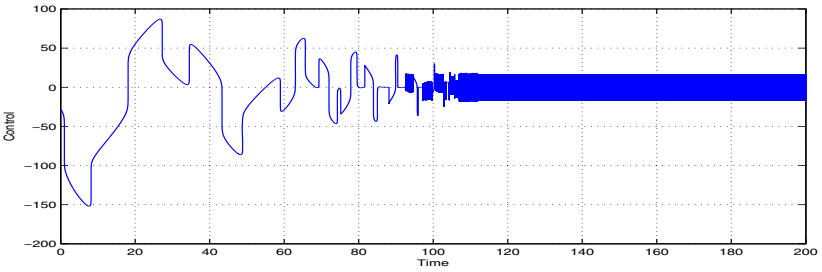

Fig. 20. Graphs of the control input (11) with exponents $\gamma_0 = 1/10$, $\gamma_1 = 1/10$, $\gamma_2 = 1/5$ for the system states (10) with initial conditions $x_{10} = 1000$, $x_{20} = -1000$

6. Consider a system (10) and a modified nonhomogeneous super-twisting regulator (8) with another set of the control gains $\lambda_0 = 0.2$, $\lambda_1 = 10$, $\lambda_2 = \lambda_3 = 20$, $\alpha = 1$:

$$u(t) = -\lambda_0 \mid \int_{t_0}^{t} x_1(s)ds \mid^{1/4} sign(\int_{t_0}^{t} x_1(s)ds) - \lambda_1 \mid x_1(t) \mid^{1/4} sign(x_1(t))$$

$$-\lambda_2 \mid x_2(t) \mid^{1/4} sign(x_2(t)) - \lambda_3 \mid x_3(t) \mid^{1/4} sign(x_3(t)) - \alpha \int_{t_0}^{t} sign(x_3(s))ds, \quad (12)$$

The initial conditions are assigned as $x_{10} = 1000$, $x_{20} = 1000$. The obtained results are shown in Fig. 21. Figure 22 depicts the graph of the control input. The results for the initial conditions $x_{10} = 1000$, $x_{20} = -1000$ are demonstrated in Figure 23. Figure 24 depicts the graph of the control input.

7. Consider a 3D system (10) with disturbance $\xi(t) = \sin(1000t)$. The modified nonhomogeneous super-twisting regulator (11) is applied with the control gains selected as $\lambda_0 = \lambda_1 = \lambda_2 = 20$, $\lambda_3 = 10$, $\alpha = 1$. The initial conditions are assigned as $x_{10} = x_{20} = x_{30} = 1000$ $x_{10} = 1000$. The obtained results are shown in Fig. 25. Figure 26 depicts the graph of the control input. Figure 27 shows the results for the initial conditions $x_{10} = x_{30} = 1000$, $x_{20} = -1000$. Figure 28 depicts the graph of the control input.

8. Consider a 3D system (10) with disturbance $\xi(t) = \sin(1000t)$. The modified nonhomogeneous super-twisting regulator (11) is applied with the control gains selected as $\lambda_0 = 0.2$, $\lambda_1 = 10$, $\lambda_2 = \lambda_3 = 20$, $\alpha = 1$. The initial conditions are assigned as $x_{10} = x_{20} = x_{30} = 1000$ $x_{10} = 1000$. The obtained results are shown in Fig. 29. Figure 30 depicts the graph of the control input. Figure 31 shows the results for the initial conditions $x_{10} = x_{30} = 1000$, $x_{20} = -1000$. Figure 32 depicts the graph of the control input.

The examples 1–8 clearly demonstrate that sufficient conditions similar to those given in [25] for the control gains in Theorem 2 and 4 would be too conservative, and the finite-time convergence takes place with much relaxed values. In particular, the value of constant L in this example is equal to 1000, due to high-frequency sinusoidal oscillations $\sin(1000t)$.

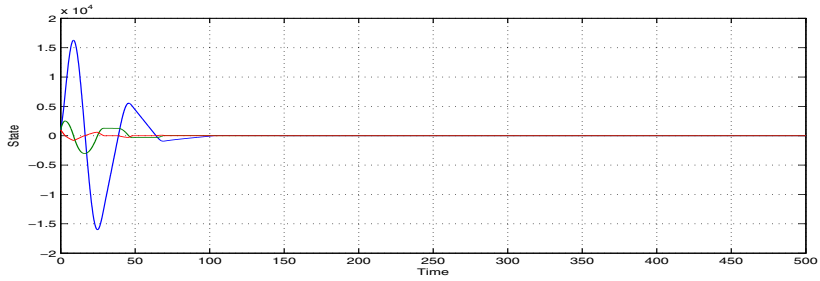

Fig. 21. Graphs of the system states (10) upon applying the control law (12) with exponents $\gamma_0 = \gamma_1 = \gamma_2 = 1/4$ and initial conditions $x_{10} = 1000$, $x_{20} = 1000$

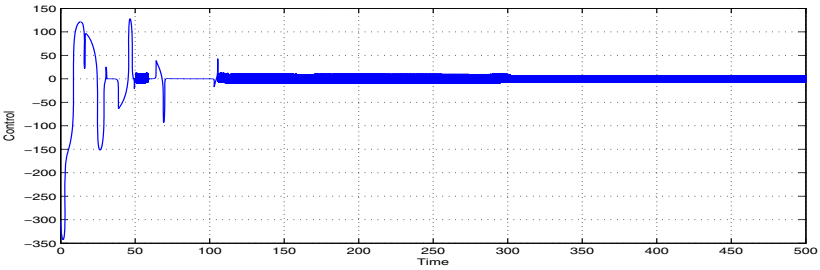

Fig. 22. Graphs of the control input (12) for the system states (10) with exponents $\gamma_0 = \gamma_1 = \gamma_2 = 1/4$ and initial conditions $x_{10} = 1000$, $x_{20} = 1000$

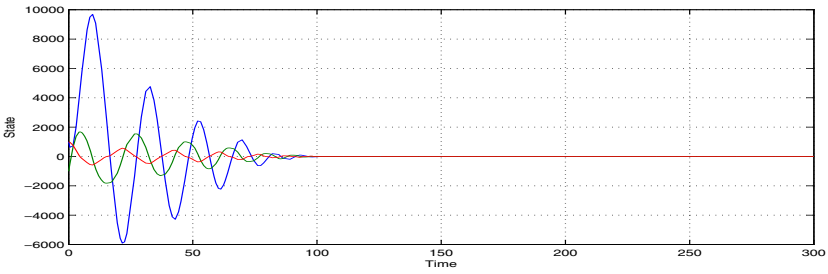

Fig. 23. Graphs of the system states (10) upon applying the control law (12) with exponents $\gamma_0 = \gamma_1 = \gamma_2 = 1/4$ and initial conditions $x_{10} = 1000$, $x_{20} = -1000$

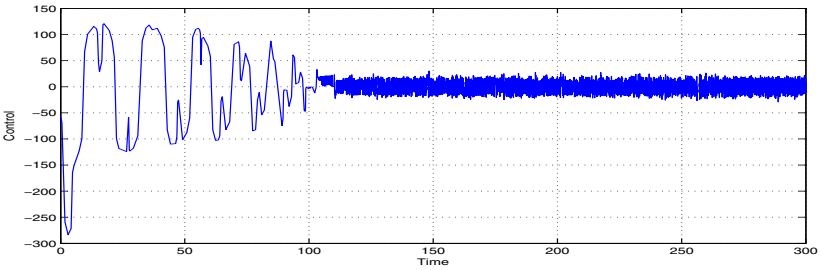

Fig. 24. Graphs of the control input (12) for the system states (10) with exponents $\gamma_0 = \gamma_1 = \gamma_2 = 1/4$ and initial conditions $x_{10} = 1000$, $x_{20} = -1000$

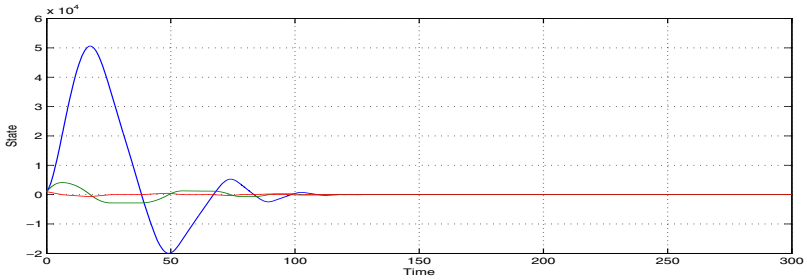

Fig. 25. Graphs of the system states (10) with disturbance $\xi(t) = \sin(1000t)$ upon applying the control law (11) with exponents $\gamma_0 = 1/10$, $\gamma_1 = 1/10$, $\gamma_2 = 1/5$ and initial conditions $x_{10} = 1000$, $x_{20} = 1000$

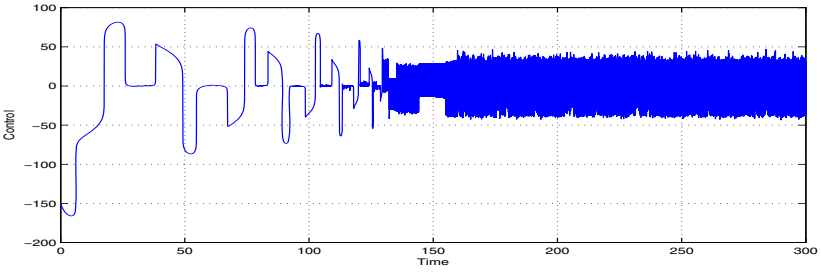

Fig. 26. Graphs of the control input (11) for the system states (10) with disturbance $\xi(t) = \sin(1000t)$, exponents $\gamma_0 = 1/10$, $\gamma_1 = 1/10$, $\gamma_2 = 1/5$, and initial conditions $x_{10} = 1000$, $x_{20} = 1000$

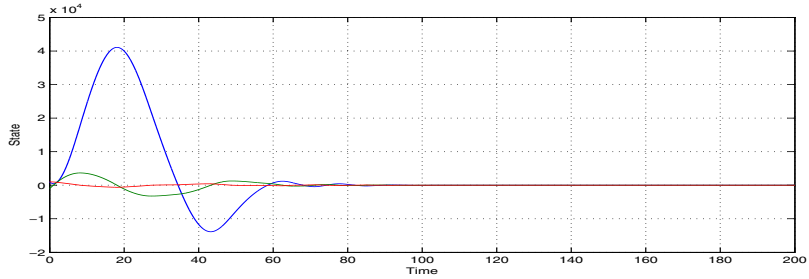

Fig. 27. Graphs of the system states (10) with disturbance $\xi(t) = \sin(1000t)$ upon applying the control law (11) with exponents $\gamma_0 = 1/10$, $\gamma_1 = 1/10$, $\gamma_2 = 1/5$ and initial conditions $x_{10} = 1000$, $x_{20} = -1000$

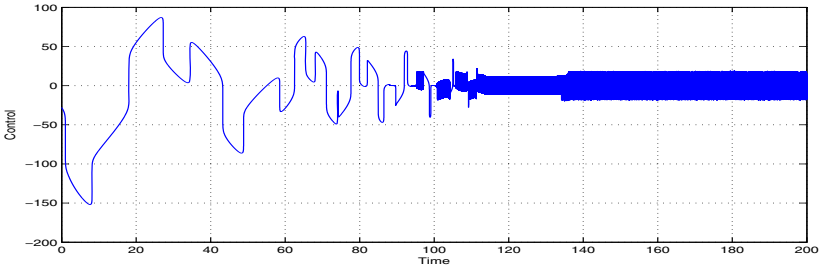

Fig. 28. Graphs of the control input (11) for the system states (10) with disturbance $\xi(t) = \sin(1000t)$, exponents $\gamma_0 = 1/10$, $\gamma_1 = 1/10$, $\gamma_2 = 1/5$, and initial conditions $x_{10} = 1000$, $x_{20} = -1000$

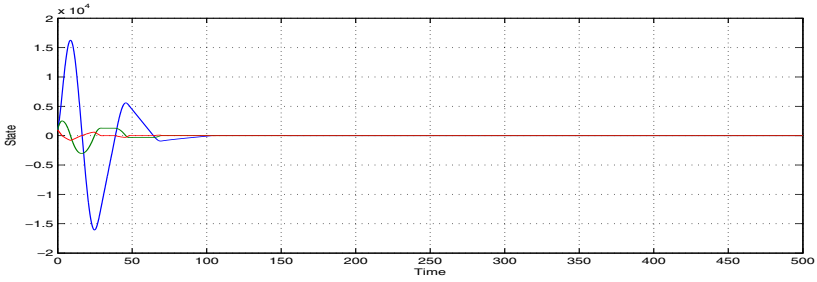

Fig. 29. Graphs of the system states (10) with disturbance $\xi(t) = \sin(1000t)$ upon applying the control law (11) with exponents $\gamma_0 = \gamma_1 = \gamma_2 = 1/4$ and initial conditions $x_{10} = 1000$, $x_{20} = 1000$

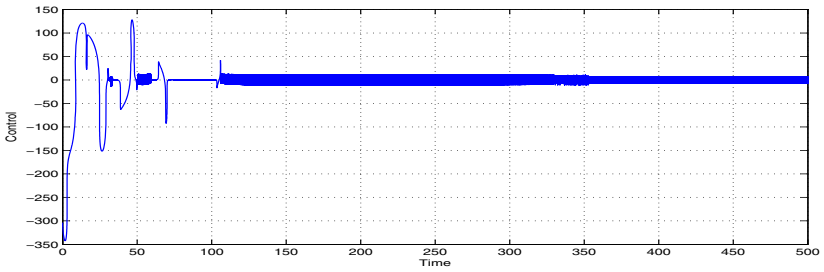

Fig. 30. Graphs of the control input (11) for the system states (10) with disturbance $\xi(t) = \sin(1000t)$, exponents $\gamma_0 = \gamma_1 = \gamma_2 = 1/4$, and initial conditions $x_{10} = 1000$, $x_{20} = 1000$

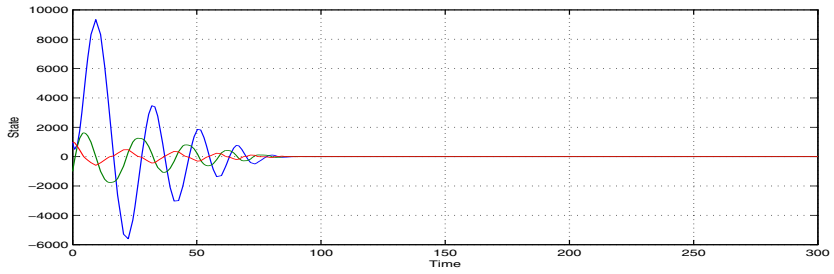

Fig. 31. Graphs of the system states (10) with disturbance $\xi(t) = \sin(1000t)$ upon applying the control law (11) with exponents $\gamma_0 = \gamma_1 = \gamma_2 = 1/4$ and initial conditions $x_{10} = 1000$, $x_{20} = -1000$

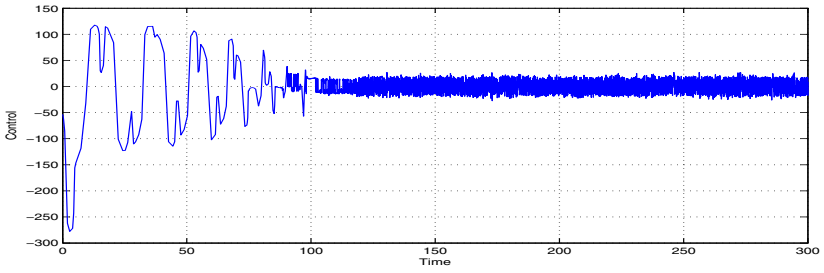

Fig. 32. Graphs of the control input (11) for the system states (10) with disturbance $\xi(t) = \sin(1000t)$, exponents $\gamma_0 = \gamma_1 = \gamma_2 = 1/4$, and initial conditions $x_{10} = 1000$, $x_{20} = -1000$

7 Conclusions

This chapter presents a nonhomogeneous continuous super-twisting algorithm for systems of dimension more than one, which is globally convergent to the origin for a finite time for any initial condition and also robust with respect to disturbances with a bounded changing rate. The designed technique generalizes the seminal continuous super-twisting algorithm, which was proven to be highly effective for stabilization of both system state and its derivative, to systems of dimension more than one. This advance leads to a possibility of applying a continuous finite-time stabilization control law to technical plants, where a conventional sliding mode control cannot be reliably employed due to effects pertinent to its discontinuous nature, such as short circuiting. Typical examples of technical devices, where the designed technique could be used to provide fault-tolerant systems, include induction motors, wind turbines, rolling mills, wireless network systems, and many others.

Acknowledgments. The first author expresses the special gratitude to Professor Okyay Kaynak for his always helpful orientation and support in many aspects of the professional life. In particular, the service as a technical editor for IEEE/ASME Transactions on Mechatronics under supervision of Prof. Kaynak as the Editor-in-Chief of this journal has been resulting in invaluable experience in improving the editorial standards and making contributions to the community.

References

1. Utkin, V.I.: Sliding Modes in Control and Optimization. Springer (1992)
2. Levant, A.: Sliding mode and sliding accuracy in sliding mode control. International Journal of Control 58, 1247–1263 (1993)
3. Levant, A.: Robust exact differentiation via sliding mode technique. Automatica 34, 379–384 (1998)
4. Kayacan, E., Oniz, Y., Kaynak, O.: A grey system modeling approach for sliding-mode control of antilock braking system. IEEE Trans. on Industrial Electronics 56, 3244–3252 (2009)
5. Xia, Y., Zhu, Z., Fu, M., Wang, S.: Attitude tracking of rigid spacecraft with bounded disturbances. IEEE Trans. on Industrial Electronics 57, 647–659 (2010)
6. Xia, Y., Zhu, Z., Fu, M.: Back-stepping sliding mode control for missile systems based on extended state observer. IET Control Theory and Applications 5, 93–102 (2011)
7. Kayacan, E., Cigdem, O., Kaynak, O.: Sliding mode control approach for online learning as applied to type-2 fuzzy neural networks and its experimental evaluation. IEEE Trans. on Industrial Electronics 59, 3510–3520 (2012)
8. Gao, H., Zhan, W., Karimi, H.R., Yang, X., Yin, S.: Allocation of actuators and sensors for coupled-adjacent-building vibration attenuation. IEEE Trans. on Industrial Electronics 60, 5792–5801 (2013)
9. Zhu, Z., Xu, D., Liu, J., Xia, Y.: Missile guidance law based on extended state observer. IEEE Trans. on Industrial Electronics 60, 5882–5891 (2013)
10. Li, H., Jing, X., Karimi, H.R.: Output-feedback-based control for vehicle suspension systems with control delay. IEEE Trans. on Industrial Electronics 61, 436–446 (2014)
11. Wu, L., Shi, P., Gao, H.: State estimation and sliding-mode control of Markovian jump singular systems. IEEE Trans. on Automatic Control 55, 1213–1219 (2010)
12. Ma, L., Wang, Z., Bo, Y., Guo, Z.: Robust H_∞ sliding mode control for nonlinear stochastic systems with multiple data packet losses. Intern. Journal of Robust and Nonlinear Control 22, 473–491 (2012)

13. Wu, L., Su, X., Shi, P.: Sliding mode control with bounded L_2 gain performance of Markovian jump singular time-delay systems. Automatica 48, 1929–1933 (2012)
14. Hu, J., Wang, Z., Gao, H., Stergioulas, L.K.: Robust sliding mode control for discrete stochastic systems with mixed time delays, randomly occurring uncertainties, and randomly occurring nonlinearities. IEEE Trans. on Industrial Electronics 59, 3008–3015 (2012)
15. Yin, S., Luo, H., Ding, S.X.: Real-time implementation of fault-tolerant control systems with performance optimization. IEEE Trans. on Industrial Electronics 61, 2402–2411 (2014)
16. Yin, S., Ding, S.X., Haghani, A., Hao, H., Zhang, P.: A comparison study of basic data-driven fault diagnosis and process monitoring methods on the benchmark Tennessee Eastman process. Journal of Process Control 22, 1567–1581 (2012)
17. Polyakov, A., Poznyak, A.: Lyapunov function design for finite-time convergence analysis: Twisting controller for second-order sliding mode realization. Automatica 45, 444–448 (2009)
18. Polyakov, A., Poznyak, A.: Reaching time estimation for super-twisting second order sliding mode controller via Lyapunov function design. IEEE Trans. on Automatic Control 54, 1951–1955 (2009)
19. Moreno, J.A., Osorio, M.: Strict Lyapunov functions for the super-twisting algorithm. IEEE Trans. on Automatic Control 57, 1035–1040 (2012)
20. Bhat, S.P., Bernstein, D.S.: Geometric homogeneity with applications to finite-time stability. Mathematics of Control, Signals, and Systems 17, 101–127 (2005)
21. Levant, A.: Homogeneity approach to high-order sliding mode design. Automatica 41, 823–830 (2005)
22. Orlov, Y.: Finite-time stability and robust control synthesis of uncertain switched systems. SIAM Journal on Control and Optimization 43, 1253–1271 (2005)
23. Filippov, A.F.: Differential Equations with Discontinuous Righthand Sides. Kluwer Academic Publishers, Dordrecht (1988)
24. Perruquetti, W., Floquet, T., Moulay, E.: Finite-time observers: applications to secure communication. IEEE Trans. on Automatic Control 53, 356–360 (2008)
25. Basin, M.V., Rodriguez-Ramirez, P.: A super-twisting algorithm for systems of dimension more than one. IEEE Trans. on Industrial Electronics 61, 6472–6480 (2014)

A Appendix

A.1 Lemma 1

Consider a dynamic system (1) of dimension two. Then, the modified nonhomogeneous super-twisting control law (5) yields finite-time convergence of both states $x_1(t)$ and $x_2(t)$ to to a point $[x_{1f}, 0]$.

Proof. The system (1),(5) can be recast as

$$\dot{x}_1(t) = x_2(t), \quad x_1(t_0) = x_{10}, \tag{13}$$

$$\dot{x}_2(t) = -\lambda_0 \mid \int_{t_0}^{t} x_1(s)ds \mid^{\gamma_0} sign(\int_{t_0}^{t} x_1(s)ds) - \lambda_1 \mid x_1(t) \mid^{\gamma_1} sign(x_1(t)) -$$

$$-\lambda_2 \mid x_2(t) \mid^{\gamma_2} sign(x_2(t)) + x_3(t), \quad x_2(t_0) = x_{20},$$

$$\dot{x}_3(t) = -\alpha sign(x_2(t)), \quad x_3(t_0) = 0.$$

Consider the following subsystem:

$$\dot{x}_1(t) = x_2(t), \quad x_1(t_0) = x_{10}, \tag{14}$$
$$\dot{x}_2(t) = -\lambda_1 \mid x_1(t) \mid^{\gamma_1} sign(x_1(t)) - \lambda_2 \mid x_2(t) \mid^{\gamma_2} sign(x_2(t)) + x_3(t), \quad x_2(t_0) = x_{20},$$
$$\dot{x}_3(t) = -\alpha sign(x_2(t)), \quad x_3(t_0) = 0.$$

The vector field f in the right-hand side of (14) can be represented as the sum of two vector fields, $f = g_1 + g_2$, where $g_1 = [x_2, -\lambda_1 \mid x_1(t) \mid^{\gamma_1} sign(x_1(t)) - \rho\lambda_2 \mid x_2(t) \mid^{\gamma_2} sign(x_2(t)), 0]$, $\rho \in (0,1)$, and $g_2 = [0, -(1-\rho)\lambda_2 \mid x_2(t) \mid^{\gamma_2} sign(x_2(t)) + x_3(t), -\alpha sign(x_2(t))]$. The field g_1 provides the finite-time stability at a point $[0,0,x_3(t_0)]$ in view of Lyapunov function $V(x_1,x_2) = \lambda_1(1/(\gamma_1+1)) \mid x_1(t) \mid^{\gamma_1+1} + (1/2) \mid x_2(t) \mid^2$. The field g_2 corresponds to a super-twisting algorithm [3], which converges to a point $[x_{1f},0,0]$ for a finite time. The finite-time convergence of the entire system (13) at a point $[x_{1f},0,x_3(t_0)]$ is derived following the arguments of Theorem 7.4 in [20], replacing there a "homogeneous" system with a "finite-time convergent" one, and taking into account that the Lyapunov function for super-twisting has a continuous total derivative in time along the trajectory, so the results of Theorem 6.2, Lemma 4.2 and the inequalities (34)-(36) from [20] hold for a finite-time convergent system.

Note that the term $\lambda_0 \mid \int_{t_0}^t x_1(s)ds \mid^{\gamma_0} sign(\int_{t_0}^t x_1(s)ds)$ in (13) satisfies a Lipschitz condition everywhere except for the initial time moment t_0. The finite-time convergence of the system (13) follows from the fact that a super-twisting algorithm still converges for a finite time in the presence of disturbances satisfying a Lipschitz condition, under certain restrictions for control gains $\lambda_0, \lambda_1, \lambda_2 > 0$, $\alpha > 0$ [3]. ■

A.2 Lemma 2

Consider a dynamic system (7) of dimension $n > 2$. Then, the modified nonhomogeneous super-twisting control law (8) yields finite-time convergence of the states $x_1(t), x_2(t) \ldots, x_n(t)$ to a point $[x_{1f}, 0, \ldots, 0]$.

Proof is given by induction. Let us assume that the lemma assertion is true for a system (7) of dimension n. Consider now a system of dimension $n+1$:

$$\dot{x}_0(t) = x_1(t), \quad x_0(t_0) = x_{00}, \tag{15}$$
$$\dot{x}_1(t) = x_2(t), \quad x_1(t_0) = x_{10},$$
$$\dot{x}_2(t) = x_3(t), \quad x_2(t_0) = x_{20},$$
$$\ldots$$
$$\dot{x}_n(t) = -v_{-1}(t) - v_0(t) - v_1(t) - v_2(t) - \ldots - v_n(t) - v_{n+1}(t), \quad x_n(t_0) = x_{n0},$$

where

$$v_{-1}(t) = \lambda_{-1} \mid \int_{t_0}^t x_0(s)ds \mid^{\gamma_{-1}} sign(\int_{t_0}^t x_0(s)ds),$$
$$v_i(t) = \lambda_i \mid x_i(t) \mid^{\gamma_i} sign(x_i(t)), \quad i = 0, \ldots, n,$$
$$v_{n+1}(t) = \alpha \int_{t_0}^t sign(x_n(s))ds,$$

and $\gamma_{-1} \in (0,1)$, $\lambda_{-1} > 0$.

Note that the term $v_{-1}(t)$ in (15) satisfies a Lipschitz condition everywhere except for the initial time moment t_0. The finite-time convergence of the system (15) to a point $[x_{0f}, x_{1f}, 0, \ldots, 0]$ follows from the induction premise, Lemma 1, and the fact that a super-twisting algorithm still converges for a finite time in the presence of disturbances satisfying a Lipschitz condition, under certain restrictions for control gains $\lambda_i > 0$, $i \in -1, \ldots, n$, $\alpha > 0$ [3]. Then, it follows from the equations (15) that $x_{1f} = 0$. Thus, the equilibrium point is given by $[x_{1f}, 0 \ldots, 0, 0]$ and located in the manifold $x_1 = x_2 = \ldots = x_n = 0$. ■

A.3 Proof of Theorem 1

The system (1),(5) can be recast introducing a new fictitious variable x_0:

$$\begin{gathered} \dot{x}_0(t) = x_1(t), \quad x_0(t_0) = 0, \\ \dot{x}_1(t) = x_2(t), \quad x_1(t_0) = x_{10}, \\ \dot{x}_2(t) = -\lambda_0 \mid \int_{t_0}^{t} x_1(s)ds \mid^{\gamma_0} sign(\int_{t_0}^{t} x_1(s)ds) - \lambda_1 \mid x_1(t) \mid^{\gamma_1} sign(x_1(t)) - \\ -\lambda_2 \mid x_2(t) \mid^{\gamma_2} sign(x_2(t)) - \alpha sign(x_2(t)), \quad x_2(t_0) = x_{20}. \end{gathered} \tag{16}$$

The theorem assertion follows directly from Lemma 2 applied to the system (16). ■

A.4 Proof of Theorem 2

The system (6) can be recast, introducing a new fictitious variable x_0, as the system (16) with a disturbance $\xi(t)$ present in the last equation for $x_2(t)$. The theorem assertion follows from Lemma 2 applied to the resulting system and the fact that a super-twisting algorithm converges for a finite time in the presence of disturbances satisfying a Lipschitz condition, under certain restrictions for control gains [3]. ■

A.5 Proof of Theorem 3

The system (7) can be recast introducing a new fictitious variable x_0:

$$\begin{gathered} \dot{x}_0(t) = x_1(t), \quad x_0(t_0) = 0, \\ \dot{x}_1(t) = x_2(t), \quad x_1(t_0) = x_{10}, \\ \dot{x}_2(t) = x_3(t), \quad x_2(t_0) = x_{20}, \\ \ldots \\ \dot{x}_n(t) = -v_0(t) - v_1(t) - v_2(t) - \ldots - v_n(t) - v_{n+1}(t), \quad x_n(t_0) = x_{n0}. \end{gathered} \tag{17}$$

The theorem assertion follows directly from Lemma 2 applied to the system (17). ■

A.6 Proof of Theorem 4

The system (9) can be recast, introducing a new fictitious variable x_0, as the system (17) with a disturbance $\xi(t)$ present in the last equation for $x_2(t)$. The theorem assertion follows from Lemma 2 applied to the resulting system and the fact that a super-twisting algorithm converges for a finite time in the presence of disturbances satisfying a Lipschitz condition, under certain restrictions for control gains [3]. ■

Global Multivariable Hybrid Estimator for Nonuniform Relative Degree Systems with Uncertainties and Disturbances

Liu Hsu[1], Eduardo V.L. Nunes[1],
Tiago Roux Oliveira[2], and Alessandro Jacoud Peixoto[1]

[1] Dept. of Electrical Engineering
COPPE/Federal University of Rio de Janeiro,
Rio de Janeiro, RJ, Brazil
{eduardo,jacoud,liu}@coep.ufrj.br
[2] Dept. of Electronics and Telecommunication Engineering,
State University of Rio de Janeiro - UERJ
Rio de Janeiro, RJ, Brazil
tiagoroux@uerj.br

Abstract. In this chapter, we propose an output feedback sliding mode controller to solve the problem of global exact output tracking for a class of uncertain multivariable nonlinear plants with disturbances. In order to cope with the nonuniform arbitrary relative degree, we propose a hybrid estimation scheme which combines through switching a high-gain observer and a set of locally exact differentiators. Norm observers for the unmeasured state are employed to dominate the disturbances since they may be state dependent. Thus, uniform global exponential practical stability and ultimate exact tracking are guaranteed with a peaking free control signal, despite the use of high-gain observers. An example is presented to illustrate the application of the proposed scheme in the presence of unmodeled dynamics and measurement noise.

Keywords: Sliding mode control, uncertain systems, disturbances, output feedback, global exact tracking, high-gain observers, high order sliding modes.

1 Introduction

The stabilization and tracking control for nonlinear systems are longstanding problems that have still been studied in recent years. Several difficulties can be pointed out, such as: the ill-defined relative degree condition [6], nonminimum phase [2], the presence of perturbations and uncertainties [1, 4, 9, 35]. In particular, the use of output feedback sliding mode control (SMC) for exact tracking of multivariable disturbed systems with arbitrary relative degree is a challenging problem in this context [15]. This scenario is even more problematic if global stability properties are also pursued [29]. For instance, to compensate the relative degree, High-Gain Observers (HGO) [11], [12, 8] can be used. However, global or semi-global stability results were obtained only with residual output errors [24].

X. Yu and M. Önder Efe (eds.), *Recent Advances in Sliding Modes*,
Studies in Systems, Decision and Control 24, DOI: 10.1007/978-3-319-18290-2_10

Recently, nonglobal exact output tracking controllers based on higher order sliding modes (HOSM) were considered by several authors (e.g., [2, 13, 15, 30]). In [30], a second order sliding mode controller was proposed for nonlinear systems with uniform relative degree two. In [15], an output feedback SMC was developed for MIMO (Multi-Input-Multi-Output) systems of any relative degree with uniformly bounded and matched nonlinearities. Local asymptotic tracking of causal nonminimum phase nonlinear systems with non-uniform arbitrary relative degree was considered in [2]. In [13], the authors used nested quasi-continuous HOSM to allow finite-time exact compensation of unmatched perturbations.

In this chapter, we solve the *global* exact output tracking problem for a class of *uncertain MIMO nonlinear* plants with *non-uniform* arbitrary relative degree and disturbances. The class considered here encompasses those in [1, 3, 10, 13], with the advantage of guaranteeing global stability properties. The afore mentioned problem using output feedback SMC had remained unsolved for this class of plants.

The result is achieved by generalizing a hybrid estimation scheme, originally proposed for SISO plants in [27], to a multivariable framework. The hybrid estimation scheme selects through switching between a MIMO HGO and a multivariable extension of a robust exact differentiator (RED) based on HOSM. As a result, the error system becomes uniformly globally exponentially practically stable [27] with respect to a small residual set and ultimately converges to zero.

New assumptions must be made for the multivariable case, which make the problem more involved and not easy to be solved. For instance, in [29] it is assumed that there exists a known matrix multiplier S_p for the high frequency gain (HFG) matrix K_p such that $K_pS_p + S_p^TK_p^T > 0$, whilst in [27] just the knowledge of the scalar HFG k_p sign is needed. Here, we consider a diagonally stable assumption that is less restrictive than the one made in [29].

In our previous results, only uniformly bounded input disturbances were considered. In this chapter, the matched disturbances may be linearly growth dependent on the unmeasured state. Moreover, the output-feedback methodology for disturbance domination is also new since norm state observers are introduced. To avoid peeking in the control signal such norm state observers are derived from the input-output filters commonly used in model reference adaptive control (MRAC).

The hybrid nonlinear filter is constructed using a high-gain observer combined with the robust exact differentiator instead of lead filters applied before. The replacement of lead filters used in [27, 29] by a high-gain observer in the hybrid estimation scheme is motivated by the HGO improved robustness to unmodeled dynamics, as discussed in [25, 22, 28].

1.1 Preliminaries

In what follows, all κ's denote positive constants. $\pi(t)$ denotes an exponentially decaying function, i.e., $|\pi(t)| \leq Ke^{-\lambda t}, \forall t$, where K possibly depends on the system initial conditions and λ is a (generic) positive constant. $|\cdot|$ stands for the Euclidean norm for vectors, or the induced norm for matrices. $\|f(t)\|$ denotes

$\operatorname{ess\,sup}\{|f(t)|, t \geq 0\}$, and $\|f_{[t_1,t_2]}\| = \sup_{t\in[t_1,t_2]}|f(t)|, 0 \leq t_1 \leq t_2$. Here, Filippov's definition for the solution of discontinuous differential equations is assumed [14]. For the sake of simplicity, "s" will represent either the Laplace variable or the differential operator (d/dt), according to the context.

2 Problem Statement

Consider an uncertain MIMO nonlinear plant described by:

$$\dot{x} = A_p x + B_p[u + d(x,t)], \qquad y = H_p x, \tag{1}$$

where $x \in \mathbb{R}^n$ is the state, $u \in \mathbb{R}^m$ is the input, $y \in \mathbb{R}^m$ is the output and $d(x,t) \in \mathbb{R}^m$ is a state dependent uncertain nonlinear disturbance. The uncertain matrices A_p, B_p and H_p belong to some compact set, such that the necessary uncertainty bounds to be defined later are available for design. The following basic assumptions are usual in MIMO adaptive control:

(A1) $G(s) = H_p(sI - A_p)^{-1}B_p$ is minimum phase and has full rank.

(A2) The linear subsystem is controllable and observable.

(A3) The observability index ν of $G(s)$ (see [21]), or an upper bound of ν, is known.

We also make the following assumptions that are discussed and motivated in [29, 28].

(A4) The left interactor matrix $\Xi(s)$ (see [19]) is diagonal and $G(s)$ has a known global vector relative degree $\{\rho_1, \ldots, \rho_m\}$ (i.e., $\Xi(s) = \operatorname{diag}\{s^{\rho_1}, \ldots, s^{\rho_m}\}$). The matrix $K_p \in \mathbb{R}^{m\times m}$, finite and nonsingular, is referred to as the *high frequency gain* (HFG) matrix and satisfies $K_p = \lim_{s\to\infty} \Xi(s)G(s)$.

(A5) A nonsingular matrix S_p is known such that $-K_pS_p$ is diagonally stable, i.e. there exists a diagonal matrix $D > 0$ such that $DK + K^TD = -Q$, with $Q = Q^T > 0$ and $K = -K_pS_p$.

To achieve global exact tracking using only output feedback the following assumption is made.

(A6) The input disturbance $d(x,t)$ is assumed to be uncertain, locally integrable and norm bounded by $|d(x,t)| \leq k_x|x| + k_d$, $\forall x, t$, where $k_x, k_d \geq 0$ are *known* scalars.

Note that the relative degree of system (1) depends only on the linear part, being independent of the disturbance d. Although this assumption restricts the class of disturbances coped with, it represents a challenge in the context of output-feedback sliding mode control since global stability and exact tracking are still pursued.

Let the reference signal $y_m(t) \in \mathbb{R}^m$ be generated by the following reference model

$$y_m = W_m(s)\, r, \quad W_m(s) = \operatorname{diag}\left\{(s+\gamma_1)^{-1}, \ldots, (s+\gamma_m)^{-1}\right\} L^{-1}(s), \tag{2}$$

where $\gamma_j > 0$ $(j = 1, \cdots, m)$, $r(t) \in \mathbb{R}^m$ is an arbitrary uniformly bounded piecewise continuous reference signal and

$$L(s) = \operatorname{diag}\{L_1(s), L_2(s), \ldots, L_m(s)\}, \tag{3}$$

with $L_j(s)=s^{(\rho_j-1)}+l^{[j]}_{\rho_j-2}s^{(\rho_j-2)}+\cdots+l^{[j]}_1 s+l^{[j]}_0$ $(j=1,\ldots,m)$ being Hurwitz polynomials and the superscript $^{[j]}$ indicating that a parameter belongs to $L_j(s)$. The transfer function matrix $W_m(s)$ has the same vector relative degree as $G(s)$ and its HFG is the identity matrix.

The main objective is to find a control law u such that the output error $e:=y-y_m$ tends asymptotically to zero, for arbitrary initial conditions. When the plant is known and $d(t)\equiv 0$, a control law which achieves the matching between the closed-loop transfer function matrix and $W_m(s)$ is given by $u^*=\theta^{*^T}\omega$, where the parameter matrix is written as $\theta^*=\left[\theta_1^{*^T}\ \theta_2^{*^T}\ \theta_3^{*^T}\ \theta_4^{*^T}\right]^T$, with $\theta_1^*,\theta_2^*\in\mathbb{R}^{m(\nu-1)\times m},\theta_3^*,\theta_4^*\in\mathbb{R}^{m\times m}$ and the regressor vector $\omega=[\omega_u^T\ \omega_y^T\ y^T\ r^T]^T$ $(w_u,w_y\in\mathbb{R}^{m(\nu-1)})$ is obtained from I/O state variable filters given by:

$$\omega_u=A(s)\Lambda^{-1}(s)u\,,\quad \omega_y=A(s)\Lambda^{-1}(s)y\,, \tag{4}$$

where $A(s)=[Is^{\nu-2}\ \ Is^{\nu-3}\ \cdots\ Is\ \ I]^T$, $\Lambda(s)=\lambda(s)I$ with $\lambda(s)$ being a monic Hurwitz polynomial of degree $\nu-1$. The matching conditions require that $\theta_4^{*T}=K_p^{-1}$.

Consider the following realization of (4)

$$\dot\omega_u=\Phi\omega_u+\Gamma u\,,\quad \dot\omega_y=\Phi\omega_y+\Gamma y\,,\quad \Phi\in\mathbb{R}^{m(\nu-1)\times m(\nu-1)},\quad \Gamma\in\mathbb{R}^{m(\nu-1)\times m} \tag{5}$$

where $\det(sI-\Phi)=\det(\Lambda(s))=[\lambda(s)]^m$. Define the state vetor $X=[x^T,\omega_u^T,\omega_y^T]^T$ with dynamics described by $\dot X=A_0X+B_0u+B_0'd,\ y=H_oX$. Then, adding and subtracting $B_0\theta^{*T}\omega$ and noting that there exist matrices Ω_1 and Ω_2 such that $\omega=\Omega_1X+\Omega_2r$, one has

$$\dot X=A_cX+B_cK_p[\theta_4^{*T}r+u-u^*]+B_0'd\,,\qquad y=H_oX\,, \tag{6}$$

where $A_c=A_0+B_0\theta^{*T}\Omega_1$ and $B_c=B_0\theta_4^{*T}$. Notice that (A_c,B_c,H_o) is a non-minimal realization of $W_m(s)$. For analysis purposes, the reference model can be described by

$$\dot X_m=A_cX_m+B_cK_p[\theta_4^{*T}r-d_f]+B_0'd,\quad y_m=H_oX_m\,, \tag{7}$$

the equivalent input disturbance $d_f=W_d(s)d$, where

$$W_d(s)=[W_m(s)K_p]^{-1}\,\bar W_d(s),\qquad \bar W_d(s)=H_o\,(sI-A_c)^{-1}\,B_0'\,. \tag{8}$$

Thus, $y_m=W_m(s)K_p\left[\theta_4^{*T}r-W_d(s)d\right]+\bar W_d(s)d$, it is straightforward to conclude that $y_m=W_m(s)\,r$. Thus, the error dynamics with state $x_e:=X-X_m$ is given by:

$$\text{state space:}\ \ \dot x_e=A_c\,x_e+B_cK_p[u-\theta^{*^T}\omega+d_f],\qquad e=H_o\ x_e, \tag{9}$$

$$\text{input-output form:}\quad e=W_m(s)K_p\left[u-\theta^{*^T}\omega+d_f\right]\,. \tag{10}$$

Remark 1. The error equations (9) and (10) are similar to those found in some of our previous works, e.g., [27] and [29]. However, in this chapter, a key difference must be highlighted: the equivalent input disturbance $d_f(x,t)$ is state-dependent. The control design tools proposed in [27] and [29] are not able to cope with the lack of a norm bound for $d_f(x,t)$, since the plant state is not available for feedback. Thus, here we use norm state observers to obtain a norm bound for $d_f(x,t)$, as discussed in the next section.

3 Norm State Observer and Norm Bound for Equivalent Disturbance

Considering Assumption (A6) and applying [17, Lemma 3] to (6), it is possible to find $k_x^* > 0$ such that, for $k_x \in [0, k_x^*]$ a norm bound for X and x can be obtained through *first order approximation filters* (FOAFs) (see details in [17]). Thus, one has $|x(t)| \leq \hat{x}(t) + \hat{\pi}(t)$, where

$$\hat{x}(t) := \frac{1}{s+\lambda_x}[c_1 k_d + c_2|\omega(t)|]\,, \tag{11}$$

with $c_1, c_2, \lambda_x > 0$ being appropriate constants that can be computed by the optimization methods described in [7]. As in [17], the exponentially decaying term $\hat{\pi}$ accounts for the system initial conditions. Reminding that $d_f = W_d(s)d$ it is clear that $|d_f| \leq |W_d(s) * d|$, *modulo* an exponential decaying term depending on the initial conditions. Moreover, from (A6) and (11), one has $|d(x,t)| \leq k_x\hat{x}(t) + k_d$, *modulo* $\hat{\pi}$ term, and one can write $|d_f| \leq \hat{d}_f + \hat{\pi}_f$, where $\hat{\pi}_f$ is an exponentially decaying term,

$$\hat{d}_f(t) := \frac{c_f}{s+\lambda_f}[k_x\hat{x}(t) + k_d]\,, \tag{12}$$

and $\frac{c_f}{s+\lambda_f}$ is a FOAF designed for $W_d(s)$, with adequate positive constants c_f and λ_f.

4 Unit Vector Control Design

For systems with uniform relative degree one, i.e. $\rho_1 = \rho_2 = \ldots \rho_m = 1$, the main idea is to close the control loop with a nominal control together with a unit vector control (UVC) term to cope with uncertainties and disturbances:

$$u = (\theta^{\text{nom}})^T\omega - \varrho(t)S_p\frac{e}{|e|}\,, \quad e \in \mathbb{R}^m,\ S_p \in \mathbb{R}^{m\times m},\ \varrho \in \mathbb{R}\,, \tag{13}$$

where θ^{nom} is the nominal value for θ^*, S_p satisfies (A5) and the modulation function $\varrho(t) \geq 0$ is designed to induce a sliding mode on the manifold $e = 0$ and is such that:

$$\varrho(t) \geq (1+c_d)\left|S_p^{-1}\left[(\theta^{\text{nom}} - \theta^*)^T\omega - d_f\right]\right| + \delta\,, \quad c_d, \delta > 0 \tag{14}$$

where c_d is an appropriate constant and δ can be arbitrarily small. Note that the nominal control signal allows the reduction of the modulation function amplitude if $|\theta^{\rm nom} - \theta^*|$ is small. Since A_p, B_p and H_p belong to some known compact set, an upper bound $\bar{\theta} \geq |\theta^{\rm nom} - \theta^*|$ can be obtained. Thus, a possible choice for the modulation function to satisfy (14) is given by

$$\varrho(t) = (1 + c_d) \left|S_p^{-1}\right| \left[\bar{\theta} \left|\omega\right| + \left|d_f\right|\right] + \delta. \tag{15}$$

For relative degree one plants, $W_m(s) = \text{diag}\left\{(s+\gamma_1)^{-1}, \ldots, (s+\gamma_m)^{-1}\right\}$ $(L(s) = I_m)$ and since $-K_p S_p$ is diagonally stable, by applying Lemma 1 in the appendix, one can conclude that the above scheme is uniformly globally exponentially stable and the output error e becomes identically zero after some finite time. For higher relative degree plants, one could use the operator $L(s)$ defined in (3), to overcome the relative degree obstacle. The operator $L(s)$ is such that $L(s)G(s)$ and $L(s)W_m(s)$ have uniform vector relative degree one. The ideal sliding variable $\sigma = L(s)e \in \mathbb{R}^m$ is given by

$$\sigma = \begin{bmatrix} e_1^{(\rho_1 - 1)} + \cdots + l_1^{[1]} \dot{e}_1 + l_0^{[1]}\ e_1 \\ \vdots \\ e_m^{(\rho_m - 1)} + \cdots + l_1^{[m]} \dot{e}_m + l_0^{[m]} e_m \end{bmatrix} = \begin{bmatrix} \sum_{i=0}^{\rho_1 - 1} l_i^{[1]} h_1^T A_c^{(i)} x_e \\ \vdots \\ \sum_{i=0}^{\rho_m - 1} l_i^{[m]} h_m^T A_c^{(i)} x_e \end{bmatrix} = \bar{H} x_e\,, \tag{16}$$

where $h_j \in \mathbb{R}^{n+2m(\nu-1)}$ is the j-th row of H_o matrix and the second equality is derived from Assumption (A4) and (9). Notice that $\{A_c, B_c, \bar{H}\}$ is a nonminimal realization of $L(s)W_m(s)$. If the control signal is given by $u = (\theta^{nom})^T \omega - \varrho(t) S_p \frac{\sigma}{|\sigma|}$, with modulation function $\varrho(t)$ satisfying (14), then the closed-loop error system is uniformly globally exponentially stable and the ideal sliding variable σ becomes identically zero after some finite time, according to Lemma 1 in the appendix. However, σ is not directly available to implement the control law.

5 Unit Vector Control Using a High-Gain Observer

Consider the minimal order observer-form [21] realization $\{A_M,\ B_M,\ C_M\}$ of the model $W_m(s)$. Then, the external dynamics of the error equation (9) can be rewritten as

$$\dot{\xi} = A_M \xi + B_M K_p \Big[u - {\theta^*}^T \omega + d_f + \pi_\eta\Big], \quad e = C_M \xi\,, \quad \xi \in \mathbb{R}^{\rho_t}, \quad \rho_t = \sum_{i=1}^{m} \rho_i \tag{17}$$

where the initial condition $\xi(0)$ and the exponentially decaying signal $\pi_\eta(t) \in \mathbb{R}^m$ are adequate for representing the initial condition of the observable but

uncontrollable modes in (9). The unavailable state ξ can be estimate by means of an HGO given by:

$$\dot{\hat{\xi}} = A_M\hat{\xi} + B_M K_p^{\text{nom}} u - \left[\Gamma(\varepsilon^{-1}) - H_a\right]\tilde{e}, \quad \tilde{e} = C_M\hat{\xi} - e\,, \tag{18}$$

where $\varepsilon \in \mathbb{R}$, $\Gamma(\varepsilon^{-1})$, $H_a \in \mathbb{R}^{\rho_t \times m}$, $A_M \in \mathbb{R}^{\rho_t \times \rho_t}$, $B_M \in \mathbb{R}^{\rho_t \times m}$, $C_M \in \mathbb{R}^{m \times \rho_t}$, $\varepsilon > 0$, $\tilde{e} \in \mathbb{R}^m$ is the observer output error $K_p^{\text{nom}} \in \mathbb{R}^{m \times m}$ is the nominal value of the gain K_p, $\Gamma(\varepsilon^{-1}) = \text{block diag}\{\Gamma_\varepsilon^{[1]}, \ldots, \Gamma_\varepsilon^{[m]}\}$, with $(\Gamma_\varepsilon^{[j]})^T = \left[\dfrac{\bar{a}_{\rho_j-1}^{[j]}}{\varepsilon} \;\ldots\; \dfrac{\bar{a}_1^{[j]}}{\varepsilon^{\rho_j-1}} \; \dfrac{\bar{a}_0^{[j]}}{\varepsilon^{\rho_j}}\right]$, $H_a = \text{block diag}\,\{H_a^{[1]}, \ldots, H_a^{[m]}\}$, with $H_a^{[j]} = \left[a_{\rho_j-1}^{[j]} \;\ldots\; a_0^{[j]}\right]^T$ and $L_j(s)(s + \gamma_j) = s^{\rho_j} + a_{\rho_j-1}^{[j]} s^{\rho_j-1} + \ldots a_1^{[j]} s + a_0^{[j]}$. The coefficients $\bar{a}_i^{[j]}$ in the observer feedback matrix, must be chosen such that $N_a^{[j]}(s) = s^{\rho_j} + \bar{a}_{\rho_j-1}^{[j]} s^{\rho_j-1} + \cdots + \bar{a}_0^{[j]}$ is Hurwitz. It is possible to design a matrix $\bar{H}_M$ such that $\{A_M, B_M, \bar{H}_M\}$ is a realization of the SPR transfer function $L(s)W_m(s)$. Thus, for plants of higher relative degree, σ can be estimated by:

$$\hat{\sigma}_h = \bar{H}_M\hat{\xi}, \qquad \bar{H}_M \in \mathbb{R}^{m \times \rho_t} \tag{19}$$

Defining the estimation error state as $\tilde{\xi} = \hat{\xi} - \xi$, one has:

$$\dot{\tilde{\xi}} = A_\xi(\varepsilon^{-1})\tilde{\xi} + B_M K_p^{nom}\bar{U}, \quad \tilde{\xi}_h = \bar{H}_M\tilde{\xi}\,, \tag{20}$$

where $A_\xi(\varepsilon^{-1}) = \text{block diag}\{A_\xi^{[1]}, \ldots, A_\xi^{[m]}\}$, $B_M = \text{block diag}\{B_M^{[1]}, \ldots, B_M^{[m]}\}$, $\tilde{\xi}_h = \hat{\sigma}_h - \sigma$, $\bar{H}_M = \text{block diag}\,\{\bar{H}_M^{[1]}, \ldots, \bar{H}_M^{[m]}\}$, $\bar{U} = \left[I - (K_p^{nom})^{-1}K_p\right]u + (K_p^{nom})^{-1}K_p(\theta^{*^T}\omega - d_f - \pi_\eta)$, with

$$A_\xi^{[j]} = \begin{bmatrix} -\frac{\bar{a}_{\rho_j-1}^{[j]}}{\varepsilon} & 1 & \ldots & 0 \\ \vdots & \vdots & \ddots & \vdots \\ -\frac{\bar{a}_1^{[j]}}{\varepsilon^{\rho_j-1}} & 0 & 0 & 1 \\ -\frac{\bar{a}_0^{[j]}}{\varepsilon^{\rho_j}} & 0 & 0 & 0 \end{bmatrix}, \; B_M^{[j]} = \begin{bmatrix} 0 \\ \vdots \\ 0 \\ 1 \end{bmatrix}, \; (\bar{H}_M^{[j]})^T = \begin{bmatrix} 0 & 0 & \ldots & 0 & 1 \\ 0 & 0 & \ldots & 1 & a_{\rho_j-1} \\ \vdots & \vdots & \iddots & \vdots & \vdots \\ 0 & 1 & \ldots & a_3 & a_2 \\ 1 & a_{\rho_j-1} & \ldots & a_2 & a_1 \end{bmatrix}^{-1} \begin{bmatrix} 1 \\ l_{p_j-2}^{[j]} \\ \vdots \\ l_1^{[j]} \\ l_0^{[j]} \end{bmatrix}.$$

Replacing σ by its estimate $\hat{\sigma}_h$ and considering the presence of an absolutely continuous uniformly bounded output disturbance β_α of order ε, i.e., $\hat{\sigma}_h + \beta_\alpha$, the plant input is given by:

$$u = (\theta^{nom})^T\omega - \varrho(t)S_p\frac{\hat{\sigma}_h + \beta_\alpha}{|\hat{\sigma}_h + \beta_\alpha|}\,. \tag{21}$$

Consider the reference model (2)–(3) and the plant (1) with input signal (21) and modulation function defined in (15) satisfying (14). The following theorem states that the complete error system is uniformly globally exponentially practically stable.

Theorem 1. *Consider the complete error system (9), (16), (20) and (21), with state* $z^T = \left[x_e^T \ \tilde{\xi}^T\right]$. *Suppose that assumptions (A1) to (A6) hold and that the disturbance* $\beta_\alpha(t)$ *is absolutely continuous and bounded by* $|\beta_\alpha(t)| \leq \varepsilon K_R$, *where* $K_R > 0$ *is a constant. Then, for sufficiently small* $\varepsilon > 0$, *there exist constants* $c_z, a > 0$ *such that* $|z(t)| \leq c_z e^{-a(t-t_0)} |z(t_0)| + O(\varepsilon)$ *holds* $\forall z(t_0), \forall t \geq t_0 > 0$. *(Proof: see Appendix.)* ■

6 MIMO Robust Exact Differentiator (MIMO RED)

In the previous section, a UVC using an HGO to estimate σ was analyzed. From Theorem 1, the convergence of the error state is only guaranteed to a residual set of order ε. To achieve exact tracking, one can use a MIMO extension of the robust exact differentiator (RED) proposed in [23]. A similar approach was considered in [16] to build a MIMO RED based observer. The idea is to use a RED of order $p_j = \rho_j - 1$ for each output $e_j \in \mathbb{R},\ j = 1, \ldots, m$ as follows:

$$\begin{aligned}
\dot{\zeta}_0^{[j]} &= v_0^{[j]}, \qquad v_0^{[j]} = -\lambda_0^{[j]} C_{\rho_j}^{[j]\frac{1}{p_j+1}} \left|\zeta_0^{[j]} - e_j(t)\right|^{\frac{p_j}{p_j+1}} \operatorname{sgn}(\zeta_0^j - e_j(t)) + \zeta_1^{[j]} \\
&\vdots \\
\dot{\zeta}_i^{[j]} &= v_i^{[j]}, \qquad v_i^{[j]} = -\lambda_i^{[j]} C_{\rho_j}^{[j]\frac{1}{p_j-i+1}} \left|\zeta_i^{[j]} - v_{i-1}^{[j]}\right|^{\frac{p_j-i}{p_j-i+1}} \operatorname{sgn}(\zeta_i^{[j]} - v_{i-1}^{[j]}) + \zeta_{i+1}^{[j]}, \\
&\vdots \\
\dot{\zeta}_{p_j}^{[j]} &= -\lambda_{p_j}^{[j]} C_{\rho_j}^{[j]} \operatorname{sgn}(\zeta_{p_j}^{[j]} - v_{p_j}^{[j]}),
\end{aligned} \tag{22}$$

where $C_{\rho_j}^{[j]}$ is a known constant such that $|e_j^{(\rho_j)}(t)| \leq C_{\rho_j}^{[j]}$. A superscript $^{[j]}$ is used to indicate that a particular parameter or variable belongs to a RED related with e_j. If the parameters $\lambda_i^{[j]}$ are properly recursively chosen[1], then the equalities

$$\zeta_0^{[j]} = e_j(t);\ \zeta_i^{[j]} = e_j^{(i)}(t), \quad j = 1, \ldots, m; \quad i = 1, \ldots, p_j$$

are established in finite time [23]. Thus, using a MIMO RED, composed by m REDs of order $\rho_j - 1$ for each output e_j, the following estimate for σ can be obtained:

$$\hat{\sigma}_r^T = \left[\zeta_{\rho_1-1}^{[1]} + \cdots + l_1^{[1]}\zeta_1^{[1]} + l_0^{[1]}\zeta_0^{[1]} \ \ldots \ \zeta_{\rho_m-1}^{[m]} + \cdots + l_1^{[m]}\zeta_1^{[m]} + l_0^{[m]}\zeta_0^{[m]}\right]. \tag{23}$$

Then, a control signal $u = (\theta^{nom})^T\omega - \varrho(t) S_p \hat{\sigma}_r / |\hat{\sigma}_r|$ could be used. However, only local convergence of the error state to zero could be guaranteed, since the convergence of the REDs requires that the signals $e_j^{(\rho_j)}(t),\ j = 1, \ldots, m$ are uniformly bounded [23, 24].

[1] In particular, the following choice is valid for $p_j \leq 3$: $\lambda_0^{[j]} = 5, \lambda_1^{[j]} = 3, \lambda_2^{[j]} = 1.5, \lambda_3^{[j]} = 1.1$. For more details, see [23].

Remark 2. Parameters $C_{\rho_j}^{[j]}$ are related to the size of the region D_R in the error space, where the differentiator convergence can be guaranteed. The larger $C_{\rho_j}^{[j]}$, the larger is the size of D_R and higher sensitivity to input noises and sampling time.

7 Global RED Based Unit Vector Controller (GRED-UVC)

Here, we propose an output feedback SMC, named Global RED based Unit Vector Controller (GRED-UVC), which is based on a multivariable hybrid estimation scheme, named GRED, that combines through switching the HGO estimate (19) with the MIMO RED estimate (23) according to:

$$\hat{\sigma}_g = \alpha(\tilde{\nu}_{rh})\ \hat{\sigma}_h + [1 - \alpha(\tilde{\nu}_{rh})]\ \hat{\sigma}_r\,, \tag{24}$$

where $\tilde{\nu}_{rh} = \hat{\sigma}_r - \hat{\sigma}_h$ is the difference between both estimates. The *switching function* (SF) $\alpha(\tilde{\nu}_{rh})$ is a continuous, state dependent modulation which assumes values in the interval $[0, 1]$ and allows the controller to smoothly change from one estimator to the other.

The underlying idea of the GRED-UVC is to guarantee that the closed-loop error system is global exponential stable with respect to a small residual set of order ε, irrespective of the MIMO RED convergence, and in addition to ensure that ultimately only the MIMO RED is used to estimate σ after its convergence is achieved. To this end, the *switching law* $\alpha(\cdot)$ is proposed so that the resulting system becomes equivalent to a UVC using an HGO with a uniformly bounded output disturbance of order ε as in (21), i.e. $|\hat{\sigma}_g - \hat{\sigma}_h| \leq \varepsilon K_R$. Thus, global practical stability is guaranteed, according to Theorem 1, independently of the MIMO RED behavior, provided its signals remain bounded. This condition is a consequence of Theorem 1 and the fact that the variables of each individual RED (22) cannot escape in finite time, which is ensured by [27, Lemma 1]. Therefore, the error state is globally driven into an invariant compact set D_R, where the convergence of the MIMO RED can be guaranteed and an upper bound $\bar{\xi}_h$ for the HGO estimation error $\tilde{\xi}_h$ can be determined. The *switching law* $\alpha(\cdot)$ is designed as follows:

$$\alpha(\tilde{\nu}_{rh}) = \begin{cases} 0, & |\tilde{\nu}_{rh}| < \epsilon_M - \Delta \\ (|\tilde{\nu}_{rh}| - \epsilon_M + \Delta)/\Delta, & \epsilon_M - \Delta \leq |\tilde{\nu}_{rh}| < \epsilon_M \\ 1, & |\tilde{\nu}_{rh}| \geq \epsilon_M \end{cases} \tag{25}$$

where $0 < \Delta < \epsilon_M$ is a boundary layer used to smoothen the switching function, and $\epsilon_M := \varepsilon K_R$ with K_R being an appropriate positive design parameter, which is selected such that $\epsilon_M - \Delta > \bar{\xi}_h$. This means that, if K_R is properly tuned, then after some finite time only the MIMO RED remains active ($\alpha = 0$), providing exact estimation of the ideal sliding variable σ, as desired.

The GRED-UVC control law is given by:

$$u = (\theta^{nom})^T \omega - \varrho(t) S_p \frac{\hat{\sigma}_g}{|\hat{\sigma}_g|}\,, \tag{26}$$

where the modulation function $\varrho(t)$ satisfies (14).

Consider the plant (1) and the reference model (2)–(3). The control law is given by (26) with modulation function ϱ defined in (15) satisfying (14) and the GRED estimate $\hat{\sigma}_g$ given by (24) being a convex combination of the estimates provided by the HGO (19) and the MIMO RED (23). The switching function $\alpha(\cdot)$ is defined in (25). The proposed control scheme in Fig. 1 guarantees global stability properties with ultimate exact tracking, as stated in the following theorem.

Theorem 2. *Suppose that assumptions (A1) to (A6) hold. For sufficiently small $\varepsilon > 0$, the closed-loop error system described by (9), (16), (20) and (21) is uniformly globally exponentially practically stable with respect to a residual set of order ε. Moreover, for $\lambda_i^{[j]}$, $j = 1, \ldots, m$, $i = 0, \ldots, \rho_j - 1$, and K_R properly chosen, the estimation of the ideal sliding variable σ becomes exact, being made exclusively by the MIMO RED ($\alpha(\cdot) = 0$) after some finite time. Then, the closed-loop error state $z^T = \left[x_e^T \ \tilde{\xi}^T\right]$, and hence the output tracking error e, converge exponentially to zero. (Proof: see Appendix.)* ■

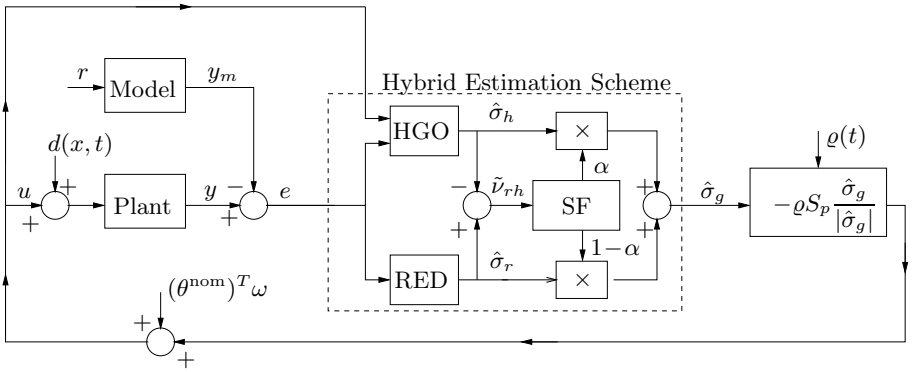

Fig. 1. GRED-UVC proposed control scheme.

Remark 3. ***(Absence of Peaking)*** As it is well known, HGO estimates may contain peaking [32]. Indeed, the HGO estimation error $\tilde{\xi}$ will contain a transient term which eventually exhibit an impulsive-like behavior, where the transient peaks to $\mathcal{O}(1/\varepsilon)$ values before it decays rapidly to zero. This behavior is known as the *peaking phenomenon* [32]. However, in the proposed scheme, the peaking phenomenon is circumvented since the modulation function is implemented using only well conditioned (without peaking) signals, the regressor vector ω and the norm observer estimate $\hat{x}$, while the unit vector control (UVC) term blocks the eventual peaking present in $\hat{\sigma}_g$ to u in (26).

8 Simulation Results

In order to illustrate the proposed control strategy, we consider a nonlinear plant with non-uniform relative degree ($\rho_1 = 2$, $\rho_2 = 3$) described by (1), with $A_p = \begin{bmatrix} -2 & 3 & 0 & 0 & 0 \\ 1 & 0 & 0 & 0 & 0 \\ 1 & 2 & -6 & -11 & -6 \\ 0 & 0 & 1 & 0 & 0 \\ 0 & 0 & 0 & 1 & 0 \end{bmatrix}$, $B_p^T = \begin{bmatrix} 1 & 0 & 0 & 0 & 0 \\ 0 & 0 & 1 & 0 & 0 \end{bmatrix}$, $H_p = \begin{bmatrix} 0 & \kappa & 0 & \kappa & 3\kappa \\ 0 & 0 & 0 & 0 & 1 \end{bmatrix}$, $G(s) = \begin{bmatrix} \frac{\kappa(s+2)}{(s-1)(s+1)(s+3)} & \frac{\kappa}{(s+1)(s+2)} \\ \frac{1}{(s-1)(s+1)(s+3)^2} & \frac{1}{(s+1)(s+2)(s+3)} \end{bmatrix}$, where the constant $\kappa \in [4, 10]$ is uncertain and $K_p = \begin{bmatrix} \kappa & \kappa \\ 0 & 1 \end{bmatrix}$ is the linear subsystem HFG matrix. The input disturbance is considered uncertain for control design and is given by $d(x) = \left[0.2\cos(t)\sin(x_2\, x_3)|x_4| \quad \frac{1}{2\pi}\left(e^{-|x_5|}|x_1| + |x_2|\right)\right]^T$. This particular choice is motivated by the example considered in [11]. The reference signal and model are chosen as $r = [\sin(t) \;\; \sin(0.5t)]$ and $W_m(s) = \text{diag}\left\{\frac{1}{(s+1)^2}, \frac{1}{(s+1)^2(s+2)}\right\}$. To perform the simulations, the actual parameter κ is set to 10, while $\kappa^{nom} = 7$ is chosen for control purposes. For $\kappa^{nom} = 7$ and $\kappa \in [4, 10]$, it follows that $\left|(\theta^{\text{nom}} - \theta^*)^T\right| \leq 2$ and Assumption (A5) is satisfied with $S_p = I$. Then, in (26) the modulation function $\varrho(t)$ is given by (15), with $c_d = 2.25$, $|d_f| \leq \hat{d}_f$ and $\delta = 1$. The signal $\hat{d}_f$ is obtained by the FOAF described in (12), with $k_x = 0.2$, $k_d = 1$, $c_f = 5$, $\lambda_f = 0.5$ and $\hat{x}$ is a state norm observer given by (11), with $c_1 = 1.2$, $c_2 = 2$ and $\lambda_x = 0.1$.

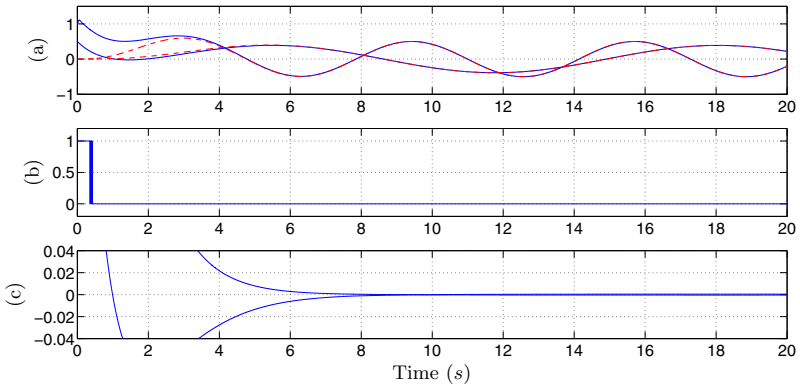

Fig. 2. (a) Tracking performance: y (—) and y_m (- -); (b) Time behavior of switching function (SF) $\alpha(\cdot)$; (c) Zoom of tracking errors $e(t)$

Other design parameters are listed as follows: I/O filters (4): $\lambda(s) = (s+2)^2$ and $\nu = 3$; $L(s) = \text{diag}\left\{(s+1), (s+1)^2\right\}$; High-gain observer (19): $\varepsilon = 0.001$;

$K_p^{nom} = K_p$ with $\kappa = 7$; $N_a^{[1]} = s^2+2s+1$, $N_a^{[2]} = s^3+3s^2+3s+1$, $H_a^{[1]} = [2\ 1]^T$, $H_a^{[2]} = [4\ 5\ 2]^T$, $\bar{H}_M^{[1]} = [-1\ 1]^T$, $\bar{H}_M^{[2]} = [4\ -2\ 1]^T$; MIMO RED (22)-(23): $\lambda_0^{[1]} = 1.5$, $\lambda_1^{[1]} = 1.1$ and $C_2^{[1]} = 30$; $\lambda_0^{[2]} = 3$, $\lambda_1^{[2]} = 1.5$, $\lambda_2^{[2]} = 1.1$ and $C_3^{[2]} = 100$; switching function (25): $\epsilon_M = 250\varepsilon$ and $\Delta = 50\varepsilon$. We consider the following plant initial conditions: $y_1(0) = 1$, $\dot{y}_1(0) = 2$, $y_2(0) = 0.5$, $\dot{y}_2(0) = -1$, $\ddot{y}_2(0) = 1$. The remaining system initial conditions are set to zero.

The Euler Method with step-size $h = 10^{-5}$ is used for numerical integration.

Fig. 2(a) shows that the GRED-UVC achieves precise tracking despite the disturbance $d(x,t)$. From the plot of $\alpha(\cdot)$ in Fig. 2(b), one notes that after a short transient only the MIMO RED remains active as expected. In practice, an advantage of the hybrid estimation scheme is that it does not require large RED parameters to guarantee global stability, thus being less sensitive to measurement noise [23] and also responsible to achieve better steady-state tracking performance.

Plant with Unmodeled Dynamics and Measurements Noise

The plant could also have a dynamic actuator with transfer matrix given by

$$G_a(s) = \begin{bmatrix} \frac{1}{\mu s+1} & 0 \\ 0 & \frac{1}{\mu s+1} \end{bmatrix}, \qquad \mu = 0.1 \tag{27}$$

Moreover, we consider that the output is corrupted by a high frequency measurement noise [34, 5, 31], so that the actual output would be given by

$$y_{noise}(t) = \begin{bmatrix} y_1(t) + 0.01\sin(200t) \\ y_2(t) + 0.01\cos(200t) \end{bmatrix}$$

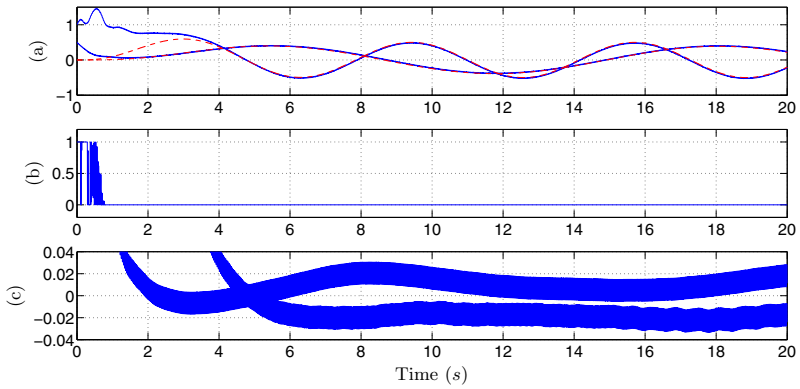

Fig. 3. (a) Tracking with unmodeled dynamics and noise: y (—) and y_m (- -); (b) Time behavior of switching function (SF) $\alpha(\cdot)$; (c) Zoom of tracking errors $e(t)$

The same control design developed for the nominal plant without unmodeled dynamics and noise is considered, except for the HGO parameter that should be adjust to cope with the high frequency noise and the switching function parameters that should also be modified. Since the errors from the estimators increases the idea is to set ε_M with a higher value so that the switching scheme can still be able to ultimately select the MIMO RED. These parameters are chosen as follows: $\varepsilon = 0.1$, $\varepsilon_M = 50\varepsilon$ and $\Delta = 10\varepsilon$ As can be seen in Fig. 3, the tracking performance of the controller under the presence of a small high-frequency noise and unmodeled dynamics remains satisfactory and the switching scheme is able to ultimately select the MIMO RED. It should be noted that if significant noise is present a degradation of the tracking performance would be expected [34, 5, 31]. The applicability of the proposed controller in real-world conditions is supported by the experiments presented in [26].

9 Conclusions

A new output feedback sliding mode tracking controller for uncertain MIMO nonlinear plants with non-uniform arbitrary relative degree in the presence of disturbances has been proposed. The controller is based on a multivariable hybrid estimation scheme, which combines a high-gain observer with locally exact differentiators in such way that uniform global exponential practical stability with respect to a small residual set is guaranteed as well as ultimate exact output tracking of a reference model. It is important to stress that since the HGO estimates are used only in the UVC term and not in the modulation, global stability is guaranteed with a peaking free control signal via norm state observers. Moreover, the scheme allows ideal sliding modes in theory, hence, chattering is precluded in the ideal case, i.e., in the absence of real life imperfections such as noise and switching delays. Indeed, the estimated sliding variable provided by the GRED, which drives the unit vector function, becomes identically zero after some finite time. Numerical simulations are presented so as to validate the analysis and show the effectiveness of the proposed technique.

Acknowledgments. The first author dedicates this work to Okyay Kaynak whom he met in 1990 at the first IEEE International Workshop on VSS, Sarajevo, starting a longstanding friendship. This is intended to express his admiration for Okyay's outstanding career which covers high impact scientific and technological contributions, highly relevant services to the Variable Structure Systems and Sliding Mode Control community, and several important awards from the IEEE.

References

[1] Angulo, M.T., Fridman, L., Levant, A.: Output-feedback finite-time stabilization of disturbed LTI systems. Automatica 48(4), 606–611 (2012)

[2] Baev, S., Shtessel, Y., Shkolnikov, I.: Nonminimum-phase output tracking in causal systems using higher-order sliding modes. IJRNC 18, 454–467 (2008)

[3] Bartolini, G., Ferrara, A., Usai, E., Utkin, V.I.: On multi-input chattering-free second-order sliding mode control. TAC 45(9), 1711–1717 (2000)
[4] Basin, M.V., Ramirez, P.C.R.: A supertwisting algorithm for systems of dimension more than one. IEEE Trans. on Ind. Electronics 61(9), 6472–6480 (2014)
[5] Bernuau, E., Efimov, D., Perruquetti, W., Polyakov, A.: On homogeneity and its application in sliding mode control. Journal of the Franklin Institute 351(4), 1866–1901 (2014), http://www.sciencedirect.com/science/article/pii/S001600321400009X; special Issue on 2010-2012 Advances in Variable Structure Systems and Sliding Mode Algorithms
[6] Chen, W.-H.: Analytic predictive controllers for nonlinear systems with ill-defined relative degree. IEE Proceedings Control Theory and Applications 148(1), 9–16 (2001)
[7] Cunha, J.P.V.S., Costa, R.R., Hsu, L.: Design of first-order approximation filters for sliding-mode control of uncertain systems. IEEE Trans. on Ind. Electronics 55(11), 4037–4046 (2008)
[8] Cunha, J.P.V.S., Costa, R.R., Lizarralde, F., Hsu, L.: Peaking free variable structure control of uncertain linear systems based on a high-gain observer. Automatica 45(11), 1156–1164 (2009)
[9] Efe, M.O., Unsal, C., Kaynak, O., Yu, X.: Variable structure control of a class of uncertain systems. Automatica 40(1), 59–64 (2004)
[10] Efimov, D., Fridman, L.: Global sliding-mode observer with adjusted gains for locally lipschitz systems. Automatica 47(3), 565–570 (2011)
[11] Emelyanov, S.V., Nisezon, K.N.: Discontinuous output feedback stabilizing an uncertain MIMO plant. Int. J. Contr. 55(1), 83–109 (1992)
[12] Esfandiari, F., Khalil, H.K.: Output feedback stabilization of fully linearizable systems. Int. J. Contr. 56, 1007–1037 (1992)
[13] Estrada, A., Fridman, L.M.: Integral HOSM semiglobal controller for finite-time exact compensation of unmatched perturbations. IEEE Trans. Aut. Contr. 55(11), 2645–2649 (2010)
[14] Filippov, A.F.: Differential equations with discontinuous right-hand side. American Math. Soc. Translations 42(2), 199–231 (1964)
[15] Floquet, T., Spurgeon, S.K., Edwards, C.: An output feedback sliding mode control strategy for MIMO systems of arbitrary relative degree. Int. J. of Robust and Nonlinear Contr. 21(2), 119–133 (2011)
[16] Fridman, L., Shtessel, Y., Edwards, C., Yan, X.G.: Higher-order sliding-mode observer for state estimation and input reconstruction in nonlinear systems. Int. J. Robust and Nonlinear Contr. 18, 399–412 (2008)
[17] Hsu, L., Costa, R.R., Cunha, J.P.V.S.: Model-reference output-feedback sliding mode controller for a class of multivariable nonlinear systems. Asian Journal of Control 5(4), 543–556 (2003)
[18] Hsu, L., Cunha, J.P.V.S., Costa, R.R., Lizarralde, F.: Multivariable output-feedback sliding mode control. In: Yu, X., Xu, J.-X. (eds.) Variable Structure Systems: Towards the 21st Century. LNCIS, pp. 283–313. Springer, Heidelberg (2002)
[19] Ioannou, P., Sun, K.: Robust Adaptive Control. Prentice-Hall (1996)
[20] Jiang, Z.P., Mareels, M.Y.: A small-gain control method for nonlinear cascade systems with dynamic uncertainties. IEEE Trans. Aut. Contr. 42(3), 292–308 (1997)
[21] Kailath, T.: Linear Systems. Prentice-Hall (1980)
[22] Khalil, H.K.: A note on the robustness of high-gain-observer-based controllers to unmodeled actuator and sensor dynamics. Automatica 41(10), 1821–1824 (2005)

[23] Levant, A.: Higher-order sliding modes, differentiation and output-feedback control. Int. J. Contr. 76(9), 924–941 (2003)
[24] Levant, A., Livne, M.: Exact differentiation of signals with unbounded higher derivatives. IEEE Trans. Aut. Contr. 57(4), 1076–1080 (2012)
[25] Mahmouda, M.S., Khalil, H.K.: Robustness of high-gain observer-based nonlinear controllers to unmodeled actuators and sensors. Automatica 38(2), 361–369 (2002)
[26] Nunes, E.V.L., Hsu, L., Lizarralde, F.: Output-feedback sliding mode control for global asymptotic tracking of uncertain systems using locally exact differentiators. In: Proc. American Contr. Conf., Minneapolis, pp. 5407–5412 (2006)
[27] Nunes, E.V.L., Hsu, L., Lizarralde, F.: Global tracking for uncertain systems using output-feedback sliding mode control. IEEE Trans. Aut. Contr. 54(5), 1141–1147 (2009)
[28] Nunes, E.V.L., Oliveira, T.R., Peixoto, A.J., Hsu, L.: Global exact tracking for uncertain multivariable systems by switching adaptation. In: Proc. of the 18th IFAC World Congress, Milano, pp. 3057–3062 (2011)
[29] Nunes, E.V.L., Peixoto, A.J., Oliveira, T.R., Hsu, L.: Global exact tracking for uncertain mimo linear systems by output feedback sliding mode control. Journal of the Franklin Institute 351(4), 2015–2032 (2014)
[30] Orlov, Y.: Finite time stability and robust control synthesis of uncertain switched systems. SIAM J. Control Optim. 43, 1253–1271 (2005)
[31] Prasov, A.A., Khalil, H.K.: A nonlinear high-gain observer for systems with measurement noise in a feedback control framework. IEEE Transactions on Automatic Control 58(3), 569–580 (2013)
[32] Sussmann, H.J., Kokotović, P.V.: The peaking phenomenon and the global stabilization of nonlinear systems. IEEE Trans. Aut. Contr. 36(4), 424–440 (1991)
[33] Utkin, V.I.: Sliding Modes in Control and Optimization. Springer (1992)
[34] Vasiljevic, L.K., Khalil, H.K.: Error bounds in differentiation of noisy signals by high-gain observers. Systems & Control Letters 57(10), 856–862 (2008), http://www.sciencedirect.com/science/article/pii/S0167691108000601
[35] Yu, X., Kaynak, O.: Sliding-mode control with soft computing: A survey. IEEE Transactions on Industrial Electronics 56(9), 3275–3285 (2009)

Appendix

The following auxiliary lemmas will be instrumental for the proof of Theorem 1.

Lemma 1. *Consider the MIMO system*

$$\sigma(t) = M(s)K[u + d(t)]\,, \tag{28}$$

where $M(s) = diag\left\{(s+\gamma_1)^{-1}, \ldots, (s+\gamma_m)^{-1}\right\}$, $\gamma_j > 0$, $K \in \mathbb{R}^{m\times m}$ *is the high frequency gain matrix and is such that* $-K$ *is diagonally stable, and* $d(t)$ *is locally integrable (LI). If* $u = -\varrho(t)\frac{\sigma}{|\sigma|}$, $\quad \varrho \geq (1 + c_d)|d(t)| + \delta$, *where* $\varrho(t)$ *is LI,* $c_d > 0$ *is an appropriate constant,* $\delta \geq 0$ *is an arbitrary constant, then, the inequality*

$$|\sigma(t)| \text{ and } |x_e(t)| \leq c|x_e(0)|e^{-\lambda t} \tag{29}$$

holds $\forall t \geq 0$ *for some positive constants* c, λ, *where* x_e *is the state of any stabilizable and detectable realization of (28) (possibly nonminimal). Moreover, if* $\delta > 0$, *then* $\sigma(t)$ *becomes identically zero after some finite time* $t_s \geq 0$.

Proof: Consider a stabilizable and detectable realization of (28) described by $\dot{x} = Ax + B(u+d)$, $\sigma = Hx$. From (28), one can obtain the normal form $\dot{\eta} = A_{11}\eta + A_{22}\sigma$, $\dot{\sigma} = A_m\sigma + K(u+d+\pi_\eta)$, where $A_m = \text{diag}\{-\gamma_1, \ldots, -\gamma_m\}$, $|\pi_\eta| \leq c_\eta |\eta(0)| e^{-\lambda_\eta t}$ and the zero dynamics given by $\dot{\eta} = A_{11}\eta$ is stable, since $M(s)$ is minimum phase. The state vector of this realization is $x_e^T = [\eta^T \ \sigma^T]$. Consider the function $V(\sigma) = \sigma^T D\sigma$, where $K^T D + DK = Q$, $Q = Q^T > 0$ for some diagonal matrix $D > 0$. The time derivative of $V(\sigma)$ can be upper bounded by $\dot{V} \leq 2\sigma^T DA_m\sigma - \varrho\frac{\sigma^T Q\sigma}{|\sigma|} + 2|DK||\sigma|(|d|+|\pi_\eta|)$, Choosing $c_d \geq 2|DK|/\lambda_{min}(Q) - 1$, it can be verified that $\dot{V} \leq -\kappa_1|\sigma|^2 - \delta|\sigma| + |\bar{\pi}_\eta||\sigma|$. Now, following the proof of Lemma 1 given in [17], one can conclude that $\sigma(t) \leq (\kappa_2 |\sigma(0)| + \kappa_3 |\eta(0)|) e^{-\bar{\lambda}t}$. Moreover, if $\delta > 0$, it can be shown that σ becomes identically zero in some finite time t_s. Since A_{11} is Hurwitz, one can further conclude that (29) holds. ■

Lemma 2. *Consider the MIMO system*

$$\dot{\sigma}(t) = A_m\sigma(t) + K[u + d(t) + \pi], \quad A_m, K \in \mathbb{R}^{m\times m} \tag{30}$$

where $A_m = diag\{-\gamma_1, \ldots, -\gamma_m\}$, $-K$ is diagonally stable, $|\pi| \leq Re^{-\lambda t}$, $u = -\varrho(t)\frac{\vartheta}{|\vartheta|}$, $d(t)$, $\pi(t)$ and $\varrho(t)$ are locally integrable, $\vartheta(t) := \sigma(t) + \beta(t)$, where $\beta(t)$ is absolutely continuous $(\forall t)$. If $\varrho(t) \geq (1 + \hat{c}_d)|d(t)|$ $\forall t$, for some appropriate $\hat{c}_d \geq 0$, then, the signals ϑ and σ are bounded by

$$|\vartheta(t)| \text{ and } |\sigma(t)| \leq \bar{c}_1|\sigma(0)|e^{-\gamma t} + \bar{c}_2\left[Re^{-min(\gamma,\lambda)t} + \|\beta\|\right] \tag{31}$$

for some positive constants $\bar{c}_1, \bar{c}_2$ and $\gamma = \min\{\gamma_1, \ldots, \gamma_m\}$. (Proof: see [28, Lemma 7] and [18, Lemma 2]) ■

A Proof of Theorem 1

In order to analyze the stability and convergence properties of the closed-loop error system, we first show that the $\tilde{\xi}$-subsystem (20) is input-to-state practically stable (ISpS) with respect to the input x_e. Applying the linear transformation $x_\xi = T(\varepsilon)\tilde{\xi}$, $T(\varepsilon) = \text{block diag}\{T_\varepsilon^{[1]}, \ldots, T_\varepsilon^{[m]}\}$ with $T_\varepsilon^{[j]} = \text{diag}\{1, \varepsilon, \ldots, \varepsilon^{\rho_j - 1}\}$, one has:

$$\dot{x}_\xi^{[j]} = \frac{1}{\varepsilon}\bar{A}_\xi^{[j]}x_\xi^{[j]} + \varepsilon^{\rho_j - 1}\bar{B}_\xi^{[j]}K_p^{nom}\bar{U}, \quad j = 1, \ldots, m \tag{32}$$

where $\bar{A}_\xi^{[j]} = \left[\begin{array}{c|c} -\bar{a}_{\rho_j-1}^{[j]} & I_{\rho_j-1} \\ \vdots & \hline \\ -\bar{a}_0^{[j]} & 0 \end{array}\right]$, $\bar{B}_\xi^{[j]} = \left[\begin{array}{c} 0_{(\rho_j - 1\times m)} \\ \hline \\ \iota_j \end{array}\right]$, ι_j is the j-th row of an identity matrix of order m and $x_\xi^T = \left[(x_\xi^{[1]})^T \ \ldots \ (x_\xi^{[m]})^T\right]$. For each state $x_\xi^{[j]}$, we consider the functions $V_j(x_\xi^{[j]}) = (x_\xi^{[j]})^T P_i x_\xi^{[j]}$, $(P_j = P_j^T > 0$ and $(\bar{A}_\xi^{[j]})^T P_j + P_j\bar{A}_\xi^{[j]} = -Q_j$, with $Q_j = Q_j^T > 0)$, From

(32), $\dot{V}_j = -\frac{1}{\varepsilon}(x_\xi^{[j]})^T Q_j x_\xi^{[j]} + 2\varepsilon^{\rho_j - 1}(x_\xi^{[j]})^T P_j \bar{B}_\xi^{[j]} K_p^{nom} \bar{U}$, which can be upper bounded by $\dot{V}_j \leq -\frac{1}{\varepsilon}\kappa_1^{[j]} \left| x_\xi^{[j]} \right|^2 + \varepsilon^{2\rho_j - 1}\kappa_2^{[j]} \left| \bar{U} \right|^2$, where $\kappa_1^{[j]} = \frac{\lambda_{min}(Q_j)}{2}$ and $\kappa_2^{[j]} = 2\frac{\left| P_j B_\xi^{[j]} K_p^{nom} \right|^2}{\lambda_{min}(Q_j)}$. Thus, one has

$$\left| x_\xi^{[j]} \right| \leq \pi_\xi^{[j]} + \varepsilon^{\rho_j} \kappa_3^{[j]} \left\| \bar{U}_{[t_0,t]} \right\| . \tag{33}$$

In what follows we show that $\bar{U}$ defined in (20) can be bounded by

$$\left\| \bar{U}_{[t_0,t]} \right\| \leq \kappa_4 \left\| x_{e_{[t_0,t]}} \right\| + \kappa_5 . \tag{34}$$

Using the relation $\omega = \Omega_1 X + \Omega_2 r$ and $x_e = X - X_m$, one has that $\omega = \Omega_1 x_e + \Omega_1 X_m + \Omega_2 r$. Now, consider the vector $\xi_e = \bar{\xi}$ - $\bar{\xi}_m$, where $\bar{\xi}^T = \left[\bar{\xi}^{[1]}, \ldots, \bar{\xi}^{[m]}\right], \bar{\xi}^{[j]} = \left[y_j \;\; \dot{y}_j \;\; \ldots \;\; y_j^{\rho_j - 1} \right]$ and $\bar{\xi}_m^T = \left[\bar{\xi}_m^{[1]}, \ldots, \bar{\xi}_m^{[m]}\right], \bar{\xi}_m^{[j]} = \left[y_{m_j} \;\; \dot{y}_{m_j} \;\; \ldots \;\; y_{m_j}^{\rho_j - 1} \right]$. Since the reference model is a stable system it can be shown that ξ_m is uniformly bounded and hence it follows that $\left|\bar{\xi}\right| \leq |\xi_e| + \kappa_m$. From (9), it can be shown that $|\xi_e| \leq \kappa_6 |x_e|$ and thus $\left|\bar{\xi}\right| \leq \kappa_6 |x_e| + \kappa_m$. Moreover, since the plant is minimum phase then it is possible to conclude that $|x| \leq \kappa_7 \left\| \bar{\xi}_{[t_0,t]} \right\|$ (*modulo* π term) by using the normal form of (1) and in addition it follows that $|x| \leq \kappa_8 \left\| x_{e_{[t_0,t]}} \right\| + \kappa_9$. From Assumption (A6), it is possible to show that $|X_m| \leq \kappa_{10} \left\| x_{[t_0,t]} \right\| + \kappa_{11}$. Thus, $|X_m| \leq \kappa_{12} \left\| x_{e_{[t_0,t]}} \right\| + \kappa_{13}$ and hence

$$|\omega(t)| \leq \kappa_{14} \left\| x_{e_{[t_0,t]}} \right\| + \kappa_{15} \tag{35}$$

From (11) and (12), it follows that $|d_f(t)| \leq \kappa_{16} \left\| \omega_{[t_0,t]} \right\| + \kappa_{17}$. Moreover, from (21) and (14), it can be shown that $|u(t)| \leq \kappa_{18} \left\| \omega_{[t_0,t]} \right\| + \kappa_{19}$, which together with (35) allows us to show that (34) holds.

From (33) and (34), one can conclude that $\left| x_\xi^{[j]} \right| \leq \pi_\xi^{[j]} + \varepsilon^{\rho_j} \kappa_\xi^{[j]} \left\| x_{e_{[t_0,t]}} \right\| + \varepsilon^{\rho_j} \kappa_{20}^{[j]}$. Since $\tilde{\xi}^{[j]} = (T_\varepsilon^{[j]})^{-1} x_\xi^{[j]}$ and $\left|\tilde{\xi}\right| \leq \left|\tilde{\xi}^{[1]}\right| + \cdots + \left|\tilde{\xi}^{[m]}\right|$, it is possible to show that

$$\left|\tilde{\xi}\right| \leq \pi_\xi + \varepsilon\kappa_\xi \left\| x_{e_{[t_0,t]}} \right\| + \varepsilon\kappa_{21} . \tag{36}$$

Thus, from Definition 1 in [27], it follows that the $\tilde{\xi}$-dynamics is ISpS with respect to the input x_e. Now, we show that the x_e-subsystem defined in (9) is ISpS with respect to the input $\tilde{\xi}$. From (10) and (16), it can be shown that $\dot{\sigma} = A_m \sigma + K_p \left[u - \theta^{*^T} \omega + d_f + \pi_\sigma \right]$, where $A_m = \text{diag}\{-\gamma_1, \ldots, -\gamma_m\}$. From (21), it follows that

$$\dot{\sigma} = A_m \sigma + K \left[u_v + d_U + \pi_\sigma \right] , \tag{37}$$

where $K = K_p S_p$, $d_U = S_p^{-1} \left[(\theta^{nom} - \theta^*)^T \omega - d_f \right]$ and $u_v = -\varrho(t)\vartheta/|\vartheta|$, with $\vartheta := \sigma + \beta$ and $\beta := \tilde{\xi}_h + \beta_\alpha$, since $\hat{\sigma}_h = \sigma + \tilde{\xi}_h$. From (20) and using the

fact that $\beta_\alpha \leq \varepsilon K_R$, the auxiliary signal $\beta(t)$ can be upper bounded by $\|\beta\| \leq \kappa_{22} \left\|\tilde{\xi}\right\| + \varepsilon K_R$. Since $\varrho(t) \geq |d_U|$ and $\beta(t)$ is absolutely continuous, applying Lemma 2 to (37), one has:

$$|\sigma(t)| \leq |\bar{\pi}_\sigma| + \kappa_{23} \left\|\tilde{\xi}_{[t_0,t]}\right\| + \bar{c}_2 \varepsilon K_R \,. \tag{38}$$

From (9) and (37) one has $\dot{x}_e = A_c x_e + B_c(\dot{\sigma} - A_m \sigma)$. Then, in order to eliminate the derivative term $\dot{\sigma}$, a variable transformation $\hat{x}_e := x_e - B_c\sigma$ is performed yielding $\dot{\hat{x}}_e = A_c \hat{x}_e + (A_c B_c - B_c A_m)\sigma$.

Thus, $\hat{x}_e$ can be upper bounded by: $|\hat{x}_e(t)| \leq \pi_{\hat{e}}(t) + \sigma_f(t)$, where $\sigma_f(t) = W_\sigma(t) * |\sigma(t)|$, with $W_\sigma(t)$ being the impulse response of a first order filter given by $W_\sigma(s) = c_\sigma/(s + \lambda_\sigma)$, where $c_\sigma > 0$, $\lambda_\sigma := \min_k\{-\mathrm{Re}(p_k)\}$, with $\{p_k\}$ being the eigenvalues of A_c. From (38) and since $|x_e| \leq |\hat{x}_e| + \kappa_{24}\,|\sigma|$, one has that

$$|x_e| \leq \pi_e + \kappa_e \left\|\tilde{\xi}_{[t_0,t]}\right\| + \varepsilon \kappa_{25} \,. \tag{39}$$

Therefore, the x_e-dynamics is ISpS with respect to the input $\tilde{\xi}$. From the small-gain theorem [20], if ε is chosen such that $\varepsilon \leq 1/(\kappa_e \kappa_\xi)$, one has that the error system with state z is globally asymptotically practically stable [27]. Moreover, since the class $\mathcal{KL}$ functions in inequalities (36) and (39) are exponentials and the ISpS gains are linear, it is possible to extend this result, proving exponential practically stability for this case (see [27] for more details). ■

B Proof of Theorem 2

The estimate given by the hybrid estimation scheme defined in (24) can be rewritten as

$$\hat{\sigma}_g(t) = \sigma(t) + \tilde{\xi}_g(t), \qquad \tilde{\xi}_g(t) = \alpha(\tilde{\nu}_{rh})\tilde{\xi}_h(t) + [1 - \alpha(\tilde{\nu}_{rh})]\,\tilde{\xi}_r(t) \,. \tag{40}$$

where $\tilde{\xi}_h(t) = \hat{\sigma}_h(t) - \sigma(t)$ and $\tilde{\xi}_r(t) = \hat{\sigma}_r(t) - \sigma(t)$ are estimation errors and σ is the ideal sliding variable defined in (16). Considering $\tilde{\xi}_g(t)$ as an output disturbance, the GRED-UVC closed-loop error system can be described by:

$$\dot{x}_e = A_c x_e + B_c K_p\,[u - {\theta^*}^T \omega + d_f], \qquad \sigma = \bar{H}\, x_e, \tag{41}$$

$$u = (\theta^{nom})^T \omega - \varrho(t) \frac{\sigma + \tilde{\xi}_g}{|\sigma + \tilde{\xi}_g|} \,. \tag{42}$$

From (25), the estimation error $\tilde{\xi}_g(t)$ can be rewritten as:

$$\tilde{\xi}_g(t) = \tilde{\xi}_h(t) + \beta_\alpha(\tilde{\nu}_{rh}(t)) \,, \tag{43}$$

where by design $\beta_\alpha(\tilde{\nu}_{rh}(t))$ is uniformly bounded by $|\beta_\alpha(\tilde{\nu}_{rh}(t))| < \epsilon_M$, with $\epsilon_M = \varepsilon K_R$. Moreover, β_α is absolutely continuous in t, since the

switching function $\alpha(\tilde{\nu}_{rh})$ is Lipschitz continuous and $\hat{\sigma}_r(t)$ and $\hat{\sigma}_h(t)$ are absolutely continuous because they are Filippov solutions. Substituting (43) into (42), it can be seen that equation (42) is equivalent to (21), where $\hat{\sigma}_h = \tilde{\xi}_h + \sigma$, with $\tilde{\xi}_h$ given by (20), σ given by (16) and e given by (9). Thus, the GRED-UVC system described by (40), (41) and (42) with switching function $\alpha(\tilde{\nu}_{rh}(t))$ defined in (25) is equivalent to the UVC using a MIMO HGO with an output disturbance $\beta_\alpha(\tilde{\nu}_{rh})$ described by (9), (16), (20) and (21), with $|\beta_\alpha(\tilde{\nu}_{rh}(t))| \leq \epsilon_M$. Thus, it is possible to conclude that Theorem 1 is valid for the GRED-UVC system and the closed-loop error system with state z is uniformly globally exponentially practically stable with respect to a residual set of order ε.

Now, we prove that the error state of the GRED-UVC ultimatelly converges to zero. According to Theorem 1, one can conclude for sufficiently small ε the error state z is steered to an invariant compact set $D_R := \{z : |z(t)| < R\}$ in some finite time $T_1 \geq 0$. Then, from (36), it follows that $\left\|\tilde{\xi}_{[T_1,t]}\right\| \leq \pi_\xi + \varepsilon\kappa_\xi R + \varepsilon\kappa_{21}$. Since $\left|\tilde{\xi}_h\right| \leq \left|\tilde{\xi}\right|$, it is straightforward to show that for some finite $T_2 \geq T_1$, $\left\|\tilde{\xi}_{h_{[T_2,t]}}\right\| \leq \bar{\xi}_h$, where $\bar{\xi}_h = \varepsilon K_h$.

Since the MIMO RED is time invariant, its initial conditions can be considered to be at $t = T_1$. From Lemma 1 in [29] the initial conditions are finite. Thus, after $t = T_1$ the conditions for convergence of the MIMO RED are satisfied and hence the estimation error $\tilde{\xi}_r(t)$ converges to zero in some finite time $T_3 > T_1$.

As K_R is chosen such that $\epsilon_M > \bar{\xi}_h + \Delta$ and from (25), it follows that after some finite time $\bar{T} = \max\{T_2, T_3\}$ the estimation of σ becomes exact and being made exclusively by the MIMO RED ($\alpha(\tilde{\nu}_{rh}) = 0$), which implies that $\tilde{\xi}_g(t) = 0, \forall t \geq \bar{T}$. In this case, an ideal sliding mode control loop [33] is formed and applying Lemma 1 to system (40)–(42), with $\varrho(t)$ satisfying (14), one can conclude that the error state z will converge exponentially to zero and σ becomes identically zero after some finite time. ■

Sliding Mode Control of Switched Stochastic Hybrid Systems

Ligang Wu, Huijun Gao, and Shen Yin

Research Institute of Intelligent Control and Systems, Harbin Institute of Technology, Harbin 150001, China
{ligangwu,hjgao,shen.yin}@hit.edu.cn

Abstract. This chapter is concerned with the sliding mode control of continuous- and discrete-time switched stochastic hybrid systems. By designing integral-type sliding surface functions, the sliding mode dynamics are established for continuous- and discrete-time systems, respectively. Then, by applying the average dwell time method and the piecewise Lyapunov function technique, sufficient conditions are proposed for the mean-square exponential stability of the sliding mode dynamics. A weighted $\mathcal{H}_\infty$ performance is also proposed for the discrete-time case. Sliding mode controllers for reaching motions of the continuous- and discrete-time switched stochastic hybrid systems are then designed, such that the trajectories of the resulting closed-loop systems can be driven onto the prescribed sliding surfaces and maintained there for all subsequent times. Finally, a numerical example is provided to illustrate the effectiveness of the proposed design scheme.

1 Introduction

Switched systems are an important class of hybrid systems, which consist of a family of subsystems described by continuous-time (or discrete-time) dynamics and these subsystems are governed by a switching signal [18]. Many real-world systems can be modelled as switched systems, for example, chemical process systems, transportation systems, computer controlled systems and communication systems. More importantly, many intelligent control strategies are designed based on the idea of switching controllers to overcome the shortcoming of the traditionally used single controller and to improve the performance [13], thus making the corresponding closed-loop systems to become switched systems. Switched systems have received increasing attention over the past few years, and a large number of papers have been reported. When focusing on stability analysis of switched systems, there are many valuable results which have appeared in the last two decades, and the interested readers may refer to some survey papers, see for example, [6, 19, 20, 21]. Considerable interests have also been devoted to synthesis problems of switched systems, including stabilization [2, 3, 5, 14, 16], robust and optimal control [8, 24, 30, 36, 37], robust filtering [1, 7, 27, 28], fault detection and fault-tolerant control [9, 26], and model approximation [10, 31].

X. Yu and M. Önder Efe (eds.), *Recent Advances in Sliding Modes*,
Studies in Systems, Decision and Control 24, DOI: 10.1007/978-3-319-18290-2_11

After more than 60 years of development, sliding mode control (SMC), as an effective robust control strategy, has been successfully applied to control of different kinds of dynamical systems, such as parametric uncertain systems [4, 17, 33], time-delay systems [11, 34], stochastic systems [22, 23], parameter-switching systems [25, 29], and singular systems [32]. To the authors' knowledge, there are few results reported on SMC of switched hybrid systems with stochastic perturbation (called switched stochastic hybrid systems). In fact, investigating this research problem would be difficult due to the fact that the probability distribution of switching is not available (that is, the switching is arbitrary subject to an average dwell time constraint, not in the form of Markovian switching as proposed in [23, 25]). Some open problems still remain unsolved when considering SMC of switched stochastic hybrid systems. In this work, we shall investigate this problem, and consider to solve the following three key issues:

- How to design an appropriate sliding surface function, with that the sliding mode dynamics exists?
- How to analyze the stability and performances of the resulted sliding mode dynamic? Specifically, how to establish the stability and performance conditions for sliding mode dynamics with less conservativeness?
- How to synthesize SMC laws so as to ensure the attraction of the sliding surface when the system changes from one mode to another under the restricted switching?

Motivated by the above questions, in this chapter, we are interested in investigating SMC problems for both continuous- and discrete-time switched stochastic hybrid systems. Firstly, by designing integral-type sliding surface functions, we obtain the sliding mode dynamics for continuous- and discrete-time cases, respectively, which are switched stochastic hybrid system with the same order as the original systems. Then, by utilizing the average dwell time approach combining with the piecewise Lyapunov function technique, sufficient conditions for the existence of the sliding mode are proposed in terms of LMIs for continuous- and discrete-time cases, and the explicit parametrization for the desired sliding surface functions are also given, respectively. Following these results, sliding mode controllers for reaching motion are synthesized such that the state trajectories of the closed-loop systems can be driven onto the prescribed sliding surfaces and maintained there for all subsequent times. Moreover, for the discrete-time system case, we consider the disturbance attenuation performance (that is, $\mathcal{H}_\infty$ performance) in the analysis of sliding mode dynamics, this is because that there are often some external disturbances involved in practical systems (for example, if the disturbance does not satisfy the so-called matching condition, it cannot be eliminated in the reaching motion phase), which constitute a source of instability or of performance degradation. Finally, a numerical example is provided to illustrate the effectiveness of the proposed SMC design scheme.

Notations. The superscript "T" denotes matrix transposition; $\mathbf{R}^n$ denotes the n-dimensional Euclidean space; the notation $P > 0$ means that P is real symmetric and positive definite; I and 0 represent the identity matrix and a zero matrix,

respectively; diag{...} stands for a block-diagonal matrix; $\lambda_{\min}(\cdot)$ ($\lambda_{\max}(\cdot)$) denotes the minimum (maximum) eigenvalue of a matrix. $\|\cdot\|$ denotes the Euclidean norm of a vector or the spectral norm of a matrix. For a vector $a = (a_i) \in \mathbf{R}^n$, $|a| \triangleq \sum_{i=1}^{n} |a_i|$ denotes the 1-norm of the vector a. $(\Omega, \mathcal{F}, \mathcal{P})$ is a probability space with Ω the sample space, $\mathcal{F}$ the σ-algebra of subsets of the sample space, and $\mathcal{P}$ the probability measure. $\mathbf{E}\{\cdot\}$ denotes the expectation operator. In symmetric block matrices or long matrix expressions, we use "$\star$" to represent a term that is induced by symmetry.

2 Continuous-Time Case

2.1 System Description and Preliminaries

Consider the continuous-time switched stochastic hybrid systems, which are established on the probability space $(\Omega, \mathcal{F}, \mathcal{P})$, and are described by

$$\begin{aligned} dx(t) = &\{A(\alpha(t))x(t) + B(\alpha(t))\,[u(t) + f(x(t), t)]\}\,dt \\ &+E(\alpha(t))x(t)d\varpi(t), \end{aligned} \tag{1}$$

where $x(t) \in \mathbf{R}^n$ is the system state vector; $u(t) \in \mathbf{R}^m$ is the control input; $\varpi(t)$ is a one-dimensional Brownian motion satisfying $\mathbf{E}\{d\varpi(t)\} = 0$ and $\mathbf{E}\left\{d\varpi^2(t)\right\} = dt$. $\alpha(t) : \mathbf{R} \to \mathcal{N}$ is a piecewise constant function of time t called a switching signal, and at a given time t, the value of $\alpha(t)$, denoted by α for simplicity, might depend on t or $x(t)$, or both, or may be generated by any other hybrid scheme. $\{(A(\alpha), B(\alpha), E(\alpha)) : \alpha \in \mathcal{N}\}$ is a family of matrices parameterized by an index set $\mathcal{N} = \{1, 2, \ldots, N\}$. Therefore, the switched stochastic hybrid system effectively switches amongst N subsystems with the switching sequence controlled by α. We assume that the value of α is unknown, but its instantaneous value is available in real time.

For each possible value $\alpha = i$ ($i \in \mathcal{N}$), we denote the system matrices associated with mode i by $A(i) = A(\alpha)$, $B(i) = B(\alpha)$ and $E(i) = E(\alpha)$, where $A(i)$, $B(i)$ and $E(i)$ are constant matrices. Corresponding to switching signal α, we have the switching sequence $\{(i_0, t_0), (i_1, t_1), \ldots, (i_k, t_k), \ldots, | \; i_k \in \mathcal{N},\ k = 0, 1, \ldots\}$ with $t_0 = 0$, which means that the i_kth subsystem is activated when $t \in [t_k, t_{k+1})$.

In addition, $f(x(t), t) \in \mathbf{R}^m$ is an unknown nonlinear function satisfying

$$\|f(x(t), t)\| \leq \psi \|x(t)\|, \quad \psi > 0.$$

For switching signal α, we revisit the average dwell time property from the following definition.

Definition 1. *[18] For any $T_2 > T_1 \geq 0$, let $N_\alpha(T_1, T_2)$ denote the number of switching of α over (T_1, T_2). If $N_\alpha(T_1, T_2) \leq N_0 + (T_2 - T_1)/T_a$ holds for $T_a > 0$, $N_0 \geq 0$, then T_a is called an average dwell time.*

Assumption 1. *The switching signal $\alpha(t)$ has an average dwell time.*

Assumption 2. *For each $i \in \mathcal{N}$, the pair $(A(i), B(i))$ in system (1) is controllable and the matrix $B(i)$ has full column rank.*

2.2 Sliding Mode Dynamics

We design the following integral sliding surface function:

$$s(t) = G(i)x(t) - \int_0^t G(i)\Big[A(i) + B(i)K(i)\Big]x(\theta)d\theta, \tag{2}$$

where $K(i) \in \mathbf{R}^{m\times n}$ are real matrices to be designed, and matrices $G(i)$ are to be chosen such that $G(i)B(i)$ are nonsingular and $G(i)E(i) = 0$ for $i \in \mathcal{N}$.

The solution of $x(t)$ can be given by

$$\begin{aligned} x(t) = x(0) &+ \int_0^t \Big[A(i)x(\theta) + B(i)\left(u(\theta) + f(x(\theta),\theta)\right)\Big]d\theta \\ &+ \int_0^t E(i)x(\theta)d\varpi(\theta). \end{aligned} \tag{3}$$

It follows from (2) and (3) that

$$\begin{aligned} s(t) = G(i)x(0) &\\ + \int_0^t G(i)\Big[&- B(i)K(i)x(\theta) + B(i)\left(u(\theta) + f(x(\theta),\theta)\right)\Big]d\theta. \end{aligned} \tag{4}$$

As is well known that when the system state trajectories reach onto the sliding surface, it follows that $s(t) = 0$ and $\dot{s}(t) = 0$. Therefore, by $\dot{s}(t) = 0$ we get the equivalent control as

$$u_{eq}(t) = K(i)x(t) - f(x(t),t). \tag{5}$$

Substituting (5) into (1), the sliding mode dynamics can be obtained as

$$dx(t) = \Big[A(i) + B(i)K(i)\Big]x(t)dt + E(i)x(t)d\varpi(t). \tag{6}$$

For notational simplicity, we define $\tilde{A}(i) \triangleq A(i) + B(i)K(i)$, then the sliding mode dynamics in (6) can be formulated as

$$dx(t) = \tilde{A}(i)x(t)dt + E(i)x(t)d\varpi(t), \tag{7}$$

Definition 2. *The sliding mode dynamics in (7) is said to be mean-square exponentially stable under $\alpha(t)$ if its solution $x(t)$ satisfies*

$$\mathbf{E}\left\{\|x(t)\|\right\} \le \eta\,\|x(t_0)\|\,e^{-\lambda(t-t_0)}, \quad \forall t \ge t_0, \tag{8}$$

for constants $\eta \ge 1$ and $\lambda > 0$.

The above analysis gives the first step of the SMC for the switched stochastic hybrid system (1). Specifically, we design an integral-type sliding surface as given in (2) so that the dynamics restricted to the sliding surface (i.e., the sliding mode dynamics) has the form of (7). The remaining problems to be addressed in this chapter can be stated as follows:

1) Stability Analysis. Given all the system matrices in (1), determine the matrices $G(i)$ and $K(i)$ in sliding surface function (2) such that the sliding mode dynamics in (7) is mean-square exponentially stable in the sense of Definition 2.
2) SMC Law Design. Synthesize a SMC law to globally drive the system state trajectories onto the predefined sliding surface $s(t) = 0$ in a finite time and maintain them there for all subsequent time.

2.3 Sliding Mode Dynamics Analysis

We present the following result for the stability of sliding mode dynamics (7).

Theorem 3. *For a given scalar $\beta > 0$, suppose that there exist matrices $P(i) > 0$ such that for $i \in \mathcal{N}$,*

$$P(i)\tilde{A}(i) + \tilde{A}^T(i)P(i) + \beta P(i) + E^T(i)P(i)E(i) < 0, \tag{9}$$

then the sliding mode dynamics in (7) is mean-square exponentially stable for any switching signal with the average dwell time satisfying $T_a > \frac{\ln \mu}{\beta}$, where $\mu \geq 1$ and satisfies

$$P(i) \leq \mu P(j), \quad i, j \in \mathcal{N}. \tag{10}$$

Moreover, an estimate of the mean-square of the state decay is given by

$$\mathbf{E}\{\|x(t)\|\} \leq \eta \|x(0)\| e^{-\lambda t}, \tag{11}$$

where

$$\begin{cases} \lambda = \dfrac{1}{2}\left(\beta - \dfrac{\ln \mu}{T_a}\right) > 0, \quad \eta = \sqrt{\dfrac{b}{a}} \geq 1, \\ a = \min\limits_{\forall i \in \mathcal{N}} \lambda_{\min}\left(P(i)\right), \quad b = \max\limits_{\forall i \in \mathcal{N}} \lambda_{\max}\left(P(i)\right). \end{cases} \tag{12}$$

Proof. Choose the following Lyapunov function candidate:

$$V(x, \alpha) = x^T(t)P(\alpha)x(t), \tag{13}$$

where $P(\alpha) > 0$, $\alpha \in \mathcal{N}$ are to be determined. Then, along the solution of the sliding mode dynamics in (7) for a fixed α, by Itô's formula, we have

$$dV(x, \alpha) = \mathscr{L}V(x_t, \alpha)dt + 2x^T(t)P(\alpha)E(\alpha)x(t)d\varpi(t),$$

where

$$\begin{aligned} \mathscr{L}V(x, \alpha) &= 2x^T(t)P(\alpha)\tilde{A}(\alpha)x(t) + x^T(t)E^T(\alpha)P(\alpha)E(\alpha)x(t) \\ &= x^T(t)\left[P(\alpha)\tilde{A}(\alpha) + \tilde{A}^T(\alpha)P(\alpha) + E^T(\alpha)P(\alpha)E(\alpha)\right]x(t). \end{aligned} \tag{14}$$

By Schur complement, LMI (9) implies

$$P(\alpha)\tilde{A}(\alpha) + \tilde{A}^T(\alpha)P(\alpha) + E^T(\alpha)P(\alpha)E(\alpha) < -\beta P(\alpha),$$

which implies from (14) that

$$\mathscr{L}V(x,\alpha) < -\beta x^T(t)P(\alpha)x(t) = -\beta V(x,\alpha).$$

Thus, we have

$$dV(x,\alpha) < -\beta V(x,\alpha)dt + 2x^T(t)P(\alpha)E(\alpha)x(t)d\varpi(t).$$

Observe that

$$\begin{aligned} d\left[e^{\beta t}V(x,\alpha)\right] &= \beta e^{\beta t}V(x,\alpha)dt + e^{\beta t}dV(x,\alpha) \\ &< e^{\beta t}\left[\beta V(x,\alpha)dt - \beta V(x,\alpha)dt + 2x^T(t)P(\alpha)E(\alpha)x(t)d\varpi(t)\right] \\ &= 2e^{\beta t}x^T(t)P(\alpha)E(\alpha)x(t)d\varpi(t). \end{aligned} \tag{15}$$

Integrate both sides of (15) from $T > 0$ to t and take expectations. Then, by some mathematical operations, we have

$$\mathbf{E}\left\{V(x,\alpha)\right\} < e^{-\beta(t-T)}\mathbf{E}\left\{V(x(T),\alpha(T))\right\}. \tag{16}$$

Now, for an arbitrary piecewise constant switching signal α, and for any $t > 0$, we let $0 = t_0 < t_1 < \cdots < t_k < \cdots$, $k = 0, 1, \ldots$, denote the switching points of α over the interval $(0, t)$. As mentioned earlier, the i_kth subsystem is activated when $t \in [t_k, t_{k+1})$. Letting $T = t_k$ in (16) gives

$$\mathbf{E}\left\{V(x,\alpha)\right\} < e^{-\beta(t-t_k)}\mathbf{E}\left\{V(x(t_k),\alpha(t_k))\right\}. \tag{17}$$

Using (10) and (13), at switching instant t_k, we have

$$\mathbf{E}\left\{V(x(t_k),\alpha(t_k))\right\} \le \mu\mathbf{E}\left\{V(x(t_k^-),\alpha(t_k^-))\right\}, \tag{18}$$

where t_k^- denotes the left limit of t_k.

Therefore, it follows from (17)–(18) and the relationship $\vartheta = N_\alpha(0,t) \le (t-0)/T_a$ that

$$\begin{aligned} \mathbf{E}\left\{V(x,\alpha)\right\} &\le e^{-\beta(t-t_k)}\mu\mathbf{E}\left\{V(x(t_k^-),\alpha(t_k^-))\right\} \\ &\le \cdots \\ &\le e^{-\beta(t-0)}\mu^{\vartheta}\mathbf{E}\left\{V(x(0),\alpha(0))\right\} \\ &\le e^{-(\beta-\ln\mu/T_a)t}\mathbf{E}\left\{V(x(0),\alpha(0))\right\} \\ &= e^{-(\beta-\ln\mu/T_a)t}V(x(0),\alpha(0)). \end{aligned} \tag{19}$$

Notice from (13) that

$$\mathbf{E}\left\{V(x,\alpha)\right\} \ge a\mathbf{E}\{\|x(t)\|^2\}, \quad V(x(0),\alpha(0)) \le b\|x(0)\|^2, \tag{20}$$

where a and b are defined in (12). Combining (19) and (20) yields

$$\mathbf{E}\left\{\|x(t)\|^2\right\} \leq \frac{1}{a}\mathbf{E}\left\{V(x,\alpha)\right\} \leq \frac{b}{a}e^{-(\beta-\ln\mu/T_a)t}\|x(0)\|^2,$$

which implies (11). By Definition 2 with $t_0 = 0$, the sliding mode dynamics in (7) is mean-square exponentially stable. This completes the proof. ■

Remark 4. A scalar β is introduced in the stability analysis of Theorem 3, this is the characteristic of the exponential stability result to the switched system by using the average dwell time approach. Here, β plays a key role in controlling the low bound of the average dwell time due to $T_a > \frac{\ln\mu}{\beta}$. From $T_a > \frac{\ln\mu}{\beta}$ we can see that when β is given a bigger value, the lower bound of the average dwell time becomes smaller with a fixed μ, which may result in the instability of the system.

Remark 5. When $\mu = 1$ in $T_a > \frac{\ln\mu}{\beta}$ we have $T_a > T_a^* = 0$, which means that the switching signal α can be arbitrary. In this case, (10) turns out to be $P(i) \leq P(j)$, $\forall i, j \in \mathcal{N}$. The only possibility for that is $P(i) = P(j) = P$, $\forall i, j \in \mathcal{N}$, and this implies that it requires a common (that is, mode-independent) Lyapunov functional for all subsystems. On the other hand, when $\mu > 1$ and $\beta \to 0$ in $T_a > \frac{\ln\mu}{\beta}$, we have $T_a \to \infty$, that is, there is no switching. In such case, the sliding mode dynamics in (7) is effectively operating at one of the subsystems all the time. We have the following result.

Corollary 6. *Suppose there is no switching in sliding mode dynamics (7) (when $\beta \to 0$ as discussed in Remark 5), that is, system (7) turn out to be a common stochastic system (thus, the parameters become $(\tilde{A}, E)$). If there exists a matrix $P > 0$ such that*

$$P\tilde{A} + \tilde{A}^T P + E^T P E < 0,$$

then the common stochastic system is mean-square asymptotically stable.

Remark 7. The mean-square asymptotic stability for the common stochastic system in Corollary 6 is consistent with the result in [35], which proves that our result in Theorem 3 has extended the result in [35] to the switched systems.

In the following, based on the result in Theorem 3, we present a solution to $K(i)$ in sliding surface function (2).

Theorem 8. *For a given scalar $\beta > 0$, suppose that there exist matrices $X(i) > 0$ and $Y(i)$ such that for $i \in \mathcal{N}$,*

$$\begin{bmatrix} A(i)X(i) + B(i)Y(i) + (A(i)X(i) + B(i)Y(i))^T + \beta X(i) & X(i)E^T(i) \\ \star & -X(i) \end{bmatrix} < 0, \tag{21}$$

then the sliding mode dynamics in (7) is mean-square exponentially stable for any switching signal with the average dwell time satisfying $T_a > \frac{\ln\mu}{\beta}$, where $\mu \geq 1$ and satisfies

$$X(i) \leq \mu X(j), \quad \forall i, j \in \mathcal{N}. \tag{22}$$

Moreover, if the above conditions are feasible, then the matrix variable $K(i)$ in (2) can be computed by

$$K(i) = Y(i)X^{-1}(i). \tag{23}$$

Proof. Let $X(i) \triangleq P^{-1}(i)$ and $Y(i) \triangleq K(i)X(i)$. Then by performing a congruence transformation to (9) with $X(i)$ and by Schur complement, the result can be obtained. ■

2.4 Sliding Mode Control Design

In this section, we synthesize a discontinuous SMC law, by which the state trajectories of the switched stochastic hybrid system (1) can be driven onto the pre-specified sliding surface $s(t) = 0$ in a finite time and then are maintained there for all subsequent time.

Theorem 9. *Consider the continuous-time switched stochastic hybrid system (1). Suppose that the sliding surface function is designed as (2) with $K(i)$ being solved by (23), then the state trajectories of system (1) can be driven onto the sliding surface $s(t) = 0$ in a finite time by the following sliding mode controller:*

$$u(t) = K(i)x(t) - \left(\varrho + \psi \left\|G(i)B(i)\right\| \left\|x(t)\right\|\right) \left(G(i)B(i)\right)^{-1} \operatorname{sign}\left(s(t)\right), \tag{24}$$

where ϱ is a positive scalar.

Proof. Choose a Lyapunov function of the following form:

$$W(t) = \frac{1}{2} s^T(t)s(t).$$

According to (4), we have

$$\dot{s}(t) = G(i)B(i)\left(-K(i)x(t) + u(t) + f(x(t), t)\right).$$

Thus, taking the derivative of $W(t)$ and considering the above equation, we have

$$\begin{aligned} \dot{W}(t) &= s^T(t)\dot{s}(t) \\ &= s^T(t)G(i)B(i)\left(-K(i)x(t) + u(t) + f(x(t), t)\right). \end{aligned} \tag{25}$$

Substituting (24) into (25) and noting $\|s(t)\| \leq |s(t)|$, we have

$$\begin{aligned} \dot{W}(t) &= s^T(t)G(i)B(i) \\ &\quad \times \left[-\left(\varrho + \psi \left\|G(i)B(i)\right\| \left\|x(t)\right\|\right) \left(G(i)B(i)\right)^{-1} \operatorname{sign}\left(s(t)\right) + f(x(t), t)\right] \\ &\leq -\left(\varrho + \psi \left\|G(i)B(i)\right\| \left\|x(t)\right\|\right) \left\|s(t)\right\| + \left\|s(t)\right\| \left\|G(i)B(i)\right\| \left\|f(x(t), t)\right\| \\ &\leq -\varrho \left\|s(t)\right\| = -\sqrt{2}\varrho W^{\frac{1}{2}}(t). \end{aligned} \tag{26}$$

It can be shown from (26) that there exists an instant $t^* = \sqrt{2W(0)}/\varrho$ such that $W(t) = 0$ (equivalently, $s(t) = 0$) when $t \geq t^*$. Thus, we can conclude that the system state trajectories can be driven onto the predefined sliding surface in a finite time. ■

3 Discrete-Time Case

3.1 System Description and Preliminaries

Consider a discrete-time switched stochastic hybrid system which can be described by the following dynamical equations:

$$\begin{cases} x(k+1) = A(\alpha(k))x(k) + B_1(\alpha(k))\left[u(k) + f(x(k),k)\right] \\ \qquad\qquad +B_2(\alpha(k))\omega(k) + E(\alpha(k))x(k)\varpi(k), \\ \quad z(k) = C(\alpha(k))x(k), \end{cases} \tag{27}$$

for $k = 1, 2, \ldots$, where $x(k) \in \mathbf{R}^n$ is the state vector; $u(k) \in \mathbf{R}^m$ represents the control input; $\omega(k) \in \mathbf{R}^p$ is the noise signal that belongs to $\ell_2[0, +\infty)$; $z(k) \in \mathbf{R}^q$ is the controlled output; $\varpi(k)$ is a zero-mean real scalar process on a probability space $(\Omega, \mathcal{F}, \mathcal{P})$ relative to an increasing family $(\mathcal{F}_k)_{k\in\mathbb{N}}$ of σ-algebras $\mathcal{F}_k \subset \mathcal{F}$ generated by $(\varpi(k))_{k\in\mathbb{N}}$. The stochastic process $\{\varpi(k)\}$ is independent, which is assumed to satisfy

$$\mathbf{E}\{\varpi(k)\} = 0, \quad \mathbf{E}\{\varpi^2(k)\} = \delta, \quad k = 0, 1, \ldots,$$

where $\delta > 0$ is a known scalar. $\alpha(k) : \mathbb{Z}^+ \to \mathcal{N}$ is a piecewise constant function of time, called a switching signal, which takes its values in the finite set $\mathcal{N}$. At an arbitrary discrete time k, the value of $\alpha(k)$, denoted by α for simplicity, might depend on k or $x(k)$, or both, or may be generated by any other hybrid scheme. We assume that the sequence of subsystems in switching signal α is unknown *a priori*, but its instantaneous value is available in real time. For the switching time sequence $k_0 < k_1 < k_2 < \cdots$ of switching signal α,the holding time between $[k_l, k_{l+1}]$ is called the dwell time of the currently engaged subsystem, where $l \in \mathcal{N}$. $\{(A(\alpha), B_1(\alpha), B_2(\alpha), C(\alpha), E(\alpha)) : \alpha \in \mathcal{N}\}$ is a family of matrices parameterized by an index set $\mathcal{N} = \{1, 2, \ldots, N\}$. For each possible value $\alpha = i$, $i \in \mathcal{N}$, we denote the system matrices associated with mode i by $A(i) = A(\alpha)$, $B_1(i) = B_1(\alpha)$, $B_2(i) = B_2(\alpha)$, $C(i) = C(\alpha)$ and $E(i) = E(\alpha)$, where $A(i)$, $B_1(i)$, $B_2(i)$, $C(i)$ and $E(i)$ are constant matrices. Corresponding to the switching signal α_k, we have the switching sequence $\{(i_0, k_0), (i_1, k_1), \ldots, (i_l, k_l), \ldots, |\ i_l \in \mathcal{N},\ l = 0, 1, \ldots\}$ with $k_0 = 0$, which means that the i_lth subsystem is activated when $k \in [k_l, k_{l+1})$.

In addition, $f(x(k), k) \in \mathbf{R}^m$ is an unknown nonlinear function satisfying

$$\|f(x(k), k)\| \leq \chi \|x(k)\|, \quad \chi > 0.$$

Definition 10. *[12] For switching signal $\alpha(k)$ and any $k_i > k_j > k_0$, let $N_\alpha(k_j, k_i)$ be the switching numbers of α over the interval $[k_j, k_i]$. If for any given $N_0 > 0$ and $T_a > 0$, we have $N_\alpha(k_j, k_i) \leq N_0 + (k_i - k_j)/T_a$, then T_a and N_0 are called average dwell time and the chatter bound, respectively.*

Here, we assume $N_0 = 0$ for simplicity as commonly used in the literature.

The following definitions are introduced, which will play key roles in deriving our main results.

Definition 11. *The discrete-time switched stochastic hybrid system in (27) with $u(k) = 0$ and $\omega(k) = 0$ is said to be mean-square exponentially stable under $\alpha(k)$ if the solution $x(k)$ satisfies*

$$\mathbf{E}\{\|x(k)\|\} \leq \eta\rho^{(k-k_0)}\|x(k_0)\|, \quad \forall k \geq k_0,$$

for constants $\eta \geq 1$ and $0 < \rho < 1$.

Definition 12. *For $0 < \beta < 1$ and $\gamma > 0$, the discrete-time switched stochastic hybrid system in (27) with $u(k) = 0$ is said to be mean-square exponentially stable with a weighted $\mathcal{H}_\infty$ performance level γ under $\alpha(k)$, if it is mean-square exponentially stable with $\omega(k) = 0$, and under zero initial condition, that is, $x(0) = 0$, it holds for all nonzero $\omega(k) \in \ell_2[0, \infty)$ that*

$$\mathbf{E}\left\{\sum_{s=k_0}^{\infty}\beta^s z^T(s)z(s)\right\} < \gamma^2\sum_{s=k_0}^{\infty}\omega^T(s)\omega(s). \tag{28}$$

3.2 Stability and $\mathcal{H}_\infty$ Performance Analysis

Firstly, we apply the average dwell time approach combined with the piecewise Lyapunov function technique to investigate the mean-square exponential stability of the following nominal system:

$$x(k+1) = A(\alpha(k))x(k) + E(\alpha(k))x(k)\varpi(k). \tag{29}$$

Theorem 13. *For a given constant $0 < \beta < 1$, suppose that there exist matrix $P(i) > 0$ such that for $i \in \mathcal{N}$,*

$$A^T(i)P(i)A(i) + \delta E^T(i)P(i)E(i) - \beta P(i) < 0, \tag{30}$$

then the discrete-time switched stochastic system in (29) is mean-square exponentially stable for any switching signal with average dwell time satisfying $T_a > T_a^* = \text{ceil}\left(-\frac{\ln\mu}{\ln\beta}\right)$, where $\mu \geq 1$ satisfies

$$P(i) \leq \mu P(j), \quad \forall i, j \in \mathcal{N}. \tag{31}$$

Moreover, an estimate of the state decay is given by

$$\mathbf{E}\{\|x(k)\|\} \leq \eta\rho^{(k-k_0)}\|x(k_0)\|, \tag{32}$$

where

$$\eta \triangleq \sqrt{\frac{b}{a}},\ \rho \triangleq \sqrt{\beta\mu^{\frac{1}{T_a}}},\ a \triangleq \min_{\forall i\in\mathcal{N}} \lambda_{\min}(P(i)),\ b \triangleq \max_{\forall i\in\mathcal{N}} \lambda_{\max}(P(i)). \tag{33}$$

Proof. Choose a mode-dependent Lyapunov function of the form:

$$V(x,\alpha) \triangleq x^T(k)P(\alpha)x(k), \tag{34}$$

where $P(\alpha) > 0$. For $k \in [k_l, k_{l+1})$, we define

$$\mathbf{E}\left\{\Delta V(x,\alpha)\right\} \triangleq \mathbf{E}\left\{V(x(k+1),\alpha) - V(x(k),\alpha)\right\},$$

and we have

$$\begin{aligned}\mathbf{E}\left\{\Delta V(x,\alpha)\right\} &= \mathbf{E}\left\{x^T(k+1)P(\alpha)x(k+1) - x^T(k)P(\alpha)x(k)\right\}\\ &= \mathbf{E}\left\{x^T(k)\left[A^T(\alpha)P(\alpha)A(\alpha) + \delta E^T(\alpha)P(\alpha)E(\alpha) - P(\alpha)\right]x(k)\right\}.\end{aligned}$$

thus, we have

$$\mathbf{E}\left\{\Delta V(x,\alpha)\right\} + (1-\beta)\mathbf{E}\left\{V(x,\alpha)\right\} \triangleq \mathbf{E}\left\{x^T(k)\Phi(\alpha)x(k)\right\}, \tag{35}$$

where

$$\Phi(\alpha) \triangleq A^T(\alpha)P(\alpha)A(\alpha) + \delta E^T(\alpha)P(\alpha)E(\alpha) - \beta P(\alpha).$$

By (30), it follows from (35) that

$$\mathbf{E}\left\{\Delta V(x,\alpha) + (1-\beta)V(x,\alpha)\right\} < 0, \quad \forall k \in [k_l, k_{l+1}). \tag{36}$$

Now, for an arbitrary piecewise constant switching signal α, and for any $k > 0$, we let $k_0 < k_1 < \cdots < k_l < \cdots, l = 1, \ldots$, denote the switching points of α over the interval $(0, k)$. As mentioned earlier, the i_lth subsystem is activated when $k \in [k_l, k_{l+1})$. Therefore, for $k \in [k_l, k_{l+1})$, it holds from (36) that

$$\mathbf{E}\left\{V(x,\alpha)\right\} < \beta^{k-k_l}\mathbf{E}\left\{V(x(k_l),\alpha(k_l))\right\}. \tag{37}$$

Using (31) and (34), we have

$$\mathbf{E}\left\{V(x(k_l),\alpha(k_l))\right\} \le \mu\mathbf{E}\left\{V(x(k_l),\alpha(k_{l-1}))\right\}. \tag{38}$$

Therefore, it follows from (37)–(38) and the relationship $\vartheta = N_\alpha(k_0,k) \le (k - k_0)/T_a$ that

$$\begin{aligned}\mathbf{E}\left\{V(x,\alpha)\right\} &\le \beta^{k-k_l}\mu\mathbf{E}\left\{V(x(k_l),\alpha(k_{l-1}))\right\}\\ &\le \cdots\\ &\le \beta^{(k-k_0)}\mu^{\vartheta}\mathbf{E}\left\{V(x(k_0),\alpha(k_0))\right\}\\ &\le (\beta\mu^{1/T_a})^{(k-k_0)}\mathbf{E}\left\{V(x(k_0),\alpha(k_0))\right\}.\end{aligned} \tag{39}$$

Notice from (34) that there exist two positive constants a and b ($a \leq b$, and they are defined in (33)) such that

$$\mathbf{E}\{V(x,\alpha)\} \geq a\mathbf{E}\left\{\|x(k)\|^2\right\},\ \mathbf{E}\{V(x(k_0),\alpha(k_0))\} \leq b\|x(k_0)\|^2. \tag{40}$$

Combining (39) and (40) yields

$$\mathbf{E}\left\{\|x(k)\|^2\right\} \leq \frac{1}{a}\mathbf{E}\{V(x,\alpha)\} \leq \frac{b}{a}(\beta\mu^{1/T_a})^{(k-k_0)}\|x(k_0)\|^2.$$

Furthermore, letting $\rho \triangleq \sqrt{\beta\mu^{1/T_a}}$, it follows that

$$\mathbf{E}\{\|x(k)\|\} \leq \sqrt{\frac{b}{a}}\rho^{(k-k_0)}\|x(k_0)\|.$$

By Definition 11, we know that if $0 < \rho < 1$, that is, $T_a > T_a^* = \text{ceil}\left(-\frac{\ln\mu}{\ln\beta}\right)$, the discrete-time switched stochastic hybrid system in (27) with $u(k) = 0$ and $\omega(k) = 0$ is mean-square exponentially stable, where function ceil(h) represents rounding real number h to the nearest integer greater than or equal to h. The proof is completed. ■

Remark 14. In Theorem 13, we propose a sufficient condition for the mean-square exponential stability condition for the considered the discrete-time switched stochastic hybrid system in (27) with $u(k) = 0$ and $\omega(k) = 0$. Here, β plays a key role in controlling the low bound of the average dwell time, which can be seen from $T_a > T_a^* = \text{ceil}\left(-\frac{\ln\mu}{\ln\beta}\right)$, specifically, if β is given a smaller value, the low bound of the average dwell time becomes smaller with a fixed μ, which may result in the instability of the system.

Remark 15. Note that when $\mu = 1$ in $T_a > T_a^* = \text{ceil}\left(-\frac{\ln\mu}{\ln\beta}\right)$ we have $T_a > T_a^* = 0$, which means that the switching signal $\alpha(k)$ can be arbitrary. In this case, (31) turns out to be $P(i) = P(j) = P, \forall i, j \in \mathcal{N}$, and the proposed approach becomes quadratic one thus conservative. In this case, the system in (27) with $u(k) = 0$ and $\omega(k) = 0$ turns out to be a discrete-time stochastic system. On the other hand, when $\beta = 1$ in $T_a > T_a^* = \text{ceil}\left(-\frac{\ln\mu}{\ln\beta}\right)$, we have $T_a = \infty$, that is, there is no switching.

Now, we investigate the weighted $\mathcal{H}_\infty$ performance for the following system:

$$\begin{cases} x(k+1) = A(\alpha(k))x(k) + B_2(\alpha(k))\omega(k) + E(\alpha(k))x(k)\varpi(k), \\ \quad z(k) = C(\alpha(k))x(k). \end{cases} \tag{41}$$

Theorem 16. *For given constants $0 < \beta < 1$ and $\gamma > 0$, suppose that there exist matrix $P(i) > 0$ such that for $i \in \mathcal{N}$,*

$$\begin{bmatrix} -\beta P(i) + C^T(i)C(i) & 0 & A^T(i)P(i) & \delta E^T(i)P(i) \\ \star & -\gamma^2 I & B_2^T(i)P(i) & 0 \\ \star & \star & -P(i) & 0 \\ \star & \star & \star & -\delta P(i) \end{bmatrix} < 0, \tag{42}$$

then the discrete-time switched stochastic system in (41) is mean-square exponentially stable with a weighted $\mathcal{H}_\infty$ performance level γ for any switching signal with average dwell time satisfying $T_a > T_a^* = \text{ceil}\left(-\frac{\ln \mu}{\ln \beta}\right)$, where $\mu \geq 1$ satisfies (31).

Proof. The proof of mean-square exponential stability can be refereed to the proof of Theorem 3. Now, we will establish the weighted $\mathcal{H}_\infty$ performance defined in (28). To this end, introduce the following index:

$$\mathcal{J} \triangleq \mathbf{E}\left\{\Delta V(x,\alpha) + (1-\beta)V(x,\alpha) + z^T(k)z(k) - \gamma^2\omega^T(k)\omega(k)\right\}, \tag{43}$$

where the Lyapunov function $V(x,\alpha)$ is given in (34). By employing the same techniques as those used in the proof of Theorem 13, and considering (42), for $k \in [k_l, k_{l+1})$ we have $\mathcal{J} < 0$. Let $\Gamma(k) \triangleq z^T(k)z(k) - \gamma^2\omega^T(k)\omega(k)$, then

$$\mathbf{E}\left\{\Delta V(x,\alpha)\right\} < \mathbf{E}\left\{-(1-\beta)V(x,\alpha) - \Gamma(k)\right\}. \tag{44}$$

Therefore, for $k \in [k_l, k_{l+1})$, it holds from (44) that

$$\mathbf{E}\left\{V(x,\alpha)\right\} < \beta^{k-k_l}\mathbf{E}\left\{V(x(k_l),\alpha(k_l))\right\} - \mathbf{E}\left\{\sum_{s=k_l}^{k-1}\beta^{k-1-s}\Gamma(s)\right\}. \tag{45}$$

Using (31) and (34), we have

$$\mathbf{E}\left\{V(x(k_l),\alpha(k_l))\right\} \leq \mu\mathbf{E}\left\{V(x(k_l),\alpha(k_{l-1}))\right\}. \tag{46}$$

Thus, by (45)–(46) we have

$$\begin{aligned}
\mathbf{E}\left\{V(x(k),\alpha(k))\right\} &< \beta^{k-k_l}\mathbf{E}\left\{V(x(k_l),\alpha(k_l))\right\} - \mathbf{E}\left\{\sum_{s=k_l}^{k-1}\beta^{k-1-s}\Gamma(s)\right\},\\
\mathbf{E}\left\{V(x(k_l),\alpha(k_l))\right\} &< \beta^{k_l-k_{l-1}}\mu\mathbf{E}\left\{V(x(k_{l-1}),\alpha(k_{l-1}))\right\}\\
&\quad -\mu\mathbf{E}\left\{\sum_{s=k_{l-1}}^{k_l-1}\beta^{k_l-1-s}\Gamma(s)\right\},\\
\mathbf{E}\left\{V(x(k_{l-1}),\alpha(k_{l-1}))\right\} &< \beta^{k_{l-1}-k_{l-2}}\mu\mathbf{E}\left\{V(x(k_{l-2}),\alpha(k_{l-2}))\right\}\\
&\quad -\mu\mathbf{E}\left\{\sum_{s=k_{l-2}}^{k_{l-1}-1}\beta^{k_{l-1}-1-s}\Gamma(s)\right\},\\
&\vdots\\
\mathbf{E}\left\{V(x(k_1),\alpha(k_1))\right\} &< \beta^{k_1-k_0}\mu\mathbf{E}\left\{V(x(k_0),\alpha(k_0))\right\}\\
&\quad -\mu\mathbf{E}\left\{\sum_{s=k_0}^{k_1-1}\beta^{k_1-1-s}\Gamma(s)\right\}.
\end{aligned}$$

Therefore, it follows from the above inequalities and the relationship $\vartheta = N_\alpha(k_0,k) \le (k-k_0)/T_a$ that

$$\begin{aligned}
\mathbf{E}\{V(x(k),\alpha(k))\} &< \beta^{k-k_l}\mathbf{E}\{V(x(k_l),\alpha(k_l))\} - \mathbf{E}\left\{\sum_{s=k_l}^{k-1}\beta^{k-1-s}\Gamma(s)\right\} \\
&< \beta^{k-k_0}\mu^{N_\alpha(k_0,k)}\mathbf{E}\{V(x(k_0),\alpha(k_0))\} \\
&\quad -\beta^{k-k_1}\mu^{N_\alpha(k_0,k)}\mathbf{E}\left\{\sum_{s=k_0}^{k_1-1}\beta^{k_1-1-s}\Gamma(s)\right\} \\
&\quad -\beta^{k-k_2}\mu^{N_\alpha(k_1,k)}\mathbf{E}\left\{\sum_{s=k_1}^{k_2-1}\beta^{k_2-1-s}\Gamma(s)\right\} - \cdots \\
&\quad -\beta^{k-k_{l-1}}\mu^2\mathbf{E}\left\{\sum_{s=k_{l-2}}^{k_{l-1}-1}\beta^{k_{l-1}-1-s}\Gamma(s)\right\} \\
&\quad -\beta^{k-k_l}\mu\mathbf{E}\left\{\sum_{s=k_{l-1}}^{k_l-1}\beta^{k_l-1-s}\Gamma(s)\right\} \\
&\quad -\mathbf{E}\left\{\sum_{s=k_l}^{k-1}\beta^{k-1-s}\Gamma(s)\right\} \\
&= \beta^{k-k_0}\mu^{N_\alpha(k_0,k)}\mathbf{E}\{V(x(k_0),\alpha(k_0))\} \\
&\quad -\mathbf{E}\left\{\sum_{s=k_0}^{k-1}\beta^{k-1-s}\mu^{N_\alpha(s,k)}\Gamma(s)\right\}. \qquad (47)
\end{aligned}$$

Under zero initial condition, that is, $x(0)=0$, (47) implies

$$\mathbf{E}\left\{\sum_{s=k_0}^{k-1}\beta^{k-1-s}\mu^{N_\alpha(s,k)}z^T(s)z(s)\right\} < \gamma^2\mathbf{E}\left\{\sum_{s=k_0}^{k-1}\beta^{k-1-s}\mu^{N_\alpha(s,k)}\omega^T(s)\omega(s)\right\}.$$

Multiplying both sides of the above inequality by $\mu^{-N_\alpha(0,k)}$ yields

$$\mathbf{E}\left\{\sum_{s=k_0}^{k-1}\beta^{k-1-s}\mu^{-N_\alpha(0,s)}z^T(s)z(s)\right\} < \gamma^2\mathbf{E}\left\{\sum_{s=k_0}^{k-1}\beta^{k-1-s}\mu^{-N_\alpha(0,s)}\omega^T(s)\omega(s)\right\}.$$

Notice that $N_\alpha(0,s) \le s/T_a$ and $T_a > -\frac{\ln\mu}{\ln\beta}$, we have $N_\alpha(0,s) \le -s\frac{\ln\beta}{\ln\mu}$. Thus, the last inequality implies

$$\begin{aligned}
\mathbf{E}\left\{\sum_{s=k_0}^{k-1}\beta^{k-1-s}\mu^{s\frac{\ln\beta}{\ln\mu}}z^T(s)z(s)\right\} &= \mathbf{E}\left\{\sum_{s=k_0}^{k-1}\beta^{k-1-s}\beta^s z^T(s)z(s)\right\} \\
&< \gamma^2\mathbf{E}\left\{\sum_{s=k_0}^{k-1}\beta^{k-1-s}\mu^{-N_\alpha(0,s)}\omega^T(s)\omega(s)\right\}
\end{aligned}$$

$$< \gamma^2 \mathbf{E}\left\{\sum_{s=k_0}^{k-1} \beta^{k-1-s}\omega^T(s)\omega(s)\right\}.$$

which yields that

$$\mathbf{E}\left\{\sum_{s=k_0}^{\infty} \beta^s z^T(s)z(s)\right\} < \mathbf{E}\left\{\sum_{s=k_0}^{\infty} \omega^T(s)\omega(s)\right\}.$$

By Definition 12, we know that system (41) is mean-square exponentially stable with a weighted $\mathcal{H}_\infty$ performance level γ. This completes the proof. ■

3.3 The Sliding Mode

We design the following sliding surface function:

$$s(k) = G(i)x(k) - G(i)\left(A(i) + B_1(i)K(i)\right)x(k-1), \tag{48}$$

where $G(i) \in \mathbf{R}^{m\times n}$ and $K(i) \in \mathbf{R}^{m\times n}$ are real matrices to be designed. Matrix $G(i)$ is designed to satisfy that $G(i)B_1(i)$ is nonsingular and $G(i)E(i) = 0$. A necessary condition for the existence of such matrix $G(i)$ is that there does not exist a common column vector in both $B_1(i)$ and $E(i)$.

As is well known, when the system trajectories reach onto the sliding surface, it follows that $s(k+1) = s(k) = 0$ (for the ideal sliding mode). Therefore, for $k \in [k_l, k_{l+1})$ (i.e., the switched system operates in one of N modes), by $s(k+1) = 0$, we have

$$\begin{aligned} s(k+1) = G(i)\Big[&A(i)x(k) + B_1(i)\left(u(k) + f(x,k)\right) + B_2(i)\omega(k) \\ &+E(i)x(k)\varpi(k)\Big] - G(i)\left(A(i) + B_1(i)K(i)\right)x(k) = 0. \end{aligned}$$

Thus, solving the above equation for $u(k)$, the equivalent control for the sliding motion is given by

$$u_{eq}(k) = K(i)x(k) - f(x,k) - \left(G(i)B_1(i)\right)^{-1} G(i)B_2(i)\omega(k). \tag{49}$$

Substituting (49) into (27), the sliding mode dynamics can be obtained as

$$x(k+1) = \hat{A}(i)x(k) + \hat{B}_2(i)\omega(k) + E(i)x(k)\varpi(k), \tag{50}$$

where

$$\begin{aligned} \hat{A}(i) &\triangleq A(i) + B_1(i)K(i), \\ \hat{B}_2(i) &\triangleq \left[I - B_1(i)\left(G(i)B_1(i)\right)^{-1} G(i)\right] B_2(i). \end{aligned}$$

In the following, we analyze the stability and performance of the sliding mode dynamics in (50) based on Theorem 16.

Proposition 17. *For given constants $0 < \beta < 1$ and $\gamma > 0$, suppose that there exist matrix $P(i) > 0$ such that for $i \in \mathcal{N}$,*

$$\begin{bmatrix} -\beta P(i) + C^T(i)C(i) & 0 & \hat{A}^T(i)P(i) & \delta E^T(i)P(i) \\ \star & -\gamma^2 I & \hat{B}_2^T(i)P(i) & 0 \\ \star & \star & -P(i) & 0 \\ \star & \star & \star & -\delta P(i) \end{bmatrix} < 0, \tag{51}$$

then the sliding mode dynamics in (50) is mean-square exponentially stable with a weighted $\mathcal{H}_\infty$ performance level γ for any switching signal with average dwell time satisfying $T_a > T_a^* = \text{ceil}\left(-\frac{\ln \mu}{\ln \beta}\right)$, where $\mu \geq 1$ satisfies (31).

Proof. The desired result can be obtained by referring to Theorem 16, and we omit its proof. ■

Proposition 18. *For given scalars $0 < \beta < 1$ and $\gamma > 0$, suppose that there exist matrices $\mathcal{P}(i) > 0$ and $\mathcal{K}(i)$ such that for $i \in \mathcal{N}$,*

$$\begin{bmatrix} -\beta\mathcal{P}(i) & 0 & (A(i)\mathcal{P}(i) + B_1(i)\mathcal{K}(i))^T & \delta\mathcal{P}(i)E^T(i) & \mathcal{P}(i)C^T(i) \\ \star & -\gamma^2 I & \hat{B}_2^T(i) & 0 & 0 \\ \star & \star & -\mathcal{P}(i) & 0 & 0 \\ \star & \star & \star & -\delta\mathcal{P}(i) & 0 \\ \star & \star & \star & \star & -I \end{bmatrix} < 0, \tag{52}$$

then the sliding mode dynamics in (50) is mean-square exponentially stable with a weighted $\mathcal{H}_\infty$ performance level γ for any switching signal with average dwell time satisfying $T_a > T_a^* = \text{ceil}\left(-\frac{\ln \mu}{\ln \beta}\right)$, where $\mu \geq 1$ satisfies

$$\mathcal{P}(i) \leq \mu\mathcal{P}(j), \quad \forall i, j \in \mathcal{N}. \tag{53}$$

Moreover, if the conditions above are feasible, the matrix $K(i)$ in (48) can be given by

$$K(i) = \mathcal{K}(i)\mathcal{P}^{-1}(i). \tag{54}$$

Proof. The desired result can be obtained by performing a congruence transformation to (51) by $\text{diag}\{\mathcal{P}(i), I, \mathcal{P}(i), \mathcal{P}(i)\}$ (where $\mathcal{P}(i) = P^{-1}(i)$) and letting $\mathcal{K}(i) = K(i)\mathcal{P}(i)$. ■

Now, we synthesize a sliding mode controller to drive the system trajectories onto the pre-defined sliding surface $s(k) = 0$. To this end, considering (27) and (48), we have

$$\begin{aligned} s(k+1) &= G(i)x(k+1) - G(i)\left(A(i) + B_1(i)K(i)\right)x(k), \\ &= G(i)\left\{A(i)x(k) + B_1(i)\left[u(k) + f(x,k)\right] + B_2(i)\omega(k)\right\} \\ &\quad -G(i)\left(A(i) + B_1(i)K(i)\right)x(k) \\ &= -G(i)B_1(i)K(i)x(k) + G(i)B_2(i)\omega(k) \\ &\quad +G(i)B_1(i)\left[u(k) + f(x,k)\right]. \end{aligned} \tag{55}$$

Theorem 19. *Consider the discrete-time switched stochastic hybrid system in (27). Suppose that the sliding surface function is designed as (48) with $K(i)$ being solved by (54), then the state trajectories of system (27) can be driven onto the sliding surface $s(k) = 0$ in a finite time by the following sliding mode controller:*

$$\begin{aligned} u(k) = (G(i)B_1(i))^{-1} \{ & -\Lambda s(k) + G(i)B_1(i)K(i)x(k) \\ & - (\varrho + \chi \|G(i)B_1(i)\| \|x(k)\| + \|G(i)B_2(i)\| \|\omega(k)\|) \operatorname{sign}(s(k))\}, \end{aligned} \tag{56}$$

where Λ is a positive definite matrix, and ϱ is a positive scalar.

Proof. Setting $\Delta s(k) = s(k+1) - s(k)$, and then considering (55), we have

$$\begin{aligned} \Delta s(k) &= s(k+1) - s(k) \\ &= -G(i)B_1(i)K(i)x(k) + G(i)B_2(i)\omega(k) \\ &\quad + G(i)B_1(i)\left[u(k) + f(x,k)\right] - s(k). \end{aligned} \tag{57}$$

Substituting (56) into (57) yields

$$\begin{aligned} \Delta s(k) = & -(\Lambda + I)s(k) + G(i)B_2(i)\omega(k) + G(i)B_1(i)f(x,k) \\ & - (\varrho + \chi \|G(i)B_1(i)\| \|x(k)\| + \|G(i)B_2(i)\| \|\omega(k)\|) \operatorname{sign}(s(k)). \end{aligned} \tag{58}$$

Choose a Lyapunov function of the following form:

$$V(k) = \frac{1}{2} s^T(k) s(k). \tag{59}$$

Thus, considering (58) and $\|s(k)\| \le |s(k)|$, we have

$$\begin{aligned} \Delta V(k) &= s^T(k)\Delta s(k) + \frac{1}{2}\Delta s^T(k)\Delta s(k) \\ &= s^T(k)\left[-(\Lambda + I)s(k) + G(i)B_2(i)\omega(k) + G(i)B_1(i)f(x,k)\right] \\ &\quad - (\varrho + \chi \|G(i)B_1(i)\| \|x(k)\| + \|G(i)B_2(i)\| \|\omega(k)\|) |s(k)| \\ &\quad + \frac{1}{2}\Delta s^T(k)\Delta s(k) \\ &\le -s^T(k)(\Lambda + I)s(k) - \varrho\|s(k)\| + \frac{1}{2}\Delta s^T(k)\Delta s(k). \end{aligned}$$

Since Λ is a positive definite matrix to be tuned, an appropriate Λ can be selected large enough such that $\Delta V(k) < 0$ as while as $s(k)$ being within a certain bounded region containing the equilibrium point. Then $\Delta s(k)$ is reasonable bounded although it is not asymptotically convergent to zero, which shows that the trajectory of (27) can be driven onto the sliding surface by the control law (56) and be maintained there. This completes the proof. ■

4 An Illustrative Example

Consider system (1) with $N = 2$ and the following parameters:

$$A(1) = \begin{bmatrix} -1.1 & 0.7 & -2.1 \\ 1.8 & -0.5 & -0.7 \\ 0.2 & 2.0 & 0.5 \end{bmatrix}, \; E(1) = \begin{bmatrix} 0.3 & 0.1 & 0.1 \\ 0.1 & 0.3 & 0.3 \\ 0.2 & 0.1 & 0.1 \end{bmatrix}, \; B(1) = \begin{bmatrix} 1.2 \\ 0.8 \\ 0.5 \end{bmatrix},$$

$$A(2) = \begin{bmatrix} 1.1 & 0.9 & 1.0 \\ 0.2 & 0.5 & -0.6 \\ 0.3 & 0.6 & -0.4 \end{bmatrix},\ E(2) = \begin{bmatrix} 0.2 & 0.1 & 0.2 \\ 0.1 & 0.3 & 0.1 \\ 0.2 & 0.2 & 0.2 \end{bmatrix},\ B(2) = \begin{bmatrix} 0.5 \\ 1.2 \\ 0.4 \end{bmatrix}.$$

Suppose $\beta = 0.5$ and $f(x(t), t) = 0.5\exp(-t)\sin(\sqrt{x_1^2(t) + x_2^2(t) + x_3^2(t)})$ (thus ψ can be chosen as $\psi = 0.5$). Our aim is to design the SMC law $u(t)$ in (24) such that the resulting closed-loop system is stable for $T_a > T_a^* = 0.1$ (the allowable minimum of μ is $\mu_{\min} = 1.0513$). Solving conditions (21)–(23) in Theorem 8, we have

$$K(1) = \begin{bmatrix} -0.4406 & -2.6407 & -1.9182 \end{bmatrix},$$
$$K(2) = \begin{bmatrix} -2.9942 & -0.7920 & -1.5538 \end{bmatrix}.$$

We choose $G(1) = \begin{bmatrix} 5 & 1 & -8 \end{bmatrix}$ and $G(2) = \begin{bmatrix} 4 & 2 & -5 \end{bmatrix}$. Thus, the sliding surface function defined in (2) is given by

$$s(t) = \begin{cases} s(t,1) = \begin{bmatrix} 5 & 1 & -8 \end{bmatrix} x(t) \\ \qquad\qquad - \displaystyle\int_0^t \begin{bmatrix} -6.5338 & -20.3939 & -20.5708 \end{bmatrix} x(\theta) d\theta, \quad i = 1, \\ s(t,2) = \begin{bmatrix} 4 & 2 & -5 \end{bmatrix} x(t) \\ \qquad\qquad - \displaystyle\int_0^t \begin{bmatrix} -3.8862 & -0.3008 & 1.0708 \end{bmatrix} x(\theta) d\theta, \quad i = 2, \end{cases}$$

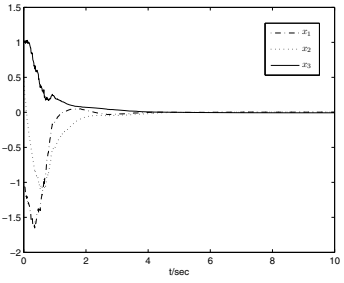

(a) States of the closed-loop system

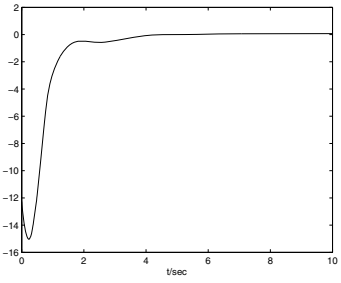

(b) Sliding surface function

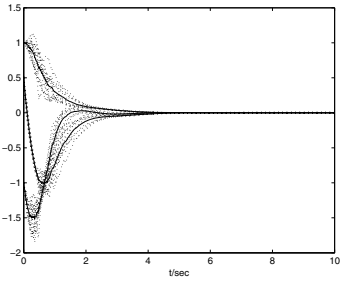

(c) Individual paths and the average of the states of the closed-loop system

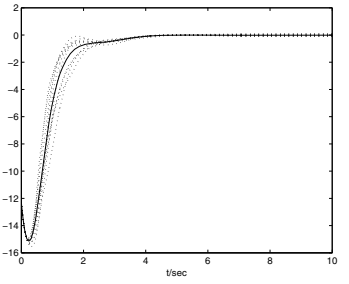

(d) Individual paths and the average of the sliding surface function

Fig. 1. Simulation results

and the SMC law designed in (24) can be computed as

$$u(t) = \begin{cases} u(t,1) = \left[-0.4406 \ -2.6407 \ -1.9182\right] x(t) \\ \qquad\quad -0.3571\left(\varrho + 1.4\left\|x(t)\right\|\right) \mathrm{sign}\left(s(t,1)\right), \ \ i = 1, \\ u(t,2) = \left[-2.9942 \ -0.7920 \ -1.5538\right] x(t) \\ \qquad\quad -0.4167\left(\varrho + 1.2\left\|x(t)\right\|\right) \mathrm{sign}\left(s(t,2)\right), \ \ i = 2. \end{cases}$$

Set the initial condition be $x(0) = \left[-1 \ \ 0.5 \ \ 1\right]^T$ and $\varrho = 0.5$. By using the discretization approach [15], we simulate the standard Brownian motion. Some initial parameters are given as follows: the simulation time $t \in [0, T^*]$ with $T^* = 10$, the normally distributed variance $\delta t = \frac{T^*}{N^*}$ with $N^* = 2^{11}$, the step size $\Delta t = \rho \delta t$ with $\rho = 2$, and the number of discretized Brownian paths $p = 10$. Figs. 1(a)–1(b) display the simulation results along an individual discretized Brownian path. Specifically, Fig. 1(a) shows the states of the closed-loop system, and the sliding surface function is given in Fig. 1(b). Figs. 1(c)–1(d) are, respectively, the simulation results on $x(t)$ and $s(t)$ along 10 individual paths (dotted lines) and the average over 10 paths (solid line).

5 Conclusions

The problems of SMC of continuous- and discrete-time switched stochastic hybrid system have been investigated in this chapter, respectively. For both continuous- and discrete-time cases, integral sliding surface functions have been designed, and sufficient conditions for the existence of sliding mode have been established in terms of LMIs, and the explicit parametrization of the desired sliding surface functions has also been given. Then, SMC laws for reaching motion have been synthesized to drive the state trajectories of the closed-loop systems onto the predefined sliding surface in a finite time. A numerical example has been provided to illustrate the effectiveness of the proposed design scheme for the continuous-time case.

Acknowledgement. The authors firstly met Prof. Kaynak at a seminar at Harbin institute of Technology (HIT) in 2003, at which time the three authors were PhD candidate, Master and Bachelor students at HIT respectively. It is our great honor to have known our best senior friend since then and have a chance to begin with an excellent cooperation experience in our lives. Recall that in 2003 Prof. Kaynak served as President of IEEE Industrial Electronics Society (IES) and was awarded as Honorary Professor at HIT. He was the first person as our respectful mentor, who opened us the door to the scientific world from both spiritual and practical levels. Since then, the authors have collaborated our research work, organized international academic conferences sponsored by IES, established the first IEEE IES chapter in mainland China, supervised excellent students from HIT and then recommended them to leading universities worldwide etc. For more than ten years, the authors and Prof. Kaynak have got along

like a family not only from the academic cooperation but more from attitudes towards life. The authors like Okay, Pervin and their daughter and are sincerely pound of their success. A father is a treasure, a brother is a comfort, but Okyay is both. The most fortune for the authors is to know him and continue the story during our lifetime.

References

1. Alessandri, A., Baglietto, M., Battistelli, G.: A maximum-likelihood Kalman filter for switching discrete-time linear systems. Automatica 46(11), 1870–1876 (2010)
2. Allerhand, L.I., Shaked, U.: Robust stability and stabilization of linear switched systems with dwell time. IEEE Trans. Automat. Control 56(2), 381–386 (2011)
3. Cheng, D., Guo, L., Lin, Y., Wang, Y.: Stabilization of switched linear systems. IEEE Trans. Automat. Control 50(5), 661–666 (2005)
4. Choi, H.H.: On the existence of linear sliding surfaces for a class of uncertain dynamic systems with mismatched uncertainties. Automatica 35(10), 1707–1715 (1999)
5. Colaneri, P., Geromel, J.C., Astolfi, A.: Stabilization of continuous-time switched nonlinear systems. Systems and Control Letters 57(1), 95–103 (2008)
6. Decarlo, R.A., Branicky, M.S., Pettersson, S., Lennartson, B.: Perspectives and results on the stability and stabilizability of hybrid systems. Proceedings of The IEEE 88(7), 1069–1082 (2000)
7. Deaecto, G.S., Geromel, J.C., Daafouz, J.: Trajectory-dependent filter design for discrete-time switched linear systems. Nonlinear Analysis – Hybrid Systems 4(1), 1–8 (2010)
8. Deaecto, G.S., Geromel, J.C., Daafouz, J.: Dynamic output feedback $\mathcal{H}_\infty$ control of switched linear systems. Automatica 47(8), 1713–1720 (2011)
9. Du, D., Jiang, B., Shi, P.: Active fault-tolerant control for switched systems with time delay. International Journal of Adaptive Control and Signal Processing 25(5), 466–480 (2011)
10. Gao, H., Lam, J., Wang, C.: Model simplification for switched hybrid systems. Systems and Control Letters 55(12), 1015–1021 (2006)
11. Han, X., Fridman, E., Spurgeon, S.K.: Sliding mode control in the presence of input delay: a singular perturbation approach. Automatica 48(8), 1904–1912 (2012)
12. Hespanha, J.P., Morse, A.S.: Stability of switched systems with average dwell time. In: Proc. 38th Conf. Decision Control, Phoenix, AZ, pp. 2655–2660 (1999)
13. Hespanha, J.P., Morse, A.S.: Switching between stabilizing controllers. Automatica 38(11), 1905–1917 (2002)
14. Hetel, L., Daafouz, J., Iung, C.: Stabilization of arbitrary switched linear systems with unknown time-varying delays. IEEE Trans. Automat. Control 51(10), 1668–1674 (2006)
15. Higham, D.J.: An algorithmic introduction to numerical simulation of stochastic differential equations. SIAM Review 43(3), 525–546 (2001)
16. Ishii, H., Francis, B.A.: Stabilizing a linear system by switching control with dwell time. IEEE Trans. Automat. Control 47(12), 1962–1973 (2002)
17. Kim, K.-S., Park, Y., Oh, S.-H.: Designing robust sliding hyperplanes for parametric uncertain systems: a Riccati approach. Automatica 36(7), 1041–1048 (2000)
18. Liberzon, D.: Switching in Systems and Control. Birkhauser, Boston (2003)

19. Liberzon, D., Morse, A.S.: Basic problems in stability and design of switched systems. IEEE Control Systems Magazine 19(5), 59–70 (1999)
20. Lin, H., Antsaklis, P.J.: Stability and stabilizability of switched linear systems: a survey of recent results. IEEE Trans. Automat. Control 54(2), 308–322 (2009)
21. Michel, A.N.: Recent trends in the stability analysis of hybrid dynamical systems. IEEE Trans. Circuits and Systems – I: Fundamental Theory and Applications 46(1), 120–134 (1999)
22. Niu, Y., Ho, D.W.C., Lam, J.: Robust integral sliding mode control for uncertain stochastic systems with time-varying delay. Automatica 41(5), 873–880 (2005)
23. Niu, Y., Ho, D.W.C., Wang, X.: Sliding mode control for Itô stochastic systems with Markovian switching. Automatica 43(10), 1784–1790 (2007)
24. Seatzu, C., Corona, D., Giua, A., Bemporad, A.: Optimal control of continuous-time switched affine systems. IEEE Transactions on Automatic Control 51(5), 726–741 (2006)
25. Shi, P., Xia, Y., Liu, G.P., Rees, D.: On designing of sliding-mode control for stochastic jump systems. IEEE Trans. Automat. Control 51(1), 97–103 (2006)
26. Wang, D., Wang, W., Shi, P.: Robust fault detection for switched linear systems with state delays. IEEE Trans. Systems, Man, and Cybernetics, Part B: Cybernetics 39(3), 800–805 (2009)
27. Wu, L., Ho, D.W.C.: Reduced-order $\mathcal{L}_2$-$\mathcal{L}_\infty$ filtering of switched nonlinear stochastic systems. IET Control Theory and Applications 3(5), 493–508 (2009)
28. Wu, L., Lam, J.: Weighted $\mathcal{H}_\infty$ filtering of switched systems with time-varying delay: average dwell time approach. Circuits Systems and Signal Processing 28(6), 1017–1036 (2009)
29. Wu, L., Lam, J.: Sliding mode control of switched hybrid systems with time-varying delay. Int. J. Adapt. Control Signal Process 22(10), 909–931 (2008)
30. Wu, L., Qi, T., Feng, Z.: Average dwell time approach to $\mathcal{L}_2$-$\mathcal{L}_\infty$ control of switched delay systems via dynamic output feedback. IET Control Theory and Applications 3(10), 1425–1436 (2009)
31. Wu, L., Zheng, W.X.: Weighted $\mathcal{H}_\infty$ model reduction for switched hybrid systems with time-varying delay. Automatica 45(1), 186–193 (2009)
32. Wu, L., Zheng, W.X.: Passivity-based sliding mode control of uncertain singular time-delay systems. Automatica 45(9), 2120–2127 (2009)
33. Wu, Y., Yu, X.: Variable structure control design for uncertain dynamic systems with disturbances in input and output channels. Automatica 35(2), 311–319 (1999)
34. Xia, Y., Jia, Y.: Robust sliding-mode control for uncertain time-delay systems: an LMI approach. IEEE Trans. Automat. Control 48(6), 1086–1091 (2003)
35. Xu, S., Chen, T.: Robust $\mathcal{H}_\infty$ control for uncertain stochastic systems with state delay. IEEE Trans. Automat. Control 47(12), 2089–2094 (2002)
36. Zhai, G., Lin, H., Kim, Y., Imae, J., Kobayashi, T.: $\mathcal{L}_2$ gain analysis for switched systems with continuous-time and discrete-time subsystems. International Journal of Control 78(15), 1198–1205 (2005)
37. Zhao, J., Hill, D.J.: On stability, $\mathcal{L}_2$-gain and $\mathcal{H}_\infty$ control for switched systems. Automatica 44(5), 1220–1232 (2008)

Sliding Mode Control for Unmanned Aerial Vehicles Research

Mehmet Önder Efe

Department of Computer Engineering, Hacettepe University,
Beytepe TR-06800, Ankara, Turkey
onderefe@ieee.org

Abstract. This chapter focuses on the applications of Sliding Mode Control (SMC) in unmanned aerial vehicle applications. It considers small scale vehicles and its autopilot as a sliding mode controller. The needs of the reality are discussed and a simulation example is given to support the claims. It is seen that robustness property of sliding mode control is an important feature in applications subject to uncertainty and imprecision. Unmanned aerial vehicle applications therefore best suit the discussion of the versatility of sliding mode control technique.

1 Introduction

The research on the applications of Unmanned Aerial Vehicles (UAVs) has been a hot topic of the previous 20 years. The rapid advances in the Very Large Scale Integration (VLSI), electronics, Microelectromechanical Systems (MEMS) and signal processing and single chip Application Specific Integrated Circuit (ASIC) solutions motivate the construction of lightweight vehicles having some payload to perform a specific task. Today, UAV design and development is considered by a wide range of researchers from senior level student to experienced engineers working for UAV companies. A good indicator of the growing interest to fly without human is illustrated in Fig. 1, where the results of a *Web of Science* searches are shown. The search is made by the keyword "unmanned aerial vehicle" and the total number of documents were counted for each year. The trend shows that we will see more interesting UAV applications in the future and UAVs will continue to be the subject of research papers/projects and commercial/military applications.

A UAV is a flying robot having its own power supply, having no human pilot and maintaining the flight through an appropriate scheduling of aerodynamic forces either autonomously or by remote control. The UAV systems are capable of being invisible to radars and of performing formation flight. With such properties, a UAV system is cheap enough to sacrifice and powerful enough to carry sensors, camera and communication systems and lightweight weapons. More importantly, a UAV can maintain the flight beyond the limits of a human pilot.

The formal categorization of UAVs is made in according to their maximum altitude and endurance. Figure 2 illustrates the classes of UAVs, namely mini, tactical, operative and strategic UAVs are today being considered by academia, industry and governments

X. Yu and M. Önder Efe (eds.), *Recent Advances in Sliding Modes*,
Studies in Systems, Decision and Control 24, DOI: 10.1007/978-3-319-18290-2_12

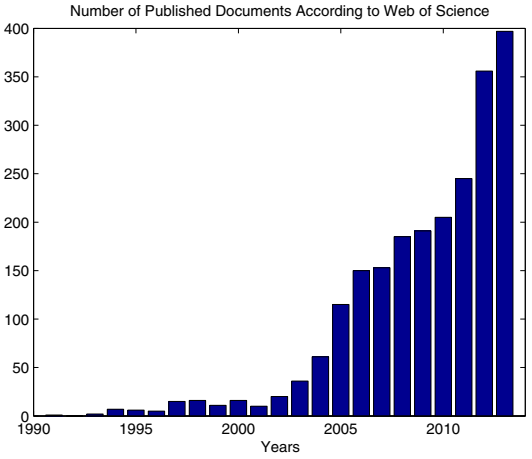

Fig. 1. The trend of UAV research outcomes since 1991

for purposes ranging from agriculture to military applications. The complexity of systems is the highest for the strategic UAVs whereas that for mini and micro UAVs is minimal. The focus of this work is the use of SMC for mini UAVs.

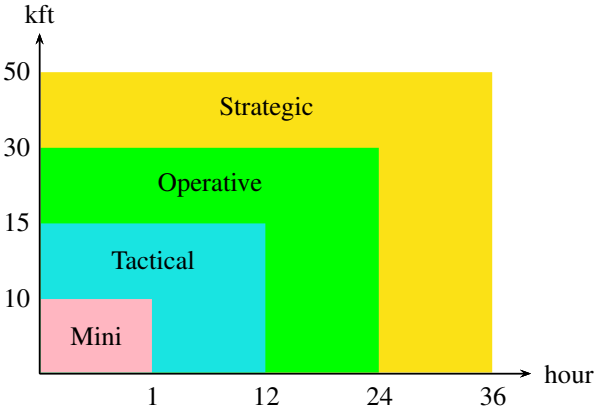

Fig. 2. Categorization of UAVs according to their maximum altitude and endurance

Such kinds of small scale and highly versatile systems are used in a wide spectrum of applications. For instance, collecting information (imaging, pursuit, searching, video acquisition and reconnaissance), security, surveillance, control (smuggling prevention), targeting, meteorologic and agricultural applications, traffic management and steering, telemetry (remote sizing) and crisis management after natural disasters are some of the examples at a first glance.

Accomplishing these high level missions with UAV systems is critically dependent upon the performance at low level command and control schemes. This fact has made the design, prototyping, implementation and manufacturing of autopilot systems a growing industry. The choice of the autopilot for a UAV system may depend upon the mission statement yet, regardless of the mission statement, the vehicle must be robust enough to cope with the difficulties of the operating environment. SMC systems are very well known for their robustness against disturbances and invariances during the sliding mode. The technique is known also as Variable Structure Control (VSC) as the system during the sliding regime operates in a predefined subset of the phase space.

Conceptually, the controller design in this framework is based on the nominal representation of the system about which the bounds of the uncertainties are assumed to be available. The decision mechanism operates on the basis of switching on the different sides of a decision boundary, which is called the sliding hypersurface [1–3], and the goal of the design is to enforce the error vector toward this hypersurface during the reaching phase. Once the error vector is confined to the sliding hypersurface, it obeys the behavior imposed by the set of equations describing the hypersurface, i.e. sliding mode starts and the error vector converges to origin. The control strategy is therefore called sliding mode control in the related literature, [1–3]. During the sliding mode, the control system becomes insensitive to the disturbances and uncertainties unless the decision mechanism violates the physical limits for maintaining the sliding motion.

SMC strategy has been applied successfully in a wide variety of design problems ranging from the control of motion control systems, and chemical processes to the control of chaotic systems. Hung et al., [1], review the control strategy for linear and nonlinear systems and discuss the design for systems represented in canonical forms. Another systematic examination of SMC approach is presented in [4], in which the practical aspects of SMC design are assessed for both continuous-time and discrete-time cases and a special consideration is given to the finite switching frequency, limited bandwidth actuators and parasitic dynamics. Misawa discusses the SMC design for discrete-time systems in [5] for the linear case and in [6] for the nonlinear case with unmatched uncertainties, Sabanovic et al. [7] elaborate the chattering free SMC design, Bartolini et al. [8] formulate the chattering-free SMC for MIMO systems, and Erbatur et al. [9] investigate the robustness properties of SMC technique on a 2-DOF direct drive SCARA robot.

An extensive range of application domains of the SMC scheme with robustness properties motivate us to design the low level control laws for the quadrotor rotorcraft system considered in this chapter and by some other researchers. For example Castillo et al. [10, 11] perform real time experiments and assess the performance of a nonlinear controller. In [12], classical PID controller is considered and model based design is experimented. Hanford et al., [13], present a simple closed loop equipped with MEMS sensors and PIC based processing unit. Hoffman et al., [14], achieve the formation control by SMC technique and focuse on collision and obstacle avoidance by extracting the state variables with a Kalman filter. Vision based control of the quadrotor rotorcraft system is studied in [15], which exploits the Moiré patterns, and in [16], which utilizes double cameras. Camlica dwells on a linear quadratic controller in [17], and Waslander puts an emphasis on the insufficiency of classical control methods and

proposes the integral SMC associated with reinforcement learning to achieve multi agent control. In [19], vehicle stabilization based on the backstepping technique is presented with successful results.

The current SMC design problem is involved with coupled and highly nonlinear dynamics, noisy observations and demanding performance requirements. The organization of the chapter is as follows: The dynamic model of the vehicle is presented in the next section, the SMC technique is presented in the third section, behavior control is discussed next, simulation results and concluding remarks are given at the end of the paper.

2 Quadrotor UAV Dynamics

A sketch of the quadrotor rotorcraft system studied in this study is shown in Fig. 3, where the Euler angles and the cartesian coordinate frame are shown. The equations of motion are given in (1) and the values of some variables seen are tabulated in Table 1.

$$M\ddot{x} = -us_\theta \tag{1a}$$
$$M\ddot{y} = uc_\theta s_\phi \tag{1b}$$
$$M\ddot{z} = uc_\theta c_\phi - Mg \tag{1c}$$
$$\ddot{\psi} = \tilde{\tau}_\psi \tag{1d}$$
$$\ddot{\theta} = \tilde{\tau}_\theta \tag{1e}$$
$$\ddot{\phi} = \tilde{\tau}_\phi \tag{1f}$$

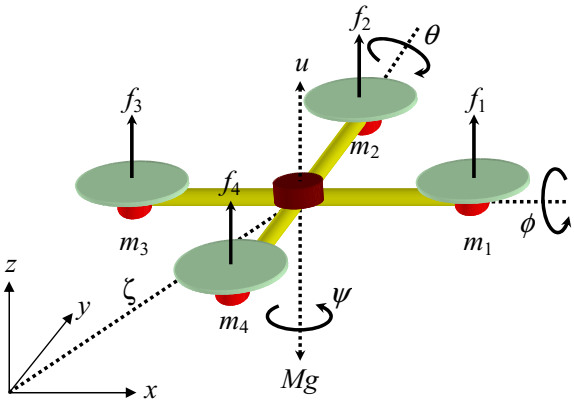

Fig. 3. General view of the quadrotor rotorcraft system

where $s\theta$ is an abbreviation for $\sin\theta$ while $c\theta$ stands for $\cos\theta$.

$$\tilde{\tau} = \begin{pmatrix} \tilde{\tau}_\psi \\ \tilde{\tau}_\theta \\ \tilde{\tau}_\phi \end{pmatrix} = \mathbb{J}^{-1}(\tau - C(\eta,\dot{\eta})\dot{\eta}) \tag{2}$$

Here $\eta = \begin{pmatrix} \psi & \theta & \phi \end{pmatrix}^{\mathrm{T}}$, $\mathbb{J}(\eta) = T_\eta^{\mathrm{T}} \mathbf{I} T_\eta$ and

$$T_\eta = \begin{pmatrix} -s_\theta & 0 & 1 \\ c_\theta s_\phi & c_\phi & 0 \\ c_\theta c_\phi & -s_\phi & 0 \end{pmatrix} \tag{3}$$

$$\mathbf{I} = \begin{pmatrix} I_{xx} & 0 & 0 \\ 0 & I_{yy} & 0 \\ 0 & 0 & I_{zz} \end{pmatrix} = \begin{pmatrix} I_{xx} & 0 & 0 \\ 0 & I_{xx} & 0 \\ 0 & 0 & 2I_{xx} \end{pmatrix} \tag{4}$$

The Coriolis and centripetal vector denoted by $C(\eta,\dot{\eta})$ is defined as below and computed as given by (31).

$$C(\eta,\dot{\eta}) = \dot{\mathbb{J}} - \frac{1}{2}\frac{\partial}{\partial\eta}(\dot{\eta}^{\mathrm{T}}\mathbb{J}) \tag{5}$$

$$\mathbb{J} = I_{xx}\begin{pmatrix} 1 + c_\theta^2 c_\phi^2 & -c_\theta s_\phi c_\phi & -s_\theta \\ -c_\theta s_\phi c_\phi & 2 - c_\phi^2 & 0 \\ -s_\theta & 0 & 1 \end{pmatrix} \tag{6}$$

$$\dot{\mathbb{J}} = I_{xx}\begin{pmatrix} \dot{\theta}s_{2\theta}c_\phi^2 + \dot{\phi}s_{2\phi}c_\theta^2 & \dot{\theta}s_\theta s_\phi c_\phi - \dot{\phi}c_{2\phi}c_\theta & \dot{\theta}c_\theta \\ \dot{\theta}s_\theta s_\phi c_\phi - \dot{\phi}c_{2\phi}c_\theta & \dot{\phi}s_{2\phi} & 0 \\ \dot{\theta}c_\theta & 0 & 0 \end{pmatrix} \tag{7}$$

$$\begin{aligned} C_{1,1} &= C_{1,2} = C_{1,3} = 0 \\ C_{2,1} &= I_{xx}(\dot{\psi}c_\phi^2 s_{2\theta} + \dot{\theta}s_\phi c_\phi s_\theta - \dot{\phi}c_\theta) \\ C_{2,2} &= I_{xx}\dot{\psi}s_\phi c_\phi s_\theta \\ C_{2,3} &= -I_{xx}\dot{\psi}c_\theta \\ C_{3,1} &= -I_{xx}(\dot{\psi}c_\theta^2 s_{2\phi} + \dot{\theta}c_\theta c_{2\phi}) \\ C_{3,2} &= -I_{xx}(\dot{\psi}c_\theta c_{2\phi} - \dot{\theta}s_{2\phi}) \\ C_{3,3} &= 0 \end{aligned} \tag{8}$$

where $I_{xx} = I_{yy} = m\ell^2$, $I_{zz} = 2m\ell^2$. Model inputs and the aerodynamic forces (f_i) created by each propeller are related to each other as described below.

$$\tau_{\psi} = \sum_{i=1}^{4} \tau_{m_i} \tag{9a}$$

$$\tau_{\theta} = (f_3 - f_1)\ell \tag{9b}$$

$$\tau_{\phi} = (f_2 - f_4)\ell \tag{9c}$$

$$u = \sum_{i=1}^{4} f_i \tag{9d}$$

In the above, $f_i = k\omega_i^2$ and $k > 0$ is a motor gain, ω_i denotes the angular velocity of ith motor. (See [10, 11] for details).

Table 1. Physical Parameters of the Quadrotor UAV

m_i	Motor weight	0.08 kg
m_b	Battery weight	0.20 kg
M	Total weight of the vehicle	0.52 kg
ℓ	Distance from motors to COG	0.205 m
g	Gravitational acceleration	9.81 m/s^2

The difficulties in the control of such an aerial robot is that the differential equations describing it are nonlinear and coupled. Further, the system is an underactuated one making the control a challenge under the presence of modeling uncertainties, imperfect observations and the mathematical difficulties. In the next section, we consider the SMC technique and then its application to the UAV considered here,[20].

3 An Overview of Sliding Mode Control

Assume that the plant under control has the structure described in (10), where ξ and $\dot{\xi}$ are the states, and δ is the control input.

$$\ddot{\xi} = F\left(\xi, \dot{\xi}\right) + G\left(\xi, \dot{\xi}\right)\delta \tag{10}$$

where $G\left(\xi, \dot{\xi}\right) \neq 0$. The design problem is to enforce the behavior of the system states towards the desired trajectories, which are known. Denote the reference trajectories by ξ_r and $\dot{\xi}_r$ and the tracking errors by $e_{\xi} = \xi - \xi_r$ and $\dot{e}_{\xi} = \dot{\xi} - \dot{\xi}_r$.

The crux of the SMC scheme is the definition of a sliding manifold, along which the sliding motion is to take place. This quantity is denoted by s and is defined as below

$$\begin{aligned} s &= \left(\frac{\mathrm{d}}{\mathrm{d}t} + \lambda\right) e_{\xi} \\ &= \dot{e}_{\xi} + \lambda e_{\xi} \end{aligned} \tag{11}$$

where $\lambda > 0$ is the slope of the sliding line[1]. If a control law enforces the trajectories in the phase space such that $s = 0$ holds true, then the errors converge asymptotically to the origin as prescribed by $\dot{e}_\xi = -\lambda e_\xi$, whose solution is $e_\xi(t) = e_\xi(0)\mathrm{e}^{-\lambda t}$.

In order to demonstrate stability, adopt the Lyaponuv function candidate given as

$$V = \frac{1}{2}s^2 \tag{12}$$

The time derivative of the Lyapunov function in (12) can be computed as follows

$$\begin{aligned}
\dot{V} &= s\dot{s} \\
&= s\left(\ddot{e}_\xi + \lambda \dot{e}_\xi\right) \\
&= s\left(\ddot{\xi} - \ddot{\xi}_r + \lambda \dot{e}_\xi\right) \\
&= s\left(F\left(\xi, \dot{\xi}\right) + G\left(\xi, \dot{\xi}\right)\delta - \ddot{\xi}_r + \lambda \dot{e}_\xi\right)
\end{aligned} \tag{13}$$

We would like to have $\dot{V} = s\dot{s} \leq -\sigma|s|$ with σ being a positive constant. Dropping the arguments of the functions F and G, and equating $F + G\delta - \ddot{\xi}_r + \lambda \dot{e}_\xi$ to $-\sigma \mathrm{sgn}(s)$ and solving for δ yields

$$\delta = \frac{1}{G}\left(-\sigma \mathrm{sgn}(s) - \lambda \dot{e}_\xi + \ddot{\xi}_r - F\right) \tag{14}$$

which ensures $\dot{s} = -\sigma \mathrm{sgn}(s)$ and $\dot{V} = -\sigma|s|$ is achieved in the closed loop. The control law in (14) has two properties.

- If an initial condition, say $(e_\xi(0), \dot{e}_\xi(0))$ is not on the sliding hypersurface characterized by $s = 0$, it is forced towards the hypersurface. In other words, the sliding hypersurface is an attractor and the regime until it is reached is called the *reaching mode*.
- If a trajectory is trapped into the sliding hypersurface, the system in the closed loop behaves exactly as how the sliding regime prescribes. During this regime, the closed loop control system becomes insensitive to disturbances to the extent allowed by the design, and this mode is known as the *sliding mode*.

With such a control law, one naturally questions the selection of $\sigma > 0$. Assume the plant given in (10) is a nominal plant, on which the SMC law is based. If the real plant has uncertainties that enter the right hand side of (10) as below;

$$\ddot{\xi} = F\left(\xi, \dot{\xi}\right) + G\left(\xi, \dot{\xi}\right)\delta + \Delta\left(\xi, \dot{\xi}, t\right) \tag{15}$$

then the application of the control signal computed for the nominal plant would yield the following result

$$\dot{s} = -\sigma \mathrm{sgn}(s) + \Delta(\cdot) \tag{16}$$

[1] In the current problem the system dynamics is a second order one, therefore the sliding manifold is a line. In general, λ is mentioned as the slope parameter determining the speed of convergence during the sliding regime.

Clearly if $\sigma > \sup_{\xi,\dot{\xi},t} |\Delta(\xi,\dot{\xi},t)|$ then $s\dot{s} < 0$ is ensured. The practical interpretation of this is as follows: For large σ, the result stipulates that larger uncertainties are tolerable however one has to consider the system specific details, e.g. time constants to determine the best σ since a large value of σ will require very fast hitting the sliding hypersurface as formulated by $t_h \leq \frac{|s(0)|}{\sigma}$, the proof of which is straightforward.

In the practical applications of SMC systems, the original sign function is smoothed by utilizing the approximation $\mathrm{sgn}(s) \approx \frac{s}{|s|+\varepsilon}$, where $\varepsilon > 0$. Since the sliding mode entails $s \approx 0$, the noise in the observed quantities becomes highly effective and the controller can generate unnecessarily large control signals. This is known as the chattering in the related literature, [3]. Utilizing the above approximation introduces a boundary layer and eliminates the undesired chattering phenomenon significantly, [3]. This paper adopts the same strategy in computing the sign of the quantity s. In the next section, we present the design of SMC for the considered UAV system.

4 Control of the Vehicle Behavior

The control of the vehicle behavior is scrutinized under three subtitles as discussed below. The underlying idea is to compute the desired value of the Euler angles and quickly drive these angles to their desired values. In Fig. 4, the general structure of the control system is shown, where the reference angle generation is followed by the angle controllers thereby resulting in desired behavioral response.

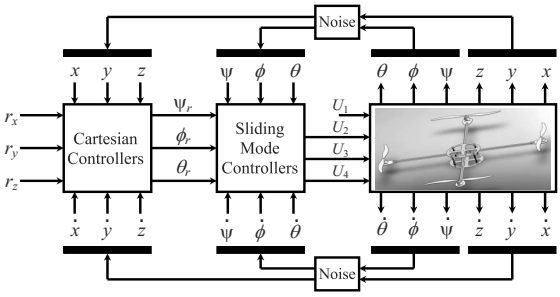

Fig. 4. The block diagram of the control system structure

4.1 SMC of the Yaw Angle (ψ) and Altitude (z)

Denote the desired altitude by z_r, the desired velocity in z-direction by $\dot{z}_r$ and the desired acceleration by $\ddot{z}_r$. Define $e_z := z - z_r$, $\dot{e}_z := \dot{z} - \dot{z}_r$ and $s_z := \dot{e}_z + \lambda_z e_z$.

With these definitions, the controller postulated below will drive the vehicle to the desired altitude.

$$u = M \frac{\ddot{z}_r - \lambda_z \dot{e}_z - \sigma_z \frac{s_z}{|s_z|+\varepsilon} - \mu_z s_z + g}{c_\theta c_\phi} \tag{17}$$

The control law above is accompanied by the following selection with $\psi_r = 0$.

$$\tilde{\tau}_\psi = -6\dot{\psi} - 9(\psi - \psi_r) \tag{18}$$

The SMC law in (17) and the stabilizing law in (18) result in the maintenance of the desired altitude.

4.2 SMC of the Roll Angle (ϕ) and y-Position

Denote the desired position in y-direction by y_r, the desired velocity by $\dot{y}_r$ and the desired acceleration by $\ddot{y}_r$. Define $e_y := y - y_r$, $\dot{e}_y := \dot{y} - \dot{y}_r$ and $s_y := \dot{e}_y + \lambda_y e_y$. Define the reference roll angle value as

$$\phi_r := \tan^{-1}\left(\frac{\ddot{y}_r - \lambda_y \dot{e}_y - \sigma_y \frac{s_y}{|s_y|+\varepsilon} - \mu_y s_y}{\ddot{z}_r - \lambda_z \dot{e}_z - \sigma_z \frac{s_z}{|s_z|+\varepsilon} - \mu_z s_z + g}\right) \tag{19}$$

Clearly the control input u in (17) keeps the desired altitude and the behavior in z-direction obeys $\dot{s}_z = -\sigma_z \frac{s_z}{|s_z|+\varepsilon} - \mu_z s_z$. As soon as the transient regime in z direction and ψ angle ends, the dynamic behavior in y-direction is governed by

$$\ddot{y} = \left(\ddot{z}_r - \lambda_z \dot{e}_z - \sigma_z \frac{s_z}{|s_z| + \varepsilon} - \mu_z s_z + g\right) \tan\phi \tag{20}$$

Obviously for $\phi \equiv \phi_r$, we would have $\dot{s}_y = -\sigma_y \frac{s_y}{|s_y|+\varepsilon} - \mu_y s_y$, then one could drive $\phi \to \phi_r$ as quickly as possible and would ensure the stability in y-direction too. The control of the roll angle is achieved by choosing

$$\tilde{\tau}_\phi = -10\dot{\phi} - 25(\phi - \phi_r) \tag{21}$$

4.3 SMC of the Pitch Angle (θ) and x-Position

Denote the desired position in x-direction by x_r, the desired velocity by $\dot{x}_r$ and the desired acceleration by $\ddot{x}_r$. Define $e_x := x - x_r$, $\dot{e}_x := \dot{x} - \dot{x}_r$ and $s_x := \dot{e}_x + \lambda_x e_x$. Define the reference pitch angle value as

$$\theta_r := \tan^{-1}\left(-\frac{\ddot{x}_r - \lambda_x \dot{e}_x - \sigma_x \frac{s_x}{|s_x|+\varepsilon} - \mu_x s_x}{\ddot{z}_r - \lambda_z \dot{e}_z - \sigma_z \frac{s_z}{|s_z|+\varepsilon} - \mu_z s_z + g} \cos\phi\right) \tag{22}$$

The choice of u in (17) makes the behavior in x-direction as follows:

$$\ddot{x} = \left(\ddot{z}_r - \lambda_z \dot{e}_z - \sigma_z \frac{s_z}{|s_z| + \varepsilon} - \mu_z s_z + g\right) \frac{\tan\theta}{\cos\phi} \tag{23}$$

If $\theta \equiv \theta_r$, we would have $\dot{s}_x = -\sigma_x \frac{s_x}{|s_x|+\varepsilon} - \mu_x s_x$, then one could drive $\theta \to \theta_r$ as quickly as possible and would ensure the stability in x-direction too. The control of the Euler angle θ is achieved by setting

$$\tilde{\tau}_\theta = -10\dot{\theta} - 25(\theta - \theta_r) \tag{24}$$

Briefly, in order to achieve a desired response in the Cartesian space, as illustrated in Fig. 4, the desired values for the Euler angles are computed and the orientation of the UAV is driven to those particular values which eventually drives the vehicle to the target position in cartesian coordinate system.

5 Simulation Studies

Two sets of simulation scenarios have been studied. In the first scenario, the reference trajectories of the vehicle change only in one direction while the other two coordinates are maintained at a constant value. This results in movements along the vertices of rectangular volumes in the cartesian space. The second scenario illustrates the results obtained when the quadrotor rotorcraft system is desired to move along a continuously changing trajectory designed for takeoff.

In Table 2, the parameters of the SMC law and the simulations are summarized. One should note that for such applications the selection of the best parameter set is a matter of the design specifications as well as the capabilities of the vehicle under investigation. After a short period of fine tuning by trial and error, we have fixed the values to the tabulated values.

Table 2. Simulation Parameters

Δt	Simulation stepsize	0.1 sec.
T	Simulation time (Flight time)	1300 sec.
σ_p	Variance of positional noise	1e-5
σ_v	Variance of velocity noise	1e-5
$\sigma_x,\sigma_y,\sigma_z$	Reaching law parameter	0.1
μ_x,μ_y,μ_z	Reaching law parameter	0.05
$\lambda_x,\lambda_y,\lambda_z$	Slope parameters	0.1
ε	Sign function smoothing par.	0.050

The results of the first scenario are illustrated in Fig. 5, where the UAV system follows the reference trajectory very precisely. In the simulations, we have assumed that the actuators are able to respond quickly and accurately, and we have not enforced limits on the control signals. Further, we assume observation noise corrupting the measurements. In the simulations, all velocities are assumed to be zero and positions are $x(0) = -1.5$, $y(0) = 1$ and $z(0) = 0$ for Cartesian positions; and $\psi(0) = 0.16$ rad., $\theta(0) = 0.19$ rad. and $\phi(0) = -0.17$ rad. Under these conditions, the obtained results have been found satisfactory.

With the same initial conditions and controller settings, the reference profile is changed to the one given below.

$$x_r(t) = \begin{cases} 0 & t < 200 \text{ sec.} \\ \frac{t-200}{6}\sin\left(\frac{2\pi t}{200}\right) & t \geq 200 \text{ sec.} \end{cases} \tag{25}$$

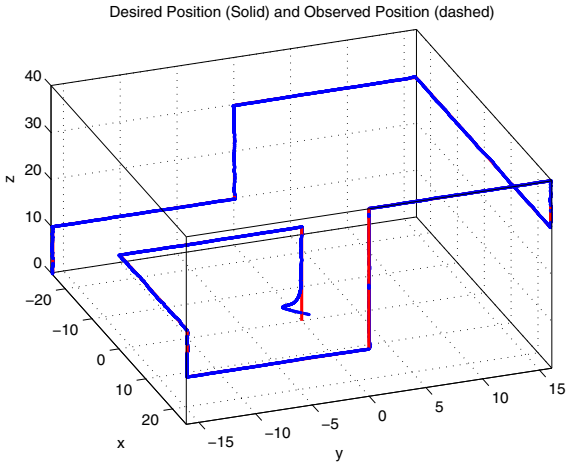

Fig. 5. Desired and observed trajectories when the flight path is discontinuous

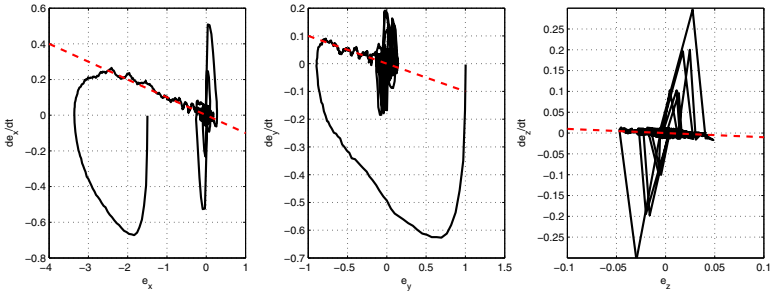

Fig. 6. Phase space behavior when the flight path is discontinuous

$$y_r(t) = \begin{cases} 0 & t < 200 \text{ sec.} \\ \frac{t-200}{6}\cos\left(\frac{2\pi t}{200}\right) & t \geq 200 \text{ sec.} \end{cases} \tag{26}$$

$$z_r(t) = \frac{t}{50} + 1 \tag{27}$$

The results obtained with these command signals are shown in Fig. 7 and Fig. 8. Clearly the vehicle takes off and follows a spiral trajectory as the altitude is gradually increased. The trajectory tracking ability is found to be very promising in this scenario too. Clearly, the simultaneous changes in the command signals causes a difficulty for the controller presented, yet, it displays certain degrees of robustness against such difficulties and the adverse effects of the observation noise are alleviated successfully. The effect of sudden changes in the command signals is also visible from the phase space behaviors shown in Fig. 8.

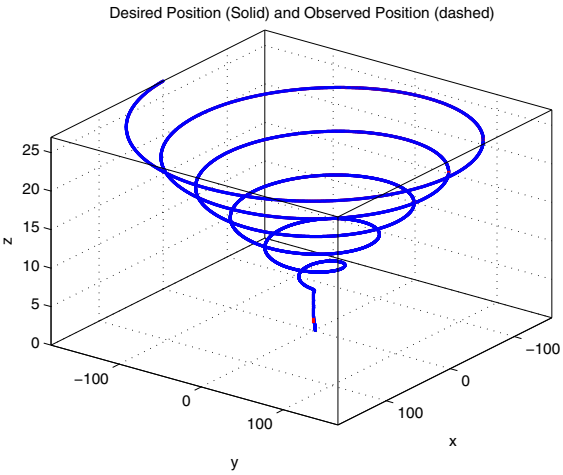

Fig. 7. Desired and observed trajectories when the flight path is continuous

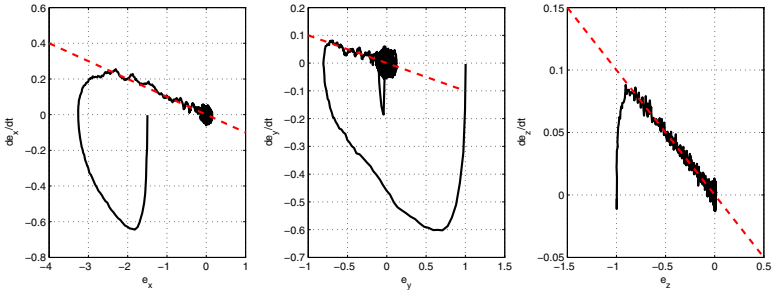

Fig. 8. Phase space behavior when the flight path is continuous

6 A Discussion of the Variants of SMC Technique

6.1 Intelligent and Adaptive Sliding Mode Control Techniques

Sliding mode control has benefited from the solutions offered in the realm of neural networks, fuzzy logic, support vector machines, evolutionary computation and the like. The essence of this collaboration lies in the fact that physical systems have mathematical models that are based on some assumptions. However, these assumptions are not met fully in reality and a mismatch appears in between the reality and the model. Inevitably, the engineer's resource is the model upon which the closed loop is designed, yet the controller staying in the loop is expected to alleviate difficulties caused by the model mismatch. Despite the presence of numerous approaches based on hard computing, the solutions offered by intelligent and adaptive systems theory assume that there are some numerical data that can be exploited toward the design of a learning control

system. Indeed, having significant amount of nonlinearity and redundancy, neural networks and fuzzy systems introduce an massively interconnected structure into the loop, where the controller can adapt itself to meet the desired performance specifications.

If we consider this discussion for the design and implementation of SMC systems, obtaining an a priori information about the functional details of the plant under control via a number of numerical data is considered as a good initial condition to start adaptation. Today, very powerful tuning algorithms are known and any SMC scheme can exploit the power of those when an unknown or uncertain function is available in the design. A detailed discussion and a list of most relevant literature on intelligent and adaptive SMC approaches can be found in [21–23].

Another avenue exploiting the robustness property of sliding mode control is to use the technique in the adaptation law of computationally intelligent systems. The dynamics of the update law is designed using the switching nature of sliding mode control and the tuning dynamics becomes robust against instantaneous spikes prescribed by the conventional laws thereby providing a smoother convergence to desired solutions, [24].

6.2 Fractional Order SMC Technique

The birth of fractional calculus goes back to 1695, with a letter from Leibniz to L'Hôpital, asking the meaning of derivative of order $\frac{1}{2}$. For few centuries the developments in the calculus of fractional mathematics have remained in theory yet with the advances in the high speed computing technology, the operators of fractional domain has become visible in applications covering a wide range from all disciplines, [26]. The two popular definitions of fractional order differintegration are by Riemann-Liouville and Caputo. Though both of them produce the same results, Caputo's definition is more suitable for the control systems engineering.

Caputo's definition of the fractional order differentiation is given in (28), where $\beta \in \Re^+$ is the order of the differentiation and $\Gamma(\beta) = \int_0^t e^{-t} t^{\beta-1} \mathrm{d}t$ is the Gamma function.

$$\mathbf{D}^{\beta} u(t) = \frac{1}{\Gamma(m-\beta)} \int_0^t \frac{\mathbf{D}^m u(\tau)}{(t-\tau)^{\beta+1-m}} \mathrm{d}\tau,\ m-1 \leq \beta < m \tag{28}$$

Now consider the fractional order state space system

$$\begin{aligned} x_i^{(\beta_i)} &= x_{i+1},\ \ i = 1,2,\ldots,n-1 \\ x_n^{(\beta_n)} &= F(\cdot) + G(\cdot)u \end{aligned} \tag{29}$$

where $0 < \beta_i < 1$ are the fractional differentiation orders, $F(\cdot)$ and $G(\cdot)$ are functions of the state variables. Consider a given reference trajectory $d_1 = r$, possessing the fractional derivatives $d_i = r^{(Q_i)}, Q_i = \sum_{k=1}^{i-1} \beta_k,\ \ i = 2,3,\ldots,n$ all being finite. Define the state tracking errors $e_i := x_i - d_i$. Choose a sliding hypersurface $s := e_n + \sum_{i=1}^{n-1} \lambda_i e_i$ such that the dynamics described by $s = 0$ is stable. Now differentiate s at order β_n. This yields

$$\begin{aligned} s^{(\beta_n)} &:= e_n^{(\beta_n)} + \sum_{i=1}^{n-1} \lambda_i e_i^{(\beta_n)} = f(\cdot) + g(\cdot)u - d_n^{(\beta_n)} + \sum_{i=1}^{n-1} \lambda_i e_i^{(\beta_n)} \\ &:= -\sigma \mathrm{sgn}(s) \end{aligned} \tag{30}$$

Solving the control signal would let us have

$$u = \frac{d_n^{(\beta_n)} - F(\cdot) - \sum_{i=1}^{n-1} \lambda_i e_i^{(\beta_n)} - \sigma \mathrm{sgn}(s)}{G(\cdot)} \tag{31}$$

Indeed, the application of this signal forces the reaching dynamics $s^{(\beta_n)} = -\sigma \mathrm{sgn}(s)$, which enforces $ss^{(\beta_n)} = -\sigma|s| < 0, \quad s \neq 0$. Obtaining $s^{(\beta_n)}(t)s(t) < 0$ can arise in the following cases. In the first case, $s(t) > 0$ and the integral $\int_0^t \frac{s(\xi)}{(t-\xi)^\beta}\, \mathrm{d}\xi$ is monotonically decreasing. In the second case $s(t) < 0$ and the integral $\int_0^t \frac{s(\xi)}{(t-\xi)^\beta}\, \mathrm{d}\xi$ is monotonically increasing. In both cases, the signal $|s(t)|$ is forced to converge the origin faster than $t^{-\beta}$. A natural consequence of this is to observe a very fast reaching phase as the signal $t^{-\beta}$ is a very steep function around $t \approx 0$. In conventional sense, one can have the following equalities to see the closed loop stability, [27].

$$s^{(\beta_n)} = -\sigma \mathrm{sgn}(s) \tag{32}$$

Defining the fractional differintegration operator of order β by $\mathbf{D}^{(\beta)}$, integrating both sides by order β_n yields (33), and differentiating once at order unity gives (34).

$$s = -\sigma \mathbf{D}^{(-\beta_n)} \mathrm{sgn}(s) \tag{33}$$

$$\dot{s} = -\sigma \mathbf{D}^{(1-\beta_n)} \mathrm{sgn}(s) \tag{34}$$

According to [27], $\mathrm{sgn}(\mathbf{D}^{(1-\beta_n)} \mathrm{sgn}(s)) = \mathrm{sgn}(s)$ and this proves that the chosen form of the control signal causes $s\dot{s} \leq 0$. This result practically tells us that the locus described by $s = 0$ is an attractor, and when confined to this subspace, the errors tend towards the origin and the closed loop systems displays certain degrees of robustness to uncertainties and becomes insensitive to disturbances entering the system through control channels, [25].

6.3 Backstepping SMC Technique

Backstepping method is one of the approaches adopted in the control of mini UAVs. The dynamics of the vehicle is suitable to apply the backstepping technique as it requires an iterative design procedure. The control law obtained at the final stage necessitates the knowledge of functional details embodying the vehicle dynamics and integrating the scheme with SMC introduces robustness to alleviate plant-model mismatch. In the literature, significant amount of work considering the backstepping SMC is reported and some of which are devoted to the quadrotor particular form.

Consider the dynamic system

$$\dot{x}_i = x_{i+1}, \quad i = 1, 2, \ldots, n \tag{35}$$

$$\dot{x}_n = F(x_1, x_2, \ldots, x_n) + G(x_1, x_2, \ldots, x_n)u, \quad G \geq 0 \tag{36}$$

Let r_i be the reference signal and the goal of the feedback control is to enforce $x_i \to r_i$ and we have $\dot{r}_i = r_{i+1}$ for $i = 1, 2, \ldots, n-1$. Choose the control law given by

$$u = -\frac{1}{G(x_1, x_2, \ldots, x_n)} \left(F(x_1, x_2, \ldots, x_n) - \dot{r}_n - \dot{A}_n + z_{n-1} + k_n z_n \right) \tag{37}$$

where $k_n > 0$, $A_1 = 0$ and $z_0 = 0$. With these initial values, the intermediate variables can be iterated as given below.

$$A_{i+1} = -k_i z_i + \dot{A}_i - z_{i-1}, \;\; i = 1, 2, \ldots, n-1 \tag{38}$$

With such a control law, the following stability result is obtained.

$$\sum_{i=1}^{n} z_i \dot{z}_i = \sum_{i=1}^{n} -k_i z_i^2 \tag{39}$$

This result shows asymptotic stability in the space spanned by the variables $z_1, z_2, \ldots, z_n$.

In ordinary SMC, the differences between the state variables and the corresponding reference signals are considered as the variables of the phase space. When the backstepping technique is blended with SMC, phase space variables are defined in terms of z_is and the nested structure of the design procedure is followed similar to the discussion presented above, [28]. The closed loop system, while controlled by a backstepping type of a nonlinear controller, exhibits the desired features of SMC scheme.

7 Conclusions

Sliding mode control, since its birth, has been an interesting research topic for many researchers. The robustness and invariance properties of the scheme has made it appealing when the design environment is subject to uncertainties. Unmanned aerial vehicles is another hot topic in control engineering and mechatronics. Having this picture in the front, researchers have used the SMC not only for autopiloting, but also in the design of adaptation laws. This work briefly describes the state of the art for SMC and unmanned aerial vehicles research and considers the extensions with intelligence, adaptiveness, non-integer designs and iterative nonlinear control designs. As a robust feedback control scheme, SMC can easily be integrated into many such domains and in the future, its use in aggressive maneuver UAVs, robust and intelligent autopilots and enhanced autonomy based on vision feedback will be the focus of research.

Acknowledgements. This work is devoted to Professor Okyay Kaynak, who is one of the leading researchers in Turkey, who contributed a lot to the theory and practice of sliding mode control and its applications utilizing logic, heuristics and intelligence. Professor Kaynak retires in 2015 yet he has a lot to do for those pursuing his career line. Thanks him not only for technical achievements but also for his service to the community.

References

1. Hung, J.Y., Gao, W., Hung, J.C.: Variable Structure Control: A Survey. IEEE Trans. on Industrial Electronics 40, 2–22 (1993)
2. Utkin, V.I.: Sliding Modes in Control Optimization. Springer, New York (1992)
3. Slotine, J.-J.E., Li, W.: Applied Nonlinear Control. Prentice-Hall, New Jersey (1991)
4. Young, K.D., Utkin, V.I., Özgüner, Ü.: A Control Engineer's Guide to Sliding Mode Control. IEEE Transactions on Control Systems Technology 7, 328–342 (1999)
5. Misawa, E.A.: Discrete-Time Sliding Mode Control: The Linear Case. Transactions of the ASME, Journal of Dynamic Systems, Measurement, and Control 119, 819–821 (1997)
6. Misawa, E.A.: Discrete-Time Sliding Mode Control for Nonlinear Systems With Unmatched Uncertainties and Uncertain Control Vector. Transactions of the ASME, Journal of Dynamic Systems, Measurement, and Control 119, 503–512 (1997)
7. Sabanovic, A., Sabanovic, N., Jezernik, K., Wada, K.: Chattering Free Sliding Modes. In: Proc. of the 3rd Workshop on Variable Structure Systems and Lyapunov Design, Napoly, Italy, pp. 143–148 (1994)
8. Bartolini, G., Ferrera, A., Usai, E., Utkin, V.I.: On Multi-Input Chattering-Free Second-Order Sliding Mode Control. IEEE Trans. on Automatic Control 45, 1711–1717 (2000)
9. Erbatur, K., Kaynak, O., Sabanovic, A.: A Study on Robustness Property of Sliding Mode Controllers: A Novel Design and Experimental Investigations. IEEE Transactions on Industrial Electronics 46, 1012–1018 (1999)
10. Castillo, P., Lozano, R., Dzul, A.E.: Stabilization of a Mini Rotorcraft with Four Rotors. IEEE Control Systems Magazine, 45–55 (December 2005)
11. Castillo, P., Lozano, R., Dzul, A.E.: Modelling and Control of Mini Flying Machines. Springer (2005)
12. Bouabdallah, S., Noth, A., Siegwart, R.: PID vs LQ Control Techniques Applied to an Indoor Micro Quadrotor. In: Proc. of 2004 IEEE/RSJ Int. Conf. on. Intelligent Robots and Systems, Sendai, Japan, September 28 - October 2 (2004)
13. Hanford, S.D., Long, L.N., Horn, J.F.: A Small Semi-Autonomous Rotary-Wing Unmanned Air Vehicle (UAV). AIAA2005-7077 (2005)
14. Hoffmann, G., Rajnarayan, D.G., Waslander, S.L., Dostal, D., Jang, J.S., Tomlin, C.J.: The Stanford testbed of Autonomous Rotorcraft for Multi Agent Control (STARMAC). In: Proc. of The 23rd Digital Avionics Systems Conference (DASC 2004), Salt Lake City, Utah, USA, October 24-28 (2004)
15. Tournier, G.P., Valentiy, M., Howz, J.P.: Estimation and Control of a Quadrotor Vehicle Using Monocular Vision and Moiré Patterns. In: AIAA Guidance, Navigation, and Control Conference and Exhibit, AIAA2006-6711, Keystone, Colorado, USA, August 21-24 (2006)
16. Altuğ, E., Ostrowski, J.P., Taylor, C.J.: Quadrotor Control Using Dual Camera Visual Feedback. In: Proc. of the 2003 IEEE Int. Conf. on Robotics & Automation, Taipei, Taiwan, September 14-19, pp. 4294–4299 (2003)
17. Çamlıca, F.B.: Demonstration of a Stabilized Hovering Platform for Undergraduate Laboratory. M.S. Thesis, Middle East Technical University, Ankara, Turkey (2004)
18. Waslander, S.L., Hoffmann, G.M., Jang, J.S., Tomlin, C.J.: Multi-Agent Quadrotor Testbed Control Design: Integral Sliding Mode vs. Reinforcement Learning. In: IEEE/RSJ Int. Conf. on Intelligent Robots and Systems, Edmonton, Alberta, Canada, August 2-6, pp. 468–473 (2005)
19. Hamel, T., Mahony, R., Lozano, R., Ostrowski, J.: Dynamic Modelling and Configuration Stbilization for an X4-Flyer. In: 15th IFAC Triennial World Congress, Barcelona, Spain (2002)

20. Efe, M.Ö.: Robust Low Altitude Behavior Control of a Quadrotor Rotorcraft Through Sliding Modes. In: The 15th Mediterranean Conf. on Control and Automation (MED 2007), Paper# T23-035, Athens, Greece (2007)
21. Yu, X., Kaynak, O.: Sliding Mode Control with Soft Computing: A Survey. IEEE Transactions Industrial Electronics 56(9), 3275–3285 (2009)
22. Kaynak, O., Erbatur, K., Ertugrul, M.: The Fusion of Computationally Intelligent Methodologies and Sliding Mode Control – A Survey. IEEE Transactions on Industrial Electronics 48(1), 4–17 (2001)
23. Ertugrul, M., Kaynak, O.: Neuro Sliding Mode Control of Robotic Manipulators. Mechatronics 10(1-2), 239–263 (2000)
24. Topalov, A., Kaynak, O.: On-Line Learning in Adaptive Neurocontrol Schemes with a Sliding Mode Algorithm. IEEE Transactions on Systems, Man and Cybernetics, Part B 31(3), 445–450 (2001)
25. Efe, M.Ö.: Fractional Order Sliding Mode Controller Design for Fractional Order Dynamic Systems. In: Güvenç, Z.B., Baleanu, D., Machado, J.A.T. (eds.) New Trends in Nanotechnology and Fractional Calculus Applications, pp. 463–470. Springer,
26. Efe, M.Ö.: Fractional Order Systems in Industrial Automation–A Survey. IEEE Transactions on Industrial Informatics 7(4), 582–591 (2011)
27. Vinagre, B.M., Calderón, A.J.: On fractional sliding mode control. In: Proc. of the 7th Portuguese Conference on Automatic Control (CONTROLO 2006), Lisbon, Portugal, September 11-13 (2006)
28. Ramirez-Rodriguez, H., Parra-Vega, V., Sanchez-Orta, A., Garcia-Salazar, O.: Robust Backstepping Control Based on Integral Sliding Modes for Tracking of Quadrotors. Journal of Intelligent and Robotic Systems 73, 51–66 (2014)

Selected Problems of Discontinues Control of Inverter Fed Induction Motor Drives

Dariusz L. Sobczuk and Marian P. Kazmierkowski

Institute of Control & Industrial Electronics, Warsaw University of Technology, Poland
{sobczuk,mpk}@isep.pw.edu.pl

Abstract. In this Chapter a combined discontinues sliding mode control (SMC) with feedback linearization control (FLC) applied for voltage source inverter-fed induction motor are presented. The FLC guarantees the exactly decoupling of the motor speed and rotor flux control. Thus this control method gives a possibility to get very good behavior in both dynamic and steady states. The SMC approach assures direct control of inverter legs and allows using a simple table instead of performing PWM online calculation. Moreover, the SMC is robust to drive uncertainties. The good behaviour of rotor flux and mechanical speed Sliding Mode Observers (SMO) is the important feature of the system. Therefore, the presented approaches are very useful in a variety of applications and, in particular, in drive systems, robotics and power electronics.

Keywords: induction motor control, discontinuous control, variable structure control, sliding mode control, sliding mode observers, feedback linearization, speed sensorless control, rotor flux observers, voltage source inverters.

1 Introduction and Overview

DC motors by their construction allow for a completely decoupled control of the flux-forming current in exciting winding and the torque producing current in armature winding. Thanks to the complete separation of control winding and mechanical commutator operation, a very simple and low computing time control algorithms can be applied for high performance industrial DC drives. Contrary, the induction motor (IM) has simple construction, high reliability, low cost, and it can operates in aggressive or volatile environments (no problems with spark and corrosion). However, the IM with multi-phase winding and cage rotor is high order nonlinear dynamic system with internal coupling and therefore, it's flux and torque cannot easy be controlled separately. Moreover, some state variables, rotor currents and fluxes, are directly not measurable. Additionally, rotor resistance (due to heating) and magnetising inductance (due to saturation) varies considerably with a significant impact on the system dynamics. Therefore, for high dynamic performance IM drives, complex control algorithms have to be used. Nevertheless, the advancements in semiconductor power electronic devices and Digital Signal Processors (DSP) enabled to apply IM in variable speed applications. Implementation of new control techniques in drive systems has made IM a reasonable alternative to DC motors.

X. Yu and M. Önder Efe (eds.), *Recent Advances in Sliding Modes,*
Studies in Systems, Decision and Control 24, DOI: 10.1007/978-3-319-18290-2_13

The most popular high performance IM vector control method, known as *Field Oriented Control* (FOC) has been proposed by Blaschke [1]. In this method the IM equations are transformed in a coordinate system that rotates with the rotor flux vector. These new coordinates are called *field coordinates*. In field coordinates – only for the constant rotor flux amplitude - there is a *linear relationship* between control variables and speed [12]. Alternative to the FOC is the *feedback linearization control* (FLC) [2]. The application of this approach can take many forms, depending on the choice of variables used for the linearization. Marino *et al.* [3, 4] have proposed a nonlinear transformation of the IM state variables, so that in the new coordinates, the speed and rotor flux amplitude are decoupled by feedback. Note, that using the *feedback linearization* approach strictly linear and strictly decoupled system are obtained. Next, for the decoupled linear system several control algorithms could be applied. One of the important requirements in the control system is robustness against changing of object parameters. In this case the discontinues control such as *Sliding Mode Control* (SMC) could be used.

The SMC creates a large group of theoretical research works and it's applications. Basically, the SMC is a type of control using the Variable Structure Systems (VSS). The first works in these fields started in 50th of the 20th century in the Soviet Union and were developed in 60th and 70th (Emelyanow, 1967 [5], Itkis, 1976 [8], Utkin, 1977 [6]) and still are continued. While it is impossible, in this connection, to quote all the relevant publications, mention should be made of the research group where much of the important works in this area has been done. These include those led by Professors Kaynak [16-23, 28, 30], Utkin [6,7, 38], Sabanovic [23, 29, 31], Slotine [26, 27], Levant [14, 15], Orlowska-Kowalska [34], Boldea [37] and others.

This chapter is divided into four sections. In section 2 the theoretical basics of the SMC will be introduced. In section 3 the application of feedback linearization to IM control will be presented. In Section 4 two algorithms will be presented. At first the sliding mode control will be used to control IM linearized in feedback [10]. The application of sliding mode control to such a system allows creating the direct control algorithms of the inverter [11]. Secondly, the Sliding Mode Observer (SMO) of rotor flux and mechanical speed used in the linearized IM control will be described [13].

2 Sliding Mode Control (SMC)

2.1 Introduction

At the beginning of 80th started more and more often applying the SMC methods in the various practical systems. Thus, the SMC methods found application in:

- systems of automatic control in planes (Singh, 1989) [24],
- control of servomechanisms (Hikita, 1988) [25],
- design observers (Slotine, de Wit, 1991) [26],
- control robots (Slotine, Sastry, 1983) [27] and (Kaynak et al. 1984) [28],
- control electric motors and in power electronics (Sabanovic, Izosimov, 1981) [29],

- current control in power converters (Kaynak, Sabanovic, 1994) [31],
- speed sensorless control (Lascu, Boldea, 2009) [37] and (Comanescu, 2009) [40],

and many others.

Later, a second order SMC (2-SMC) was proposed by A. Levant [14,15] and Bartolini [32]. The 2-SMC is sometimes called SMC without chattering, because this disadvantageous phenomenon of classical first order SMC is strongly limited.

Since in this book there are a few earlier theoretical chapters which cover the basics of SMC, the content of Section 2 is reduced to focus only on the specifics needed for control of induction motors discussed later.

2.2 SMC for Linear Systems

Let us assume, that the object is described by matrix equation:

$$\dot{\boldsymbol{x}} = \boldsymbol{A}\boldsymbol{x} + \boldsymbol{b}u \tag{1}$$

where:

$$\boldsymbol{A} \in R^{n \times n};\ \boldsymbol{b}, \boldsymbol{x}, \in R^{n};\ u \in R. \tag{2}$$

For SMC description the single input and single output (SISO) object can be written in the canonical form:

$$\begin{aligned} \dot{x}_i &= x_{i+1} \qquad \text{for i} = 1,2,\ldots,\text{n} - 1 \\ \dot{x}_n &= -\sum_{i=1}^{n} a_i x_i + u \end{aligned} \tag{3}$$

Let us assume that aim of control is zeroing of the output $y = x_1$. Let u will be a function of the vector x with discontinuity surface determined by the equation $s = 0$, where

$$s = \sum_{i=1}^{n} c_i x_i,\ c_i = const,\ c_n = 1 \tag{4}$$

If trajectories are directed at the surface s = 0, then SMC occurred. The sufficient condition is:

$$\begin{aligned} &\lim_{s \to 0^+} \dot{s} < 0 \\ &\lim_{s \to 0^-} \dot{s} > 0 \end{aligned} \tag{5}$$

It means that if s is positive, then its derivative should be negative and if s is negative, then its derivative should be positive. So, when the Eq.(5) is fulfilled,

trajectories will be attracted to the sliding surface. Thus, the resulting equation of the system working with SMC is as follows:

$$\begin{aligned} \dot{x}_i &= x_{i+1} \qquad \text{for i} = 1,2,\ldots,\text{n - 2} \\ \dot{x}_{n-1} &= -\sum_{i=1}^{n} \text{c}_i x_i \end{aligned} \tag{6}$$

Note, that these equations are not dependent from control parameters but only from parameters c_i.

The main problem is to select control to meet the following properties:

- the sliding mode must exist in all points of the surface s = 0,
- control should provide reaching this surface.

In the case of classical SM, the switching function, used in control is function sign().

$$sign(s) = \begin{cases} +1 \quad if \ s \geq 0 \\ -1 \quad if \ \ s < 0 \end{cases} \tag{7}$$

So the control of the SISO system is equal :

$$\text{u}=\text{V}_\text{m}\ \text{sign(s)} \tag{8}$$

3 Feedback Linearization Control (FLC) of Induction Motor

The induction motor equations in per unit (pu) system is described in the following form:

$$\dot{\boldsymbol{x}} = \boldsymbol{f}(\boldsymbol{x}) + u_{\text{s}\alpha}\,\boldsymbol{g}_\alpha + u_{\text{s}\beta}\,\boldsymbol{g}_\beta \tag{9}$$

Where

$$\boldsymbol{f}(\boldsymbol{x}) = \begin{bmatrix} -\alpha\psi_{\text{r}\alpha} - \omega_\text{m}\psi_{\text{r}\beta} + \alpha x_\text{M} i_{\text{s}\alpha} \\ \omega_\text{m}\psi_{\text{r}\alpha} - \alpha\psi_{\text{r}\beta} + \alpha x_\text{M} i_{\text{s}\beta} \\ \alpha\beta\,\psi_{\text{r}\alpha} + \beta\omega_\text{m}\psi_{\text{r}\beta} - \gamma i_{\text{s}\alpha} \\ -\beta\omega_\text{m}\psi_{\text{r}\alpha} + \alpha\beta\,\psi_{\text{r}\beta} - \gamma i_{\text{s}\beta} \\ \mu(\psi_{\text{r}\alpha} i_{\text{s}\beta} - \psi_{\text{r}\beta} i_{\text{s}\alpha}) - \dfrac{m_\text{L}}{\tau_\text{M}} \end{bmatrix} \tag{10}$$

$$\boldsymbol{g}_\alpha = [0,\ 0,\ 1/\sigma\text{x}_\text{s},\ 0,\ 0]^\text{T},\ \boldsymbol{g}_\beta = [0,\ 0,\ 0,\ 1/\sigma\text{x}_\text{s}\ ,\ 0]^\text{T} \tag{11}$$

$$\boldsymbol{x} = [\psi_{\text{r}\alpha},\ \psi_{\text{r}\beta},\ i_{\text{s}\alpha},\ i_{\text{s}\beta},\ \omega_\text{m}]^\text{T} \tag{12}$$

and $\alpha = r_r/x_r$; $\beta = x_M/(\sigma x_s x_r)$; $\gamma = (r_s x_r^2 + r_r x_M^2)/(\sigma x_s x_r^2)$; $\mu = x_M/(\tau_M x_r)$; $\sigma = 1 - x_M^2/(\sigma x_s x_r)$,

where motor parameters r_r, r_s are rotor and stator resistance in pu. system, and x_r, x_s, x_M, are rotor, stator and main inductance in pu. system.

Note that ω_m, $\psi_{r\alpha}$, $\psi_{r\beta}$, are not directly dependent on control signals $u_{s\alpha}$, $u_{s\beta}$. In this case it is easy to choose two variables dependent on $\boldsymbol{x}$ only. Now the feedback linearization procedure will be applied. So we can define [2]:

$$\phi_1(x) = \psi_{r\alpha}^2 + \psi_{r\beta}^2 = \psi^2 \tag{13}$$

$$\phi_2(x) = \omega_m \tag{14}$$

Let $\phi_1(\boldsymbol{x})$, $\phi_2(\boldsymbol{x})$ are the output variables. The aim of control is to obtain:

- constant flux amplitude,
- reference angular speed.

Part of the new state variables we can choose according to (13), (14). So, the full definition of new coordinates is given by [3, 4]:

$$\begin{aligned} z_1 &= \phi_1(\boldsymbol{x}) \\ z_2 &= L_f \phi_1(\boldsymbol{x}) \\ z_3 &= \phi_2(\boldsymbol{x}) \\ z_4 &= L_f \phi_2(\boldsymbol{x}) \\ z_5 &= \arctan\left(\frac{\psi_{r\beta}}{\psi_{r\alpha}}\right) \end{aligned} \tag{15}$$

Where $L_f h$ is the *Lie derivative* of h with respect to a vector field f : $L_f h = (\nabla h)^T \boldsymbol{f}$

Note, that the fifth variable cannot be linearizable and the linearization can be only partial. Denote:

$$\phi_3(\boldsymbol{x}) = z_5 \tag{16}$$

then the dynamic of the system is given by:

$$\begin{aligned} \dot{z}_1 &= z_2 \\ \dot{z}_2 &= L_f^2 \phi_1(\boldsymbol{x}) + L_{g\alpha} L_f \phi_1(\boldsymbol{x})\ u_{s\alpha} + L_{g\beta} L_f \phi_1(\boldsymbol{x})\ u_{s\beta} \\ \dot{z}_3 &= z_4 \\ \dot{z}_4 &= L_f^2 \phi_2(\boldsymbol{x}) + L_{g\alpha} L_f \phi_2(\boldsymbol{x})\ u_{s\alpha} + L_{g\beta} L_f \phi_2(\boldsymbol{x})\ u_{s\beta} \\ \dot{z}_5 &= L_f^2 \phi_3(\boldsymbol{x}) \end{aligned} \tag{17}$$

In the further part of this section we will consider the system consists of the first four equations, because the fifth variable is only responsible for the zero dynamics of the system. We can define linearizing feedback as [4]:

$$\begin{bmatrix} u_{s\alpha} \\ u_{s\beta} \end{bmatrix} = \mathbf{D}^{-1} \left\{ \begin{bmatrix} -L_f^2 \phi_1 \\ -L_f^2 \phi_2 \end{bmatrix} + \begin{bmatrix} v_1 \\ v_2 \end{bmatrix} \right\} \tag{18}$$

$\boldsymbol{D}$ is given by:

$$\boldsymbol{D} = \begin{bmatrix} L_{g\alpha} L_f \phi_1 & L_{g\beta} L_f \phi_1 \\ L_{g\alpha} L_f \phi_2 & L_{g\beta} L_f \phi_2 \end{bmatrix} \tag{19}$$

After simple calculation, with the assumption that det($\boldsymbol{D}$) ≠ 0 what means that $\psi_r \neq 0$, the following equation is fulfilled:

$$\boldsymbol{D}^{-1} = \frac{\sigma x_s}{2\alpha\mu x_M \psi_r^2} \begin{bmatrix} \mu\psi_{r\alpha} & -2\alpha x_M \psi_{r\beta} \\ \mu\psi_{r\beta} & -2\alpha x_M \psi_{r\alpha} \end{bmatrix} \tag{20}$$

and $L_f^2\phi_1$, $L_f^2\phi_2$ are equal:

$$\begin{aligned} L_f{}^2\phi_1 = {} & 2\alpha \left[(2\alpha + \alpha\beta x_M (\psi_{r\alpha}{}^2 + \psi_{r\beta}{}^2) + \alpha x_M{}^2 (i_{s\alpha}{}^2 + i_{s\beta}{}^2) - \right. \\ & \left. (\gamma x_M + 3\alpha x_M) (\psi_{r\alpha} i_{s\alpha} + \psi_{r\beta} i_{s\beta}) + x_M \omega_m (\psi_{r\alpha} i_{s\beta} - \psi_{r\beta} i_{s\alpha}) \right] \end{aligned} \tag{21}$$

$$\begin{aligned} L_f{}^2\phi_2 = {} & -\mu \left[\omega_m (\psi_{r\alpha} i_{s\alpha} + \psi_{r\beta} i_{s\beta}) + \beta\omega_m (\psi_{r\alpha}{}^2 + \psi_{r\beta}{}^2) + \right. \\ & \left. (\gamma + \alpha) (\psi_{r\alpha} i_{s\beta} - \psi_{r\beta} i_{s\alpha}) \right] \end{aligned} \tag{22}$$

The resulting system is described by the equations:

$$\begin{aligned} \dot{z}_1 &= z_2 \\ \dot{z}_2 &= v_1 \\ \dot{z}_3 &= z_4 \\ \dot{z}_4 &= v_2 \end{aligned} \tag{23}$$

So, the block diagram of the linearized system is shown in the Fig. 1(b)

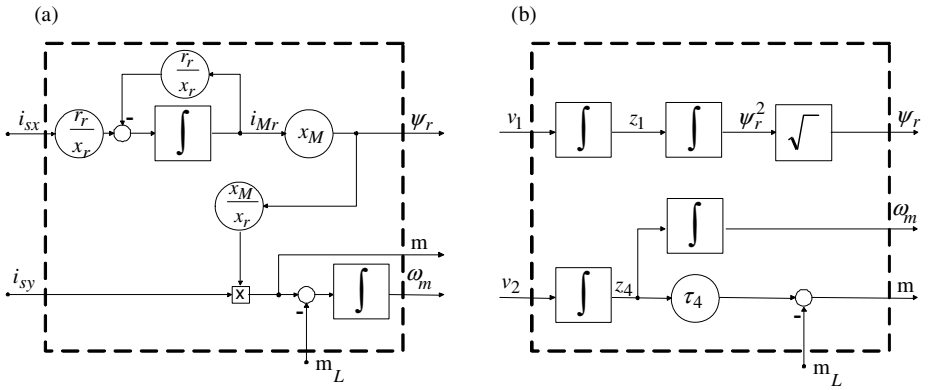

Fig. 1. Block diagram of induction motor: a) in x-y field coordinates, b) with new control signals v_1, v_2 (feedback linearization)

Control signals can be calculated by the following formulas:

$$v_1 = k_{11}\,(z_1 - z_{1\mathrm{ref}}) - k_{12} z_2 \tag{24}$$

$$v_2 = k_{21}\,(z_3 - z_{3\mathrm{ref}}) - k_{22} z_4 \tag{25}$$

where coefficients k_{11}, k_{12}, k_{21}, k_{22} are chosen to determinate closed loop system dynamic.

Control algorithm consists of two steps (Fig. 2):

- calculations v_1 ,v_2 according to Eq. (24), Eq. (25),
- calculations $u_{s\alpha}$, $u_{s\beta}$ according to Eq. (18).

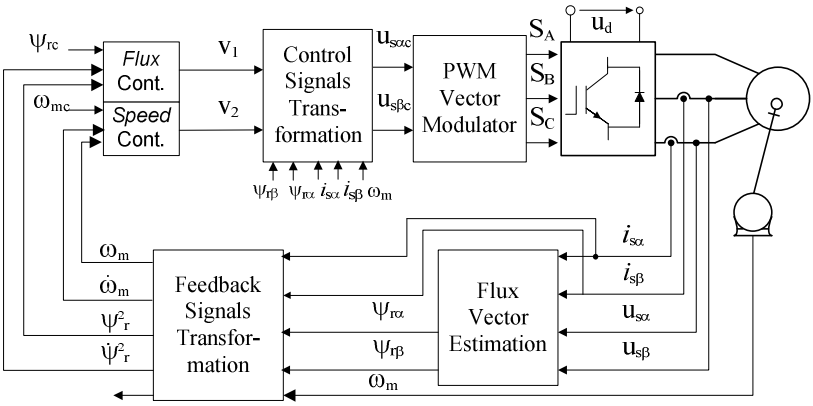

Fig. 2. Block diagram of Feedback Linearization Control (FLC) of inverter fed IM

Application of the feedback linearization method gives us a possibility to get very good behaviour in steady and dynamical states. The main features and advantages of the presented control are:

- with control variables v_1, v_2 the FLC guarantee the exactly decoupling of the motor speed and rotor flux control in both dynamic and steady states.
- the FLC is implemented in a state feedback fashion and needs more complex signal processing (full information about motor state variables and load torque is required).

One should notice, that in contrast to the classical FOC system, where the control variables i_{sx}, i_{sy}, (see the block diagram in Fig. 1a) are not directly influences to the output variables m and ψ_r , in the FLC approach control variables v_1, v_2, (see the block diagram in Fig. 1b) causes that the system is directly and fully decoupled. However, the transformation and new control variables v_1, v_2 used in the FLC have no so direct physical meaning as i_{sx}, i_{sy} (flux and torque current, respectively) in the FOC system.

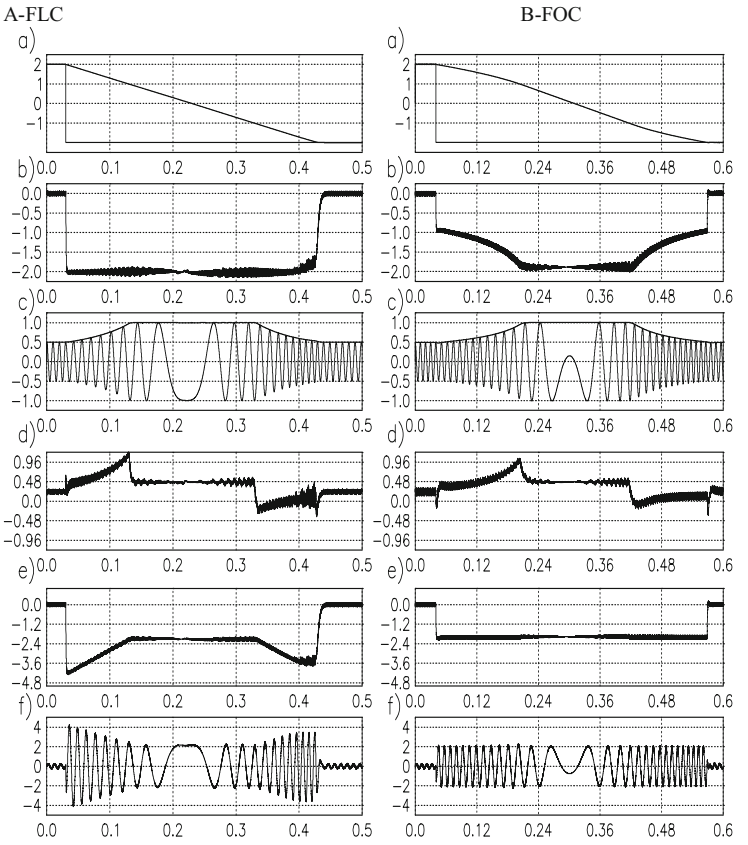

Fig. 3. Comparison of speed reversal including field weakening of induction motor controlled via feedback linearization (left) with classical field oriented control (right). From the top: a) actual and reference speed (ω_{mref}, ω_m) b) torque m, c) flux component and amplitude ($\psi_{r\alpha}$, ψ_r), d) flux current i_{sx}, e) torque current i_{sy}, f) current component $i_{s\beta}$.

Fig. 3. shows oscillograms illustrating comparison of speed reversal including field weakening of IM controlled via feedback linearization with classical FOC.

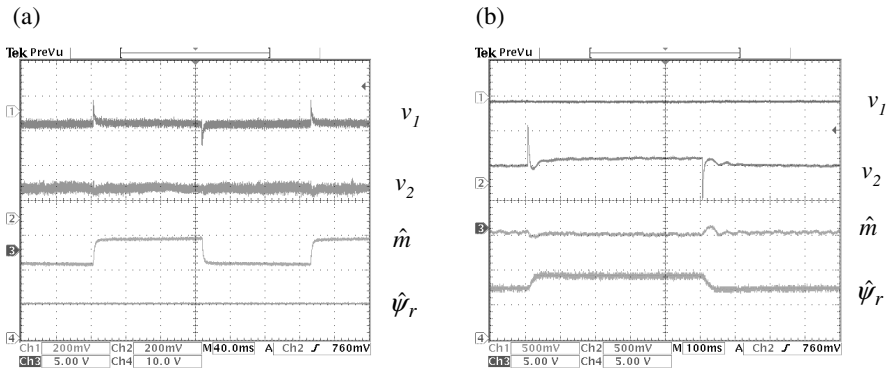

Fig. 4. Experimental oscillograms illustrating decoupling performance with new control variables v_1, v_2 in the FLC scheme of Fig. 2; (a) torque tracking, (b) flux amplitude tracking

The experimental oscillograms showing control signal v_1, which controls flux amplitude and control signal v_2, which controls electromagnetic torque are presented in Fig. 4. These results were measured on the laboratory setup with 3 kW IM, Mitsubishi 1200V and 50A IGBT inverter and dSPACE DS1102 control board. Note that well decoupling of flux and torque control as well as perfect flux amplitude and torque tracking performances are achieved.

4 Sliding Mode Feedback Linearization Control of Induction Motor

4.1 Introduction

In this section two application examples of SMC for induction motor (IM) will be shown. At first the SMC is used to control of feedback linearized IM. The SMC application for such a system gives us the possibility creating the direct control algorithms of the transistor inverter. Secondly, the Sliding Mode Observer (SMO) of rotor flux vector and speed used in the feedback linearized induction motor will be described.

4.2 Feedback Linearization with Sliding Mode

In many publications the SMC is applied to FOC controlled IM [3, 4]. In this section application of the sliding mode technique to the resulting linear system obtained by feedback linearization is described. The robustness and the discontinuous nature of

Variable Structure Control permits to use this control technique to the inverter-fed induction motor drives.

In SMC [7] the system structure is switched when the system state crosses the predetermined discontinuity line, so that the plant state slides along the reference trajectory. The design of SMC requires a suitable control law. The simplest way to solve this problem is to use bang-bang controller. In this case the absolute value of the control command v is constant and the sign is given by the sign of a commutation function s as follows:

$$v = v_{max}\ \mathrm{sgn}(s) \tag{24}$$

The controller gain v_{max} can be evaluated based on the existing condition of sliding mode Eq. (5).

In the case of linearized IM, there are two error signals:

$$e_1 = z_{1ref} - z_1 \tag{25a}$$
$$e_2 = z_{3ref} - z_3 \tag{25b}$$

where z_1 and z_3 are given in equations (3.5) – (3.7). Two sliding lines are defined as:

$$\begin{aligned} s_1 &= e_1 + \tau_1 \dot{e}_1 \\ s_2 &= e_2 + \tau_2 \dot{e}_2 \end{aligned} \tag{26}$$

giving two control signals:

$$v_1 = v_{1max}\ \mathrm{sgn}(s_1) \tag{27a}$$
$$v_2 = v_{2max}\ \mathrm{sgn}(s_2) \tag{27b}$$

Note that for each vector v_1, v_2 the conditions of Eq. (5) must be fulfilled and this gives us possibilities to choose a vector pattern for inverter control.

In many papers [2-4], [33-36], where the nonlinear control of induction motor is described, the inverter model does not take into account. However, in the case of two-level three-phase inverter, it is easy to show that using SMC approach one can find the voltage vector, from the set of eight possible vectors, which assure the correct system behaviour (i.e. according to sliding mode conditions). It is obvious that this approach is easy to extend for multilevel inverters.

The simplest way of producing the inverter switch states is to check all possibilities and choose this one, which fulfil the sliding mode conditions. The algorithm could be performed in different ways using an appropriate Switching Table in the scheme shown in Fig. 5 (algorithm 1).

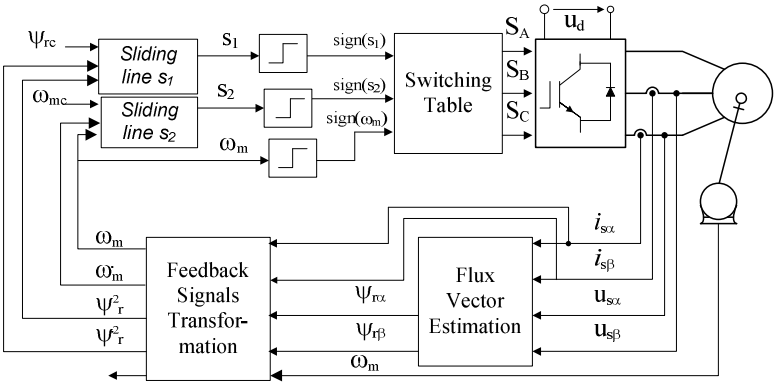

Fig. 5. The sliding mode control with switching table applied to the feedback linearized inverter-fed induction motor

Table 1. Switching table in classical sliding mode

sector	$s_2>0$, $s_1>0$	$s_2>0$, $s_1<0$	$s_2<0$, $s_1>0$	$s_2<0$, $s_1<0$
1	2	3	6	5
2	3	4	1	6
3	4	5	2	1
4	5	6	3	2
5	6	1	4	3
6	1	2	5	4

where sectors are defined by the angle of the rotor flux vector as shown in Table 2.

Table 2. Definition of rotor flux sectors

$-\pi/6<\varphi_{\psi r}<\pi/6$	1
$\pi/6<\varphi_{\psi r}<\pi/2$	2
$\pi/2<\varphi_{\psi r}<5\pi/6$	3
$5\pi/6<\varphi_{\psi r}<7\pi/6$	4
$7\pi/6<\varphi_{\psi r}<3\pi/2$	5
$3\pi/2<\varphi_{\psi r}<11\pi/6$	6

The algorithm could be modified in such a way, that in some situations we can choose zero vector instead of active vectors. In this case the sign of mechanical speed is taken to account, and the switching table is shown in Table 3 (algorithm 2).

This approach is correct in steady state, but not correct in transients, because the SMC condition is not fulfilled in every time instance. In transient state another modification could be used. Inside the ε-neighborhood the algorithm with modification will be used and outside this region the algorithm which strictly fulfilled the sliding mode conditions will be applied (algorithm 3).

Table 3. Switching table in modified sliding mode

sect.	$\omega_m>0$, $s_2>0$, $s_1>0$	$\omega_m>0$, $s_2>0$, $s_1<0$	$\omega_m s_2<0$	$\omega_m<0$, $s_2<0$, $s_1>0$	$\omega_m<0$, $s_2<0$, $s_1<0$
1	2	3	0	6	5
2	3	4	0	1	6
3	4	5	0	2	1
4	5	6	0	3	2
5	6	1	0	4	3
6	1	2	0	5	4

The simulations of these algorithms are performed. The oscillograms obtained for FLC with sinusoidal PWM and with linear speed and rotor flux controllers as well as for FLC with sliding mode (algorithm 1) are shown in Fig. 6A and 6B. These oscillograms show the steady state behaviour of the above systems. As can be seen from figure 6B, it exists torque stress in some time instances. To guarantee better performance one can apply algorithm 2 presented in the Table 3. In Fig. 6C the simulation results obtained for SMC with modification are shown. When compare stator voltage vector path $u_{s\beta}(u_{s\alpha})$ of Fig. 6B and Fig. 6C, it can be seen that modified SMC algorithm select only neighbour voltage vectors. This guarantees elimination of the torque stress like in the case of operation with sinusoidal PWM (Fig. 6A).

In Fig. 7 the transient response to speed reference step change is presented. The simulated oscillograms obtained for FLC with sinusoidal PWM and with linear speed and rotor flux controllers as well as for FLC with modified sliding mode (algorithm 3) are shown. These oscillograms show the dynamic behaviour of the above systems, which are similar to each other.

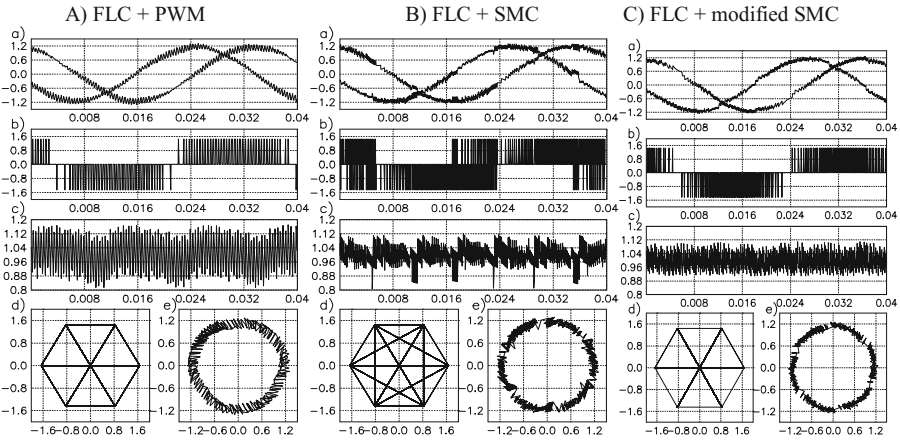

Fig. 6. Steady state operation of the induction motor controlled via feedback linearization with linear feedback and PWM (A), with SMC (B), and with modified SMC (C): a) stator currents $i_{s\alpha}$, $i_{s\beta}$, b) stator voltage $u_{s\beta}$, c) electromagnetic torque m, d) stator voltage vector path $u_{s\beta}(u_{s\alpha})$, e) stator current vector path $i_{s\beta}(i_{s\alpha})$

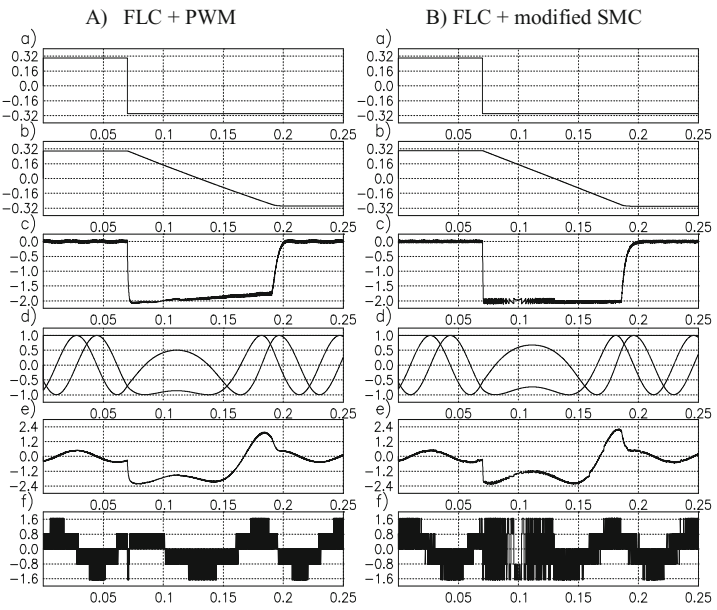

Fig. 7. Transients to step change of the reference speed with induction motor controlled via feedback linearization with linear feedback and PWM (A) and with modified SMC (B); a) reference speed ω_{mref}, b) actual speed ω_m, c) electromagnetic torque m, d) rotor flux components and absolute value ($\psi_{r\alpha}$, $\psi_{r\beta}$, ψ_r), e) stator current component $i_{s\alpha}$, f) stator voltage component $u_{s\alpha}$

4.3 Sliding Mode Observers

4.3.1 Application of Sliding Mode Observers

The sliding mode condition should be fulfilled, which imply the convergence to the prescribed surface. The main advantage of SMC is the robustness of the system. The sliding mode could be applied to observers in which the discontinues terms are used. In this section the Sliding Mode Observers (SMO) used for induction motor are presented. Recently many papers devoted to this topic were written [37] – [43]. In this work two different observers are presented, the parallel and serial SMO.

The parallel Sliding Mode Observer of rotor flux we can calculate using following formulas:

$$\begin{aligned}
\frac{d\hat{\psi}_{r\alpha}}{dt} &= -\alpha\hat{\psi}_{r\alpha} - \omega_m\hat{\psi}_{r\beta} + \alpha x_M i_{s\alpha} + kV_\alpha \\
\frac{d\hat{\psi}_{r\beta}}{dt} &= -\alpha\hat{\psi}_{r\beta} + \omega_m\hat{\psi}_{r\alpha} + \alpha x_M i_{s\alpha} + kV_\beta \\
\frac{d\hat{i}_{s\alpha}}{dt} &= \alpha\beta\hat{\psi}_{r\alpha} + \beta\omega_m\hat{\psi}_{r\beta} - \gamma\hat{i}_{s\alpha} + \frac{1}{\sigma x_s}u_\alpha + V_\alpha \\
\frac{d\hat{i}_{s\beta}}{dt} &= \alpha\beta\hat{\psi}_{r\beta} - \beta\omega_m\hat{\psi}_{r\alpha} - \gamma\hat{i}_{s\beta} + \frac{1}{\sigma x_s}u_\beta + V_\beta
\end{aligned} \tag{28}$$

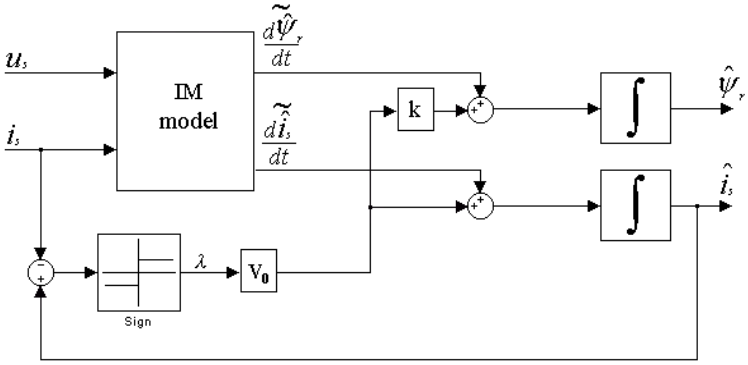

Fig. 8. Parallel Sliding Mode Flux Observer

where $\hat{\psi}_{r\alpha}$, $\hat{\psi}_{r\beta}$, $\hat{i}_{s\alpha}$, $\hat{i}_{s\beta}$ are estimated values of the rotor flux and stator currents, k is a positive convergence rate coefficient and V_α, V_β are discontinues functions of the current errors:

$$\begin{aligned} V_\alpha &= -V_0 sign(\bar{i}_{s\alpha}) = -V_0 sign(\hat{i}_{s\alpha} - i_{s\alpha}) \\ V_\beta &= -V_0 sign(\bar{i}_{s\beta}) = -V_0 sign(\hat{i}_{s\beta} - i_{s\beta}) \end{aligned} \tag{29}$$

and V_0>0.

The block scheme of this observer is presented in Fig. 8.

The serial SMO is based on current observer which is calculated by following formula:

$$\begin{bmatrix} \dot{\hat{i}}_{s\alpha} \\ \dot{\hat{i}}_{s\beta} \end{bmatrix} = \frac{x_M}{\sigma x_s x_r} \begin{bmatrix} \lambda_{r\alpha} \\ \lambda_{r\beta} \end{bmatrix} - \frac{r_s}{\sigma x_s} \begin{bmatrix} \hat{i}_{s\alpha} \\ \hat{i}_{s\beta} \end{bmatrix} + \frac{1}{\sigma x_s} \begin{bmatrix} u_{s\alpha} \\ u_{s\beta} \end{bmatrix} \tag{30}$$

and in this case the flux observer is

$$\begin{bmatrix} \dot{\hat{\psi}}_{r\alpha} \\ \dot{\hat{\psi}}_{r\beta} \end{bmatrix} = -\begin{bmatrix} \lambda_{r\alpha} \\ \lambda_{r\beta} \end{bmatrix} \tag{31}$$

$$\begin{aligned} \lambda_{r\alpha} &= -V_0 sign(\bar{i}_{s\alpha}) = -V_0 sign(\hat{i}_{s\alpha} - i_{s\alpha}) \\ \lambda_{r\beta} &= -V_0 sign(\bar{i}_{s\beta}) = -V_0 sign(\hat{i}_{s\beta} - i_{s\beta}) \end{aligned} \tag{32}$$

and $V_0 > 0$.

The scheme of this observer is presented in Fig. 9.

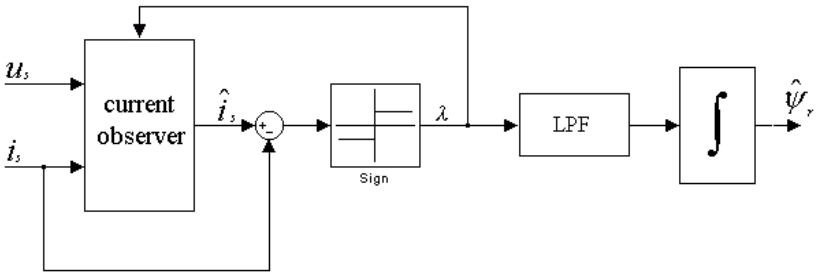

Fig. 9. Serial Sliding Mode Flux Observer

Knowing the estimated current, estimated rotor flux, and λ function values, we can express estimated rotor speed as [39]:

$$\hat{\omega}_m = \frac{\hat{\psi}_{r\beta} \cdot \lambda_{r\alpha} - \hat{\psi}_{r\alpha} \cdot \lambda_{r\beta} - \alpha x_M (\hat{i}_{s\beta}\hat{\psi}_{r\alpha} - \hat{i}_{s\alpha}\hat{\psi}_{r\beta})}{\hat{\psi}_{r\alpha}^2 + \hat{\psi}_{r\beta}^2} \tag{33}$$

4.3.2 SMO Results

The simulated and experimental oscillograms were obtained for FLC with space vector PWM and with Sliding Mode Flux Observers (Fig. 10).

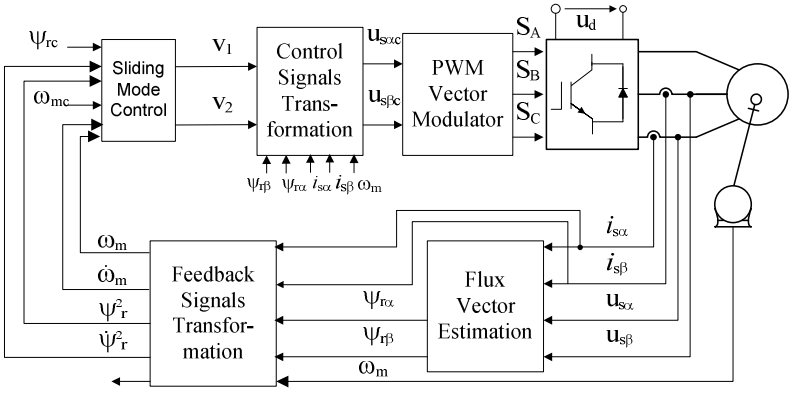

Fig. 10. Control of induction motor via feedback linearization with SM observers

Simulation of two described flux vector estimators is shown in Fig. 11 and Fig. 12 (steady state operation) and Fig. 13 and Fig. 14 (dynamic behaviour). It can be seen, that the parallel flux estimator has lower flux estimation error then serial one.

These oscillograms confirm the good dynamic behaviour of the system, and the correct operation of Sliding Mode Flux Observers. Additionally, using a serial SMO there is possible to obtain mechanical speed (33). It should be noted, that for estimation of the rotor flux in FLC scheme (Fig. 10) the parallel SM observer is used.

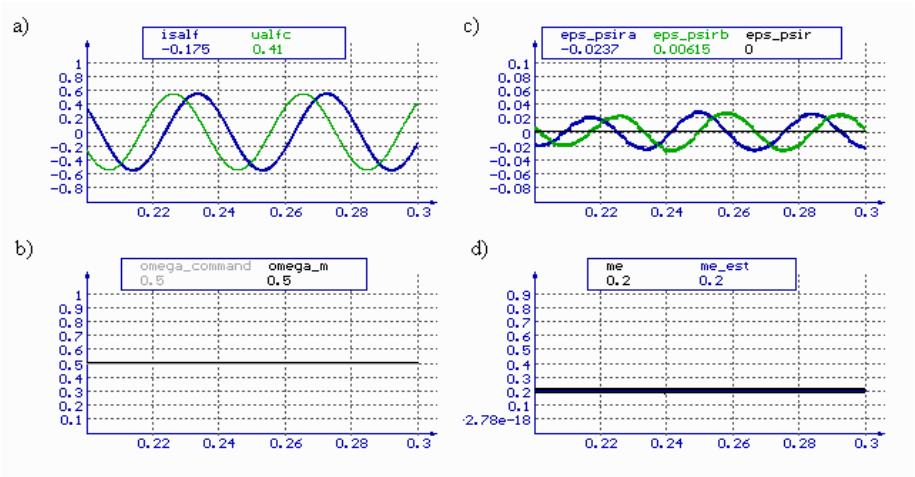

Fig. 11. Simulation results for steady state operation (ω_m=0.5 i m_L=0.2) for parallel SMO a) current and voltage, b) speed and speed command, c) flux estimation errors, d) electromagnetic torque

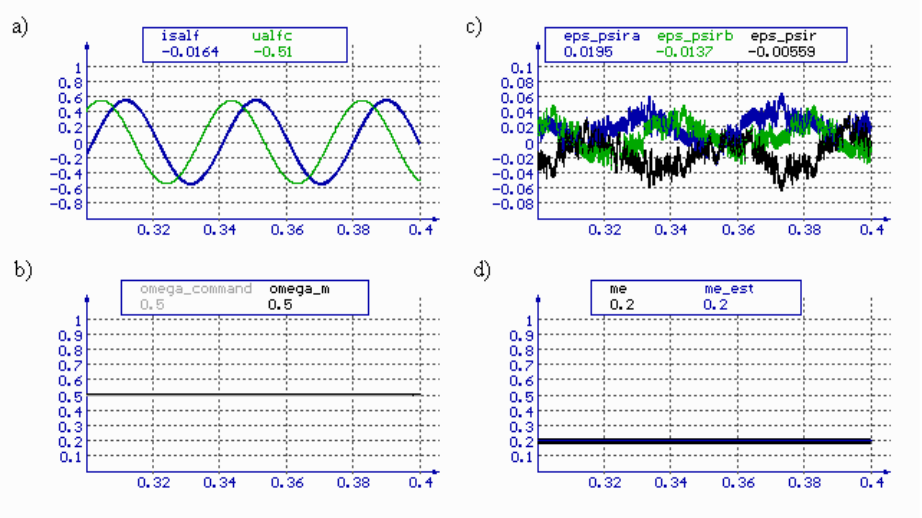

Fig. 12. Simulation results for steady state operation (ω_m=0.5 i m_L=0.2) for serial SMO a) current and voltage, b) speed and speed command, c) flux estimation errors, d) electromagnetic torque

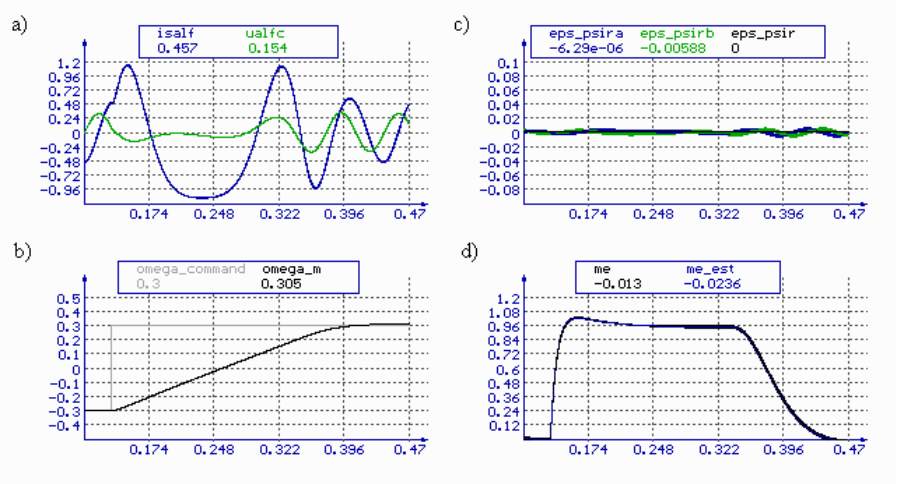

Fig. 13. Dynamic behavior. The speed reversal ω_m=-0,3 0,3 for parallel SMO. a) current and voltage, b) speed and speed command, c) flux estimation errors, d) electromagnetic torque.

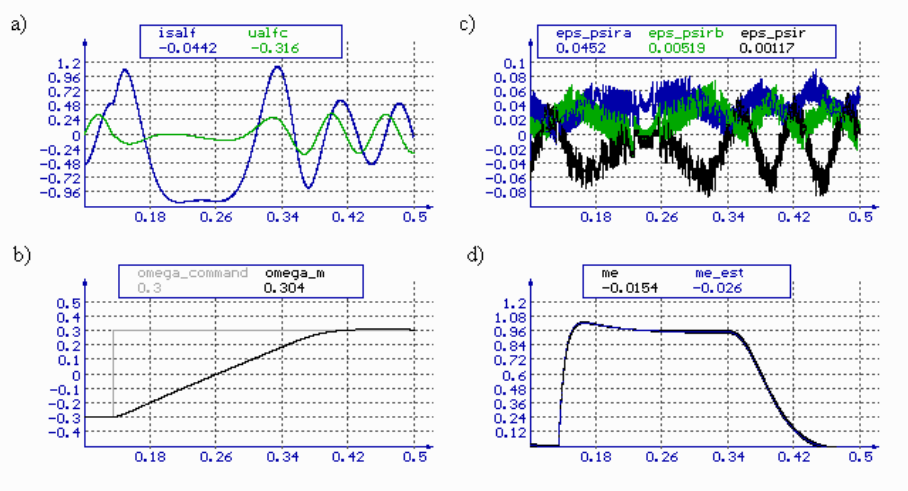

Fig. 14. Dynamic behavior. The speed reversal ω_m=-0,3 0,3 for serial SMO. a) current and voltage, b) speed and speed command, c) flux estimation errors, d) electromagnetic torque.

5 Summary and Conclusions

This chapter presents several applications of sliding mode control (SMC) and sliding mode observers (SMO) for voltage sourced inverter-fed feedback linearized induction motor drives. Main features and advantages of described algorithms can be summarized as follows.

- The feedback linearization control (FLC) guarantees the exactly decoupling of the motor speed and rotor flux control in both steady and transient states. Since in the FLC chosen variables (ω_m, ψ_r^2) and its derivative ($\dot{\omega}_m$, $\dot{\psi}_r^2$) are used as new coordinates - this approach is well suited for sliding mode speed and position controllers. The SMC is robust. Therefore, the combination of these two methods allows achieving the advantages of both algorithms: decoupled and robust control system.
- SMC assures direct control of inverter legs and allows using a simple table instead of performing complicated online calculation.
- In speed sensorless systems the good behaviour of rotor flux and mechanical speed SMOs is the important feature which allows achieving very good performances.

Thus, the sliding mode and feedback linearization, both together and separately, offer an interesting perspective in future research. These approaches are also a good alternative to other modern solutions, such as predictive and adaptive systems, and soft computing. SMOs are frequently used in drive systems. The SM based controllers work well in switching systems, and are recommended for systems which parameters are variable or not accurately set. Therefore, one can say that these approaches are very useful in a variety of applications, in particular, in the drive systems, robotics and power electronics.

Acknowledgments. It is our great honour and pleasure to dedicate this work to Prof. Okyay Kaynak to commemorate his life time achievements and services to profession. He is one of the most prominent and world-recognized researchers in the area of computational intelligence, intelligent control and mechatronics. Marian Kazmierkowski is grateful for a long help and cooperation in various activities in the IEEE Industrial Electronics Society, especially, as Prof. Kaynak was Vice president (1999-2001) and President (2002-2003).

References

[1] Blaschke, F.: The principle of field-orientation as applied to the Transvector closed-loop control system for rotating-field machines. Siemens Review 34, 217–220 (1972)
[2] Isidori, A.: Nonlinear Control Systems, 2nd edn. Communications and Control Engineering. Springer, Berlin (1989)
[3] Marino, R., Peresada, S., Valigi, P.: Adaptive partial feedback linearization of induction motors, in. In: Proceedings of the 29th Conference on Decision and Control, Honolulu, Hawaii, pp. 3313–3318 (1990)
[4] Marino, R., Valigi, P.: Nonlinear control of induction motors: a simulation study, in. In: Proceedings of the European Control Conference, Grenoble, France, pp. 1057–1062 (1991)
[5] Emelyanov, S.V.: Variable Structure Control Systems, Nauka, Moskwa (1967)
[6] Utkin, V.I.: Variable structure systems with sliding modes: a survey. IEEE Trans. on Automatic Control 22(2), 212–222 (1977)
[7] Utkin, V.I.: Sliding modes and their applications in variable structure systems, Moscow (1981)

[8] Itkis, Y.: Control Systems with Variable Structure. Wiley, New York (1976)
[9] Sobczuk, D.L.: Nonlinear control for induction motor. In: Proceedings of the PEMC 1994, pp. 684–689 (1994)
[10] Kazmierkowski, M.P., Sobczuk, D.L.: High performance induction motor control via feedback linearization. In: Proceedings of the ISIE 1995, pp. 633–638 (1995)
[11] Kazmierkowski, M.P., Sobczuk, D.L.: Sliding mode feedback linearized control of PWM inverter fed induction motor. In: Proceedings of the IEEE IECON Conference, pp. 244–249 (1996)
[12] Kazmierkowski, M.P., Krishnan, R., Blaabjerg, F.: Control in Power Electronics. Academic Press, San Diego (2002)
[13] Sobczuk, D.L., Malinowski, M.: Feedback Linearization Control of Inverter Fed Induction Motor –with Sliding Mode Speed and Flux Observers. In: Proceedings of the IECON 2006, Paris, France, pp. 1299–1304 (2006)
[14] Levantovsky, L.V.: Second order sliding algorithms: their realization. Dynamics of Heterogenous Systems, pp. 32–43. Inst. for System Studies, Moscow (1985)
[15] Levant, A. (LV Levantovsky) Sliding order and sliding accuracy in sliding mode control. International Journal of Control 58(6), 1247–1263 (1993)
[16] Sarpturk, S., Istefanopulos, Y., Kaynak, O.: On the stability of discrete-time sliding mode control systems. IEEE Trans. on Automatic Control 32(10), 930–932 (1987)
[17] Kaynak, O., Erbatur, K., Ertugrul, M.: The fusion of computationally intelligent methodologies and sliding-mode control-a survey. IEEE Transactions on Industrial Electronics 48(1), 4–17 (2001)
[18] Xinghuo, Y., Kaynak, O.: Sliding-Mode Control With Soft Computing: A Survey. IEEE Transactions on Industrial Electronics 56(9), 3275–3285 (2009)
[19] Kaynak, O.: Discrete – Time Sliding Mode Control in the Presence of System ucertainty. International Journal of Control 57(5), 1177–1189 (1993)
[20] Efe, M.O., Kaynak, O., Wilamowski, B.M.: Stable training of computationally intelligent systems by using variable structure systems technique. IEEE Transactions on Industrial Electronics 47(2), 487–496 (2000)
[21] Erbatur, K., Kaynak, O.: Use of adaptive fuzzy systems in parameter tuning of sliding-mode controllers. IEEE/ASME Trans. on Mechatronics 6(4), 474–482 (2001)
[22] Topalov, A.V., Kaynak, O.: Online learning in adaptive neurocontrol schemes with a sliding mode algorithm. IEEE Transactions on Systems, Man, and Cybernetics, Part B: Cybernetics 31(3), 445–450 (2001)
[23] Erbatur, K., Kaynak, O., Sabanovic, A.: A study on robustness property of sliding-mode controllers: a novel design and experimental investigations. IEEE Transactions on Industrial Electronics 46(5), 1012–1018 (1999)
[24] Singh, S.N.: Asymptotically decoupled discontinuous control of systems and non-linear aircraft maneuver. IEEE Trans. on Aeronautic Electronic Systems 25(3), 380–391 (1989)
[25] Hikita, H.: Servomechanisms based on sliding mode control. International Journal of Control 48(2), 435–441 (1988)
[26] Slotine, J.J., Canudas de Wit, C.: Sliding Observers for Robot Manipulators. Automatica 27(5), 859–864 (1991)
[27] Slotine, J.J., Sastry, S.S.: Tracking control of nonlinear systems using sliding surfaces with application to robot manipulators. International Journal of Control 38(2), 465–492 (1983)
[28] Kaynak, O., Harashima, F., Hashimoto, H.: Variable structure systems theory, as applied to sub-time optimal position control with an invariant trajectory. Trans. Inst. Elect. Eng. Jpn. E (104), 47–52 (1984)

[29] Sabanovic, A., Izosimov, D.B.: Applications of sliding modes to induction motor control. IEEE Trans. on Industry Applications 17(1), 41–49 (1981)
[30] Topalov, A.V., Cascella, G.L., Giordano, V., Cupertino, F., Kaynak, O.: Sliding Mode Neuro-Adaptive Control of Electric Drives. IEEE Transactions on Industrial Electronics 54(1), 671–679 (2007)
[31] Sabanovic-Behlilovic, N.: Šabanovic A, Jezernik K, Kaynak OM Current control in three-phase switching converters and AC electrical machines, in Proc. of the 20th International Conference on Industrial Electronics, Control and Instrumentation, IEEE IECON'94. In: Proc. of the 20th International Conference on Industrial Electronics, Control and Instrumentation, IEEE IECON 1994, vol. 1, pp. 581–586 (1994)
[32] Bartolini, G., Ferrara, A., Usai, E.: Applications of a sub-optimal discontinuous control algorithm for uncertain second order systems. Int. J. of Robust and Nonlinear Control 7(4), 299–310 (1997)
[33] Rashed, M., MacConnell, P.F.A., Stronach, A.F.: Nonlinear adaptive state-feedback speed control of a voltage-fed induction motor with varying parameters. IEEE Transactions on Industry Applications 42(3), 723–732 (2006)
[34] Orlowska-Kowalska, T., Dybkowski, M., Szabat, K.: Adaptive Sliding-Mode Neuro-Fuzzy Control of the Two-Mass Induction Motor Drive Without Mechanical Sensors. IEEE Trans. on Ind. Electronics 57(2), 553–564 (2010)
[35] Rashed, M., Goh, K.B., Dunnigan, M.W., MacConnell, P.F.A., Stronach, A.F., Williams, B.W.: Sensorless second-order sliding-mode speed control of a voltage-fed induction-motor drive using nonlinear state feedback. IEE Proceedings of Electric Power Applications 152(5), 1127–1136 (2005)
[36] El-Sousy, F.F.M.: Adaptive Dynamic Sliding-Mode Control System Using Recurrent RBFN for High-Performance Induction Motor Servo Drive. IEEE Transactions on Industrial Informatics 9(4), 1922–1936 (2013)
[37] Lascu, C., Boldea, I., Blaabjerg, F.: A Class of Speed-Sensorless Sliding-Mode Observers for High-Performance Induction Motor Drives. IEEE Transactions on Industrial Electronics 56(9), 3394–3403 (2009)
[38] Rao, S., Buss, M., Utkin, V.: Simultaneous State and Parameter Estimation in Induction Motors Using First- and Second-Order Sliding Modes. IEEE Transactions on Industrial Electronics 56(9), 3369–3376 (2009)
[39] Yongchang, Z., Zhengming, Z., Ting, L., Liqiang, Y., Wei, X., Jianguo, Z.: A comparative study of Luenberger observer, sliding mode observer and extended Kalman filter for Sensorless vector control of induction motor drives. In: Proceedings of the ECCE IEEE, pp. 2466–2473 (2009)
[40] Comanescu, M.: An Induction-Motor Speed Estimator Based on Integral Sliding-Mode Current Control. IEEE Transactions on Industrial Electronics 56(9), 3414–3423 (2009)
[41] Rehman, H., Derdiyok, A., Guven, M.K., Xu, L.: A new current model flux observer for wide speed sensorless control of an Induction Machine. IEEE Transaction on Power Electronics 17(6), 1041–1048 (2002)
[42] Gadoue, S.M., Giaouris, D., Finch, J.W.: MRAS Sensorless Vector Control of an Induction Motor Using New Sliding-Mode and Fuzzy-Logic Adaptation Mechanisms. IEEE Trans. on Energy Conversion 25(2), 394–402 (2010)
[43] Zhang, X.: Sensorless Induction Motor Drive Using Indirect Vector Controller and Sliding Mode Observer for Electric Vehicle. IEEE Transactions on Vehicular Technology 62(7), 3010–3018 (2013)

Tensor Product Model Transformation Based Sliding Mode Design for LPV Systems

Péter Korondi[1], Csaba Budai[1], Hideki Hashimoto[2], and Fumio Harashima[3]

[1] Budapest University of Technology and Economics,
Faculty of Mechanical Engineering,
Department of Mechatronics, Optics and Mechanical Engineering Informatics
Muegyetem rkp. 3., 1111 Budapest, Hungary
{korondi,budaicsaba}@mogi.bme.hu
[2] Dept. of EECE, Chuo University
1-13-27 Kasuga Bunkyo-ku, Tokyo 112-8551 Japan
hashimoto@elect.chuo-u.ac.jp
[3] Tokyo Metropolitan University
1-1Minami-Osawa Hachioji-Shi, Tokyo 192-0397, Japan
harashima-fumio@tmu.ac.jp

Abstract. The main contribution of this chapter is a new sliding mode design for nonlinear systems. This method is based on Tensor Product Model Transformation. It is partially extension and combination of the classical optimal manifold design for linear (or linearized) system and sector sliding mode control. This new approach enables a systematic design and decomposition of optimal sliding sector by the High Order Singular Value Decomposition (HOSVD)-based canonical description of a wide class of nonlinear systems. Two design examples and experimental results of a DSP-controlled single-degree-of-freedom motion-control system are presented.

Keywords: Sector sliding mode, Tensor Product model based transformation, LPV systems.

1 Introduction

Sliding mode control of variable structure systems has a special role in the field of robust control. On one hand, the exact description of sliding mode needs advanced mathematics, which was established by [3], [4] in the early sixty's. On the other hand, it is quite easy to implement in most engineering systems ([18], [22]), a simple relay is satisfactory in most cases. The main utility of sliding mode in control design problems is to decouple the highly coupled nonlinear dynamics, and to desensitize the performance to variations of the unknown system parameters.

The initial works on sliding mode control were followed by a large number of research papers in robotic manipulator control, in motor drive control and in the field of power electronics since they are typical variable structure systems.

X. Yu and M. Önder Efe (eds.), *Recent Advances in Sliding Modes*,
Studies in Systems, Decision and Control 24, DOI: 10.1007/978-3-319-18290-2_14

The sliding mode is applied for disturbance rejection [12] and substantial efforts placed in integration of sliding mode control with soft computing [36].

Nowadays sliding mode control is one of the most popular robust control methods for the engineering systems ([2], [30], [28]). However, despite the theoretical predictions of superb closed-loop system performance of sliding mode, some of the experimental work indicated that sliding mode has limitations in practice, due to the need for a high sampling frequency to reduce the high-frequency oscillation phenomenon about the sliding mode manifold, collectively referred to as "chattering". In most of the experimental work involving sliding mode ([35]), the effort spent on understanding the theoretical basis of sliding mode control is generally minimized, while a great deal of energy was invested in empirical techniques to reduce chattering.

Sliding sector was introduced by [5], [6], [24] as a promising method to reduce the chattering. Another approach of sliding sector is proposed by [31], [17]. The systematic sliding manifold design for linear systems was proposed by [25]. As an extension of that method, various linear control design methods based on state feedback (pole placement, LQ optimal, frequency shaped method, $\mathcal{H}_\infty$) were proposed for optimal sliding manifold design.

A new HOSVD-based canonical description of a wide class of nonlinear systems was proposed by [1] which enables a systematic controller design for a wide class of nonlinear systems. A new approach of sliding sector design will be proposed in this chapter, which enables a systematic and tractable design for linear parameter variant (LPV) systems as well. This chapter will propose and investigate the combination of three concepts: sector sliding mode control [31], the classical surface design for the linear systems [25] and the TP model transformation (see in Fig. 1)). The first initial works were published in [13], [15].

2 Brief Overview of a Sliding-Mode Controller Design for Linear Time Invariant Systems

The design of a sliding-mode controller consists of three main steps. First is the design of the sliding surface, the second step is the design the control law which holds the system trajectory on the sliding surface, and the third and key step is the chattering-free implementation.

2.1 Sliding Manifold Design for Linear Time Invariant Systems

The following linear time invariant (LTI) system is considered; first the reference signal is supposed to be constant and zero.

$$\begin{aligned} \dot{x}(t) &= Ax(t) + Bu(t) \\ y(t) &= Cx(t) + Du(t) \end{aligned}, \tag{1}$$

where $x(t) \in \mathbb{R}^n$ is the state, $u(t) \in \mathbb{R}^m$ is the input and $y(t) \in \mathbb{R}^l$ is the output with $l \leq n$ and A, B, C, D are constant matrices of suitable dimensions.

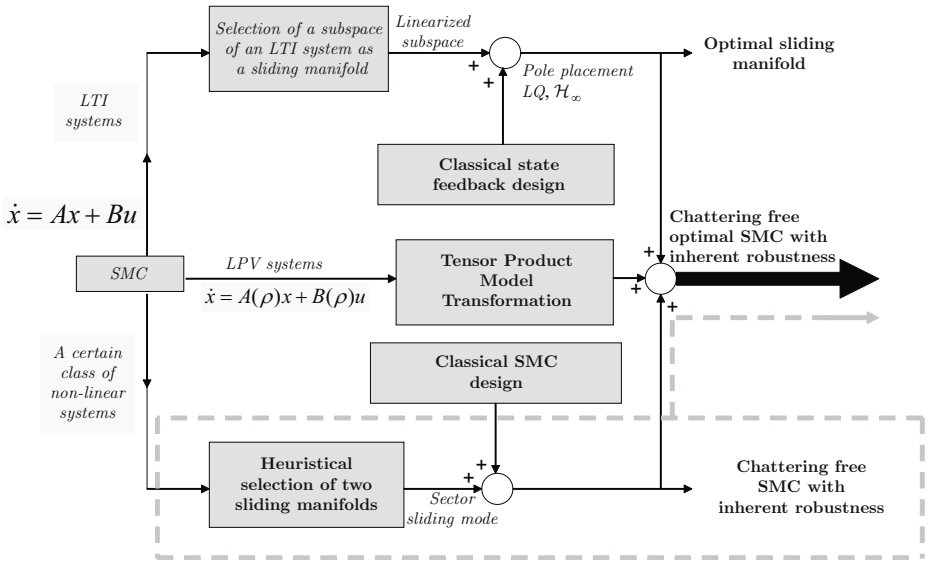

Fig. 1. Sliding mode control

The LTI system in Eq. (1) can be transformed to a regular form [20]:

$$\begin{bmatrix} \dot{x}_1 \\ \dot{x}_2 \end{bmatrix} = \begin{bmatrix} A_{11} & A_{12} \\ A_{21} & A_{22} \end{bmatrix} \begin{bmatrix} x_1 \\ x_2 \end{bmatrix} + \begin{bmatrix} 0 \\ B_2 \end{bmatrix} u, \tag{2}$$

where $x_1 \in \mathbb{R}^{n-m}$, $x_2 \in \mathbb{R}^m$.

The switching surfaces of the sliding mode, where the control vector components have discontinuities, can be written in the following form

$$\sigma = x_2 + Kx_1 \ , \quad \sigma \in \mathbb{R}^m. \tag{3}$$

When sliding mode occurs, $\sigma = 0$ and $x_2 = -Kx_1$. The design problem of the sliding surfaces can be regarded as a linear state feedback control design for the following subsystem:

$$\dot{x}_1 = A_{11}x_1 + A_{12}x_2. \tag{4}$$

In Eq. (4), x_2 can be considered as the input of the subsystem. A state feedback controller $x_2 = -Kx_1$ for this subsystem gives the switching surface of the whole variable structure system (VSS) controller. In sliding mode

$$\dot{x}_1 = (A_{11} - A_{12}K)\, x_1. \tag{5}$$

Various linear control design methods based on state feedback are applicable to the design of the switching surfaces. Recently, many papers have appeared on optimal sliding surface design.

Table 1. Summary of Optimal Switching Surface Design

Method	Cost Function	Design Parameter
LQ [27],[26]	$J = \int_0^\infty \left(x_1(t)^{\mathrm{T}} Q x_1(t) + x_2^{\mathrm{T}} R x_2\right) \mathrm{d}t$	Q R
Frequency shaped LQ [33]	$J = \frac{1}{2\pi} \int_{-\infty}^{\infty} \left(x_1^*(j\omega) Q x_1(j\omega) + x_2^*(j\omega) R(\omega^2) x_2(j\omega)\right) \mathrm{d}\omega$	Q $R(\omega^2) = W_2^*(j\omega) W_2(j\omega)$
$\mathcal{H}_2, \mathcal{H}_\infty$ [11]	$J = \|G_{zw}\|_2, \|G_{zw}\|_\infty$ (G_{zw} is the transfer matrix of the generalized plant)	weights of control input and error, ...

Linear Quadratic Approach. According to LQ design [27],[26], the cost function (6) is minimized by solving the well known Riccati equation to achieve the optimal feedback gain for subsystem (4):

$$J = \int_{t_s}^{\infty} (x_1^{\mathrm{T}} Q x_1 + 2 x_1^{\mathrm{T}} N x_2 + x_2^{\mathrm{T}} R x_2)\, \mathrm{d}t. \tag{6}$$

where t_s is the time at which sliding mode begins. (For simplicity, $N = 0$ is assumed.) The LQ optimal sliding surface is given by

$$\sigma = x_2 + K_{LQ} x_1, \quad K_{LQ} = R^{-1} A_{12}^{\mathrm{T}} P, \tag{7}$$

where $P > 0$ is a unique solution of the following Riccati equation

$$P A_{11} + A_{11}^{\mathrm{T}} P - P A_{12} R^{-1} A_{12}^{\mathrm{T}} P + Q = 0. \tag{8}$$

Frequency Shaped LQ Approach. The frequency shaped sliding mode [33] comes from frequency shaped LQ method [7]. Frequency shaped LQ approach is based on frequency dependent weights. The cost function (6) can be written in the frequency domain using Perseval's theorem as

$$J = \frac{1}{2\pi} \int_{-\infty}^{\infty} x_1^{\mathrm{T}}(j\omega) Q x_1(j\omega) + x_2^{\mathrm{T}}(j\omega) R x_2(j\omega)\, \mathrm{d}\omega. \tag{9}$$

In the time domain (6), Q and R are constant matrices. If instead of a constant R, a frequency dependent weight matrix $R(\omega^2)$ is introduced, control inputs for certain frequencies can be amplified or suppressed. We can choose R to have high-pass characteristics for reduction of high frequency control inputs of the subsystem (4).

This idea is realized using state space representation. The frequency dependent weight $R(\omega^2)$ must be a rational function of ω^2 to solve this problem [7]. The transfer matrix $W(s)$ is defined as

$$R(\omega^2) = W^*(j\omega) W(j\omega), \tag{10}$$

where $W^*(s)$ stands for the conjugate transpose of $W(s)$. The subsystem (4) should be augmented by the states (written in the vector x_w) of $W(s)$. $W(s)$ has the following state space representation

$$\begin{aligned} \tilde{u} &= W(s)x_2 \\ \tfrac{\mathrm{d}}{\mathrm{d}t}x_w &= A_w x_w + B_w x_2. \\ \tilde{u} &= C_w x_w + D_w x_2 \end{aligned} \tag{11}$$

Then the cost function (9) with a frequency dependent weight matrix $R(\omega^2)$ can be rewritten in the time domain as

$$J = \int_0^\infty x_a^{\mathrm{T}} Q_a x_a + 2x_a^{\mathrm{T}} N_a x_2 + x_2^{\mathrm{T}} R_a x_2 \,\mathrm{d}t, \tag{12}$$

where $\dot{x}_a = A_a x_a + B_a x_2$, $x_a = \begin{bmatrix} x_w & x_1 \end{bmatrix}^{\mathrm{T}}$, $A_a = \mathrm{diag}(A_w, A_{11})$, $B_a = \begin{bmatrix} B_w & A_{12} \end{bmatrix}^{\mathrm{T}}$, $Q_a = \mathrm{diag}(C_w^{\mathrm{T}} C_w, Q)$, $N_a = \begin{bmatrix} C_w^{\mathrm{T}} D_w & 0 \end{bmatrix}^{\mathrm{T}}$, $R_a = D_w^T D_w$.

Minimization of this cost function with cross term between state and control input is formulated as solving following Riccati equation

$$P_a A_a + A_a^{\mathrm{T}} P_a - (P_a B_a + N_a) R_a^{-1} (B_a^{\mathrm{T}} P_a + N_a^{\mathrm{T}}) + Q_a = 0. \tag{13}$$

The optimal switching plane is written using the solution of this Riccati equation as

$$\sigma = x_2 + K_{FS} x_a, \quad K_{FS} = R_a^{-1}(B_a^{\mathrm{T}} P_a + N_a^{\mathrm{T}}). \tag{14}$$

$\mathcal{H}_\infty$ Optimal Control Approach. Recently, linear control theory is well developed especially in the field of robust control. $\mathcal{H}_\infty$ optimal control theory is an excellent result of this development. Hashimoto [11] introduces $\mathcal{H}_\infty$ control methods for the optimal sliding surface design based on $\mathcal{H}_\infty$ norm.

The control goal is formulated through a norm minimization of the generalized plant $G(j\omega)$, where $\mathcal{H}_\infty$ norms are used to formulate the cost function. If $G(j\omega)$ is a stable transfer matrix in the frequency domain, than the $\mathcal{H}_\infty$ norms are

$$\|G(s)\|_\infty = \sup_\omega \sigma_{\max}[G(j\omega)]. \tag{15}$$

Various linear control design methods based on state feedback (pole placement, LQ optimal, frequency shaped method, $\mathcal{H}_\infty$) were proposed for (5) to design the switching surfaces in the last decade. The main problem is that these methods are not suitable for a non-linear system which is more challenging. The solution can be the Tensor Product model transformation.

2.2 Control Law

To ensure that the system remains in the sliding mode ($\sigma = 0$) the condition

$$\dot{\sigma}\sigma < 0 \tag{16}$$

should hold. The simplest control law which can lead to sliding mode is the relay:

$$u = M \cdot \text{sign}(\sigma) \tag{17}$$

This is easy to realize by power electronic circuits. The relay type of controller can directly control the semiconductor switching elements, but it does not ensure the existence of sliding mode for the whole state space, and relatively big values of M is necessary which might cause a severe chattering phenomenon. This control law is preferable if the controller's sample frequency is nearly equal to the maximum switching frequency of semiconductor switching elements.

If sliding mode exists then there is a continuous control, so-called "equivalent" control, u_{eq}, which can hold the system on the sliding manifold. It can be calculated from $\dot{\sigma} = 0$

$$\begin{aligned} \dot{\sigma} &= \dot{x}_2 + K\dot{x}_1 = 0 \\ \dot{\sigma} &= A_{21}x_1 + A_{22}x_2 + B_2u + K(A_{11}x_1 + A_{12}x_2) = 0 \end{aligned} \tag{18}$$

u_{eq} can be expressed from (18)

$$u_{eq} = -\left((A_{21} + KA_{11})x_1 + (A_{22} + KA_{12})x_2\right)/B_2 \tag{19}$$

In the practice, there is never perfect knowledge of the whole system and its parameters. Only $\hat{u}_{eq}$, the estimation of u_{eq}, can be calculated. Since u_{eq} does not guarantee the convergence to the switching manifold in general, a discontinuous term is usually added to $\hat{u}_{eq}$.

$$u = \hat{u}_{eq} + M \cdot \text{sign}(\sigma) \tag{20}$$

The control laws (20) do not control the semiconductor switching elements directly; additional PWM is needed. Usually, this is no problem since the switching frequency of the semiconductor elements can be much higher than the sampling frequency of the fastest digital controller.

2.3 Chattering Free Implementation, Sector Sliding Mode

The chattering in the basic sliding mode control is essentially due to the requirement that the system state must stick to the switching surface. (detailed in [31]) There are several solutions for elimination of chattering. Here the sector sliding mode is discussed since it can be extended for TP model based sliding mode control.

Obviously this requirement is too restrict when only finite switching rate is available. Replacing the switching surface to the sliding sector may enable the system state to move continuously.

To implement the proposed approach, two sliding surfaces are defined first

$$\sigma_r = x_2 + K_r x_1 = 0 \quad r = 1, 2 \tag{21}$$

Then the two sliding surfaces divide the whole state space into three regions defined as

Definition 1. *Classical sector*

$$\begin{aligned}\mathcal{R}_1 &= \{x \,|\, \sigma_1(x) > 0 \text{ and } \sigma_2(x) > 0\}\\ \mathcal{R}_2 &= \{x \,|\, \sigma_1(x) < 0 \text{ and } \sigma_2(x) < 0\}\\ \mathcal{R}_3 &= \{x \,|\, \sigma_1(x)\sigma_2(x) \leq 0\}\end{aligned} \tag{22}$$

Here the region $\mathcal{R}_3$ is the sliding sector.

The control strategy of the proposed modified sliding mode control method is

$$u = u_{eq} + u_d, \tag{23}$$

where u_{eq} is the continuous "equivalent" and u_d is defined as

$$u_d = \begin{cases} M \text{sign}\left(\frac{\sigma_1+\sigma_2}{2}\right) & \mathbf{x} \in \mathcal{R}_1 \cup \mathcal{R}_2 \\ M\frac{\sigma_1+\sigma_2}{|\sigma_1|+|\sigma_2|}, & \mathbf{x} \in \mathcal{R}_3 \end{cases} \tag{24}$$

As shown in Fig. 2, let's represent the sector by the a surface of

$$\sigma = x_2 + Kx_1 = 0, \tag{25}$$

where $K = \frac{K_1+K_2}{2}$.

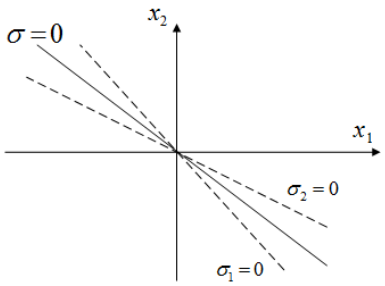

Fig. 2. Sliding sectors (In case of $n = 2$)

3 Sliding-Mode Controller Design for Linear Parameter Varying (LPV) System

The three main steps of sliding mode design discussed in the previous chapter are extended here for LPV systems.

3.1 Sliding Surface Design Based on Tensor Product Model Transformation

This section is intended to discuss the fundamental of tensor product (TP) models. Consider a parametrically varying dynamical system

$$\begin{aligned} \dot{x}(t) &= A(p(x))x(t) + B(p(x))u(t) \\ y(t) &= C(p(x))x(t) + D(p(x))u(t) \end{aligned}, \tag{26}$$

with input $u\,(t)$, output $y\,(t)$ and state vector $x\,(t)$. The system matrix

$$S(p(x)) = \begin{pmatrix} A(p(x)) & B(p(x)) \\ C(p(x)) & D(p(x)) \end{pmatrix}, \quad S(p(x)) \in \mathbb{R}^{(n+1)\times(n+1)} \tag{27}$$

is a parameter-varying object, where $p(x) \in \Omega$ is time varying N-dimensional parameter vector, and is an element of the closed hypercube $\Omega = [a_1, b_1] \times [a_2, b_2] \times \cdots \times [a_N, b_N] \in \mathbb{R}^N$. The parameter $p(x)$ includes some elements of $x(t)$.

The TP model transformation starts with the given LPV model (27). First a numerical discretization is performed over a hyper-rectangular grid on Ω. The system is known in the discrete points and an interpolation technique is necessary between the discrete points. The next step is reduction of the discrete model by High Order Singular Value Decomposition [1], [21], which results in the TP model representation:

$$S(p(x)) = \sum_{r=1}^{R} w_r(p(x))S_r, \tag{28}$$

where $w_r(p(x))$ are weighting coefficients and

$$S_r = \left(\begin{pmatrix} A_{11r} & A_{12r} \\ A_{21r} & A_{22r} \end{pmatrix} \begin{pmatrix} 0 \\ B_{2r} \end{pmatrix} \right) \begin{pmatrix} C_r & D_r \end{pmatrix}. \tag{29}$$

There are several selections of $w_r(p(x))$ and S_r, from now on the canonical form is applied [1] when

$$w_r\,(p\,(x)) \in [0, 1] \quad \text{and} \quad \sum_{r=1}^{R} w_r(p(x)) = 1. \tag{30}$$

For further details about TP model transformation, refer to [1].

Since there are R system components S_r a sliding surface is designed for each of them.

$$\sigma_r = x_2 + K_r x_1 = 0. \tag{31}$$

There are three cases:

- The nonlinearity is only inside of subspace (4)
- The nonlinearity is only outside of subspace (4)
- The nonlinearity is inside and outside of subspace (4)

The actual sliding mode design depends on the above cases.

3.2 Control Law for Tensor Product Model Based Sliding Mode

If the nonlinearity is only inside of subspace (4), than the same poles are selected for each subspace (4) and the sliding surfaces are calculated for the selected poles in the each component system.

If the nonlinearity is only outside of subspace (4), than the equivalent control is selected in such a way that

$$\hat{u}_{eq} = u_{eq1} = u_{eq2} \cdots = u_{eqR}, \tag{32}$$

where u_{eqi} is calculated for each system S_r according to (19)

$$u_{eqi} = -\frac{(A_{21i} + K_i A_{11i})x_1 + (A_{22i} + K_i A_{12i})x_2}{B_{2i}}. \tag{33}$$

Note, u_{eqi} is not the real equivalent control signal, and (32) itself cannot definite the sliding surface.

If the nonlinearity is inside and outside of subspace (4), than the combination of the above two solution is applied.

3.3 Sliding Mode Design Based on Tensor Product Transformation

The sliding sector design method can be extended for nonlinear systems given in the form of (28).

The definition of the three regions can be extended in the following way

Definition 2. *TP based sector*

$$\begin{aligned} \mathcal{R}_1 &\in \{x \,|\, \bigcap_{r=1}^{R} \sigma_r(x) < 0\} \\ \mathcal{R}_2 &\in \{x \,|\, \bigcap_{r=1}^{R} \sigma_r(x) > 0\} \\ \mathcal{R}_3 &\in \{x \,|\, \bigcup_{i,j}^{R} \sigma_i(x)\sigma_j(x) \leq 0\} \end{aligned} \tag{34}$$

Here the region $\mathcal{R}_3$ is a sliding sector. $R = 5$ in case of Fig. 3.

A modified version of (24) is applied

$$u = u_c + u_d \tag{35}$$

where u_c is a feed forward compensation term based on the estimation of the "equivalent" control according to (4). u_d is a switching term to suppress the system parameter variations and disturbances.

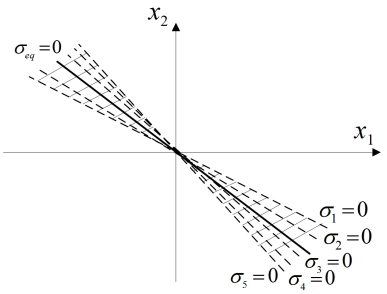

Fig. 3. Sliding sectors (In case of $n = 2$ and $R = 5$)

$$\begin{aligned} u_c &= \hat{u}_{eq} \\ u_d &= \begin{cases} -M\text{sign}\left(\sigma_{eq}\right) & \text{if } \; x \in \mathcal{R}_1 \cup \mathcal{R}_2 \\ -M\left(\frac{\sigma_{eq}}{\sum_{r=1}^{R} w_r(p(X_s)|\sigma_r|}\right) & \text{if } \; x \in \mathcal{R}_3 \end{cases} \\ \sigma_{eq} &= w_r(p(X_s)\sigma_r) \end{aligned} \tag{36}$$

where X_s is the value of x at a properly selected point of the sliding sector and σ_{eq} is the equivalent surface of the sliding sector.

3.4 Robustness of the Proposed Method

The stability of the proposed sliding sector can be checked by the Lyapunov function candidate

$$V = \frac{\sigma_{eq}^2}{2} \tag{37}$$

To define $\dot{V}$, the value of $\dot{\sigma}_{eq}$ is necessary. Outside of the sector (in $\mathcal{R}_1$ and $\mathcal{R}_2$), according to (19), (36) and the (30)

$$\dot{\sigma}_{eq} = -\sum_{r=1}^{R} w_r(p(X_s)B_{2r}M\text{sign}\left(\sigma_{eq}\right) \quad \dot{V} = \sigma_{eq}\dot{\sigma}_{eq} < 0 \tag{38}$$

According to (38), $\dot{V}$ is always negative outside of the sector. It means the system trajectory enters into the sector in finite time. In side of the sector

$$\begin{gathered} \dot{\sigma}_{eq} = -\sum_{r=1}^{R} w_r(p(X_s)B_{2r}M\frac{\sigma_{eq}}{\sum_{r=1}^{R} w_r(p(X_s)|\sigma_r|} \\ \dot{V} = \sigma_{eq}\dot{\sigma}_{eq} \leq 0 \end{gathered} \tag{39}$$

Since $\dot{V} = 0$ implies $\sigma_{eq} = 0$, the sector sliding mode inherits the most important characteristic of classical sliding mode. As the system state approaches the middle of the sector the absolute value of the discontinuous term is getting smaller that ensures the chattering free applications.

4 Applications

The experimental system consists of a conventional DC servo gear motor with encoder feedback and variable inertia load coupled by a relatively rigid shaft, as shown in Fig. 4 and the structure can be seen in Fig. 5. The controller is implemented using a DSP as the computation engine. The main source of nonlinearity is the friction. The harmonic gear connected to the motor has relative big friction, which is modeled in two different ways. In case of the first model, the nonlinearity (the friction term) is only outside of subspace (4). In case of the second model, the nonlinearity (the friction term) is only inside of subspace (4). Since the same system is used the results of two cases are quite similar. The aim of the two solutions is to show examples for two basic cases, when the friction term is only inside or outside of subspace (4). The main difference between the two approaches is that the armature inductance of the servo motor is ignored in the first case and it is calculated in the second case. In the course of control design, the flexibility of the shaft is ignored. The effect of $mass_d$ is considered as a disturbance. A TPTool (`http://tptool.sztaki.hu`), a free MATLAB Toolbox for Tensor-Product Model Transformation is used for numeric calculation. The toolbox is available for download together with documentation and examples.

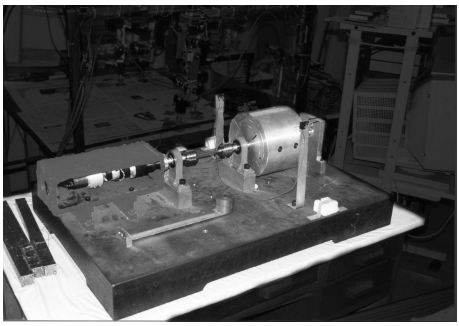

Fig. 4. The experimental system

4.1 The Friction Term Is Only Outside of Subspace (4)

System Equations. The state variables are the shaft position θ and the shaft angular velocity ω, the control signal u is the motor voltage.The model calculated

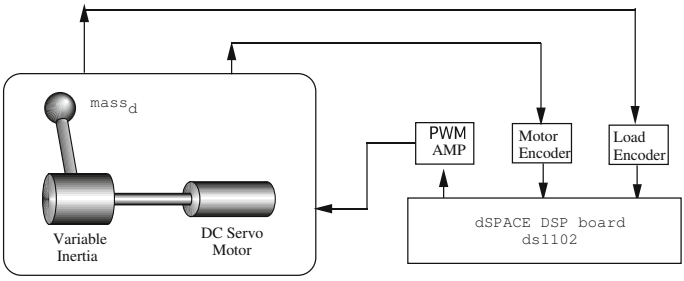

Fig. 5. System structure

from the nominal parameters of the system is as follows (when the friction is ignored)

$$\begin{pmatrix} \dot{\theta} \\ \dot{\omega} \end{pmatrix} = \begin{pmatrix} 0 & 1 \\ 0 & -76 \end{pmatrix} \begin{pmatrix} \theta \\ \omega \end{pmatrix} + \begin{pmatrix} 0 \\ 18 \end{pmatrix} u \tag{40}$$

Coulomb has nonlinear characteristic, which is modeled in the following way

$$u = u' \left(1 - \frac{1}{|u'| + 2.7} \right) \tag{41}$$

where u' is the control signal of the original linear system. The first part of the correction of the control signal in (41) is achieved empirically. It is quite straightforward to explain. The Coulomb friction torque is independent of the input voltage of the motor. If the input voltage is small the effect of the Coulomb friction is relative big. As you increase the absolute value of the motor voltage, the effect of Coulomb friction is getting relatively smaller and smaller. The second (dynamic) term is necessary because of TP model transformation.

The system matrix

$$S(p(x)) = \begin{pmatrix} 0 & 1 & 0 \\ 0 & -76 & p(x) \\ 1 & 0 & 0 \end{pmatrix}, \tag{42}$$

where

$$p(x) \equiv p(u) = 18 - \frac{18}{2.7\mathrm{abs}(u) + 1}. \tag{43}$$

The parameter vector is

$$\Omega = [u_{\min}, u_{\max}] = [-22, 22]. \tag{44}$$

Since equidistant sampling is applied and the sampling density must be high around zero voltage, the interval Ω is sampled at 1370 grid points. The sampled system is arranged into a tensor

$$S_u = \begin{pmatrix} S_1 & S_2 & \cdots & S_{1370} \end{pmatrix} \in \mathbb{R}^{137 \times (3 \times 3)} \tag{45}$$

where tensor S_u has only two singular values (1061.6 and 31.7). That is why the above nonlinear system can be modelled by weighted combination of two linear systems

$$S_1 = \begin{pmatrix} 0 & 1 & 0 \\ 0 & -76 & 17.7 \\ 1 & 0 & 0 \end{pmatrix} \quad \text{and} \quad S_2 = \begin{pmatrix} 0 & 1 & 0 \\ 0 & -76 & 13.9 \\ 1 & 0 & 0 \end{pmatrix}. \tag{46}$$

The two weighing coefficients as a function of the control are shown in Fig. 6.

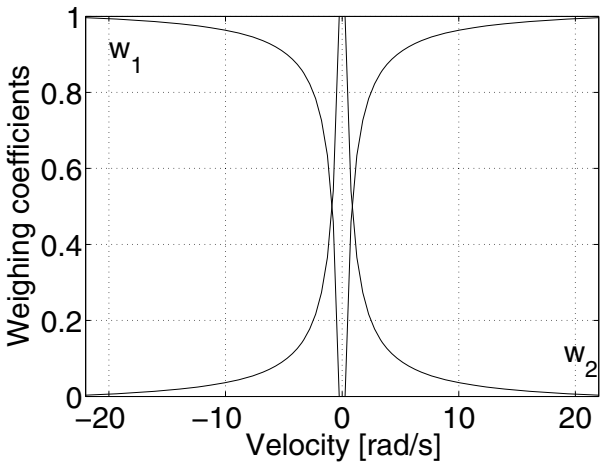

Fig. 6. The weighing coefficients as a function of the control signal

Sliding Surface Design. Since a second-order model is applied, the sliding "surface" is a sliding line that can be described by a scalar parameter K_r in (31). The subspace of the sliding surface (5) is

$$\omega = -K_r\theta \;\text{ where }\; r = 1, 2 \tag{47}$$

The sliding surface is

$$\sigma_r = \omega + K_r\theta = 0 \;\text{ where }\; r = 1, 2 \tag{48}$$

According to (36) and (40)

$$\hat{u}_{eq} = -\frac{(-76 + K_r)x_2}{B_{2r}}. \tag{49}$$

where the values of B_{2r} can be read from (46). One equation cannot definite two parameters. The sliding surface is carefully designed (i.e. pole K is selected according to [16]) to satisfy both fast response both vibration suppression for the both systems. $K = 15$ in [16], the sector around that value is selected. If $K_1 = 8$ than $K_2 = 22$ according to (49) which is acceptable. X_p is selected in such a way that $w_1(p(X_s)) = 0.5$, $w_2(p(X_s)) = 0.5$.

4.2 The Friction Term Is Only Inside of Subspace (4)

System Equations. The state variables are the shaft position, θ, the shaft angular velocity, ω, and the armature current, i, the control signal is the motor voltage u.

$$\begin{pmatrix} \dot{\theta} \\ \dot{\omega} \\ \dot{i} \end{pmatrix} = \begin{pmatrix} 0 & 1 & 0 \\ 0 & 0 & \frac{K_t}{J} \\ 0 & -\frac{K_\omega}{L_a} & -\frac{R_a}{L_a} \end{pmatrix} \begin{pmatrix} \theta \\ \omega \\ i \end{pmatrix} + \begin{pmatrix} 0 \\ 0 \\ \frac{1}{L_a} \end{pmatrix} u \tag{50}$$

Here J is the inertia of the motion control system, K_t and K_ω are the torque constant and the back-EMF constant, respectively, R_a and L_a are the resistance and the inductance of the armature. The effect of $mass_d$ is considered as a disturbance. The viscous, Coulomb and Stribeck frictions were modelled in the following way,

$$\dot{\omega} = -\underbrace{\frac{F_v}{J}\omega}_{\text{viscous term}} - \underbrace{\left(\frac{2F_c}{J(1+e^{-500\omega})} - \frac{F_c}{J}\right)}_{\text{Coulomb term}} - \underbrace{\left(\frac{\frac{2(F_s-F_C)}{1+e^{-500\omega}} - (F_s-F_C)}{J(1+(\omega/\omega_s)^2)}\right)}_{\text{Stribeck term}} + \underbrace{\frac{K_t}{J}i}_{\substack{\text{term for} \\ \text{electric} \\ \text{torque}}} \tag{51}$$

where the second two terms are nonlinear and the signum function is approximated as

$$\text{sign}(\omega) = \frac{2}{(1+e^{-500\omega})} - 1 \tag{52}$$

F_v was given in the data sheet of the servo motor, F_c, F_s and ω_s were determined through testing. Fig. 7 shows the simulated Stribeck curve. The model calculated from the rated parameters of the system is:

$$\begin{pmatrix} \dot{\theta} \\ \dot{\omega} \\ \dot{i} \end{pmatrix} = \begin{pmatrix} 0 & 1 & 0 \\ 0 & p(t) & 42 \\ 0 & -4600 & -2450 \end{pmatrix} \begin{pmatrix} \theta \\ \omega \\ i \end{pmatrix} + \begin{pmatrix} 0 \\ 0 \\ 1100 \end{pmatrix} u$$
$$\mathbf{S}(p(t)) = \begin{pmatrix} 0 & 1 & 0 & 0 \\ 0 & p(t) & 42 & 0 \\ 0 & -4600 & -2450 & 1100 \\ 1 & 0 & 0 & 0 \end{pmatrix} \tag{53}$$

where

$$p(t) \equiv p(\omega) = -\frac{F_v}{J} - \frac{2F_c}{\omega J(1+e^{-500\omega})} - \frac{F_c}{\omega J} - \frac{\frac{2(F_s-F_C)}{1+e^{-500\omega}} - (F_s-F_C)}{\omega J(1+(\omega/\omega_s)^2)} \tag{54}$$

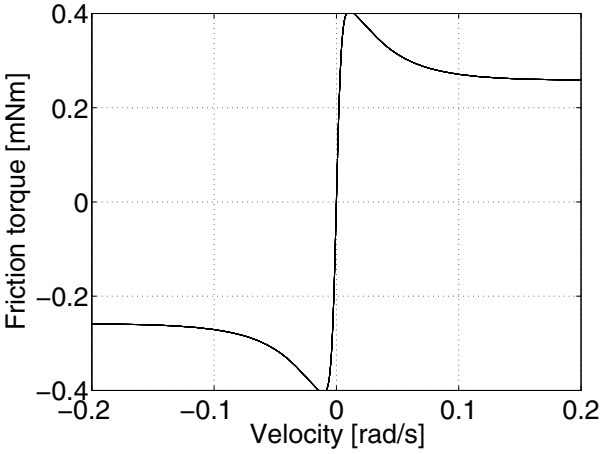

Fig. 7. Simulated Stribeck curve

where $\Omega = [\omega_{min}, \omega_{max}] = [-4, 4]$ Since equidistant sampling is applied and the sampling density must be high around zero velocity, the interval Ω is sampled at 1370 grid points (even number is necessary to avoid division by zero). The sampled system is arranged into a tensor

$$\mathbf{S}_\omega = \left(\mathbf{S}^1 \; \mathbf{S}^2 \; \cdots \; \mathbf{S}^{1370} \right) \in \mathbb{R}^{1370 \times (4 \times 4)} \tag{55}$$

where tensor , S_ω, has only two singular values ($197.32 * 10^3$ and $10.61 * 10^3$). That is why the above nonlinear system can be modelled by two linear systems (it is a significant reduction of $\mathbf{S}_\omega \in \mathbb{R}^{1370 \times 4 \times 2}$):

$$\mathbf{S}^1(p(t)) = \begin{pmatrix} 0 & 1 & 0 & 0 \\ 0 & -19.3 & 42 & 0 \\ 0 & -4600 & -2450 & 1100 \\ 1 & 0 & 0 & 0 \end{pmatrix} \tag{56}$$

$$\mathbf{S}^2(p(t)) = \begin{pmatrix} 0 & 1 & 0 & 0 \\ 0 & -3151.8 & 42 & 0 \\ 0 & -4600 & -2450 & 1100 \\ 1 & 0 & 0 & 0 \end{pmatrix} \tag{57}$$

The weightings ($w_1(\omega)$ and $w_2(\omega)$) are functions of the velocity as shown in Fig. 8 The shape of the weighting functions is quite straightforward to explain. The nonlinear friction terms are modelled using a varying viscosity coefficient, which is represented by the s_{22} element in the system matrix. S_1 with small viscous coefficient dominates at high speed, where the Coulomb friction is relatively small. The S_2 system matrix with very large viscous coefficient dominates at low speed, where the Coulomb friction is comparatively large.

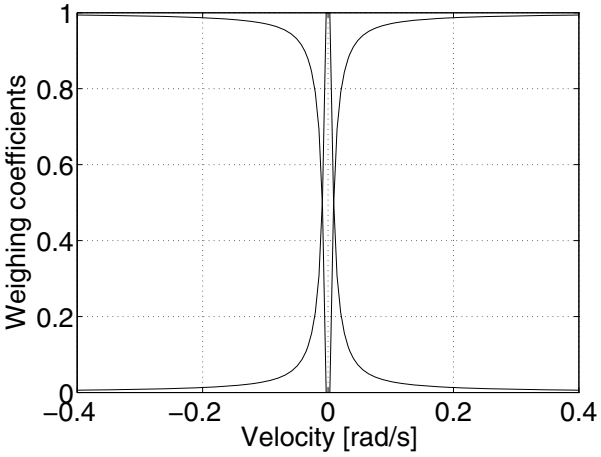

Fig. 8. The weighting coefficients as function of velocity

The subspace of the sliding surface (5) is

$$\begin{pmatrix} \dot{\theta} \\ \dot{\omega} \end{pmatrix} = \begin{pmatrix} 0 & 1 \\ 0 & s_{22} \end{pmatrix} \begin{pmatrix} \theta \\ \omega \end{pmatrix} - \begin{pmatrix} 0 \\ 42 \end{pmatrix} \begin{pmatrix} k_1 & k_2 \end{pmatrix} \begin{pmatrix} \theta \\ \omega \end{pmatrix} \tag{58}$$

The state feedback controller is designed by pole placement. The poles of the sliding surface are selected as

$$Poles = (-15 \quad -1500) \tag{59}$$

The first pole is related to the closed loop "mechanical" time constant.
Using the MATLAB toolbox for pole placement

$$\begin{aligned} K_1 &= (5359 \;\; 357) \\ K_2 &= (5359 \;\; 433) \end{aligned} \tag{60}$$

Because of that big values the effect of the third state variable i is ignorable according to (31).

4.3 Experimental Results

The normalized form of the two sliding sectors in the two design examples are quite similar as it was expected. There is no significant difference in the experimental results in the two cases that is why the experimental results of the first case and a conventional controller are compared in Fig. 9-Fig. 13.

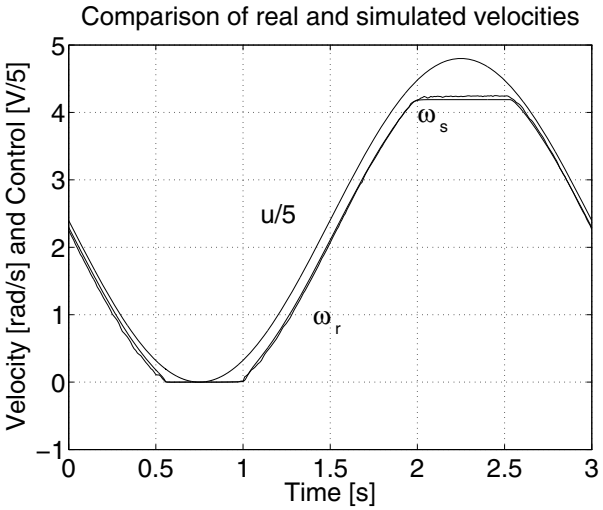

Fig. 9. The open loop response

The nonlinearity of the system is borne from the huge friction of the harmonic gear. To verify the friction model, the real and simulated velocities (ω_r, ω_s) are compared in Fig. 9, where the input voltage of the motor is a shifted sinusoid with amplitude of 12 V (open loop response). Note, the voltage input is divided by 5 to use the same scale as the speed. It can be seen in the Fig. 9, if the motor is in standstill, at least 2 V should be switched across the motor to start it. On the other hand, the motor is stick, if the input voltage is under 1.2 V. The power electronic PWM unit is saturated at 22 V. It is also a kind of nonlinearity which could be handled using a TP model. Because this chapter concentrates on sliding sector design, only the nonlinearity of the friction is handled by TP model.

The chattering of the classical sliding mode and the chattering free response of the sector sliding mode control can be compared in Fig. 10. and Fig. 11.

After entering into the sector, the trajectory reaches the surface ($\sigma_{eq} = 0$) gradually and smoothly, in case of sector sliding mode. The phase trajectory of the conventional sliding mode controller reaches the sliding surface directly and earlier than that of the sector sliding mode controller. After reaching the surface, the trajectory chatters around the surface. In Fig. 13, the system enters into the sliding sector approximately at $t = 0.5s$ ($\sigma_1 = 0$) in case of the sector sliding mode control. The main difference appears in the control activity. Two control signals are compared in Fig. 12. The conventional sliding mode is very robust but it needs intensive control action (see in Fig. 12), which causes significant audio noise as well. The sampling rate was quite rare. $T_{sampling} = 10ms$. The chattering could be reduced by increasing the sampling frequency but this chapter

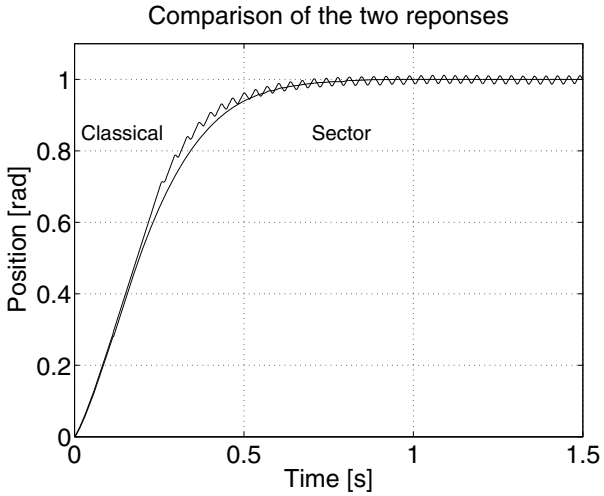

Fig. 10. Comparison of the position responses

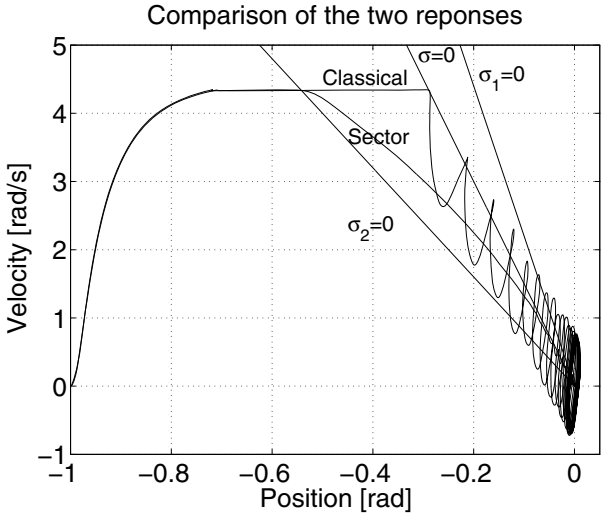

Fig. 11. Comparison of the trajectories

demonstrates that the reduction of chattering (the intensity of the control action and the audio noise) is significant at the same sampling rate, if the TP based sector sliding mode (Fig. 12) is applied instead of the traditional sliding mode control. The oscillation in the control signal is caused by the friction (Fig. 12. $t = 0.5 - 08s$).

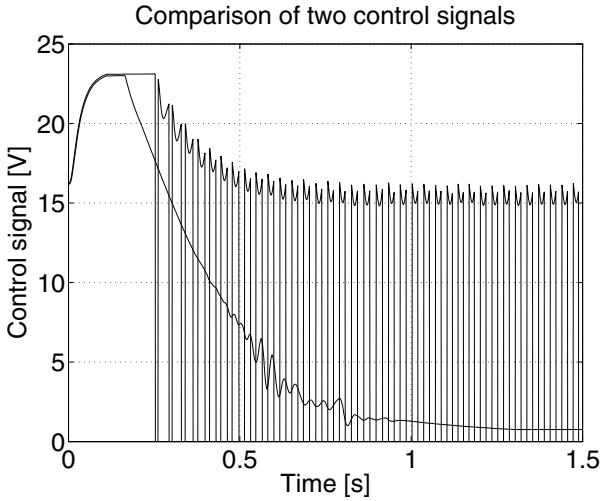

Fig. 12. Comparison of the two control signals

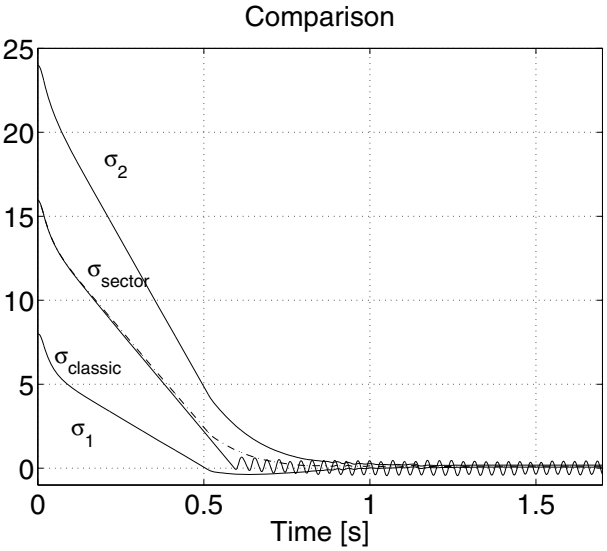

Fig. 13. Distance from the sliding surfaces

5 Conclusion

In this chapter, a modified variable structure control strategy with continuous switching control has been developed in detail for the nonlinear system with uncertainty. The control strategy can be regarded as the extension of conventional

VSS based sliding mode control method through expanding the switching surface to the sliding sector. The sliding sector is designed by a tensor product model transformation. The major advantage of the proposed control scheme is the introduction of the continuous switching control which successfully achieves smooth control response and retains the robustness of sliding mode control simultaneously. Both theoretical analysis and simulations demonstrate the attractiveness and the asymptotic stability of the sliding sector with the use of the proposed switching control which is essentially an interpolated control.

Acknowledgments. This chapter is dedicated to Okyay Kaynak since he and the authors of this chapter are in a big family. Our languages, Japanese, Turkish and Hungarian have the same root and maybe that is why we always feel that we can understand each other better.

The first author of the chapter meet Okyay in 1989 in a conference entitled as East-West Technological Bridge and feels "bridge" a kind of motto that expresses the relationship of this little group. Especially that after Okyay he got the chance to stay in the Harashima-Hashimoto Laboratory. During the years all authors spent some very determinative time in the laboratory called as the Mecca of Sliding Mode Control, which also created similarity among them and strengthen their relationship.

References

1. Baranyi, P.: TP model transformation as a way to LMI based controller design IEEE Trans Ind. Electron 51(2), 387–400 (2004)
2. Cheng, K.H., Hsu, C.F., Lin, C.M., Lee, T.T., Li, C.: Fuzzy Neural Sliding-Mode Control for DC DC Converters Using Asymmetric Gaussian Membership Functions. IEEE Trans. Ind. Electron 54(3), 1528–1536 (2007)
3. Filippov, A.G.: Application of the Theory of Differential Equations with Discontinuous Right-hand Sides to Non-linear Problems in Automatic Control. In: 1st IFAC Congress, pp. 923–925 (1960)
4. Filippov, A.G.: Differential Equations with Discontinuous Right-hand Side. Ann. Math. Soc. Trans. 42, 199–231 (1964)
5. Furuta, F.: Variable structure control with sliding sector. Systems and Control Letters 14, 145–152 (1990)
6. Furuta, K., Pan, Y.: Variable structure control with sliding sector. Automatica 36, 211–228 (2000)
7. Gupta, N.K.: Frequency-shaped cost functionals: Extension of linear-quadratic-gaussian design. Journal of Guidance and Control 3(6), 529–535 (1980)
8. Harashima, F., Hashimoto, H., Kondo, S.: MOSFET Converter-fed position servo system with sliding mode control. IEEE Trans. Industrial Electronics 32(3), 238–244 (1986)
9. Hashimoto, H., Maruyama, K., Harashima, F.: A microprocessor based robot manipulator control with sliding mode. IEEE Trans on Industrial Electronics 34(1), 11–18 (1987)
10. Hashimoto, H., Utkin, V.I.: VSS Observer for linear time varying system. Proc. of IEEE IECON, 34–39 (1990)

11. Hashimoto, H., Konno, Y.: Variable Structure and Lyapunov Contro. In: Sliding Surface Design in the Frequency Domain, pp. 75–86 (1993)
12. Kaynak, O., Harashima, F.: Disturbance Rejection by Means of Sliding Mode. IEEE Trans on Industrial Applications 32(1), 85–87 (1985)
13. Korondi, P.: Sliding Sector Design Based on Tensor Product Model Transformation. Transactions on Automatic Control and Computer Science 51(2), 1–6 (2006)
14. Korondi, P.: Tensor Product Model Transformation-based Sliding Surface Design. Acta Polytechnica Hungarica 3(4), 23–36 (2006)
15. Korondi, P., Xu, J.-X., Hashimoto, H.: Sector Sliding Mode Design Based on Tensor Product Model Transformation. In: International Conference on Intelligent Engineering Systems (INES 2007), pp. 253–258 (2007)
16. Korondi, P., Hashimoto, H.: Sliding Mode Design for Motion Control. Studies in Applied Electromagnetics and Mechanics, vol. 16, pp. 1–12 (2000)
17. Korondi, P., Xu, X.-J., Hashimoto, H.: Sector Sliding Mode Controller for Motion Control. In: 8th Conference on Power Electronics and Motion Control, vol. 5, pp. 254–259 (1998)
18. Lin, F.J., Teng, T.L., Shieh, P.H.: Intelligent Sliding-Mode Control Using RBFN for Magnetic Levitation System. IEEE Trans. Ind. Electron 54(3), 1752–1762 (2007)
19. Lin, H.-N., Kuroe, Y.: Decoupling Control of DD Robot Manipulators by VSS Disturbance Observer In National Convention Record I, pp. 61–766. I.E.E. Japan - Industry Applications Society (1993)
20. Lukuyanov, A.G., Utkin, V.I.: Method of reducing equations of dynamic systems to regular form. Automation and Remote Control 42(1), 413–420 (1981)
21. Petres, Z., Baranyi, P., Korondi, P., Hashimoto, H.: Trajectory tracking by TP model transformation: case study of a benchmark problem. IEEE Trans. Ind. Electron 54(3), 1654–1663 (2007)
22. Ryvkin, S., Schmidt-Obermoeller, R., Steimel, A.: Sliding-Mode-Based Control for a Three-Level Inverter Drive. IEEE Trans. Ind. Electron 55(11), 3828–3835
23. Sabanovic, A., Izosimov, D.: Application of sliding modes to induction motor control. IEEE Trans Industrial Appl 17(1), 41–49 (1981)
24. Suzuki, S., Pan, Y., Furuta, K., Hatakeyama, S.: Invariant Sliding Sector for Variable Structure Control. Asian Journal of Control 7(2), 124–134 (2005)
25. Utkin, V.I.: Variable Structure Control Optimization Springer (1999)
26. Utkin, V.I., Young, K.D.: Methods for Constructing Discontinuous Planes in Multidimensional Variable Structure Systems. Automation and Remote Control 31(10), 1466–1470 (1978)
27. Utkin, V.: I Variable Structure Control Optimization. Springer (1992)
28. Veselic, B., Drazenovic, P.B., Milosavljevic, C.: High-Performance Position Control of Induction Motor Using Discrete-Time Sliding-Mode Control. IEEE Trans Ind Electron 55(11), 3809–3817 (2008)
29. Xu, J.-X., Hashimoto, H., Harashima, F.: On Design of VSS Observer for Nonlinear Systems. Trans Society of Instrumentation and Control Engineers 25(2), 20–26 (1989)
30. Xu, J.-X., Abidi, K.: Discrete-Time Output Integral Sliding-Mode Control for a Piezomotor-Driven Linear Motion Stage. IEEE Trans. Ind. Electron 55(11), 3917–3926 (2008)
31. Xu, J.-X., Lee, T.-H., Wang, M., Yu, X.H.: On the design of variable structure controllers with continuous switching control. International Journal of Control 65(5), 409–431 (1996)
32. Young, K.D. (ed.): Variable Structure Control for Robotics and Aerospace Applications Elsevier Science Publishers (1993)

33. Young, K.D., Özgüner, Ü.: Frequency Shaping Compensator Design for Sliding Mode In Special Issue on Sliding Mode Control. International Journal of Control (1993)
34. Young, K.D.: Controller Design for Manipulator Using Theory of Variable Structure Systems. IEEE Trans on Systems, Man and Cybernetics 8(2), 101–109 (1978)
35. Yildiz, Y., Sabanovic, A., Abidi, K.: Sliding-Mode Neuro-Controller for Uncertain Systems. IEEE Trans Ind Electron 54(3), 1676–1685 (2007)
36. Yu, X., Kaynak, O.: Sliding Mode Control with Soft Computing: A Survey. IEEE Trans. Indust Electronics 56(9), 3275–3285 (2009)

Sliding Mode Control for a Robotic Fish

Jian-Xin Xu

National University of Singapore
elexujx@nus.edu.sg

Abstract. In this chapter, a sliding mode control scheme is designed for a biomimetic robotic fish, in which parameter uncertainties and external disturbances present. The Carangiform robotic fish consists of N links and $N-1$ joints, and its dynamic model of motion is given in terms of Lagrangian mechanics. Through this model, the relationship between the motion of the fish and the torques applied is made clear. By giving particular reference angles of joints, forward locomotion is obtained as a kind of trajectory tracking task. Due to the presence of parameter uncertainties and environmental disturbances especially from fluid dynamics, we adopt sliding mode control (SMC) to warrant a robust control performance. Comparisons are carried out between SMC and traditional computed torque control, and results of numerical examples validate the effectiveness of SMC when performing the tracking task in joint space.

Keywords: sliding mode control, robotic fish, Carangiform, underactuation.

1 Introduction

With increasing underwater activities, such as underwater archaeology, leakage detection, military reconnaissance [2], Autonomous Underwater Vehicle (AUV) is receiving more and more attention [3]. Traditional AUV, usually thrusted by rotatory propellers, may not be satisfactory in efficiency and maneuverability. Thus, new type of AUV is needed. During the long period time of nature selection, fish have evolved body structures and swimming patterns that highly adapt to aquatic environments [4]. Actually, they are more advanced swimming machines with higher efficiency, more remarkable maneuverability and less noise than conventional AUV.

Inspired by these appealing merits, researchers developed many theories and numerous robotic fish prototypes to study and mimic the way that real fish moves. Generally, swimming modes of fish are classified into three main categories: Anguilliform, Carangiform and Thunniform [5,6]. In Anguilliform mode, the whole body participates in large amplitude undulations. While in Carangiform swimming, the fish body undulations are confined to the last third of the body length, and in Thunniform, the undulation proportion is even less. Elongated body theory (EBT) [7,8], assuming sinusoidal motion of the fish body, was principally used to study steady state propulsion. In [9] a four-link robotic fish

X. Yu and M. Önder Efe (eds.), *Recent Advances in Sliding Modes*,
Studies in Systems, Decision and Control 24, DOI: 10.1007/978-3-319-18290-2_15

is designed and implemented with a PID controller and a fuzzy logic controller to control the speed and orientation respectively. In [10], a neuronal model and a mechanical model of fish swimming are presented, and the two models are combined together by the transformation of the motoneuron activity to mechanical forces and feedback of fish movements to stretch receptors. Based on the quasi-steady fluid flow theory, fish's propulsion model was established in [11,12], and nonlinear control method was investigated for trajectory stabilization of the robotic fish.

Due to the complexity of modeling interaction force between fish body and water, most existing works considered steady speed of the robotic fish [7,8], and the dynamic process remains not handled. Moreover, little attention was paid to parameter uncertainties in the fish model in existing works. In this chapter, we present a links-and-joints based robotic fish model. Motion dynamics is derived from Lagrangian formulation. Two kinds of control laws, computed torque control, and sliding mode control, are designed and applied. It is shown that, by designing particular reference joint angles, forward locomotion of Carangiform fish is achieved. Further, Parameter uncertainties and external disturbances are handled successfully by sliding mode control.

The chapter is organized as follows. In Section 2, the mechanical model of the robotic fish and dynamics of the system are given. In Section 3, locomotion patterns and reference trajectories are briefly introduced. In Section 4, the formulation of the actual system is first given, which contains uncertainties and disturbances. Next, a sliding mode controller is designed with the analysis on the stability. In Section 5, numerical examples are provided to validate the effectiveness of the controller. Section 6 concludes the chapter with a brief summary.

2 Dynamic Model of the Robotic Fish

In this section, an Carangiform fish (carps, mackerels) model is given to study its motion and control problems. From a biological perspective, in this swimming mode, only the latter part of the fish body participates in large amplitude undulations, while the amplitude of the undulation of the former part is small, which is different from the way that Anguilliform fish moves. The most remarkable characteristic in moving process of Carangiform fish is that there exists a body wave, traveling from head to tail [7]. Obviously, the traveling direction of the body wave in the fish is backwards, which is opposite to the direction that fish moves forward.

2.1 Fish Body Prototype

As shown in Fig. 1, we select the central line, which locates at the center of the fish body and stretches from head to tail, to represent the Carangiform fish, and we use links and joints to mimic its shape. The fish consists of N links and $N-1$ joints, where two connective links are connected by one joint. There is one motor on each joint, which exerts torques to its neighbor links.

Fig. 1 shows the top view of the central curve of the Carangiform fish. xoy is the world coordinates system. The position and orientation of each link i are described by three coordinates x_i, y_i and ϕ_i: x_i and y_i denote the position of the midpoint of link i, while ϕ_i denotes the angle from $+x$-axis to link i. The links are numbered from head to tail (see Fig. 1b). Each link i is impacted by two types of external forces: hydrodynamic forces w_i and torques τ_i, τ_{i-1} (see Fig. 2).

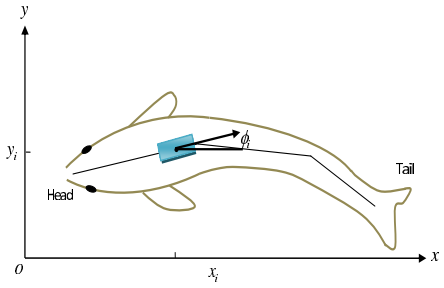

(a) The position(x_i, y_i) and orientation ϕ_i of each link i

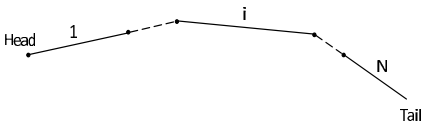

(b) Numbering of links

Fig. 1. Sketch map of the Carangiform robotic fish model. (a) Position and orientation representation. (b) Link numbering.

2.2 Hydrodynamic Force

When there is relative motion between the fish and the surrounding fluid, fluid is displaced and hydrodynamic force arises. The force can be obtained through surface integrals of vector force per area around the fish body. Since this force is related with the geometry of the object immersed in water and relative velocity between the object and water, in principle, the exact force distribution can be obtained by solving the Navier-Stokes equation. However, the calculation is quite complicated and time consuming [6]. In [10], the force is simplified and easy to

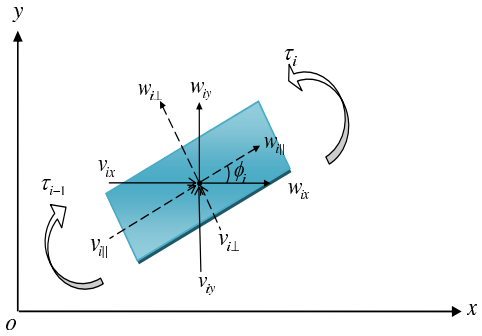

Fig. 2. External forces acting on link i

compute. As shown in Fig. 2, we adopt a simplified approximation of this force as (1) and (2) indicate

$$w_{i\perp} = -f_{i\perp}(v_{i\perp})^2 sgn(v_{i\perp}) \tag{1}$$

$$w_{i\parallel} = -f_{i\parallel}(v_{i\parallel})^2 sgn(v_{i\parallel}) \tag{2}$$

where $v_{i\perp}$, $v_{i\parallel}$ are parallel component and perpendicular component of the velocity v_i, and $f_{i\perp}$, $f_{i\parallel}$ are the water resistance coefficients in corresponding directions. The notation $sgn(\cdot)$ represents $+1$ if the element in the parentheses is positive or -1 if negative. Based on the geometric relationship (refer to Fig. 2), we have $v_{i\perp} = -v_{ix}\sin\phi_i + v_{iy}\cos\phi_i$, $v_{i\parallel} = v_{ix}\cos\phi_i + v_{iy}\sin\phi_i$, $w_{ix} = -w_{i\perp}\sin\phi_i + w_{i\parallel}\cos\phi_i$, $w_{iy} = w_{i\perp}\cos\phi_i + w_{i\parallel}\sin\phi_i$, where v_{ix}, v_{iy} are projection of the velocity v_i on x-axis and y-axis; w_{ix}, w_{iy} are projection of the hydrodynamic force w_i on x-axis and y-axis, respectively. All of them are scalars. Hydrodynamic forces experienced by all the links can be calculated the same way.

Since the link velocity v_i can be possibly in any direction, it is arduous to find each water resistance coefficient f in corresponding direction. Fortunately, f remains unchanged in the direction of paralleling the link, as well as in the perpendicular direction. Thus, we calculate the hydrodynamic forces in such a way that the need of the value of f in arbitrary direction is avoided.

2.3 Lagrangian Formulation of the Mechanical Model

In this part, we give dynamics of the fish model. Details of derivation see [1].

First, we define coordinates vector $\mathbf{p} \in \Re^{3N}$ as

$$\mathbf{p} = [x_1, y_1, \phi_1, x_2, y_2, \phi_2, \cdots, x_N, y_N, \phi_N]^T$$

where the notation $(\cdot)^T$ denotes transpose of a vector or a matrix $(\cdot)$. The constraints in the system can be formulated in a matrix form

$$\mathbf{g}(\mathbf{p}) = \begin{bmatrix} x_1 + \frac{l_1}{2}\cos\phi_1 - x_2 + \frac{l_2}{2}\cos\phi_2 \\ y_1 + \frac{l_1}{2}\sin\phi_1 - y_2 + \frac{l_2}{2}\sin\phi_2 \\ x_2 + \frac{l_2}{2}\cos\phi_2 - x_3 + \frac{l_3}{2}\cos\phi_3 \\ y_2 + \frac{l_2}{2}\sin\phi_2 - y_3 + \frac{l_3}{2}\sin\phi_3 \\ \vdots \\ x_{N-1} + \frac{l_{N-1}}{2}\cos\phi_{N-1} - x_N + \frac{l_N}{2}\cos\phi_N \\ y_{N-1} + \frac{l_{N-1}}{2}\sin\phi_{N-1} - y_N + \frac{l_N}{2}\sin\phi_N \end{bmatrix} = 0$$

where l_i is the length of link i, $\mathbf{g}(\mathbf{p}) \in \Re^{2(N-1)}$.

Define $J(\mathbf{p})$ as the Jacobian of the constraints matrix $\mathbf{g}(\mathbf{p})$

$$J(p) = \frac{\partial \mathbf{g}(\mathbf{p})}{\partial \mathbf{p}}$$

where $J(\mathbf{p}) \in \Re^{2(N-1)\times 3N}$. The external forces vector, that acts on individual coordinate of $\mathbf{p}$, is

$$\begin{aligned} \mathbf{w} = [&w_{1x}, w_{1y}, \tau_1, w_{2x}, w_{2y}, \tau_2 - \tau_1, \cdots, \\ &w_{Nx}, w_{Ny}, -\tau_{N-1}]^T \end{aligned} \tag{3}$$

where $\tau_i - \tau_{i-1}$ represents the total torque exerted on link i. It is worth noting that $\tau_0 = \tau_N = 0$, since there are no torques at the endpoints.

The system dynamics is then given as

$$\ddot{\mathbf{p}} = A(\mathbf{p})\dot{\mathbf{p}} + B(\mathbf{p})\mathbf{w} \tag{4}$$

where $A(\mathbf{p}) = -M^{-1}J^T(JM^{-1}J^T)^{-1}\dot{J}$, $B(\mathbf{p}) = M^{-1}[I - J^T(JM^{-1}J^T)^{-1}JM^{-1}]$, $A(\mathbf{p}) \in \Re^{3N\times 3N}$, $B(\mathbf{p}) \in \Re^{3N\times 3N}$, $M \in \Re^{3N\times 3N}$ is the mass matrix and it can be written as

$$M = diag\{m_1, m_1, I_1, m_2, m_2, I_2, \cdots, m_N, m_N, I_N\}$$

where m_i is the mass and I_i is the moment of inertia of link i. The notation $diag\{\}$ represents that M is a diagonal matrix, and the diagonal elements are in the braces. I is identity matrix with the same dimension as M.

The dynamics (4) contains all the acceleration terms, of which we are more interested in angular acceleration terms $\ddot{\phi}_i$. By partitioning (4), we obtain dynamics of ϕ

$$\ddot{\phi} = A_1(\mathbf{p})\dot{\mathbf{p}} + B_1(\mathbf{p})\mathbf{w}_x + B_2(\mathbf{p})\mathbf{w}_y + B_3(\mathbf{p})B_\tau\tau \tag{5}$$

$$\begin{aligned} \text{where} \qquad \phi &= [\phi_1, \phi_2, \cdots, \phi_N]^T \\ \mathbf{w}_x &= [w_{1x}, w_{2x}, \cdots, w_{Nx}]^T \\ \mathbf{w}_y &= [w_{1y}, w_{2y}, \cdots, w_{Ny}]^T \\ \tau &= [\tau_1, \tau_2, \cdots, \tau_{N-1}]^T \\ B_\tau &= \begin{bmatrix} 1 & 0 & \cdots & 0 \\ -1 & 1 & \ddots & \vdots \\ 0 & -1 & \ddots & 0 \\ \vdots & \ddots & \ddots & 1 \\ 0 & \cdots & 0 & -1 \end{bmatrix} \end{aligned}$$

and $A_1(\mathbf{p}) \in \Re^{N\times 3N}, B_1(\mathbf{p}) \in \Re^{N\times N}, B_2(\mathbf{p}) \in \Re^{N\times N}, B_3(\mathbf{p}) \in \Re^{N\times N}$ are corresponding coefficient matrices obtained from matrix $A(\mathbf{p})$, $B(\mathbf{p})$ in (4). It is worth noting that the dimension of τ is $N-1$, one less than the total number of links N.

3 Gait Generation for the Robotic Fish

In this section, three locomotion patterns of Anguilliform fish are investigated. We adopt the control torques τ derived from computed torque control method [1]

$$\begin{aligned} \tau = \quad & (B_\tau^T B_3 B_\tau)^{-1} B_\tau^T [\ddot{\phi}_r + k_1(\phi_r - \phi) + k_2(\dot{\phi}_r - \dot{\phi}) \\ & -(A_1 \dot{\mathbf{p}} + B_1 \mathbf{w}_x + B_2 \mathbf{w}_y)] \end{aligned} \tag{6}$$

where $\phi_r = [\phi_{1r}, \phi_{2r}, \cdots, \phi_{Nr}]^T$, ϕ_{jr} $(j = 1, 2, \cdots, N)$ is orientation of link j, and k_1, k_2 are coefficients relating to feedback terms. Here we choose $k_1 = 10$, $k_2 = 1$.

3.1 Forward Gait

We define that the reference $\phi_{j,r}$ that assumes the following form

$$\phi_{j,r} = A_m(j) \cdot \sin[\omega t + (2-j)\theta] \tag{7}$$

where $j = 1, 2, \cdots, N$. t denotes time instant. $A_m(j), \omega$ are the amplitude and angular frequency of $\phi_{j,r}$ respectively, and θ is the phase lead of link i comparing with its latter one. Note that in Carangiform fish, the amplitude of the body wave gradually increases from its head to its tail, thus we have the following relation: $A_m(1) < \cdots < A_m(j) < \cdots < A_m(N)$.

In this case, we choose $A_m(j) = 0.15\pi$, $\omega = 2\pi$, $\theta = \frac{\pi}{2}$. x_1 trajectory with respect to time is shown in Fig. 3.

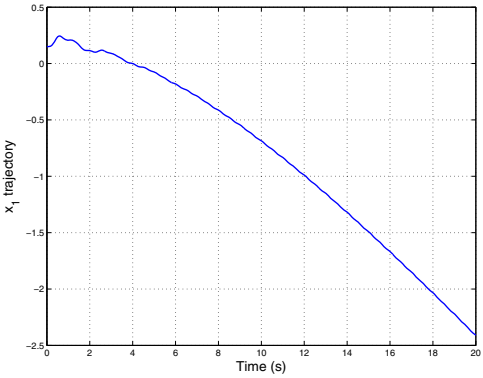

Fig. 3. x trajectory of forward motion

3.2 Backward Gait

Despite conducting forward motion, Anguilliform fish can also move backwards. In this case, the direction of the body wave is opposite to that of the forward locomotion case, i.e., the wave moves forwards. Thus, the movement of the former part of the body has a phase lag than its latter one. The reference $\phi_{j,r}$ now assumes the following form

$$\phi_{j,r} = A_m(j) \cdot \sin[\omega t - (2-j)\theta] \tag{8}$$

In this case, we choose $A_m(j) = 0.15\pi$, $\omega = 2\pi$, $\theta = \frac{\pi}{2}$. x trajectory with respect to time is shown in Fig. 4.

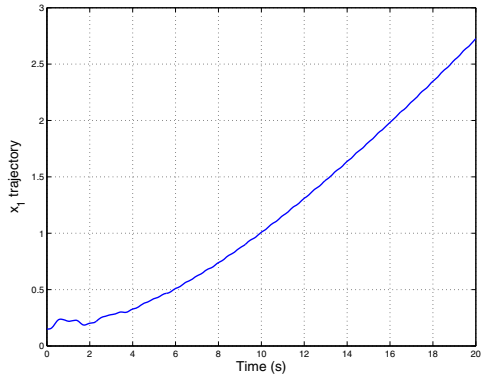

Fig. 4. x trajectory of backward motion

3.3 Turning Gait

In previous two cases, the reference angles are symmetric about zero, thus the fish neither deflects to left nor to right, but moves in a straight line. While in turning locomotion, in order to let the fish turn, we add deflections on the reference angles:

$$\phi_{j,r} = A_m(j) \cdot \sin[\omega t + (2 - j)\theta] + \gamma(j) \tag{9}$$

where $\gamma(j)$ represents angle deflection added on different joints. By using computed torque control, the fish can achieve turning movement. In this case, we choose $A_m(j) = 0.15\pi$, $\omega = 2\pi$, $\theta = \frac{\pi}{2}$, and the deflection $\gamma = [\frac{\pi}{4}\ \frac{\pi}{6}\ \frac{\pi}{12}\ 0]$. $x - y$ trajectory of the fish is shown in Fig. 5. Now we change ω, while remaining other

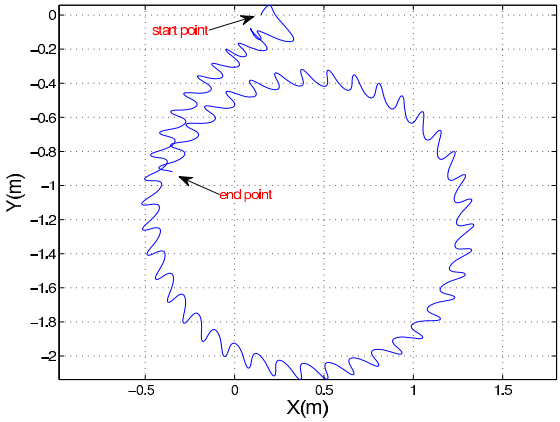

Fig. 5. $x - y$ trajectory of the fish

parameters the same as previous, then we can explore the effects of ω on the turning diameter and turning period of the fish. The result is shown in Table 1. From the table, we find that when ω increases, the turning period decreases correspondingly, while there is no noticeable change on the turning diameter. These phenomena may be due to the fact that, when ω increases, the turning angular velocity of the fish also increases, thus the turning period drops. From another point of view, the linear velocity of the fish also increases as ω increases.

Table 1. Effect of ω on Turning Diameter D and Turning Period P

ω(rad/s)	π	1.5π	2π	2.5π	3π
D(m)	1.84	1.83	1.83	1.82	1.82
P(sec)	77.9	52	39	31.2	25.3

Since both the angular velocity and the linear velocity of the fish increase, as a trade-off of these two variables, the turning diameter remains almost the same.

4 Sliding Mode Control Design for the Robotic Fish System

Modeling inaccuracies always exist and have strong adverse effects on control systems. Thus, any practical design must address them explicitly [13]. Otherwise, the control law may lose effect since the actual parameters deteriorate the performance of the whole system. Here we adopt sliding mode control, which belongs to robust controllers. In this robotic fish system, it is obvious that the number of actuators is one less than that of reference inputs. In other words, this robotic fish is under-actuated, and therefore, special consideration is taken on matched as well as unmatched components when we design the sliding mode control law.

4.1 Parameter Uncertainties

In the robotic fish model we constructed, many parameters involve uncertainties. These uncertainties either come from inaccuracy in the modeling, or come from unpredictable influence of surroundings. The water resistance coefficient f can be affected by many factors, such as different velocities of fish with respect to the environment. Thus, it is rather an estimated parameter than an accurate one. The mass matrix M can be measured accurately on ground, but when the fish comes into water, M becomes inaccurate because of added mass effect. Though we cannot know the exact information of the interested parameters due to complex factors, those parameters always change in a predictable range. This is reasonable because every parameter has its own physical meaning, thus it neither blows up to infinity nor becomes too small. Then, we can always give an upper bound and a lower bound for each parameter.

We define that

$$F_\perp = diag\{f_{1\perp}, f_{2\perp}, \cdots, f_{N\perp}\}$$
$$F_\parallel = diag\{f_{1\parallel}, f_{2\parallel}, \cdots, f_{N\parallel}\}$$

Assume that there exist parameter uncertainties on M, $F_\perp$ and $F_\parallel$, and their norms are bounded.

For derivation convenience, we define that

$$\mathbf{v}_{\perp\sin} = [v_{1\perp}^2 sgn(v_{1\perp}) \sin\phi_1, \cdots, v_{N\perp}^2 sgn(v_{N\perp}) \sin\phi_N]^T$$
$$\mathbf{v}_{\perp\cos} = [v_{1\perp}^2 sgn(v_{1\perp}) \cos\phi_1, \cdots, v_{N\perp}^2 sgn(v_{N\perp}) \cos\phi_N]^T$$
$$\mathbf{v}_{\parallel\sin} = [v_{1\parallel}^2 sgn(v_{1\parallel}) \sin\phi_1, \cdots, v_{N\parallel}^2 sgn(v_{N\parallel}) \sin\phi_N]^T$$
$$\mathbf{v}_{\parallel\cos} = [v_{1\parallel}^2 sgn(v_{1\parallel}) \cos\phi_1, \cdots, v_{N\parallel}^2 sgn(v_{N\parallel}) \cos\phi_N]^T$$

Then, hydrodynamic forces $\mathbf{w}_x$ and $\mathbf{w}_y$ can be written as

$$\mathbf{w}_x = F_\perp \mathbf{v}_{\perp\sin} - F_\parallel \mathbf{v}_{\parallel\cos} \tag{10}$$

$$\mathbf{w}_y = -F_\perp \mathbf{v}_{\perp\cos} - F_\parallel \mathbf{v}_{\parallel\sin} \tag{11}$$

where $\mathbf{w}_{x0}, \mathbf{w}_{y0}$ are nominal values of $\mathbf{w}_x, \mathbf{w}_y$. From a practical point of view, the coordinate $\mathbf{p}$ and its derivative $\dot{\mathbf{p}}$ are always bounded, which indicates that both $A(\mathbf{p})$ and $B(\mathbf{p})$ are bound, because $A(\mathbf{p})$ and $B(\mathbf{p})$ are functions of $\mathbf{p}$ and $\dot{\mathbf{p}}$. Together with the fact that $F_\perp$ and $F_\parallel$ are bounded, we thus know that $\mathbf{w}_x$ and $\mathbf{w}_y$ are bounded from (10) and (11).

4.2 External Disturbances

Besides parameter uncertainties, we have to take into account environmental disturbances when considering system dynamics. Disturbances are always existing in the robotic fish system, no matter in outdoor or indoor environments. In outdoor environment, such as seas or rivers, the robotic fish will experience unpredictable currents or waves, which are generated by winds or heat exchange, either beneath or on the surface of the water. In indoor environment, such as a water tank, the robotic fish will experience the reflection wave from the water container, which are generated by the swimming motion of the fish itself.

In general, these disturbances can be both additive and multiplicative to the dynamic equations of motion. However, the additive disturbances are a good approximation for most marine control applications [14]. Hence, we assume that the disturbances have additive format in this work.

The disturbances function as external forces, which are similar to $\mathbf{w}_x$, $\mathbf{w}_y$ and τ in (5). Since the disturbances adhere to the original external forces and they are additive, (5) can be written as follows

$$\begin{aligned}\ddot{\phi} = {} & A_1(\mathbf{p})\dot{\mathbf{p}} + B_1(\mathbf{p})(\mathbf{w}_x + \mathbf{d}_x) + B_2(\mathbf{p})(\mathbf{w}_y + \mathbf{d}_y) \\ & + B_3(\mathbf{p})B_\tau(\tau + \mathbf{d}_\tau)\end{aligned} \tag{12}$$

where $\mathbf{d}_x \in \Re^N$ and $\mathbf{d}_y \in \Re^N$ are the disturbance vectors in the directions of x-axis and y-axis, respectively, $\mathbf{d}_\tau \in \Re^{N-1}$ is the disturbance vector on the torque τ. In practice, $\mathbf{d}_x$, $\mathbf{d}_y$ and $\mathbf{d}_\tau$ will change in a reasonable range.

Note that among the parameter uncertainties and external disturbances that appear in (12), only $\mathbf{d}_\tau$ is matched, while all the others are unmatched, because they are not in the range space of the input matrix $B_3(\mathbf{p})B_\tau$.

4.3 Sliding Mode Control Law Design

Generally, there are two standard steps in sliding mode control design: 1) a sliding surface is given such that system on it manifests desired behavior; 2) a discontinuous control law is utilized to drive the system states into that surface and stay on it for all future time [15].

The sliding mode control law is composed of two parts. The first part is used to handle the nominal model, while the second is used to handle system uncertainties. Since there are not enough number of actuators to track all the reference inputs, we have to make a trade-off when setting the control objective, i.e., tracking the same number of reference inputs as that of actuators. In this model, the number of actuators, i.e., the number of torques, applied on the fish is $N-1$. Thus, we make the dimension of the sliding surface be $N-1$.

Before designing the sliding surface, we first define angular error and its derivative

$$\mathbf{e} = \phi_{New} - \phi_{rNew} \qquad \dot{\mathbf{e}} = \dot{\phi}_{New} - \dot{\phi}_{rNew}$$

where $\phi_{New} = [\phi_1, \phi_2, \cdots, \phi_{N-1}]^T$, representing the first $N-1$ actual joint angles, and $\phi_{rNew} = [\phi_{1r}, \phi_{2r}, \cdots, \phi_{(N-1)r}]^T$, representing the first $N-1$ reference joint angles. The dynamics of ϕ_{New} is

$$\begin{aligned}\ddot{\phi}_{New} &= A_2(\mathbf{p})\dot{\mathbf{p}} + B_4(\mathbf{p})(\mathbf{w}_x + \mathbf{d}_x) + B_5(\mathbf{p})(\mathbf{p})(\mathbf{w}_y + \mathbf{d}_y) \\ &\quad + B_6(\mathbf{p})B_\tau(\tau + \mathbf{d}_\tau) \\ &= A_{2n}(\mathbf{p})\dot{\mathbf{p}} + B_{4n}(\mathbf{p})\mathbf{w}_{xn} + B_{5n}(\mathbf{p})\mathbf{w}_{yn} \\ &\quad + B_{6n}(\mathbf{p})B_\tau\tau + \mathbf{d}(\mathbf{p}, \tau, t) \end{aligned} \tag{13}$$

where $A_2(\mathbf{p})$, $B_4(\mathbf{p})$, $B_5(\mathbf{p})$, $B_6(\mathbf{p})$, are submatrices obtained from matrix $A(\mathbf{p})$, $B(\mathbf{p})$ in (4), corresponding to $\ddot{\phi}_{New}$, and $A_{2n}(\mathbf{p})$, $B_{4n}(\mathbf{p})$, $B_{5n}(\mathbf{p})$, $B_{6n}(\mathbf{p})$ are their nominal values. $\mathbf{d}(\mathbf{p}, \tau, t) = (A_2 - A_{2n})\dot{\mathbf{p}} + (B_4\mathbf{w}_x - B_{4n}\mathbf{w}_{xn} + B_4\mathbf{d}_x) + (B_5\mathbf{w}_y - B_{5n}\mathbf{w}_{yn} + B_5\mathbf{d}_y) + (B_6B_\tau\tau - B_{6n}B_\tau\tau + B_6B_\tau\mathbf{d}_\tau)$, represents the difference between the actual terms and nominal terms. In the expression of $\mathbf{d}(\mathbf{p}, \tau, t)$, all the terms are bounded, thus we assume that the norm of it has an upper bound

$$||\mathbf{d}(\mathbf{p}, \tau, t)|| \leq d_{\max}$$

From the definition of $\mathbf{e}$, we set the control objective as tracking the first $N-1$ reference inputs. Next, we define the sliding surface as

$$\sigma = C\mathbf{e} + \dot{\mathbf{e}} \tag{14}$$

where C is a diagonal matrix whose entries are positive scalars.

Assume that information of the coordinate vector $\mathbf{p}$ and its velocity $\dot{\mathbf{p}}$ is available by means of vision or other measurement system. Now, we give the control law. As stated before, the control law consists of two parts

$$\tau = \tau_0 + \tau_s \tag{15}$$

$$\begin{aligned}\tau_0 = (B_{6n}B_\tau)^{-1}[&\ddot{\phi}_{rNew} - C(\dot{\phi}_{New} - \dot{\phi}_{rNew}) \\ &-(A_{2n}\dot{\mathbf{p}} + B_{4n}\mathbf{w}_{xn} + B_{5n}\mathbf{w}_{yn})]\end{aligned} \tag{16}$$

$$\tau_s = -\rho(B_{6n}B_\tau)^{-1}\frac{\sigma}{||\sigma||} \tag{17}$$

where $\rho = d_{\max} + \eta$, η is a positive constant. τ_0 is used to handle nominal model, τ_s is used to handle the uncertainties.

Then, we have the following theorem.

Theorem 1. *Consider the nonlinear system (13) associated with the chosen sliding surface $\sigma = \mathbf{0}$. Under the control law (15)-(17), the sliding surface will be reached in finite time.*

Proof. First we define the Lyapunov function

$$V = \frac{1}{2}\sigma^T\sigma$$

Differentiating it, we obtain

$$\begin{aligned}\dot{V} &= \sigma^T\dot{\sigma} = \sigma^T(C\dot{\mathbf{e}} + \ddot{\mathbf{e}}) \\ &= \sigma^T[C(\dot{\phi}_{New} - \dot{\phi}_{rNew}) - \ddot{\phi}_{rNew} + (A_2\dot{\mathbf{p}} + B_4\mathbf{w}_x \\ &\quad + B_4\mathbf{d}_x + B_5\mathbf{w}_y + B_5\mathbf{d}_y + B_6B_\tau\tau + B_6B_\tau\mathbf{d}_\tau)] \\ &= \sigma^T[C(\dot{\phi}_{New} - \dot{\phi}_{rNew}) - \ddot{\phi}_{rNew} \\ &\quad + (A_{2n}\dot{\mathbf{p}} + B_{4n}\mathbf{w}_{xn} + B_{5n}\mathbf{w}_{yn} + B_{6n}B_\tau\tau) + \mathbf{d}]\end{aligned}$$

Substituting (15), (16) and (17) into $\dot{V}$, one obtains

$$\begin{aligned}\dot{V} &= -\rho||\sigma|| + \sigma^T\mathbf{d} \le -\rho||\sigma|| + ||\sigma|| \cdot ||\mathbf{d}|| \\ &\le -\rho||\sigma|| + d_{\max}||\sigma|| = -\eta||\sigma||\end{aligned}$$

It is obvious that $\dot{V}$ is negative definite. By Lyapunov theorem for stability, the equilibrium at the origin $\sigma = \mathbf{0}$ is asymptotically stable. If $\phi_{New}(t=0)$ is off $\phi_{rNew}(t=0)$ in the beginning, the sliding surface is reached in a finite time $t_{reach} \le \|\sigma(t=0)\|_\infty/\eta$, where $\|(\cdot)\|_\infty$ denotes the $\infty-$norm of $(\cdot)$. After the system reaches the sliding surface $\sigma = \mathbf{0}$, it stays there. In the sliding mode, $\sigma(t) = \mathbf{0}$, $\dot{\sigma}(t) = \mathbf{0}$, the equivalent control is $\tau_{eq} = (B_6B_\tau)^{-1}[\ddot{\phi}_{rNew} - C(\dot{\phi}_{New} - \dot{\phi}_{rNew}) - (A_2\dot{\mathbf{p}} + B_4\mathbf{w}_x + B_4\mathbf{d}_x + B_5\mathbf{w}_y + B_5\mathbf{d}_y + B_6B_\tau\mathbf{d}_\tau)]$. (14) gives the dynamics of $\mathbf{e}$, which contains the first three angular errors. Since all entries of the diagonal matrix C are chosen to be positive scalars, it is easy to show that on the sliding surface, each single element of $\mathbf{e}$ always converges to 0, thus yielding the result that the first $N-1$ reference inputs can be tracked. ∎

5 Numerical Examples

Forward motion is the most common locomotion pattern of Carangiform fish (in this work, all the examples are given by using forward locomotion). If the fish moves forward, there exists a body wave traveling backwards. Since the wave travels from its head to tail, the head is preceding the tail affected by the wave. More generally, the movement of the former part of the body has a phase lead than the latter one, and it is reflected in the phase difference among the link

orientation angle ϕ_j $(j = 1, \cdots, N)$. For the reason that the backward moving wave has the same oscillating frequency at different places, we suppose each ϕ_j follow the same angular frequency. Following these considerations, we let the reference $\phi_{j,r}$ assume the form (7).

In this model, we select $N = 3$, i.e., the robotic fish consists of three links. The first link is the longest, and the third link is the shortest. Their length proportion is referred to [2]. Table 2 shows mechanical parameters of the links, where l_i, m_i, I_i are the length, mass and moment of inertia of link i respectively, $f_{i\perp}$ and $f_{i\parallel}$ are estimated water resistance coefficients [10]. Their SI units are $m(meter)$, kg, $kg \cdot m^2$, Ns^2/m^2, Ns^2/m^2.

Table 2. Mechanical Parameters of the Links

Link #	l_i	m_i	I_i	$f_{i\perp}$	$f_{i\parallel}$
1.	0.15	0.45	1.4603×10^{-3}	2.7	2.70
2.	0.108	0.168	2.721×10^{-4}	5.4	1.40
3.	0.0975	0.1236	1.632×10^{-4}	5.4	1.141

Based on (7), we give the reference angles $\phi_{j,r}$. Since this robotic fish is essentially an underactuated system, tracking of arbitrary number of reference inputs is impossible. However, by reference planning approach in [1], which conducts equilibrium analysis at the neighborhood of the equilibrium point, this problem can be handled. Following this method and the relation between the amplitudes of the body wave, we choose $\theta = 2.003$, $A_m(1) = 0.3142$, $A_m(2) = 0.3227$, $A_m(3) = 1.0090$. Other parameter is appropriately chosen as $\omega = 2\pi$. In this section, the above set of parameters (θ, A_m, ω), applies to all scenarios, and we only consider the forward moving case due to space limitation.

For simplicity, we suppose that the parameter uncertainties are in the following form: $M = (1 + \alpha)M_0$, $F_\perp = (1 + \beta_1)F_{\perp 0}$, $F_\parallel = (1 + \beta_2)F_{\parallel 0}$, where $\alpha = 0.2$, $\beta_1 = 0.2$, $\beta_2 = 0.2$. The disturbances parameters are: $\mathbf{d}_x = 10^{-3} \times [1 + \sin t, -2 + \cos t, 0.5 - 2\sin t]^T$, $\mathbf{d}_y = 10^{-3} \times [0.2 + 0.3\sin t, 1 + 2\cos t, 0.3 - 4\sin t]^T$, $\mathbf{d}_\tau = 10^{-3} \times [0.2 + 0.2\sin t, 0.1 - 0.2\cos t]^T$. Chattering phenomenon always exists in sliding mode control, which is a character of it. To have a smoother control signal, we replace $\frac{\sigma}{\|\sigma\|}$ in (17) with a saturation function $sat(\sigma)$.

$$sat(\sigma) = \begin{cases} \dfrac{\sigma}{||\sigma||}, & \text{if } ||\sigma|| > \epsilon, \\ \dfrac{\sigma}{\epsilon}, & \text{otherwise.} \end{cases}$$

and here we choose $\epsilon = 0.1$

In the first scenario, we use sliding mode control, and select the parameters as $C = diag\{10, 1\}$ (a diagonal matrix), $d_{\max} = 40$, $\eta = 0.1$. At time $t = 0$, the fish is still, and its three links are aligned on x-axis with its head at the origin, which means $\mathbf{p} = [0.15\ 0\ 0\ 0.45\ 0\ 0\ 0.75\ 0\ 0\ 1.05\ 0\ 0]^T$. The control torques are shown in Fig. 6.

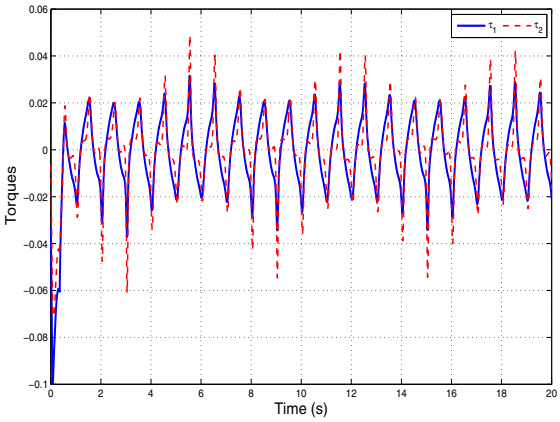

Fig. 6. Scenario 1: Torques trajectory (Sliding mode control)

In the second scenario, we use computed torque control method [1] in (19).

$$\begin{aligned}\tau = \quad & (B_\tau^T B_3 B_\tau)^{-1} B_\tau^T [\ddot{\phi}_r + k_1(\phi_r - \phi) + k_2(\dot{\phi}_r - \dot{\phi}) \\ & -(A_1 \dot{\mathbf{p}} + B_1 \mathbf{w}_x + B_2 \mathbf{w}_y)] \end{aligned} \tag{19}$$

where $\phi_r = [\phi_{1r}, \phi_{2r}, \cdots, \phi_{Nr}]^T$ is the vector of reference angles for all the links, and k_1, k_2 are coefficients relating to feedback terms. Here we choose feedback gains $k_1 = 10$, $k_2 = 1$. Other parameters and initial condition are the same as the first scenario. The comparison of angular error between sliding mode controller and computed torque controller is shown in Fig. 7. It is obvious that by SMC method, the first two joint angular errors quickly converge to 0 after a short period of time. The third joint angular error changes around 0 but cannot converge. While by computed torque method, the three joint angular errors are much larger than those obtained from SMC method, and none of them converge to 0 in the end.

In the third scenario, we still use sliding mode control. Note that the chattering phenomenon exists in the second scenario, which is a character of sliding mode control. To have a smoother control signal, we replace $\frac{\sigma}{||\sigma||}$ in (17) with a saturation function $sat(\sigma)$

$$sat(\sigma) = \begin{cases} \dfrac{\sigma}{||\sigma||}, & \text{if } ||\sigma|| > \epsilon_1, \\ \dfrac{\sigma}{\epsilon_1}, & \text{otherwise.} \end{cases}$$

and here we choose $\epsilon_1 = 0.1$, with other parameters and initial condition are the same as the first scenario. The control torques are shown in Fig. 8, and the comparison of angular errors between using saturation function and sign function is shown in Fig. 9.

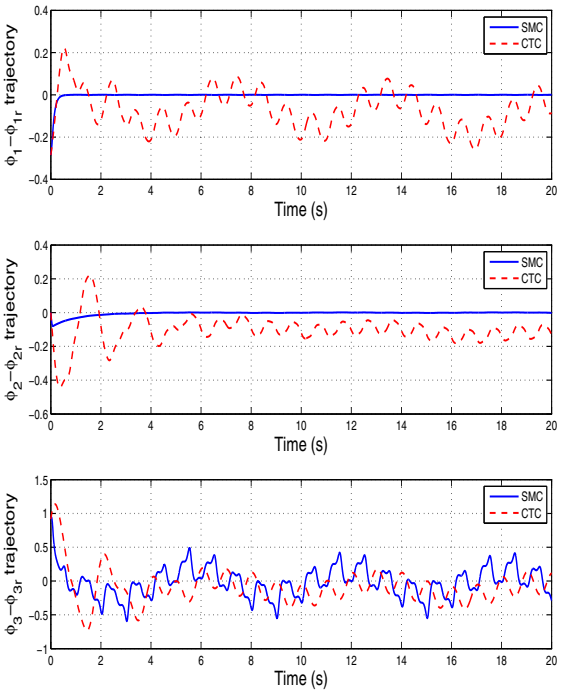

Fig. 7. Comparison of angular error between Scenario 1: sliding mode control (SMC) and Scenario 2: computed torque control (CTC)

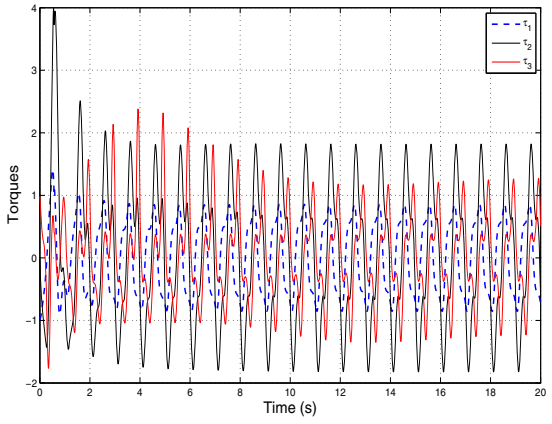

Fig. 8. Scenario 3: Torques trajectory (Sliding mode control using saturation function, with parameters $A_m = 0.15\pi, \omega = 2\pi, \theta = 2.1682, C = I_3, \epsilon_1 = 0.1, \epsilon_2 = 2$)

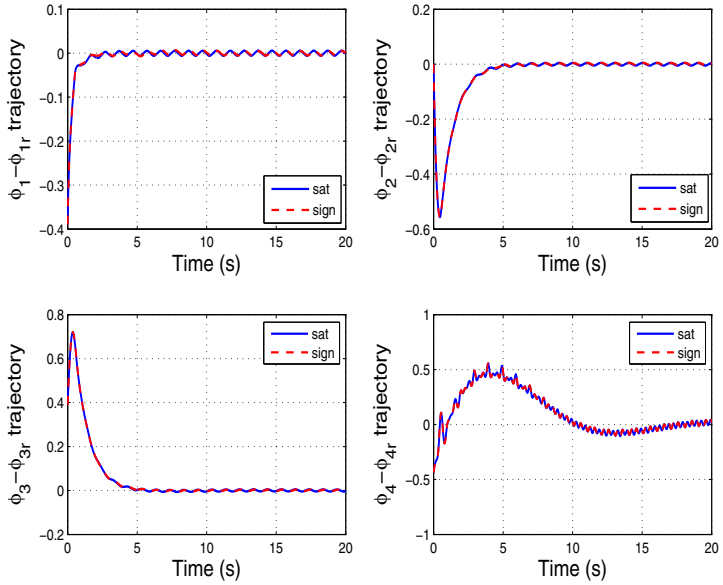

Fig. 9. Comparison of angular errors between Scenario 3: SMC with saturation function and Scenario 1: SMC with sign function

Comparing those scenarios, we find that when there exist parameter and unmodeled uncertainties, computed torque control cannot work very well, because the error between the actual joint angles and reference joint angles are large and always exists. When we use sliding mode control, the first two reference inputs can be perfectly tracked, thus we achieve the goal in Sec. IV-B when designing the sliding surface.

In Scenario 1, though ϕ_{1r} and ϕ_{2r} can be tracked accurately, perfect tracking of ϕ_{3r} cannot be promised theoretically. The fundamental reason is that the system is underactuated, i.e., the number of actuators in the system is fewer than the number of independent physical variables, which means arbitrary number of trajectory tracking is impossible. Furthermore, robustness can not be guaranteed for unmatched uncertainties or disturbances.

6 Conclusion

In this chapter, the dynamic model of the Carangiform robotic fish is first given. Based on the fact that body wave exists on the body of a traveling fish, we give the reference angles for all the links' orientation by using sinusoidal functions. We find that when the former reference angle has a phase lead compared with

the latter one, the fish moves forward. Sliding mode control is proposed to handle the actual system model, which takes into account parameter uncertainties and external disturbances. SMC design can promise theoretically that angular error of the first two links converge to zero. Numerical results show that the effectiveness of SMC to resist uncertainties, and better tracking performance is obtained compared with that using computed torque control.

Acknowledgement. This chapter is dedicated to Okyay Kaynak to commemorate his life time impactful research and scholarly achievements and his services to the profession. I got to know Okyay since 1987 when he visited Professor Fumio Harashima's Laboratory, University of Tokyo. I was a PhD student of Professor Harashima's at that time working on SMC. I benefited a lot from his visit. I still remember the situation where Okyay and I sat together debugging a simulation program run on a 286 computer, and finally obtained meaningful results with his predictive SMC algorithm. I still remember, when Okyay was about to leave Japan at the end of his visit, he kissed my face. This is the only kiss I have had from a gentleman so far in my life!

References

1. Xu, J.-X., Niu, X.-L.: Analytical control design for a biomimetic robotic fish. In: IEEE International Symposium on Industrial Electronics, pp. 864–869 (2011)
2. Yu, J., Wang, L., Tan, M.: Geometric optimization of relative link lengths for biomimetic robotic fish. IEEE Transactions on Robotics 23, 382–386 (2007)
3. Zhou, C., Tan, M., Cao, Z., Wang, S., Creighton, D., Gu, N., Nahavandi, S.: Kinematic modeling of a bio-inspired robotic fish. In: IEEE International Conference on Robotics and Automation, pp. 695–699 (2008)
4. Zou, K., Wang, C., Xie, G., Chu, T., Wang, L., Jia, Y.: Cooperative control for trajectory tracking of robotic fish. In: American Control Conference, pp. 5504–5509 (2009)
5. Sfakiotakis, M., Lane, D., Davies, J.: Review of fish swimming modes for aquatic locomotion. IEEE Journal of Oceanic Engineering 24, 237–252 (1999)
6. Colgate, J., Lynch, K.: Mechanics and control of swimming: a review. IEEE Journal of Oceanic Engineering 29, 660–673 (2004)
7. Lighthill, M.J.: Aquatic animal propulsion of high hydromechanical efficiency. Journal of Fluid Mechanics 44, 265–301 (1970)
8. Lighthill, M.J.: Large-amplitude elongated-body theory of fish locomotion. Proceedings of the Royal Society of London. Series B, Biological Sciences. 179, 125–138 (1971)
9. Yu, J.Z., Tan, M., Wang, S., Chen, E.: Development of a biomimetic robotic fish and its control algorithm. IEEE Transactions on Systems Man and Cybernetics Part B: Cybernetics 34, 1798–1810 (2004)
10. Ekeberg, O.: A combined neuronal and mechanical model of fish swimming. Biological Cybernetics 69, 363–374 (1993)
11. Morgansen, K.A., Duidam, V., Mason, R.J., Burdick, J.M., Murray, R.M.: Nonlinear control methods for planar carangiform robot fish locomotion. In: IEEE International Conference on Robotics and Automation, vol. 1, pp. 427–434 (2001)

12. Morgansen, K.A., Vela, P.A., Burdick, J.W.: Trajectory stabilization for a planar carangiform robot fish. In: IEEE International Conference on Robotics and Automation, vol. 1, pp. 756–762 (2002)
13. Slotine, J., Li, W.: Applied nonlinear control. Prentice-Hall (1991)
14. Fossen, T.: Guidance and control of ocean vehicles. Wiley (1995)
15. Cao, W., Xu, J.X.: Nonlinear integral-type sliding surface for both matched and unmatched uncertain systems. IEEE Transaction on Automatic Control 49, 1355–1360 (2004)

Variable Structure Control of a Perturbed Crane: Parametric Resonance Case Study

Carlos Vázquez[1], Joaquin Collado[2], and Leonid Fridman[3]

[1] Department of Applied Physics and Electronics,
Umeå University, SE-901 87 Umeå, Sweden
carlos.vazquez@umu.se
https://sites.google.com/site/carlosvazquezcontact/
[2] Department of Automatic Control,
CINVESTAV-IPN, Av.IPN 2508, 07360 México City, México
jcollado@ctrl.cinvestav.mx
[3] Department of Control Engineering and Robotics,
Engineering Faculty, UNAM, C.P. 04510 México City, México
lfridman@unam.mx
http://verona.fi-p.unam.mx/~lfridman/

Abstract. An under-actuated 5 degrees of freedom parametrically excited crane is the subject of study. In particular, a control methodology is proposed in order to avoid the parametric resonance effect and at the same time to attenuate the load oscillations, ensuring precise load transfer during the load movement despite model uncertainties and un-modeled dynamic actuators. The nonlinear controllers proposed in this chapter are motivated by the Super-Twisting and Twisting algorithms and the design uses the vector and non-smooth Lyapunov function approaches providing the stability of the overall closed-loop system. The experiments conducted over a laboratory platform, including a comparison with a PID controller, resemble quite well the simulations, verifying the obtained results.

Keywords: Parametric Resonance, Ship Onboard Crane, Twisting and Super-Twisting Algorithms, Vector and Non-smooth Lyapunov Functions, Under-Actuated Systems.

1 Introduction

The maneuvering with overhead crane systems has become the main part in many industrial activities where the efficiency in the cargo transportation process is crucial. This has motivated an intensive research on modeling and control during the last decades. A brief summary can be found in [1]. Cranes are under-actuated mechanical systems and the accelerations needed to move the trolley induce high oscillations in the payload. The measurement of these oscillations, in order to use feedback, is not trivial. On the other hand, measurements of the states are limited on industrial cranes where just the position of the trolley is available, in most of the cases, complicating the control design. In addition, uncertainties and external perturbations occur during regular operation conditions, degrading the overall control performance and increasing the risk of damages and accidents, see [39]. In particular, if the crane is installed on a ship, the

X. Yu and M. Önder Efe (eds.), *Recent Advances in Sliding Modes*,
Studies in Systems, Decision and Control 24, DOI: 10.1007/978-3-319-18290-2_16

wave-induced motions may contain significant energy close to the natural frequency of the free swinging load, or even twice its value. These kinds of variations are the cause of parametric resonance[1], see [1] and [54]. This phenomenon is not exclusive to this case, several mechanical, electrical and electromechanical systems are subject to parametric resonances, see [41]. There are a few methods for controlling the parametric resonance phenomena: active, semi-active and feedback controllers, where detuning the resonance condition requires the study of linear periodic systems, see [41] and [8]. Moreover, the subject of parametric resonance is still far from being fully understood and this chapter represents a step forward in that direction.

1.1 State of the Art

For shipboard cranes, the resulting load oscillation, which can reach 30-40 degrees may bring the load into a dangerous condition for the ship, the cargo and the crew. For this reason, operation of the shipboard crane is not allowed if the sea state is not acceptable. Moreover, there are reports that this phenomenon has been observed at full scale, even in moderate sea states, see [53]. Since much time and money can be wasted waiting for acceptable sea conditions, it is important to develop new schemes capable of transferring cargo in marginal conditions where the significant wave height may vary around one meter, or 10% of the maximum rope length, see [53] and [20]. On the other hand, new methods of operating the shipboard cranes are not implemented in the field if the stability is not guaranteed.

Three fundamental architectures of shipboard cranes have been presented in literature: the US Navy crane, ship cranes with Maryland rigging system and the mooring system, see [23], [22] and [32] respectively. In [23], using the flatness property, a feedback controller was proposed which only needs motor measurements. The combination of a feedforward and feedback controllers was presented in [22]. In both schemes the parametric resonance risk is not considered. Some methods to measure the payload oscillations have been proposed in [46], [43] and [9], opening new possibilities to include the payload oscillation measurements in real environments. Other control strategies are based on delayed feedback, see [20] and [32]. However, the mentioned approaches are not suitable in the presence of perturbations or unmodeled dynamics. In this context, in [3] the Suboptimal Second Order Sliding Mode Control was successfully applied for an overhead crane system of three degrees of freedom. Also, an Output Feedback Scheme was proposed in [5]. An extension for the decoupled three dimensional case was implemented in [42] using the Super-Twisting algorithm. In [38] a sliding mode antisway control of an offshore container crane was proposed. The case of periodic variation in the base support has been considered in [50], [51] and [36].

1.2 Methodology

The design of control laws under the presence of heavy uncertainty conditions is one of the main problems of modern control theory. In this scenario, the sliding mode (SM)

[1] *Parametric resonance* occurs when the frequency ω with which the parameter varies is close to any value $2\omega_0/n$, where ω_0 is the natural frequency and n is any integer, see [54].

methodology offers very good robustness/insensitivity properties against a wide variety of external disturbances as well as model uncertainties, see [47], [6], [21], [55], [15]. The main disadvantage of the SM controllers is the so-called *chattering effect*, a high frequency commutation in the control signal. This discontinuous input of high frequency is not suitable for the majority of the actuators. For this purpose, High Order Sliding Modes (HOSM) have been proven to reduce the *chattering effect* without compromising the SM robustness/insensitivity properties, see [28], [29], [4], [44] and [10].

In order to deal with unmatched perturbations two directions have been taken: the minimization of unmatched perturbations in combination with robust schemes, see [11] and the compensation via observer and sliding-surface designs, see [17], [16] and [14]. In our study, the case of periodic variations and the presence of parametric resonance is considered. We introduced a new sliding surface and the proposed control scheme is formed by two components: the Twisting and Super-Twisting algorithms. Both Second Order Sliding Mode Controllers has been widely studied by the control research community during the last two decades, see [28], [30] and [47].

1.3 Main Contribution

This chapter presents the modeling and control of a five degrees of freedom overhead-crane system under the presence of parametric resonance. Two methods are introduced which are motivated by the Twisting and Super-Twisting algorithms, together with the appropriate design of the sliding surface. The trolley and payload angular positions are assumed to be available for measurement and their corresponding derivatives are obtained via differentiators. In summary:

- The model of a parametrically excited crane is presented. The crane is modeled as a spherical pendulum attached to a moving support which is parametrically excited. By using the appropriate small angle assumptions, the model results in a time-varying system which is decoupled and symmetric with respect to the traveling and traversing motions of the crane. This model includes two time-varying parameters: the periodic oscillation in the base support and the rope length variation.
- The design of a new sliding surface is proposed together with the design of a Super-Twisting Algorithm (STA) achieving the desired tracking, chattering alleviation, oscillation attenuation and the avoidance of *parametric resonance*. The design of the sliding surface is inspired by the work of [3] and the robustness of the zero dynamics stability is improved using the method of Hill infinite determinants. The convergence time to the sliding surface is estimated with the non-differentiable Lyapunov function approach. The obtained results are validated experimentally on a Laboratory Inteco^{TM} 3D crane with a cam mechanism adaptation to produce the parametric excitation.
- A new control law is proposed which is formed by two components: a linear and nonlinear controller. The nonlinear component is discontinuous and is motivated by the Twisting algorithm. However, in our case the theoretical switching frequency is finite and we are not enforcing the sliding modes, see [19]. The ultimate bounded

stability analysis of the overall closed-loop system, which includes two interconnected dynamics: the error of the trolley position and the payload oscillation, is achieved with the design of a non-smooth vector Lyapunov function, see [7], [26] and [33].

1.4 Chapter's Structure

The remainder of this chapter is organized as follows. The mathematical model and problem statement is described in Section 2. In Section 3 the design of a super-twisting algorithm is presented. In Section 4 the vector Lyapunov approach is introduced. Simulations and experiments are shown in both sections 3 and 4, where the obtained results are validated experimentally over a Laboratory Inteco^{TM} 3D crane with a cam mechanism adaptation. Finally in section 5, the conclusions are drawn for this study.

2 Mathematical Model

The considered overhead crane system consists of a spherical pendulum attached to a moving support, the trolley, which is parametrically excited. Moving a suspended load along a pre-specified path is not an easy task since the system is under-actuated and the parametric resonance risk is present. Without parametric excitation the crane is asymptotically stable for any configuration and loads. On the contrary, in the presence of parametric excitation, there are some excitation frequencies and lengths in the rope that makes the crane exponentially unstable.

The coordinate representation is shown in Figure 1. Here, XYZ is the fixed coordinate system and $X_1Y_1Z_1$ is the trolley coordinate system which moves with the trolley. In the fixed coordinate system the trolley position is $(x,y,z = a\cos(\omega_1 t + \eta))$ where z is the parametric perturbation. This perturbation represents the vertical component of the regular waves of the sea, which is simulated by a cam mechanism attached to the laboratory crane as is shown in Figure 2. The swing angles projected on X_1Z_1 and Y_1Z_1 planes are θ_x and θ_y, respectively; β is the swing angle measured from X_1Z_1 plane. The load is considered as a point mass and the mass and stiffness of the rope are neglected.

The position of the load in the fixed coordinate system is: $(x_m, y_m, z_m) = (x + l\sin\theta_x\cos\beta, y + l\sin\beta, z - l\cos\beta\cos\theta_x)$, where x, y, l, θ_x and β are defined as the generalized coordinates to describe the motion. The Lagrangian $L = T - P$ is formed by the kinetic and potential energies of the crane and its load, $T = \frac{1}{2}m(\dot{x}_m^2 + \dot{y}_m^2 + \dot{z}_m^2) + \frac{1}{2}m_c(\dot{x}^2 + \dot{y}^2) + \frac{1}{2}m_r(\dot{x}^2)$, $P = mgl(1 - \cos\theta_x\cos\beta)$. Rayleigh's dissipation function is given by: $R = \frac{1}{2}(\mu_x\dot{x}^2 + \mu_y\dot{y}^2 + \mu_l\dot{l}^2)$, where μ_x, μ_y and μ_l are the viscous friction coefficients associated with the x, y and l motions. The equations of motion of the crane system are obtained by inserting L and R into Lagrange's equations associated with the generalized coordinates:

$$\begin{aligned}(m_c + m_r + m)\ddot{x} + \mu_x\dot{x} + ml\cos\theta_x\cos\beta\,\ddot{\theta}_x - ml\sin\theta_x\sin\beta\,\ddot{\beta} \\ +m\sin\theta_x\cos\beta\,\ddot{l} + 2m\cos\theta_x\cos\beta\,\dot{l}\dot{\theta}_x - 2m\sin\theta_x\sin\beta\,\dot{l}\dot{\beta} \\ -ml\sin\theta_x\cos\beta\,\dot{\theta}_x^2 - 2ml\cos\theta_x\sin\beta\,\dot{\theta}_x\dot{\beta} - ml\sin\theta_x\cos\beta\,\dot{\beta}^2 = f_x,\end{aligned} \tag{1}$$

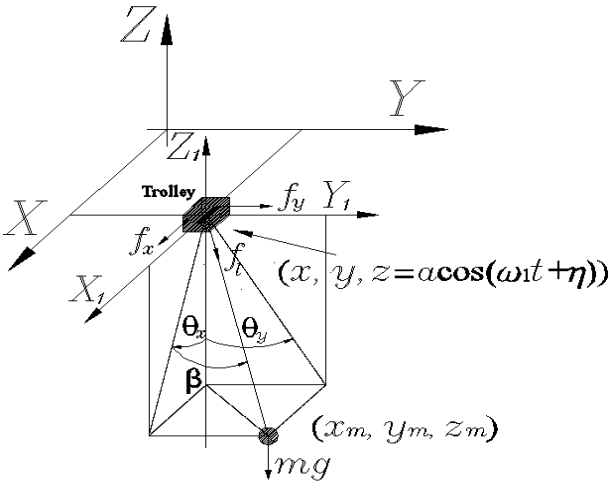

Fig. 1. Coordinate system

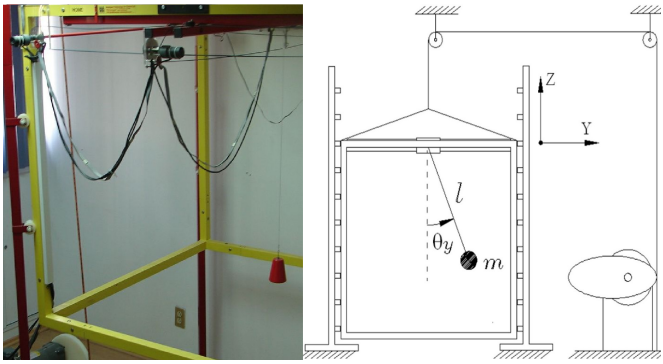

Fig. 2. Laboratory platform

$$l^2 m\ddot{\theta}_x \cos^2\beta + lm\ddot{x}\cos\theta_x \cos\beta - 2l^2 m\dot{\theta}_x\dot{\beta}\cos\beta\sin\beta + 2lml\dot{\theta}_x\cos^2\beta + lm(g+\ddot{z})\cos\beta\sin\theta_x = 0, \tag{2}$$

$$(m_c+m)\ddot{y} + \mu_y\dot{y} + ml\cos\beta\ddot{\beta} + ml\sin\beta\ddot{l} + 2m\cos\beta\dot{l}\dot{\beta} - ml\sin\beta\dot{\beta}^2 = f_y, \tag{3}$$

$$l^2 m\ddot{\beta} + lm\ddot{y}\cos\beta - lm\ddot{x}\sin\theta_x\sin\beta + 2ml\dot{l}\dot{\beta} + l^2 m\dot{\theta}_x^2\cos\beta\sin\beta + lm(g+\ddot{z})\cos\theta_x\sin\beta = 0, \tag{4}$$

$$m\ddot{l} + m\sin\theta_x\cos\beta\ddot{x} + \mu_l\dot{l} + m\sin\beta\ddot{y} - ml\cos^2\beta\dot{\theta}_x^2 - ml\dot{\beta}^2 - m(g+\ddot{z})\cos\beta\cos\theta_x = f_l. \tag{5}$$

Setting $q = [x, \theta_x, y, \beta, l]^T$, system (1)-(5) can be represented by the following matrix-vector form:

$$M(q)\ddot{q} + D\dot{q} + C(\dot{q},q)\dot{q} + G(q,t) = F \ , \tag{6}$$

where the driving force F, the damping matrix D and the gravitational force vector $G(q,t)$ are defined as $F = [f_x, 0, f_y, 0, f_l]^T$, $D = \mathrm{diag}(\mu_x, 0, \mu_y, 0, \mu_l)$ and $G = [0, lm(g + \ddot{z})\cos\beta\sin\theta_x, 0, lm(g + \ddot{z}(t))\cos\theta_x\sin\beta, -m(g + \ddot{z})\cos\beta\cos\theta_x]^T$, respectively.

Remark 1

The 5×5 matrix $M(q)$ can be readily obtained from the $\ddot{q}$ terms and is positive definite when $l > 0$ and $|\beta| < \frac{\pi}{2}$; the 5×5 Coriolis and centrifugal force matrix $C(\dot{q},q)$ satisfies $\dot{M}(q) - 2C(\dot{q},q) = -(\dot{M}(q) - 2C(\dot{q},q))^T$ and can be found from the q and $\dot{q}$ terms.

2.1 Model Simplification

In practice, the maximum acceleration of overhead cranes is much smaller than the gravitational acceleration and the rope length is kept constant or slowly varying while the cranes are in motion. In this chapter we adopt the model simplification proposed in [27], where the practical cases: $|\ddot{x}| \ll g$, $|\ddot{y}| \ll g$ and $|\ddot{l}| \ll g$ and the small angles assumptions: $\cos\theta_x \simeq 1$, $\cos\beta \simeq 1$, $\sin\theta_x \simeq \theta_x$ and $\sin\beta \simeq \beta$ are considered; furthermore $\beta = \arctan(\cos\theta_x \tan\theta_y)$, and $\theta_x \simeq 0 \Rightarrow \beta \simeq \arctan(\tan\theta_y) = \theta_y$. For small oscillations, the linear equations for the parametrically excited crane under the action of gravity and inertia forces are:

$$M_x\ddot{x} + \mu_x\dot{x} - 2m\dot{l}\dot{\theta}_x - m(g + \ddot{z})\theta_x = f_x, \tag{7}$$

$$\ddot{\theta}_x + \frac{2}{l}\dot{l}\dot{\theta}_x + \frac{1}{l}(g + \ddot{z})\theta_x = -\frac{\ddot{x}}{l}, \tag{8}$$

$$m_c\ddot{y} + \mu_y\dot{y} - 2m\dot{l}\dot{\theta}_y - m(g + \ddot{z})\theta_y = f_y, \tag{9}$$

$$\ddot{\theta}_y + \frac{2}{l}\dot{l}\dot{\theta}_y + \frac{1}{l}(g + \ddot{z})\theta_y = -\frac{\ddot{y}}{l}, \tag{10}$$

$$m\ddot{l} + \mu_l\dot{l} - m(g + \ddot{z}) = f_l, \tag{11}$$

where m_c is the trolley mass, m is the load mass, m_r is the girder mass, $M_x = m_c + m_r$, g is the gravitational acceleration and μ_x, μ_y and μ_l are the viscous damping coefficients associated with the x, y and l motions, respectively.

Remark 2

The system parameters considered in this chapter are: $m = 1\,\mathrm{kg}$, $m_c = 0.6\,\mathrm{kg}$, $m_r = 1\,\mathrm{kg}$, $\mu_x = 3.1\,\mathrm{kg/s}$, $\mu_y = 4.1\,\mathrm{kg/s}$ and $\mu_l = 4.1\,\mathrm{kg/s}$.

Remark 3

In the parametrically excited crane, shown in Figure 2, the parametric resonance phenomenon appears when the frequency ω_1 of z is twice the natural frequency, i.e., $\omega_1 = 2\omega_0 = 2\sqrt{g/l_0}$, see [54] and [34]. Figure 3 shows the exponential growth due to the parametric resonance in the laboratory overhead crane with the cam mechanism adjusted to $\omega_1 = 6.26\,\mathrm{rad/s}$ and $a = 0.06\,\mathrm{m}$. When the oscillations are greater than 40°, the nonlinear dynamic phenomena are dominant and limit the oscillations. See the experiment video at the URL [49].

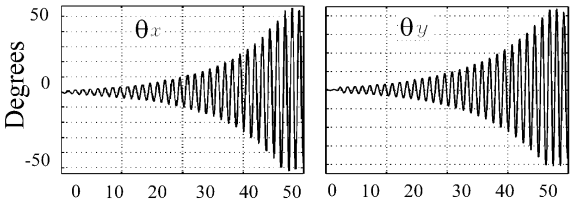

Fig. 3. Experiment: Parametric resonance ($\omega_1 = 2\omega_0$)

In conclusion, the three-dimensional overhead crane consists of the travel dynamics (7) and (8), the traverse dynamics (9) and (10), and the independent load hoisting dynamics (11). The travel and traverse dynamics are decoupled and symmetric, which means that the control of the three-dimensional overhead crane is transformed into a control problem of two independent two-dimensional overhead cranes having the same load hoisting dynamics. In this work, using the travel dynamics, the control law will be designed, and it will be used for the control of both the traveling and traversing motions. An independent controller, will be the responsible for the control of the load hoisting dynamic represented by equation (11).

2.2 Design of Trajectories

The control objective is to move the payload from the initial position $(x_0, \bar{l})$ to a final desired position, along a pre-specified smooth trajectory keeping the swing angle sufficiently small in the presence of parametric variations on the base support. Two trajectories are designed in order to avoid a known obstacle, one for the car position and other for the rope length position, as shown in Figure 5.

The reference for the car position $r_{\mathrm{ref}}(t)$, $r = x, y$, is required to be three times differentiable, and the derivatives need to be Lipschitz continuous. Such trajectory is given by:

$$r_{\mathrm{ref}}(t) = \begin{cases} a_0 + a_1 t + a_2 t^2 + a_3 t^3 + a_4 t^4 + a_5 t^5 + a_6 t^6 + a_7 t^7, & t \le t_f, \\ x_f, & t > t_f, \end{cases} \tag{12}$$

the constants a_i, $i = 1,2,3,4,5,6,7$ should be calculated. Based on the crane dimensions, we choose: $t_0 = 0$, $t_f = 6$, $r_0 = 0.1$ and $r_f = 0.7$; then, in order to satisfy the

relations: $r_{\text{ref}}(t_0) = r_0$, $r_{\text{ref}}(t_f) = r_f$, $\dot{r}_{\text{ref}}(t_0) = \ddot{r}_{\text{ref}}(t_0) = \dddot{r}_{\text{ref}}(t_0) = 0$ and $\dot{r}_{\text{ref}}(t_f) = \ddot{r}_{\text{ref}}(t_f) = \dddot{r}_{\text{ref}}(t_f) = 0$, we obtain: $a_0 = 0.1$, $a_1 = a_2 = a_3 = 0$, $a_4 = 0.0162$, $a_5 = -0.006481$, $a_6 = 0.0009002$ and $a_7 = -0.00004286$.

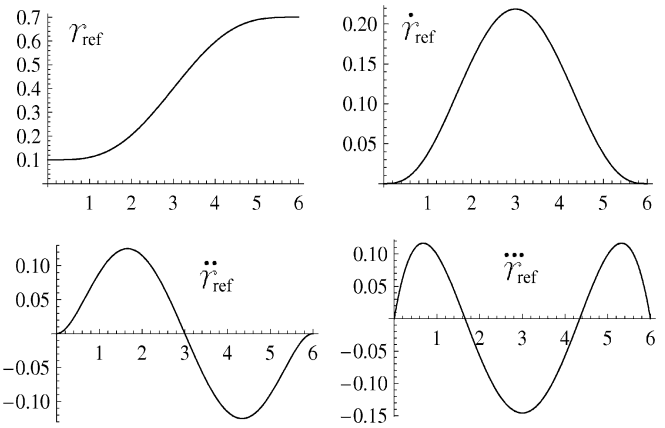

Fig. 4. Trajectory for the car position and its derivatives

Remark 4

The suggested trajectory is three times differentiable and its derivatives $\dot{r}_{\text{ref}}(t)$, $\ddot{r}_{\text{ref}}(t)$ and $\dddot{r}_{\text{ref}}(t)$ are Lipschitz continuous. These conditions will be required in the STA design.

For the rope length we consider the reference function:

$$l_{\text{ref}}(t) = \begin{cases} L(1+\varepsilon\cos(\omega_2 t)), & 0 < \omega_2 t \le t_a, \\ l_f = L(1+\varepsilon), & t_a < \omega_2 t \le t_b, \\ L(1+\varepsilon\cos(\omega_2 t - t_b - \pi)), & t_b < \omega_2 t \le t_f, \end{cases} \tag{13}$$

The frequency ω_2 is given by $\omega_2 = \frac{1}{p}\omega_0$ with $p > 0$ an integer. In this paper we consider $L = 1.25$, $\varepsilon = 0.16$ and $\omega_2 = \frac{1}{4}\omega_0$.

3 Super-Twisting Algorithm

The STA is one of the popular algorithms among the second order sliding mode controllers and is characterized for belonging to the class of Lipschitz continuous controllers, which is suitable for mechanical and electromechanical systems. The STA is used for plants with relative degree one and the derivative of the sliding surface is not required, see [28] and [30]. Moreover, new results in the field of sliding mode control theory offer a methodology to construct Lyapunov functions for the STA in order to estimate the convergence time to the sliding surface, see [45].

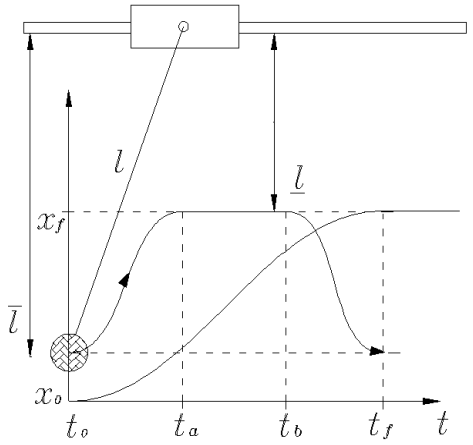

Fig. 5. Trajectories for the car position and rope length

In this section, based on the travel dynamics, equations (7) and (8), we propose using the STA in order to attenuate the payload oscillations and to eliminate the *parametric resonance* in a parametrically excited crane. Additionally, the robustness stability of the zero dynamics is improved with the Hill infinity determinants. This is important because the overall system is under-actuated and at least two degrees of freedom would result in *parametric resonance*.

3.1 Sliding Output

Two degrees of freedom must be controlled by using one control action, thus, the first step is the design of a suitable sliding output that includes the two variables, x and θ_x; motivated by the sliding output designed in [3], we proposed:

$$\sigma(t) = k_d\dot{e}(t) + k_p e(t) + k_i \int_0^t e(t)d\tau - k_1\theta_x(t) - k_p k_1 \int_0^t \theta_x(t)d\tau, \tag{14}$$

where $e(t) = x(t) - x_{\text{ref}}(t)$ is the position error and new integral terms were added. Note that the relative degree with respect to $\sigma(t)$ is one. In the following, we will omit the dependence on time. Then the derivative of σ is given by:

$$\dot{\sigma} = \frac{k_d}{M_x} f_x + g_0(\theta_x, \dot{\theta}_x, e, \dot{e}) + d(t), \tag{15}$$

with: $g_0 = (k_p - \frac{\mu_x}{M_x})\dot{e} + k_i e - k_1\dot{\theta}_x + (\frac{mg}{M_x} - k_p k_1)\theta_x$ and $d(t) = -k_d(\ddot{x}_{ref} + \frac{\mu_x}{M_x}\dot{x}_{ref})$, where $M_x = m_c + m_r$. Now defining:

$$f_x = \frac{M_x}{k_d}(u_x - g_0), \tag{16}$$

we obtain:

$$\dot{\sigma} = u_x + d(t), \tag{17}$$

Then the sliding mode enforcement will be designed in order to compensate the Lipschitz continuous perturbation $d(t)$. If g_0 is not available, another possibility is to use a sliding mode observer in order to obtain the estimation of g_0, see [13]. Taking into account $\dot{\sigma} = 0$ and the system dynamics (7) and (8), the obtained zero dynamics for the payload and the car, respectively, are:

$$l\ddot{\theta}_x + (\alpha + \beta\omega_1^2\cos(\omega_1 t + \eta))\theta_x + (2\dot{l} + 2\mu)\dot{\theta}_x - \frac{k_p}{k_d}\dot{e} - \frac{k_i}{k_d}e = -\ddot{x}_{ref}, \tag{18}$$

$$\ddot{e} + \frac{k_p}{k_d}\dot{e} + \frac{k_i}{k_d}e - k_1\dot{\theta}_x - (k_p k_1 - \frac{mg}{M_x})\theta_x = 0, \tag{19}$$

where: $2\mu = \frac{k_1}{k_d}$ and $\alpha = g + \frac{k_p k_1}{k_d}$. With the designed trajectory, see Figure 4, the term $\ddot{x}_r$ is bounded, Lipschitz continuous and it vanish at the finite time $t_f = 6$. The zero dynamics stability depends on the homogeneous equations:

$$l\ddot{\theta}_x + (\alpha + \beta\omega_1^2\cos(\omega_1 t + \eta))\theta_x + (2\dot{l} + 2\mu)\dot{\theta}_x - \frac{k_p}{k_d}\dot{e} - \frac{k_i}{k_d}e = 0, \tag{20}$$

$$\ddot{e} + \frac{k_p}{k_d}\dot{e} + \frac{k_i}{k_d}e - k_1\dot{\theta}_x - (k_p k_1 - \frac{mg}{M_x})\theta_x = 0. \tag{21}$$

The stability of the zero dynamics (20)-(21) and the sliding mode enforcement via the STA will be studied in the next two subsections.

3.2 Zero Dynamics

In this section we study the stability of the zero dynamics (20)-(21). The stability is affected by amplitude β and the rope length variation, $l(t)$. With the proposed reference, l_r, the rope length variation, is in the interval $\underline{l} \leq l(t) \leq \overline{l}$. Moreover, it has the form $l(t) = L(1 + \varepsilon\cos(\omega_2 t))$, where $\varepsilon = \frac{\overline{l}-\underline{l}}{\overline{l}+\underline{l}} < 1$ and $L = \frac{\underline{l}+\overline{l}}{2}$. Also, we should note that $\frac{1}{l(t)} = \frac{1}{L}(1 + l_\varepsilon(t))$ where $l_\varepsilon(t) = \sum_{i=1}^{\infty}(-1)^i(\varepsilon\cos\omega_2 t)^i$ and $|l_\varepsilon(t)| \leq \frac{\varepsilon}{1-\varepsilon} = \varepsilon_l$.

Setting:

$$q = [q_1, q_2, q_3, q_4]^T, \tag{22}$$

with $q_1 = l\theta_x$, $q_2 = \dot{q}_1$, $q_3 = e$ and $q_4 = \dot{e}$, equations (20)-(21) are rewritten in the next matrix form:

$$\dot{q} = A_0 q + \Delta A q, \tag{23}$$

with:

$$A_0 = \begin{bmatrix} 0 & 1 & 0 & 0 \\ -\frac{\alpha}{L} & -\frac{2\mu}{L} & \frac{k_i}{k_d} & \frac{k_p}{k_d} \\ 0 & 0 & 0 & 1 \\ k_p k_1 - \frac{mg}{M_x} & k_1 & -\frac{k_i}{k_d} & -\frac{k_p}{k_d} \end{bmatrix} \text{ and } \Delta A = \begin{bmatrix} 0 & & 0 & 0 \\ -\psi(t) & -\delta(t) & 0 & 0 \\ 0 & 0 & 0 & 0 \\ 0 & 0 & 0 & 0 \end{bmatrix}, \tag{24}$$

where:

- $\psi(t) = -\frac{\alpha l_\varepsilon}{L} - \frac{1+l_\varepsilon}{L}(2\frac{\mu\dot{l}}{l} + \ddot{l} + \beta\omega_1^2\cos(\omega_1 t + \eta))$.
- $\delta(t) = -2\frac{\mu l_\varepsilon}{L}$.

and $\Delta A q$ represents the time-varying perturbation.

Theorem 1. *Let the Lyapunov function be $V = \frac{1}{2}q^T Pq$, where $P = P^T > 0$ is the solution of the Lyapunov equation: $A^T P + PA = -I_n$, then the exponential stability of system (23) is guaranteed if the following condition is satisfied:*

$$\frac{\|\Delta Aq\|}{\|q\|} \leq \frac{1}{\lambda_{\max}[P]}, \tag{25}$$

where $\lambda_{\max(\min)}[\cdot]$ denotes the operation of taking the largest (smallest) eigenvalue of some symmetric matrix. The Euclidean norm of a vector q and the induced norm of a matrix A are denoted by $\|q\|$ and $\|A\|$ respectively.

The perturbation $\Delta A(t)$ is bounded, and we have $|\Delta A_{ij}| \leq E_{ij}$, then condition (25) is transformed into:

$$e_{\max} \leq \frac{1}{n\lambda_{\max}[P]}, \tag{26}$$

where $e_{\max} \triangleq \max_{i,j} E_{ij}$. See [40] and [52] for the proof. With the right selection of parameters k_p, k_d, k_i and k_1, matrix A_0 is Hurwitz and the Lyapunov matrix equation $A_0^T P + PA_0 = -2I_n$ must be solved for robustness. For example, setting the following control parameters:

$$k_p = .1,\ k_d = 1,\ k_i = .1\ k_1 = 1.58, \tag{27}$$

and solving the Lyapunov equation with the command *lyap* in Matlab, condition (26) is transformed into $e_{\max} \leq 0.00039$ which in general is very conservative. In order to improve the maximum allowed bound of the perturbation, we will use the method of the infinite Hill determinants, [31] and [37]. We need to study two cases:

- Constant rope length: $l = L > 0$, L a constant.
- Variable rope length: $l = L(1 + \varepsilon \cos \omega_2 t)$.

3.2.1 Constant Length

Setting the control parameters as in (27), A_0 is Hurwitz and the condition $e_{\max} \leq 0.00039$ implies the exponential stability of system (23). In order to improve the stability of the zero dynamics, we should consider the condition of parametric resonance $\omega_1 = 2\omega_0$. In this case from equation (20) we obtain the Mathieu equation. Now, considering $\eta = 0$ and scaling the time with $t = \frac{1}{\omega_0}\tau$, where $\omega_0^2 = \frac{g}{L}$, we obtain the normalized Mathieu equation:

$$\ddot{\theta}_x + 2\mu\,\dot{\theta}_x + (\alpha + \beta \cos 2\tau)\theta_x = 0, \tag{28}$$

where $2\mu = \frac{1}{\sqrt{g}L}(\frac{k_1}{k_d})$ and $\alpha = (1 + \frac{k_p k_1}{g k_d})$. Usually, the stability of Mathieu's equation is given in terms of its parameters (α, β) as a stability chart. By Floquet theorem, system (28) has a solution of the form $\theta_x = e^{\rho t} p(t)$, where $p(t) = p(t+T)$ and ρ is one characteristic exponent. This solution can be expressed in Fourier series:

$$\theta_x = \sum_{n=-\infty}^{\infty} p_n e^{(\rho + 2in)t}, \tag{29}$$

where the p_n coefficients are constants. Substituting (29) in equation (28) we obtain:

$$\begin{array}{l} \sum_{n=-\infty}^{\infty}\{(\alpha + 2\mu(\rho + 2in) + (\rho + 2in)^2)p_n e^{(\rho+2in)t}\} \\ +\frac{1}{2}\beta \sum_{n=-\infty}^{\infty}\{p_n e^{(\rho+2i(n-1))t} + p_n e^{(\rho+2i(n+1))t}\} = 0. \end{array} \tag{30}$$

Equating each of the coefficients of the exponential terms to zero, we obtain the following infinite set of linear algebraic homogeneous equations for the p_n:

$$\frac{1}{2}\beta p_{n-1} + Q(n)p_n + \frac{1}{2}\beta p_{n+1} = 0, \tag{31}$$

where $Q(n) = \alpha + 2\mu(\rho + 2in) + (\rho + 2in)^2$. From Floquet's theorem, the set of equations (31) must have a nontrivial solution. If the infinite determinant $\Delta(\rho)$, formed by (31), is identically zero, the infinite set of equations have a solution different to the trivial for the p_n coefficients. From (31) we obtain the infinite determinant $\Delta(\rho)$:

$$\Delta(\rho) = \begin{vmatrix} .. & . & . & . & & . & . & .. \\ .. & \frac{\beta}{2} & Q(-2) & \frac{\beta}{2} & 0 & 0 & 0 & .. \\ .. & 0 & \frac{\beta}{2} & Q(-1) & \frac{\beta}{2} & 0 & 0 & .. \\ .. & 0 & 0 & \frac{\beta}{2} & Q(0) & \frac{\beta}{2} & 0 & .. \\ .. & 0 & 0 & 0 & \frac{\beta}{2} & Q(1) & \frac{\beta}{2} & .. \\ .. & 0 & 0 & 0 & 0 & \frac{\beta}{2} & Q(2) & .. \\ .. & . & . & . & & . & . & .. \end{vmatrix}$$

The determinant $\Delta(\rho)$ results in a polynomial of infinity degree. The roots of this polynomial, ρ_i, are spaced periodically in the ρ_i plane. Then, all the independent solutions are represented through those characteristic exponents, ρ_i. Considering the three central rows and columns, the convergent infinite determinant $\Delta(\rho)$ can be approximated by truncation, see [12], we have $\Delta(\rho, n) =$

$$\begin{vmatrix} Q(-n) & \frac{\beta}{2} & 0 & . & . & . & . & .. \\ \frac{\beta}{2} & Q(-(n-1)) & \frac{\beta}{2} & 0 & . & . & . & .. \\ .. & . & . & . & . & . & . & .. \\ .. & 0 & 0 & \frac{\beta}{2} & Q(0) & \frac{\beta}{2} & 0 & .. \\ .. & . & . & . & & . & . & .. \\ .. & . & 0 & \frac{\beta}{2} & Q(n-1) & \frac{\beta}{2} & 0 & .. \\ .. & . & . & . & 0 & 0 & \frac{\beta}{2} & Q(n) \end{vmatrix}$$

The transitions curves separating stable solutions from the unstable ones, correspond to $\rho = 0$, i.e. periodic solutions with period π, or $\rho = \pm i$, i.e. periodic solutions with period 2π. In Figure 6, these regions where obtained evaluating the truncated determinant $\Delta(\rho, n)$, considering $n = 5$; the shaded regions correspond to unbounded solutions of equation (28) and the white regions correspond to bounded solutions. The boundaries between the two regions are called transitions curves where one solution is either π or 2π periodic, see [54]. The shaded regions are known as Arnold tongues or resonance zones and in such regions the solution of equation (28) grows exponentially, see [2]. Figure 6 shows the Arnold tongues for equation (28) for different system parameters and in order to guarantee the stability for maximum expected amplitude of the waves we need to fix the set point in a stable region. For more details about the method of infinite Hill determinants, see [31], [12] and [37].

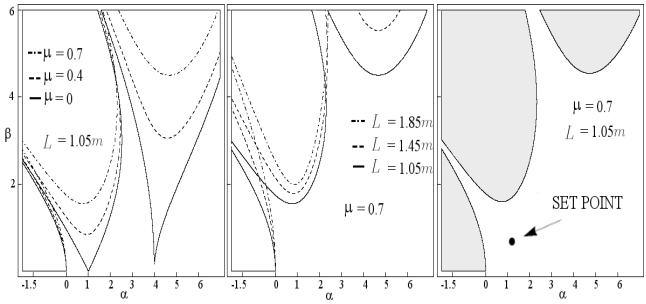

Fig. 6. Arnold tongues, Mathieu equation

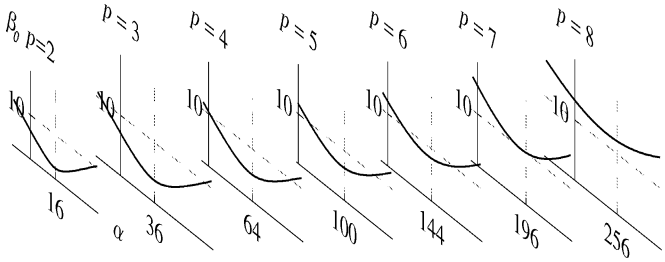

Fig. 7. Arnold tongues, Ince equation

3.2.2 Variable Length

Considering the case of parametric resonance $\omega_1 = 2\omega_0$, normalizing time $t = \frac{2p}{\omega_0}\tau$ and setting $l = L(1 + \varepsilon \cos \omega_2 t)$ with $\omega_2 = \frac{1}{p}\omega_0$, equation (20) become the normalized Ince equation:

$$l\ddot{\theta}_x + 2\dot{l}\dot{\theta}_x + 2\mu\dot{\theta}_x + [\alpha + \beta_0 \cos 4p\tau]\theta_x = 0, \tag{32}$$

where: $\beta_0 = \frac{p^2}{g}\beta$, $2\mu = (\frac{2p}{\sqrt{gL}})(\frac{k_1}{k_d})$ and $\alpha = (2p)^2(1 + \frac{k_p k_1}{g k_d})$. Following the procedure of infinite determinant of Hill, we obtain the stability chart in terms of the parameters (α, β). Figure 7 shows the Arnold tongues that emanate from $\alpha = (2p)^2$ for different values of p, i.e. different values of ω_2. Figure 8 shows the Arnold tongue that will be considered in the experiment.

3.3 STA Design

The input force u_x for the STA is given as a sum of two components:

$$u_x = -\lambda |\sigma|^{\frac{1}{2}} \text{sign}(\sigma) + f_1, \tag{33}$$

where: $\dot{f}_1 = -\gamma \text{sign}(\sigma)$. Note that the STA does not need the measurement of $\dot{\sigma}$. Substituting the control law (33) in equation (17) we have:

$$\begin{aligned} \dot{\sigma} &= -\lambda |\sigma|^{\frac{1}{2}} \text{sign}(\sigma) + f_1 + d, \\ \dot{f}_1 &= -\gamma \text{sign}(\sigma), \end{aligned} \tag{34}$$

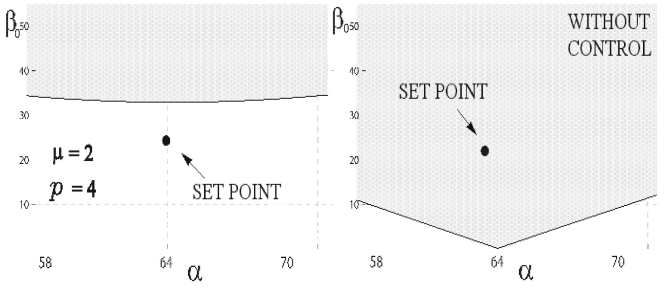

Fig. 8. Arnold tongues for Ince equation

By means of the transformation:

$$\xi = d - \gamma \int_0^t \text{sign}(\sigma) d\tau, \tag{35}$$

system (34) may be rewritten as

$$\begin{aligned} \dot{\sigma} &= -\lambda |\sigma|^{\frac{1}{2}} \text{sign}(\sigma) + \xi, \\ \dot{\xi} &= -\gamma \text{sign}(\sigma) + \dot{d}, \end{aligned} \tag{36}$$

where $|\dot{d}| \leq c$. A necessary condition of convergence is $\gamma > c$, if in addition, we select the gain λ sufficiently large, the appearance of a Second Order Sliding Mode is guaranteed after a finite time transient, i.e. $\sigma = \xi = 0$ in system (36). A very crude condition is $2(\gamma + c)^2/(\lambda^2(\gamma - c)) < 1$, see [45, Theorem 4.6, p. 159.]. In [35], a Lyapunov function is introduced that permits the design of λ and γ providing the estimation of convergence time. Recently, in [48], it was demonstrated that for any $\kappa > 0$, $\kappa = \gamma - c$, and $\delta > 0$, there exists λ^* such that σ is reduced to zero in finite time less than $(\sigma(0)/\kappa) + \delta$, if $\lambda > \lambda^*$. The convergence time cannot be less than $e_1(0)/\kappa$.

Now, based on the methodology presented in [35], we define $\zeta = [|\sigma|^{\frac{1}{2}} \text{sign}(\sigma), \xi]^T$ in order to design the following candidate Lyapunov function:

$$V = \tfrac{1}{2} \zeta^T P \zeta, \; P = \begin{bmatrix} \rho_1 & -\rho_2 \\ -\rho_2 & \rho_3 \end{bmatrix}, \tag{37}$$

where ρ_1, ρ_2 and ρ_3 are positive constants. This Lyapunov function is differentiable almost everywhere. If the inequalities $\rho_1 > 0$, $\rho_3 > 0$ and $\rho_1 \rho_3 - \rho_2^2 > 0$, then $V(\zeta)$ is positive definite and radially unbounded, i.e.,

$$\frac{1}{2} \lambda_{\min}[P] ||\zeta||_2^2 \leq V(\zeta) \leq \frac{1}{2} \lambda_{\max}[P] ||\zeta||_2^2, \tag{38}$$

Its time derivative along the solutions of the system is:

$$\dot{V} = -\frac{1}{2} |\sigma|^{-\frac{1}{2}} (\zeta^T Q_0 \zeta + \dot{d}(-\rho_2 \zeta_1^2 + \rho_3 \zeta_1 \zeta_2) \text{sign}(\sigma)), \tag{39}$$

where:

$$Q_0 = \begin{bmatrix} \rho_1\lambda - \rho_2\gamma & -\rho_1 - \rho_2\lambda + 2\rho_3\gamma \\ -\rho_1 - \rho_2\lambda + 2\rho_3\gamma & \rho_2 \end{bmatrix}. \tag{40}$$

Moreover, taking into account:

$$| \dot{d} | \leq k_{\max}(| x_r^{(3)} | + | \ddot{x}_r |) = c \tag{41}$$

where the constant $k_{\max} = \max\{k_d, \frac{k_d \mu_x}{M_x}\}$, we obtain:

$$\dot{V} \leq -\frac{1}{2}|\sigma|^{-\frac{1}{2}} \zeta^T Q_1 \zeta,$$

with:

$$Q_1 = \begin{bmatrix} \rho_1\lambda - \rho_2\gamma - (\rho_3 - 2\rho_2)c & -\rho_1 - \rho_2\lambda + 2\rho_3\gamma \\ -\rho_1 - \rho_2\lambda + 2\rho_3\gamma & \rho_2 - \rho_3 c \end{bmatrix} \tag{42}$$

Now, setting $Q_1 = I_{2\times 2}$, and considering $P > 0$, we obtain the relations:

- $\rho_2 > 1$, $\rho_3 = \frac{-1+\rho_2}{c}$ and $\rho_1 > \frac{c\rho_2^2}{\rho_2 - 1}$.
- $\lambda = \frac{2\rho_3 + \rho_2\rho_1 + 2\rho_3(\rho_3 - 2\rho_2)c}{2\rho_3\rho_1 - \rho_2^2}$ and $\gamma = \frac{\rho_1 + \rho_2\lambda}{2\rho_3}$.

Considering that $||\zeta||_2^2 = |\sigma| + |\zeta|^2$ is the Euclidean norm of ζ and using the fact that:

$$|\sigma|^{\frac{1}{2}} \leq ||\zeta||_2 \leq \frac{V^{\frac{1}{2}}}{\lambda_{\min}^{\frac{1}{2}}[P]}, \tag{43}$$

we obtain:

$$\dot{V} \leq -\phi V^{\frac{1}{2}}, \tag{44}$$

where $\phi = \frac{\lambda_{\min}^{\frac{1}{2}}[P]\lambda_{\min}[Q_1]}{\lambda_{\max}[P]}$. From the solution of (44), it follows that $\xi(t)$ converges to zero in finite time and reaches that value at most after $T = \frac{2V^{\frac{1}{2}}(\xi(0))}{\phi}$. Previous analysis has proven the following:

Theorem 2. *If condition (41) is satisfied together with:*

$$\rho_2 > 1,\ \rho_3 = \frac{-1+\rho_2}{c},\ \rho_1 > \frac{c\rho_2^2}{\rho_2 - 1}, \tag{45}$$

and defining the controller gains:

$$\lambda = \frac{2\rho_3 + \rho_2\rho_1 + 2\rho_3(\rho_3 - 2\rho_2)c}{2\rho_3\rho_1 - \rho_2^2},\ \gamma = \frac{\rho_1 + \rho_2\lambda}{2\rho_3}, \tag{46}$$

the zero state $\sigma = \dot{\sigma} = 0$ of system (36) is uniformly global finite time stable with the time of convergence $T = \frac{2V^{\frac{1}{2}}(\zeta(0))}{\phi}$ where $\phi = \frac{\lambda_{\min}^{\frac{1}{2}}[P]}{\lambda_{\max}[P]}$.

3.4 Simulations

Simulations were performed in Matlab-Simulink considering the nonlinear model (7)-(11) and the proposed control scheme. The case of *parametric resonance* is considered, i.e. $\omega_1 = 2\omega_0$, moreover the amplitude β and the phase η are unknown. An independent PI controller, $f_l = 15e_1(t) + \int_0^t e_1(t)d\tau$ with $e_1(t) = l(t) - l_{\text{ref}}(t)$, is responsible for the control of the rope length. In the time intervals $t_0 < t < t_a$ and $t_b < t < t_f$, the zero dynamics correspond to Ince equation (32) and Figure 8 shows the set point. In the time interval $t_a < t < t_b$ the zero dynamics correspond to Mathieu equation and Figure 6 shows the set point. In both cases, we selected the set point according to the worst case, i.e., the minimum length available, $\underline{l} = (L - \varepsilon) = 1.05m$, and the maximum expected amplitude of β, $\beta = 0.21m$. The design of control parameters is achieved in two stages:

1. Sliding surface design. The sliding output (14) depends on the parameters k_d, k_p, k_i and k_1. The design of these parameters is achieved using the Arnold tongues, Figures 6 and 7.
   - With $p = 4$ and $\beta = .21$ we have $\beta_0 = 6.5$.
   - Setting $k_p = 0.1$, $k_i = 0$ and $k_d = 1$, one has $\alpha = (2p)^2(1 + \frac{k_p k_1}{g})$, which implies $\alpha = 65.04$
   - $2\mu = (\frac{2p}{\sqrt{g\underline{L}}})(\frac{k_1}{k_d})$; setting $\mu = 2$ and $p = 4$ one obtains $k_1 = \frac{2\mu k_d\sqrt{g\underline{L}}}{2p} = 0.43$.
   - From Figure 8 the set point: $(\alpha, \beta_0) = (64, 6.5)$ belongs to a stable region.
   - In the arrival phase we have $2\mu = \frac{1}{\sqrt{g\underline{l}}}(\frac{k_1}{k_d})$; setting $\mu = 0.7$ one obtains, $k_1 = 2\mu\sqrt{g\underline{l}} = 5.45$ and $\alpha = 1 + \frac{k_p k_1}{g k_d} = 1.05$. From Figure 6 the point $(\alpha, \beta) = (.21, 1.05)$ belongs to a stable region.
2. Design of control parameters (λ, γ) of Super-Twisting algorithm. The control parameters should be designed using Theorem 2.
   - First the bound of $\dot{d}$ is given by (41); in this case with the trajectory presented in Figure 4, we have $\dot{d} = 0.775(|\ddot{x}_r| + |\dddot{x}_r|) \leq 0.775(0.2 + 0.2) \leq c = 1$.
   - Setting $\rho_2 = 2$ we have $\rho_3 = \frac{-1+\rho_2}{c} = 1$.
   - Finally setting $\rho_1 = (1.1)\frac{c\rho_2^2}{\rho_2 - 1} = 4.4$, we obtain $\lambda = 1$ and $\gamma = 3.2$ by theorem 2.

The simulation was performed using the obtained control parameters and the results are presented in Figure 9.

3.5 Experiments

Experiments were performed on the laboratory crane, shown in Figure 2, with $\omega_1 = 2\omega_0$. The laboratory crane has the values of $(x, \theta_x, y, \theta_y, l)$ available for measurement, and they are interfaced to a personal computer through an Inteco$^{\text{TM}}$ Data Acquisition Board. The control algorithms are implemented in a Matlab/Simulink$^{\text{TM}}$ environment. The derivatives $(\dot{x}, \dot{\theta}_x, \dot{y}, \dot{\theta}_y)$ are obtained through sliding mode differentiators. The obtained results are presented in Figure 10. Notice how well the experimental results in Figure 10 and the simulations results shown in Figure 9 resemble each other.

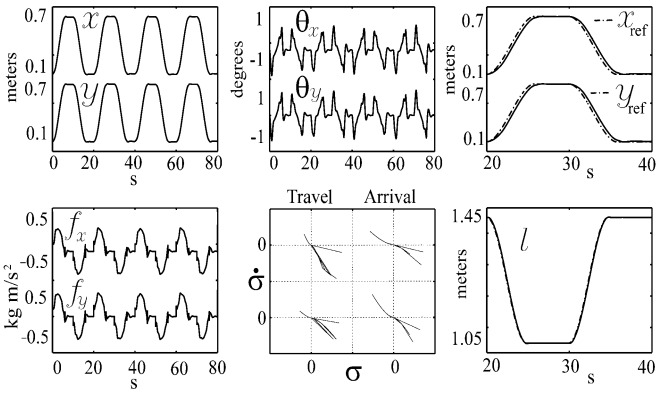

Fig. 9. Simulation with the STA

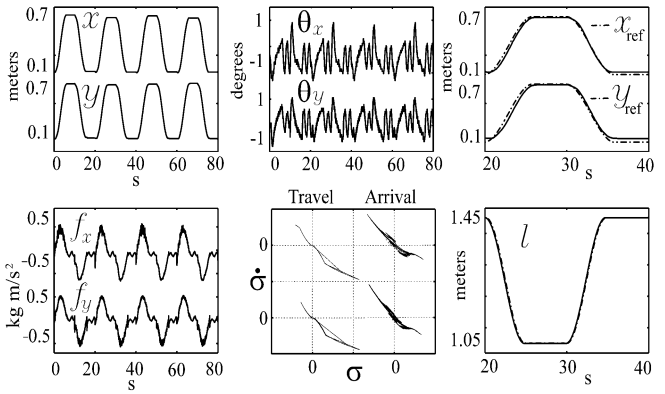

Fig. 10. Experiment with the STA

4 Vector Lyapunov Approach

The problem of time varying perturbations, periodic or not periodic, is a very important one for all kinds of control applications. In this section we will review some basic results concerning the Lyapunov stability theory for systems subject to time varying perturbations and the Vector Lyapunov Method used in this chapter.

4.1 Nonlinear Time Varying Perturbation

Consider the system,

$$\dot{x} = Ax + g(x,t), \tag{47}$$

where x and $g(x,t)$ are $n-$dimensional vectors and $g(0,t) = 0\ \forall t$; $g(x,t)$ represents the time-varying perturbation.

Theorem 3. *Let the Lyapunov function be $V = \frac{1}{2}x^T Px$, where $P = P^T > 0$ is the solution of the Lyapunov equation: $A^T P + PA = -I_n$, then the stability of system (47) is guaranteed if the following condition is satisfied:*

$$\frac{\|g(x,t)\|}{\|x(t)\|} \leq \frac{1}{\lambda_{\max}[P]}, \tag{48}$$

where $\lambda_{\max(\min)}[\cdot]$ denotes the operation of taking the largest (smallest) eigenvalue of some symmetric matrix. The Euclidean norm of a vector x and the induced norm of a matrix A are denoted by $\|x\|$ and $\|A\|$ respectively. See [40] for the proof of (48).

In the case of a linear time-varying perturbation:

$$g(x,t) = \Delta A(t)x, \tag{49}$$

where the perturbation $\Delta A(t)$ is bounded by, $|\Delta A_{ij}| \leq E_{ij}$, the condition (48) is transformed into:

$$e_{\max} \leq \frac{1}{n\lambda_{\max}[P]}, \tag{50}$$

where $e_{\max} \triangleq \max_{i,j} E_{ij}$. See [40] and [52] for the proof.

4.2 Second Order System

The study of second order systems is of fundamental interest because they are present in a great variety of physical phenomena. Moreover, if one of the parameters of a linear system is time varying, periodic or non-periodic, the classical theory for stability analysis, Routh-Hurwitz, Nyquist or Root-Locus, are not applicable and the complexity of the control problem is increased, see [54]. In addition, the design of Lyapunov functions for linear time varying systems is more difficult than it is for time-invariant systems. A particular case of system (47) is given by:

$$A = \begin{bmatrix} 0 & 1 \\ -\psi_0 & -\delta_0 \end{bmatrix}, \quad g(x,t) = \begin{bmatrix} 0 & 0 \\ -\Delta\psi & -\Delta\delta \end{bmatrix} x, \tag{51}$$

where matrix A is Hurwitz and the coefficients $\Delta\psi$ and $\Delta\delta$ are bounded, moreover:

- $\psi(t) = \psi_0 + \Delta\psi(t) > 0$ and $\delta(t) = \delta_0 + \Delta\delta(t) > 0$.
- $\underline{\psi} = \psi_0 - \| \Delta\psi(t) \|_\infty$ and $\overline{\psi} = \psi_0 + \| \Delta\psi(t) \|_\infty$.
- $\underline{\delta} = \delta_0 - \| \Delta\delta(t) \|_\infty$ and $\overline{\delta} = \delta_0 + \| \Delta\delta(t) \|_\infty$.
- $\| \dot{\psi}(t) \|_\infty \leq \beta_0$ and $\| \dot{\delta}(t) \|_\infty \leq \beta_1$.

In order to study the stability of (51) consider the Lyapunov function $V(x,t) = \frac{1}{2}x^T P(t)x$ with:

$$P(t) = \begin{bmatrix} \phi\psi(t) + \delta(t) & 1 \\ 1 & \phi \end{bmatrix}, \tag{52}$$

If $\phi > 0$, $\psi(t) > 0$, $\delta(t) > 0$ and $\phi(\phi\underline{\psi} + \underline{\delta}) > 1$ then $P(t) > 0$. Now $\dot{V}(x,t)$ is given by,

$$\dot{V}(x,t) = -x^T \begin{bmatrix} \psi(t) - \frac{1}{2}(\phi\dot{\psi} + \dot{\delta}) & 0 \\ 0 & \phi\delta(t) - 1 \end{bmatrix} x, \tag{53}$$

where:

$$\underline{\psi} > \frac{1}{2}(|| \dot{\psi} ||_\infty \phi + || \dot{\delta} ||_\infty) \text{ and } \underline{\delta} > \frac{1}{\phi}, \tag{54}$$

which implies $\dot{V}(t,x) \leq 0$.

Remark 1. In general, condition (50) is conservative. In some applications we have control of the parameters ψ_0 and δ_0 and the stability condition (54) gives better results for (51).

4.3 Vector Lyapunov Functions

In this section we present the basic result of the vector Lyapunov function method used in this paper, see [26] and [7] for details and further extensions. Consider the system, given by:

$$\dot{x} = f(t,x), \tag{55}$$

where x and $f(x,t)$ are $n-$dimensional vectors. Moreover, the function $f(x,t)$ is piecewise continuous. The precise meaning of the solution of differential equation (55) with a piecewise continuous right-hand side is defined in the sense of Filippov, [18]. Stability of system (55) will be studied via vector Lyapunov functions. For any vector Lyapunov function $V \in C[\mathbb{R}_+ \times \mathbb{R}^n, \mathbb{R}^N_+]$ we define the function,

$$D^+V(t,x) = \lim_{h \to 0^+} \sup \frac{1}{h}[V(t+h, x+hf(t,x)) - V(t,x)], \tag{56}$$

for $(t,x) \in \mathbb{R}_+ \times \mathbb{R}^n$. One could also utilize other generalized derivatives, for example,

$$D_-V(t,x) = \lim_{h \to 0^-} \inf \frac{1}{h}[V(t+h, x+hf(t,x)) - V(t,x)], \tag{57}$$

We note that if $V \in C^1[\mathbb{R}_+ \times \mathbb{R}^n, \mathbb{R}^N_+]$, then $D^+V = D_-V = \dot{V}$, where:

$$\dot{V}(t,x) = \frac{\partial}{\partial t}V(t,x) + \frac{\partial}{\partial x}V(t,x)f(t,x). \tag{58}$$

In general $V(t,x)$ may not belong to C^1, but satisfies the Lipschitz condition in the neighborhood of each point of this domain and the composite function $V(t,x)$ is absolutely continuous for any solution $x(t)$ of (55). Its time derivative is given by (58) almost everywhere, wherever the function $f(t,x)$ is continuous and $\frac{\partial}{\partial x}V(t,x)$ exists, see [18]. Let us consider the comparison system,

$$\dot{W} = g(t,W), \;\; W(t_0) = W_0 \geq 0, \tag{59}$$

where $g \in C[\mathbb{R}_+ \times \mathbb{R}^n, \mathbb{R}^N]$ and $g(t,W)$ is quasimonotone nondecreasing in W. Let us recall that inequalities between vectors are component wise and quasimonotonicity of $g(t,W)$ means that $W \leq R, W_i = R_i$ for $1 \leq i \leq N$ implies $g_i(t,W) \leq g_i(t,R)$. The crucial step in the vector Lyapunov function is to assume that,

$$D^+V(t,x) \leq g(t,V(t,x)). \tag{60}$$

Furthermore, in order to apply the method to specific problems it is necessary to know the properties of the solutions of system (59), which is difficult in general. In the present section we will consider the linear comparison system,

$$g(t,W(t,x)) = AW(t,x) + b, \tag{61}$$

where stability properties are given by the matrix $A = [a_{ij}]_{n\times n}$ and the vector $b = [b_{i1}]_{n\times 1}$.

Theorem 4. *Assume that:*

1. $g(t,W)$ *has the form of (61).*
2. $V \in C[\mathbb{R}_+ \times \mathbb{R}^n, \mathbb{R}^N]$, $V(t,x)$ *is locally Lipschitz in* x *and the function* $V_0(t,x) = \sum_{i=1}^{N} V_i(t,x)$ *is positive definite and decreasing.*
3. $f(t,x)$ *is piecewise continuous and*

$$D^+V(t,x) \leq g(t,V(t,x)).$$

Then the stability properties of the trivial solution of

$$\dot{W} = g(t,W), \;\; W(t_0) \geq 0, \tag{62}$$

imply the corresponding stability properties of the trivial solution of (55). See [26] for the proof.

Corollary 1. *In Theorem 4,*

- $g(t,W) \equiv 0$ *is admissible to yield uniform ultimate bounded stability.*
- $g(t,W) = AW + b$, *with A Hurtwitz and* $b > 0$ *is admissible to imply uniform strong ultimate bounded stability. See [25] for the proof.*

The vector Lyapunov function method offers a very flexible mechanism since each function can satisfy less rigid requirements, see [7], [26] and [33]. Due to the fact that a given large system may be decomposed into interconnected subsystems to determine the stability of the system from the stability properties of the subsystems and the nature of the interconnections, in some situations several Lyapunov functions result naturally and employing more Lyapunov functions yields better results.

4.4 Control Design

In this section, using the travel dynamics, described by equations (7) and (8), we will design a twisting controller in order to attenuate the load oscillations and eliminate the parametric resonance in the shipboard crane. The actual case does not yield a standard application of the sliding mode control methodology since the crane system is underactuated and subject to parametric resonance.

The position variable x is the output of subsystem (7) and θ_x is the output of subsystem (8); both outputs have relative degree two and both are available. Besides, in equation (8) and (10), the term $\frac{1}{l}$ is included which can be represented by the next expression:

$$\frac{1}{l} = \frac{1}{l_0}(1 + l_\varepsilon(t)) \leq \frac{1}{l_0}(1 + |l_\varepsilon|), \tag{63}$$

where $l_\varepsilon(t) = \sum_{i=1}^{\infty}(-1)^i(\varepsilon\cos\omega_2 t)^i$, $l_0 = \frac{\bar{l}+\underline{l}}{2}$, and $\mid l_\varepsilon \mid \leq \frac{\varepsilon}{1-\varepsilon} = \varepsilon_l$. Finally, setting $\theta_1 = \theta_x$, $\theta_2 = \dot{\theta}_x$, $e_x = x - x_r$, $e_v = \dot{x} - \dot{x}_r$ and defining $\theta = [\theta_1, \theta_2]^T$, $e = [e_x, e_v]^T$ and $f_x = l_0 M_x u_x$, equations (7) and (8) have the next state-space representation:

$$\begin{bmatrix}\dot{e}\\ \dot{\theta}\end{bmatrix} = \begin{bmatrix}A_{11} & A_{12}(t)\\ A_{21}(t) & A_{22}(t)\end{bmatrix}\begin{bmatrix}e\\ \theta\end{bmatrix} + \begin{bmatrix}b_1\\ b_2(t)\end{bmatrix}u_x + \begin{bmatrix}d_1(t)\\ d_2(t)\end{bmatrix}. \tag{64}$$

The time varying matrices can be decomposed into:

- $d_1(t) = b_1\Delta d_1$.
- $d_2(t) = b_{20}\Delta d_2$.
- $b_2(t) = b_{20}(1 + l_\varepsilon(t))$.
- $A_{21}(t) = b_{20}\Delta A_{21}$.
- $A_{22}(t) = A_{220} + b_{20}\Delta A_{22}$.
- $A_{12}(t) = b_1\Delta A_{12}$.

Where: $A_{11} = \begin{bmatrix}0 & 1\\ 0 & -\frac{\mu_x}{M_x}\end{bmatrix}$, $\Delta A_{12} = \begin{bmatrix}\frac{m(g+\ddot{z})}{M_x} & \frac{2m\dot{l}}{M_x}\end{bmatrix}$, $\Delta d_1 = -\ddot{x}_r - \frac{\mu_x}{M_x}\dot{x}_r$, $b_1 = \begin{bmatrix}0\\ l_0\end{bmatrix}$,

$A_{220} = \begin{bmatrix}0 & 1\\ -\omega_0^2 & 0\end{bmatrix}$, $b_{20} = \begin{bmatrix}0\\ -1\end{bmatrix}$, $\Delta d_2 = -\frac{\mu_x}{lM_x}\dot{x}_r$, $\Delta A_{21} = \begin{bmatrix}0 & -\frac{\mu_x(1+l_\varepsilon(t))}{l_0 M_x}\end{bmatrix}$,

$\Delta A_{22} = \begin{bmatrix}\Delta\psi_\theta(t) & \Delta\delta_\theta(t)\end{bmatrix}$, $\Delta\psi_\theta(t) = \frac{M_x+m}{M_x}(\frac{\ddot{z}}{l_0} + (\omega_0^2 + \frac{\ddot{z}}{l_0})l_\varepsilon(t) + \frac{m}{M_x+m}\omega_0^2)$

and $\Delta\delta_\theta(t) = 2\frac{\dot{l}}{l_0}(1+l_\varepsilon)(\frac{m+M_x}{M_x})$.

The described crane has two degrees of freedom, x and θ_x, and must be controlled by using one control action. The next step is to design a suitable control input that includes the two control components.

$$u_x = -K_e e + K_\theta\theta + \rho(e,\theta), \tag{65}$$

where $K_e = [k_{e1}, k_{e2}]$ and $K_\theta = [k_{\theta 1}, k_{\theta 2}]$ are the corresponding gains of the linear part of the control law and $\rho(e,\theta)$ corresponds to the twisting controller,

$$\rho(e,\theta) = -K\overline{\text{sign}}(e) + R\overline{\text{sign}}(\theta), \tag{66}$$

where:

- $R = [r_1, r_2]$, and $\overline{\text{sign}}(\theta) = [\text{sign}(\theta_1), \text{sign}(\theta_2)]^T$.
- $K = [k_1, k_2]$ and $\overline{\text{sign}}(e) = [\text{sign}(e_x), \text{sign}(e_v)]^T$.

The closed-loop version of (64) with control laws (65)-(66):

$$\begin{bmatrix}\dot{e}\\ \dot{\theta}\end{bmatrix} = \begin{bmatrix}\bar{A}_{11} & b_1\Delta\bar{A}_{12}\\ b_2(K_x + \Delta A_{21}) & \bar{A}_{22} + b_2\Delta A_{22}\end{bmatrix}\begin{bmatrix}e\\ \theta\end{bmatrix} + \begin{bmatrix}b_1\\ b_2\end{bmatrix}\rho(e,\theta) + \begin{bmatrix}b_1\Delta d_1\\ b_{20}\Delta d_2\end{bmatrix}, \tag{67}$$

with $\bar{A}_{11} = A_{11} - b_1 K_e$, $\bar{A}_{22} = A_{220} - b_{20}K_\theta$, $\Delta\bar{A}_{12} = \Delta A_{12} + K_\theta$. The next properties are satisfied:

- The pair (A_{11}, b_1) is controllable.
- The pair (A_{220}, b_{20}) is controllable.
- $\bar{A}_{11}^T P_e + P_e\bar{A}_{11} = -Q_e$.

where P_e and Q_e are symmetric positive definite matrices. Under these assumptions and using the vector Lyapunov function approach, the stability of the closed loop system will be studied in the next part of this section.

4.5 Stability Analysis

Now we propose the vector Lyapunov function, $V = [V_e, V_\theta]^T$, with: $V_e = \frac{1}{2}e^T P_e e + l_0 k_1 \gamma |e_x|$ and $V_\theta = \frac{1}{2}\theta^T P_\theta(t)\theta + r_1\phi|\theta_1|$, and the matrices P_e and $P_\theta(t)$:

$$P_e = \begin{bmatrix} \gamma\psi_e + \delta_e & 1 \\ 1 & \gamma \end{bmatrix}, \quad P_\theta(t) = \begin{bmatrix} \phi\psi_\theta(t) + \delta_\theta(t) & 1 \\ 1 & \phi \end{bmatrix},$$

with:

- $\psi_e = k_{e1} l_0 > 0$; $\delta_e = k_{e2} l_0 + \frac{\mu_x}{M_x} > 0$.
- $\psi_\theta(t) = \psi_{\theta 0} + \Delta\psi_\theta(t) > 0$; $\overline{\psi_\theta} = \psi_{\theta 0} + || \Delta\psi_\theta ||_\infty$.
- $\psi_{\theta 0} = \omega_0^2 + k_{\theta 1}$; $\underline{\psi_\theta} = \psi_{\theta 0} - || \Delta\psi_\theta ||_\infty$.
- $\delta_\theta(t) = \delta_{\theta 0} + \Delta\delta_\theta(t) > 0$; $\delta_{\theta 0} = k_{\theta 2}$.
- $\underline{\delta_\theta} = \delta_{\theta 0} - || \Delta\delta_\theta ||_\infty$; $\overline{\delta_\theta} = \delta_{\theta 0} + || \Delta\delta_\theta ||_\infty$.

Functions V_e and V_θ are definite positive if the next conditions are satisfied:

- $\gamma > 0$, $\gamma\psi_e + \delta_e > 0$ and $\gamma\psi_e + \delta_e > \frac{1}{\gamma}$.
- $\phi > 0$, $\phi\psi_{\theta 0} + \delta_{\theta 0} > \phi || \Delta\psi_\theta ||_\infty + || \Delta\delta_\theta ||_\infty + \frac{1}{\phi}$.

Function V_θ satisfies the next inequality:

$$\frac{1}{2}\theta^T \underline{P_\theta}\theta < V_\theta < \frac{1}{2}\theta^T \overline{P_\theta}\theta + r_1\phi \mid \theta_1 \mid, \tag{68}$$

where: $\underline{P_\theta} = \begin{bmatrix} \underline{\psi_\theta}\phi + \underline{\delta_\theta} & 1 \\ 1 & \phi \end{bmatrix}$ and $\overline{P_\theta} = \begin{bmatrix} \overline{\psi_\theta}\phi + \overline{\delta_\theta} & 1 \\ 1 & \phi \end{bmatrix}$. Functions V_e and V_θ are positive definite and decrescent:

$$\lambda_{\min}[P_e]||e||_2^2 \leq V_e \leq \overline{\gamma}(||e||_2^2 + |e_x|), \tag{69}$$

$$\lambda_{\min}[\underline{P_\theta}]||\theta||_2^2 \leq V_\theta \leq \overline{\phi}(||\theta||_2^2 + |\theta_1|), \tag{70}$$

where $\overline{\gamma} = \max\{\lambda_{\max}[P_e], l_0 k_1\}$, $\overline{\phi} = \max\{\lambda_{\max}[\overline{P_\theta}], r_1\phi\}$. Now taking the derivative to the right of V_e, we have:$D^+V_e \leq -e^T Q_e e + e^T P_e b_1 \Delta\bar{A}_{12}\theta + e^T P_e b_1 R\overline{\text{sign}}(\theta) + + e^T P_e b_1 \Delta d_1 - e^T P_e b_1 K\overline{\text{sign}}(e)$. The corresponding matrix Q_e is given by:

$$Q_e = \begin{bmatrix} l_0 k_{e1} & 0 \\ 0 & \gamma(l_0 k_{e2} + \frac{\mu_x}{M_x}) - 1 \end{bmatrix}.$$

Taking the absolute value of the terms with indefinite sign: $D^+V_e \leq -\lambda_{\min}[Q_e](||e||_2^2 + |e_x|) + +||P_e b_1||_\infty ||\Delta\bar{A}_{12}||_\infty ||e||_1 ||\theta||_1 + \varepsilon_1 ||e||_1$, where:

- $||P_e b_1||_\infty = l_0\gamma$.
- $\varepsilon_1 = l_0\gamma(r_1 + r_2) + l_0\gamma||\Delta d_1||_\infty - \underline{k}$.
- $\underline{k} = \min\{l_0(k_1 - k_2 - \frac{\lambda_{\min}[Q_e]}{l_0}), l_0\gamma k_2\}$.
- $k_1 > k_2 > \frac{\lambda_{\min}[Q_e]}{l_0}$.
- $r_1 > r_2 > k_1 + k_2 \Rightarrow 0 < \varepsilon_1 << 1$.

All norms in $\mathbb{R}^n$ are equivalent, for example if $z \in \mathbb{R}^n$ we have $||z||_2 \leq ||z||_1 \leq \sqrt{n}||z||_2$. Considering the last inequality:

$$D^+V_e \leq -\lambda_{\min}[Q_e](||e||_2^2 + |e_x|) + +2l_0\gamma||\Delta\bar{A}_{12}||_\infty||e||_2||\theta||_2 + \sqrt{2}\varepsilon_1||e||_2.$$

Now we can rewrite the last expression in terms of V_e and V_θ:

$$D^+V_e \leq -\frac{\lambda_{\min}[Q_e]}{\overline{\gamma}}V_e + (2l_0\gamma c_0||\Delta\bar{A}_{12}||_\infty V_\theta^{\frac{1}{2}} + \sqrt{2}\varepsilon_e)V_e^{\frac{1}{2}}, \tag{71}$$

where $c_0 = (\lambda_{\min}[P_e]\lambda_{\min}[\underline{P_\theta}])^{-\frac{1}{2}}$ and $\varepsilon_e = \varepsilon_1(\lambda_{\min}[P_e])^{-\frac{1}{2}}$. Finally setting the change of variables $W_1^2 = V_e$ and $W_2^2 = V_\theta$ we have:

$$D^+W_1 \leq -\frac{\lambda_{\min}[Q_e]}{2\overline{\gamma}}W_1 + l_0\gamma c_0||\Delta\bar{A}_{12}||_\infty W_2 + \frac{1}{\sqrt{2}}\varepsilon_e. \tag{72}$$

Expression (72) will be used to construct the comparison system. Now taking the derivative to the right of V_θ, and considering the bounds of l, $\dot{l}$, ψ_θ and δ_θ, we have: $D^+V_\theta \leq -\frac{1}{2}\theta^T Q_\theta(t)\theta - \phi_2(r_1 - r_2)|\theta_1| - \phi(r_2 - \varepsilon_l r_1)|\theta_2| + (1+\varepsilon_l)\phi(||K_x||_\infty + ||\Delta A_{21}||_\infty)||e||_1||\theta||_1 + (1+\varepsilon_l)\phi(||K||_\infty + ||\Delta d_2||_\infty)||\theta||_1$, where the corresponding matrix $Q_\theta(t)$ is given by:

$$Q_\theta = \begin{bmatrix} \psi_\theta - \frac{1}{2}(\dot{\psi}_\theta\phi + \dot{\delta}_\theta) & 0 \\ 0 & \delta_\theta\phi - 1 \end{bmatrix},$$

Moreover, $x^T\underline{Q_\theta}x \leq x^T Q_\theta x \leq \frac{1}{2}x^T\overline{Q_\theta}x$ where:

$$\underline{Q_\theta} = \begin{bmatrix} \underline{\psi_\theta} - \frac{1}{2}(||\dot{\psi}_\theta||_\infty\phi + ||\dot{\delta}_\theta||_\infty) & 0 \\ 0 & \underline{\delta}_\theta\phi - 1 \end{bmatrix},$$

$$\overline{Q_\theta} = \begin{bmatrix} \overline{\psi_\theta} - \frac{1}{2}(||\dot{\psi}_\theta||_\infty\phi + ||\dot{\delta}_\theta||_\infty) & 0 \\ 0 & \overline{\delta}_\theta\phi - 1 \end{bmatrix}.$$

In order to have $Q_\theta > 0$ we need to satisfy:

$$\underline{\psi_\theta} > \frac{1}{2}(||\dot{\psi}_\theta||_\infty\phi + ||\dot{\delta}_\theta||_\infty) \text{ and } \underline{\delta_\theta} > \frac{1}{\phi}, \tag{73}$$

which implies, $D^+V_\theta \leq -\lambda_{\min}[\underline{Q}_\theta]||\theta||_2^2 - (r_1 - r_2)|\theta_1| - \phi(r_2 - \varepsilon_l r_1)|\theta_2| + (1+\varepsilon_l)\phi(||K_x||_\infty + ||\Delta A_{21}||_\infty)||\theta||_1||e||_1 + (1+\varepsilon_l)\phi(||K||_\infty + ||\Delta d_2||_\infty)||\theta||_1$. Now, setting:

- $r_1 > r_2 > \varepsilon_l r_1$, $r_2 > \lambda_{\min}[\underline{Q}_\theta]$ and $||e||_1 < c$.
- $\underline{r} = \min\{(r_1 - r_2 - \lambda_{\min}[\underline{Q}_\theta]), \phi(r_2 - \varepsilon_l r_1)\}$.

We obtain: $D^+V_\theta \leq -\lambda_{\min}[\underline{Q}_\theta](||\theta||_2^2 + |\theta_1|) - \varepsilon_\theta||\theta||_1$, with:

$$\varepsilon_\theta = \underline{r} - (1+\varepsilon_l)\phi((||K_x||_\infty + ||\Delta A_{21}||_\infty)c + ||K||_\infty + ||\Delta d_2||_\infty).$$

Then, we have two cases:

$$D^+V_\theta \leq \begin{cases} -\underline{\phi}(||\theta||_2^2 + ||\theta||_1) & \text{if } \varepsilon_\theta > 0, \\ -\underline{\lambda}_{\min}[\underline{Q}_\theta](||\theta||_2^2 + |\theta_1|) + |\varepsilon_\theta|||\theta||_1 & \text{if } \varepsilon_\theta \leq 0, \end{cases}$$

where $\underline{\phi} = \min\{\lambda_{\min}[\underline{Q}_\theta], \varepsilon_\theta\}$; rewriting the last expression in terms of V_θ:

$$D^+V_\theta \leq \begin{cases} -(\underline{\phi}/\overline{\phi})V_\theta & \text{if } \varepsilon_\theta > 0, \\ -(\lambda_{\min}[\underline{Q}_\theta]/\overline{\phi})V_\theta + \frac{|\varepsilon_\theta|}{\sqrt{2}}V_\theta^{\frac{1}{2}} & \text{if } \varepsilon_\theta \leq 0. \end{cases}$$

Finally, considering the previous change of variables, we obtain:

$$D^+W_2 \leq \begin{cases} -\frac{1}{2}(\underline{\phi}/\overline{\phi})W_2 & \text{if } \varepsilon_\theta > 0, \\ -\frac{1}{2}(\lambda_{\min}[\underline{Q}_\theta]/\overline{\phi})W_2 + \frac{|\varepsilon_\theta|}{\sqrt{2}} & \text{if } \varepsilon_\theta \leq 0. \end{cases} \tag{74}$$

Now from (72) and (74) we have the comparison system:

$$\dot{W} = AW + b, \tag{75}$$

where $W = [W_1, W_2]^T$, and:

$$A = \begin{bmatrix} -\frac{1}{2}\underline{\gamma}/\overline{\gamma} & \overline{l}\overline{\gamma}_3||K_\theta||_\infty \\ 0 & -\frac{1}{2}\lambda_{\min}[\underline{Q}_\theta]/\overline{\phi} \end{bmatrix}, \; b = \begin{bmatrix} \frac{\varepsilon_e}{\sqrt{2}} \\ \frac{\varepsilon_\theta}{\sqrt{2}} \end{bmatrix}, \qquad \text{if } \varepsilon_\theta \leq 0,$$

$$A = \begin{bmatrix} -\frac{1}{2}\underline{\gamma}/\overline{\gamma} & \overline{l}\overline{\gamma}_3||K_\theta||_\infty \\ 0 & -\frac{1}{2}\underline{\phi}/\overline{\phi} \end{bmatrix}, \; b = \begin{bmatrix} \frac{\varepsilon_e}{\sqrt{2}} \\ 0 \end{bmatrix}, \qquad \text{if } \varepsilon_\theta > 0.$$

Matrix A is Hurwitz and upper triangular, which implies ultimate bounded stability of e and θ. Moreover if $\varepsilon_\theta > 0$ we have exponential stability for θ.

4.6 Simulation

Simulations were performed in Matlab/Simulink^{TM} considering the proposed control scheme and the nonlinear model, equations (1)-(5). In simulations we consider the case of parametric resonance, i.e. $\omega_1 = 2\omega_0$. The phase η and the amplitude a are unknown parameters, but amplitude a is bounded by the maximum expected amplitude of the waves. Additionally, an initial payload swing is considered in the simulation, including the initial conditions $x(0) = y(0) = 0.1m$, $\dot{x}(0) = \dot{y}(0) = 0$, $\theta_x(0) = -6^\circ$, $\dot{\theta}_x = 11.4^\circ/s$, $\beta(0) = 6^\circ$ and $\dot{\beta} = 5.7^\circ/s$. An independent generalized twisting controller is responsible for the control of the rope length, i.e. $f_l = -10e_l - 5\dot{e}_l - 15\text{sign}(e_l) - 12\text{sign}(\dot{e}_l)$, where $e_l = l - l_r$. The design parameters for the travel and traverse dynamics are:

- $a \leq 0.145$, i.e. 10% of $\overline{l}$
- $r_1 = 0.2$, $r_2 = 0.18$, $k_1 = 0.16$ and $k_2 = 0.08$.
- $k_{e1} = 6$, $k_{e2} = 8$, $k_{\theta 1} = 10$ and $k_{\theta 2} = 11$.

With these parameters expressions (73) are satisfied. Moreover, $\varepsilon_e = 0.1$ and $\varepsilon_\theta = 0.1$. For practical purposes the sign function can be approximated by $\text{sign}(x) \approx \frac{x}{|x|+\delta}$, with $\delta \ll 1$. We consider $\delta = 0.001$. The obtained results are presented in Figure 11 and Figure 12 shows the control forces.

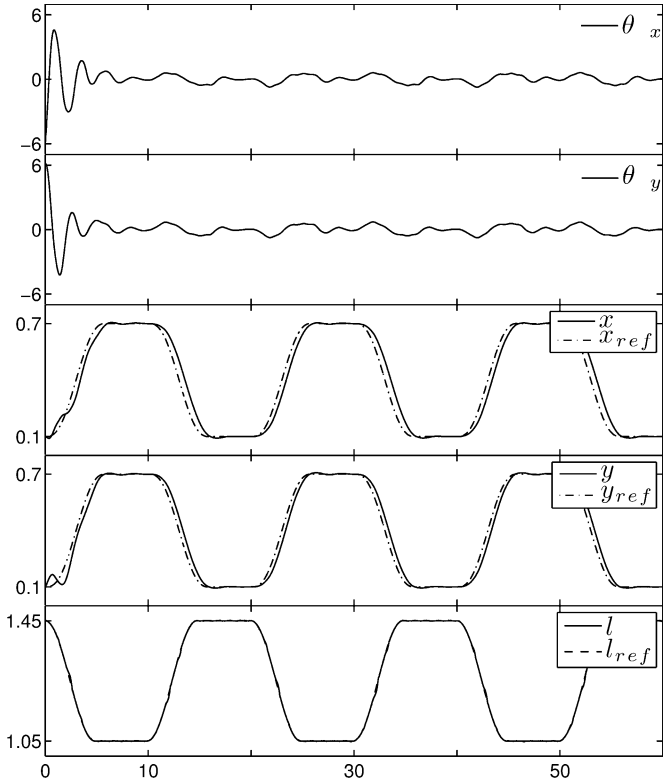

Fig. 11. Simulation: trolley position and rope length (meters); and payload oscillations (degrees) vs time (seconds)

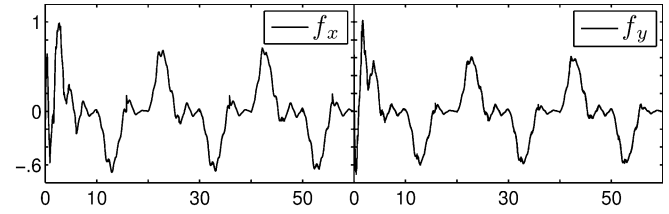

Fig. 12. Simulation: control actions (kg m/s^2) vs time (s)

4.7 Experiment

Experiments were performed in a Laboratory Inteco^{TM} 3D crane, with a cam mechanism adaptation, shown in Figure 2, adjusted to $\omega_1 = 2\omega_0 = 6.26$ rad/s and $a = 0.06$m. The laboratory crane has the variables $(x, \theta_x, y, \theta_y, l)$ available for measurement through encoders, and they are interfaced to a personal computer with an Inteco^{TM} Data Acquisition Board. The control algorithms are implemented on Matlab/Simulink^{TM} environment. The measurement of the velocities, $(\dot{x}, \dot{\theta}_x, \dot{y}, \dot{\theta}_y)$, is not available; however,

we can compute the velocities from the position measurements, see [56]. For this purpose, the velocity signal is obtained with $\frac{s}{(Ts+1)^2}$, where the filter constant T is adjusted experimentally, in this case we choose $T = 0.5$. The system frequency as well as the switching frequency is above 0.4Hz which is less than the filter frequency of 2Hz, then by the classical theory of singular perturbations is not necessary to include the filter dynamic in the model, see [24]. The obtained results are presented in Figure 10. Figure 14 shows the control forces. In the experiment, as well as in Simulation, an initial payload swing was introduced. The videos of the experiments, Figures 3 and 13 are available at the URL [49]. Notice how well the experimental results, illustrated in Figure 13, resemble the corresponding simulation in Figure 11. For comparison purposes we implemented the control law (65) neglecting the discontinuous term $\rho(e,\theta)$; in this form this control law corresponds to the PD control. Additionally, we implemented the PID control provided by INTECO^{TM}. This control law has the form: $f_m = k_{pm}e_m + k_{dm}\dot{e}_m + k_{im}\int_0^t e_m d\tau + k_m\theta_m$ for $m = x, y$ and $f_l = k_{pl}e_l + k_{dl}\dot{e}_l + k_{il}\int_0^t e_l d\tau$. The considered parameters are: $k_{px} = k_{py} = k_{pl} = 10$, $k_{dx} = 2$, $k_{dy} = k_{dl} = 1$, $k_{ix} = 10$,

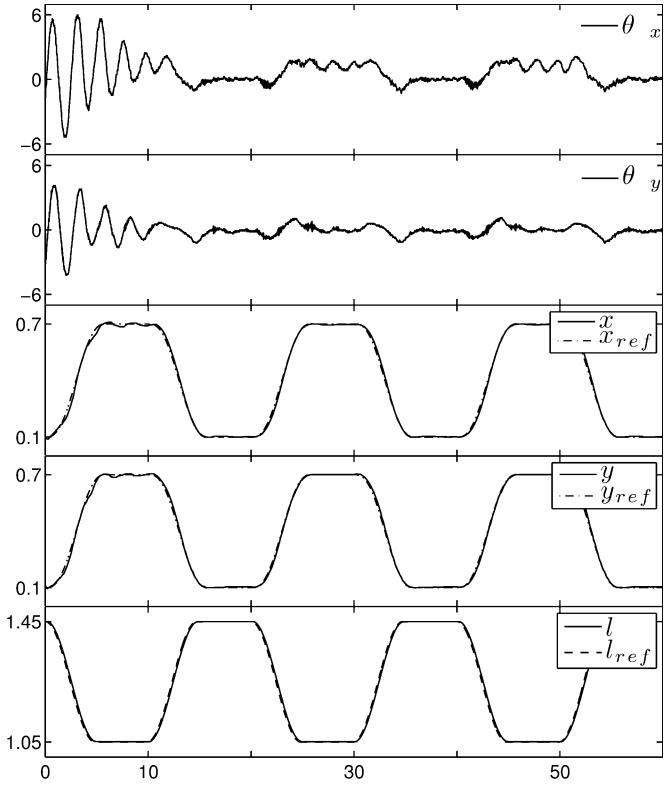

Fig. 13. Experiment: trolley position and rope length (meters), payload oscillations (degrees) vs time (seconds)

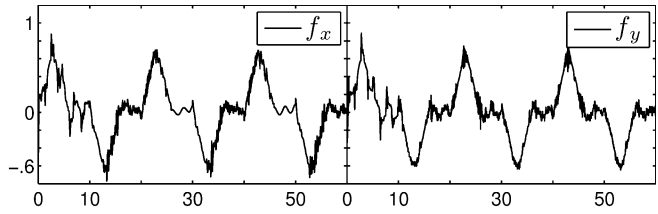

Fig. 14. Experiment: control actions (kg m/s^2) vs time (s)

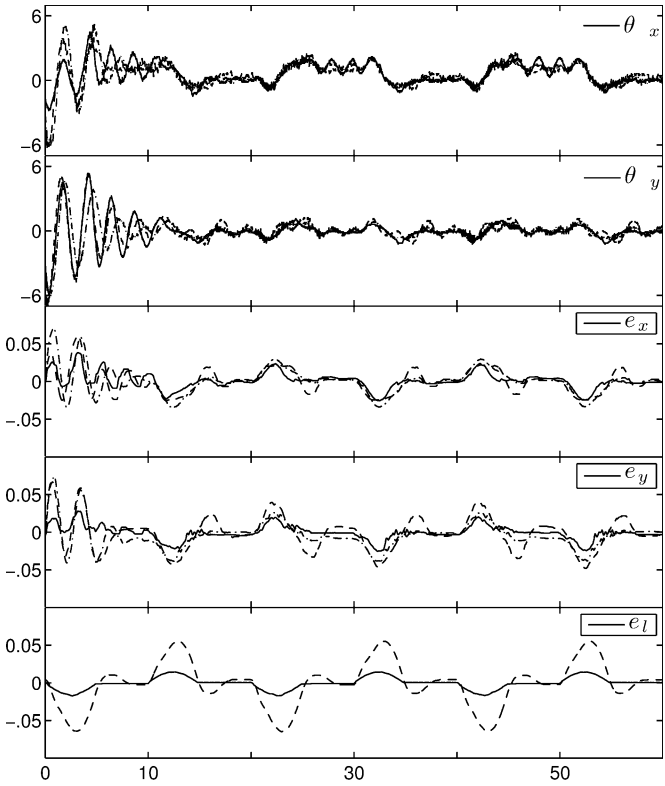

Fig. 15. Experiment: Comparison of position errors (meters), payload oscillations (degrees) with our scheme (-), PD control (-.) and PID control (- -)

$k_{iy} = 15$, $k_{il} = 20$ and $k_x = k_y = 10$. We adjust the parameters in order to add the same attenuation for the oscillations as is shown in Figure 15. This Figure shows the oscillations θ_x and θ_y, and the position errors for the positions x, y and l obtained with the PID control (- -), PD control (-.) and the generalized twisting controller (-) presented in this chapter. The generalized twisting controller not only avoids the parametric resonance effect but also provides better performance, reducing the positions errors, as we can observe in Figure 15.

Remark 5

Since syntonization rules do not exist for the PID controller in order to avoid the parametric resonance, it could be possible, for some frequencies and some rope lengths, that the parametric resonance effect appears with the PID controller. Besides, the proposed controller is supported by the vector Lyapunov method, and the stability is guaranteed.

5 Conclusions

We presented a solution to the problem of tracking, oscillation attenuation and avoidance of parametric resonance in a parametrically excited crane. We modeled the crane as a pendulum with an oscillating support, obtaining the Mathieu and Ince equations in the established zero dynamics. Stability is ensured by analyzing the corresponding Arnold tongues. Furthermore, the STA was proposed in order to guarantee the Lipschitz continuous property of the control law as well as the estimation of the time convergence rate.

On the other hand, based on the vector Lyapunov function approach a new controller has been introduced. The proposed controller is formed by two components, one of them is discontinuous motivated by the "Twisting" algorithm. In this case, we are not enforcing the sliding modes. The method of vector Lyapunov functions was successful and provides the ultimate bounded stability conditions for the closed loop system.

We tested and validated the proposed controllers in a laboratory crane which includes a cam mechanism adaptation, obtaining good results. Extensions of "Twisting" and "Super-Twisting" algorithms applied to most general linear periodic systems as well as the almost periodic case are considered for future work.

Acknowledgement. With this chapter the authors want to acknowledge the contribution of Professor Okyay Kaynak in the development of sliding mode control. His energy, his willing and abilities to help to all of colleagues, the excellent organization VSS08 workshop pushing the VSS community to reach the high level results. Thank you Okyay!

The authors also want to acknowledge the CONACyT grant 132125 and PAPIIT grant 113613 and Postdoctoral Program of UNAM.

References

1. Abdel-Rahman, E.M., Nayfeh, A.H.: Dynamics and Control of Cranes: A Review. Journal of Vibration and Control 9, 863–908 (2003)
2. Arnol'd, V.I.: Remarks on the perturbation theory for problems of Mathieu type. Russian Math. Surveys 38(4), 215–233 (1983)
3. Bartolini, G., Pisano, A., Usai, E.: Second-order sliding-mode control of container cranes. Automatica 38, 1783–1790 (2002)
4. Bartolini, G., Pisano, A., Usai, E.: A survey of applications of second order sliding mode control to mechanical systems. International Journal of Control 76, 875–892 (2003)

5. Bartolini, G., Pisano, A., Usai, E.: Output-feedback control of container cranes: a comparative analysis. Asian Journal of Control 5, 578–593 (2003)
6. Bartoszewicz, A., Kaynak, O., Utkin, V.I.: Guest Editorial: Industrial Applications of Sliding Mode Control: Part I. IEEE Trans. Indust. Electron 55(11), 3806–3808 (2008)
7. Bellman, R.: Vector Lyapunov Functions. J. SIAM Control Ser. A 1(1), 32–34 (1962)
8. Bittanti, S., Colaneri, P.: Periodic Systems: Filtering and Control. Springer, London (2009)
9. Björkbom, M., Nethi, S., Eriksson, L.M., Jäntti, R.: Wireless control system design and co-simulation. Control Engineering Practice 19, 1075–1086 (2011)
10. Boiko, I.: Discontinuous Control Systems: Frequency-Domain Analysis and Design. Birkhäuser, Boston (2009)
11. Castaños, F., Fridman, L.: Analysis and Design of Integral Sliding Manifolds for Systems With Unmatched Perturbations. IEEE Transaction on Automatic Control 51, 853–858 (2006)
12. Cooley, W.W., Clark, R.N., Buckner, R.C.: Stability in Linear Systems Having a Time-Variable Parameter. IEEE Transactions on Automatic Control AC 9, 426–434 (1964)
13. Davila, J., Fridman, L., Levant, A.: Second order Sliding-Mode Observer for Mechanical System. IEEE Transactions on Automatic Control 50, 1785–1789 (2005)
14. Davila, J.: Exact Tracking Using Backstepping Control Design and High-order Sliding Modes. IEEE Transactions on Automatic Control 58, 2077–2081 (2013)
15. Erbatur, K., Kaynak, O., Sabanovic, A.: A Study on Robustness Property of Sliding Mode Controllers: A Novel Design and Experimental Investigations. IEEE Trans. Indust. Electron. 46(5), 1012–1018 (1999)
16. Ferreira, A., Bejarano, F.J., Fridman, L.: Unmatched uncertainties compensation based on high-order sliding mode observation. International Journal of Robust and Nonlinear Control 23, 754–764 (2013)
17. Ferreira, A., Punta, E., Fridman, L., Bartolini, G., Delprat, S.: Nested backward compensation of unmatched perturbations via HOSM observation. Journal of the Franklin Institute 351, 2397–2410 (2014)
18. Filippov, A.F.: Differential equations with discontinuities right-hand sides. Kluwer Academic Publishers, Dordrecht (1988)
19. Fridman, L.: Slow periodic motions in variable structure systems. International Journal of Systems Science 33(14), 1145–1155 (2002)
20. Henry, R.J., Masoud, Z.N., Nayfeh, A.H., Mook, D.T.: Cargo pendulation reduction on ship mounted cranes via Boom-Luff angle actuation. Journal of Vibration and Control 7, 1253–1264 (2001)
21. Kaynak, O., Bartoszewicz, A., Utkin, V.I.: Guest Editorial: Industrial Applications of Sliding Mode: Control Part II. IEEE Transactions on Industrial Electronics 56(9), 3271–3274 (2009)
22. Kimiaghalam, B., Homaifar, A., Bikdash, M.: Feedback and Feedforward Control Law for a ship Crane with Maryland Rigging System. In: IEEE Proceedings of the American Control Conference (2000)
23. Kiss, B.: Control of a reduced size model of US Navy crane using only motor position sensors. In: Isidori, A., Lamma, F., Respondek, W. (eds.) Nonlinear Control in the Year 2000. 259, vol. LNCIS, pp. 1–12. Springer, Heidelberg (2000)
24. Kokotović, P., Khalil, H., O'Reilly, J.: Singular Perturbation Methods in Control. SIAM (1999)
25. Lakshmikantham, V., Leela, S., Martynyuk, A.A.: Practical stability of nonlinear systems. World Scientific. Pub. Co. Inc, Singapore (1990)
26. Lakshmikantham, V., Matrosov, V.M., Sivasundaram, S.: Vector Lyapunov Functions and Stability of Nonlinear Systems. Kluwer Academic Publishers, Dordrecht (1991)
27. Ho-Hoon, L.: Modeling and Control of a Three-Dimensional Overhead Crane. Journal of Dynamic Systems, Measurement, and Control 120, 471–476 (1998)

28. Levant, A.: Sliding order and sliding accuracy in sliding mode control. International Journal of Control 58(6), 1247–1263 (1993)
29. Levant, A.: High order sliding modes, differentiation and output feedback control. International Journal of Control 76(9), 924–941 (2003)
30. Levant, A.: Principles of 2-sliding mode design. Automatica 43, 576–586 (2007)
31. Magnus, W., Winkler, S.: Hill's Equation. John Wiley and Sons, Inc., New York (1966)
32. Masoud, Z.N., Nayfeh, A.H., Mook, D.T.: Cargo pendulation reduction of ship-mounted cranes. Nonlinear Dynamics 35, 299–311 (2004)
33. Michel, A.N., Waing, K., Hu, B.: Qualitative theory of dynamical systems: The role of stability preserving mappings. Marcel Dekker Inc., New York (2001)
34. Minorsky, N.: Parametric Excitation. Journal of Applied Physics 22, 49–54 (1951)
35. Moreno, J.A., Osorio, M.: Strict Lyapunov Functions for the Super-Twisting Algorithm. IEEE Transactions on Automatic Control 57, 1035–1040 (2012)
36. Moreno-Ahedo, L., Collado, J., Vázquez, C.: Parametric Resonance Cancellation Via Reshaping Stability Regions: Numerical and Experimental Results. IEEE Transactions on Control Systems Technology 22(2), 753–760 (2014)
37. Nayfeh, A.H., Mook, D.T.: Nonlinear Oscillations (Wiley Classics Library). John Wiley and Sons, Inc, London (1995)
38. Ngo, Q.H., Hong, K.S.: Sliding-Mode Antisway Control of an Offshore Container Crane. IEEE/ASME Transactions on Mechatronics 17, 201–209 (2002)
39. Ngo, Q.H., Hong, K.S.: Dynamics of the container crane on a mobile harbor. Ocean Engineering 53, 16–24 (2012)
40. Patel, R.V., Toda, M.: Quantitative measures of robustness for multivariable systems. In: Proc. of Joint Automatic Control Conference TP 8-A (1980)
41. Peña-Ramirez, J., Fey, R., Nijmeijer, H.: An Introduction to Parametric Resonance. In: Fossen, T.I., Nijmeijer, H. (eds.) Parametric Resonance in Dynamical Systems, pp. 1–13. Springer (2012)
42. Pisano, A., Scodina, S., Usai, E.: Load swing suppresion in the 3-dimensional overhead crane via second-order sliding-modes. In: The 11th International Workshop on Variable Structure Systems, pp. 452–457 (2010)
43. Schaub, H.: Rate-based ship-mounted crane payload pendulation control system. Control Engineering Practice 16, 132–145 (2008)
44. Shtessel, Y., Shkolnikov, I., Levant, A.: Smooth second order sliding modes: missile guidance. Automatica 43(8), 1470–1476 (2007)
45. Shtessel, Y., Edwards, C., Fridman, L., Levant, A.: Sliding Mode Control and Observation. Birkäuser, New York (2014)
46. Todd, M.D., Vohra, S.T., Leban, F.: Dynamical measurement of ship crane load pendulation. In: Conference Proceedings Oceans MTS/IEEE, pp. 1230–1236 (1997)
47. Utkin, V., Guldner, J., Shi, J.: Sliding Mode Control in Electromechanical Systems. Taylor and Francis, London (2009)
48. Utkin, V.: On Convergence Time and Disturbance Rejection of Super-Twisting Control. IEEE Transactions on Automatic Control 58, 2013–2017 (2013)
49. Videos of Experiments, `https://sites.google.com/site/carlosvazquezcontact/videos/parametrically-excited-crane`
50. Vázquez, C., Collado, J., Fridman, L.: Control of a Parametrically Excited Crane: A Vector Lyapunov Approach. IEEE Transactions on Control Systems Technology 21(6), 2332–2340 (2013)

51. Vázquez, C., Collado, J., Fridman, L.: Super twisting control of a parametrically excited overhead crane. Journal of the Franklin Institute 351(4), 2283–2298 (2014)
52. Weinmann, A.: Uncertain Models and Robust Control. Springer, New York (1991)
53. Witz, J.A.: Parametric Excitation of Crane Loads in Moderate Sea States. Ocean Engineering 22(4), 411–420 (1995)
54. Yakubovich, V.A., Starzhinskii, V.M.: Linear Differential Equations with Periodic Coefficients. John Wiley and Sons Inc., New York (1975)
55. Yu, X., Kaynak, O.: Sliding Mode Control with Soft Computing: A Survey. IEEE Trans. Indust. 9, 3275–3285 (2009)
56. Åström, K.J., Block, D.J., Spong, M.W.: The Reaction Wheel Pendulum. Morgan and Claypool Publishers (2007)

Controlling the Pitch and Yaw Angles of a 2-DOF Helicopter Using Interval Type-2 Fuzzy Neural Networks

Mojtaba Ahmadieh Khanesar[1] and Erdal Kayacan[2]

[1] Department of Electrical and Control Engineering,
Faculty of Electrical and Computer Engineering, Semnan University, Semnan, 35131, Iran
ahmadieh@semnan.ac.ir
[2] School of Mechanical & Aerospace Engineering, Nanyang Technological University,
50 Nanyang Avenue, Singapore 639798
erdal@ntu.edu.sg

Abstract. Due to not only having strong nonlinear inter-couplings in its model but also being an open-loop unstable system, control of a 2-degree of freedom (DOF) helicopter is a challenging task. This chapter deals with the decentralized control of the Quanser 2-DOF helicopter system by designing an interval type-2 fuzzy neural network for the control of the pitch and yaw angles by using a sliding mode control theory-based training algorithm. The proposed control method is known as feedback error learning in which an intelligent controller, a type-2 fuzzy neural network in this case, works in parallel with a conventional PD controller. In the proposed scheme, on one hand, the conventional PD controller is responsible to maintain the stability of the system until the intelligent controller takes the responsibility of controlling the system. On the other hand, the intelligent controller learns the system dynamics online with a sliding mode control-theory based learning algorithm. The simulation results show that without having neither a priori knowledge about the mathematical model of the system nor its parameters, the proposed control algorithm is able to track the reference signals for both yaw and pitch angles without giving a steady state error. In addition, the simulation results show the superiority of the proposed control scheme over its type-1 counterpart in the presence of noise in the system. In addition to its robustness, the sliding mode control theory-based learning algorithm has additional advantages such as having no matrix manipulations or partial derivatives which makes the overall training and control algorithm computationally simple and fast when compared to other methods, e.g. gradient-descent based methods.

Keywords: 2-DOF helicopter, sliding mode control theory-based learning algorithm, type-2 fuzzy neural network, feedback error learning.

1 Introduction

Over the last decades, control of helicopters has received more attention among other aerial vehicles due to their abilities of performing agile maneuvers in relatively small spaces and being able to take-off and land on small areas vertically. These features

X. Yu and M. Önder Efe (eds.), *Recent Advances in Sliding Modes*,
Studies in Systems, Decision and Control 24, DOI: 10.1007/978-3-319-18290-2_17

make helicopters more versatile aerial vehicles for short distance transportation when compared to fixed wing aerial vehicles. Consequently, helicopters have found wide application areas, e.g. traffic surveillance, air-sea rescue, fire fighting, teleoperation, visual servoing/tracking, etc. [12, 33]. Howbeit, helicopter dynamics are highly nonlinear with having strong cross-couplings in their models as well as being open loop unstable systems. Hence, helicopters are benchmark nonlinear systems since their control is a challenging task [4].

In addition to inherent complexities in helicopter models, identification of these systems is not a straight forward and easy task. In most of the cases, determination of parameters of a helicopter model require specific experiments and each experiment needs to be repeated many times to get more accurate identification results which is an expensive and time-consuming task. In order to reduce the number of experiments and simplify the identification process, a simpler method is proposed in [40]. In the mentioned investigation, an implementation of soft computing methodologies, genetic algorithm and fuzzy logic theory, is proposed for the identification and control of 2-DOF nonlinear helicopter model (Humusoft CE 150). Another challenge of controlling helicopters is that these systems are subject to inherent and external uncertainties, such as operating under windy environments. What is more, suppression of moments caused by the variation in loading conditions affect helicopter flight control system adversely [3]. These moments are listed in [3] as weight variations, turbulence in the fuel tank, coolant tanks and hydraulic fluid tanks. Similarly, any abrupt and unforeseen changes during the flight may cause disturbance torques in the system, e.g. change of center of gravity due to passenger or load changes. Since the fuselage acts as a pendulum suspended from the rotor, the ideal condition for the helicopter is to keep its horizontal position in hovering flight. The mentioned disturbances will change the center of gravity of the helicopter which will cause a change in the angle at which it is hung from the support point resulting in additional torques in the system [31].

The simplest case for a given disturbance is a bias resulting in a steady state error in the control system. The error can be compensated by using an integral action [42]. However, the disturbances in a helicopter system mentioned above are more complicated and hard to model, and they must be dealt with sophisticated control methods. In the case of dealing with a 2-DOF helicopter, the control is even more complicated than having a conventional helicopter. The reason for the mentioned complexity is that the simplicity in the mechanical designs comes at a price of the complexity in the model. More specifically, in order to simplify the mechanical structure, 2-DOF helicopter is designed in a way that the blades of the rotors have a fixed angle of attack, but the speeds of the rotors are manipulated to control the system [3]. As a consequence, 2-DOF helicopter has significant cross-coupled nonlinearities. Hence, 2-DOF helicopters have been used as a benchmark system for several advanced control algorithms. In [2], a new sliding surface is proposed to handle cross-coupling affects in the system, and it is shown that the designed controller provides robustness against cross-coupling as well as performance along with the freedom to operate the system in nonlinear range. An adaptive super-twisting control for a 2-DOF helicopter has been proposed in [36]

with a nonlinear extended state observer for estimating non-measurable states and external disturbances. The experimental results show that the proposed control scheme increases robustness under non-modeled dynamics and external disturbances. In [10], nonlinear predictive control for tracking control of 2-DOF helicopter is proposed, and it is claimed that while the nonlinear controller can control the system with a high accuracy, its linear counterpart is unable to stabilize the system. In [28], two multivariable model predictive control strategies, selfish and solidary, are investigated for the control of 2-DOF helicopter system, and its results are compared with the ones by using a linear quadratic regulator. It is reported that the main differences between selfish and solidary control arise at the moment that the constraints are active. In [27], the control of a 2-DOF helicopter is performed by using a feedback linearization technique, e.g. input-output linearization.

All the control algorithms listed above have tried to improve their performances by using more sophisticated algorithms, such as being MIMO instead of SISO or using nonlinear models instead of using linear models, etc. However, it is to be noted that all these designs are model-based controllers, and they need an accurate mathematical model of the system. However, as explained before, to obtain an accurate mathematical of the helicopter systems is a time consuming and challenging task. When the mathematical model of the system is not precisely known, model-free control methods may be preferable since they do not need the mathematical model of the system. These approaches are conceptually simple and they lessen the need for physical and mathematical knowledge of the system. Artificial neural networks are universal approximators, and they have been implemented very successfully in the identification and control of nonlinear dynamic systems. By using their learning ability, neural networks can learn the system dynamics online and provide better performances when compared to conventional model-based control algorithms. For instance, in [12], neural backstepping and neural sliding mode block control techniques are proposed in order to control the pitch and yaw positions of a 2-DOF helicopter. It is reported that although both controllers are able to show good performance, the block control technique presents slightly better performance when compared to backstepping algorithm.

Among model-free approaches, fuzzy logic systems are one of the most popular methods because of their strength to model expert and experienced human knowledge. When the expert knowledge about a system is not complete and/or sufficient, fuzzy neural networks (FNNs) can be used to learn more about the system than is available through the expert. Basically, FNNs are learning machines that find the fuzzy logic system parameters (i.e., fuzzy sets, fuzzy rules) by exploiting approximation techniques from neural networks [25]. Thus, FNNs can simultaneously use expert human knowledge and learn from measured input/output data [35, 41]. There are two types of FNNs: type-1 and type-2 which differ in their membership functions (MFs). The MFs in T1FNN are totally crisp, while they are themselves fuzzy in type-2 fuzzy neural networks (T2FNN). Therefore, the antecedents and consequent parts in T2FNNs are interval rather than a single value resulting in interval and uncertain rule bases. This uncertain rule base of T2FNN makes it possible to model and minimize the drawbacks

of uncertainties of real world systems. Moreover, T2FNNs have more degrees of freedom and are capable of controlling the system with higher performance specially in the presence of measurement noise [1, 19, 21, 23, 37]. Regardless of being type-1 or type-2, FNNs are also preferred to control 2-DOF helicopters. For instance, in [4], a FNN structure with parameterized conjunctions are used to control the desired pitch and yaw angles of a 2-DOF helicopter, and its performance is compared with a PID controller. It is concluded that the FNN structure gives a fast transient response and low RMSE value as compared to the conventional PID controller.

The earlier FNN controllers (regardless of using type-1 or type-2 MFs) suffer from the lack of rigorous stability analysis which is the most important consideration in the design of a controller. This is the main reason why some researchers have made use of classical control approaches in the design of FNN based controllers. This combination makes it possible to simultaneously benefit from the flexibility and general function approximation property of FNNs and guaranteed stability analysis of classical control methods [20]. Feedback-error-learning (FEL) is one of first introductions of classical methods to FNN controllers which was first developed by Kawato in an effort to establish a stable controller which can learn the inverse dynamic of the system under control [15]. This structure comprises a fixed classical controller to ensure the stability of the system and an adaptive intelligent feed-forward controller in parallel to the fixed controller which improves the performance of the controller. The outputs of the fixed feedback controller is regarded as the error signal and is used to train the inverse model of the plant [34]. From a control theoretic viewpoint, FEL falls in adaptive control technique categories [9]. Stability analysis of FEL is considered in several papers. In [29] the stability of FEL for stable and stably invertible linear systems is proved. In [30] the stability property of FEL for a class of nonlinear dynamical systems is considered. In addition, stable FEL approaches based on sliding mode control (SMC) method are considered in several papers [8, 18]. To date, several implementations of FEL in industrial plants have been reported. For example in [1] and [11], FEL scheme is used to control an n-degrees of freedom robotic manipulator and an anti-lock breaking system respectively. It has been shown that FEL method can increase the overall performance of the system by learning the system dynamics online.

The fusion of SMC with intelligent control approaches has been widely investigated for the control nonlinear systems in recent years [8, 13, 18, 24, 26, 32]. SMC is widely known to be a robust control method for the systems with nonlinearities, uncertain parameters and bounded input disturbances [22]. Although it shows robustness against nonlinear features of the system, SMC suffers from some drawbacks such as chattering, measurement noise and conservative control signal [7, 17]. In addition, the design of an ideal SMC needs an exact model of the system which is not readily on hand and/or it includes uncertainties almost in all cases [26]. To cope with these problems, SMC is used in a combination with intelligent approaches e.g. FNNs. Because of proven general function approximation property, flexibility and capability of using human knowledge of FNNs, this structure is one of the most important structures used to overcome drawbacks of SMC [8, 18, 26]. On the other hand, FNN can benefit from the mathematical stability analysis of SMC if it is used in combination with SMC.

In this study, a novel FEL scheme is proposed to control the yaw and pitch angles of a 2-DOF helicopter in which a T2FNN works in parallel with a PD controller for each subsystem, namely yaw and pitch dynamics. The output of the PD controller is used to train the T2FNN which has two inputs: the error and the time derivate of the error. The MFs considered for the system are Gaussian type-2 membership functions with uncertain variance. The sliding mode theory-based parameter update rules are derived for such a structure, and the stability of the learning algorithm is proved by using an appropriate Lyapunov function. The required conditions for the stability of the system are also derived. In addition, an adaptive learning rate for the training of the parameters of T2FNN is introduced. Using this adaptive learning rate, it is shown that a prior knowledge about the upper bound of the states of the system and their derivatives is no longer needed. This is the most important superiority of the current approach over similar SMC based training of FNN and T2FNN. Another benefit of the current approach over the similar methods reported in literature is that the training method proposed in this paper does not include any derivative of states of the system. This is also very important feature because the derivative of the states of the system amplifies the noise power significantly. The simulation results show that the proposed approach can control the 2-DOF helicopter even in the presence of measurement noise and uncertainties which necessarily exist in the model of the system. The performance of the T2FNN is also compared with that of its type-1 counterpart in the presence of noise. It is shown that T2FNN can control the system with smaller error when there is measurement noise in the system. It is also shown that the states of the system follow the predefined sliding motion.

2 System Description

In Fig. 1, a 2-DOF helicopter system is shown. There exist two DC motor driven propellers, one for the pitch and the other for the yaw dynamics, which are mounted on a fixed base in the system. While the front propeller is responsible for controlling the elevation of the helicopter nose about the pitch axis, the back propeller controls the side to side motions of the helicopter about the yaw axis. While the inputs to the system are the voltages applied to the front and the back propellers, the output of the system is the pitch and the yaw angles in radians. The system can freely rotate around the yaw axis angle about 360 degrees [14]. When the helicopter is at rest, the pitch angle is equal to $-40.5°$and its motion is restricted between $-40.5°$and $40.5°$. The thrust forces F_p and F_y shown in Fig. 1 are generated at the distances u_p and u_y from the pitch and the yaw axes, respectively [14]. The aim of the controlled system is to be able to track time varying desired trajectories in the pitch and yaw axes. The nonlinear dynamic equations of motion are given as follows [14]:

$$\begin{aligned}(J_p + ml^2)\ddot{\theta} &= K_{pp}V_{m,p} + K_{py}V_{m,y} - mglcos\theta - B_p\dot{\theta} \\ &\quad - ml^2 sin\theta cos\theta\,\dot{\psi}^2 \\ (J_y + ml^2cos^2\theta)\ddot{\psi} &= K_{yp}V_{m,p} + K_{yy}V_{m,y} - B_y\dot{\psi} + 2ml^2 sin\theta cos\theta\,\dot{\psi}\dot{\theta}\end{aligned} \tag{1}$$

Table 1. Description of the parameters

	Description	Values
J_p	Total moment of inertia about pitch axis	$0.0384 kgm^2$
J_y	Total moment of inertia about yaw axis	$0.0431 kgm^2$
l	Center of mass length along helicopter body from pitch axis	$0.1855m$
K_{pp}	Thrust torque constant acting on pitch axis from pitch propeller	$0.2041 Nm/V$
K_{py}	Thrust torque constant acting on pitch axis from yaw propeller	$0.0068 Nm/V$
K_{yp}	Thrust torque constant acting on yaw axis from pitch propeller	$0.0219 Nm/V$
K_{yy}	Thrust torque constant acting on yaw axis from yaw propeller	$0.072 Nm/V$
g	Gravitational constant	$9.81 m/s^2$
B_p	Viscous damping about pitch axis	$0.8 N/V$
B_y	Viscous damping about yaw axis	$0.318 N/V$
m	Total moving mass of the helicopter	$1.3872 kg$
$V_{m,p}$	Voltage apply to pitch motor	$\pm 24V$
$V_{m,y}$	Voltage apply to yaw motor	$\pm 15V$

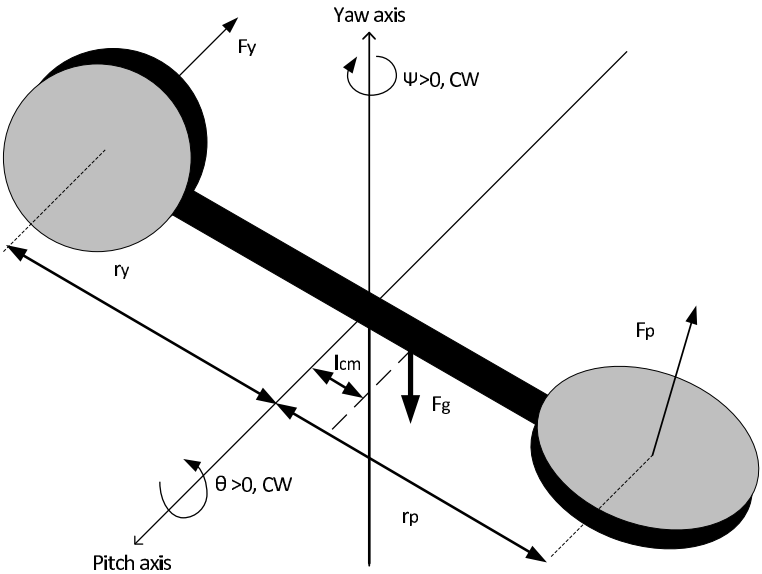

Fig. 1. Free body diagram of 2-DOF helicopter

3 The Adaptive Interval Type-2 Fuzzy Neural Network Control Framework

3.1 The Control Scheme

In this subsection, the proposed sliding mode T2FNN is presented. Figure 2 shows the control scheme.

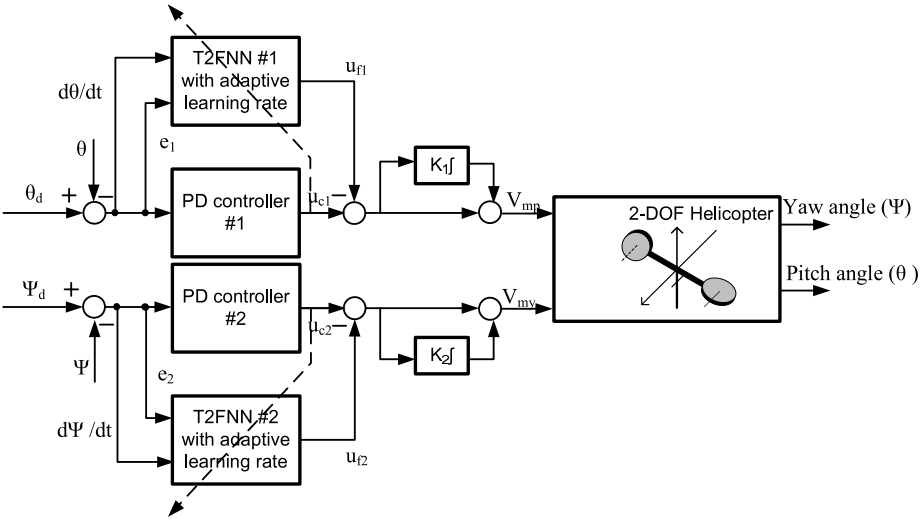

Fig. 2. Block diagram of the proposed fuzzy neural network scheme

The PD controller is responsible for the global asymptotic stability of the system in compact space and sliding manifold for the states of the system. The PD control law is described as follows:

$$u_c = k_P e + k_D \dot{e} \tag{2}$$

in which e is the feedback error, k_P and k_D are the gains of the PD controller. The process of finding the optimal values for the PD controller seems as to find a point on a 2-D surface. This is a difficult task in real life. However, our method works with all the PD coefficients which keeps the stability of the system. So, our method seems like to find a circle in a 2-D surface. The latter case is, of course, more practical when compared to the former case. The interior of the mentioned circle is the stability region of the overall system.

Type-2 Fuzzy Neural Network (T2FNN). The T2FNN considered here benefits from type-2 membership functions in the premise part and crisp numbers for the consequent part. This structure is called A2-C0 fuzzy system [6] and it is shown in Fig. 2. The T2FNN has two inputs and one output serving as a feedback controller.

The fuzzy *if-then* rule R_{ij} of a zero-order TS model with two input variables where the consequent part has a constant value and is defined as follows:

$$R_{ij}\text{: } \textit{If } e \text{ is } \widetilde{A}_{1i,k} \text{ and } \dot{e} \text{ is } \widetilde{A}_{2j}, \textit{ then } u_f = f_{ij}$$

where f_{ij} are constant values which are updated during training. In this paper, for T2FNN, type-2 MF Gaussian with uncertain standard deviation (please see Fig. 4) are used. The mathematical expression for the membership function is expressed as:

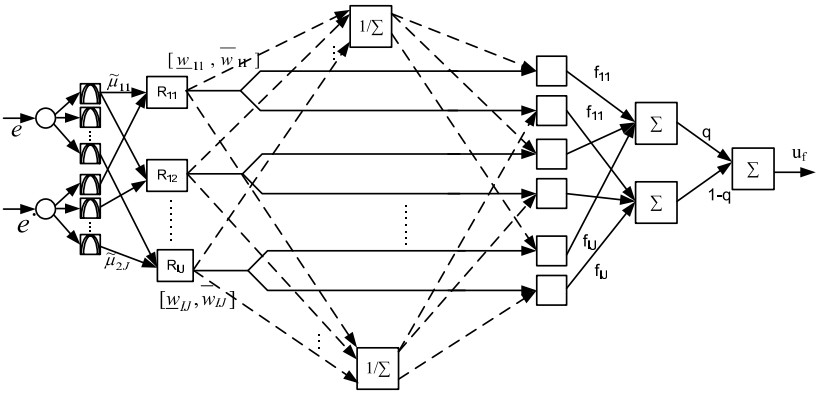

Fig. 3. Structure of T2FNN

$$\tilde{\mu}(x) = \exp\left[-\frac{(x-c)^2}{\sigma^2}\right] \tag{3}$$

where c and σ are the *center* and the *standard deviation* of the type-2 MF and x is the input.

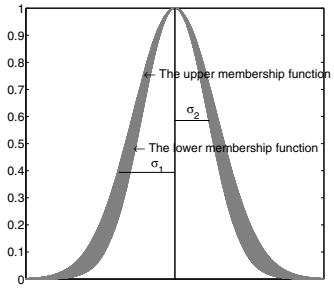

Fig. 4. Type-2 fuzzy membership function with uncertain value for its standard deviation

Using uncertain values for σ the type-2 MF has a footprint of uncertainty which is bounded with an upper and lower MF. The upper and the lower MFs are denoted as: $\overline{\mu}(x)$ and $\underline{\mu}(x)$, respectively. The firing strength of the rule R_{ij} is obtained as a T-norm of the membership functions in the premise part (by using a multiplication operator):

$$\underline{W}_{ij} = \underline{\mu}_{1i}(e)\underline{\mu}_{2j}(\dot{e}) \tag{4}$$

$$\overline{W}_{ij} = \overline{\mu}_{1i}(e)\overline{\mu}_{2j}(\dot{e}) \tag{5}$$

The Gaussian membership functions $\underline{\mu}_{1i}(e)$, $\overline{\mu}_{1i}(e)$, $\underline{\mu}_{2j}(\dot{e})$, and $\overline{\mu}_{2j}(\dot{e})$ of the inputs e and $\dot{e}$ in the above expression are of the following form:

$$\underline{\mu}_{1i}(e) = \exp\left[-(\frac{e-c_{1i}}{\underline{\sigma}_{1i}})^2\right] \tag{6}$$

$$\overline{\mu}_{1i}(e) = \exp\left[-(\frac{e-c_{1i}}{\overline{\sigma}_{1i}})^2\right] \tag{7}$$

$$\underline{\mu}_{2j}(\dot{e}) = \exp\left[-(\frac{\dot{e}-c_{2j}}{\underline{\sigma}_{2j}})^2\right] \tag{8}$$

$$\overline{\mu}_{2j}(\dot{e}) = \exp\left[-(\frac{\dot{e}-c_{2j}}{\overline{\sigma}_{2j}})^2\right] \tag{9}$$

where the real constants $\underline{\sigma}, \overline{\sigma} > 0$ and c are among the tunable parameters of the above T2FNN structure.

Hence, (4) and (5) can be rewritten as follows:

$$\underline{W}_{ij} = \exp\left[-(\frac{e-c_{1i}}{\underline{\sigma}_{1i}})^2 - (\frac{\dot{e}-c_{2j}}{\underline{\sigma}_{2j}})^2\right] \tag{10}$$

$$\overline{W}_{ij} = \exp\left[-(\frac{e-c_{1i}}{\overline{\sigma}_{1i}})^2 - (\frac{\dot{e}-c_{2j}}{\overline{\sigma}_{2j}})^2\right] \tag{11}$$

The computational output of A2-C0 structure as it is proposed in [5] is used to determine the output of TSK T2FNN.

$$u_f = \frac{q\sum_{i=1}^{I}\sum_{j=1}^{J} f_{ij}\underline{W}_{ij}}{\sum_{i=1}^{I}\sum_{j=1}^{J}\underline{W}_{ij}} + \frac{(1-q)\sum_{i=1}^{I}\sum_{j=1}^{J} f_{ij}\overline{W}_{ij}}{\sum_{i=1}^{I}\sum_{j=1}^{J}\overline{W}_{ij}} \tag{12}$$

After the normalization of (12), the output signal of the fuzzy neural network will acquire the following form:

$$u_f = q\sum_{i=1}^{I}\sum_{j=1}^{J} f_{ij}\widetilde{\underline{W}}_{ij} + (1-q)\sum_{i=1}^{I}\sum_{j=1}^{J} f_{ij}\widetilde{\overline{W}}_{ij} \tag{13}$$

where $\widetilde{\underline{W}}_{ij}$ and $\widetilde{\overline{W}}_{ij}$ are the normalized values of the lower and the upper outputs corresponding to ij node of the second hidden layer of the network:

$$\widetilde{\underline{W}}_{ij} = \frac{\underline{W}_{ij}}{\sum_{i=1}^{I}\sum_{j=1}^{J}\underline{W}_{ij}} \tag{14}$$

$$\widetilde{\overline{W}}_{ij} = \frac{\overline{W}_{ij}}{\sum_{i=1}^{I}\sum_{j=1}^{J}\overline{W}_{ij}} \tag{15}$$

$\underline{\widetilde{W}}(t)=\left[\underline{\widetilde{W}}_{11}(t)\ \underline{\widetilde{W}}_{12}(t)\ldots\underline{\widetilde{W}}_{21}(t)\ \ldots\ \underline{\widetilde{W}}_{ij}(t)\ \ldots\ \underline{\widetilde{W}}_{IJ}(t)\right]^T$ are the vector of the normalized lower output signals of the neurons from the second hidden layer of the first and the second T2FNNs respectively; $\overline{\widetilde{W}}(t)=\left[\overline{\widetilde{W}}_{11}(t)\ \overline{\widetilde{W}}_{12}\ (t)\ldots\overline{\widetilde{W}}_{21}(t)\ \ldots\ \overline{\widetilde{W}}_{ij}(t)\ \ldots\ \overline{\widetilde{W}}_{IJ}(t)\right]^T$ is the vector of the normalized upper output signals of the neurons from the second hidden layer of the IT2FNNs;
$\underline{\sigma}_1=[\underline{\sigma}_{11}\ldots\underline{\sigma}_{1i}\ldots\underline{\sigma}_{1I}]^T$, $\underline{\sigma}_2=\left[\underline{\sigma}_{21}\ldots\underline{\sigma}_{2j}\ldots\underline{\sigma}_{2J}\right]^T$, are vectors of the tuning parameters $\underline{\sigma}$ of the lower bounds of type-2 Gaussian MFs with uncertain variance. $\overline{\sigma}_1=[\overline{\sigma}_{11}\ldots\overline{\sigma}_{1i}\ldots\overline{\sigma}_{1I}]^T$, $\overline{\sigma}_2=\left[\overline{\sigma}_{21}\ldots\overline{\sigma}_{2j}\ldots\overline{\sigma}_{2J}\right]^T$, are vectors of the tuning parameters $\overline{\sigma}$ of the upper bounds of type-2 Gaussian MFs with uncertain variance. $c_1=[c_{11}\ldots c_{1i}\ldots c_{1I}]^T$ and $c_2=\left[c_{21}\ldots c_{2j}\ldots c_{2J}\right]^T$ are vectors of the tuning parameters c of the lower and upper bounds of type-2 Gaussian MFs with uncertain variance.

It is assumed that due to the control scheme adopted Fig. 2, where the conventional controller serves to guarantee global asymptotic stability in compact space, the input signals $e(t)$ and $\dot{e}(t)$, and their time derivatives can be considered bounded:

$$|e(t)|\leq B_e,\quad |\dot{e}(t)|\leq B_e\quad |\ddot{q}(t)|\leq B_{\dot{e}}\qquad \forall t \tag{16}$$

where B_e and $B_{\dot{e}}$ are assumed to be some unknown positive constants. The adaptation law for the tunable parameters is considered such that $\underline{\sigma}$, $\overline{\sigma}$, and c of the Gaussian membership functions are bounded as follows:

$$\begin{gathered}\underline{B}_\sigma\leq\|\underline{\sigma}_1\|\leq\overline{B}_\sigma,\quad \underline{B}_\sigma\leq\|\underline{\sigma}_2\|\leq\overline{B}_\sigma,\\ \|c_1\|\leq B_c,\quad \|c_2\|\leq B_c\end{gathered} \tag{17}$$

$$\begin{gathered}\underline{B}_\sigma\leq\|\overline{\sigma}_1\|\leq\overline{B}_\sigma,\quad \underline{B}_\sigma\leq\|\overline{\sigma}_2\|\leq\overline{B}_\sigma,\\ \|\overline{c}_1\|\leq B_c,\quad \|\overline{c}_2\|\leq B_c\left\|\overline{f}_{ij}\right\|\leq B_f\end{gathered} \tag{18}$$

where $\underline{B}_\sigma$, $\overline{B}_\sigma$, B_c and B_f are some unknown positive constants.

Similar to the previous case, it follows that $0<\underline{\widetilde{W}}_{ij}<1$ and $0<\overline{\widetilde{W}}_{ij}<1$. In addition, by definition, $\sum_{i=1}^{I}\sum_{j=1}^{J}\underline{\widetilde{W}}_{ij}=1$ and $\sum_{i=1}^{I}\sum_{j=1}^{J}\overline{\widetilde{W}}_{ij}=1$. It is also considered that, u and $\dot{u}$ are bounded signals too, *i.e.*

$$|u(t)|\leq B_u,\quad |\dot{u}(t)|\leq B_{\dot{u}}\quad \forall t \tag{19}$$

where B_u and $B_{\dot{u}}$ are two unknown positive constants. In similar previous papers e.g. [8, 16, 18, 38] it is assumed that the upper bounds defined by (16), (17), (18) and (19) are known. But in the current paper, using an adaptive learning rate, these parameters are no more needed to be known. This is the main improvement of the current approach with respect to above mentioned papers.

3.2 The Sliding Mode Theory-Based Learning Algorithm

The zero value of the learning error coordinate $u_c(t)$ can be defined [39] as time-varying sliding surface,*i.e.*,

$$S_c\left(u_f,u\right)=u_c\left(t\right)=u_f\left(t\right)+u\left(t\right) \tag{20}$$

which is the condition that the T2FNN is trained to become a nonlinear regulator to obtain the desired response during the tracking-error convergence movement by compensating the nonlinearity of the controlled plant. The sliding surface for the nonlinear system under control $S_p\left(e,\dot{e}\right)$ is defined as:

$$S_p\left(e,\dot{e}\right)=\dot{e}+\chi e \tag{21}$$

with χ_k being a constant determining the slope of the sliding surface.

Definition: A sliding motion will appear on the sliding line $S_c\left(u_f,u\right)=u_c\left(t\right)=0$ after a time t_h, if the condition $S_c(t)\dot{S}_c(t)=u_c\left(t\right)\dot{u}_c\left(t\right)<0$ is satisfied for all t in some nontrivial semi-open subinterval of time of the form $[t,t_h)\subset(-\infty,t_h)$.

It is desired to design an online learning algorithm for the parameters of T2FNN such that the sliding mode condition of the above definition is enforced.

The Parameter Update Rules For T2FNN

Theorem 1: If the adaptation laws for T2FNN parameters are chosen as:

$$\dot{c}_{1i}=-\beta_1\frac{\overline{\sigma}_{1i}^2}{e-c_{1i}}sgn(u_c) \tag{22}$$

$$\dot{c}_{2j}=-\beta_1\frac{\overline{\sigma}_{2j}^2}{\dot{e}-c_{2j}}sgn(u_c) \tag{23}$$

$$\dot{\underline{\sigma}}_{1i}=-\beta_1\frac{\underline{\sigma}_{1i}^3}{(e-c_{1i})^2}sgn(u_c) \tag{24}$$

$$\dot{\underline{\sigma}}_{2j}=-\beta_1\frac{\underline{\sigma}_{2j}^3}{(\dot{e}-c_{2j})^2}sgn(u_c) \tag{25}$$

$$\dot{\overline{\sigma}}_{1i}=-\beta_1\frac{\overline{\sigma}_{1i}^3}{(e-c_{1i})^2}sgn(u_c) \tag{26}$$

$$\dot{\overline{\sigma}}_{2j}=-\beta_1\frac{(\overline{\sigma}_{2j})^3}{(\dot{e}-c_{2j})^2}sgn(u_c) \tag{27}$$

$$\dot{f}_{ij}=-\alpha\frac{q\widetilde{\underline{W}}_{ij}+(1-q)\widetilde{\overline{W}}_{ij}}{(q\widetilde{\underline{W}}+(1-q)\widetilde{\overline{W}})^T(q\widetilde{\underline{W}}+(1-q)\widetilde{\overline{W}})}sgn(u_c) \tag{28}$$

$$\dot{\alpha}=\gamma_1\left|u_c\right|-\nu\gamma_1\alpha \tag{29}$$

then, given an arbitrary initial condition $u_c(0)$, the learning error $u_c(t)$ will converge firmly to zero during a finite time t_h.

Proof: See appendix A.

There is a relation between the sliding line S_p and $u_c(t)$ (the classical controller signal). If χ is taken as $\chi = \frac{k_P}{k_D}$, the following equation is obtained.

$$S_c = u_c = k_D\dot{e} + k_P e = k_D\left(\dot{e} + \frac{k_p}{k_D}e\right) = k_D S_p \tag{30}$$

Remark: Equation (30) indicates that the convergence of S_c towards zero guarantees the convergence of S_p towards zero and there exists a sliding motion in the states of the system.

4 Simulation Results

The 2-DOF helicopter system is controlled using the proposed T2FNN which is previously shown in Fig. 2. The parameters of the model considered in this study can be time varying and the measurements are subject to noise. In order to have a better comparison, the results obtained by the proposed method are compared with its type-1 counterpart. 2-DOF helicopter is a MIMO nonlinear system and two independent controllers are designed to control the pitch and the yaw axes. From the physical model of the 2-DOF helicopter, the yaw axes can be controlled by appropriate selection of $V_{m,y}$ while $V_{m,p}$ can be used to control the helicopter in pitch axes. The error (e_p) is calculated as the difference between the measured yaw angle and its desired value. This value and its time derivative are fed to the yaw controller which benefits from the structure which is discussed completely in the previous sections. The premise part of the T2FNN is composed of three Gaussian type-2 membership functions with uncertain variance for each input and hence the type-2 fuzzy system benefits from nine rules. These membership functions are distributed in the closed interval of $[-0.5, 0.5]$ initially and evolved during the training to find their optimal positions.

Figure 5 shows the step response of the controller for both pitch and yaw subsystems. The sample time of the controller is considered to be equal to $0.1msec$. As can be seen from the figure, although the 2-DOF helicopter suffers from a non-minimum phase dynamics, the proposed method is able to control it with a satisfactory performance. The non-minimum phase characteristic of the system causes an undershoot in the response in the first few miliseconds. However, the amplitude of this undershoot is no more than micro radians.

Figure 6 depicts the response of the controller when the reference signal is sinusoid. As can be seen from the figure, the response of the system for a sinusoidal reference signal is also satisfactory. In order to show the superiority of T2FNN in the presence of white Gaussian noise in the system over its type-1 counterpart, another simulation is performed in which the standard deviation of the noise is considered to be 0.0075. The experiments are performed 10 times. The mean value of the integral of squared error obtained in these experiments are equal to 1.98 for type-1 neuro-fuzzy system and 1.79 for T2FNN which shows 9.6% improvement in the favor of T2FNN. Moreover, the standard deviations of the integral of the squared error are obtained as 0.27 and 0.29 for T2FNN and its type-1 counterpart, respectively. The results obtained for the standard deviations also show that the results obtained using T2FNN are more consistent than that of type-1 neuro-fuzzy system.

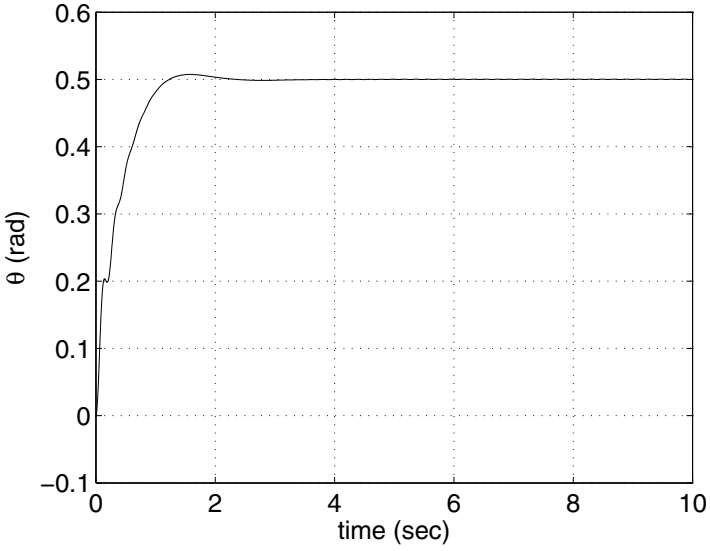

(a)

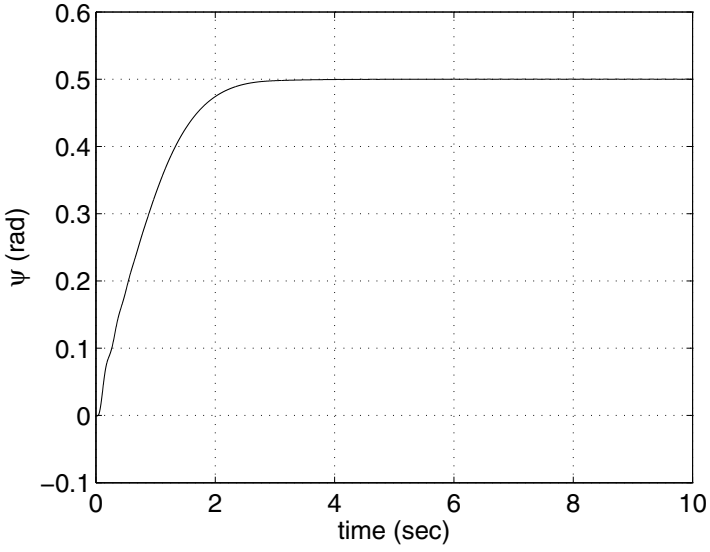

(b)

Fig. 5. The step response of the proposed controller for 5(a) pitch 5(b) yaw axes

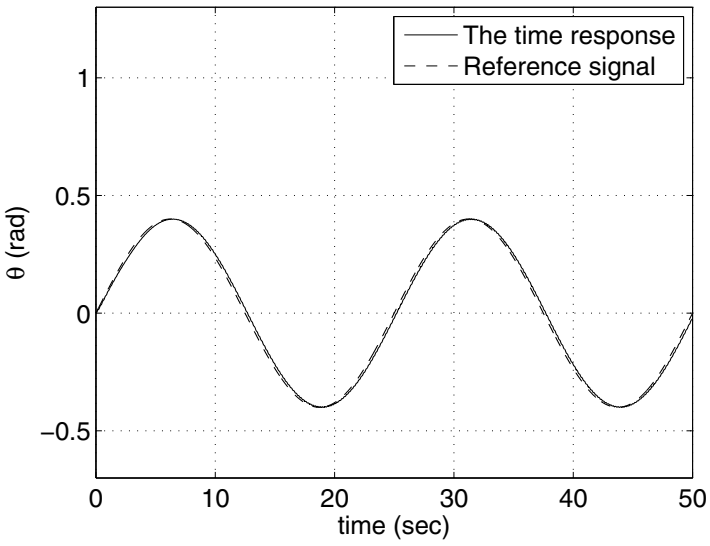

(a)

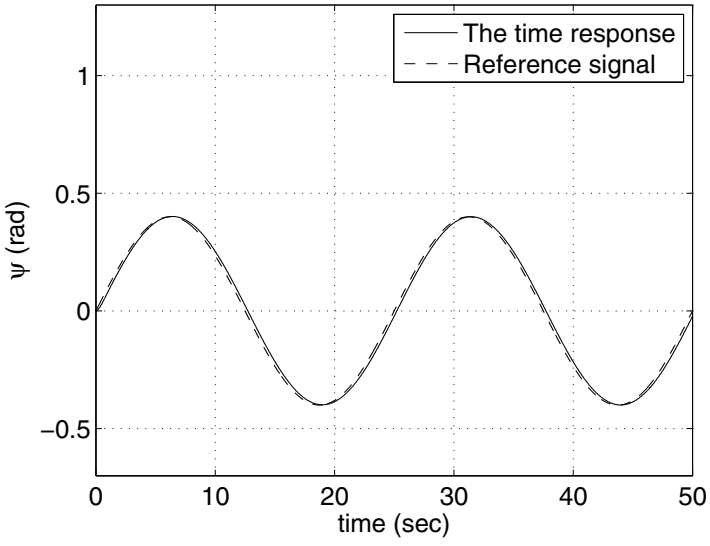

(b)

Fig. 6. The sinusoidal response of the proposed controller for 6(a) pitch 6(b) yaw axes

When using a PD controller, abrupt changes in the reference signal may produce large control signal values resulting in an instability in the system. This behavior is well-known in control theory that a PD controller is sensitive to the measurement noise in the system. However, in real-life applications, PD controller is not applied to the system directly but its output is filtered before applying it to the system. In this investigation, PD controllers with such a filter are preferred to avoid the issues explained above especially for the noisy responses.

Acknowledgement. This book chapter could not be written to its fullest without Prof. Okyay Kaynak, who was guiding us in the area of intelligent controllers and their applications in real life as well as sliding mode control theory and its use in the tuning of inteligent controllers. He challenged and encouraged us throughout not only our time spent studying under his supervision in Bogazici University but also a continuing support in our research.

5 Conclusions

The main goal of this study is to design a sliding mode control theory-based T2FNN controller for the control of yaw and pitch angles of a 2 DOF helicopter. The controller introduced in this study benefits from Gaussian membership functions with uncertain variance. A novel proof for the stability of the controller using an appropriate Lyapunov function is proposed. In addition, the designed controller benefits from an adaptive learning rate which makes it possible to control the system with less priori knowledge about the system. It is to be noted that by the use of such an adaptive parameter, it is possible to initialize the learning rate by a small value and this parameter converges to its true value during adaptation. Hence, the learning rate does not become bigger than needed. The simulation results show that the proposed method is able to control the system with a satisfactory performance. Furthermore, white Gaussian noise is added to the measurements of yaw and pitch angles of the system. The results of these simulations show that T2FNN outperforms T1FNN when there exists noise in the system. Hence, the proposed controller is a superior choice over its type-1 counterpart in the presence of measurement noise in the system.

References

1. Ahmadieh Khanesar, M., Kayacan, E., Teshnehlab, M., Kaynak, O.: Extended kalman filter based learning algorithm for type-2 fuzzy logic systems and its experimental evaluation. IEEE Transactions on Industrial Electronics PP(99), 1 (2011)
2. Ahmed, Q., Bhatti, A., Iqbal, S.: Nonlinear robust decoupling control design for twin rotor system. In: 7th Asian Control Conference, ASCC 2009, pp. 937–942 (August 2009)
3. Ahmed, Q., Bhatti, A., Iqbal, S., Kazmi, I.: 2-sliding mode based robust control for 2-dof helicopter. In: 2010 11th International Workshop on Variable Structure Systems (VSS), pp. 481–486 (June 2010)
4. Aras, A., Kaynak, O.: Trajectory tracking of a 2-dof helicopter system using neuro-fuzzy system with parameterized conjunctors. In: 2014 IEEE/ASME International Conference on Advanced Intelligent Mechatronics (AIM), pp. 322–326 (July 2014)

5. Begian, M., Melek, W., Mendel, J.: Stability analysis of type-2 fuzzy systems. In: IEEE International Conference on Fuzzy Systems, FUZZ-IEEE 2008. IEEE World Congress on Computational Intelligence, pp. 947–953 (June 2008)
6. Biglarbegian, M., Melek, W., Mendel, J.M.: On the stability of interval type-2 tsk fuzzy logic control systems. IEEE Transactions on Systems, Man, and Cybernetics, Part B: Cybernetics 40(3), 798–818 (2010)
7. Chiang, M.H.: The velocity control of an electro-hydraulic displacement-controlled system using adaptive fuzzy controller with self-tuning fuzzy sliding mode compensation. Asian Journal of Control 13(4), 492–504 (2011), http://dx.doi.org/10.1002/asjc.350
8. Cigdem, O., Kayacan, E., Khanesar, M., Kaynak, O., Teshnehlab, M.: A novel training method based on variable structure systems theory for fuzzy neural networks. In: 2011 IEEE Symposium on Computational Intelligence in Control and Automation (CICA), pp. 44–51 (April 2011)
9. Doya, K., Kimura, H., Miyamura, A.: motor control: neural models and systems theory. Int. J. Appl. Math. Comput. Sci. 11(1), 77–104 (2001)
10. Dutka, A., Ordys, A., Grimble, M.: Non-linear predictive control of 2 dof helicopter model. In: Proceedings of the 42nd IEEE Conference on Decision and Control, vol. 4, pp. 3954–3959 (December 2003)
11. Er, M.J., Liew, K.C.: Control of adept one scara robot using neural networks. IEEE Transactions on Industrial Electronics 44(6), 762–768 (1997)
12. Hernandez-Gonzalez, M., Alanis, A., Hernandez-Vargas, E.: Decentralized discrete-time neural control for a quanser 2-dof helicopter. Applied Soft Computing 12(8), 2462–2469 (2012)
13. Huang, T., Javaherian, H., Liu, D.: Nonlinear torque and air-to-fuel ratio control of spark ignition engines using neuro-sliding mode techniques. International Journal of Neural Systems 21(03), 213–224 (2011)
14. Quanser Inc.: Quanser 2-DOF Helicopter Manual (2010)
15. Kawato, M., Gomi, H.: A computational model of four regions of the cerebellum based on feedback-error learning. Biological Cybernetics 68, 95–103 (1992)
16. Kayacan, E., Cigdem, O., Kaynak, O.: Sliding mode control approach for online learning as applied to type-2 fuzzy neural networks and its experimental evaluation. IEEE Transactions on Industrial Electronics 59(9), 3510–3520 (2012)
17. Kaynak, O., Erbatur, K., Ertugnrl, M.: The fusion of computationally intelligent methodologies and sliding-mode control-a survey. IEEE Transactions on Industrial Electronics 48(1), 4–17 (2001)
18. Khanesar, M., Kayacan, E., Kaynak, O., Teshnehlab, M.: An online training algorithm based on the fusion of sliding mode control theory and fuzzy neural networks with triangular membership functions. In: 2011 8th Asian Control Conference (ASCC), pp. 617–622 (May 2011)
19. Khanesar, M., Kayacan, E., Teshnehlab, M., Kaynak, O.: Analysis of the noise reduction property of type-2 fuzzy logic systems using a novel type-2 membership function. IEEE Transactions on Systems, Man, and Cybernetics, Part B: Cybernetics 41(5), 1395–1406 (2011)
20. Khanesar, M., Kaynak, O., Teshnehlab, M.: Direct model reference takagi-sugeno fuzzy control of siso nonlinear systems. IEEE Transactions on Fuzzy Systems 19(5), 914–924 (2011)
21. Khanesar, M., Teshnehlab, M., Kayacan, E., Kaynak, O.: A novel type-2 fuzzy membership function: application to the prediction of noisy data. In: 2010 IEEE International Conference on Computational Intelligence for Measurement Systems and Applications (CIMSA), pp. 128–133 (September 2010)
22. Khanesar, M., Teshnehlab, M., Shoorehdeli, M.: Sliding mode control of rotary inverted pendulm. In: Mediterranean Conference on Control Automation, MED 2007, pp. 1–6 (June 2007)

23. Khanesar, M.A., Kaynak, O., Teshnehlab, M.: Statistical results to show the superiority of type two fuzzy logic systems over type one counterparts under noisy conditions. In: Proceedings of the IEEE International Symposium on Industrial Electronics, ISIE 2012, pp. 905–910 (May 2012)
24. Kim, H.G., Oh, S.Y.: Locally activated neural networks and stable neural controller design for nonlinear dynamic systems. International Journal of Neural Systems 06(01), 91–106 (1995)
25. Kruse, R.: Fuzzy neural network. Scholarpedia 3(10), 6043 (2008)
26. Lon-Chen Hung, H.Y.C.: Decoupled sliding-mode with fuzzy-neural network controller for nonlinear systems. International Journal of Approximate Reasoning 46, 74–97 (2007)
27. Lopez-Martinez, M., Diaz, J.M., Ortega, M., Rubio, F.: Control of a laboratory helicopter using switched 2-step feedback linearization. In: American Control Conference Proceedings of the 2004, vol. 5, pp. 4330–4335 (June 2004)
28. Medina, R., Hernandez, A., Ionescu, C., De Keyser, R.: Evaluation of constrained multivariable epsac predictive control methodologies. In: 2013 European Control Conference (ECC), pp. 530–535 (July 2013)
29. Miyamura, A., Kimura, H.: Stability of feedback error learning scheme. Systems and Control Letters 45(4), 303–316 (2002)
30. Nakanishi, J., Schaal, S.: Feedback error learning and nonlinear adaptive control. Neural Networks 17(10), 1453–1465 (2004)
31. Padfield, G.: Helicopter Flight Dynamics: The Theory and Application of Flying Qualities and Simulation Modeling. AIAA education series, American Institute of Aeronautics and Astronautics (2007)
32. Parma, G.G., Menezes, B.R.D., Braga, A.P.: Neural networks learning with sliding mode control: The sliding mode backpropagation algorithm. International Journal of Neural Systems 09(03), 187–193 (1999)
33. Perez-D'Arpino, C., Medina-Melendez, W., Fermin-Leon, L., Bogado, J., Torrealba, R., Fernandez-Lopez, G.: Generalized bilateral mimo control by states convergence with time delay and application for the teleoperation of a 2-dof helicopter. In: 2010 IEEE International Conference on Robotics and Automation (ICRA), pp. 5328–5333 (May 2010)
34. Ruan, X., Dinga, M., Gong, D., Qiaoa, J.: On-line adaptive control for inverted pendulum balancing based on feedback-error-learning. Neurocomputing 70(4-6), 770–776 (2007)
35. Sadighi, A., Jong Kim, W.: Adaptive-neuro-fuzzy-based sensorless control of a smart-material actuator. IEEE/ASME Transactions on Mechatronics 16(2), 371–379 (2011)
36. Salas, O., Castaeda, H., DeLeon-Morales, J.: Observer-based adaptive super twisting control strategy for a 2-dof helicopter. In: 2013 International Conference on Unmanned Aircraft Systems (ICUAS), pp. 1061–1070 (May 2013)
37. Sepulveda, R., Castillo, O., Melin, P., Montiel, O., Aguilar, L.: Evolutionary optimization of interval type-2 membership functions using the human evolutionary model. In: IEEE International Fuzzy Systems Conference, 2007. FUZZ-IEEE 2007, London, UK, pp. 1–6 (2007)
38. Topalov, A.V., Oniz, Y., Kayacan, E., Kaynak, O.: Neuro-fuzzy control of antilock braking system using sliding mode incremental learning algorithm. Neurocomputing 74, 1883–1893 (2011)
39. Utkin, V.I.: Sliding Modes in Control Optimization. Springer (1992)
40. Velagic, J., Osmic, N.: Identification and control of 2dof nonlinear helicopter model using intelligent methods. In: 2010 IEEE International Conference on Systems Man and Cybernetics (SMC), pp. 2267–2275 (October 2010)
41. Yu, W., Li, X.: Automated nonlinear system modeling with multiple fuzzy neural networks and kernel smoothing. International Journal of Neural Systems 20(05), 429–435 (2010)
42. Zarikian, G., Serrani, A.: Harmonic disturbance rejection in tracking control of euler-lagrange systems: An external model approach. IEEE Transactions on Control Systems Technolog 15(1), 118–129 (2007)

Appendix A

The stability analysis of the learning algorithm is considered in this section. The following variables are defined.

$$A_{1i} = \left[-(\frac{e - c_{1i}}{\underline{\sigma}_{1i}})^2 \right] \tag{31}$$

$$U_{1i} = \left[-(\frac{e - c_{1i}}{\overline{\sigma}_{1i}})^2 \right] \tag{32}$$

$$A_{2j} = \left[-(\frac{\dot{e} - c_{2j}}{\underline{\sigma}_{2j}})^2 \right] \tag{33}$$

$$U_{2j} = \left[-(\frac{\dot{e} - c_{2j}}{\overline{\sigma}_{2j}})^2 \right] \tag{34}$$

Considering (6)-(9) we have:

$$\dot{\underline{\mu}}_{1i}(e) = -2A_{1i}\dot{A}_{1i}\underline{\mu}_{1i}(e) \tag{35}$$

$$\dot{\overline{\mu}}_{1i}(e) = -2U_{1i}\dot{U}_{1i}\overline{\mu}_{1i}(e) \tag{36}$$

$$\dot{\underline{\mu}}_{2j}(\dot{e}) = -2A_{2j}(\dot{A}_{2j})\underline{\mu}_{2j}(\dot{e}) \tag{37}$$

$$\dot{\overline{\mu}}_{2j}(\dot{e}) = -2U_{2j}(\dot{U}_{2j})\overline{\mu}_{2j}(\dot{e}) \tag{38}$$

In addition considering (14) and (15), the time derivatives of $\underline{\widetilde{W}}_{ij}$ and $\overline{\widetilde{W}}_{ij}$ are obtained as:

$$\begin{aligned} \underline{\widetilde{W}}_{ij} = \frac{\underline{W}_{ij}}{\sum_{i=1}^{I}\sum_{j=1}^{J}\underline{W}_{ij}} \Rightarrow \dot{\underline{\widetilde{W}}}_{ij} = & \frac{(\underline{\mu}_{1i}(e)\underline{\mu}_{2j}(\dot{e}))'(\sum_{i=1}^{I}\sum_{j=1}^{J}\underline{W}_{ij})}{(\sum_{i=1}^{I}\sum_{j=1}^{J}\underline{W}_{ij})^2} \\ & - \frac{(\underline{W}_{ij})(\sum_{i=1}^{I}\sum_{j=1}^{J}\underline{\mu}_{1i}(e)\underline{\mu}_{2j}(\dot{e}))'}{(\sum_{i=1}^{I}\sum_{j=1}^{J}\underline{W}_{ij})^2} \end{aligned} \tag{39}$$

$$\begin{aligned} \overline{\widetilde{W}}_{ij} = \frac{\overline{W}_{ij}}{\sum_{i=1}^{I}\sum_{j=1}^{J}\overline{W}_{ij}} \Rightarrow \dot{\overline{\widetilde{W}}}_{ij} = & \frac{(\overline{\mu}_{1i}(e)\overline{\mu}_{2j}(\dot{e}))'(\sum_{i=1}^{I}\sum_{j=1}^{J}\overline{W}_{ij})}{(\sum_{i=1}^{I}\sum_{j=1}^{J}\overline{W}_{ij})^2} \\ & - \frac{(\overline{W}_{ij})(\sum_{i=1}^{I}\sum_{j=1}^{J}\overline{\mu}_{1i}(e)\overline{\mu}_{2j}(\dot{e}))'}{(\sum_{i=1}^{I}\sum_{j=1}^{J}\overline{W}_{ij})^2} \end{aligned} \tag{40}$$

Since $\underline{\widetilde{W}}_{ij} = (\underline{W}_{ij})/(\sum_{i=1}^{I}\sum_{j=1}^{J}\underline{W}_{ij})$ and $\overline{\widetilde{W}}_{ij} = (\overline{W}_{ij})/(\sum_{i=1}^{I}\sum_{j=1}^{J}\overline{W}_{ij})$ we have:

$$\begin{aligned}\dot{\underline{\widetilde{W}}}_{ij} &= \frac{\dot{\underline{\mu}}_{1i}(e)\underline{\mu}_{2j}(\dot{e}) + \underline{\mu}_{1i}(e)\dot{\underline{\mu}}_{2j}(\dot{e})}{\sum_{i=1}^{I}\sum_{j=1}^{J}\underline{W}_{ij}} \\ &- \frac{(\underline{\widetilde{W}}_{ij})(\sum_{i=1}^{I}\sum_{j=1}^{J}(\dot{\underline{\mu}}_{1i}(e)\underline{\mu}_{2j}(\dot{e}) + \underline{\mu}_{1i}(e)\dot{\underline{\mu}}_{2j}(\dot{e}))}{(\sum_{i=1}^{I}\sum_{j=1}^{J}\underline{W}_{ij})} \\ &= \frac{-2A_{1i}\dot{A}_{1i}\underline{\mu}_{1i}(e)\underline{\mu}_{2j}(\dot{e}) - 2A_{2j}\dot{A}_{2j}\underline{\mu}_{1i}(e)\underline{\mu}_{2j}(\dot{e}))}{\sum_{i=1}^{I}\sum_{j=1}^{J}\underline{W}_{ij}} \\ &- \frac{(\underline{\widetilde{W}}_{ij})\sum_{i=1}^{I}\sum_{j=1}^{J} -2A_{2j}\dot{A}_{2j}\underline{\mu}_{1i}(e)\underline{\mu}_{2j}(\dot{e}))}{\sum_{i=1}^{I}\sum_{j=1}^{J}\underline{W}_{ij}} \\ &- \frac{(\underline{\widetilde{W}}_{ij})\sum_{i=1}^{I}\sum_{j=1}^{J}(-2A_{1i}\dot{A}_{1i}\underline{\mu}_{1i}(e)\underline{\mu}_{2j}(\dot{e}))}{\sum_{i=1}^{I}\sum_{j=1}^{J}\underline{W}_{ij}}\end{aligned} \tag{41}$$

and further:

$$\dot{\underline{\widetilde{W}}}_{ij} = -\underline{\widetilde{W}}_{ij}\dot{\underline{N}}_{ij} + \underline{\widetilde{W}}_{ij}\sum_{i=1}^{I}\sum_{i=1}^{J}\underline{\widetilde{W}}_{ij}\dot{\underline{N}}_{ij} \tag{42}$$

$$\dot{\overline{\widetilde{W}}}_{ij} = -\overline{\widetilde{W}}_{ij}\dot{\overline{N}}_{ij} + \overline{\widetilde{W}}_{ij}\sum_{i=1}^{I}\sum_{i=1}^{J}\overline{\widetilde{W}}_{ij}\dot{\overline{N}}_{ij} \tag{43}$$

in which:

$$\dot{\underline{N}}_{ij} = 2A_{1i}\dot{A}_{1i} + 2A_{2j}\dot{A}_{2j}, \dot{\overline{N}}_{ij} = 2U_{1i}\dot{U}_{1i} + 2U_{2j}\dot{U}_{2j} \tag{44}$$

$$\dot{A}_{1i} = \frac{(\dot{e} - \dot{c}_{1i})\underline{\sigma}_{1i} - (e - \underline{c}_{1i})\dot{\underline{\sigma}}_{1i}}{\underline{\sigma}_{1i}^2}, \dot{A}_{2j} = \frac{(\ddot{e} - \dot{\underline{c}}_{2j})\underline{\sigma}_{2j} - (\dot{e}_k - \underline{c}_{2j})\dot{\underline{\sigma}}_{2j}}{\underline{\sigma}_{2j}^2}$$

$$\dot{U}_{1i} = \frac{(\dot{e} - \dot{\overline{c}}_{1i})\overline{\sigma}_{1i} - (e - \overline{c}_{1i})\dot{\overline{\sigma}}_{1i}}{\overline{\sigma}_{1i}^2}, \dot{U}_{2j} = \frac{(\ddot{e} - \dot{\overline{c}}_{2j})\overline{\sigma}_{2j} - (\dot{e} - \overline{c}_{2j})\dot{\overline{\sigma}}_{2j}}{\overline{\sigma}_{2j}^2}$$

it is possible to use Maclaurin series expansion to obtain following equations.

$$\frac{\dot{x}_1 - \dot{c}_{1i}}{\underline{\sigma}_{1i}} = \frac{\dot{e} - \dot{c}_{1i}}{\underline{\sigma}_{1i} - \overline{\sigma}_{1i} + \overline{\sigma}_{1i}} = \frac{\dot{e} - \dot{c}_{1i}}{\overline{\sigma}_{1i}}\left(1 - \underbrace{\frac{\underline{\sigma}_{1i} - \overline{\sigma}_{1i}}{\overline{\sigma}_{1i}} + \frac{(\overline{\sigma}_{1i} - \underline{\sigma}_{1i})^2}{\underline{\sigma}_{1i}^2} + H.O.T}_{D_{1i}}\right) \tag{45}$$

and:

$$\frac{e - c_{1i}}{\underline{\sigma}_{1i}} = \frac{e - c_{1i}}{\underline{\sigma}_{1i} - \overline{\sigma}_{1i} + \overline{\sigma}_{1i}} = \frac{e - c_{1i}}{\overline{\sigma}_{1i}}\left(1 - \frac{\underline{\sigma}_{1i} - \overline{\sigma}_{1i}}{\overline{\sigma}_{1i}} + \frac{(\overline{\sigma}_{1i} - \underline{\sigma}_{1i})^2}{\underline{\sigma}_{1i}} + H.O.T\right) \tag{46}$$

Using (45), we have:

$$A_{1i}\dot{A}_{1i} = U_{1i}\dot{U}_{1i} + \frac{(\dot{e}-\dot{c}_{1i})}{\overline{\sigma}_{1i}}\frac{(e-c_{1i})}{\overline{\sigma}_{1i}}\left(2D_{1i}+D_{1i}^2\right) \tag{47}$$

and similarly using (46) we obtain that:

$$A_{2j}\dot{A}_{2j} = U_{2j}\dot{U}_{2j} + \frac{(\ddot{e}-\dot{c}_{2j})}{\overline{\sigma}_{2j}}\frac{(\dot{e}-c_{2j})}{\overline{\sigma}_{2j}}\left(2E_{2j}+E_{2j}E_{2j}^2\right) \tag{48}$$

in which:

$$E_{2j} = -\frac{\underline{\sigma}_{2j}-\overline{\sigma}_{2j}}{\overline{\sigma}_{2j}} + \frac{(\underline{\sigma}_{2j}-\overline{\sigma}_{2j})^2}{\overline{\sigma}_{2j}^2} + H.O.T \tag{49}$$

It can be proved that $|D_{1i}|$ and $|E_{2j}|$ are bounded as $|D_{1i}| < B_D$ and $E_{2j} < B_E$. In order to analyze the stability of the controller with adaptive learning rate, the following Lyapunov function is proposed.

$$V_c = \frac{1}{2}u_c^2(t) + \frac{1}{2\gamma_1}(\alpha-\alpha^*)^2 \tag{50}$$

The time derivative of the Lyapunov function (50) is derived as:

$$\dot{V}_c = u_c\dot{u}_c = u_c(\dot{u}_f+\dot{u}) + \frac{\dot{\alpha}}{\gamma_1}(\alpha-\alpha^*) \tag{51}$$

Since:

$$\begin{aligned} u_f &= \frac{q\sum_{i=1}^{I}\sum_{j=1}^{J} f_{ij}\underline{W}_{ij}}{\sum_{i=1}^{I}\sum_{j=1}^{J}\underline{W}_{ij}} + \frac{(1-q)\sum_{i=1}^{I}\sum_{j=1}^{J} f_{ij}\overline{W}_{ij}}{\sum_{i=1}^{I}\sum_{j=1}^{J}\overline{W}_{ij}} \\ &= q\sum_{i=1}^{I}\sum_{j=1}^{J} f_{ij}\widetilde{\underline{W}}_{ij} + (1-q)\sum_{i=1}^{I}\sum_{j=1}^{J} f_{ij}\widetilde{\overline{W}}_{ij} \end{aligned} \tag{52}$$

and:

$$\dot{u}_f = q\sum_{i=1}^{I}\sum_{j=1}^{J}(\dot{f}_{ij}\widetilde{\underline{W}}_{ij} + f_{ij}\dot{\widetilde{\underline{W}}}_{ij}) + (1-q)\sum_{i=1}^{I}\sum_{j=1}^{J}(\dot{f}_{ij}\widetilde{\overline{W}}_{ij} + f_{ij}\dot{\widetilde{\overline{W}}}_{ij}) \tag{53}$$

one obtains:

$$\begin{aligned} \dot{u}_f = {} & q\sum_{i=1}^{I}\sum_{j=1}^{J}\left(\left(-\widetilde{\underline{W}}_{ij}\dot{\underline{K}}_{ij} + \widetilde{\underline{W}}_{ij}\sum_{i=1}^{I}\sum_{j=1}^{J}\widetilde{\underline{W}}_{ij}\dot{\underline{K}}_{ij}\right)f_{ij} + \widetilde{\underline{W}}_{ij}\dot{f}_{ij}\right) \\ & + (1-q)\sum_{i=1}^{I}\sum_{j=1}^{J}\left(\left(-\widetilde{\overline{W}}_{ij}\dot{\overline{K}}_{ij} + \widetilde{\overline{W}}_{ij}\sum_{i=1}^{I}\sum_{j=1}^{J}\widetilde{\overline{W}}_{ij}\dot{\overline{K}}_{ij}\right)f_{ij} + \widetilde{\overline{W}_{ij}}\dot{f}_{ij}\right) \end{aligned} \tag{54}$$

Considering adaptation for sigma and center we have:

$$\begin{aligned}\dot{V}_c = u_c \Bigg(& q \sum_{i=1}^{I} \sum_{j=1}^{J} \Bigg(2 \Bigg(-\underline{\widetilde{W}}_{ij} \left(\frac{\dot{e}}{\underline{\sigma}_{1i}} A_{1i} + \frac{\ddot{e}}{\underline{\sigma}_{2j}} A_{2j} \right) \\ & + \underline{\widetilde{W}}_{ij} \sum_{i=1}^{I} \sum_{j=1}^{J} \underline{\widetilde{W}}_{ij} \left(\frac{\dot{e}}{\underline{\sigma}_{1i}} A_{1i} + \frac{\ddot{e}}{\underline{\sigma}_{2j}} A_{2j} \right) \Bigg) f_{ij} + \underline{\widetilde{W}}_{ij} \dot{f}_{ij} \Bigg) \\ & + q \sum_{i=1}^{I} \sum_{j=1}^{J} \Bigg(2 \Bigg(-\underline{\widetilde{W}}_{ij} \left(2D_{1i} + D_{1i}^2 + 2D_{2j} + D_{2j}^2 \right) \\ & + \underline{\widetilde{W}}_{ij} \sum_{i=1}^{I} \sum_{j=1}^{J} \underline{\widetilde{W}}_{ij} \left(2D_{1i} + D_{1i}^2 + 2D_{2j} + D_{2j}^2 \right) \Bigg) f_{ij} \Bigg) \\ & + (1-q) \sum_{i=1}^{I} \sum_{j=1}^{J} \Bigg(2 \Bigg(-\overline{\widetilde{W}}_{ij} \left(\frac{\dot{e}}{\overline{\sigma}_{1i}} A_{1i} + \frac{\ddot{e}}{\overline{\sigma}_{2j}} A_{2j} \right) \\ & + \overline{\widetilde{W}}_{ij} \sum_{i=1}^{I} \sum_{j=1}^{J} \overline{\widetilde{W}}_{ij} \left(\frac{\dot{e}}{\overline{\sigma}_{1i}} A_{1i} + \frac{\ddot{e}}{\overline{\sigma}_{2j}} A_{2j} \right) \Bigg) f_{ij} + \overline{\widetilde{W}}_{ij} \dot{f}_{ij} \Bigg) + \dot{u} \Bigg) \\ & + \frac{\dot{\alpha}}{\gamma_1} (\alpha - \alpha^*) \end{aligned} \tag{55}$$

Considering assumptions (17) and (18), (55) can be rewritten as:

$$\begin{aligned} \dot{V}_c &\leq 4B_r |u_c| + u_c \left(\sum_{i=1}^{I} \sum_{j=1}^{J} \dot{f}_{ij} (q \underline{\widetilde{W}}_{ij} + (1-q) \overline{\widetilde{W}}_{ij}) + \dot{u} \right) + \frac{\dot{\alpha}}{\gamma_1} (\alpha - \alpha^*) \\ &\leq 4B_r |u_c| - \alpha^* |u_c| + (\alpha^* - \alpha) |u_c| + |u_c| B_{\dot{u}} + \frac{\dot{\alpha}}{\gamma_1} (\alpha - \alpha^*) < 0 \end{aligned} \tag{56}$$

in which:

$$B_r = B_f \left(\frac{3B_D + 3B_E + B_{\dot{e}}^2 + B_{\dot{e}}^2 + B_c B_e + B_c B_{\dot{e}}}{\underline{B}_\sigma^2} \right) \tag{57}$$

using the adaptation law for α as:

$$\dot{\alpha} = \gamma_1 |u_c| - \nu \gamma_1 \alpha$$

and taking α^* as:

$$B_{\dot{u}} + 4B_r < \frac{1}{2} \alpha^*$$

we have:

$$\dot{V}_c \leq -\frac{1}{2} \alpha^* |u_c| + \nu \alpha (\alpha - \alpha^*) \tag{58}$$

$$= -\frac{1}{2} \alpha^* |u_c| + \nu (\alpha - \alpha^*)^2 - \frac{\nu \alpha^{*2}}{4} \tag{59}$$

Furthermore:

$$\dot{V}_c \leq -\frac{1}{2}\alpha^* |u_k| + \nu(\alpha - \alpha^*)^2 \tag{60}$$

Therefore, the Lyapunov function u_c converges exponentially until $|u_c| \leq 2\frac{\nu}{\alpha^*}(\alpha - \alpha^*)^2$ and the parameters of the controller are bounded. Consequently the system states converge to a compact set R in which:

$$R = \left\{ u \,|\, |u| \leq 2\frac{\nu}{\alpha^*}(\alpha - \alpha^*)^2 \right\} \tag{61}$$

It should be noted that this region can be chosen to be as small as desired by choosing a proper value for ν. Consequently, u can be made as small as desired.

Fuzzy Control of Direct Drive Manipulators

Kemalettin Erbatur

Sabancı University Mechatronics Engineering Program
Tuzla, Istanbul, Turkey
erbatur@sabanciuniv.edu

Abstract. Direct drive motors, sometimes referred to a torque motors are speciality servo actuators which posess high torque capacity without the necessity of gears. The author worked on a number of direct drive robots and their control methods since early 1990s when Professor Okyay Kaynak taught him fundamentals of fuzzy control and gave him the opportunity of experimental work on direct drive robotics. This chapter presents samples of the studies of the author on indirect fuzzy control implemented on direct drive robots between 1993 and 2012. The role of on-line controller parameter adaptation for sliding mode trajectory controllers, force controllers and for the integration of visual servoing and force control is discussed with case studies.

1 Introduction

A direct drive motor is one directly coupled to the load it drives. This configuration avoids gear coupling effects. The best known effect of gears is the backlash. Also gear flexibility can be a shortcoming of employing reduction between the motor and the load. There applications where positioning accuracy is critical and these nonlinear effects can not be tolerated. The direct coupling alleviates these problems on the cost of two drawbacks. i)Torque amplification capacity of the reductor is lost. ii) Measuring resolution, also multiplied by the reduction ratio is compromised. Typical industrial servo motors are equipped with 1024-4096 increments per revolution rotary resolvers or encoders and this resolution is usually adequate for applications with gears or transmission mechanisms like ball screws. However, they are hardly suitable for direct drive applications. These drawbacks lead to a speciality design servo application motor. The general name coined to the type came from its way of coupling to the load: "Direct drive." "Torque motor" is another term to describe the same machine, reflecting the fact that the lack of gears is compansated for by the high torque capacity of the motor.

A direct drive motor, unlike the common servo motor architecture in the industry, usually has a low axial length / diameter ratio around 1 or less. It has higher torque and less speed compared with an equal weight servo motor. It's encoder system is designed superior to other servos. The lack of the gear reductor support in encoder resolution is taken account for with a huge number of increments per revolution. 400000 to 1000000 increments per revolution are quite common in current direct

X. Yu and M. Önder Efe (eds.), *Recent Advances in Sliding Modes,*
Studies in Systems, Decision and Control 24, DOI: 10.1007/978-3-319-18290-2_18

drive products. The weaknesses of lacking the gears in the envisaged application area are therefore eliminated by hardware design and encoder superiority.

Still, there is another threat in front of the implementation of the direct drive motor in robotics applications. The absence of reduction mechanisms in its application area makes the motor highly backdrivable. While desiable in a number of applications, backdrivability in the joints of an articulated manipulator means pronounced coupling efects. The dynamics equations of a robotic manipulator are highly nonlinear with sinificant interlink coupling effects. The velocity and acceleration, as well as the position of one joint can affect those of another joint. The interlink coupling effects are minimized for robots with high gear ratios. However, these effects are quite significant when direct drive motors are employed at the joints. This is where manipulator control methods come into the picture. The advantages of the direct drive motors can be exploited by employing control methods which cope with adverse effects of link-to-link coupling. The same fact makes the direct drive robot an ideal test bed for robot control methodologies.

In robotic manipulator trajectory control, as a robust control strategy, Sliding Mode Control (SMC) has many useful properties in coping with the problems of non-linearity, coupling effects and changing parameters even in cases where the knowledge on the plant dynamics is extremely limited.

Fuzzy control systems, as tools against the problems of uncertainty and vagueness, incorporate human experience into the task of controlling a plant. When employed in robotic trajectory control, they mainly play one of two roles in the controller structure. One of them is to compute the control signal by fuzzy rules. The other is to tune, adapt or schedule the parameters of other control mechanisms to accomplish better performance in face of uncertainties and different operating points.

Fuzzy control, when used in combination with sliding mode control (SMC) systems, usually aim to alleviate implementation difficulties of sliding mode controllers or to intelligently tune the controller parameters. This methodology is termed "indirect fuzzy control" since, the basic design and implementation philosophy of SMCs is followed to a great extent and FL systems are used to fulfil a secondary function [1]. In this chapter, methods which combine fuzzy systems with sliding mode controllers to solve the chattering problem of sliding mode control for robotic applications are reviewed. In these methods, special attention is paid to schemes that eliminate chattering without a degradation of the tracking performanceSections 2 and 3 present two case studies [2, 3] with fuzzy tuned sliding mode control implemented on direct drive SCARA type robots.

Force control of robotic manipulators is becoming more and more important in applications that involve interaction with the environment. Depending on the nature of the task at hand, different control algorithms can be suitable to be implemented. In Section 4, the task of reaching an object by the robot tool and applying a constant force on it is considered as a case study [4]. This task is one of the typical manipulation operations. A fuzzy logic scheduling approach, which smoothly changes the control action between two force control schemes, is reviewed. The first force control method is admittance control, which is suitable to be used in the phase of approaching the work piece. The second one is an explicit force control strategy, integral force control, suitable for force regulation when the manipulator tool is in contact with the work piece. The fuzzy controller scheduling approach is tested via experimental work on a direct drive SCARA-type manipulator.

Vision and force sensors provide rich information which can enable robots to execute complex tasks. However, the integration of these two types of sensors with different nature is not straightforward. Section 5 defines a manipulation task as a case study problem [5]. In this problem, a constant magnitude normal force is to be exerted at a point fixed on an object which is free to rotate. Visual servoing and explicit force control techniques are applied next in the task frame formalism to achieve this objective. Disadvantages of the constant parameter controllers are addressed and a solution in which controller gains are tuned with fuzzy logic systems is presented. The solution is in the hybrid control category. Experiments are carried out on a two degrees of freedom (DOF) direct drive robot.

The chapter is concluded in Section 6.

2 Fuzzy On-Line Tuning of Sliding Mode ControllerParameters

The control mechanism in this section is presented for systems in the following form.

$$\dot{x}_1 = f_1(x_1, x_2) \tag{1}$$

$$\dot{x}_2 = f_2(x_1, x_2) + B(x_1, x_2)u + B(x_1, x_2)d_d(t) \tag{2}$$

In this state space description $x_1 \in R^{n-m}$, $x_2 \in R^m$, $u \in R^m$, $rank(B) = m$. d_d is the disturbance. The components of the control input and the derivative of x_2 are bounded with known bounds. The aim is to push the states of the system into the set *S* defined by

$$S = \{x : \phi(t) - s_a(x) = s(x,t) = 0\} \tag{3}$$

Here, *x* is the state vector formed by augmenting x_1 and x_2. The function $\phi(t)$ is the time varying part of the sliding function vector $s(x,t)$. It contains reference inputs to be applied to the controlled plant. $s_a(x)$ denotes the state dependent part of $s(x,t)$:

$$s_a = G_1 x_1 + G_2 x_2 \tag{4}$$

The matrix G_2 is of rank *m.* By employing the Lyapunov function candidate

$$V = s^T s / 2 \tag{5}$$

it can be shown that the control law

$$u = \underbrace{-d_d + (G_2 B)^{-1}\left[\phi - G_2 f_2 - G_1 f_1\right]}_{u_{eq}} + (G_2 B)^{-1} Ds \tag{6}$$

can force the derivative of this Lyapunov function to be of the form

$$\dot{V} = -s^T Ds \tag{7}$$

where D is positive definite. For robotic manipulators, the matrix B is the same as the inverse of the positive definite manipulator inertia matrix and G_2 has the rank m. Therefore, the existence of the inverse of the matrix G_2B is guaranteed. It can be noted that when the part of the control input in (6) designated by u_{eq} is applied to the system, the derivative of the sliding function s will be zero. Such a control is termed "equivalent control" in sliding mode control terminology. Thus the control input can be written as

$$u = u_{eq} + (G_2B)^{-1} Ds \tag{8}$$

It can be also be shown [6-11] that the above equation can be put into the recursive form

$$u(t) = u(t^-) + (G_2B)^{-1}(Ds + \dot{s})\big|_{t=t^-} \tag{9}$$

$$t^- = t - T \tag{10}$$

where, $(G_2B_2)^{-1}(Ds + \dot{s})\big|_{t=t^-}$ is the updating term and T is a very small time interval corresponding to the sampling interval in digital implementation.

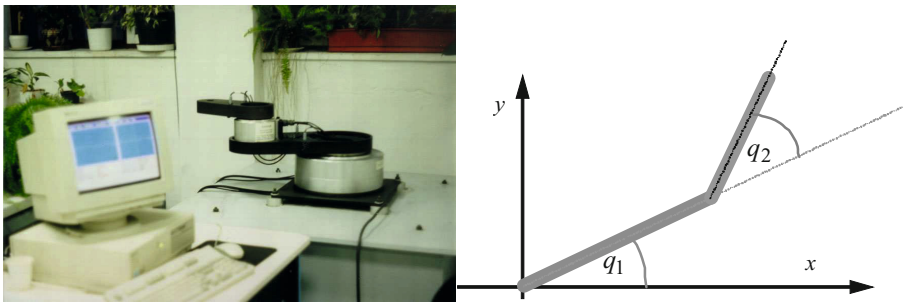

Fig. 1. The direct drive manipulator

On the sliding manifold, $u(t^-)$ becomes the same as the equivalent control. Since the control is bounded, the saturation function is added to the control law above:

$$u(t) = \mathrm{sat}\left(u(t^-) + (G_2B)^{-1}(Ds + \dot{s})\big|_{t=t^-}\right) \tag{11}$$

The performance of the control algorithm is checked by experimental investigations on a direct drive two degrees of freedom SCARA type arm shown in Fig. 1. Various mass, length and inertia parameters of the arm and the direct drive motors given in [3]. A floating point DSP based system was used to control the arm . C language servo routines are compiled and downloaded onto the DSP. This makes short sampling times possible even for the most complicated adaptation scheme

considered in this section. The torque motors used on base and elbow joints provide position signals with a resolution of 153600 pulses/rev.

The angular positions and their derivatives are selected as the states variables:

$$q = x_1 \text{ and } \dot{q} = x_2 \tag{12}$$

The following state equations are then obtained.

$$\dot{x}_1 = x_2, \quad \dot{x}_2 = \ddot{q} = J^{-1}(x_1)\left[u(t) - W(x_1, x_2) - F\right] \tag{13}$$

Here, J is the inertia matrix of the manipulator and W represents the centripetal and Coriolis matrix. F stands for the friction effects. The second equation above can also be written as

$$\dot{x}_2 = -J^{-1}(x_1)\left[W(x_1, x_2) + F\right] + J^{-1}(x_1)u(t) \tag{14}$$

With a comparison of (13) and (14) with (1) and (2) we obtain

$$f_1(x_1, x_2) = x_2, \quad f_2(x_1, x_2) = -J^{-1}(x_1)\left[W(x_1, x_2) + F\right], \quad B = J^{-1}(x_1). \tag{15}$$

The design of the sliding surface can be carried out as follows:

$$s = \phi(t) - s_a(q, \dot{q}) \tag{16}$$

with

$$\phi(t) = G_1 q_d + G_2 \dot{q}_d \tag{17}$$

where q_d is the desired position vector. It can be noted that s is a function of position and velocity errors. With the definition of position error as

$$e = \begin{pmatrix} e_1 \\ e_2 \end{pmatrix} = q_d - q, \tag{18}$$

the following expression can be obtained for the sliding function s.

$$s(x,t) = \begin{pmatrix} s_1 \\ s_2 \end{pmatrix} = G_1 e + G_2 \dot{e} \tag{19}$$

The matrices G_1 and G_2 used in this design are

$$G_1 = \begin{pmatrix} c_{11} & 0 \\ 0 & c_{22} \end{pmatrix} \equiv C, \quad G_2 = \begin{pmatrix} 1 & 0 \\ 0 & 1 \end{pmatrix} \tag{20}$$

where c_{11} and c_{22} are positive constants. Here, the introduction of the matrix C is solely for notational simplicity. It can be noted that the sliding surface in the four-dimensional state space can be identified by two independent sliding lines in two-dimensional phase planes. The slopes of these lines are $-c_{11}$ and $-c_{22}$. We also obtain

$$(G_2 B)^{-1} = J(q) \,. \tag{21}$$

Hence, the following control rule is obtained with a nominal inertia term J_n

$$u((k+1)T) = u(kT) + K\, J_n (Ds + \dot{s})\big|_{t=kT} \tag{22}$$

In this expression, T is the control cycle time. K is a diagonal gain matrix with positive entries used for tuning and D is chosen diagonal as well.

$$K = \begin{pmatrix} K_{11} & 0 \\ 0 & K_{22} \end{pmatrix}, \; D = \begin{pmatrix} d_{11} & 0 \\ 0 & d_{22} \end{pmatrix} \tag{23}$$

In discrete time, Euler approximation is used for the derivative of the sliding function.

An obvious difficulty in the implementation of the control scheme described above is the selection of the controller parameters. Fuzzy adaptation methods are developed for the two-link manipulator described above. In this approach, specifically, the selection of the sliding surface specified by the diagonal matrix C, the positive definite matrix D and gain K are carried out by fuzzy adaptation rules. These are termed C adaptation, D adaptation and gain adaptation, respectively. The three kinds of parameter adaptation methods are applied separately. By these schemes, parameters are varied continuously. Figures 4 and 5 schematically demonstrate the idea behind the adaptation of C and D matrices. For C adaptation, the slopes of the sliding lines are varied by considering the absolute position error (Fig. 3). The tracking performance of the sliding controller depends highly upon the value of the sliding line slope. A large value for the sliding line slope ensures good tracking performance but a too large slope can cause instability. By increasing slope when the absolute error gets small, good tracking can be achieved without causing overshoot or instability. The use of fuzzy rules is proposed for the adaptation. The effect of adapting the parameters of the D matrix is illustrated in Fig. 4. The curve labeled 1 corresponds to the case with a large d_{kk} value (k=1, 2). System states reach the sliding line in short time but make an overshoot. After a while and possibly many sliding line crossovers, the line is followed very closely to achieve zero error. The curve labeled 2 reflects the case with a small D parameter. No undesirable overshoot is observed, but, the sliding line is reached after a long time, may be near the origin. Both of these cases are unwanted since the objective in sliding mode control is to force the system states onto the sliding line as fast as possible and to ensure that they stay there forever. The third curve in the phase plane can be obtained via fuzzy adaptation by increasing D parameters only when states are close to the sliding line. The absolute value of the sliding variable s_k will be the measure of closeness to the line. The performance and robustness of the controller is affected by the selection of the gain matrix K. High gain can easily cause chattering whereas small values of the gains K_{kk} lead to the degradation of the tracking performance. The fuzzy adaptation algorithm below balances the chattering and error in the system and tunes the gain parameter in such a way to get the best tracking without chattering. Absolute value of

position error, absolute value of the sliding function *s* and the chattering variable, which is defined below, are chosen as input linguistic variables. Triangular membership functions are employed. A one-dimensional rule base with six rules is used for the *C* parameter adaptation. The absolute value of the error is used as the input of the adaptation scheme. Similarly, a one-dimensional rule base with six inputs are used for the *D* parameter adaptations too. For this type adaptation, however, the absolute value of the scalar sliding variable for the corresponding joint replaces the absolute value of the joint position error of the joint. Again triangular membership functions are used. For the adaptation of the parameters of the gain matrix *K* to avoid chattering, a measure for the chattering in the system has to be devised. Since the sliding mode control algorithm is applied in discrete time, the following measure can be used for this purpose.

$$\Gamma_k(t) = \sum_{l=0}^{30} \left| u(t - lT) - u(t - (l+1)T) \right| \tag{24}$$

In this expression, Γ_k is the measure of chattering in joint *k*, taken as the cumulative absolute change in control input in the last 30 control cycles. The rule base consisted of 36 rules in 6x6 formation in the computation of the parameters K_{kk} and the rule base is repeated for each joint.

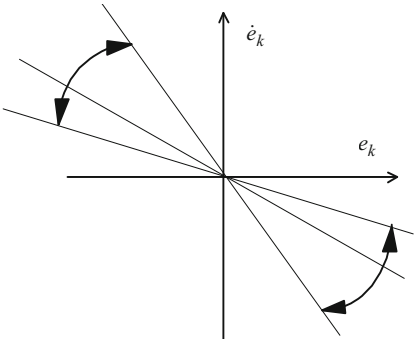

Fig. 2. C parameter adaptation

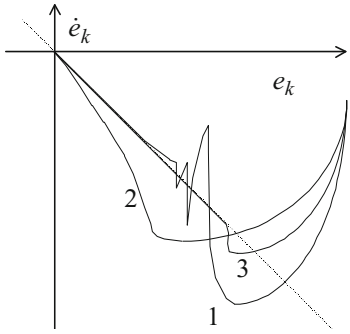

Fig. 3. D parameter adaptation

Chattering and absolute joint position error are employed as the inputs. Different form the *C* and *D* adaptations, the fuzzy system of the *K* computation compute the increment ΔK_{kk} on the gain parameters to be added every computational cycle. It should be noted that in gain adaptation what is calculated is the incremental change to the gain, whereas *D* and *C* adaptations give the exact values of *C* and *D* parameters as outputs. Rate limiters are put at the outputs of these adaptations. It is observed that this method works successfully. As a summary the adapted parameters are computed as follows.

$$c_{kk} = H_k^C \frac{\sum_{i=1}^{6} r_{c_i} \mu_{ae_i^c}(|e_k|)}{\sum_{i=1}^{6} \mu_{ae_i^c}(|e_k|)}, \quad d_{kk} = H_k^D \frac{\sum_{i=1}^{6} r_{d_i} \mu_{as_i}(|s_k|)}{\sum_{i=1}^{6} \mu_{as_i}(|s_k|)},$$
$$\Delta K_{kk} = H_k^K \frac{\sum_{i=1}^{6}\sum_{j=1}^{6} R_{g_{i,j}} \mu_{ch_i}(|\Gamma_k|)\mu_{ae_j^g}(|e_k|)}{\sum_{i=1}^{6}\sum_{j=1}^{6} \mu_{ch_i}(|\Gamma_k|)\mu_{ae_j^g}(|e_k|)} \tag{25}$$

The constants H_k^C, H_k^D and H_k^K are tuning factors for the robot joint *k*. The letters *C*, *D* and *K* indicate in which adaptation they are used. μ with the appropriate describing subscript stands for a membership function. *r* or *R* are symbols used for rule strengths.

To test the applicability and performance of the parameter adaptation schemes experimental investigations are carried out with the direct drive manipulator. A control cycle period of 1.3 ms is used in the experiments. The reference curve is obtained by integrating a "1-cosine" curve and thus smooth position and velocity references are given to the system. This represents a smoothed step reference of 1.2 radians, reached in a 1.5 s rising time. The same reference is applied to both joints. Only elbow results are presented here. Similar results are obtained for the base joint. In Fig. 5, it can be observed with the gain adaptation fuzzy system that in the first second, chattering is high and therefore the gain parameter is decreased. When chattering diminishes, the gain is increased to remove the steady state error. The parameter converges when acceptable chattering and error ranges are reached. These ranges are specified in the rule base for the gain adaptation. This algorithm removes steady state error without introducing too much chattering.

C parameter adaptation is presented in Fig. 6. The performance with this adaptation method is similar to that obtained with the gain adaptation algorithm. By increasing the parameters c_{kk} when the joint position errors get close to zero, the steady state errors are reduced without chattering in the control signals. To demonstrate the adaptation in the *D* parameters, a different reference input is employed. This is a step of 0.04 radians height. The reason why step inputs are used is that, compared with the reference trajectories without initial position error, they create a better test framework to observe the phase plane behavior. Fig. 7 shows the error, control and phase plane trajectory curves for the elbow with and without *D* adaptation. Reference steps are applied at t = 0.13 sec. The figure indicates that the elbow phase plane trajectory without the *D* adaptation moves about the sliding line but does not converge to it before zero error is reached. Therefore the desired error dynamics are only roughly obtained. To assure that the trajectories converge to the sliding lines quickly, the fuzzy *D* adaptation algorithm is implemented. The results are presented in Fig. 7, on

the right hand side. The elbow phase plane trajectory converges rapidly to sliding line without significant overshoot. Considerable amount of control effort is observed to keep system motion on the sliding line, as the parameter d_{kk} is increased by the fuzzy parameter computation when the phase plane motion is close to the sliding line. Fig. 8 indicates that the adapted *D* parameter converges to its final value as the joint position error converges to zero.

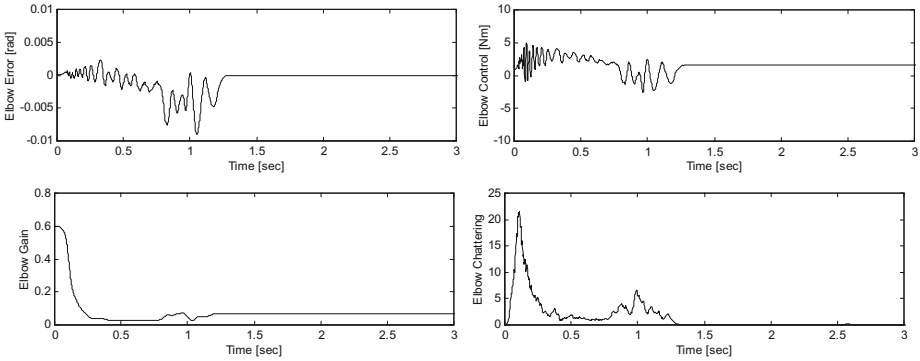

Fig. 4. Elbow position error, control torque, adapted parameter and chattering indicator in gain adaptation

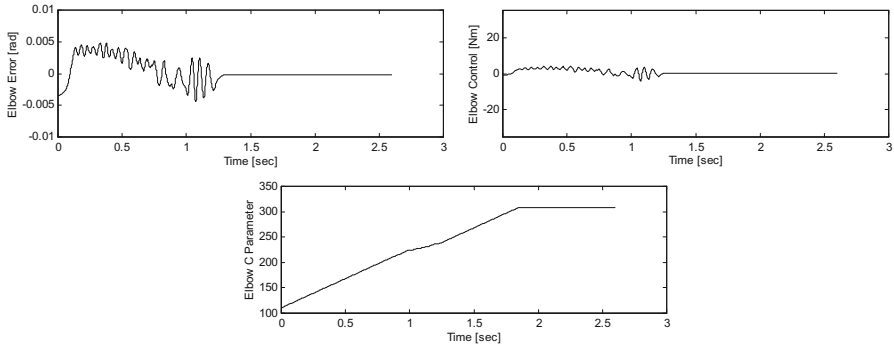

Fig. 5. Elbow error curve, control input and adapted parameter with *C* adaptation

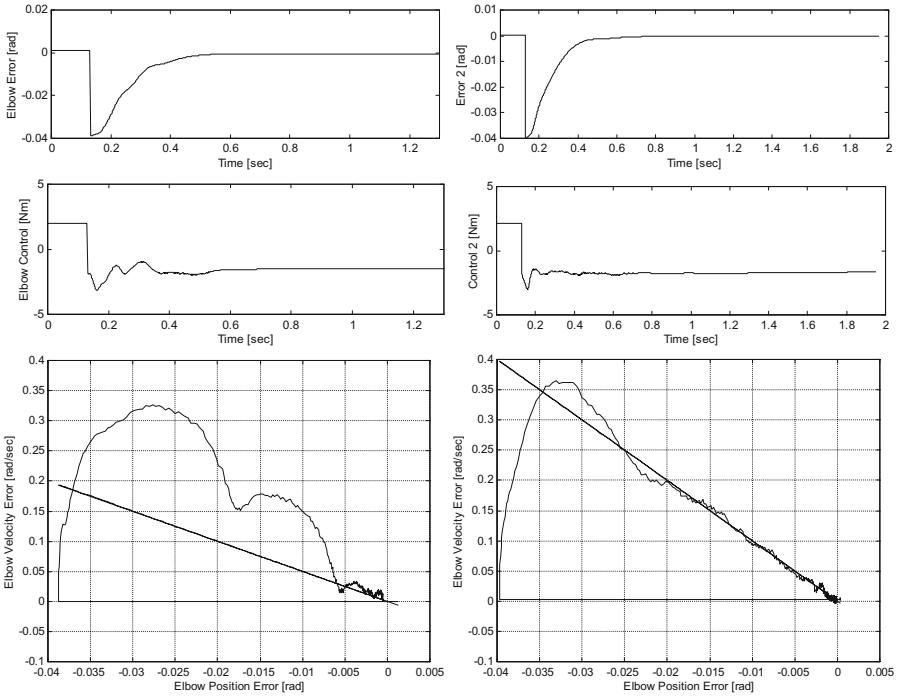

Fig. 6. Elbow error curve, control input and phase plane trajectory without *D* adaptation (on the left). Elbow error curve, control input and phase plane trajectory with *D* adaptation (on the right).

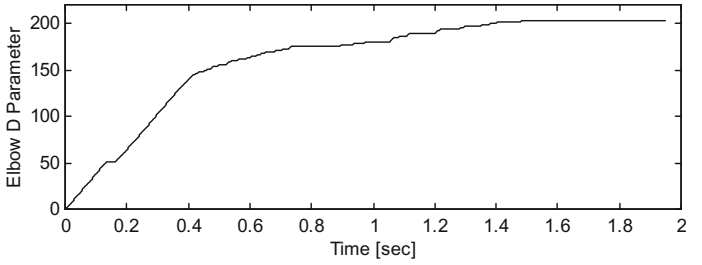

Fig. 7. Adapted parameter in *D* adaptation

3 Fuzzy Adaptation Tuning of Sliding Mode Boundary Layer Thickness

In this section, a SMC method with a varying boundary layer thickness is reviewed. For simplicity, second order SISO systems are focused on. The controller is derived for the systems with the form

$$\ddot{x} = f(X) + b(X)u \,. \tag{26}$$

Here, X is an augmented vector of the scalar state variables x, $\dot{x}$, defined as

$$X = \begin{bmatrix} x & \dot{x} \end{bmatrix}^T \,. \tag{27}$$

u is the control input and the input gain $b(X)$ takes strictly positive values. The tracking error is defined by

$$e = x_d - x \tag{28}$$

where x_d is the desired value for x. The sliding variable s is defined as

$$s(e) = \dot{e} + \lambda e \tag{29}$$

and the desired dynamic response for this system is given by $s = 0$. λ is a positive number for stability. If s can be forced to zero, the desired dynamics can be attained and the tracking error will converge to zero with the dynamics dictated by $\dot{e} + \lambda e = 0$, which corresponds to a line with slope $-\lambda$ in the phase plane. A Lyapunov function candidate V of s is chosen as

$$V = \tfrac{1}{2} s^2 \,. \tag{30}$$

The control law is constructed such that the sliding line is attractive for the state trajectories. This, can be guaranteed if the derivative of V can be shown to be negative definite. This derivative can also be written as,

$$\dot{V} = s(\ddot{x}_d - f(X) - b(X)u + \lambda \dot{e}) \,. \tag{31}$$

The negative definiteness of $\dot{V}$ can be achieved by control input

$$u = \frac{1}{b(X)} \left(\ddot{x}_d + \lambda \dot{e} - f(X) + Hs + K(X)\text{sign}(s) \right) \tag{32}$$

where the "sign" stands for the signum function. H is a constant which is chosen strictly positive for stability. $K(X)$ is a state dependent gain which also takes only positive values. Since $f(X)$ and $b(X)$ cannot be known exactly, their estimates $\hat{f}(X)$ and $\hat{b}(X)$ are used in the control law. Using estimates, the control law becomes

$$u = \frac{1}{\hat{b}(X)} \left(\ddot{x}_d + \lambda \dot{e} - \hat{f}(X) + Hs + K(X)\text{sign}(s) \right). \tag{33}$$

If the bound of the uncertainties on $f(X)$ and $b(X)$ are known, the gain $K(X)$ can be selected adequately high to assure robustness in face of these uncertainties. Let $F(X)$ be a known upper bound on $f(X)$ with

$$\left| f(X) - \hat{f}(X) \right| \le F(X). \tag{34}$$

Also, let $b_{\min}(X)$ and $b_{\max}(X)$ be known lower and upper bounds for $b(X)$:

$$b_{\min}(X) \le b(X) \le b_{\max}(X). \tag{35}$$

Let $\beta(X)$ be defined by $\beta(X) = \sqrt{b_{\max}(X)/b_{\min}(X)}$. Suppose that we use the geometric mean of the upper and lower bounds of $b(X)$ as an estimate: $\hat{b}(X) = \sqrt{b_{\min}(X) b_{\max}(X)}$. Let $\hat{u} \equiv \ddot{x}_d + \lambda \dot{e} - \hat{f}(X)$ and choose the gain $K(X)$ such that

$$K(X) \ge \beta(X) F(X) + (\beta(X) - 1)\left|\hat{u}\right|. \tag{36}$$

With this choice of control parameters, it can be shown than the derivative $\dot{V}$ of the Lyapunov function candidate will be negative definite [3]. The sign function requires infinite switching frequency, in the theory, to keep the system states on the sliding line. However, because of some factors like actuator limitations and delays which are inevitable when the controller is implemented on digital computers, infinite frequency switching cannot be realized. As a result, frequent state trajectory jumps across the sliding line are observed. Such frequent jumps are called chattering in the sliding mode control terminology. It can also be identified as high frequency and high amplitude oscillations in the control input and velocity signals in the motion control field. Many modifications of the original control law are proposed to alleviate the chattering problem. The most simple and popular solution is the so called boundary layer approach in which the sign function is replaced by a saturation function (Fig. 9). Then the control input becomes

$$u = \frac{1}{\hat{b}(X)} \left(\ddot{x}_d + \lambda \dot{e} - \hat{f}(X) + Hs + K(X) \mathrm{sat}_{\phi}(s) \right). \tag{37}$$

The parameter ϕ defines the thickness of the boundary layer as shown in Fig. 9.

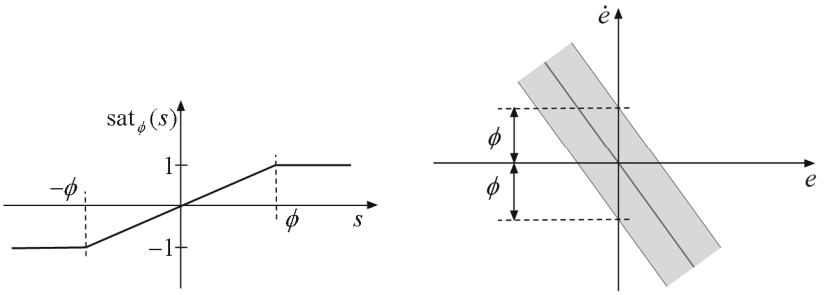

Fig. 8. The saturation function and the boundary layer

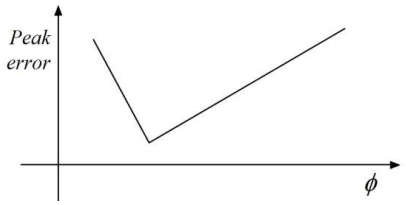

Fig. 9. Typical boundary layer thickness versus error relation

Outside the boundary layer, in effect, the unmodified sliding mode control is used. Therefore, this control, as discussed above, pushes system trajectories towards the sliding line.

In the digital implementation, even when the classical sliding mode controller with the signum function is employed, tracking performance cannot be guaranteed. The zigzag behavior is observed even for small values of the boundary layer thickness ϕ. For larger values of ϕ chattering disappears, however, with increasing ϕ, the tracking performance deteriorates. This suggests that there is a critical value of ϕ, such that below this value chattering occurs and above this value the tracking performance becomes worse (Fig. 10). In the boundary layer approach, this puts the limits of the achievable performance, assuming that all other controller parameters are kept the same. Such a limiting value for the thickness of the boundary level can be found experimentally by trial and error. However, this value may be highly dependent on the reference trajectory and the load conditions employed in the experimental tuning. Therefore, the value of the boundary layer thickness should be varying according to the chattering level in the control signal in order to achieve the best performance possible without causing chattering. To this end, a measure of chattering, Γ, is introduced:

$$\Gamma = |\dot{u}| . \tag{38}$$

$|\dot{u}|$, the absolute value of the derivative of the control signal is obtained by Euler approximation in the digital implementation. Equipped with this measure of chattering, a fuzzy parameter adjustment method which relates the boundary layer thickness ϕ to the control activity can be devised. The main idea is summarized as below.

(i) When chattering occurs, the boundary thickness should be increased to force the control input to be smoother. (ii) The boundary layer thickness should be decreased if the control activity is low. This is since, in order to obtain best tracking performance, some amount of activity in control is needed and our aim is to operate the system at the limit of chattering. Low control activity can be identified by small values of the chattering variable Γ. (iii) When the absolute value of the sliding variable is low, the phase trajectory is close to the sliding line and hence a steep saturation function (narrow boundary layer) is likely to introduce chattering effect. (iv) When the absolute value of the sliding variable is high, the phase trajectory is far away from the sliding line and hence a steep saturation function is desirable to decrease the duration of the reaching phase.

The method proposed in this paper employs fuzzy systems for the online tuning of ϕ. Fuzzy systems, as also mentioned previously, are natural choices to exploit verbal descriptions (like the four guidelines above) of the plant or problem to obtain control or adaptation mechanisms. Table I and Fig. 11 describe the four fuzzy rules used in the tuning. In Table I the subscript "NB" stands for negative big, "NS" is negative small and "PB" is positive big. The following defuzzification rule is employed.

$$\Delta\phi = \frac{\mu_{Big|s|}(|s|)\mu_{Small\,\Gamma}(\Gamma)\Delta\phi_{NB} + \mu_{Big|s|}(|s|)\mu_{Big\,\Gamma}(\Gamma)\Delta\phi_{NS} + \mu_{Small|s|}(|s|)\mu_{Big\,\Gamma}(\Gamma)\Delta\phi_{PB}}{\mu_{Big|s|}(|s|)\mu_{Small\,\Gamma}(\Gamma) + \mu_{Big|s|}(|s|)\mu_{Big\,\Gamma}(\Gamma) + \mu_{Small|s|}(|s|)\mu_{Small\,\Gamma}(\Gamma) + \mu_{Small|s|}(|s|)\mu_{Big\,\Gamma}(\Gamma)} \tag{39}$$

This function characterizes a fuzzy system with singleton fuzzification, product inference rule and center average defuzzifier. Finally, ϕ is updated by at every control cycle k:

$$\phi(k) = \phi(k-1) + \Delta\phi(k-1) \tag{40}$$

Table 1. The Fuzzy Rule Base

$\lvert s\rvert$ \ Γ	Small Γ	Big Γ
Big $\lvert s\rvert$	$\Delta\phi_{NB}$ *Rule A*	$\Delta\phi_{NS}$ *Rule C*
Small $\lvert s\rvert$	0 *Rule D*	$\Delta\phi_{PB}$ *Rule B*

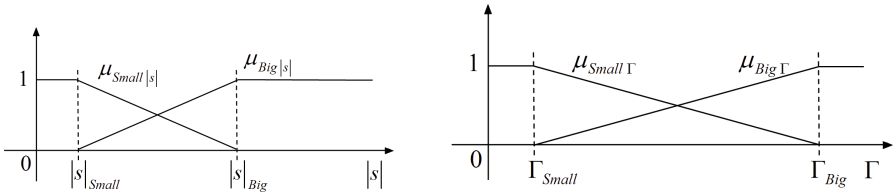

Fig. 10. The membership functions

The choice of the rule base and the membership functions satisfies the conditions (i) - (iv) above. The rules summarized in Table I are restated below.

If Γ is small and $|s|$ is big, then decrease ϕ with the high rate $\Delta\phi_{NB}$.

If Γ is big and $|s|$ is small, then increase ϕ with the high rate $\Delta\phi_{PB}$

If Γ is big and $|s|$ is big, then decrease ϕ with the low rate $\Delta\phi_{NS}$.

If Γ is small and $|s|$ is small, then do not change ϕ.

It is quite intuitive that, because small chattering and small $|s|$ are desirable conditions, the thickness which achieves them should not be changed. Note the shapes

of the Small Γ and Small $|s|$ membership functions. They assume the value 1 in their respective neighborhoods of zero. These regions close to zero act as a dead-zone which stops the evolution of ϕ by commanding zero $\Delta\phi$. For the convergence of ϕ, this dead-zone characteristics is quite useful. The membership corner positions Γ_{Small} and $|s|_{Small}$ act as borders of the dead-zone, and hence, they are very important design parameters. They convey the control engineer's notion of the acceptable performance and the acceptable level of chattering into the controller design. Whenever the pair ($\Gamma, |s|$) leaves the dead-zone, nonzero $\Delta\phi$ will be computed in (39) and ϕ will continue evolving.

The SMC method described above is implemented with and without the online fuzzy tuning of the parameter ϕ. The robustness of this algorithm is tested by several experiments using additional weights mounted on the robot tool tip in order to introduce modeling uncertainties. A two-dof direct drive manipulator built at Sabanci University Robotics Laboratory is shown in Fig. 12. This manipulator is used as the test bed in the experimental studies. A dSPACE 1102 DSP-based system is used to control the arm. The user interface software runs on a PC. C language servo routines are compiled in this environment and downloaded to the DSP. The Yokogawa Dynaserv direct drive motors used at base and elbow joints provide position measurement signals with a resolution of 1024000 pulses/rev. The base motor torque capacity is 200 Nm and that of the elbow motor is 40 Nm. The dynamics equation of the robot can be expressed as

$$\left(\begin{bmatrix} J_1 & 0 \\ 0 & J_2 \end{bmatrix} + D(q_1, q_2)\right)\begin{bmatrix} \ddot{q}_1 \\ \ddot{q}_2 \end{bmatrix} + \left(C(q_1, q_2, \dot{q}_1, \dot{q}_2) + \begin{bmatrix} B_1 & 0 \\ 0 & B_2 \end{bmatrix}\right)\begin{bmatrix} \dot{q}_1 \\ \dot{q}_2 \end{bmatrix} + \begin{bmatrix} F_{c1} \\ F_{c2} \end{bmatrix} = \begin{bmatrix} \tau_1 \\ \tau_2 \end{bmatrix}. \quad (41)$$

In (41), q_1 is the base joint angular position and q_2 is the angular position of the elbow as shown in Fig. 12. J_1 and J_2 are the rotor inertia values for the base and elbow joints, respectively. D is the manipulator inertia matrix and C represents the matrix for centripetal and Coriolis effects. B_1 and B_2 are constant viscous friction coefficients for the two joints. F_{c1} and F_{c2} stand for the Coulomb friction torques. The robot is controlled by the joint actuation torques τ_1 and the various link length, mass and inertia parameters are described in [3]. Since this control law is derived for single input single output (SISO) systems, it is applied to the robot joints in an independent joint control scheme. Simplified SISO equations of motion are obtained from (41) with fixed effective inertia and effective damping parametersand the control law is applied as is (37).

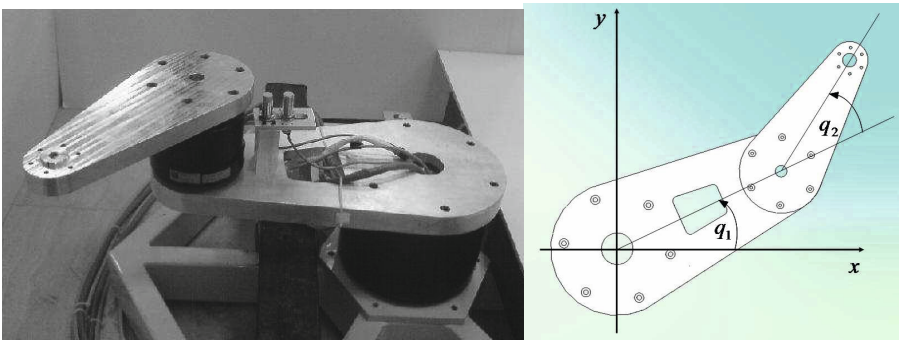

Fig. 11. The direct drive SCARA type robot arm

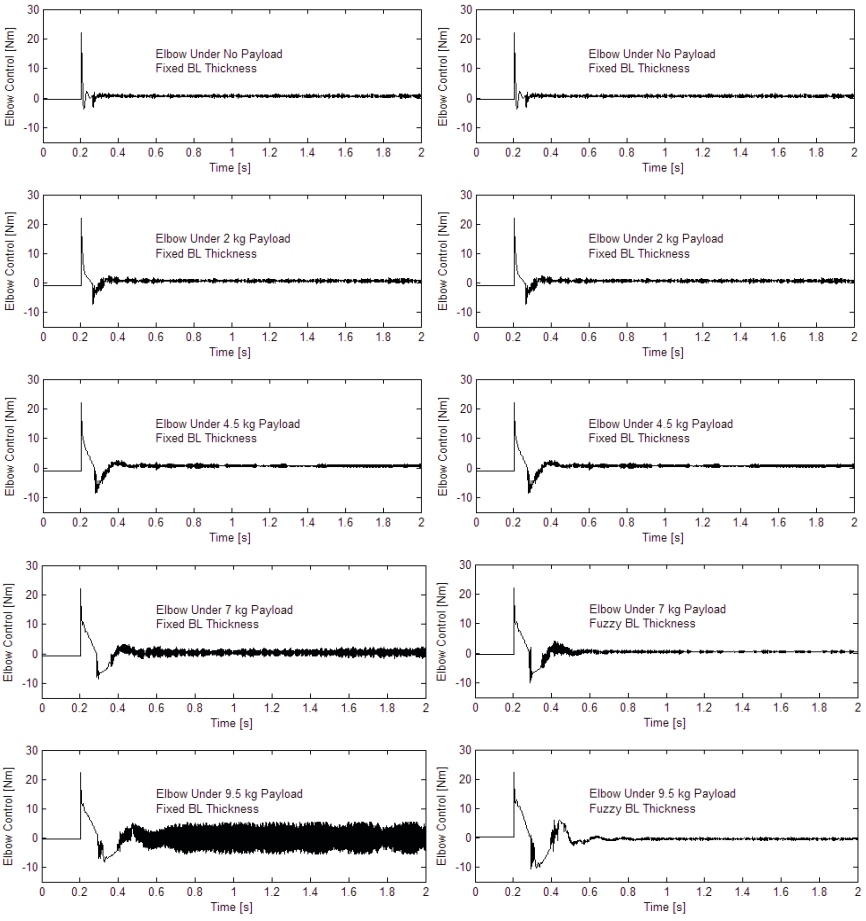

Fig. 12. Control signals in experiments with various payload values with and without fuzzy ϕ parameter tuning

The next step in the SMC application is the selection of the controller gain function $K_1(X_1)$ and controller parameters H_1, λ_1 and ϕ_1 for the base. The discussion above states the condition (36) on $K_1(X_1)$ for robust performance. However, it should be noted that in practice, we are faced with another constraint when assigning $K_1(X_1)$. This constraint is chattering which is not considered in the design of the control law. Large values of $K_1(X_1)$ cause chattering even when a boundary layer is employed. Therefore, rather than seeking uncertainty bounds for f_1 and b_1, manual tuning of the parameters which will achieve acceptable performance with limited chattering is carried out in this work. This is a trial and error based process. Also, because it is more suitable for manual tuning, not a function varying over the domain of X_1, but a constant value K_1 is used for $K_1(X_1)$. The gains H_1, λ_1 and ϕ_1 are manually tuned too. The control law for the elbow is obtained similarly. The control parameters are obtained by manual tuning. It should be noted that these parameters are obtained for the fixed boundary layer SMC method. This method and the SMC method in which ϕ is determined online by fuzzy rules are compared in the experiments. In the SMC with the fuzzy boundary layer thickness, the parameters other than ϕ are kept constant.

A control cycle time of 1 ms is used. The position reference trajectory consists of step joint references of 0.1 rad applied to the two joints. The initial condition corresponds to a stationary pose with extended elbow. Below, we present results for the elbow joint. However, the step references are applied simultaneously to the joints and similar results are obtained for the base joint. The strength of this online tuning system becomes apparent when tested under changing operating conditions. Experiments are carried out with 2 kg, 4.5 kg, 7 kg and 9.5 kg payloads. Fig. 13 shows the elbow control signals in ten experiments. The results with fixed ϕ are shown on left hand side and the ones with the fuzzy ϕ method are shown on the right. The payload increases from 0 to 9.5 kg from the top plots to the bottom in Fig. 13. With increasing payload, the task of the controller becomes more difficult. Keeping a heavier load on the sliding line is more demanding than the task in the zero payload case. The fixed ϕ parameter SMC method acts with high control activity and chattering phenomenon emerges. The oscillations on the control signal become more and more significant with increasing payload. The five plots on the right hand side show the control signals with the fuzzy SMC method. When these plots are compared with the corresponding left column plots with the same payload, it can be observed that the level of chattering or ringing is kept the same, independent from the weight of the payload. The fuzzy tuning on ϕ regulates the control effort. The initial value of the boundary layer thickness was zero in all five experiments with fuzzy tuning. We also observed that the steady state value of ϕ increased with increasing payload. It should also be noted that the steady state error did not change significantly in the ten experiments of Fig. 13. It was less than 10^{-4} rads in all cases. The proposed fuzzy tuning method adjusts the boundary layer thickness successfully and this makes the use of the SMC controller practical even under changing payloads.

4 Online Control Scheme Scheduling in Robot Force Control by a Fuzzy Logic System

This section defines a manipulation case study and describes the admittance and integral force controllers used in the reaching and contact phases in a force control problem. The operation of approaching an object with the robot tool tip, establishing contact and exerting a desired constant amount of force is a typical manipulation task. The phase when the contact is established is quite important in this task. Large overshoots over the desired contact force can be observed. Fig. 14 illustrates such a manipulation task with the CAD model of the experimental direct drive manipulator. The "tool" is a bolt which is fixed vertically on a six-axis force sensor mounted to the end of the elbow link. In Fig. 14.a, the manipulator is in its initial position. Starting from this configuration, the tool tip travels towards the work piece. In Fig. 14.b he contact is established. The main concern of the control algorithm in this phase is force regulation. It is intuitive to expect that the best performing controller structures for the phases of approach and contact should be of different nature, since the control problems are different. Although in many manipulation applications, the workpiece will be a rigidly fixed one, the task description in this paper does not exclude moving or free-to-move workpieces. In this problem definition, the exact position of the workpiece contact surface is only roughly known, with a precision of a few centimeters.

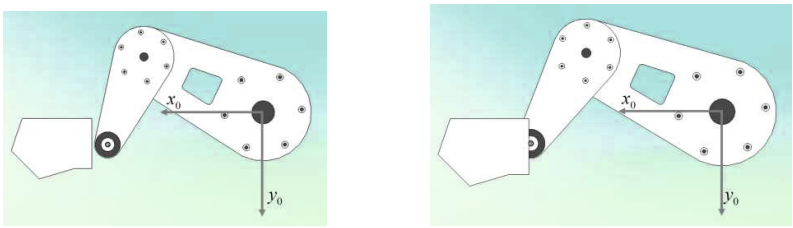

a) b)

Fig. 13. The manipulation task. The robot starts its motion off the surface of the workpiece. It moves towards it and establishes contact. The contact force should be regulated at a desired constant value after the establishment of the contact.

In the task considered in this section, in the approach phase and for the contact establishment with the surface, admittance control is used as the main control method. Amass-spring-damper model is used to compute the variation of the tool tip x-directional Cartesian position reference as expressed in the robot base coordinate frame (Fig.14). For the sake of simplicity, the $y-$directional motion is kept constant in the position control mode, with a constant Cartesian position reference:

$$y_{ref} = y_0 \tag{42}$$

Here, y_0 is constant value. The x-directional Cartesian reference increases smoothly to reach the workpiece. Specifically, a reference of the form

$$x_{ref} = x_0 + (x_f - x_0)(1-\cos(\omega t))/2 \tag{43}$$

is implemented in the experiments. x_0 and x_f are the initial and final values of the x -directional reference, respectively. The "speed" of this reference is adjusted by setting the angular frequency ω in (43). In order to track the reference trajectory described in (42, 43), the inverse kinematics problem for the planar elbow manipulator is solved with the elbow-right configuration assumption [12] and joint position references $q_{ref} = \begin{bmatrix} q_{1_{ref}} & q_{2_{ref}} \end{bmatrix}^T$ which correspond to the Cartesian references x_{ref} and y_{ref} are computed. A joint space PID controller is employed to track the joint position references obtained in this way:

$$\tau = K_p(q_{ref} - q) + K_d(\dot{q}_{ref} - \dot{q}) + K_i \int (q_{ref} - q)dt \tag{44}$$

Here, q represents the actual joint position vector. K_p, K_d and K_i are diagonal matrices with positive entries and they stand for the proportional, derivative and integral gain matrices, respectively. τ is the vector of joint control torques. The variation of the x -directional Cartesian position reference under admittance control is denoted by $c(t)$ where t stands for the continuous time. The reference varies as

$$x_{ref}^{applied}(t) = x_{ref}(t) - c(t)). \tag{45}$$

The modified reference variable $x_{ref}^{applied}(t)$ then replaces $x_{ref}(t)$ in (2). The Laplace transform $C(s)$ of $c(t)$ is related to that of the sensed x -directional force $F_e(t)$ as

$$C(s) = \frac{F_e(s)}{Ms^2 + Bs + K} \tag{46}$$

where M, B and K are the parameters which define the behavior of the tool tip in contact with the workpiece. This equation is discretized by Tustin approximation and converted into a difference equation which is suitable for the on-line computation of $c(kT)$ by a computer, where T is the sampling period and k is a discrete time sampling index. Admittance control offers a performance equivalent to position control during the approach in free space. Since exact location of the workpiece is only very roughly known to the controller, the final position target is set, again roughly, inside the workpiece. If the controller parameters are tuned appropriately, under admittance control, once the robot is in contact with the workpiece surface, it responds quickly without overshoots and keeps the contact. However, this strategy is not useful for controlling the force applied in the steady state, since parameters on which this force depends also determine the stability of the robot and its first impact behavior against the workpiece. Varying the parameters in order to obtain the desired force, we would deteriorate the stability and smoothness of the establishment of the contact. For the steady state, a more appropriate strategy is the integral control. The integral force controller integrates the error between a desired steady state constant force level and the actual (sensed) force exerted by the tool-tip. The integral force

error F_{int} is multiplied then by the integral action constant K_{iF} to compute the Cartesian control force F_c:

$$F_{\text{int}} = \int (F_{ref} - F_e) dt \tag{47}$$

$$F_c = K_{iF} F_{\text{int}} \tag{48}$$

F_{ref} in (6) is the two dimensional vector

$$F_{ref} = \begin{bmatrix} F_{ref_x} & 0 \end{bmatrix}^T \tag{49}$$

where F_{ref_x} is the constant force reference in the x-direction mentioned above. By (49), a force reference of 0 N is applied in the y-direction. Then the torque to be applied on the robot joints is computed as [12]:

$$\tau = J_M^T F_c \tag{50}$$

The integral in (6) is computed by a digital approximation.

Once the contact is settled, integral force control prevents loosing contact with the surface; provides zero steady state error for a constant reference force and it is more stable and accurate than proportional action force controllers. On the other hand, when the initial tool tip position is in free space, integral force control generates undesired large accelerations. Also, after an approach phase where the integral control is active, this control causes contact force overshoots. In this case the force error integral will grow during the approach since no (or very small) force is sensed in free space and there will always be a nonzero and positive force error. The impact force when reaching the workpiece can be excessive. The magnitude of this force depends on the initial distance between surface and tool-tip. With this motivation, it is proposed to use the admittance control dominantly in the reaching phase and the integral control as the primary controller after the establishment of the contact with a smooth transition between the controllers dictated by a fuzzy scheduler.

There are three objectives to be reached with the proposed fuzzy scheduling system:

1) Avoiding a brusque impact when reaching the surface of the workpiece.
2) Avoiding the application of integral control while the tool-tip is not in stable contact with the workpiece.
3) Switching the control action from admittance into integral force control without causing a large force overshoot, once the tool-tip is in stable contact with the workpiece.

In order to achieve a controller-to-controller transition a weighting variable, $W(kT)$, is introduced. This variable varies between 0 and 1 and when $W(kT) = 1$ only admittance control is applied. Similarly, at the other extreme, that is, when $W(kT) = 0$ the applied control input is computed purely by integral force control

action. A linear combination of the two controllers' outputs is applied for cases in which $W(kT) \in (0,1)$. In other words, the two controllers are combined with the relation

$$\tau = W\tau_a + (1-W)\tau_i, \tag{51}$$

where τ_a and τ_i are the admittance and integral force control actions, respectively. With formulation in the above equation, the task of the fuzzy system is to determine $W(kT)$ at every sampling instant k.

In order to identify sudden changes in force, the following measure of contact force activity, denoted by Γ is introduced.

$$\Gamma(kT_\Gamma) = \sum_{i=0}^{N_\Gamma} \left| \overline{F}((k-i)T_\Gamma) - \overline{F}((k-i-1)T_\Gamma) \right| \rho(i) \tag{52}$$

Here, T_Γ is the sampling period for the computation of Γ. Again it is a multiple of the controller sampling period T. N_Γ is the number of samples used in the computation and ρ is a variable which indicates whether the force is changing direction or not. A force difference which keeps the same direction (increasing or decreasing) from sample to sample is added up to contribute to Γ.

$$\begin{aligned} &\rho(i) = 1 \quad if \quad \left[\overline{F}((k-i)T_\Gamma) - \overline{F}((k-i-1)T_\Gamma)\right]\left[\overline{F}((k-i-1)T_\Gamma) - \overline{F}((k-i-2)T_\Gamma)\right] > 0 \\ &\rho(i) = 0 \quad if \quad \left[\overline{F}((k-i)T_\Gamma) - \overline{F}((k-i-1)T_\Gamma)\right]\left[\overline{F}((k-i-1)T_\Gamma) - \overline{F}((k-i-2)T_\Gamma)\right] \le 0 \end{aligned} \tag{53}$$

The third input of the fuzzy scheduler, W is also a useful one since it provides valuable information about in which mode the control algorithm is. In order to apply the most suitable control scheme at every moment the following guidelines are developed:

(i) If the integral force control is dominant (if W is small) and the average force is small, it may be the case that the integral force control is active with the robot tooltip in free space. Admittance control should be made dominant and the weight of integral control should be decreased quickly to avoid unnecessary force error integration. (ii) If the admittance controller is dominant (W close to 1), the average force is large and rate of change of the average force is small, we can infer that the contact is well established and increase the weight of the integral controller gradually to reach a steady state and desired level of force without large overshoots.

(iii) No change in W is necessary in other conditions.

Formulated as fuzzy rules, these guidelines can be written as:

1) If W is small, Γ is small and $\overline{F}$ is small, then W should be increased with a big increment

2) If W is small, Γ is big and $\overline{F}$ is small, then W should be increased with a big increment

3) If W is big, Γ is small and $\overline{F}$ is big, then W should be decreased with a small decrement

4) In any other case, W should be kept constant.

Fig. 15 shows the membership functions. Product inference rule and center average defuzzification is applied.

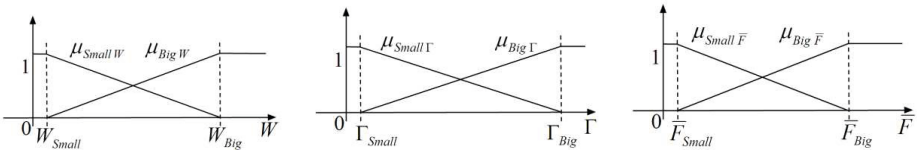

Fig. 14. Membership functions for W , Γ and $\bar{F}$

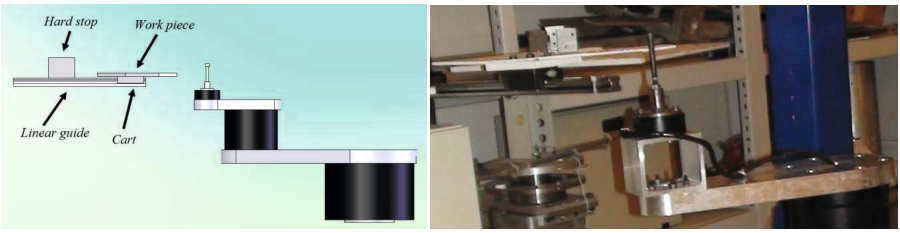

Fig. 15. The sliding work piece

A constant force reference is applied and the task is to reach the workpiece and to regulate force at this constant reference. In order to test the control algorithms under different working conditions two manipulation scenarios are prepared. In the first one the workpiece is kept rigidly fixed, and in the other one the workpiece is initially free-to-move on a linear guide until the motion range of the linear slide comes to an end when the workpiece is stopped by a hard stopper. In this scenario the robot firstly works against the friction of the linear guide, and then against the effectively fully fixed workpiece, after its stop (Fig. 16).

The F_{ref} is set as 12 N. In order to simplify computations, the workpiece assembly is arranged in a particular position, so as to make the x -direction of the robot base frame and the normal to the workpiece surface coincide. Fig. 17 shows the experimental results obtained by the fuzzy scheduling for the rigidly fixed workspace case. With the impact of the contact, an increasing average force and high force activity is observed. The fuzzy rule base decides to decrease the weight of the admittance control and increase that of the integral controller. The admittance controller weight chances from one to zero. This smooth change keeps admittance control active for a while after the contact establishment too. Fig. 18 shows the performance of the fuzzy scheduling with the sliding work piece. Actually the motion in this case is divided into three phases rather than into two. The first phase is that of reaching the workpiece. In the second one the workpiece is pushed by the robot and the force sensor reads nonzero force values due to the friction on the linear guide. In the third phase of this motion sequence, the hard stop of the linear guide is reached and the workpiece poses a solid obstacle in touch with the robot tool tip. Basically, the operation of the scheduler remained the same as in the case with the fixed workpiece. The scheduler adjusts the controller contribution weight W by evaluating

the average force and activity variables together with the current weight of the controllers to avoid the misinterpretation of slightly rising contact forces (due to friction) as the forces of an established rigid contact. The performance of the force control system with the fuzzy scheduler with fixed and sliding workpieces is quite similar. This suggests that the performance of this control system is not affected severely by working condition variations of this kind.

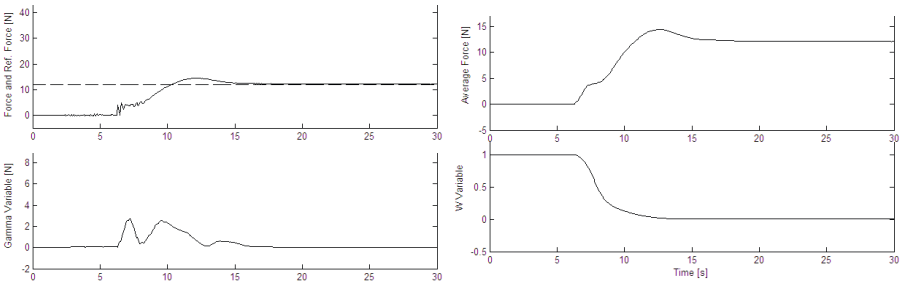

Fig. 16. Fixed workpiece. Plots of the evolution of the measured force and the fuzzy system variables

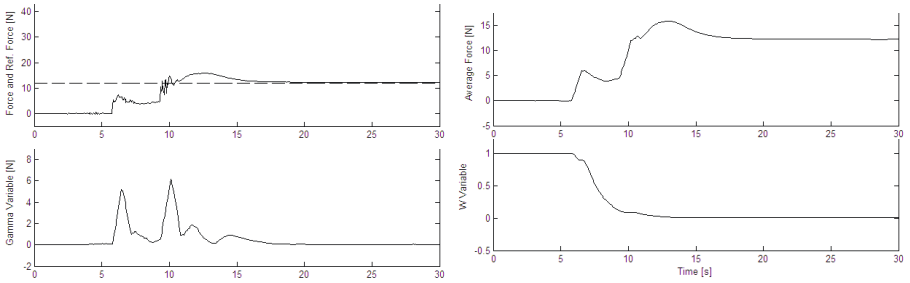

Fig. 17. Constrained motion of the workpiece on the linear guide. Plots of the evolution of the measured force and the fuzzy system variables.

5 Visual Servoing and Force Control Integration by Fuzzy Parameter Adjustment

Fig. 19 shows the scenario of a manipulation task with a free to rotate object. From left to the right, the task description goes through following phases: In the first phase, robot tool tip starts far away from the workpiece, like the point I in Fig. 19 a). The aim of the robot is to apply a constant magnitude force on the point O normal to the edge of the workpiece where O is located. This is a planar manipulation task. To accomplish this aim, robot should approach to point O perpendicularly. First the robot should be brought on the y -axis as shown in Fig. 19 a). As the tool tip reaches

the y-axis, robot should approach to the workpiece by following the y-axis as shown in Fig. 19 b). When a contact with the workpiece is sensed, desired constant force should be exerted on the workpiece in normal direction as shown in Fig. 19 c). The robot is also expected to continue exerting the force reference, and should reestablish the contact in the case of a contact loss. The workpiece is free to rotate about the pivot point P. In the experiments, the workpiece is rotated intentionally about this point in order to create contact losses. This phase is shown in Fig. 19 d). This is the most demanding phase for a control system, because application of forces on points on the edge of the workpiece other than the location indicated by the black point in Figure 19 is undesired. The interaction of the robot tool tip with the workpiece can be in many different ways while it moves from point O to point $\overline{O}$ in Fig. 19 d). However, our target in control synthesis is to achieve an interaction which fulfills demands described above. Firstly, we design a fixed parameter controller for the problem definition stated in the previous section. This controller is based on the task frame approach. The origin of the task frame is attached on the contact point of the workpiece. Hybrid control is applied with a visual servoing component in the direction tangent to the straight edge of the workpiece and force control component normal to this straight edge. Since a force normal to its contour is to be applied on the workpiece, the orientation of the task frame can be identified with the slope of the edge detected on the workpiece by vision system. The x, y-axis and origin O shown in Fig. 19 describe the task frame. For force control, an explicit force controller in PI structure is used [13], [14]. The force error is defined as the difference between the task space force reference F^r and the measured interaction force F:

$$e_F = (F^r - F) \,. \tag{54}$$

The "selected force error" is then obtained by

$$e_{FS} = S(F^r - F) \,, \tag{55}$$

where the diagonal matrix S is called the selection matrix.

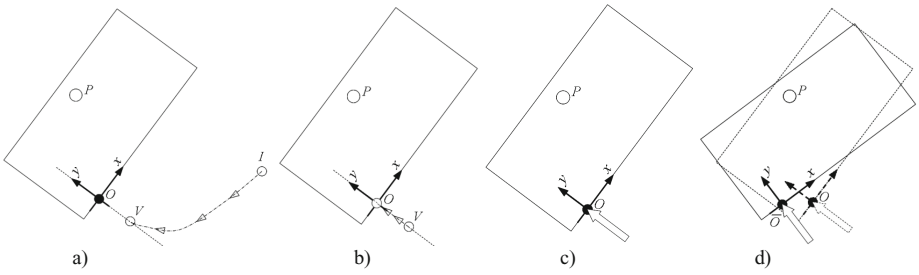

Fig. 18. The manipulation scenario

The entries of the matrix S specify the force controlled task space directions. If the i^{th} direction is a force controlled one, then the i^{th} diagonal term s_{ii} of S is equal to 1 and it is equal to 0 otherwise. The force control law is expressed as

$$F_F^c = K_{p_F} e_{FS} + K_F \int e_{FS} dt \,. \tag{56}$$

In (55), F_F^c stands for the Cartesian control force defined in the task space. K_{p_F} is the diagonal proportional force control gain matrix and K_F is the diagonal integral gain matrix:

$$K_{p_F} = \begin{bmatrix} K_{p_F x} & 0 \\ 0 & K_{p_F y} \end{bmatrix}, \qquad K_F = \begin{bmatrix} K_{F^x} & 0 \\ 0 & K_{F^y} \end{bmatrix}. \tag{57}$$

The control F_F^c is then transformed into robot joint torques by using the robot Jacobian J_R as,

$$u_F = J_R^T(q) R_w^t F_F^c \tag{58}$$

where q is the vector of joint positions and R_w^t is the rotation matrix between the task frame and the world frame attached to the base link of the manipulator. u_F stands for the force control component in the joint control torques. The vision based position control adopted in this section is in the so-called "dynamic look-and-move" control category. In dynamic look-and-move approach, visual servoing generates position references for an inner position control loop based on joint encoder feedback. Task space errors e_V^x and e_V^y (measured in pixels) for visual servoing are defined in Fig. 20. Augmenting them together, the task space position error e_V is obtained:

$$e_V = \begin{bmatrix} e_V^x \\ e_V^y \end{bmatrix}. \tag{59}$$

Its "selected" version is obtained by

$$e_{VS} = (I - S) e_V \tag{60}$$

where I stands for the identity matrix. The position errors in the force controlled directions are ignored. The visual servoing rule in the image space is defined as,

$$F_V^c = K_V e_{VS} \tag{61}$$

In (61), F_V^c is the task space control force vector generated by visual servoing and K_V is the gain

$$K_V = \begin{bmatrix} K_V^x & 0 \\ 0 & K_V^y \end{bmatrix}. \tag{62}$$

The output of the visual control, F_V^c, should be interpreted in the following way. Because of our choice of the visual control structure as dynamic look-and-move, we

are not using this vector as a Cartesian control force to be converted to joint torques via a Jacobian-Transpose relation. Rather, this vector is used to generate world frame Cartesian tool tip position references. F_V^c is regarded as the task space velocity demand for the visual servoing task. It is expressed firstly in the image frame coordinates by multiplying it by the rotation matrix relating the task frame coordinates to the image frame coordinates and then using the rotation matrix relating image frame and world frame coordinates, it is represented in world frame:

$$v^r = R_w^i R_i^t F_V^c \tag{63}$$

Here v is the task space velocity demand in m/sec. J_I is the image Jacobian which includes camera intrinsic parameters. The position reference p^r in the world frame is obtained by integrating this velocity demand as in the following equation.

$$p^r = \int v^r dt \tag{64}$$

Let p be the actual Cartesian position of the robot tool. (p is obtained through joint encoder readings and forward kinematics with the position control loop sampling rate, which is higher than the camera sampling rate.) Defining e_P, the Cartesian position error expressed in the world frame, by $e_P = p^r - p$, a PID position controller is used to generate a Cartesian control force for the robot tool as below.

$$F_P^c = K_{P_P} e_P + K_{I_P} \int e_P dt + K_{D_P} \dot{e}_P . \tag{65}$$

This force is reflected to joint control torques by the use of the manipulator Jacobian:

$$u_P = J_R^T F_P^c . \tag{66}$$

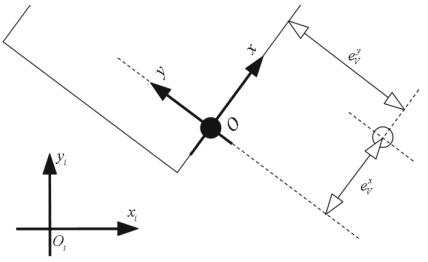

Fig. 19. Visual servoing errors

As in the case of u_F, u_P is a component in the joint control torque vector. The joint control vector u is finally computed as

$$u = u_F + u_P . \tag{67}$$

Our task is the application of a normal force to a workpiece. We divided this task into two phases: i) Reaching phase and ii) manipulation phase. In the reaching phase, the tool tip of the robot is brought near the force application point using visual servoing in task frame. In this phase the both of the task frame directions are visually controlled. Therefore, the selection matrix S is given by

$$S = \begin{bmatrix} 0 & 0 \\ 0 & 0 \end{bmatrix}. \tag{68}$$

In the reaching phase, the visual servoing gain in x direction is specified higher than the visual servoing gain in y direction, in order to quickly bring the tool tip to the line of concern (task frame y-axis). After intersecting it, the robot tool moves along with the y axis of the task frame and touches the surface of the workpiece. The contact is sensed by the force sensor by measuring the force in y-direction in task space. A force threshold is employed for the contact detection. With the contact, second phase begins. In the second phase hybrid position/force control guided by visual servoing is applied. Along the y direction force control is applied, and visual servoing is implemented along the x direction. This corresponds to the following selection matrix.

$$S = \begin{bmatrix} 0 & 0 \\ 0 & 1 \end{bmatrix}. \tag{69}$$

Since the problem definition involves a free-to-rotate workpiece, after the reaching phase, the object is manually rotated around the pivot point P shown in Fig. 19. In this phase, even if there appears a position error in x-direction, the controller continues applying force. This results with the application of force on undesired points of the workpiece. High values for visual servoing gains may be suggested as a solution of this problem. With high control gains, visual servoing can push the x-direction position error quickly to zero. However, using a high gain values can result with overshoot and oscillations. As another problem, if force control continues when the contact is lost, some hard impacts are inevitable. Though hard impacts can be avoided by using very low force control gains, low gains result in a very slow force control reaction. The dominant control gain in force control is K_F. According to [13] an effective use of the explicit force control scheme can be obtained by selecting a K_F value much larger than K_{p_F}. Therefore the gain K_F is chosen for tuning the force controller by fuzzy rules. In the vision control law the only gain is K_V, and this gain is tuned by a fuzzy system. The main principles of the tuning are as follows.

(i) If the position error is big and force error is small, then this means that the robot is applying the reference force to an undesired point. The robot should be brought on the line of concern (task space y-axis) without applying too much force on the workpiece. To accomplish this force gain should be decreased, and vision gain should be increased. (ii) If the position error is small and force error is big, this means the robot is at the right position, but force control gain is too low that the desired force value has not reached yet. To overcome this, force control gain should be increased.

And also to avoid fast movements in tangential direction, motion in visually guided direction should be softened. (iii) If both position and force error are big, this means the workpiece went through a large motion. In this case, the force gain should be decreased rapidly and visual servoing should be increased. (iv) If both of the position error and force error are small, then there is no need to change the control gains.

These four principles can be implemented by two independently running fuzzy tuning systems for the two controller gains mentioned above. The rule bases for these fuzzy systems for K_F and K_V are summarized in Tables II and III, respectively. Note that the tuning is carried out for the "active" entries of the gain matrices corresponding to the force and vision controlled directions chosen by the selection matrix S. Fig. 21 shows the membership functions for the input variables. "Δ" in the notation for the rule strengths signifies that, instead of computing the control gains directly, incremental changes in the control gains are computed by the fuzzy systems. Center average defuzzification with singleton fuzzification and product inference rule is implemented. Finally, K_{F^y} and K_{V^x} are obtained by

$$K_{F^y}(k+1) = K_{F^y}(k) + \Delta K_{F^y}(k) \qquad K_{V^x}(k+1) = K_{V^x}(k) + \Delta K_{V^x}(k) \tag{70}$$

In (70) k is the computation cycle of the digital controller. When the error in x direction is reduced via visual servoing, according to the fuzzy rules, force control gain begins to rise. If there is a nonzero position error in y -direction in that instance, this fuzzy tuned control system cannot avoid a hard impact. The two-dof direct drive manipulator built at Sabanci University Robotics Laboratory is used in the experiments (Fig. 22). A 6-axis force sensor is assembled at the tip of link 2. A M8 stud is mounted on top of this device, concentric with it, and used as the tool in the experiments. The camera which overlooks the scene has a resolution of 320x240 pixels. The workpiece, a polymer sheet of 10 mm thickness with rectangular shape is pivoted around a vertical axis, and is free to rotate. Soft linear springs attached to the workpiece from both sides keep the orientation of it fixed when no external forces are applied on it. The integrated visual/force control is tested in a hybrid approach with a fuzzy gain tuning. The task frame orientation is identified with the angle α between the image frame and task frame x-axes in Fig. 20, and this angle is termed "task angle."

The results obtained with the approach are shown in Fig. 23. In this approach undesired sheer forces are overcome by fuzzy gain scheduling. With fuzzy tuning, when there appears a position error in x- direction, visual servoing gain in x-direction begins to climb where force control gain drops rapidly. As the position error decreases to some specified degree which is defined by the fuzzy rule, force control gain rises.

Table 2. The Fuzzy Rule Base for Tuning the y-Direction Force Gain

e_{F^y} \ e_{V^x}	Small e_{V^x}	Big e_{V^x}
Big e_{F^y}	$\Delta K_{F^y PS}$	$\Delta K_{F^y NB}$
Small$_f$	0	$\Delta K_{F^y NS}$

Table 3. The Fuzzy Rule Base for Tuning the x-Direction Visual Control Gain

e_{F^y} \ e_{V^x}	Small e$_v$	Big e$_v$
Big e$_f$	$\Delta K_{V^x NS}$	$\Delta K_{V^x PS}$
Small$_f$	0	$\Delta K_{V^x PS}$

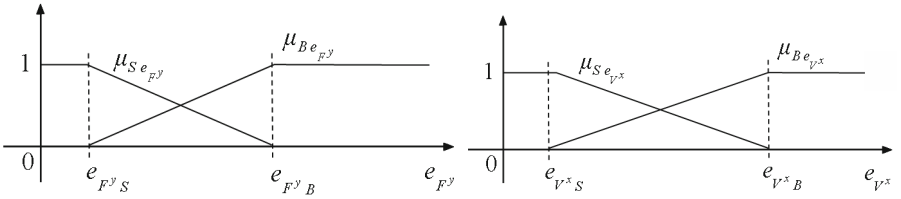

Fig. 20. Membership functions used in the fuzzy inference of the first fuzzy tuning system

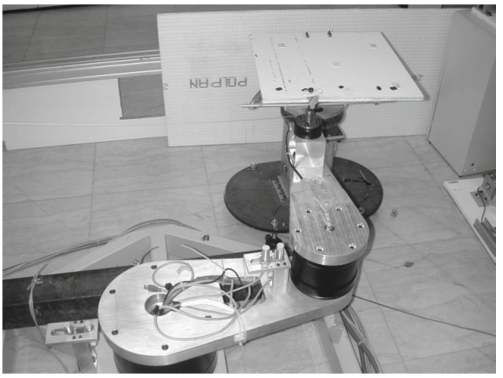

Fig. 21. The experimental setup. This scene is overlooked by the camera which is fixed at a location above the workpiece. The robot is equipped by a 6-axis force sensor at its tool tip.

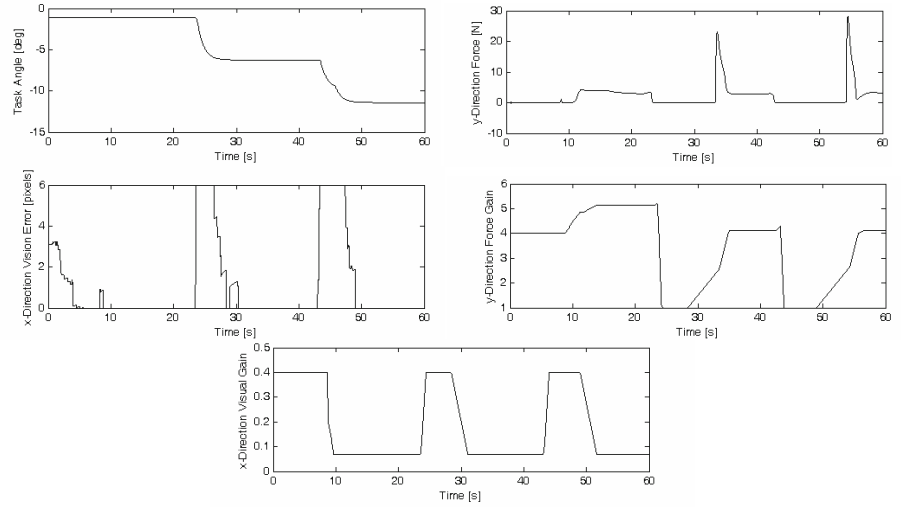

Fig. 22. Task angle, y-direction force, and x-direction visual servoing error and the tuned controller gains in the fuzzy tuning approach

6 Conclusion

On-line fuzzy parameter adeptation techniques for position, force and visual control applications implemented on direct drive manipulators are reviewd as case studies in this chapter.

Fuzzy adaptive sliding mode control of a direct drive manipulator is considered in Section 2. Three different fuzzy logic based adaptation schemes are proposed. Implementation results with these algorithms applied separately reveal that the methods presented improve the performance of the original algorithm. Another important aspect is that there is no need for an off-line tuning of controller parameters when the adaptation schemes are used. Faster convergence to desired trajectories can be obtained, without the need for off-line tuning of control parameters. Furthermore, dependency on a particular reference signal is avoided.

Sliding mode controller structures with boundary layers are widely used to solve the chattering problem. However, tracking performance is degraded when a too wide boundary layer is used and chattering prevails when the boundary layer is too narrow. The determination of a suitable boundary layer thickness which can eliminate chattering and at the same time achieve acceptable performance is an important design issue. Section 3 reviewed an online fuzzy tuning method to adjust the thickness of the boundary layer. The thickness of the boundary layer is obtained without the offline trial and error processes. The online algorithm reacts to changes in the sliding variable and the chattering level to adjust the boundary layer thickness continuously. This enables the controller to perform under changing operating conditions without chattering. The results are verified by experiments with various payload values on a direct drive robot. The performance and chattering elimination properties of the proposed method make it a candidate for industrial applications.

Section 4 concentrated on a manipulation problem as a case study. In this task the robot tool tip should travel in free space to reach the surface of a workpiece and after reaching it, it should exert a desired constant value of normal force on it. Two simple structured and robust control techniques are chosen as dominant controllers in the two phases mentioned. These are the admittance control and integral force control for the reaching and force regulation phases, respectively. A fuzzy logic system for smooth switching between the controllers is proposed. Experimental studies are carried out on a direct drive SCARA type manipulator. Different working conditions are introduced by working with free-to-move workpieces as well as with rigidly fixed ones. The experimental results indicate that the fuzzy scheduler is applicable to a wide range of working conditions.

A hybrid vision/force control approach with fuzzy logic tuned controller gains is discussed in Section 5. It is seen that with online fuzzy tuning, the system behaves more stable and avoids sheer forces. The results show that fuzzy logic can be very useful in this kind of integration of control methodulogies.

In the case studies above fuzzy parameter adaptation performed well in on-line tuning, in providing the controllers with an adaptive nature and in combining control methodologies for exploiting their benefits and avoiding their drawbacks. It can be stated that these techniques can be employed in demanding industrial applications of direct drive motors and direct drive robotics.

Acknowledgement. I met Professor Okyay Kaynak first in 1989, in the venue of a post-Chernobyl nuclear energy conference, as a sophomore student in electronics engineering, working in the local organization of the meeting. Next year I found myself Professor Kaynak's conference organization staff for the 1990 IEEE International Workshop on Intelligent Motion Control. Since then I am working in the field of intelligent motion control. I have built my first robot control system as his advisee in 1992, published my first paper in 1994 with his co-authorship, finished my Ph.D. work under his supervision with about 25 more co-authored papers in 2000. He is surely the most influential figure in my professional life. I am indebted, however, not solely for his guidance on technical matter. He was always a motivating and promoting supervisor. So he was after my graduation too. As a faculty member, I am tyring to meet the standarts set by him, in motivating students and opening new doors for them.

References

1. Kaynak, O., Erbatur, K., Ertugrul, M.: The fusion of computationally intelligent methodologies and sliding mode control - A survey. IEEE Trans. Ind. Electron 48(1), 4–17 (2001)
2. Erbatur, K., Kaynak, O., Sabanovic, A., Rudas, I.: Fuzzy adaptive sliding mode control of a direct drive robot. Robot Auton Syst. 19(2), 215–227 (1996)
3. Erbatur, K., Calli, B.: Adaptive fuzzy boundary layer tuning for sliding mode controllers and its application on a direct drive robot. Soft Computing - A Fusion of Foundations, Methodologies and Applications 13(11), 1099–1111 (2009)
4. Perez Plius, M., Yilmaz, M., Seven, U., Erbatur, K.: Fuzzy controller scheduling for robotic manipulator force control. In: Proceedings of the 12th IEEE International Workshop on Advanced Motion Control, Sarajevo, Bosnia and Herzegovina, March 25-27 (2012)
5. Çallı, B., Erbatur, K., Ünel, M.: Visual servoing and force control integration with fuzzy parameter adjustment. In: Proceedings of the 11th IASTED International Conference on Intelligent Systems and Control, Orlando, November 16-18, pp. 633–808 (2008)
6. Sabanovic, A., Sabanovic, N., Jezernik, K., Wada, K.: Chattering free sliding modes. In: Proceedings of the Third Workshop on Variable Structure Systems and Lyapunov Design, Napoly, Italy, pp. 143–148 (September 1994)
7. Sabanovic, A., Jezernik, K., Kaynak, O.: Chattering free sliding modes in robotic manipulators control. Mechatronics 1(1) (1994)
8. Erbatur, K., Kaynak, O., Sabanovic, A.: An experimental evaluation of chattering free sliding mode control as applied to the control of a direct drive manipulator. In: Proceedings of the Industrial Power Electronics Conference, Yokohama, pp. 226–231 (1995)
9. Erbatur, K., Kaynak, O., Sabanovic, A.: A novel variable structure control as applied to the control of a direct drive manipulator. In: Proceedings of the European Control Conference, Rome, pp. 196–201 (1995)
10. Erbatur, K., Kaynak, O., Sabanovic, A.: A study on robustness property of sliding mode controllers. IEEE Trans. Ind. Electron 46(5), 1012–1018 (1999)
11. Erbatur, K., Kaynak, O., Sabanovic, A.: Robot trajectory control in cartesian space via sliding modes. In: Proceedings of the IEEE Industrial Electronics Conference, vol. 2, pp. 766–771 (1996)
12. Spong, M.W., Vidyasagar, M.: Robot dynamics and contro. John Wiley & Sons, Inc. (1989)
13. Volpe, R., Khosla, P.: An experimental evaluation and comparison of explicit force control strategies for robotic manipulators. In: Proceedings of the American COntrol Conference, Chicago IL, pp. 758–764 (June 1992)
14. Volpe, R., Khosla, P.: ‘A theoretical and experimental investigation of explicit force control strategies for manipulators. IEEE Trans. Auto Contr. 38(11), 1634–1650 (1993)

Model Reduction for Sliding Mode Control of Rapid Thermal Processing System

Tengfei Xiao and Han-Xiong Li

Department of Systems Engineering and Engineering Management,
City University of Hong Kong, Hong Kong SAR, China
xiaotf2012@gmail.com,
mehxli@cityu.edu.hk

Abstract. In order to control the temperature on the wafer in a rapid thermal processing system, we develop a reduced model of the dynamic based on the spectrum of the system operator and then develop a sliding mode controller for the system. The dominant modes of the system are extracted through the analysis of the spectrum. Galerkin's method is utilized to construct the reduced model of the system with the dominant modes as the trial functions. Then, sliding mode controller is designed based on the reduced model. Simulations are performed by comparing the high-order model with the proposed reduced model and applying the control scheme to the system. Simulation results show that the proposed reduced model has relatively small order but the same ability to model the process and the sliding mode control actions can heat the wafer to a desired temperature with a uniform distribution.

1 Introduction

Rapid thermal processing (RTP) is a mainstream technique in the manufacturing of semiconductor. RTP has large advantage over batch furnaces processing with its smaller thermal mass. The RTP technique was firstly applied to implantation annealing, on GaAs in an inert ambient [1]. In [2], the technique was further utilized on Si to activate ion implanted dopants, remove defects, and regrow amorphized silicon, with minimal diffusion of the dopant atoms. [3] generalized various applications of the RTP which include silicidation, gate dielectric formation, gas reflow, metal alloying, shallow junction dopant diffusion and multilayer deposition. It was pointed out in this work that RTP is not only a superior alternative to furnace processing, but it is also the only way to perform certain crucial steps in the processing of compound semiconductor devices such as highmobility transistors, resonant tunneling devices, and high-efficiency solar cells.

Dedicated equipment design, efficiency temperature measure and control technique are needed in the development of the RTP. The following sections will present some current methods of the equipment design, temperature measure and temperature control. The problem of modeling arises in the design of measurement sensor and controller. We will introduce some existing modeling methods for RTP system and their weaknesses in section 1.3.

X. Yu and M. Önder Efe (eds.), *Recent Advances in Sliding Modes*,
Studies in Systems, Decision and Control 24, DOI: 10.1007/978-3-319-18290-2_19

1.1 Equipment Design

The components of an RTP system needed to be designed are energy source, the process chamber, the gas panel and the wafer transfer system etc. In this section, we will focus our effect to review the dominant techniques used to design the energy source and the process chamber.

1.1.1 Energy Source

In the commercially available RTP systems, there are three basically heating sources. Two are lamp sources: tungsten filament lamp and long-arc noble gas discharge lamp. The third type is the continuous resistive heat source.

The tungsten lamp is made up of a linear double-ended quartz tube and a tungsten filament contained in it which is resistively heated. In order to increase the filaments color temperature, halogen gas rather than inner gas is chosen to be the fill gas. The chemical and physical mechanisms can be found in [4] where experiments were performed.

The second type of heating source is the long-arc lamp. Most of the long-arc lamps used in the RTP systems are the dc water-wall argon lamps [5,6]. This kind of lamp has advantage over the tungsten-halogen lamp and conventional arc lamps for that it provides high power output and has the ability to change power levels rapidly. Annealing experiments using the water-wall lamp have shown that good activation and essentially complete removal of implant damage can be achieved. In [7], it is pointed out that the vary rapid heating and cooling rates obtainable with the water-wall lamp offer a great deal of flexibility in the time/temperature cycles used for annealing.

The third type of heating source is the classical resistive heating. A resistively heated silicon carbide bell jar is used as the reaction chamber and the heat source [8]. There exists a well-defined temperature gradient in the bell jar. The wafer is moved up and down to a position which corresponds to a certain process temperature.

1.1.2 Process Chamber

There are three basic chamber designs employed in the commercially available systems: the cold wall, the warm wall and hot wall design.

The schematic of the cold wall chamber is shown in the Figure 1. The cold wall chamber is made using metals like aluminum, stainless steel or other alloy which are sometimes coated with a thin quartz layer. Because the chamber is water cooled, it is referred to as a cold wall system. The strength of using the cold wall chamber is that there is no potential secondary radiation source which complicates temperature measurement as the chamber walls are kept at a fixed temperature. However, the weakness of using the cold wall chamber is that the wall can be contaminated by parasitic deposition which cause particles and decrease temperature uniformity [9].

The second chamber design is the warm wall chamber which is made up of quartz envelop. As the quartz envelop is air cooled, it is referred to as a warm wall chamber. The wall of the chamber is kept at a significantly lower temperature than the wafer. The schematic of warm wall chamber is shown in Figure 2. The advantage of the warm wall chamber is that it minimizes metal contamination from the metal chamber. However, preheat cycles are needed in this type of system as the warm wall has thermal memory effects.

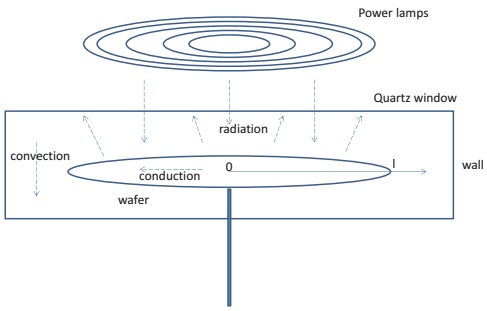

Fig. 1. Schematic diagram of the RTP system

The third type of chamber design is the hot wall chamber with its bell-jar shaped silicon carbide [8]. The temperature of the wall is higher than the wafer as it serves as the uniform heat radiator to the wafer in the hot wall chamber. A schematic of hot wall chamber can be found in Figure 3.

1.2 Temperature Measure

There are basically two methods of temperature measurement in the RTP systems: an absolute method and an optical method. The absolute method uses a thermocouple which contact with the wafer directly to measure the temperature while the optical method uses a noncontact pyrometer as the measurement tool. The optical method is preferred to absolute method because it can minimize foreign objects in contact with wafers. Most of todays RTP systems use the optical method to measure the temperature of the wafer.

However, the major problem of using the pyrometer is that the measurement can be affected by some sources of error. The first order radiation which comes from the heat source or from the reflectors and the second order radiation which is reflected off the silicon wafer can disturb the Lambertian radiation from the hot wafer.

There are two primary methods to solve this problem. The fundamental idea of the first approach is to avoid the overlap of the spectral wavelength distribution of the radiation from the heat source with the bandpass wavelength range of the sensor. In [10], there was a strong absorption peak in the lamp which does not emit radiation beyong 1.4m while the band-pass of the pyrometer is 1.4-1.5m.

The fundamental idea of the second approach is to exclude the interfering radiation from the heat source to the pyrometer. The pyrometer views the wafer through a window of materials like calcium fluoride [11]. The window absorbs radiation of a specific wavelength and composes a selective narrow-band absorption filter.

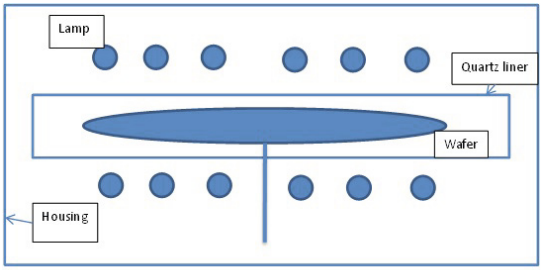

Fig. 2. Schematic diagram of the RTP system

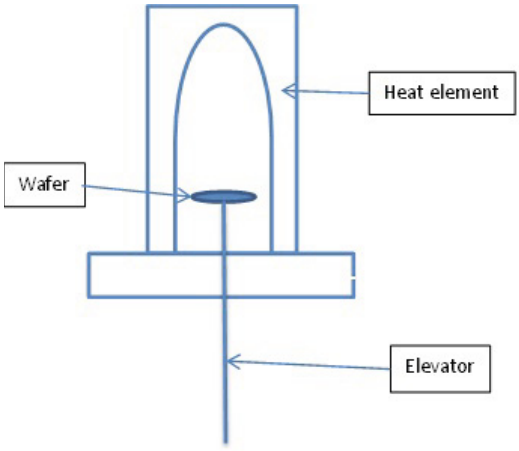

Fig. 3. Schematic diagram of the RTP system

1.3 Modeling of Temperature

The model of the system plays an important role in the design of the measurement sensor and controller. There are numerous works [12–16] proposing model of the RTP system. In [12], two-dimensional model was used to simulate rapid thermal processing process where the dominant factors governing heat transfer and fluid flow inside the reactor were identified. Then a finite-difference method was used to get the numerical solution of the system. [13] developed a numerical model that incorporated radiative and convective heat transfer and then thermal stresses were analyzed. Nonlinear numerical model was proposed in [15] and control method was developed.

One weak point of the above models is that the orders of the models are relatively high. A reduced model is demanded for most designs of sensor and controller. There are a few works [17–19] proposing some model reduction methods for the RTP system. [17] and [18] extracted the low-order models using the proper orthogonal decomposition (POD) method. [19] made use of the excellent predictive capabilities of the reduced model to optimize power inputs to achieve a desired polysilicon deposition thickness.

However, the data-based POD method is a non-causal procedure, meaning that the models cannot be derived before the system response is known. In this work, a causal analytical method based on the spectrum of the system operator is presented for the model reduction of the RTP system. The dominant modes of the system are firstly obtained and the system can be partitioned into two subsystem: the dominant slow system and a remaining fast subsystem. By ignoring the affection of the fast subsystem with the Galerkin's method, a reduced model with relatively low order is obtained.

1.4 Temperature Control

First research effects focus on the temperature accuracy of the wafer in the steady state. However, with the development of the manufacturing of semiconductor, temperature uniformity in the transient states is required. It was shown in [20] that the temperature uniformity was limited by radiation loss at the wafer edge in the stationary state and by non-uniform illumination of the wafer during ramp-up. Structures on wafers were also potential sources for non-uniform heating. In the case of wafers with patterned over-layers on the front side, [21] showed the non-uniformity of the temperature experimentally and theoretically and also claimed that highly reflective reflectors at the front side of the wafer may help. In [22], a use of a gradient in the reflection coefficient in the reflector was proposed to compensate for edge dissipation. We will propose a sliding mode control method in this work to heat the wafer in the RTP system to a desired temperature with an uniform distribution.

The work is organized as follows. In section 2, a model formulation using physical principles is presented. The methodology of model reduction is proposed in section 3. The sliding mode control method is given in Section 4. Section 5 gives the simulation results of the proposed reduced model and control schemes. Section 5 concludes the work.

2 Model Formulation

The system we deal with in this work is the same as in the [23] which is named as Steag CVD system. The system has halogen lamps above which are arranged in five zones as the heating system. The silicon wafer is placed on a rotating support to decrease the temperature distribution in different azimuths. The reaction chamber is closed from above by a quartz window, which allows for radiative heating of the wafer, while at the same time permits wafer processing under vacuum. Figure 1 illustrates a schematic diagram of the RTP system.

There are three types of heat transfer on the wafer: conduction, convection and radiation which are presented as q_k, q_c and q_r respectively in the following energy balance equation of the wafer in the rapid thermal processing chamber.

$$\rho C \frac{\partial \bar{T}}{\partial t} = q_k + q_c + q_r \tag{1}$$

where ρ is the wafer density, $\bar{T}$ is the wafer temperature pertaining to position and time, C is the specific heat, and t is the time.

2.1 Conduction

As mentioned above, the wafer is placed on a rotating support and the dynamic is identical along the positions with the same radius. The polar angle of the position thus can be ignored and the full three-dimensional model (in radius, polar angle and thickness) can be reduced into a two-dimensional one (in radius and thickness). And because the wafer is very thin, we ignore the thickness of the wafer and consider the upper of the wafer only. The two-dimensional model can be further reduced into a one-dimensional model(in radius). With these assumptions, the conduction on the wafer can be expressed as:

$$q_k = \frac{k}{R^2}\frac{\partial}{\partial x}\left(\frac{\partial \bar{T}}{\partial x}\right) \tag{2}$$

where x is the radius coordinate, and k is the thermal conductivity.

2.2 Convection

Considering the boundary condition, we have

$$k\frac{\partial \bar{T}}{\partial x} = 0 \text{ at } x = 0 \tag{3}$$

and due to the convection on the edge of the wafer, we obtain

$$\frac{k}{R}\frac{\partial \bar{T}}{\partial x} = -h_e(\bar{T} - \bar{T}_w) \text{ at } x = 1 \tag{4}$$

where h_e is the convective heat transfer coefficient at the wall, $\bar{T}_w$ is the wall temperature, and R is the radial length of the wafer.

2.3 Radiation

The energy on the upper surface of the wafer comes from the radiation of the lamp and the heat exchange between the wafer and quartz window as follows:

$$q_r = \frac{\varepsilon}{Z}q(x,t) - \frac{F\varepsilon\sigma}{Z}\left(\bar{T}^4 - \bar{T}_a^4\right) \tag{5}$$

where ε is the emissivity of the upper surface, Z is the thickness of the wafer, $q(x,t)$ is the heat transfer from the lamp to a given point at x, F is the reflective coefficient of the upper surface, and $\bar{T}_a$ is the temperature of the quartz window.

The radiation from the lamps to the wafer can be expressed as a function of view factor. The view factor in RTP system can be derived from the system geometry as:

$$V_j = \frac{1}{2}\left(\frac{x^2 + d^2 - r_i^2}{\left[x^2 + d^2 + r_i^2\right]\sqrt{1 - \frac{4x^2 r_i^2}{\left[x^2+d^2+r_i^2\right]^2}}} - \frac{x^2 + d^2 - r_o^2}{\left[x^2 + d^2 + r_o^2\right]\sqrt{1 - \frac{4x^2 r_o^2}{\left[x^2+d^2+r_o^2\right]^2}}}\right) \tag{6}$$

Table 1. Heating System Arrangement

Zone	r_{in} (cm)	r_{out} (cm)
1	0	1.35
2	1.85	4.55
3	5.05	7.75
4	8.25	10.95
5	11.45	14.15

where r_i and r_o are the radiuses of inner ring and outer ring of the power lamp zones respectively. The power lamps are divided into five zones with their r_i and r_o as shown in Table 1.

The total energy from the lamps to the wafer can be derived with the view factor as

$$q(x,t) = \sum_{j=1}^{5} V_j u(j,t) \tag{7}$$

where j is the ring number, $u(j,t)$ is the power of different zones.

For convenience, we can define dimensionless variables $T = \frac{\bar{T}-T_e}{T_e}$, $T_a = \frac{\bar{T}_a-T_e}{T_e}$, $T_w = \frac{\bar{T}_w-T_e}{T_e}$ where T_e is the temperature of the environment. The energy balance then becomes:

$$\frac{\partial T}{\partial t} = \frac{k}{R^2\rho C}\frac{\partial}{\partial x}\left(\frac{\partial T}{\partial x}\right) - \frac{F\varepsilon\sigma}{Z\rho CT_e}\left((T_eT+T_e)^4 - (T_eT_a+T_e)^4\right) + \frac{\varepsilon}{Z\rho CT_e}\sum_{j=1}^{5} Vu(j,t) \tag{8}$$

with the boundary conditions:

$$\frac{\partial T}{\partial x} = 0 \text{ at } x = 0 \tag{9}$$

$$\frac{\partial T}{\partial x} = -\frac{h_eR}{k}(T - T_w) \text{ at } x = 1 \tag{10}$$

and initial condition:

$$T = T_{ini} \text{ when } t = 0 \tag{11}$$

The system parameters can be found in Table 2.

3 Model Reduction

3.1 Spectrum of the System Operator

Before introducing the Galerkin's method, we first define the spectrum of the system in order to derive the dominant modes of the system. Considering the convection at the edge of wafer, we define $PT = \frac{\partial}{\partial x}\left(\frac{\partial T}{\partial x}\right)$, with boundary conditions:

$$\frac{\partial T}{\partial x} = 0 \text{ at } x = 0 \tag{12}$$

Table 2. Parameters for RTP system

Parameter	Meaning	Value
$k(\frac{W}{cmK})$	the thermal conductivity	0.6211 at 600K
$\rho(\frac{kg}{cm^3})$	the wafer density	2.3
$C(\frac{J}{gK})$	the heat capacity	0.7894 at 600K
F	the reflective coefficient	1
ε	the emissivity	0.7
$\sigma(\frac{W}{cm^2K^4})$	the Stephan-Bolzman constant	5.674×10^{-12}
$Z(cm)$	the wafer thickness	0.0525
$T_e(K)$	the temperature of the environment	300
$\overline{T}_a(K)$	the temperature of the quartz window	300
$\overline{T}_w(K)$	the temperature of the wall	300
$R(cm)$	the radius of the wafer	12

$$\frac{\partial T}{\partial x} = -e(T - T_w) \text{ at } x = 1 \tag{13}$$

Considering the eigenvalue problem $PT = \lambda_k \phi_k$, we have the following results. The eigenvalues are real and the corresponding eigenfunctions may be chosen to be real. After analysis, we can get the spectrum of the system. We define θ as the positive roots of

$$\tan(\theta) = -e/\theta \tag{14}$$

and have $\lambda = -\theta^2$.The corresponding eigenfunctions are:

$$\phi = \sqrt{\int_0^1 \cos^2(\theta x) dx} \cos(\theta x) \tag{15}$$

3.2 Galerkin's Method

We now turn to the Galerkin's method.

The solution of the RTP system can be represented by

$$T(x,t) = \sum_{k=1}^{\infty} T_k(t)\phi_k(x) \tag{16}$$

Projecting the state variable in Hilbert space onto a finite dimension subspace

$$T_N(x,t) = P_N T \equiv \sum_{k=1}^{N} T_k(t)\phi_k(x) \tag{17}$$

and an infinite dimension subspace

$$T_R(x,t) = P_R T \equiv \sum_{k=N+1}^{\infty} T_k(t)\phi_k(x) \tag{18}$$

and then projecting the system (8) onto the finite dimension subspace, we have

$$\begin{aligned} P_N\frac{\partial T}{\partial t} = {} & \frac{k}{R^2\rho C}P_N\frac{\partial}{\partial x}\left(\frac{\partial T}{\partial x}\right) - \frac{F\varepsilon\sigma}{Z\rho CT_e}P_N\left((T_e(T_N+T_R)+T_e)^4 - (T_eT_a+T_e)^4\right) \\ & + \frac{\varepsilon}{Z\rho CT_e}P_N\sum_{j=1}^{5}V_j u(j,t) \end{aligned} \tag{19}$$

If the infinite part T_R is ignored, the following approximated subsystem is obtained:

$$\begin{aligned} \frac{\partial T_N}{\partial t} = {} & \frac{k}{R^2\rho C}\frac{\partial}{\partial x}\left(\frac{\partial T_N}{\partial x}\right) - \frac{F\varepsilon\sigma}{Z\rho CT_e}P_N\left((T_eT_N+T_e)^4 - (T_eT_a+T_e)^4\right) \\ & + \frac{\varepsilon}{Z\rho CT_e}P_N\sum_{j=1}^{5}V_j u(j,t) \end{aligned} \tag{20}$$

In order to get the best approximation, we define the residual as

$$\begin{aligned} R = {} & \frac{\partial T_N}{\partial t} - \frac{k}{R^2\rho C}\frac{\partial}{\partial x}\left(\frac{\partial T_N}{\partial x}\right) + \frac{F\varepsilon\sigma}{Z\rho CT_e}P_N\left((T_eT_N+T_e)^4 - (T_eT_a+T_e)^4\right) \\ & - \frac{\varepsilon}{Z\rho CT_e}P_N\sum_{j=1}^{5}V_j u(j,t) \end{aligned} \tag{21}$$

By using the Galerkins method, we set the test function $\varphi_k = \phi_k$ and make $\langle R, \varphi_k\rangle = 0$ at $k = 1,\ldots,N$. Then we have the following reduced system model

$$\begin{aligned} \dot{T}_k = {} & \frac{k}{R^2\rho C}\left\langle\frac{\partial}{\partial x}\left(\frac{\partial T_N}{\partial x}\right),\phi_k\right\rangle - \frac{F\varepsilon\sigma}{Z\rho CT_e}\left\langle P_N\left((T_eT_N+T_e)^4 - (T_eT_a+T_e)^4\right),\phi_k\right\rangle \\ & + \frac{\varepsilon}{Z\rho CT_e}\left\langle P_N\sum_{j=1}^{5}V_j u(j,t),\phi_k\right\rangle \end{aligned} \tag{22}$$

for $k = 1,\ldots,N$.
Because we use the eigenfunctions as the basis functions, we have

$$\left\langle\frac{\partial}{\partial x}\left(\frac{\partial T_N}{\partial x}\right),\phi_k\right\rangle = \lambda_k T_k \tag{23}$$

for $k = 1,\ldots,N$.
We have the following reduced system

$$\begin{aligned} \dot{T}_k = {} & \frac{k}{R^2\rho C}\lambda_k T_k - \frac{F\varepsilon\sigma}{Z\rho CT_e}\left\langle P_N\left((T_eT_N+T_e)^4 - (T_eT_a+T_e)^4\right),\phi_k\right\rangle \\ & + \frac{\varepsilon}{Z\rho CT_e}\left\langle P_N\sum_{j=1}^{5}V_j u(j,t),\phi_k\right\rangle \end{aligned} \tag{24}$$

for $k = 1,\ldots,N$.

4 Sliding Mode Control

We can rewrite the reduced model as follows:

$$\dot{\mathbf{T}} = A\mathbf{T} + F(\mathbf{T}) + B\mathbf{u}(t) \tag{25}$$

where

$$\mathbf{T} = [T_1, T_2, \cdots, T_N]^T$$

$$A = \frac{k}{R^2 \rho C} \begin{bmatrix} \lambda_k & & \\ & \ddots & \\ & & \lambda_N \end{bmatrix}$$

$$F(\mathbf{T}) = -\frac{F\varepsilon\sigma}{Z\rho C T_e} \begin{bmatrix} \left\langle (T_e T_N + T_e)^4 - (T_e T_a + T_e)^4, \phi_1 \right\rangle \\ \vdots \\ \left\langle (T_e T_N + T_e)^4 - (T_e T_a + T_e)^4, \phi_N \right\rangle \end{bmatrix}$$

$$B = \frac{\varepsilon}{Z\rho C T_e} \begin{bmatrix} \langle P_N V_1, \phi_1 \rangle & \cdots & \langle P_N V_m, \phi_1 \rangle \\ & \ddots & \\ \langle P_N V_1, \phi_N \rangle & \cdots & \langle P_N V_m, \phi_N \rangle \end{bmatrix}$$

and

$$\mathbf{u}(t) = [u(1,t), \cdots, u(m,t)]^T \tag{26}$$

Based on the reduced model of the RTP system, we propose a sliding mode control algorithm in this section to control the temperature on the wafer to a desired one. Firstly, a sliding surface is chosen linearly as:

$$S = D\mathbf{T} \tag{27}$$

where $D \in \mathbb{R}^{m \times N}$ is a parameter matrix.

The sliding mode control algorithm is composed of two term

$$\mathbf{u} = u_{eq} + \Delta u \tag{28}$$

where u_{eq} is given as:

$$u_{eq} = -(DB)^{-1} D[A\mathbf{T} + F(\mathbf{T})] \tag{29}$$

to guarantee that $\dot{S} = 0$ when $S = 0$ and

$$\Delta u = -k\,\mathrm{sign}(S). \tag{30}$$

k is a suitable gain chosen to eliminate the perturbation effect. In this algorithm, we require that $(DB)^{-1}$ exists. Fortunately, this is satisfied in the model of RTP system we consider.

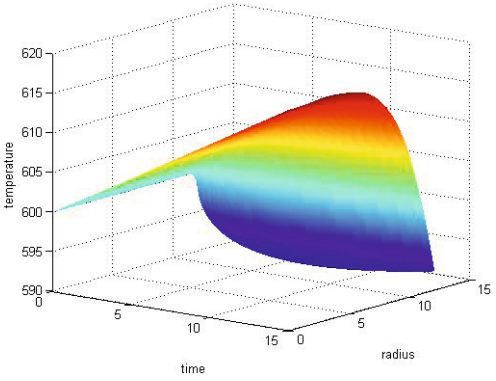

Fig. 4. High-order model

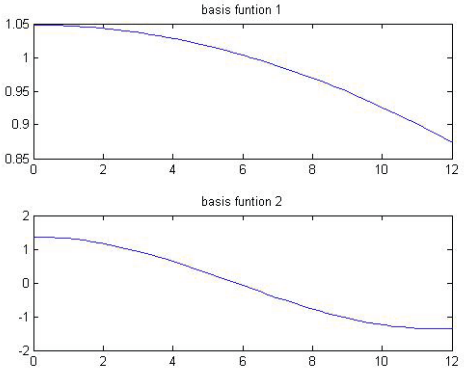

Fig. 5. Basis functions

5 Simulation

The simulation is composed of two parts. In the first part, we compare the reduced model with the high-order model to show the capacity of the model we obtain with Galerkin's method. In the second part, we apply the sliding mode control scheme to the RTP system to show the effectiveness of the control algorithm.

5.1 Capacity of the Reduced Model

Firstly, we construct a high-order model with finite-difference method to represent the dynamic of the RTP process. The partial differential equation of the wafer temperature is discretized with finite differences in the spatial dimension with 50 points. A model of 50 dimensions is obtained. The model runs for 15s with fixed lamps power. The time evolution of the temperature is illustrated in Figure 4.

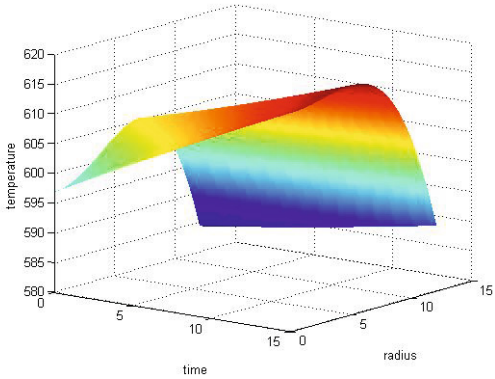

Fig. 6. Proposed low-order reduced model

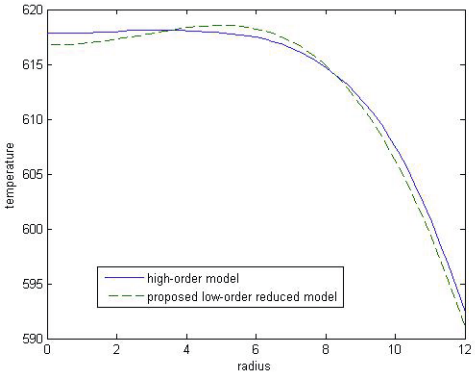

Fig. 7. Comparison of two models as $t = 15s$

Then, a simulation on the proposed low-order reduced model (24) is performed. We choose two basis functions and thus the reduced model has dimension of 2. The model also runs for 15s with the identical lamps power as before. The dominant modes we get using the spectrum are shown in Figure 5. And the temperature profile of the proposed model is shown in Figure 6.

Comparing two models at the time 15s, we have the result shown in Figure 7. From that, we find these two models have the identical ability to model the RTP, while the model we propose has dimension much lower.

5.2 Sliding Mode Control for the RTP System

In this part, we apply the sliding mode control algorithm we proposed in the last section to the RTP system. The temperature on the wafer is required to rise from 850K to 900K in a few seconds. In the simulation, D is selected as the identity matrix and k is chosen

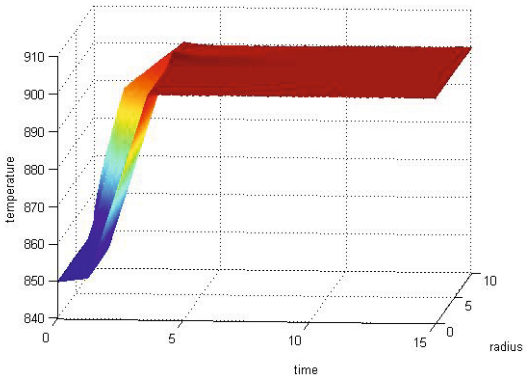

Fig. 8. Temperature distribution when applying the sliding mode control to the system

as $\begin{bmatrix} 2 & 2 \\ 2 & -2 \end{bmatrix}$. We can see from Figure 8. that the control actions successfully heat the wafer from 850K to 900K with a uniform temperature distribution.

6 Conclusion

A spectrum-based reduced model is proposed to model a RTP process and a sliding mode control based on the reduced model is developed in this work. Firstly, a model in the form of partial differential equation is constructed using the physical principles. Then, dominant modes are extracted by applying the spectrum of the operator of the system. Based on the dominant modes, a reduced model is obtained by using the Galerkin's method. The proposed model has much lower dimension compared to other methods such as finite-difference method. However, from the numerical simulations, we find that they have similar ability to model the process. The approach seems very promising for model reduction of RTP process. At last, based on the reduced model, we successfully design the sliding mode control scheme to control the system. Simulation results show that the control actions can heat the temperature on the wafer in RTP system to a desired one with a uniform temperature distribution.

Acknowledgment. Authors would like to thank Professor Okyay Kaynak for his generous help and guidance in the past years and dedicate this chapter to commemorate his life time outstanding research achievements and contributions to the profession.

References

1. Surridge, R.K., Sealy, B.J.: Comparison of sn-ion-implanted, ge-ion-implanted, se-ion-implanted and te-ion-implanted gaas. Journal of Physics D-Applied Physics 10, 911–917 (1977)
2. Sedgwick, T.O.: Short-time annealing. Journal of the Electrochemical Society 130, 484–493 (1983)

3. Singh, R.: Rapid isothermal processing. Journal of Applied Physics 63, R59–R114 (1988)
4. Coaton, J.R., Fitzpatrick, J.R.: Tungsten-halogen lamps and regenerative mechanisms. IEE Proceedings-A-Science Measurement and Technology 127, 142–148 (1980)
5. Rehmet, M.: Xenon lamps. IEE Proceedings-A-Science Measurement and Technology 127, 190–195 (1980)
6. Walsh, P.J., Kermani, A.: Electrical characterization of cw xenon arcs at moderate currents. Journal of Applied Physics 61, 4484–4491 (1987)
7. Gelpey, J.C., Stump, P.O.: Rapid annealing using the water-wall arc lamp. Nuclear Instruments and Methods in Physics Research Section B-Beam Interactions with Materials and Atoms 6, 316–320 (1985)
8. Lee, C.H., Chizinsky, G.: Rapid thermal-processing using a continuous heat-source. Solid State Technology 32, 43–44 (1989)
9. Kim, K.B., Maillot, P., Morgan, A.E., Kermani, A., Ku, Y.H.: Formation of beta-sic at the interface between an epitaxial si layer grown by rapid thermal chemical vapor-deposition and a si substrate. Journal of Applied Physics 67, 2176–2179 (1990)
10. Fulcher, M.R., Kwor, R., Ricker, R.E., Ho, C.C., Gelpey, J.C.: Tem study of rapid thermal annealed sb-implanted si. Journal of the Electrochemical Society 330, C329–C330 (1986)
11. Sheets, R.E.: Automatic cassette to cassette radiant impulse processor. Nuclear Instruments and Methods in Physics Research Section B-Beam Interactions with Materials and Atoms 6, 219–223 (1985)
12. Chatterjee, S., Trachtenberg, I., Edgar, T.F.: Mathematical-modeling of a single-wafer rapid thermal reactor. Journal of the Electrochemical Society 139, 3682–3689 (1992)
13. Lord, H.A.: Thermal and stress analysis of semiconductor wafers in a rapid thermal processing oven. IEEE Transactions on Semiconductor Manufacturing 1, 105–114 (1988)
14. Kakoschke, R., Bussmann, E., Foll, H.: Modeling of wafer heating during rapid thermal-processing. Applied Physics A-Materials Science and Processing 50, 141–150 (1990)
15. Cho, W., Edgar, T.F., Lee, J.: Nonlinear model identification for temperature control in single wafer rapid thermal processing. Industrial and Engineering Chemistry Research 47, 4791–4796 (2008)
16. Kakoschek, R., BuMann, E.: Simulation of temperature effects during rapid thermal processing. In: MRS Proceedings Symposium B Rapid Thermal Annealing/Chemical Vapor Deposition and Integrated Processing (1989)
17. Banerjee, S., Cole, J.V., Jensen, K.F.: Designing reduced-order models for rapid thermal processing systems. Journal of the Electrochemical Society 145, 3974–3981 (1998)
18. Banerjee, S., Cole, J.V., Jensen, K.F.: Nonlinear model reduction strategies for rapid thermal processing systems. IEEE Transactions on Semiconductor Manufacturing 11, 266–275 (1998)
19. Theodoropoulou, A., Adomaitis, R.A., Zafiriou, E.: Model reduction for optimization of rapid thermal chemical vapor deposition systems. IEEE Transactions on Semiconductor Manufacturing 11, 85–98 (1998)
20. Kakoschek, R., BuMann, E.: Simulation of temperature effects during rapid thermal processing. In: MRS Proceedings Symposium B Rapid Thermal Annealing/Chemical Vapor Deposition And Integrated Processing (1989)
21. Vandenabeele, P., Maex, K., De Keersmaecker, R.: Impact of patterned layers on temperature non-uniformity during rapid thermal processing for vlsi-applications. In: MRS Proceedings Symposium B Rapid Thermal Annealing/Chemical Vapor Deposition and Integrated Processing (1989)
22. Hill, C., Jones, S., Boys, D.: Rapid thermal annealing - theory and practice. In: Levy, R. (ed.) Reduced Thermal Processing For ULSI, Springer, US (1989)
23. Dassau, E., Grosman, B.: Lewin DaR Modeling and temperature control of rapid thermal processing. Computers and Chemical Engineering 30, 686–697 (2006)

A Classification and Overview of Sliding Mode Controller Sliding Surface Design Methods

Sezai Tokat[1], M. Sami Fadali[2], and Osman Eray[3]

[1] Computer Engineering Department, Pamukkale University, Denizli, 20070, Turkey
stokat@pau.edu.tr
[2] Electrical Engineering Department, University of Nevada - Reno, 89557, NV, USA
fadali@unr.edu
[3] Korkuteli Vocational School, Akdeniz University, Korkuteli, Antalya, 07800, Turkey
oeray@akdeniz.edu.tr

Abstract. Sliding mode control provides insensitivity to parameter variations and complete rejection of disturbances. However, this property is only valid in the sliding phase. Sliding surface design can be used to improve controller performance by minimizing or eliminating the time to reach the sliding phase. In this study, we review and classify the methods available in the literature for sliding surface design focusing on single-input systems.

Keywords: sliding mode control, sliding surface design, linear and nonlinear sliding surface.

1 Introduction

The state-space trajectory of a sliding mode control system can be divided into two parts representing two different modes of system operation. The trajectories start from a given initial condition off the sliding surface and tend towards the sliding surface. The part of the trajectory before reaching the sliding surface is known as the reaching or hitting mode and its duration is called the reaching time. When the trajectories converge to the sliding surface, the sliding mode starts. In general, the design of a sliding mode controller (SMC) involves the design of a sliding surface that represents desired stable dynamics and a control law that guarantees the reaching mode and sliding mode. The system trajectories are sensitive to parameter variations and disturbances during the reaching mode of the trajectory but are insensitive in sliding mode.

The design problem in systems with discontinuous control laws can usually be reduced to the selection of the parameters of the sliding surfaces that completely determine the performance of the control system [1]. Thus, there are various sliding surface design strategies in the literature to improve SMC performance by minimizing or even eliminating the reaching mode [2, 3]. This study surveys and classifies continuous-time SMC studies based on their different sliding surface design methods. The terminology used in the SMC literature can sometimes be confusing making it hard to understand, compare and classify design approaches. For instance, a sliding

X. Yu and M. Önder Efe (eds.), *Recent Advances in Sliding Modes,*
Studies in Systems, Decision and Control 24, DOI: 10.1007/978-3-319-18290-2_20

surface with a linear combination of state variables can be called a nonlinear sliding surface as the dynamics of the sliding phase may become a nonlinear trajectory as a result of other parameters such as time-varying ones. However time-varying parameters do not introduce nonlinearities in terms of state variables. We therefore classify sliding surface design methods according to properties such as dimension, linearity, time dependence, and the nature of their moving algorithm. The first classification is arranged based on the number of sliding surfaces to be designed which in turn depends on the number of input variables. For single-input systems, the sliding surface is scalar while for multi-input systems it is a vector. Another property is the time dependence of the sliding surface. If the parameters of the sliding surface during the operation of the system are stationary with respect to time, it is called a constant sliding surface. In conventional SMC, the sliding surface is naturally constant. However, a time-varying function can also be used for defining a sliding surface to obtain a time-varying sliding surface. If the changes in the parameters of the time-varying sliding surface are all functions of the continuous-time variable *t*, they are called continuously-moving sliding surfaces. If any parameter change is made at discrete time instants, the sliding surface is a discretely-moving sliding surface. If the sliding surface is defined by a linear function of the state variables, the sliding surface is linear; otherwise, it is nonlinear.

The remainder of this chapter is organized as follows. In Section 2, the notation and structure of the conventional SMC are explained. Then, in Section 3, sliding surface design methods are presented based on the above classification. Section 4 provides conclusions and suggestions for future work.

2 Conventional Continuous-Time Sliding Mode Control

A single-input non-autonomous dynamic open-loop system of order *n* can be given as

$$x^{(n)}(t) = f(\mathbf{x},t) + b(\mathbf{x},t).u(t) + d(\mathbf{x},t) \tag{1}$$

where $\mathbf{x}(t) = [x(t) \quad \dot{x}(t) \quad ... \quad x^{(n-1)}(t)]^T$ is the state vector with $x^{(n-1)}(t)$ denoting the $(n\text{-}1)^{\text{th}}$ derivative of $x(t)$ with respect to time, $u(t)$ is the input signal, $d(\boldsymbol{x},t)$ is a time-dependent disturbance with known upper bound and $f(\mathbf{x},t)$ and $b(\mathbf{x},t)$ are functions determining the system characteristics. For single-input systems, the commonly used sliding surface for the tracking problem can be defined as

$$s(\mathbf{e}) = \mathbf{c}\mathbf{e}(t) \tag{2}$$

where $\mathbf{c}=[\ c_{n-1}\ c_{n-2} ... \ c_1\ 1] \in \Re^{1xn}$ is a vector with strictly positive real elements that determine the coefficients of the sliding surface, $\mathbf{e}(t) \in \Re^{nx1}$ is the tracking error defined as $\mathbf{e}(t) \triangleq \mathbf{x}(t) - \mathbf{x}_d(t) = [e(t) \quad \dot{e}(t) \quad ... e^{(n-1)}(t)]^T$ where $\mathbf{x}_d(t)$ is the desired trajectory. For second order systems, (2) can be written as

$$s(\mathbf{e}) = \dot{e}(t) + c_1 e(t) \tag{3}$$

which gives a linear function of the error with slope c_1. A homogeneous differential equation that has a unique solution is obtained by setting $s(\mathbf{e})=0$. Thus, the error will asymptotically reach zero with an appropriate control law that keeps the trajectory on the sliding surface. Since it is necessary and sufficient to differentiate (2) or (3) once for the input $u(t)$ to appear, this is a first order stabilization problem based on $s(\mathbf{e})$. Lyapunov's direct method can be used to obtain the control law that keeps $s(\mathbf{e})$ at zero and a candidate Lyapunov function is

$$V(s)=\frac{1}{2}s^2(\mathbf{e}) \tag{4}$$

with $V(0)=0$, $V(s)>0$ for $\forall s(\mathbf{e})>0$. A sufficient condition for the stability of the system is

$$\dot{V}(s)=\frac{1}{2}\frac{\mathrm{d}}{\mathrm{d}t}s^2(\mathbf{e})\le-\eta\left|s(\mathbf{e})\right| \tag{5}$$

where η is a strictly positive real constant that determines the convergence velocity of the trajectory to the sliding surface [4]. The inequality (5) ensures that the distance to the sliding surface decreases along all trajectories and consequently, the system is stable. Therefore, (5) is called the reaching condition for the sliding surface. By substituting (3) into (5) and omitting the arguments of the dependent variables one obtains

$$s.(f+b.u+d-\ddot{x}_d+c_1\dot{e})\le-\eta\left|s\right| \tag{6}$$

A control input satisfying the reaching condition can be chosen as

$$u(t)=-b^{-1}(\hat{f}(\mathbf{x},t)-\ddot{x}_d(t)+c_1\dot{e}(t))-k\,\mathrm{sign}(s(\mathbf{e}))\triangleq u_{eq}(t)+u_{dis}(t) \tag{7}$$

where $\hat{f}$ is the estimated state equation, k is the discontinuous control gain that is a strictly positive real constant with a lower bound dependent on the estimated system parameters and bounded external disturbances. The function sign(.) denotes the signum function defined as follows

$$\mathrm{sign}(s)=\begin{cases}-1 & \text{if } s<0\\ +1 & \text{if } s>0\end{cases} \tag{8}$$

Note that at $s=0$, (8) is undefined. In SMC design, this definition is adequate since (8) provides opposite signs in the neighbourhood of $s=0$, that is

$$\lim_{s\to0^-}\dot{s}>0 \quad \text{and} \quad \lim_{s\to0^+}\dot{s}<0 \tag{9}$$

The control input $u(t)$ in (7) consists of two parts. The first part, u_{eq} is a continuous term known as the *equivalent control.* It is based on the estimated system parameters and it compensates the estimated undesirable dynamics of the system. The second part

with the signum function is the *discontinuous control* law, u_{dis} that requires infinite switching on the part of the control signal and actuator at the intersection of the error state trajectory and the sliding surface. Thus, the trajectory is forced to always move towards the sliding surface [1].

3 Sliding Surface Design Methods

Designing the sliding surface is a powerful method to improve system performance. It is also possible to shorten the reaching time and thus lessen the effect of disturbances by increasing the amplitude of the discontinuous control gain k in (7). This reduces the reaching time by increasing the amplitude of the control signal during the reaching mode. However, the gain increase has negative effects such as high sensitivity to unmodeled system dynamics, undesired high amplitude chattering, and actuator saturation. Therefore, increasing the discontinuous control gain is generally undesirable for physical systems and is not a viable alternative to sliding surface design.

A good trade-off between reaching time and speed of response is obtained by changing the parameters of the sliding surface. We discuss surface design methodologies for selecting these parameters next.

3.1 Linear Constant Sliding Surface

Conventional sliding mode control (SMC) has linear constant sliding surfaces and the sliding surface parameters directly determine the system performance [1]. For example, for second order systems in the form of single-input non-autonomous dynamic open-loop system (1) simulations for $f(\mathbf{x},t)=\dot{x}$, $b(\mathbf{x},t)=1$ and $d(\mathbf{x},t)=0$ give underdamped, critically damped or overdamped system responses with different values of sliding surface parameter c_1 as shown in Figure 1.

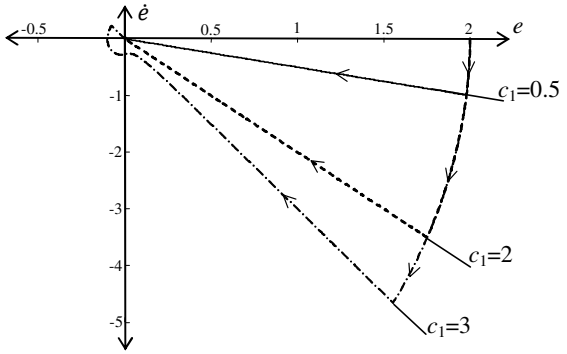

Fig. 1. Error state-space responses obtained with different c_1 parameters

For small values of c_1, the reaching time is small but the system dynamics is slow. For larger values of c_1, the system response becomes faster but the reaching time

increases. Thus, the same feedback controllers may either result in a stable system or may lead to instability depending on the switching rule applied.

An upper bound of c_1 for physical systems is determined by each of three main factors: the frequency of the lowest unmodeled structural resonant mode, neglected time delays, and the sampling rate. The first two bounds are directly related to the physical system characteristics but the sampling rate bound depends on the available technology and the performance of the control algorithm. The upper bound on the sliding surface parameter c_1 is chosen as the minimum of these three bounds. Smaller c_1 values give longer tracking times. Therefore, the lower limit of c_1 directly depends on the maximum allowable tracking time. To achieve the desirable closed loop performance, the switching rule must be appropriately chosen considering the upper and lower limits. The determination of the parameters of the constant scalar sliding surface is an important step in the sliding mode control strategy. Generally, these parameters are selected either by empirical rules or by trial and error. However, optimization methods can be used to obtain the constant parameters and improve the system performance [5].

For the conventional SMC introduced in Section 2, the sliding surface (2) naturally results in a PD sliding surface. An integral action can also be included to obtain PID control structures. The integral action is typically used with a boundary layer SMC because the integral term can eliminate the steady-state error resulting from the boundary layer. Slotine and Spong [6] added an integral term to the sliding surface as follows

$$s(\mathbf{e}) = k_d \dot{e} + k_p e + k_I \int_0^t e(\tau) d\tau \tag{10}$$

where k_d must be non-zero for a causal input-output relation [7]. Stepanenko et al. [8] proposed a sliding surface where the integral action is active only when the system enters a predetermined region to avoid overshoot as a result of large initial errors.

Integral action is not only used with boundary layer SMC. For instance, in [9, 10] integral action is used to eliminate the reaching time. Without using the conventional equivalent control term and analyzing the global asymptotic stability for the robot arm, Jafarov et al. [11] improved the simulation performance given in [8]. The effectiveness of integral sliding surfaces has been demonstrated with various experimental set-ups such as DC motor control [12, 13].

3.2 Linear Discretely-Moving Sliding Surface

Conventional SMC has reaching and sliding modes, and if the initial state is far from the sliding surface, the system may have an undesirable and unpredictable transient response. Hence, we need to minimize the reaching time by decreasing the distance between the sliding surface and the initial state. This is achieved by decreasing the magnitudes of the sliding surface parameter vector **c** in (2). However, large parameters are required to reduce the steady state error. Time-varying linear sliding surfaces provide a compromise between reaching time and steady-state error. Although they

naturally have a linear structure in state space, their variation with time brings a nonlinear trajectory in sliding mode [14].

An important study about linear and time-varying sliding surfaces is the rotation and shifting schemes of Choi et al. [15]. They initially choose the sliding surface parameters to pass through arbitrary initial conditions then move the sliding surface towards a predetermined final sliding surface. This reduces the time during which the disturbances affect the system and reduces sensitivity to parameter variations and external disturbances. For trajectory tracking with second order systems, the sliding surface is defined in [15] as

$$\hat{s}(\mathbf{e},t) = \dot{e}(t) + c_1(t)e(t) - \alpha(t) = 0 \tag{11}$$

In stable regions, α is chosen zero and only $c_1 > 0$ is adjusted to obtain the desired dynamics. On the other hand, in unstable regions, c_1 is constant as in conventional SMC and α is adjusted to provide the shifting scheme. Thus, no reaching mode exists in stable regions and the system is insensitive to uncertainties including parameter variations and external disturbance. The SMC without reaching mode is called *global SMC* [16] or total SMC [10]. To place the surface near the current state, the sliding surface is rotated at discrete steps. The newly calculated sliding surface is fixed for a determined time instance in discretely-moving algorithms. This time period is known as the dwelling time and it is another controller parameter that must be adjusted to preserve robustness, subject to hardware capabilities. When the initial conditions are in the unstable regions, if the rotation process is applied, $c_1(t_0)$ becomes negative and $e(t)=e(t_0)\exp(-c_1(t_0)t)$ becomes unbounded. In this case, the trajectory moves away from the origin until the sliding surface enters the stable region. By applying the rotation scheme in unstable regions the system can also be taken to the equilibrium state. Nevertheless, rotation in the unstable region increases the reaching time. In [15], the shifting scheme was proposed for unstable regions to avoid this situation. The rotation and shifting schemes in [15] were extended and implemented for second order nonlinear systems with both disturbances and parameter variations [17].

The moving algorithms can be easily determined with respect to the stable and unstable regions for second order systems and the algorithm works until a predefined final sliding surface is reached. However, the determination of the rotation and shifting regions is more complex for higher order systems. Roy and Olgac [18] arranged (11) for n^{th} order systems and moved the sliding surface represented by the initial conditions and the final sliding surface parameters. Robust stability for parameters in the bounded ranges of the rotation scheme can be tested using Kharitinov's theorem [19]. The rotation scheme is used if the system is robustly stable for this range. Otherwise, the shifting scheme is used. The experimental results of discretly shifting and rotating schemes are also demonstrated for single-phase PWM inverters [20].

In another study for higher order systems, Park and Choi [21] assumed that all the desired eigenvalues λ_{di} of the sliding surface $\hat{s}(\mathbf{e},t)$ are equal to $\lambda_d(t)$ to simplify the difficulties arising for higher order systems. The rotation and shifting schemes are obtained by adjusting $\lambda_d(t)$ and $\alpha(t)$. In discretely-moving sliding surfaces, as the

sliding surface is taken to be constant during the dwelling time, the derivatives of the sliding surface parameters **c** in (2) is not necessary for the calculation of the control law. Therefore, the control law calculated for conventional SMC is used. This is an advantage of discretely-moving sliding surfaces.

3.3 Linear Continuously-Moving Sliding Surface

In discretely-moving sliding surfaces, the sliding surface is fixed during the dwelling time but has a discontinuity at the end of each dwelling period. The discontinuity causes sensitivity to disturbances. Slotine [22] introduced the continuously-moving sliding surface to eliminate this. He used the time derivatives of the sliding surface parameter to calculate the control input $u(t)$. Salamci et al. [23] approximated the nonlinear system by a linear time-varying system and designed linear continuously-moving sliding surfaces to minimize a specified optimization criterion.

Bartoszewicz [24] also considered the dwelling time in discretely-moving sliding surfaces for second order systems and defined the sliding surface as a function of time. The sliding surface parameter $c_1(t)$ and shifting parameter $\alpha(t)$ in (11) are written as first degree polynomials of time. The rotation and shifting schemes are then obtained by choosing the polynomial parameters. When $c_1(t)$ is varied at a constant value, the amount of rotation differs with the current value of $c_1(t)$. Therefore, Tokat [25] directly used angular information to define the rotation scheme. The continuously-moving sliding surface for second order systems is obtained in [26] as a shifting scheme using $s(\mathbf{e})$ in (3) and a quadratic polynomial as follows

$$\hat{s}(\mathbf{e},t) = s(\mathbf{e}) + \begin{cases} a_1 t^2 + a_2 t + a_3, & t \le t_b \\ 0, & t > t_b \end{cases} \tag{12}$$

where c_1 in $s(\mathbf{e})$ and $t_b > 0$, a_1, a_2, a_3 and are constant design parameters. When $a_1=0$ as in [24], the time-dependent shifting in stable regions is directly proportional to time. Thus, (12) is called a *constant-velocity* sliding surface. Otherwise, the sliding surface is shifted to the conventional sliding surface as a quadratic function of time and the speed of convergence to the conventional sliding surface increases as time passes. In the quadratic case, (12) is called a *constant-acceleration* sliding surface. The state can be initially set on the sliding surface by adjusting the design parameters. The new idea in (12) is continuously shifting the sliding surface until time t_b. The idea is also applied to third order systems considering various input and state constraints [3]. Continuously shifting was also accomplished in [27] using (3) as

$$\hat{s}(\mathbf{e},t) = \begin{cases} s(\mathbf{e}) - c_1 (t/t_f - 1) x_{1d}, & 0 \le t \le t_b \\ s(\mathbf{e}), & t > t_b \end{cases} \tag{13}$$

where it is assumed that the desired states are fixed and the initial conditions are $(x_1(0),x_2(0))=(0,0)$. The sliding surface (13) will initially be zero and the state will be on the sliding surface. When t reaches t_b, the sliding surface is fixed as in the conventional sliding surface. In [28], sliding surfaces was proposed for second order systems

obtained by inserting a time-dependent function in the conventional sliding surface of (3) as

$$\hat{s}(\mathbf{e},t) = s(\mathbf{e}) - (\dot{v}(t) + c_1 v(t)) \tag{14}$$

where $v(t)$ is a second order differentiable, time-dependent, continuous function defined in the range $[0,+\infty)$. The sliding surface (14) starts at the initial conditions with

$$v(t) = \begin{cases} a_0 t^3 + a_1 t^2 + a_2 t + a_3, & t \le t_b \\ 0, & t > t_b \end{cases} \tag{15}$$

Time-dependent variables for shifting and rotation schemes are frequently used to obtain continuously-moving sliding surfaces and generally provide a global SMC [29]. To eliminate the reaching time for n^{th} order single-input systems in controllable canonical forms, an error function as $\hat{e}(t) = e(t) - \gamma(t)$ was used in [30] where $\gamma(t)$ is a time-dependent function that initially places the trajectories on the sliding surface. To preserve the sliding dynamics of the original system, $\gamma(t)$ must vanish as the motion of the system evolves in time. Therefore, it is chosen in an exponential form and the new sliding surface is defined as

$$\hat{s}(\mathbf{e},t) = \mathbf{c}\hat{\mathbf{e}} \triangleq \mathbf{c}\left[\hat{e}(t)\,\dot{\hat{e}}(t)\cdots\hat{e}^{(n-1)}(t)\right]^T \tag{16}$$

As a result of the linear time-dependent structure of $\hat{e}(t)$, (16) is a continuously-moving linear sliding surface. Using $\hat{e}(t)$, sliding surfaces for multi-input systems were also developed [31]. Adding an exponential time-dependent term to obtain a continuously time-varying sliding surface provides better performance and improves robustness with a simple engineering design [16, 32]. Tokat et al. [33] proposed a continuously time-varying linear sliding surface in a new (*s*-*p*) plane with the coordinates defined as the original sliding surface *s=0* in the $(e - \dot{e})$ plane and

$$p(\mathbf{e}) = \dot{e}(t) - c^{-1} e(t) = 0 \tag{17}$$

which is perpendicular to $s(\mathbf{e})=0$ in (3). A linear sliding surface is defined in the (*s*-*p*) plane as

$$\hat{s}(\mathbf{e},t) = s(\mathbf{e}) - k_s(t).p(\mathbf{e}) \tag{18}$$

where $k_s(t)$ determines the position of the proposed sliding surface. A rotating sliding surface is obtained by continuously adjusting the parameter k_s. One way of generating $k_s(t)$ is using a time dependent function with simple first-order derivatives. For example, $k_s(t)$ for stable regions can be chosen as the shifted sigmoid function

$$k_s(t) = (k_{s\max} - k_{s\min})(1 + e^{mt+a})^{-1} + k_{s\min} \tag{19}$$

where m and a are parameters that determine the shape of the function. The surface modified by adjusting the parameter $k_s(t)$ within a predefined interval [33].

Integrating fuzzy logic control and sliding mode control to achieve stability and meet desired performance criteria is an active area of research [34]. These studies can be classified in two groups. The first group use conventional sliding mode control strategies and employ fuzzy models to simplify or to improve the control mechanism. The controllers obtained using these approaches are known as sliding mode fuzzy controller (SMFC). The second group, known as fuzzy sliding mode controller (FSMC) obtains an approximate input-output relation for a conventional SMC and realizes it with a single input fuzzy logic controller (FLC). With these definitions in mind, sliding surface design using fuzzy theory can be classified as SMFC. For instance, Ha et al. [35] proposed a fuzzy logic tuning algorithm for second order systems in which the FLC generates the rotation for stable regions and the shifting for unstable regions. However, only the output error e_1 is used in the antecedents of the fuzzy rules and, consequently, rotation is only permitted in a slope-increasing direction. Komurcugil [36] used a one-input FLC structure for continuous rotation and implemented the design for a single-phase UPS inverter. Lee et al. [14] proposed a linear continuously time-varying sliding surface as in (11) with $c_1(t)$=0 for unstable regions. As this is parallel to the $e(t)$=0 plane, the sliding surface is shifted until $\alpha(t) = 0$. A Takagi-Sugeno (TS) type fuzzy model is then designed to generate $c_1(t)$ and $\alpha(t)$ for the regulation of the time-varying sliding surface. Also, a TS type fuzzy model was utilized in [37] for directly obtaining the sliding surface with rule consequents $s^i = \dot{e}(t) + c^i e(t)$ (i=1,2,...,r), where r is the number of rules, s^i, c^i are the sliding surface and the sliding surface slope for the i^{th} rule, respectively. For higher order systems, a continuously-moving linear sliding surface was proposed in [21] designing a Mamdani-type fuzzy moving algorithm based on the sliding surface design in [18]. In this algorithm, the inputs are the distance of the current state to the sliding surface and the discontinuous control gain and the output is the change in the sliding surface. The rules result in larger changes in the sliding surface when either the distances of the current state to the sliding surface or the discontinuous control gain increases [21].

Artificial neural networks have also been used for continuously time-varying sliding surface design. For instance, a radial basis function neural network was proposed in [38] to adjust the sliding surface and controller parameters. The delayed control input and system output are the inputs and the adaptive parameters are obtained online using the artificial neural network outputs.

3.4 Constant Nonlinear Sliding Surface

For large tracking errors, linear sliding surface design methods require a large control input to keep the system states on the sliding surface [39]. This is because the magnitude of the control signal is usually directly proportional to the distance between the states and reference states. Another problem with a linear sliding surface is that it replaces nonlinear dynamics with linear dynamics that may not fit the global dynamics of the controlled system.

These disadvantages can be avoided by using a nonlinear sliding surface that offers a wider variety of design alternatives than their linear counterparts [40]. Thus, a nonlinear sliding surface can provide better system performance if the nonlinearity is chosen judiciously. SMC with nonlinear sliding surfaces is called nonlinear SMC. Sliding mode control is similar to bang-bang control [41]; they both have a relay-like structure. With this similarity in mind, for a n^{th} order single-input linear time-invariant system

$$\dot{\mathbf{x}} = \mathbf{A}\mathbf{x} + \mathbf{b}u \tag{20}$$

the Hamiltonian function to obtain the time-optimal control strategy is

$$h = 1 + \mathbf{q}^T(\mathbf{A}\mathbf{x} + \mathbf{b}u) \tag{21}$$

where $\mathbf{q} \in \Re^{nx1}$ is a co-state vector. Finally, for **A**= [0 1;0 0], **b**=$[b_1\ 0]^T$, and for the minimum time problem with the constraint $|u(t)| \leq 1$, the solution of the state equations are obtained with $u = \pm 1$ as [41]

$$x_1 = \pm\frac{t^2}{2} + c_3 t + c_4, \qquad x_2 = \pm t + c_3 \tag{22}$$

If the two solutions in (22) are combined, we have

$$x_1 = \begin{cases} \dfrac{1}{2b_1}x_2^2 + c_5, & u = +1 \\ -\dfrac{1}{2b_1}x_2^2 + c_6, & u = -1 \end{cases} \tag{23}$$

Therefore, taking c_5=0, c_6=0 and defining

$$s(\mathbf{x}) = x_1 + \frac{1}{2b_1}x_2|x_2| \tag{24}$$

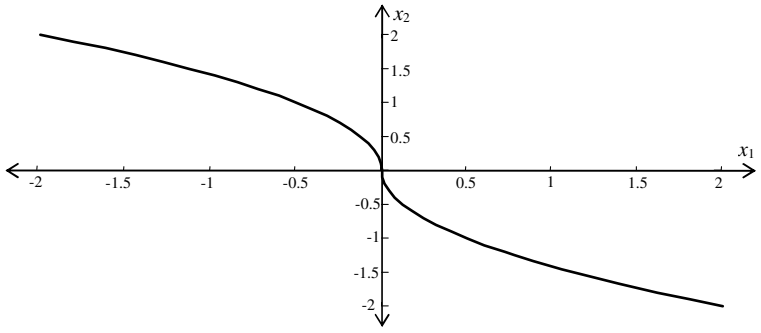

Fig. 2. The sliding surface obtained by using time-optimal control strategy

Thus, the control signal can be written in terms of (24) as $u(t)$=-sign(s). From Figure 2, it is seen that (24) has a parabolic structure obtained by combining optimal control and sliding mode control.

The first such surface as in Figure 2 was also proposed by McDonald [42] who used a linear combination of the error in the controlled variable and its square as the sliding surface function. In [39], a parabolic sliding surface was used in nonlinear SMC design and (24) was modified in [43] by scaling x_1 with a constant. All these efforts are for improving the robustness without increasing the magnitude of the control input.

Nonlinear sliding surfaces also increase the application areas of SMC. For instance, a nonlinear sliding surface was used in [44] for power systems. Cerruto et al. [45] defined the sliding trajectory for the position and speed regulator problem of electrical servo drives. The motor is stationary at t=t_0, accelerates until t=t_1, then moves with a constant speed between t_1> t >t_2. Finally, it decelerates with a maximum acceleration until the desired reference value. This scheme is appropriate for most servo applications [46]. The sliding surface proposed in [45] is given by

$$s(\mathbf{e}) = \begin{cases} a_1\dot{e}^2(t) + e(t) - e(0), & t_0 < t \le t_1 \\ \dot{e}(t) + a_2 & , \quad t_1 < t \le t_2 \\ -a_1\dot{e}^2(t) + e(t) & , \quad t_2 < t \le t_3 \\ \dot{e}(t) + a_3 e(t) & , \quad t > t_3 \end{cases} \tag{25}$$

where a_i, and t_i (i=1,2,3) are constant design parameters subject to physical system constraints. When the current state is close to the origin (t >t_3), a linear sliding surface is used in (25) to provide smooth settling behaviour. Some sytem dynamics constitutes a nonlinear underactuated system and can be represented by linear system with bounded and unmatched uncertainty. Thus, designing a nonlinear sliding surface reflecting the nonlinear dynamics of the system provides a novel sliding surface with simple and implementable control law [47]. Also, Takahashi et al [48] used SMC to obtain a special sinusoidal voltage source. An ideal sinusoidal wave has an elliptical trajectory in the current-voltage phase plane. The state variables are taken as capacitor voltage $x_1 = v_c$ and capacitor current $x_2 = i_c$. The nonlinear constant sliding surface is defined as

$$s(\mathbf{x}) = \frac{x_1^2}{V_{\max}^2} + \frac{x_2^2}{I_{\max}^2} - 1 = 0 \tag{26}$$

where s(**x**) has negative values inside the ellipsoid and positive values outside it. Thus, SMC provides robustness to variations in magnitude and frequency and better tracking of a sinusoidal reference for second order systems [48].

For a nonlinear sliding surface, different ideas can be combined in order to improve the performance. For instance Kelly [49], used a nonlinear function of the state variables in the integral term of an integral sliding surface to obtain global asymptotic stability and better performance. Su and Stepanenko [40] defined the generalized sliding surface equation as

$$\mathbf{s}(\mathbf{x}, \mathbf{x}_d, \dot{\mathbf{x}}_d, t) = \dot{\mathbf{x}} - \mathbf{v}\left(\mathbf{x}, \mathbf{x}_d, \dot{\mathbf{x}}_d, t\right) \tag{27}$$

for an n^{th} order systems with especially n inputs where $\mathbf{v} = \begin{bmatrix} v_1 & v_2 & \dots & v_n \end{bmatrix} \in \Re^{nx1}$ are design functions. The generalized sliding surface (27) includes sliding surface equations in the robot manipulator literature as each degree of freedom of a robot manipulator is powered with independent torques [40]. For example, for n=2, v_1=v_2 is defined as

$$v_i = \dot{x}_{di}(t) - \begin{cases} \dfrac{d}{1/a_1 + a_3 d} + a_2\left(x_i(t) - d\right), & if \quad x_i > d \\ \dfrac{x_i(t)}{1/a_1 + a_3 x_i(t)}, & if \quad 0 \le x_i \le d \\ \dfrac{x_i(t)}{1/a_1 - a_3 x_i(t)}, & if \quad -d \le x_i \le 0 \\ -\dfrac{d}{1/a_1 + a_3 d} + a_2\left(x_i(t) + d\right), & if \quad x_i < -d \end{cases} \tag{28}$$

and to visualize the nonlinear constant sliding surface, (28) is obtained in Figure 3 for a_1=16, a_2=4, a_3=0.2, d=0.3125. The similarity between the sliding surfaces given in Figure 3 and the parabolic sliding surface of Figure 2 obtained using optimal control is notable. Lee [50] proposed a nonlinear sliding surface with cubic polynomials and improved the system performance with respect to conventional linear SMC.

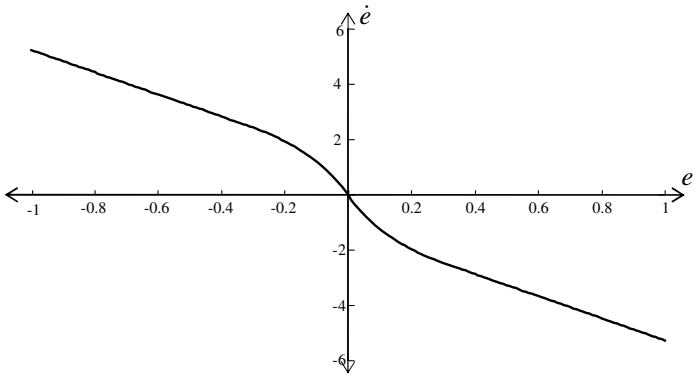

Fig. 3. Nonlinear constant sliding surface obtained with (28)

Higher order SMCs are used to retain the property of robustness and to eliminate chattering [51]. However this advantage is obtained by tuning the gain parameter which must be sufficiently high. A nonlinear sliding surface based higher order SMC is applied for controlling the position of a servomotor [52]. Comparisons with the higher order SMC using a linear switching surface shows a reduction of chattering as in the linear case with superior transient performance.

Richter [53] used polytrophic process dynamics to define a sliding surface. For ideal gases with pressure x_1 and density x_2 a polytrophic process is one in which the state of the substance is transferred from one point to another following the law

$$x_1 x_2^n = a \tag{29}$$

where $n \in \Re$ is a polytrophic exponent and $a \in \Re$ is a constant. The system that follows the thermodynamic path is defined by the sliding surface

$$s(\mathbf{x}) = x_1 x_2^n - a \tag{30}$$

In general, the tracking error is large at the early phase of the transient period and decreases as the response approaches the steady state. Exploiting this fact, a nonlinear sliding surface was proposed in [54] using a state-dependent coefficient for the conventional sliding surface (3) as

$$c_1(e) = k_1(k_2 - |e|) \tag{31}$$

where $k_2 = \max(|e|) + \varepsilon$, $\varepsilon > 0$ and k_1>0. Initially, $|e| \approx \max(|e|)$ and hence $c_1 \approx k_1 \varepsilon$. Near the desired states, the error is approximately zero and $c_1 \approx k_1 k_2$. Thus, the sliding surface changes as a function of the tracking error in continuous-time.

Another method in sliding surface design is inserting the control input term $u(t)$ in the sliding surface definition to improve performance. Sliding surfaces that depend on the states as well as the control input are called *dynamic* sliding surfaces and the associated SMCs are known as *dynamic SMC* [55]. In general, this makes the control input a nonlinear function of the states and results in nonlinear constant sliding surfaces.

Fractional order systems, in the context of SMC design, are used either to improve the control performance or to apply SMC to fractional order systems [56, 57]. A hybrid system was proposed in [58] that combines the advantages of fractional control and sliding mode control. The sliding surface is first defined for n^{th} order single-input systems as

$$s(\mathbf{e}) = c_n e + c_{n-1} D^{\alpha} e + c_{n-1} D^{1+\alpha} e + \ldots + D^{n+\alpha-1} e \tag{32}$$

where $c_i > 0$ $(i = 1,2,\ldots,n)$ are sliding surface parameters, $D^{\alpha} = d^{\alpha} / dt^{\alpha}$ with $\alpha \in \Re$ is the fractional order differintegration operator [58]. Then PD^{μ} and $PI^{\lambda}D^{\mu}$ fractional order sliding surfaces are obtained from the proposed definition (32). Tang *et al.* [59] used a fractional order PD^{μ} sliding surface for ABS to regulate the slip to a desired value.

In all linear and most nonlinear sliding surface design methods, asymptotic convergence is inevitable and error convergence to zero is achieved in infinite time. Using the concept of fractional order systems, Zak [60] proposed the *terminal attractor* concept to improve the stability characteristics of dynamic systems. If the Lipschitz condition is not satisfied at an equilibrium point, this equilibrium becomes a terminal attractor [61]. A function $f(x)$ satisfies the Lipschitz condition at x=0 if

$$\left|f(h)-f(0)\right| \le b\left|l\right| \tag{33}$$

for all $\left|l\right| < \varepsilon$, where b is independent of l. For example, given the dynamics

$$\dot{x}_1 = -\beta_1 x_1^{\frac{a_1}{b_1}} \tag{34}$$

(x_1, $\dot{x}_1$)=(0,0) is an equilibrium point. The Lipcshitz condition (33) is not satisfied and therefore the equilibrium is a terminal attractor. The solution of (34) is

$$x_1(t) = \left(x_1(0)^{\frac{b_1-a_1}{b_1}} - \frac{\beta_1(b_1-a_1)}{b_1} t \right)^{\frac{b_1}{b_1-a_1}} \tag{35}$$

The solution is obtained by integrating from zero to any time instant t. If the integral is solved until time t when the equilibrium point is reached, it can be seen that for

$$t_s = \left| \int_{x_1(0)}^{0} -\frac{1}{\beta_1} x_1^{\frac{a_1}{b_1}} dx_1 \right| = \frac{b_1}{\beta_1(a_1-b_1)} \left|x_1(0)\right|^{\frac{b_1-a_1}{b_1}} \tag{36}$$

$x_1(t_s)$=0 is obtained and that the equilibrium point is approached in finite time [61]. Similarly, it can be shown that $\dot{x}_1$ also approaches zero in finite time. The terminal SMC was first proposed for second order nonlinear dynamic systems in controllable canonical form for which the system dynamics in sliding mode are determined with (34). Thus, the terminal sliding surface is defined as

$$s(\mathbf{x}) = x_2 + \beta_1 x_1^{\frac{a_1}{b_1}} \tag{37}$$

where β_1>0 is positive real, b_1 and a_1 are odd integer constant design parameters with b_1>a_1 [62]. The sliding mode control law is chosen to provide s=0 in finite time, namely providing a stable sliding surface. The nonlinear sliding surface thus obtained is known as a *terminal* sliding surface and the control structure is known as *terminal SMC*. In terminal SMC, while the sliding surface reaches the sliding mode in finite time as in conventional SMC, the tracking error also converges to zero in finite time unlike conventional SMC. Later, the terminal sliding surface was considered in [63] for single-input n^{th} order linear systems in controllable canonical form. For single-input systems, the $(n\text{-}1)^{\text{th}}$ order sliding surface is given as

$$s(\mathbf{x}) = h_{n-2} + \beta_{n-1} h_{n-2}^{\frac{a_{n-1}}{b_{n-1}}} \tag{38}$$

where h_{n-2} function is calculated in an hierarchical structure as

$$h_1 = \dot{x}_1 + \beta_1 x_1^{\frac{a_1}{b_1}}$$
$$h_i = \dot{h}_{i-1} + \beta_i h_{i-1}^{\frac{a_2}{b_2}} \qquad i = 2,...,n-2 \tag{39}$$

where $\beta_i > 0$ are positive real numbers and $b_i > a_i$ are odd integer design parameters. If a terminal SMC is designed such that $s\dot{s} < 0$, the terminal sliding variables $h_{n-1},\ldots, h_1$ in (39) converge to zero in finite time sequentially and the system states reach the origin in finite time [64]. This finite time is equal to the sum of the reaching times of all the sliding surface variables in (38) and (39) calculated separately by the formula in (36) [63].

Terminal SMC improves the system performance and reaches the equilibrium point in finite time rather than asymptotically. However, the system may not be robust with respect to modeling uncertainties. Because of the hierarchical process steps in (39), when the initial conditions are not determined carefully, singularities may occur. To eliminate this problem, a zero value is avoided for h_i (i=0,1,..., j-1). The singularity problem for multi-input linear systems with uncertainties was investigated in [65]. The terminal SMC for nonlinear uncertain systems was examined in [66]. To remove chattering and attenuate disturbances, Yu et al [67] proposed new forms of terminal SMC with global finite-time stability and analyzed some of their properties through application to the control of robotic manipulators. To completely remove disturbances, disturbance observer based terminal SMC stuructures are also proposed [68, 69]. When the state is away from the equilibrium point, namely $x_1 > 1$, the $x_1^{a_1/b_1}$ term in the sliding surface equation (37) may not provide better system performance. The following nonlinear sliding surface eliminates this problem for second order systems in controllable canonical form

$$s(\mathbf{x}) = x_2 + \beta_1 x_1^{\frac{a_1}{b_1}} + \beta_2 x_1^{\frac{a_2}{b_2}} \tag{40}$$

where $\beta_1, \beta_2 > 0$ are real, $b_1 > a_1$ and $a_2 > b_2$ are odd integer constant design parameters [70]. For x_1 values near zero, the approximate system dynamics become $\dot{x}_1 = -\beta_1 x_1^{a_1/b_1}$ with finite-time convergence similar to (37). When x_1 values are far from zero, the system dynamics become $\dot{x}_1 = -\beta_2 x_1^{a_2/b_2}$, which has better convergence rate than conventional SMC with constant linear sliding surface. SMC with the nonlinear sliding surface (40) is called *fast terminal* SMC [70]. Both a terminal and a fast terminal sliding surface are shown in Figure 4 for parameters a_1=3, b_1=5, a_2=13, b_2=5, $\beta_1 = \beta_2 = 1$. The figure shows that for regions away from the equilibrium point the fast terminal sliding surface and thus the system states are in a faster control region. As the system converges to the equilibrium point fast terminal and terminal sliding surfaces become similar. For negative x values, the fractional power in $x^{a/b}$ terms may lead to $x^{a/b} \notin \Re$. This is avoided in the literature by some assumptions or by using extra control effort. Aghababa [71], directly proposed a nonsingular terminal SMC to avoid this problem.

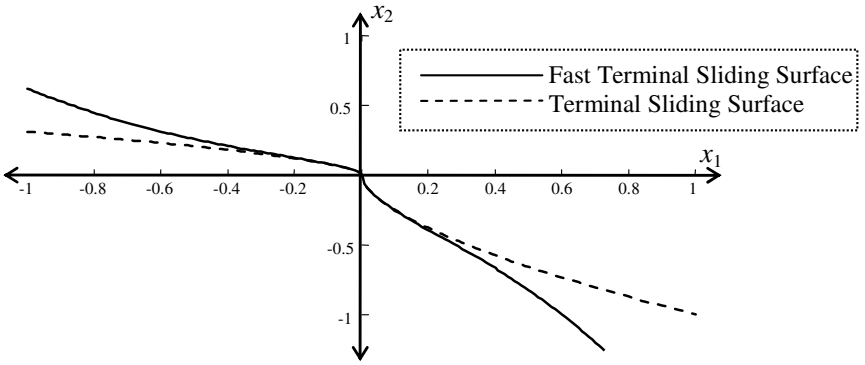

Fig. 4. Terminal and fast terminal sliding surfaces

The hierarchical structure in (39) can also be used for the control of single-input higher order nonlinear systems by rearranging it for sliding surface (40) [72]. With the help of terminal and fast terminal control structures, the error converges to zero in finite time by using constant and nonlinear sliding surfaces.

3.5 Nonlinear Discretely-Moving Sliding Surface

As surveyed in Section 3.2 and 3.3, linear sliding surfaces combined with moving algorithms result in nonlinear system trajectory. Hence, the moving schemes given for linear sliding surfaces can be also applied to nonlinear sliding surface design. Clearly, a nonlinear system trajectory can already be obtained when a nonlinear constant sliding surface is used. However, defining the whole trajectory with a nonlinear function may result in a highly nonlinear sliding surface and control input. Therefore, moving algorithms for nonlinear sliding surfaces can lessen or shorten the reaching mode by using relatively simple nonlinear functions in place of a constant nonlinear sliding surface.

Li et al. [73] considered the regulator problem for single-input second order systems and define the sliding surface for the single-input scalar case of (28). In particular, to obtain a nonlinear discretely-moving sliding surface, $v_1(e)$ was defined in [73] as a nonlinear function of the error and then obtain the nonlinear sliding surface as

$$\hat{s}(\mathbf{e},t) = \dot{e} + w_p(t)\tanh(c_1 e) \tag{41}$$

where c_1 is the sliding surface slope of the conventional linear sliding surface and w_p is a design parameter.

Using the delta-neighbourhood approach presented by Choi et al. in [15], (41) is designed as a discretely-moving nonlinear sliding surface where the parameter w_p is updated recursively. The discretely-moving nonlinear sliding surface obtained for c_1=2 and different values of w_p is given in Figure 5. The parameter w_p is adjusted until the last specified sliding surface value is reached [73].

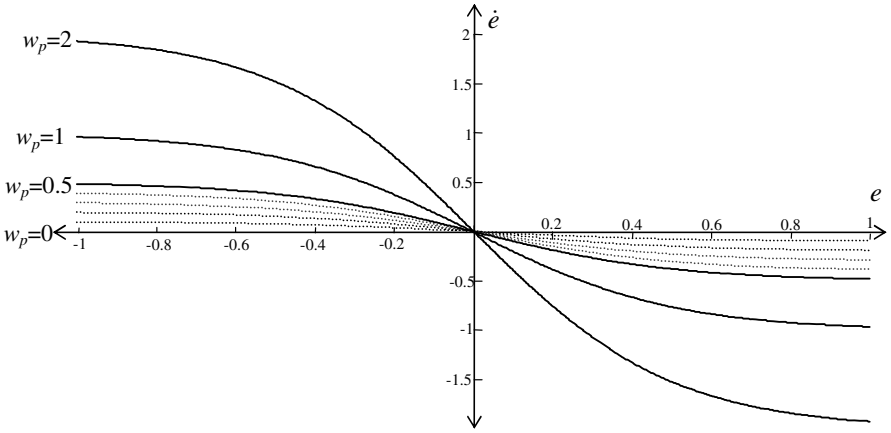

Fig. 5. Discretely-moving nonlinear sliding surfaces obtained by (41)

3.6 Nonlinear Continuously-Moving Sliding Surface

Continuously-moving sliding surfaces were developed to avoid the dwelling time of discretely-moving sliding surfaces. A sliding surface was defined in [74] using (3) as

$$\hat{s}(\mathbf{e},t) = s(\mathbf{e}) - (\dot{e}(t_0) + c_1 e(t_0)\exp\left(-a_1\left(t - t_0\right)\right) \tag{42}$$

where a_1>0 is a design parameter. They showed that for known initial conditions, the second term keeps the system on the sliding surface and eliminates the reaching mode. They also showed that the overall system is globally exponentially stable and (42) is a terminal SMC. Inspired by the terminal SMC concept, Bartoszewicz [75] also designed the following nonlinear continuously-moving sliding surface for second order nonlinear systems with state constraints

$$\hat{s}(\mathbf{e},t) = \dot{e} + \gamma(t).\text{sign}\left(e(t)\right).\left|e(t)\right|^{a_1} \tag{43}$$

In (43), a_1 and $\gamma(t)$ are design parameters where a_1 is a constant in the range $1/2 \le a_1 < 1$ and $\gamma(t)$ is a time-dependent function that becomes constant at a predetermined time instant. Combining (12) and the terminal sliding surface of (37), the continuously-moving terminal sliding surface was proposed in [26] as

$$\hat{s}(\mathbf{e},t) = \begin{cases} \dot{e}(t) + 2a_1 t + a_2 + a_4 \text{sign}(e + a_1 t^2 + a_2 t + a_3).(e + a_1 t^2 + a_2 t + a_3)^{2/3}, & t \le t_b \\ \dot{e}(t) + a_4 \text{sign}(e).(e)^{2/3} & , t > t_b \end{cases} \tag{44}$$

where t_b>0, a_1, a_2, a_3, a_4 are constant design parameters. In [76], a parabolic sliding surface was proposed using (3) and the (*s*-*p*) coordinates defined in (17) as follows

$$\hat{s}(\mathbf{e},t) = s(\mathbf{e}) - k_s(t).p^2(\mathbf{e},t), \quad (k_s=0 \quad \text{if} \quad e\dot{e} > 0) \tag{45}$$

where $k_s(t)$ provides a bending measure of the parabolic sliding surface. The nonlinear parabolic sliding surfaces obtained using (45) with different values of $k_s(t)$ function (19) is illustrated in Figure 6.

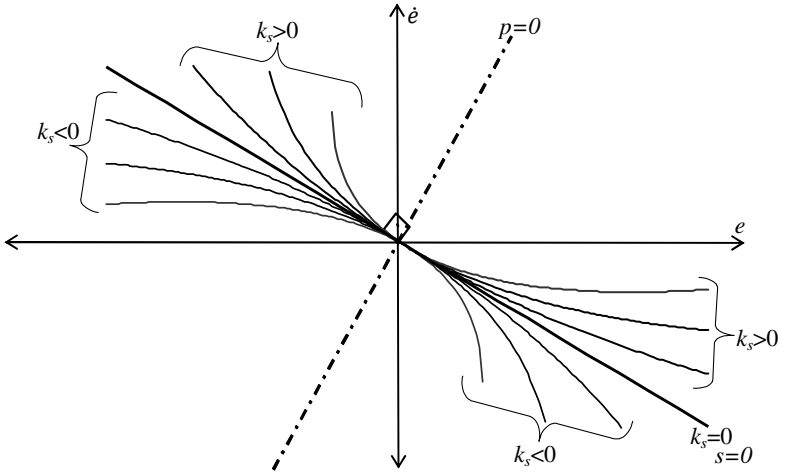

Fig. 6. Nonlinear sliding surfaces obtained by different values of k_s in (45)

4 Conclusion

In this chapter, sliding surface design methods are classified and surveyed according to their properties. In conventional sliding mode control, the sliding surface is constant and linear for simplicity. To improve system performance, moving linear sliding surfaces were proposed. The basic philosophy in moving sliding surface design is that the sliding surface parameters are initially chosen so that the sliding surface passes through the initial conditions. The reaching time which is the period where the disturbances affect the system, is reduced and the system becomes robust with respect to parameter variations and external disturbances. The moving algorithm may be discrete or continuous. In discretely-moving sliding surfaces, the sliding surface is constant for a given time period. The discontinuity at the end of this period causes sensitivity to disturbances. To overcome this, a continuously-moving sliding surface may be used. Unlike discretely-moving sliding surfaces, they require the derivatives of the sliding surface parameters to calculate the control law. This is an advantage of discretely-moving sliding surfaces.

Despite their simplicity, linear sliding surfaces have certain disadvantages. For instance, when the sliding surface is linear, the magnitude of the control input required to keep the system states on the sliding surface usually increases in direct proportion to the magnitude of the tracking error. Another problem with linear sliding surface design is the replacement of the nonlinear system characteristics with linear dynamics arising from the control law obtained by the linear sliding surface. The linear dynamics

of the linear sliding surface may not fit the global dynamics of the controlled system. Therefore, using a nonlinear sliding surface may provide better performance if the nonlinearity is appropriately selected. For instance, with the use of a special sliding surface (known as a terminal sliding surface), the tracking error converges to zero in finite time whereas convergence is asymptotic in conventional sliding mode control.

Moving algorithms for nonlinear sliding surfaces lessen or eliminate the reaching mode by using a simpler nonlinear function. Thus, similar performance is obtained by using a moving nonlinear sliding surface in place of a constant but complicated one. Because discretely-moving schemes for nonlinear sliding surfaces have the same discontinuity effects as in the linear case; various continuously-moving sliding surfaces have been developed in the literature to remove this drawback.

Compared to their linear counterparts, both constant and moving nonlinear sliding surface design methods result in analytical difficulties in sliding surface design or in determining the sliding surface parameters. For moving nonlinear sliding surfaces, it is even more complicated to geometrically predetermine the path of the sliding surface. Moreover, designing the control law and determining the stability boundaries based on nonlinear sliding surfaces are more difficult. As a consequence, the trade-off between the simplicity of the control algorithm and the desired performance improvement must be considered in choosing the sliding surface design methodology.

Acknowledgements. As being one of the first graduates of the Systems and Control Engineering Department of Bogazici University, Sezai Tokat takes immense pleasure in thanking Prof. Okyay Kaynak who taught him hard working and gave the love of control theory.

References

1. Utkin, V.I.: Sliding modes and their application in variable structure systems. MIR Publishers, Moscow (1978)
2. Bandyopadhyay, B., Deepak, F., Kim, K.-S.: Sliding Mode Control Using Novel Sliding Surfaces. LNCIS, vol. 392. Springer, Heidelberg (2009)
3. Bartoszewicz, A., Nowacka-Leverton, A.: Time-Varying Sliding Modes for Second and Third Order Systems. LNCIS, vol. 382. Springer, Heidelberg (2009)
4. Slotine, J.J.E., Li, W.: Applied nonlinear control. Prentice-Hall, Englewood Cliffs (1991)
5. Qian, D., Liu, X., Ma, M., Xu, C.: GA-based integral sliding mode control for AGC. In: Tan, Y., Shi, Y., Tan, K.C. (eds.) ICSI 2010, Part II. LNCS, vol. 6146, pp. 260–267. Springer, Heidelberg (2010)
6. Slotine, J.J.E., Spong, M.W.: Robust control with bounded input torques. Journal of Robotic Systems 2(4), 329–352 (1985)
7. Cho, D.D.: VSC of nonlinear systems: experimental case studies. In: Zinober, A.S.I. (ed.) Variable Structure and Lyapunov Control. LNCIS, vol. 193, pp. 335–364. Springer, Heidelberg (1994)
8. Stepanenko, Y., Cao, Y., Su, C.Y.: Variable structure control of robotic manipulator with PID sliding surfaces. International Journal of Robust and Nonlinear Control 8, 79–90 (1998)

9. Wai, R.J.: Adaptive sliding mode control for induction servomotor drive. IEE Proceedings-Electric Power Applications 147(6), 553–562 (2000)
10. Lin, F.J., Shyu, K.K., Wai, R.J.: Recurrent fuzzy neural network sliding mode controlled motor toggle servomechanism. IEEE/ASME Transactions on Mechatronics 6(4), 453–466 (2001)
11. Jafarov, E.M., Parlakcı, M.N.A., Istefanopulos, Y.: A New Variable Structure PID-Controller Design for Robot Manipulators. IEEE Transactions on Control Systems Technology 13(1), 122–130 (2005)
12. Eker, I.: Sliding mode control with PID sliding surface and experimental application to an electromechanical plant. ISA Transactions 45(1), 109–118 (2006)
13. Orłowska-Kowalska, T., Kami´nski, M., Szabat, K.: Implementation of a sliding-mode controller with an integral function and fuzzy gain value for the electrical drive with an elastic joint. IEEE Transactions on Industrial Electronics 57(4), 1309–1317 (2010)
14. Lee, H., Kim, E., Kang, H.J., Park, M.: Design of a sliding mode controller with fuzzy sliding surfaces. IEE Proceedings- Control Theory and Applications 145(5), 411–418 (1998)
15. Choi, S.B., Cheong, C.C., Park, D.W.: Moving switching surfaces for robust control of second order variable structure systems. International Journal of Control 58(1), 229–245 (1993)
16. Lu, Y.S., Chen, J.S.: Design of a global sliding mode controller for a motor drive with bounded control. International Journal of Control 62(5), 1001–1019 (1995)
17. Choi, S.B., Park, D.W., Jayasuriya, S.: A time-varying sliding surface for fast and robust tracking control of second order uncertain systems. Automatica 30(5), 899–904 (1994)
18. Roy, R.G., Olgac, N.: Robust nonlinear control via moving sliding surfaces: nth order case. In: Proceedings of the 36th IEEE Conference on Decision and Control, vol. 2, pp. 943–948. IEEE Press, New York (1997)
19. Barmish, B.R.: A Generalization of Kharitonov's four-polynomial concept for robust stability problems with linearly dependent coefficient perturbations. IEEE Transactions on Automatic Control 34(2), 157–165 (1989)
20. Chang, E.-C., Chang, F.-J., Lin, Y.-K.: Improved performance using discrete rotating and shifting switching manifolds of single-phase PWM inverters. In: Proceedings of the IEEE/SICE International Symposium on System Integration, December 20-22, pp. 997–1002. Kyoto University, Kyoto (2011)
21. Park, D.W., Choi, S.B.: Moving sliding surfaces for high-order variable structure systems. International Journal of Control 72(11), 960-970 (1999)
22. Slotine, J.J.E.: Sliding controller design for non-linear systems. International Journal of Control 40(2), 421–434 (1984)
23. Salamci, M.U., Ozgoren, M.K., Banks, S.P.: Sliding mode control with optimal sliding surfaces for missile autopilot design. Journal of Guidance, Control, and Dynamics 23(4), 719–727 (2000)
24. Bartoszewicz, A.: A comment on 'A time varying sliding surface for fast and robust tracking control of second-order uncertain systems'. Automatica 31(12), 1893–1895 (1995)
25. Tokat, S.: Sliding mode controlled bioreactor using a time-varying sliding surface. Transactions of the Institute of Measurement and Control 31(5), 435–456 (2009)
26. Bartoszewicz, A.: Time-varying sliding modes for second order systems. IEE Proceedings-Control Theory and Applications 143(5), 455–462 (1996)
27. Betin, F., Pinchon, D., Capolino, G.A.: A time-varying sliding surface for robust position control of a DC motor drive. IEEE Transactions on Industrial Electronics 49(2), 462–473 (2002)

28. Park, K.B., Tsuji, T.: Terminal sliding mode control of second-order nonlinear uncertain systems. International Journal of Robust and Nonlinear Control 9, 769–780 (1999)
29. Choi, H.S., Park, Y.H., Cho, Y., Lee, M.: Global sliding mode control. IEEE Control Systems Magazine 21(3), 27–35 (2001)
30. Yilmaz, C., Hurmuzlu, Y.: Eliminating the reaching phase from variable structure control. Transactions of the ASME-G: Journal of Dynamic Systems, Measurement and Control 122(4), 753–757 (2000)
31. Chang, T.H., Hurmuzlu, Y.: Sliding control without reaching phase and its application to bipedal locomotion. Journal of Dynamics, Systems, Measurement and Control 115, 447–455 (1993)
32. Hu, Q., Bo, L., Youmin, Z.: Robust attitude control design for spacecraft under assigned velocity and control constraints. ISA Transactions 52(4), 480–493 (2013)
33. Tokat, S., Eksin, I., Guzelkaya, M.: A new design method for sliding mode controllers using a linear time-varying sliding surface. Proceedings of the Institution of Mechanical Engineers, Part I: Journal of Systems and Control Engineering 216(6), 455–466 (2002)
34. Kaynak, O., Erbatur, K., Ertugrul, M.: The fusion of computationally intelligent methodologies and sliding mode control- a survey. IEEE Transactions on Industrial Electronics IE 48, 4–17 (2001)
35. Ha, Q.P., Rye, D.C., Durrant-Whyte, H.F.: Fuzzy moving sliding mode control with application to robotic manipulators. Automatica 35, 607–616 (1999)
36. Komurcugil, H.: Rotating sliding-line based sliding-mode control for single-phase UPS inverters. IEEE Transactions on Industrial Electronics 59(10), 3719–3726 (2012)
37. Iliev, B., Hristozov, I.: Variable structure control using Takagi-Sugeno fuzzy system as a sliding surface. In: Proceedings of the IEEE World Congress on Computational Intelligence, Honolulu, USA, May 12-17, pp. 644–649 (2002)
38. Akhavan, S., Jamshidi, M.: ANN-based sliding mode control for non-holonomic mobile robots. In: Proceedings of the IEEE International Conference on Control Applications, pp. 664–667. IEEE Press, New York (2000)
39. Jabbari, A., Tomizuka, M., Sakaguchi, T.: Robust nonlinear control of positioning systems with stiction. In: Proceedings of the American Control Conference, San Diego, California, USA, May 23-25, pp. 1097–1102 (1990)
40. Su, C.Y., Stepanenko, Y.: Adaptive sliding mode control of robot manipulators: general sliding manifold case. Automatica 30(9), 1497–1500 (1994)
41. Kirk, D.E.: Optimal control theory: an introduction. Prentice-Hall, Englewood Cliffs (1970)
42. McDonald, D.: Nonlinear techniques for improving servo performance. In: National Electronics Conference, vol. 6, pp. 400–421 (1950)
43. Kalaykov, I., Iliev, B.: Time-optimal sliding mode control of robot manipulator. In: Proceedings of the 26th Annual Conference of the IEEE Industrial Electronics Society, vol. 1, pp. 265–270. IEEE Press, New York (2000)
44. de Leon-Morales, J.: Sliding mode controllers and observers for electromechanical systems. In: Fridman, L., Moreno, J., Iriarte, R. (eds.) Sliding Modes. LNCIS, vol. 412, pp. 493–516. Springer, Heidelberg (2011)
45. Cerruto, E., Consoli, A., Kucer, P., Testa, A.: A fuzzy logic quasi sliding mode controlled motor drive. In: Proceedings of the IEEE International Symposium on Industrial Electronics, pp. 652–658. IEEE Press, New York (1993)
46. De Azevedo, H.R., Wong, K.P.: A fuzzy logic controller for permanent magnet synchronous machine-a sliding mode approach. In: Proceedings of the IEEE Power Conversion Conference, pp. 672–677. IEEE Press, New York (1993)

47. Kurode, S., Spurgeon, S.K., Bandyopadhyah, B., Gandhi, P.S.: Sliding mode control for slosh-free motion using a nonlinear sliding surface. IEEE/ASME Transactions on Mechatronics 18(2), 714–724 (2013)
48. Takahashi, R.H.C., Peres, P.L.D., Barbosa, L.L.S.: A sliding mode controlled sinusoidal voltage source with ellipsoidal switching surface. IEEE Transactions on Circuits and Systems-I: Fundamental Theory and Applications 46(6), 714–721 (1999)
49. Kelly, R.: Global positioning of robot manipulators via PD control plus a class of nonlinear integral actions. IEEE Transactions on Automatic Control 43(7), 934–938 (1998)
50. Lee, J.J.: Adaptive tracking control of DC servomotors. IEEE Transactions on Consumer Electronics 37(4), 905–912 (1991)
51. Fridman, L., Levant, A.: Higher order sliding modes. In: Barbot, J.P., Perruguetti, W. (eds.) Sliding Mode Control in Engineering, pp. 53–101. Marcel Dekker, New York (2002)
52. Mondal, S., Mahanta, C.: Nonlinear sliding surface based second order sliding mode controller for uncertain linear systems. Communications in Nonlinear Science and Numerical Simulation 16(9), 3760–3769 (2011)
53. Richter, H.: Tracking of a thermodynamic process using a polytropic surface as a sliding manifold. In: Proceedings of the American Control Conference, vol. 1, pp. 197–201. IEEE Press, New York (2003)
54. Lee, C.K., Kwok, N.M.: A variable structure controller with adaptive switching surfaces. In: Proceedings of the American Control Conference, vol 1, pp. 1033–1034. IEEE Press, New York (1995)
55. Sira-Ramirez, H.: On the dynamical sliding mode control of nonlinear systems. International Journal of Control 57(5), 1039–1061 (1993)
56. Efe, O., Kasnakoglu, C.: A fractional adaptation law for sliding mode control. International Journal of Adaptive Control and Signal Processing 22, 968–986 (2008)
57. Efe, O.: Fractional order sliding mode control with reaching law approach. Turkish Journal of Electrical Engineering and Computer Science 18(5), 731–747 (2010)
58. Delavari, H., Ranjbar, A.N., Ghaderi, R., Momani, S.: Fractional order control of a coupled tank. Nonlinear Dynamics 61, 383–397 (2010)
59. Tang, Y., Zhang, X.Y., Zhang, D., Zhao, G., Guan, X.P.: Fractional order sliding mode controller design for antilock braking systems. Neurocomputing 111, 122–130 (2013)
60. Zak, M.: Terminal attractors for addressable memory in neural networks. Physics Letters A 133(12), 18–22 (1988)
61. Bianchini, M., Gori, M., Maggini, M.: Does terminal attractor backpropagation guarantee global optimization? In: Marinaro, M., Morasso, P.G. (eds.) Proceedings of the International Conference on Artificial Neural Networks, vol. 1(pt. 2), pp. 377–380. Springer, London (1994)
62. Zhihong, M., Paplinski, A.P., Wu, H.R.: A robust MIMO terminal sliding mode control scheme for rigid robotic manipulators. IEEE Transactions on Automatic Control 39(12), 2464–2469 (1994)
63. Yu, X.H., Zhihong, M.: Model reference adaptive control systems with terminal sliding modes. International Journal of Control 64(6), 1165–1176 (1996)
64. Zhihong, M., Yu, X.H.: Terminal sliding mode control of MIMO linear systems. IEEE Transactions on Circuits and Systems-I: Fundamental Theory and Applications 44(11), 1065–1070 (1997)
65. Yu, X.H., Zhihong, M.: Multi-input uncertain linear systems with terminal sliding mode control. Automatica 34(3), 389–392 (1998)
66. Wu, Y., Yu, X.H., Zhihong, M.: Terminal sliding mode control design for uncertain dynamic systems. Systems and Control Letters 34, 281–287 (1998)

67. Yu, S.H., Yu, X.H., Bijan, S., Man, Z.H.: Continuous finite-time control for robotic manipulators with terminal sliding mode. Automatica 41, 1957–1964 (2005)
68. Su, J., Yang, J., Li, S.: Continuous finite-time anti-disturbance control for a class of uncertain nonlinear system. Transactions of the Institute of Measurement and Control 36(3), 300–311 (2013)
69. Yang, J., Li, S., Su, J., Yu, X.: Continuous nonsingular terminal sliding mode control for systems with mismatched disturbances. Automatica 49(7), 2287–2291 (2013)
70. Yu, X.H., Zhihong, M., Wu, Y.: Terminal sliding modes with fast transient response. In: Proceedings of the 36th IEEE Conference on Decision and Control, vol. 2, pp. 962–963. IEEE Press, New York (1997)
71. Aghababa, M.P., Sohrab, K., Alizadeh, G.: Finite-time synchronization of two different chaotic systems with unknown parameters via sliding mode technique. Applied Mathemathical Modelling 35(6), 3080–3091 (2011)
72. Yu, X.H., Zhihong, M.: Fast terminal sliding mode control design for nonlinear dynamic systems. IEEE Transactions on Circuits and Systems-I: Fundamental Theory and Applications 49(2), 261–264 (2002)
73. Li, Y.F., Eriksson, B., Wikander, J.: Sliding mode control of two-mass positioning systems. In: Proceedings of the 14th IFAC Triennial World Congress, pp. 151–156. Pergamon, Oxford (1999)
74. Kim, J.J., Lee, J.J., Park, K.B., Youn, M.J.: Design of a new time-varying sliding surface for robot manipulator using variable structure controller. Electronics Letters 29(2), 195–196 (1993)
75. Bartoszewicz, A.: Design of a nonlinear time-varying switching line for second order systems. In: Proceedings of the 37th IEEE Conference on Decision and Control, vol. 3, pp. 2404–2408. IEEE Press, New York (1998)
76. Tokat, S., Eksin, I., Guzelkaya, M., Soylemez, T.: Design of a sliding mode controller with a nonlinear time-varying sliding surface. Transactions of the Institute of Measurement and Control 25(2), 145–162 (2003)

Continuous Sliding Mode Control of a Quadrotor

Nikola G. Shakev and Andon V. Topalov

Control Systems Department, Technical University of Sofia, Branch in Plovdiv,
25 Tsanko Dyustabanov Str., 4000 Plovdiv, Bulgaria
{shakev,topalov}@tu-plovdiv.bg

Abstract. The interest into the unmanned aerial vehicles has largely increased recently. With the advances in technologies it has become possible to test efficiently and cost effectively different autonomous flight control concepts using small-scale aircrafts. In this work the stabilizing and trajectory tracking control problem of a quad-rotor helicopter using sliding mode controllers has been investigated. The well-known ability of the above control approach to stabilize under-actuated systems and to deal with existing nonlinear mismatched uncertainties in their dynamic models makes it a suitable choice for controlling rotorcrafts. The proposed method is based on the definition of several terminal attractors to establish certain relationships between variables to be maintained, thus allowing a designed continuous sliding mode controller to drive the system's trajectory to a sliding surface in a finite time. Asymptotic stability of the system's motion in the sliding mode is then achieved. The effectiveness of the adopted approach is demonstrated by the results from a simulated flight of an automatically controlled small-scale four-rotor helicopter.

Keywords: unmanned aerial vehicles, quad-rotor rotorcraft, sliding mode control, stabilization, nonlinear control.

1 Introduction

Unmanned helicopters are versatile aerial vehicles designed to operate with high agility and to be capable to work in degraded environments that include wind gusts etc. In comparison with the control approaches applicable to the classical helicopters the quad-rotor control design can be implemented more easily. Therefore, different control techniques for quadro-copters have been recently proposed and investigated in the literature. Linearization and linear quadratic regulator (LQR) [1, 2], H-infinity state-space design and feedback linearization [13, 20], model predictive control [10], backstepping control [3] and feedback control laws with saturation elements [16] are among the popular design methods.

Backstepping control approach was proposed in 1990s as a recursive procedure to design stable control laws for a wide class of nonlinear systems [12]. Its specificity is in the way it combines Lyapunov stability theory with the advanced methods from the nonlinear differential-geometric control theory. The backstepping control technique is based on the usage of some states as fictitious controls to control other states.

X. Yu and M. Önder Efe (eds.), *Recent Advances in Sliding Modes,*
Studies in Systems, Decision and Control 24, DOI: 10.1007/978-3-319-18290-2_21

The method gives the possibility to include a broad class of nonlinearities in the controller design. Its stability and error convergence have been rigorously proven. The weak side of the backstepping design procedure, however, is its computational complexity that increases with the system order due to the necessity to perform repeated differentiations of the nonlinear functions. So the method suffers from the so called ‘‘explosion of complexity”. In an attempt to diminish the above disadvantage of the backstepping control and to strengthen its robustness new design procedures based on the combination of the basic backstepping approach with other robust control techniques and with the variable structure control (VSC) or sliding mode control (SMC) approach in particular have emerged [11]. A method, similar to backstepping, called multiple sliding surface (MSS) control, has been proposed to simplify the controller design for systems where model differentiation is difficult [7, 19, 9]. An earlier work on VSC using similar hierarchical and block control principle has been also presented in [4]. MSS control has become a preferable control approach for under-actuated systems where the model structure is in cascade form [12]. It has been used to derive a control scheme for the elevation and travel angles of a 3DOF helicopter stand and for stabilizing control of a quad-rotor rotorcraft [8, 15]. A different approach has been proposed in [21], where the terminal sliding mode control has been extended to control a class of high-order SISO system. A chain-like structure of the sliding mode surfaces has been introduced where the sliding variables converge to zero in a finite time sequentially.

Sliding modes were initially discovered in variable structure systems. The VSC approach uses a discontinuous control structure to guarantee perfect tracking for a class of systems satisfying "matching" conditions and is well known for its invariance against various matched uncertainties, such as variations in the parameters of the dynamic model and existing external disturbances, when the controlled system is in sliding mode. While on the surface, however, due to the involved switching, chattering may occur which has to be removed to allow the controller to perform appropriately [6]. A common approach to avoid chattering is to smooth out the control discontinuity in a thin boundary layer neighboring the switching manifold [18, 5]. Such continuous approximation of the switching function however can provide reaching a sliding surface only asymptotically. In addition, in the case of existing disturbances and uncertainties, convergence is limited only to some vicinity of the sliding manifold [18, 5]. This problem has given impetus to the research on continuous sliding mode controllers, as a specific class that do not implement continuous approximation of the switching function [17].

The method, adopted in this investigation, is based on the definition of several terminal attractors to establish certain relationships between variables to be maintained, thus allowing a continuous sliding mode controller to drive the system’s trajectory to a sliding surface in a finite time. Asymptotic stability of the system’s motion in the sliding mode is then obtained. The proposed approach is applied to the stabilizing and trajectory tracking control problem of a quad-rotor rotorcraft where continuous sliding mode controllers have been designed for its roll, pitch, yaw angles and for the altitude control as well. The presented results from a simulated flight of an automatically controlled small-scale four-rotor rotorcraft demonstrate the effectiveness of the proposed control scheme.

2 Quadrotor Dynamics and the Adopted Control Strategy

2.1 Simplified Dynamics of the Small Size Quad-rotor Rotorcraft

The configuration of the rotors of the quad-rotor unmanned aerial vehicle is shown on fig. 1. There is one rotor at the front and at the rear, while the two others are on the sides. The front and rear rotors turn likewise (counter clockwise) whilst the left and right rotors turn the opposite way. Due to this configuration the gyroscopic effects and aerodynamic torques tend to cancel in trimmed flight. Pitch movement is obtained by increasing (reducing) the speed of the rear motor while reducing (increasing) the speed of the front motor. Roll movement is obtained similarly using the lateral motors. Yaw movement is obtained by increasing (decreasing) the speed of the front and rear motors while decreasing (increasing) the speed of the lateral motors.

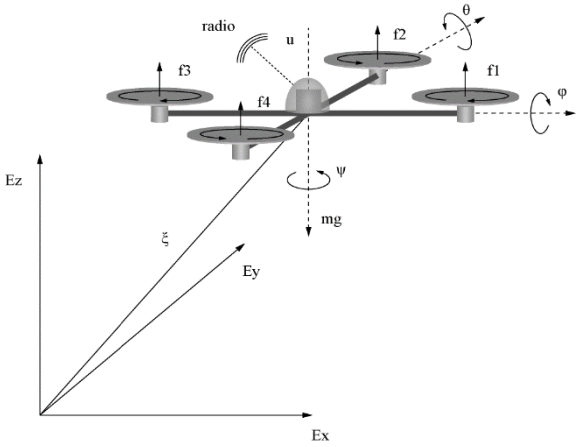

Fig. 1. Schematic representation of the quad-rotor rotorcraft

Typically the rotorcraft motion can be presented into two different frames: an inertial earth frame $\{R_E\}$ (I, E_X, E_Y, E_Z) and a frame fixed to the center of gravity of the aircraft body $\{R_B\}$ (G, x, y, z). The relative position and orientation of frame $\{R_B\}$ with respect to the frame $\{R_E\}$ can be specified by the position vector $\xi = [X\,Y\,Z]^T \in \Re^3$, describing the displacement of the rotorcraft center of mass G relative to the origin of the inertial frame and the orientation vector $\eta = [\psi\,\theta\,\phi]^T \in \Re^3$ where (ψ, θ, ϕ) are the three Euler angles (yaw, pitch, and roll) representing the orientation.

Each propeller generates vertical lifting force, denoted as f_1, f_2, f_3, f_4 respectively and

$$f_i = k\,\omega_i^2 \qquad (i = 1, 2, 3, 4) \tag{1}$$

where ω_i is the rotational speed of the propeller and k is a positive constant. The overall lifting force will be normal to the plane of propellers, and its magnitude will be:

$$u = f_1 + f_2 + f_3 + f_4 \tag{2}$$

The generalized moments caused by the four propellers are

$$\tau = \begin{bmatrix} \tau_\phi \\ \tau_\theta \\ \tau_\psi \end{bmatrix} = \begin{bmatrix} (f_4 - f_2)l \\ (f_3 - f_1)l \\ (\omega_2^2 + \omega_4^2 - \omega_1^2 - \omega_3^2)d \end{bmatrix} \tag{3}$$

where l is the distance from any motor to the center of mass and d is a drag constant.

The dynamic model of the rotorcraft can be developed using the Lagrangian form of the dynamics [2, 16, 14]. Since the Lagrangian contains no cross-terms in the kinetic energy combining $\dot{\xi}$ and $\dot{\eta}$, the Euler-Lagrange equation is partitioned into the dynamics for the ξ coordinates and the η dynamics:

$$m\ddot{X} = u(\cos(\phi)\cos(\psi)\sin(\theta) + \sin(\phi)\sin(\psi)), \tag{4}$$

$$m\ddot{Y} = u(\cos(\phi)\sin(\psi)\sin(\theta) - \sin(\phi)\cos(\psi)), \tag{5}$$

$$m\ddot{Z} = u\cos(\phi)\cos(\theta) - mg, \tag{6}$$

$$I_{zz}\ddot{\psi} = \tau_\psi - \dot{I}_{zz}\dot{\psi}, \tag{7}$$

$$I_{yy}\ddot{\theta} = \tau_\theta - \dot{I}_{yy}\dot{\theta}, \tag{8}$$

$$I_{xx}\ddot{\phi} = \tau_\phi - \dot{I}_{xx}\dot{\phi}, \tag{9}$$

where $J = diag\left(I_{xx}, I_{yy}, I_{zz}\right)$ is inertia matrix expressed in terms of the η dynamics.

In order to obtain an appropriate form of the equations (7) – (9) the following change of input variables is proposed [2, 16]

$$\tau_\psi = I_{zz}\tilde{\tau}_\psi + \dot{I}_{zz}\dot{\psi} \tag{10}$$

$$\tau_\theta = I_{yy}\tilde{\tau}_\theta + \dot{I}_{yy}\dot{\theta} \tag{11}$$

$$\tau_\phi = I_{xx}\tilde{\tau}_\phi + \dot{I}_{xx}\dot{\phi} \tag{12}$$

where $\tilde{\tau} = \left[\tilde{\tau}_\psi \ \tilde{\tau}_\theta \ \tilde{\tau}_\phi\right]^T$ are the new inputs.

Finally we obtain:

$$m\ddot{X} = u(\cos(\phi)\cos(\psi)\sin(\theta) + \sin(\phi)\sin(\psi)) \tag{13}$$

$$m\ddot{Y} = u(\cos(\phi)\sin(\theta)\sin(\psi) - \cos(\psi)\sin(\phi)) \tag{14}$$

$$m\ddot{Z} = u\cos(\phi)\cos(\theta) - mg \tag{15}$$

$$\ddot{\psi} = \tilde{\tau}_{\psi} \tag{16}$$

$$\ddot{\theta} = \tilde{\tau}_{\theta} \tag{17}$$

$$\ddot{\phi} = \tilde{\tau}_{\phi} \tag{18}$$

The generalized coordinates of the rotorcraft are: $q = \left[X\ Y\ Z\ \psi\ \theta\ \phi\right]^T \in \Re^6$

In the dynamical model (13) – (18) the total trust $u \in \Re$ and the torque $\tilde{\tau} \in \Re^3$ are the control inputs, so the quad-rotor rotorcraft is a coupled Lagrangian form under-actuated system with six outputs and four inputs.

2.2 Altitude Control of the Four Rotor Rotorcraft

The vertical displacement Z in (15) can be controlled by forcing the altitude to satisfy the dynamics of a linear system. Therefore the total trust is set [2, 16].

$$u = (r + mg)\frac{1}{\cos\phi\cos\theta} \tag{19}$$

where r is a new control input.

Introducing (19) into (15) and assuming $\cos\theta\cos\phi \neq 0$, that is, $\theta,\ \phi \in (-\pi/2, \pi/2)$ it can be obtained that

$$m\ddot{Z} = r \tag{20}$$

This equation describes the dynamics of a second order system and r has to be chosen such as to guarantee its stability and convergence.

$$r = f_Z(Z, \dot{Z}) \tag{21}$$

2.3 Yaw Angle Control Approach

The rotation of the aircraft around z axis of the body attached frame can be controlled by applying a control law of the following general form

$$\tilde{\tau}_{\psi} = f_{\psi}(\psi, \dot{\psi}) \tag{22}$$

The equation describing the rotorcraft yaw dynamics can be obtained by introducing (22) into (16):

$$\ddot{\psi} = f_{\psi}(\psi, \dot{\psi}) \tag{23}$$

Similarly, $f_\psi(\psi,\dot{\psi})$ has to be chosen such as to guarantee its stability and convergence.

2.4 Quadrotor Pitch and Roll Control Strategy

In order to reduce the dynamics coupling it is useful to design these control laws with respect to the body-fixed frame $\{R_B\}$. For $Z-Y-X$ Euler angles the transition between non-inertial coordinates (x,y,z) and inertial coordinates (X,Y,Z) can be done by the rotation matrix R [16].

$$R=\begin{bmatrix} C_\theta C_\psi & C_\psi S_\theta S_\phi - C_\phi S_\psi & C_\phi C_\psi S_\theta + S_\phi S_\psi \\ C_\theta S_\psi & S_\theta S_\phi S_\psi + C_\phi C_\psi & C_\phi S_\theta S_\psi - C_\psi S_\phi \\ -S_\theta & C_\theta S_\phi & C_\theta C_\phi \end{bmatrix} \tag{24}$$

where $S_{(\cdot)}$ and $C_{(\cdot)}$ represent $\sin(\cdot)$ and $\cos(\cdot)$ respectively.

Thus the acceleration vector can be represented as follows

$$m\begin{bmatrix}\ddot{x}\\ \ddot{y}\\ \ddot{z}\end{bmatrix} = mR^T\begin{bmatrix}\ddot{X}\\ \ddot{Y}\\ \ddot{Z}\end{bmatrix} = R^T\begin{bmatrix}m\ddot{X}\\ m\ddot{Y}\\ m\ddot{Z}\end{bmatrix} \tag{25}$$

Substituting (13)-(15), (19) and (24) in (25) one can obtain

$$m\ddot{x} = mg\sin(\theta) \tag{26}$$

$$m\ddot{y} = -mg\sin(\phi)\cos(\theta) \tag{27}$$

The roll and pitch angles are theoretically limited to $\pm\pi/2$, but in fact during the aircraft stabilization they take smaller values since the upper lift, which compensates the gravity typically is much greater than the forces producing horizontal movement during the flight. To further simplify the analysis we will impose an upper bound on $|\phi|$ and $|\theta|$ in such a way that $\sin(\theta)\approx\theta$ and $\sin(\phi)\approx\phi$. Therefore the forward (longitudinal) movement dynamics can be approximated by the subsystem (28) and the dynamics of side (lateral) movements - by subsystem (29).

$$\begin{vmatrix}\ddot{x} = g\theta\\ \ddot{\theta} = \tilde{\tau}_\theta\end{vmatrix} \tag{28}$$

$$\begin{vmatrix}\ddot{y} = -g\phi\\ \ddot{\phi} = \tilde{\tau}_\phi\end{vmatrix} \tag{29}$$

Let us denote the vector of state variables $\bar{\chi}$:

$$\begin{aligned}\bar{\chi} &= [\chi_1\ \chi_2\ \chi_3\ \chi_4\ \chi_5\ \chi_6\ \chi_7\ \chi_8\ \chi_9\ \chi_{10}\ \chi_{11}\ \chi_{12}]^T = \\ &= \left[z\ \dot{z}\ \psi\ \dot{\psi}\ (x/g)\ (\dot{x}/g)\ \theta\ \dot{\theta}\ (-y/g)\ (-\dot{y}/g)\ \phi\ \dot{\phi}\right]^T\end{aligned} \tag{30}$$

Its time derivative is:

$$\begin{aligned}\dot{\chi} &= [\dot{\chi}_1\ \dot{\chi}_2\ \dot{\chi}_3\ \dot{\chi}_4\ \dot{\chi}_5\ \dot{\chi}_6\ \dot{\chi}_7\ \dot{\chi}_8\ \dot{\chi}_9\ \dot{\chi}_{10}\ \dot{\chi}_{11}\ \dot{\chi}_{12}]^T = \\ &= [\chi_2\ (r/m)\ \chi_4\ \tilde{\tau}_\psi\ \chi_6\ \chi_7\ \chi_8\ \tilde{\tau}_\theta\ \chi_{10}\ \chi_{11}\ \chi_{12}\ \tilde{\tau}_\phi]^T\end{aligned} \tag{31}$$

The state error e_i is specified as:

$$e_i = \chi_{id} - \chi_i \quad (i = 1...12), \tag{32}$$

and χ_{id} $(i = 1...12)$ is the desired value of the state variable χ_i.

The desired values for the altitude, yaw angle, lateral displacement, and longitudinal displacement - $\chi_{1d}, \chi_{3d}, \chi_{5d}, \chi_{9d}$, respectively are set by the operator in accordance with the mission of quadrotor.

The desired values of the remaining state variables cannot be obtained directly. They have to be defined instead by the control strategy in regard to the desired behavior that the quadrotor should have. In this respect the desired values for the state variables $\chi_{id}, (i = 2,4,6,7,8,10,11,12)$ will be chosen in the design stage.

The control signals $(r, \tilde{\tau}_\psi, \tilde{\tau}_\theta, \tilde{\tau}_\phi)$ are calculated as follow:

$$\begin{aligned} r &= m(\dot{\chi}_{2d} + k_2 e_2^\gamma) \\ \tilde{\tau}_\psi &= \dot{\chi}_{4d} + k_4 e_4^\gamma \\ \tilde{\tau}_\theta &= \dot{\chi}_{8d} + k_8 e_8^\gamma \\ \tilde{\tau}_\phi &= \dot{\chi}_{12d} + k_{12} e_{12}^\gamma \end{aligned} \tag{33}$$

where k_2, k_4, k_8, k_{12} are positive; $\gamma = \frac{q}{p}$; and p, q $(p > q)$ are positive odd integers.

Let us define the following sliding variables

$$s_i(t) = \lambda_i e_i + \dot{e}_i \quad (i = 1,3,5,8) \tag{34}$$

and the following sliding surfaces respectively

$$s_i(t) = 0 \quad (i = 1,3,5,8) \tag{35}$$

3 Finite-reaching-time Continuous Sliding Mode Controller Design

3.1 Terminal Attractor

It has been shown in [22] that $z = 0$ is the terminal attractor of the system

$$\dot{z} = -k\ z^{q/p} \tag{36}$$

where $k>0$ and p,q ($p>q$) are positive odd integers. The relaxation time t_S for a solution of a system (36) is given by

$$t_S = k^{-1}\int_{z(0)}^{0}\frac{dz}{z^{q/p}} = \frac{\left|z(0)\right|^{1-q/p}}{k\ (1-q/p)} \tag{37}$$

3.2 The Altitude Subsystem

Let us first consider the vertical displacement subsystem including state variables χ_1, χ_2 and the control signal $r(t)$. The time derivative of the error $e_2(t)$ governed by the control signal $r/m = \dot{\chi}_{2d} + k_2 e_2^{\gamma}$ can be calculated by the next expression

$$\dot{e}_2 = \dot{\chi}_{2d} - \dot{\chi}_2 = \dot{\chi}_{2d} - r/m = \dot{\chi}_{2d} - \dot{\chi}_{2d} - k_2 e_2^{\gamma} = -k_2 e_2^{\gamma} \tag{38}$$

Since (38) represents the dynamics of the terminal attractor (36) the error $e_2(t)$ will converge to zero and χ_2 will converge to χ_{2d}:

$$\begin{aligned} e_2(t_{S2}) &= 0 \\ \chi_2(t_{S2}) &= \chi_{2d} \end{aligned} \tag{39}$$

The relaxation time t_{S2} taken to drive the error $e_2(0)$ to $e_2(t_{S2}) = 0$ is given by

$$t_{S2} = k_2^{-1}\int_{e_2(0)}^{0}\frac{de_2}{e_2^{\gamma}} = \frac{\left|e_2(0)\right|^{1-\gamma}}{k_2(1-\gamma)} \tag{40}$$

A Lyapunov function candidate for the sliding surface $s_1 = 0$ can be chosen as:

$$V_1 = \frac{1}{2}s_1^2 \tag{41}$$

Considering (39) for $t \geq t_{S2}$ the time derivative of error $e_1(t)$ is

$$\dot{e}_1 = \dot{\chi}_{1d} - \dot{\chi}_1 = \dot{\chi}_{1d} - \chi_2 = \dot{\chi}_{1d} - \chi_{2d} \tag{42}$$

And if we choose

$$\chi_{2d}(t) = \dot{\chi}_{1d}(t) + k_1 e_1(t) \tag{43}$$

where k_1 is a positive constant, the time derivative of V_1 can be determined as:

$$\begin{aligned} \dot{V}_1 &= \dot{s}_1 s_1 = (e_1 + \lambda_1 \dot{e}_1)(\dot{e}_1 + \lambda_1 \ddot{e}_1) = \\ &= (e_1 - \lambda_1 k_1 e_1)(-k_1 e_1 + \lambda_1 k_1^2 e_1) = \\ &= -e_1^2 k_1 (1 - \lambda_1 k_1)^2 \leq 0 \end{aligned} \tag{44}$$

The inequality (44) is satisfied and as a result the error $e_1(t)$ will converge to zero along the sliding manifold $s_1(t)=0$ and the altitude χ_1 will converge to the desired value χ_{1d}:

$$\begin{aligned} e_1 &\to 0 \\ \chi_1 &\to \chi_{1d} = z_d \end{aligned} \tag{45}$$

Remark: The relaxation time t_{S2} is actually equal to the time t_{r1} necessary for sliding variable s_1 to reach the sliding surface $s_1=0$.

$$t_{r1} = t_{s2} \tag{46}$$

The block diagram of the altitude subsystem controller is presented on fig.2.

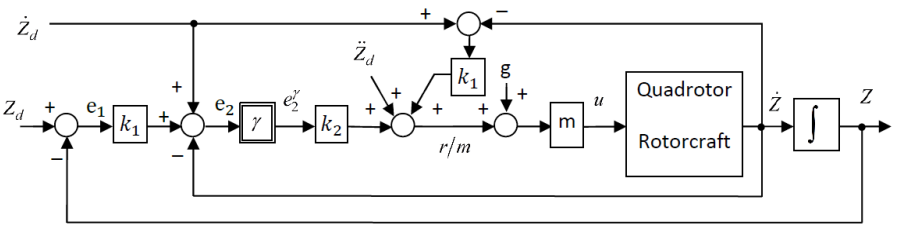

Fig. 2. Block diagram of the altitude subsystem controller

3.3 Yaw Angle Subsystem

For the yaw angle subsystem that includes state variables χ_3, χ_4 the time derivative of the error $e_4(t)$ governed by the control signal $\tilde{\tau}_\psi = \dot{\chi}_{4d} + k_4 e_4^\gamma$ can be calculated by the next expression

$$\dot{e}_4 = \dot{\chi}_{4d} - \dot{\chi}_4 = \dot{\chi}_{4d} - \tilde{\tau}_\psi = \dot{\chi}_{4d} - \dot{\chi}_{4d} - k_4 e_4^\gamma = -k_4 e_4^\gamma \tag{47}$$

Since (47) represents the dynamics of a terminal attractor, the error $e_4(t)$ will converge to zero and χ_4 will converge to χ_{4d} for a finite time t_{S4}.

$$t_{S4} = k_4^{-1} \int_{e_4(0)}^{0} \frac{de_4}{e_4^\gamma} = \frac{|e_4(0)|^{1-\gamma}}{k_4(1-\gamma)} \tag{48}$$

This means that at time t_{S4} the state variable $\chi_4(t)$ reaches the desired value $\chi_{4d}(t)$.

$$\begin{aligned} e_4(t_{S4}) &= 0 \\ \chi_4(t_{S4}) &= \chi_{4d} \end{aligned} \tag{49}$$

Similarly let us choose a Lyapunov function candidate for the sliding surface $s_3 = 0$ as:

$$V_3 = \frac{1}{2} s_3^2 \tag{50}$$

Considering (49) for $t \geq t_{S4}$ the time derivative of error the $e_3(t)$ is

$$\dot{e}_3 = \dot{\chi}_{3d} - \dot{\chi}_3 = \dot{\chi}_{3d} - \chi_4 = \dot{\chi}_{3d} - \chi_{4d} \tag{51}$$

And if we choose

$$\chi_{4d}(t) = \dot{\chi}_{3d}(t) + k_3 e_3(t) \tag{52}$$

where k_3 is a positive constant, the time derivative of V_3 can be calculated as follows:

$$\begin{aligned} \dot{V}_3 &= \dot{s}_3 s_3 = (e_3 + \lambda_3 \dot{e}_3)(\dot{e}_3 + \lambda_3 \ddot{e}_3) = \\ &= (e_3 - \lambda_3 k_3 e_3)(-k_3 e_3 + \lambda_3 k_3^2 e_3) = \\ &= -e_3^2 k_3 (1 - \lambda_3 k_3)^2 \leq 0 \end{aligned} \tag{53}$$

In case $k_3 > 0$ the inequality (53) is satisfied. As a result the error $e_3(t)$ will converge to zero along the sliding manifold $s_3 = 0$ and the yaw angle χ_3 will converge to the desired value χ_{3d}:

$$\begin{aligned} e_3 &\to 0 \\ \chi_3 &\to \chi_{3d} = \psi_d \end{aligned} \tag{54}$$

3.4 Continuous Sliding Mode Control of the Pitch and Roll Angles Subsystems

Let us first consider the subsystem describing the rotorcraft pitch angle θ and position x dynamics (state variables χ_5, χ_6, χ_7 and χ_8). The time derivative of the error $e_8(t)$ governed by the control signal $\tilde{\tau}_\theta = \dot{\chi}_{8d} + k_8 e_8^\gamma$ can be calculated by the next expression

$$\dot{e}_8 = \dot{\chi}_{8d} - \dot{\chi}_8 = \dot{\chi}_{8d} - \tilde{\tau}_\theta = \dot{\chi}_{8d} - \dot{\chi}_{8d} - k_8 e_8^\gamma = -k_8 e_8^\gamma \tag{55}$$

Since (55) represents the dynamics of a terminal attractor, the error $e_8(t)$ will converge to zero and χ_8 will converge to χ_{8d} for a finite time t_{S8}.

$$t_{S8} = k_8^{-1} \int_{e_8(0)}^{0} \frac{de_8}{e_8^\gamma} = \frac{|e_8(0)|^{1-\gamma}}{k_8(1-\gamma)} \tag{56}$$

This means that at time t_{S8} the state variable $\chi_8(t)$ reaches the desired value $\chi_{8d}(t)$ and will stay at this value until some external forces disturb it.

$$\begin{aligned} e_8(t_{S8}) &= 0 \\ \chi_8(t_{S8}) &= \chi_{8d} \end{aligned} \tag{57}$$

Substituting

$$\chi_{8d}(t) = \dot{\chi}_{7d}(t) + k_7 e_7^{\gamma}(t) \tag{58}$$

and considering (57) for $t \geq t_{S8}$ the time derivative of the error $e_7(t)$ can be calculated by the next expression

$$\dot{e}_7 = \dot{\chi}_{7d} - \dot{\chi}_7 = \dot{\chi}_{7d} - \chi_8 = \dot{\chi}_{7d} - (\dot{\chi}_{7d} + k_7 e_7^{\gamma}) = -k_7 e_7^{\gamma} \tag{59}$$

In a similar way (59) represents the dynamics of a terminal attractor. The error $e_7(t)$ will converge to zero and the state variable χ_7 will converge to χ_{7d} for a finite time interval t_{S7}.

$$t_{S7} = k_7^{-1} \int_{e_7(t_{S8})}^{0} \frac{de_7}{e_7^{\gamma}} = \frac{\left|e_7(t_{S8})\right|^{1-\gamma}}{k_7(1-\gamma)} \tag{60}$$

This means that

$$\begin{aligned} e_7(t_{S8} + t_{S7}) &= 0 \\ \chi_7(t_{S8} + t_{S7}) &= \chi_{7d} \end{aligned} \tag{61}$$

For the state variable $\chi_7(t)$ we can set the following desired value:

$$\chi_{7d}(t) = \dot{\chi}_{6d}(t) + k_6 e_6^{\gamma}(t) \tag{62}$$

This allows obtaining the next expression for the dynamics of the state error $e_6(t)$

$$\dot{e}_6 = \dot{\chi}_{6d} - \dot{\chi}_6 = \dot{\chi}_{6d} - \chi_7 = \dot{\chi}_{6d} - (\dot{\chi}_{6d} + k_6 e_6^{\gamma}) = -k_6 e_6^{\gamma} \tag{63}$$

The equation (63) again represents the dynamics of a terminal attractor and the error $e_6(t)$ will converge to zero. The state variable χ_6 will converge to χ_{6d} for a finite time t_{S6}

$$t_{S6} = k_6^{-1} \int_{e_6(t_{S8}+t_{S7})}^{0} \frac{de_6}{e_6^{\gamma}} = \frac{\left|e_6(t_{S8} + t_{S7})\right|^{1-\gamma}}{k_6(1-\gamma)} \tag{64}$$

In consequence the state variable χ_6 reaches the desired value χ_{6d} for a time t_{S6} starting at the moment of satisfying (63).

$$\begin{aligned} e_6(t_{S8} + t_{S7} + t_{S6}) &= 0 \\ \chi_6(t_{S8} + t_{S7} + t_{S6}) &= \chi_{6d} \end{aligned} \tag{65}$$

A Lyapunov function candidate for the sliding surface $s_5 = 0$ can be chosen as:

$$V_5 = \frac{1}{2} s_5^2 \tag{66}$$

Considering (65) for $t \geq t_{S8} + t_{S7} + t_{S6}$ the time derivative of the error $e_5(t)$ can be calculated by the next expression

$$\dot{e}_5 = \dot{\chi}_{5d} - \dot{\chi}_5 = \dot{\chi}_{5d} - \chi_6 = \dot{\chi}_{5d} - \chi_{6d} \tag{67}$$

And if we choose

$$\chi_{6d}(t) = \dot{\chi}_{5d}(t) + k_5 e_5(t) \tag{68}$$

where k_5 is a positive constant, the time derivative of V_5 can be determined as:

$$\begin{aligned} \dot{V}_5 &= \dot{s}_5 s_5 = (e_5 + \lambda_5 \dot{e}_5)(\dot{e}_5 + \lambda_5 \ddot{e}_5) = \\ &= (e_5 - \lambda_5 k_5 e_5)(-k_5 e_5 + \lambda_5 k_5^2 e_5) = \\ &= -e_5^2 k_5 (1 - \lambda_5 k_5)^2 \leq 0 \end{aligned} \tag{69}$$

The inequality (69) is satisfied and as a result the error $e_5(t)$ will converge to zero along the sliding manifold $s_5 = 0$. Thus the quadrotor's position χ_5 will converge to the desired position χ_{5d}:

$$\begin{aligned} e_5 &\to 0 \\ \chi_5 &\to \chi_{5d} \end{aligned} \tag{70}$$

According to the obtained results it follows that the state errors $e_8(t)$, $e_7(t)$, $e_6(t)$, $e_5(t)$ will consecutively converge to zero.

For the subsystem describing the dynamics of the roll angle ϕ and the rotorcraft's position y (state variables χ_9, χ_{10}, χ_{11} and χ_{12}), governed by the control signal $\tilde{\tau}_\phi = \dot{\chi}_{12d} + k_{12} e_{12}^{\gamma}$, it is possible in analogous manner to repeat the above analysis. As a result it can be shown in a similar way that the state errors $e_{12}(t)$, $e_{11}(t)$, $e_{10}(t)$, $e_9(t)$ will consecutively converge to zero.

4 Simulation Results

The performance of the proposed finite-reaching-time continuous sliding mode controllers has been evaluated by conducting flight simulations with an automatically controlled small-scale quadrotor. They have been carried in the Matlab/Simulink programming environment. The simplified dynamic model of the four rotor rotorcraft described by the equations (13) – (18) has been used.

The proposed continuous sliding mode control strategy has been tested in two consecutive simulation experiments. The first one has considered the rotorcraft stabilization problem. During it the step responses of all subsystems have been investigated. The quadrotor has been expected to execute separate lateral, longitudinal and altitude displacements at a distance of 2 meters and also to rotate around Z axis at an angle of $\pi/2$ rad. The following desired values of the state variables have been set accordingly:

$$\begin{aligned} \chi_{1d} &= 2; \\ \chi_{3d} &= \pi/2; \\ \chi_{5d} &= 2; \\ \chi_{9d} &= 2; \end{aligned} \tag{71}$$

The controller parameters have been chosen as follow

$$\begin{aligned} & k_1 = 1; \quad k_2 = 1; \\ & k_3 = 1; \quad k_4 = 1; \\ & k_5 = 0.1; \quad k_6 = 0.5; \quad k_7 = 1; \quad k_8 = 8; \\ & k_9 = 0.1; \quad k_{10} = 0.5; \quad k_{11} = 1; \quad k_{12} = 8; \\ & \gamma = q/p; \quad q = 17; \quad p = 19; \end{aligned} \tag{72}$$

The obtained results are shown on figures 3 - 10. Fig. 3 represents the error between the desired and the current altitude $e_1(t)$, as well as the error between the desired and current vertical velocities $e_2(t)$. It has to be noted that the desired value for the vertical velocity has not been fixed, but it has been calculated instead in accordance with equation (34). The phase trajectories of $e_1(t)$ and $e_2(t)$ are shown on fig. 4. In a similar manner fig. 5 shows the evolution of the yaw angle error $e_3(t)$ and the angular velocity error $e_4(t)$, while fig. 6 represents the phase trajectories of the errors $e_3(t)$ and $e_4(t)$. Fig. 7 and fig. 8 illustrate graphically the dynamics of the pitch angle and the longitudinal displacement subsystem. That is fig. 7 represents the error between the desired and current longitudinal position $e_5(t)$, as well as the angular speed error of the pitch angle $e_8(t)$. Fig. 8 demonstrates the phase trajectories of the errors $e_5(t)$ and $e_8(t)$. The dynamics of the roll angle and lateral displacement subsystem is shown on fig. 9 and fig. 10. That is fig. 9 shows the error between the desired and the current lateral position $e_9(t)$, as well as the angular speed error of the roll angle $e_{12}(t)$. The phase trajectories are shown on fig. 10 respectively.

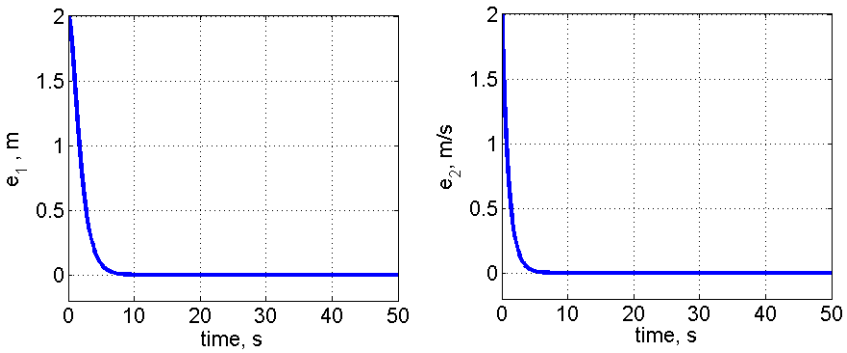

Fig. 3. The evolution of the altitude error $e_1 = z_d - z$ and the vertical speed error $e_2 = \dot{z}_d - \dot{z}$

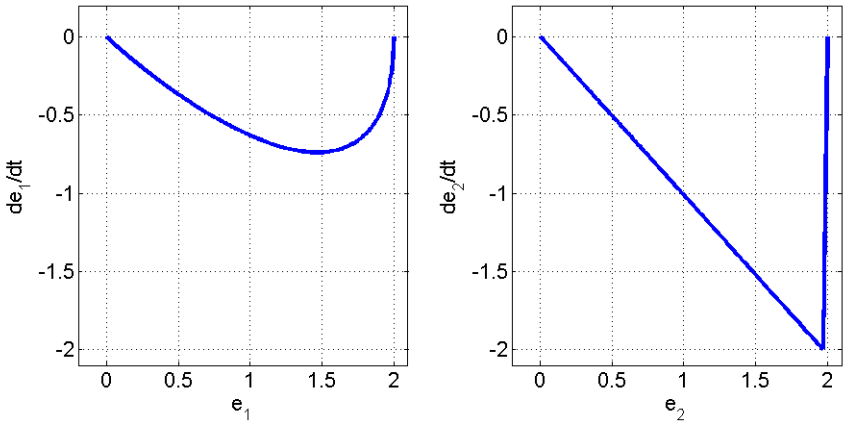

Fig. 4. The phase trajectories of the errors e_1 and e_2

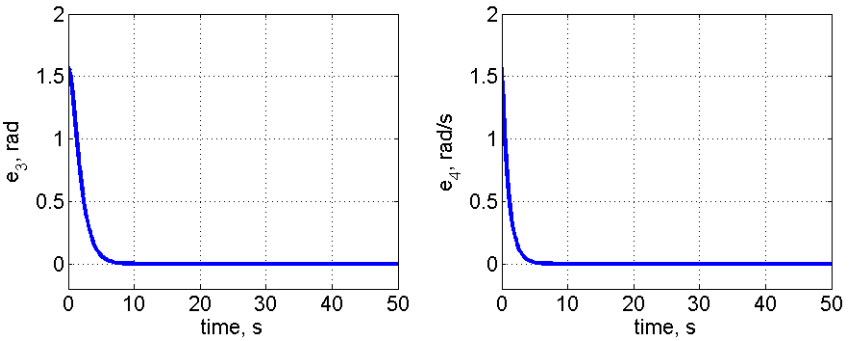

Fig. 5. The evolution of the yaw angle error $e_3 = \psi_d - \psi$ and the angular speed error $e_4 = \dot{\psi}_d - \dot{\psi}$

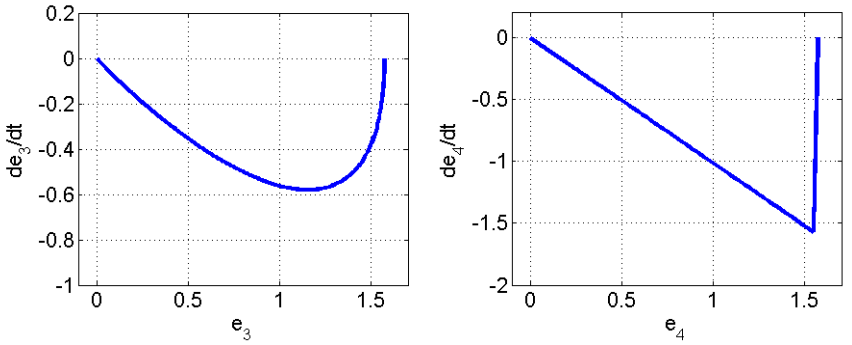

Fig. 6. The phase trajectories of the errors e_3 and e_4

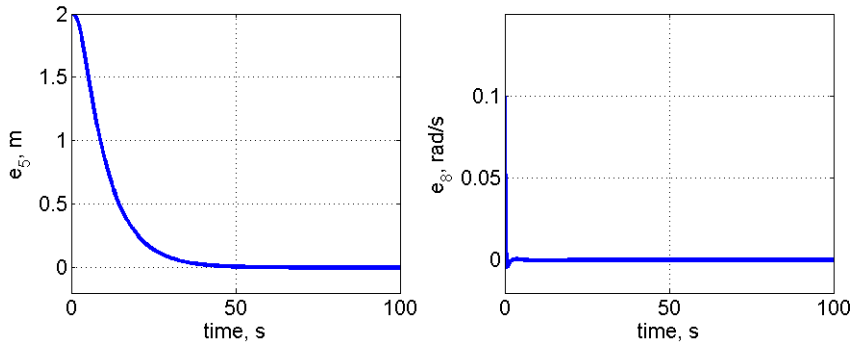

Fig. 7. The evolution of the longitudinal error $e_5 = x_d - x$ and the angular speed error of the pitch angle $e_8 = \dot{\theta}_d - \dot{\theta}$

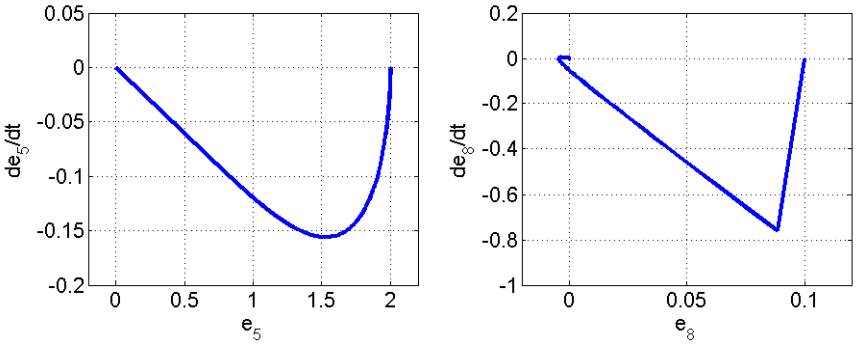

Fig. 8. The phase trajectories of the errors e_5 and e_8

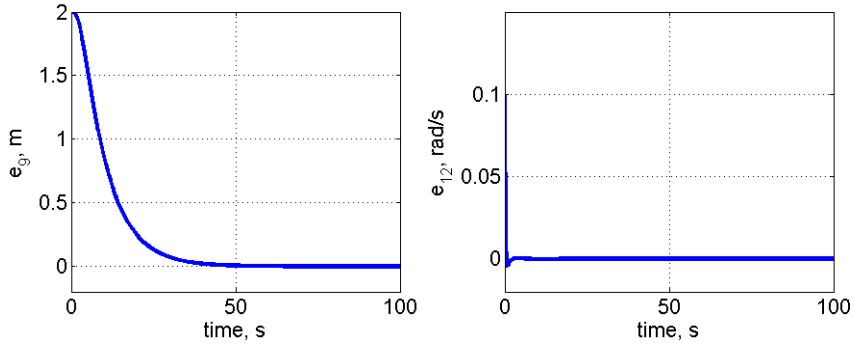

Fig. 9. The evolution of the lateral error $e_9 = y_d - y$ and the angular speed error of the roll angle $e_{12} = \dot{\phi}_d - \dot{\phi}$

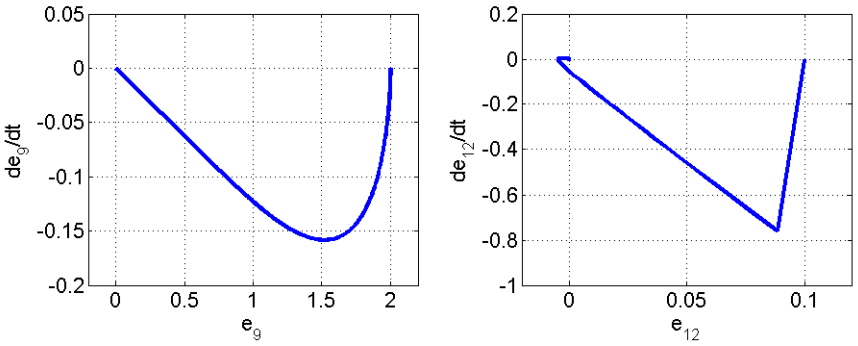

Fig. 10. The phase trajectories of the errors e_9 and e_{12}

The second simulation experiment has investigated the dynamics of the system during the trajectory tracking problem. The rotorcraft has been expected to take off and to track a circular trajectory with a radius of 1 m, situated on horizontal plane at an altitude of 2 m. Fig. 11 shows how the rotorcraft has tracked the desired trajectory in the 3D space.

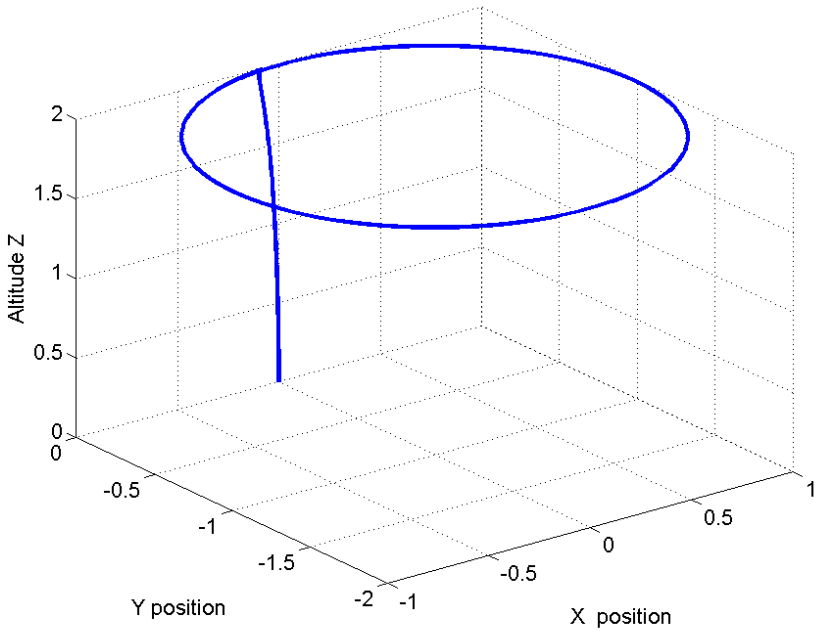

Fig. 11. The rotorcraft trajectory in 3D space during the trajectory tracking simulation experiment

The results obtained from simulations have demonstrated the good performance of the rotorcraft during the automatically guided flights using the designed continuous sliding mode controllers. The proposed method ensures high control robustness, good static and dynamic performance (features that are typical for the sliding-mode control approach). Moreover, the control complexity remains the same as for the standard control algorithms.

5 Conclusions

In this investigation a continuous SMC strategy has been successfully applied and tested to control the position and orientation of a small size quad-rotor rotorcraft during autonomous flights. The proposed method is based on the definition of several terminal attractors to establish certain relationships between variables to be maintained, thus allowing a designed continuous sliding mode controller to drive the system's trajectory to a sliding surface in a finite time. Asymptotic stability of the system's motion in the sliding mode is then achieved. The flight simulations have shown that the proposed controllers demonstrate good performance and are suitable for stabilization and implementation of trajectory tracking tasks for small size unmanned drones.

Acknowledgment. The authors gratefully acknowledge the crucial impact that their professional relationship with Professor Okyay Kaynak, has on their involvement in research in the field of variable structure systems and sliding mode control. As a friend and collaborator he has always been an inexhaustible source of new fruitful ideas and his support has been encouraging and inspiring us to investigate new problems and applications within this very interesting research area.

The authors also acknowledge the financial support for this investigation provided within the Ministry of Education and Science of Bulgaria Research Fund Project DFNI 102/6.

References

1. Bouabdallah, S., North, A., Siegwart, R.: PID vs LQ control techniques applied to an indoor micro quadrotor. In: Proc. of Int. Conf. on Intelligent Robots and Systems, pp. 2451–2456 (2004)
2. Castillo, P., Lozano, R., Dzul, A.E.: Stabilization of a mini rotorcraft with four rotors. IEEE Control Syst. Mag. 25, 45–55 (2005)
3. Das, A., Lewis, F., Subbarao, K.: Backstepping approach for controlling a quadrotor using Lagrange form dynamics. Journal of Intell. Robot. Syst. 56, 127–151 (2009)
4. Drakunov, S.V., Izosimov, D.B., Lukyanov, A.G., Utkin, V.A., Utkin, V.I.: Block control principle, Automation and Remote Control part. 1 51(5), 38–46, Automation and Remote Control part. 2 51(6), 20-31 (1990)
5. Esfandiary, F., Khalil, H.K.: Stability analysis of a continuous implementation of variable structure control. IEEE Transactions on Automatic Control 36(5), 616–619 (1991)

6. Fridman, L.: Sliding mode enforcement after 1990: Main results and some open problems. In: Fridman, L., Moreno, J., Iriarte, R. (eds.) Sliding Modes. LNCIS, vol. 412, pp. 3–57. Springer, Heidelberg (2011)
7. Greenand, J., Hedrick, J.K.: Nonlinear speed control for automotive engines. In: Proc. of 1990 American Control Conf., San Diego, CA, vol. 3, pp. 2891–2898 (1990)
8. Hamood, M.A., Akmeliawati, R., Leqowo, A.: Multiple-surface sliding mode control for 3DOF helicopter. In: Proc. of 4th Int. Conf. on Mechatronics (ICOM), Kuala Lumpur, Malaysia, May 17-19. ©2011 IEEE (2011) 978-1-61284-437-4/11
9. Hedrick, J.K., Yip, P.P.: Multiple sliding surface control: Theory and application. Journal of Dynamic Syst., Measurement, and Control 122(4), 586–593 (2000)
10. Kim, H.J., Shim, D.H., Sastry, S.: Nonlinear model predictive tracking control for rotorcraft-based unmanned aerial vehicles. In: Proc. of the American Control Conference, Anchorage, AK, May 8-10, pp. 3576–3581 (2002)
11. Koshkouei, A.J., Mills, R.E., Zinober, A.S.I.: Adaptive backstepping control. In: Yu, X., Xu, J.-X. (eds.) Variable Structure Systems: Towards the 21st Century. LNCIS, vol. 274, pp. 128–153. Springer, Heidelberg (2002)
12. Krstic, M., Kanellakopoulos, I., Kokotovic, P.: Nonlinear and Adaptive Control Design. John Wiley & Sons, Inc., New York (1995)
13. Mokhtari, A., Benallegue, A., Daachi, B.: Robust feedback linearization and GH∞ controller for a quadrotor unmanned aerial vehicle. Journal of Electr. Eng. 57(1), 20−27 (2006)
14. Naidoo, Y., Stopforth, R., Bright, G.: Quad-rotor unmanned aerial vehicle helicopter modelling & control. Int. Journal of Adv. Robotic Systems 8(4), 139–149 (2011)
15. Shakev, N.G., Topalov, A.V., Shiev, K.B., Kaynak, O.: Stabilizing multiple sliding surface control of quad-rotor rotorcraft. In: Proc. of the 9th Asian Control Conference, ASCC 2013, Istanbul, Turkey, June 23-26. ©2013 IEEE (2013) 978-1-4673-5769-2/13
16. Shakev, N.G., Topalov, A.V., Kaynak, O., Shiev, K.B.: Comparative results on stabilization of the quad-rotor rotorcraft using bounded feedback controllers. Journal of Intell. Robot. Syst. 65, 389–408 (2012)
17. Shtessel, Y.B., Buffington, J.M.: Continuous sliding mode control. In: Proc. of the American Control Conference, Philadelphia, Pennsylvania, USA, pp. 562–563 (1998)
18. Slotine, J., Li, W.: Applied Nonlinear Control. Prentice Hall, Englewood Cliffs (1991)
19. Won, M., Hedrick, J.K.: Multi-surface sliding control of a class of uncertain nonlinear systems. Int. Journal of Control 64(4), 693–706 (1996)
20. Yang, C.-D., Liu, W.-H.: Nonlinear H∞ decoupling hover control of a helicopter with parameter uncertainties. In: Proc. of American Control Conference, Denver, Colorado, June 4-6, pp. 3454−3459 (2003)
21. Yu, X., Man, Z.: Model reference adaptive control systems with terminal sliding modes. Int. Journal of Control 64, 1165–1176 (1996)
22. Zak, M.: Terminal attractors in neural networks. Neural Networks 2, 259–274 (1989)

Author Index